NON-LINEAR ANALYSIS OF REINFORCED CONCRETE STRUCTURES SUBJECTED TO TRANSIENT FORCES

By

AHMAD NICKNAM

SUBMITTED FOR THE DEGREE OF

DOCTOR OF PHILOSOPHY

AT HERIOT-WATT UNIVERSITY

ON COMPLETION OF RESEARCH IN THE

DEPARTMENT OF CIVIL AND OFFSHORE ENGINEERING

JANUARY 1994.

DEDICATION

This work is dedicated to my
wife, Mahsa and Afsoon our daughters.

I hereby declare that the work presented in this thesis was carried out by myself at Heriot-Watt University, Edinburgh, except where due acknowledgement is made, and has not been submitted for any other degree.

AHMAD NICKNAM (Candidate)

PROF. I. M. MAY (Supervisor)

28-1-94

Date

Contents

List of Tables

List of Figures

Ackowledgements

I would like to express my appreciation and thanks to my supervisor Professor I. M. May who has contributed immensely by way of encouragement, useful suggestions, many discussions and purposeful guidance throughout the entire course of this study.

Sincere thanks go to the author's friend Dr. Damangir for his encouragement and useful discussions.

The author is grateful to the staff of Bradford University and Heriot-Watt university libraries for their help in obtaining many of the papers referenced herein. Thanks are also due to the advisory staff of computer center of both universities for their assistance in computational matters.

The author acknowledges the financial support of the Tunel Arme Company during the period of this investigation (1988-1994).

My special thanks are due to my wife and two daughters Mahsa and Afsoon for their understanding, encouragement and loving support during the research period.

Abstract

The objective of this study was to investigate the non-linear finite element analysis of reinforced concrete structures under transient forces particularly seismic loading. The thesis can be broadly divided into five parts.

In the first part, the experimental evidence of rate effect on tensile strength, compressive strength and peak compressive strain of concrete is reviewed. The classical elastic, plastic and viscoplastic theories are also reviewed and Perzyna's viscoplastic model is described. A rheological model is proposed which enables the simulation of strain-rate parameters such as initial modulus of elasticity, secant modulus elasticity and peak strength of concrete. Emphasis has been concentrated on modelling the material stiffening and strengthening due to increasing strain-rate. The fluidity parameters are highlighted and the parameters involved are determined using existing experimental data.

In the second part, spatial discretisation and mass discretisation are described. A formula for producing a lumped mass matrix from a consistent mass matrix for square and rectangular elements is proposed which allows the natural frequencies to be determined more accurately than the existing methods.

The third part is devoted to a brief explanation of dynamic solution techniques. The accuracy and stability of currently used algorithms, particularly those suitable for dynamic analysis of structures under seismic loading, are discussed. Attention has been focused on the effect of algorithmic errors on structural response in direct integration schemes . The effect of spatial discretisation on the accuracy of the natural frequencies is discussed and shown by an example.

In the fourth part, the proposed model is implemented in a computer program for plane and axisymmetric problems. Two types of concrete cylindrical specimens and reinforced concrete structures under transient force are analysed and the results are compared with those obtained by other investigator where available. The ability of the model for simulation of the material stiffening and strengthening is shown.

The fifth part of the thesis describes the proposed variable mixed explicit-implicit algorithm for analysing dynamic problems under loading of long-duration. The accuracy of the algorithm is compared with the traditional explicit- implicit method by some examples.

Conclusions and recommendations for further work are presented in the last part of the thesis.

Chapter 1

1.1 Background

Concern at the high level of damage to structures and loss of life over the last number of years, particularly in Iran, due to earthquakes has been one of the driving factors behind this research.

In the past, most analytical models for reinforced concrete structures have concentrated on the static behaviour. This has included the ability to model stress softening, confinement effects, cyclic degradation of stiffness, volumetric dilatation and interaction between reinforcing steel and concrete. However, when a structure responds to impulsive loading, the local material behaviour can vary significantly. Large stress and strain gradients occur as the dynamic load propagates through the entire structure in a transient manner. The response is governed by the kinetic energy of the material. Energy is used in straining and accelerating the material and in the production of microcracks. Local material failure is produced by the growth and development of macrocracks.

In this study, attention has been focused on modelling the history-strain-rate-sensitivity of reinforced concrete structures under transient forces, particularly earthquake loading. Due to lack of experimental data, a limited number of rate-dependent parameters have been simulated and further research is required to extend the present model to incorporate all the material rate-dependent parameters.

1.1.1 Statement of the problem

Designs for reinforced concrete structures subjected to transient forces are grouped on the basis of the type of dynamic loads. The first group are designed to withstand impulsive loads of high frequency and short duration which might be due to impact from ballistic missiles, high explosive, effects of blast shock, etc. The second group are designed to resist transient forces of low to medium frequency with long duration, such as earthquake, winds, etc. Such dynamic loads cause intense local dynamic stresses which lead to local penetration, crushing and fracturing, and potentially overall structural collapse of failure.

Analytical models for such problems are required to predict the behaviour of structures under such a type of time-dependent loading. In this study, attention has been focused on modelling the second group of reinforced concrete structures.

1.1.2 Scope and objective of the present research

The aim of the research is to develop and demonstrate a numerical model to predict the non-linear behaviour of reinforced concrete structures under transient forces, particularly those due to earthquake loading.

In order to accomplish this objective, a number of idealizations such as geometry, boundary conditions and loading are to be made. Various characteristics of each idealized component are identified according to their physical properties using the laws of mechanics.

The finite element method is the most versatile and powerful method for modelling the geometry and loading. Identification of the characteristics of each modelled component depends on the availability of relevant mechanical properties. For example, the experimental data available for cracked reinforced concrete under impulsive loading does not suffice for the post-cracked behaviour of concrete to be idealized.

The principal aims of the thesis can be summarized as follows:

- To present the finite element formulation for the spatial discretisation of reinforced concrete structures and to review the finite difference formulae

for solving the simultaneous equilibrium equations of motion in dynamic problems.

- To review the available experimental data on the behaviour of concrete loaded at high strain-rates.

- To develop a history-strain-rate-dependent constitutive model for concrete.

- To review existing models for predicting the non-linear behaviour of reinforced concrete structures under rate-sensitivity loads and the strain-rate-dependent parameters used to describe the mechanical property of the material.

- To develop a model for the effects of strain-rate on the compressive and tensile strengths of concrete, the initial modulus of elasticity, the tangent modulus of elasticity and the peak strength of concrete.

- To present a rate-dependent formula in viscous problems for determining the rate-dependent parameters.

- To review the numerical algorithms currently used for solving dynamic problems and to assess their accuracy and stability.

- To discuss the appropriate method for the numerical dynamic analysis of structures under short, medium and long loading duration.

- To develop an efficient numerical algorithm with the appropriate accuracy and the minimum computational effort for solving short and long duration dynamic problems.

- To develop a versatile flexible and comprehensive computer program for the numerical dynamic analysis of reinforced concrete structures.

1.1.3 Lay-out of the thesis

Chapter 2 starts with a discussion of the available experimental observation of concrete under dynamic loading. The increase in the initial modulus of elasticity, the tangent modulus of elasticity, Poisson's ratio, the peak compressive and tensile strength of concrete under time-dependent loading are shown. The chapter continues with an explanation of the classical theories for predicting the non-linear behaviour of reinforced concrete. Damage-based models in which initiation and propagation of microcracks are monitored by a damage function are discussed. Perzyna's visco-plastic model [119], adopted in this study, is discussed and assessed. The next section of the chapter is devoted to a description of the mechanical characteristics of concrete and reinforcing steel. The constitutive laws for pre- and post-cracked concrete, the existing failure criteria, the proposed failure surface are the subjects of the next sections.

The proposed rheological model for concrete and the proposed model for predicting the effect of strain-rate on the rate-sensitive parameters, the proposed formulae for the fluidity parameters and the incremental form of the proposed uniaxial model are discussed in subsequent sections. The chapter closes with a description of the rate-sensitive function for reinforcing steel.

In chapter 3, the spatial discretisation, mass discretisation and the method for producing a lumped mass matrix from a consistent mass matrix are discussed. A new formula for producing a lumped mass matrix from a consistent mass matrix for square and rectangular elements is proposed.

Chapter 4 starts with a description of the eigenvalue problem and the superposition method. The contribution of higher modes to the structural response is discussed and illustrated with an example. The next section is devoted to finite difference schemes. The direct integration methods in the form of implicit and explicit algorithms, and the mixed explicit-implicit algorithms are the subject of the next sections and some of the currently used numerical methods are discussed. The chapter closes with a description of the non-linear solution techniques.

Chapter 5 starts with explanation of some general items and the background

to dynamic solution techniques. The assessment of the accuracy and stability of a number of numerical algorithms discussed in chapter 4 is given in the next section of this chapter. Attention is focused on the assessment of the stability conditions for implicit and explicit algorithms and the response inaccuracy caused by artificial algorithmic errors. The efficiency of the currently used numerical algorithms, with and without numerical dissipation and dispersion, are assessed and demonstrated graphically. Errors due to spatial discretisation are the subject of the next section. The chapter closes with a description of the stability condition due to material non-linearity and visco-plastic strain approximation.

Chapter 6 starts with a brief explanation of the formulae used in the proposed model for predicting the concrete behaviour under dynamic loading and continues with an explanation of the program structure and flow chart. The next section is devoted to the analysis of the compressive and tensile specimens of Hatano [10] and the compressive specimen of Ahmad [21].

The dynamic analysis of a simply supported reinforced concrete beam subjected to two suddenly applied concentrated loads is the subject of the next section. The chapter closes with the dynamic analysis of a clamped circular reinforced concrete slab under a ramp loading and a discussion of the results.

Chapter 7 starts with an explanation of the governing equations for modal superposition method, the Newmark implicit and explicit methods, the mixed implicit-explicit algorithms. The next section is devoted to a description of the proposed variable implicit-explicit algorithm. The accuracy of the above-mentioned methods are assessed and a simply supported beam under a harmonic load is analysed using using different methods. The spectral mid-span deflection of the beam obtained from the traditional mixed implicit-explicit scheme is compared with that of the proposed algorithm. The chapter closes with an analysis of a shear wall under an analytical earthquake loading.

Chapter 8 gives the conclusions obtained through this study and some recommendations for further research are made.

Chapter 2

A Numerical Model For Plain Concrete Under Transient Loading

2.1 Introduction

As a result of the inability of linearly elastic analysis to predict the behaviour of reinforced concrete structures, investigations into its non-linear behaviour have been the subject of a great deal of both experimental and theoretical research in the last two decades. The result is that there now exists a good understanding of most of the basic mechanisms at work when a reinforced concrete member is subjected to various types of loading.

To be reliable, any analysis must be capable of predicting a number of different failure mechanisms and also must be sufficiently discriminating so that the failure mechanism which would occur in the physical structure is the one which the analysis predicts.

In a non-linear finite element analysis, the failure mechanism and the load at which it occurs can be influenced by many factors. Some of these are: element type, mesh size, load type, concrete cracking and crushing, failure criteria, aggregate interlock, bond slip, action, time- dependent effects and reinforcement

yielding. Hence, a comprehensive analytical model should synthesize such phenomena along with any geometric effects if necessary in such a way that the afore-mentioned reliability is achieved.

The advent of computers and powerful numerical methods such as the finite element method have facilitated incorporation of such models into computer programs and, as a result, many sophisticated material models have been developed. These include: non-linear elasticity-based model [1], plasticity-based models [2, 3], boundary-surface plasticity models, and damage-mechanics based model [4, 41]. It should be mentioned that a significant scatter in experimental response is common even for identical specimens tested under identical conditions and the scatter becomes more in the case of dynamic tests.

Under extreme conditions, a structure may be deformed well beyond its linearly elastic range and hence a non-linear analysis becomes necessary.

Plain concrete exhibits non-linear behaviour in two major ways. First, tensile cracking produces a softening and directional material and is often the most important non-linear effect. Indeed, one could say, cracking is "the" dominant non-linear effect in reinforced concrete. Secondly, the stress-strain curve for concrete under compression becomes increasingly non-linear in uniaxial compression at stresses in excess of about 70% of the maximum stress [76].

The dynamic behaviour of concrete is relatively complex, particularly at high-rates of loading. Experimental data is very scarce because of the expense. So, until recently, the available constitutive models prohibited any realistic analytical modelling.

The objectives of this chapter are summarized as follows

- To review the experimental observations of concrete loaded at various strain-rates.
- To review the existing elastic-based, plastic-based, visco-plastic-based theories and damage modelling for predicting the behaviour of concrete, reinforcing steel under both static and strain-rate loading.

- To review the currently used methods for modelling the pre-cracked and post-cracked behaviour of concrete and also fracture mechanics under static and dynamic loading.

- To present the work carried out on the uniaxial and multiaxial compressive behaviour of concrete under static loading.

- To simulate progressive concrete cracking and the strain-rate-dependent behaviour of pre-cracked concrete.

- To incorporate strain-rate-dependent parameters to enable the prediction of a reliable time-history-dependent response of reinforced concrete structures under medium strain-rate compatible with those of seismic effects, despite the shortage of experimental data. Attention has been focused on history-strain-rate-dependent modelling of the uniaxial and biaxial behaviour of concrete in compression.

- To model the rate-dependent parameters such as the initial modulus of elasticity, the secant modulus of elasticity, the tangent modulus of elasticity and the peak strength.

- To develop a formula which enables the prediction of the history-strain-rate-dependent behaviour of reinforced concrete in two-dimensional problems.

The chapter starts with a review of experimental observations of concrete under dynamic load and continues with a description of classical constitutive theories, such as, elastic theories, fracturing theories, damage theories, plastic and visco-plastic theories. In the next sections the mechanical properties of concrete, the rate-effect on rate-dependent parameters of concrete and steel will be discussed in two parts.

The mechanical properties of plain concrete under uniaxial and biaxial loading, the constitutive laws for pre-cracked and post-cracked concrete in tension and compression are discussed in the first part.

In the second part, discussion starts with the effect of strain-rate-dependency of the relevant parameters such as modulus of elasticity, peak stress, peak strain, Poisson's ratio and ultimate strain of plain concrete in compression and the strain-rate-sensitive functions in tension. The proposed rheological model is explained in the next section. The proposed formula for predicting the strain-rate-dependent uniaxial stress-strain relation which includes an increase in the initial modulus of elasticity with increasing strain-rate and the proposed multiaxial model for predicting history-strain-rate-dependent behaviour of reinforced concrete are discussed in subsequent sections. The chapter closes with a description of the constitutive equation used for the reinforcement.

2.2 Experimental evidence for rate-effect

Despite the large number of experimental studies on the behaviour of concrete that have been carried out over a considerable period of time, knowledge about its physical and mechanical properties is still deficient, particularly under dynamic loading. The heterogeneous structure of concrete, the difficulties of experimental testing and the expense of the tests are some of the reasons for its difficulty.

Poisson's ratio is influenced by strain rate Figs. 2.1 and 2.2 and will be discussed later on.

Concrete exhibits a significant increase in both the strength and the stiffness when at an increased strain-rate Figs. 2.2- 2.20. Experimental data on the properties of concrete subjected to high strain-rates have been reported by various investigators, such as [4-10].

2.3 Concrete strain-rate-sensitive parameters

In this section, rate effects on the following strain-rate-sensitive parameters are explained briefly.

- Poisson's ratio.

- Peak Tensile Strength.
- Initial, Secant and Tangent Modulus of Elasticity.
- Peak Compressive Strength.
- The strain at peak compressive strength.
- The ultimate strain.

The Poisson's ratio for concrete under static uniaxial compressive stress ranges between 0.15-0.22, with 0.2 being representative [11]. Under uniaxial loading, the ratio of lateral strain to principal compressive strain remains constant until approximately 80% of peak stress $\acute{f}_c$, there-after, the apparent Poissons's ratio begins to increase [11].

Takeda and Tachikawa [9] have carried out experimental observations to study the rate-dependent parameters on concrete. They observed both an increase in tension strength and in the secant modulus measured at the peak stresses. Measurements were also taken of the lateral strains and an increase in the Poisson' ratio with increasing strain-rate for tensile tests was noted. However, in compressive tests, the Poisson's ratio decreased with increasing strain-rate. Figs. 2.1 A [4] and B [9] show the effect of strain-rate on the apparent Poisson's ratio.

In the experimental observations of Takeda et al. [9], the initial modulus of elasticity with increased loading rate was found to remain approximately constant, while the secant and tangent modulus of elasticity measured at the same strain-rate were observed to increase with increasing strain-rate [7, 9]. However, Mander et al. [12], Hatano [10], and Bazant et al. [6] have found that the initial modulus of elasticity changes with increasing the rate of strain.

Many investigators have conducted experiments to study the rate effect in both tension [4, 10, 12, 13, 14, 15] and flexure [5, 6, 9, 12, 14]. The experimental evidence indicates that the rate sensitivity of tensile strength is noticeably higher than that of compressive strength and that the rate sensitivity of flexural strength is in between that of tensile and compressive strength [4, 15], as shown in Fig.

2.2 [4]. It was concluded that the ultimate tensile and compressive strength of concrete under strain-rate is primarily related to the strain-rate effect on cracking. Figs. 2.3 , 2.4, 2.5 and 2.6, illustrate the rate effect on tensile strength of concrete and Fig. 2.7 shows a bounding strain-rate-effect on tensile strength of concrete [15]. Strain-rate effect on tensile strength for three types of concrete mix carried out by Hatano et al. [10] is illustrated in Fig. 2.8.

Experimental evidence has also confirmed that the compressive strength of concrete is influenced by strain-rate and it increases with increasing strain-rate. Figs. 2.9 A and B illustrates the maximum compressive stress versus strain rate for two aggregate types carried out by Malvern et al. [17] and Figs. 2.10 and 2.11 show the effect of water/cement ratio on rate-dependence in compression carried out by Jawed et al [18] and Hatano et al. [10] respectively. Figs. 2.12, 2.13 and 2.14 show the strain-rate effect on compressive strength of concrete.

The effect of strain-rate on flexural strength of concrete is shown in Figs. 2.15 and 2.16 respectively. The secant modulus of elasticity also has been observed to be strain-rate-sensitive as shown in Fig. 2.17. Fig. 2.18 gives the results of experimental observation carried out by McHenry and Schideler [19] showing how the compressive strength of concrete is affected by rate of loading.

The ultimate strain of concrete has been observed to increase with increasing strain-rate [20]. Fig. 2.19 show the stress-strain curve obtained for static and dynamic compressive loading reported by Curbanch et al. [20].

The experimental results obtained from plain and transversely confined concrete subjected to strain-rates between 32 microstrains/sec a quasi-static test, 10 000 microstrains/sec and 30 000 microstrains/sec carried out by Ahmad and Shah, [21] show that for both plain and hoop confined concrete in compression, there is an increase in the values of secant modulus of elasticity, peak stress and peak strain for high strain-rates Fig. 2.20. As can be seen the peak strain in compression increases with increasing strain-rate. An experimental ultimate dynamic strain ϵ_U has been proposed by Raid H. L. [22] in the form

$$\epsilon_u = .00350 - .00003 \times \acute{f}_c + .000114(\sigma_p - \acute{f}_c) \tag{2.1}$$

where, σ_p is the dynamic peak strength. Both σ_p and $\acute{f}_c$ are in kips. Both the compression and tension strength of reinforcing steel also have been observed to increase with increasing strain-rate Fig. 2.21 [23] and 2.22. [24]. In contrast to concrete, the rate effects on steel are approximately equal in tension and compression.

2.3.1 A review of classical constitutive theories and their application for concrete

In this section, the classical constitutive theories currently used and their application are reviewed. The effectiveness and applicability of these theories in predicting the observed behaviour of concrete and reinforced concrete under static loading will be discussed.

2.3.2 Elastic models

One of the models widely used to represent the behaviour of concrete under general types of loading during the past decades is based on elasticity theory. This approach may be categorized on the basis of the state of the stress that is modelled (uniaxial, biaxial and triaxial) and the form of constitutive relations. The degradation of concrete stiffness under loading is characterized through two different types of Hookean formulations:

- Finite (or total) material characterization in which the secant-strain formulation is used.

- Incremental (differential) material descriptions in which the stress- strain relation is modelled in tangential form (termed as hyperelastic model) which will be explained in the next section.

Hyperelastic model(Green elastic)

The classical form of hyperelasticity theory is based on the existence of a strain energy potential (W) which for the isotropic case is expressed as a scalar function of the strain invariants I_1, I_2, and I_3. The constitutive relations for a hyperelastic material can be expressed as

$$\sigma_{ij} = \frac{\partial W}{\partial \epsilon_{ij}} \tag{2.2}$$

or

$$\sigma_{ij} = C_{ijkl}\epsilon_{kl} \tag{2.3}$$

where C_{ijkl} is a function of stress-state. It can be seen that stress and strain are related one to one, hence this approach yields tangents which are identical in loading and unloading. Hyperelastic models also exhibit time-independent behaviour. Despite these shortcomings, they can model many concrete characteristics such as non-linear dilatation and strain or stress induced anisotropy and have been used for concrete [25]. In the model developed by Cedolin et al. [26], the constitutive law was constructed by using strain dependent bulk and shear moduli. The bulk modulus and shear modulus were assumed to be dependent on the first strain invariant and second strain invariant respectively, assuming the path independent of the strain energy function thus, making it a hyperelastic constitutive law.

2.3.3 Hypoelastic model

This type of constitutive relation is used to model the behaviour of materials in which the state of stress depends upon the current strain as well as on the stress path followed to reach that state. In general, the constitutive relations for a hypoelastic material can be expressed in a rate form

$$\dot{\sigma_{ij}} = F_{ij}(\dot{\epsilon_{kl}}, \sigma_{mn}) \tag{2.4}$$

However, most hypoelastic formulations are based on a simplified constitutive law which exhibits time-independent behaviour. The general linearly incremental form of such a hypoelastic constitutive law can be written as

$$d\sigma_{ij} = C_{ijkl} d\epsilon_{kl} \tag{2.5}$$

where C_{ijkl} is the fourth-order tangential material stiffness tensor that depends on the stress and/or strain tensor. Hypoelastic models of various orders can be formulated depending upon the degree of dependence of C_{ijkl} on the components of the stress tensor σ_{ij}. Coon [27] obtained reasonable agreement with uniaxial and biaxial tests for concrete, using a first order theory assuming C_{ijkl} a linear function of σ_{ij}.

Total stress/strain theory (Cauchy elastic)

In this approach, the stresses and strains are related by a unique relationship given by

$$\sigma_{ij} = F_{ij}(\epsilon_{kl}) \tag{2.6}$$

The total stress/strain model can be considered as a generalization of the hyperelastic model where the existence of a strain energy function is not postulated. The weak point of this approach arises from the point that the path independency of the strain energy is not guaranteed, which may be in some loading and unloading cycles in violation of the first law of thermodynamics. Using this theory, Kupfer and Gerstle [28, 29] have expressed the bulk and shear moduli as functions of the second invariant and obtained good agreement with biaxial test results for concrete.

Palaniswamy and Shah [30] obtained close agreement with triaxial test results for concrete by expressing the bulk modulus as a function of the first stress invariant.

2.3.4 Plasticity based model

It is well known that, concrete undergoes irreversible strains particularly at high stress level while the previously discussed constitutive theories (with some exceptions) exhibit reversible behaviour. The theory of plasticity appears to be well adapted for modelling such material behaviour which will be reviewed in this section.

Flow theory of plasticity

This theory is based on the hypothesis of a loading function also called *' the yield surface'* which encloses all stress-states under which the incremental behaviour is elastic. The loading function, which is dependent upon the current state of stress σ_{ij} and a number of hardening parameters k, can be expressed as

$$F(\sigma_{ij}, \epsilon_{ij}^{P}, k) = 0 \tag{2.7}$$

Once the stress reaches the loading surface, plastic behaviour can occur and failure occurs when the loading surface reaches the failure surface [2, 31, 32].

Yield criterion

The yield criterion determines the onset of plastic deformation and can be written in the general form

$$F(\sigma_{ij}, \epsilon^p_{ij}, k) = f(\sigma_{ij}, \epsilon^p_{ij}) - Y(k) \tag{2.8}$$

where f is the yield function which depends on the stress σ_{ij} and plastic strain components ϵ^p_{ij}, Y is the yield stress which may be related to the material history and is constant in perfectly plastic material and k is the hardening parameter. Considering only isotropic plasticity ϵ^p_{ij} is dropped in Eq. (2.8) which leads to

$$F(\sigma_{ij}, K) = f(\sigma_{ij}) - Y(K) \tag{2.9}$$

The behaviour is elastic if $F \leq 0$ and plastic if $F > 0$. Since the material behaviour is physically independent, the yield criterion is expressible in terms of any set of stress .

Many geometrical forms of loading surface have been proposed throughout the years. The Von-Mises and Modified Von-Mises criteria, under the assumptions of associated plasticity [2, 33] Fig. 2.23, has been widely used successfully for metals. Bhattachar and Weisgerber [34] have carried out some finite element analysis of reinforced concrete structures based on the Von-Mises criteria.

The Von-Mises criteria in terms of principal is written as

$$[(\sigma_1 - \sigma_2)^2 + (\sigma_2 - \sigma_3)^2 + (\sigma_3 - \sigma_1)^2]^{1/2} = Y(K) \tag{2.10}$$

The Drucker-Prager surface in principal stress space is clearly a right-circular cone whose meridian and cross section on π plane are shown in Fig. 2.24 and has the form

$$\alpha(\sigma_1 + \sigma_2 + \sigma_3) + \{[(\sigma_1 - \sigma_2)^2 + (\sigma_2 - \sigma_3)^2 + (\sigma_3 - \sigma_1)^2]/6\}^{1/2} = K' \tag{2.11}$$

A yield surface based on Dracker-Prager has been proposed by William and Warnke [35]. Green and Swanson [36] have used the Drucker-Prager yield surface combined with a volumetric-dependent cap surface. A loading surface which is elliptic in the octahedral plane and also exhibits ϕ dependence shown in Fig. 2.25, has been proposed by Nilson [37]. Both stress and strain history-dependence can be exhibited using the flow theory of plasticity. Stress induced anisotropy can also be incorporated. However, the material softening observed in concrete and time-dependent behaviour can not be modelled by the flow theory of plasticity.

Tresca states that the yielding of the material begins when the maximum shearing stress at a point reaches a critical value k which in principal stress is written as

$$\sigma_1 - \sigma_3 = 2k \tag{2.12}$$

Mohr-Coulomb states that the failure is governed by the relation,

$$| \tau | = f(\sigma) \tag{2.13}$$

where the limiting shearing stress τ in a plane is dependent only on the normal stress σ in the same plane at a point. Fig. 2.26

$$(\sigma_1 - \sigma_3)/2 + \sin\phi(\sigma_1 + \sigma_3)/2 = c\cos\phi \tag{2.14}$$

in which c is the cohesion, ϕ the friction angle and

Hardening rule

The Hardening rule establishes conditions for subsequent yielding from the previous plastic straining. The hardening rule is commonly modelled by either

- Isotropic Hardening [2] in which the yield surface is assumed to expand
- Kinematic Hardening [2] which corresponds simply to a translation preserving the initial shape. However more complex hardening rules may be obtained by a combination [2] of the above.

For simplicity, only isotropic hardening is considered which may be defined in two ways,

- Work Hardening W_p in which

$$W_p = \int \sigma_{ij} d\epsilon_{ij}^p \tag{2.15}$$

where σ_{ij} is the stress and $d\epsilon_{ij}^p$ is the plastic change and

- Strain Hardening in which the yield stress Y depends on the effective strain $\bar{\epsilon_p}$ [2]

$$\bar{\epsilon_{eff}^p} = \int [2/3(d\epsilon_{ij}^p d\epsilon_{ij}^p)]^{1/2} \tag{2.16}$$

The effective stress and effective strain will be explained in the following sections.

Flow rule

The flow rule relates stress to plastic strain increments and is assumed to be proportional to the stress gradient of plastic potential

$$d\epsilon_{ij}^p = d\lambda \frac{\partial Q}{\partial \sigma_{ij}} \tag{2.17}$$

where $d\lambda$ is a non-negative factor called the plastic multiplication. If Q is assumed to be equal to a particular yield function f then

$$d\epsilon_{ij}^p = d\lambda \frac{\partial f}{\partial \sigma_{ij}} \tag{2.18}$$

This equation is called the *' associated flow rule'* [2] and implies a normality condition between the plastic strain increment and the yield surface in principal stress space.

Matrix formulation

In this section the basic expressions of the previous section will be presented in a matrix form suitable for numerical treatment.

Assuming a three-dimensional isotropic hardening continuum we can write

$$F(\sigma, k) = f(\sigma) - Y(k) = 0 \tag{2.19}$$

Equation (2.19) may be written in incremental form as

$$dF = (\frac{\partial f}{\partial \sigma})^T . d\sigma - dY/dk . dk = 0 \tag{2.20}$$

$$d\sigma = D(d\epsilon - d\epsilon_p) = D(d\epsilon - d\lambda \frac{\partial f}{\partial \sigma}) \tag{2.21}$$

where $\sigma = \{\sigma_x, \sigma_y, \sigma_z, \sigma_{yz}, \sigma_{zx}, \sigma_{xy}\}^T$, and D is the usual 6×6 material stiffness matrix denoting $a = \frac{\partial f}{\partial \sigma}$ and $A = \frac{1}{d\lambda} \frac{dY}{dk} dk$ leads to

$$d\lambda = \frac{a^T D d\epsilon}{A + a^T D a} \tag{2.22}$$

and

$$d\sigma = D_{ep} d\epsilon \tag{2.23}$$

where

$$D_{ep} = D - \frac{D a a^T D}{A + a^T D a} \tag{2.24}$$

A general procedure for developing the incremental stiffness matrix for an elasto-plastic material model with multiple intersecting yield surfaces has been proposed by Lade and Nelson [38]. In their approach, each surface has its own associated or non-associated flow rule and is assumed to depend on work-hardening or work-softening effects. According to this procedure, models with up to five independent, simultaneously activated yield surfaces may be incrementalised.

An elasto-plastic model with a non-associated law has been proposed by Barros [39] for structural analysis problems.

Many elasto-plastic models for structural analysis problems have been proposed by investigators [38, 40-42, 44-49].

2.3.5 Endochronic theory

This theory is suitable for application to concrete for two reasons, firstly, the inelastic strains are obtained directly from the evaluation of a measure of irreversible damage referred to as intrinsic time, secondly, the ability of the theory to describe material

Valanis [49] proposed the theory for describing the mechanical behaviour of concrete. A pseudo time-scale was introduced in which the intrinsic time ξ was defined as

$$\xi = \int_0^{\epsilon} \frac{d\xi}{f(\xi)} \tag{2.25}$$

where $f(\xi)$ is a history-dependent material function. The value $d\xi$ is related to the real time increment by

$$d\xi^2 = a_{ijkl} d\epsilon_{ij} d\epsilon_{kl} + a_0 (dt)^2 \tag{2.26}$$

where a_{ijkl} is a material tensor and a_0 is a constant. The constitutive relations can be obtained by using the pseudo-time measure ξ instead of t in Eq. (2.26), as

$$\sigma_{ij}(\xi) = \sigma^0_{ij} + \int_0^{\xi} R_{ijkl}(\xi, \acute{\xi}) \frac{\partial \epsilon_{kl}}{\partial \acute{\xi}} d\acute{\xi} \tag{2.27}$$

Bazant [50] has developed the endochronic theory for concrete using a generalized Maxwell chain model which was capable of exhibiting strain hardening/softening, hysteresis effects, hydrostatic pressure sensitivity of inelastic strain, and the inelastic observed in concrete.

In spite of the fact that endochronic theory presents the possibility of modelling many of the material characteristics observed in concrete, the requirement of determining a large number of material parameters is the biggest drawback of the method.

2.3.6 Progressive fracturing theory

The constitutive models for the endochronic theory discussed above are not capable of exhibiting the progressive loss of stiffness. Dougill [51] developed a progressive fracturing theory which is well suited for modelling such softening behaviour. In the model the relations for loading and unloading are

$$\sigma_{ij} = C_{ijkl} \epsilon_{kl} \tag{2.28}$$

$$\dot{\sigma} = C_{ijkl} \dot{\epsilon}_{kl} + \dot{C}_{ijkl} \epsilon_{kl} = \dot{\sigma}^{el}_{ij} - \dot{\sigma}^{fr}_{ij} \tag{2.29}$$

In this theory, the unloading is assumed to be elastic without fracturing.

In the next section concrete properties in tension and compression will be explained.

2.4 Concrete in tension

2.4.1 Uniaxial behaviour of concrete in tension

Uniaxial tensile is commonly evaluated by either

- the split test or
- the modulus of rupture (flexural-tensile strength) or bending test.

The flexural-tensile strength determined from a modulus of rupture test tends to be higher than the tensile strength of a split cylinder which in turn tends to be higher than the tensile strength obtained from a direct tension test[52].

The tensile strength can be expressed in terms of the cylindrical compressive strength of concrete. Stevens and Collins [53] have recommended the following relation

$$\acute{f}_t = .33\sqrt{\acute{f}_c} \tag{2.30}$$

where $\acute{f}_t$ is the ultimate tensile strength in ksi and $\acute{f}_c$ is the cylindrical compressive strength of concrete in ksi.

Although the higher strength concretes appear to be relatively brittle, the lack of a descending branch may be more a function of the testing machine than of the material [54].

Johnson [55] found that, the ratio of uniaxial tensile strength to compressive strength ranges from .05 for high-strength concrete to about 0.1 for a concrete of medium strength. It was found that the tensile-strength is influenced by the aggregate type and calcareous aggregate increases the tensile strength while siliceous aggregate decreases the tensile strength of concrete. The tensile stress-strain curve is typically shown in Fig. 2.27. However, the above relations give an approximation due to scatter of test results. Fig. 2.27 shows the scatter in experimental data of split cylinder strength versus the modulus of rupture.

2.4.2 Pre-cracked concrete

In most finite element analyses of reinforced concrete structures, elastic behaviour for concrete prior to the crack formation has been adopted [56-59]. This assumption could be reliable in monotonic static loading, however, Yankelevsky et al. [60] have observed some non-linearity for plain concrete. The flexural tensile strength determined from a modulus of rupture test tends to be higher than the tensile strength of a split cylinder, which in turn tends to be higher than the tensile strength obtained from a direct tension test. An elastic behaviour has been adopted for pre-cracked concrete in this study.

2.4.3 Crack modelling in concrete

The development of constitutive models for the description of cracks in reinforced concrete structures is presently a field of rapid progress. This interest is brought about partly by the related important theoretical aspects, such as: uniqueness, stability, size effects and localization, and partly by the practical implications since the main damage to concrete structures is often caused by cracking.

In modelling reinforced concrete structures, initiation and propagation of cracks which are the major source of non-linearity must be represented properly.

Cracking is assumed to occur on the plane of maximum principal stress when this maximum principal stress reaches the ultimate tensile strength $\acute{f}_t$ then after, the concrete behaves as an orthotropic material.

Methods of incorporating this mode of failure include plasticity-based models, plastic fracture models and the simple tension cut-off model [2]. The simple tension cut-off model is the most popular one and the basis for a cut-off may be strength, maximum strain or energy.

Cracks may be represented in two distinct ways in a finite element procedure. The discrete crack model pioneered by Ngo and Scodelis [61] represents cracks as discontinuities. Although the discrete model can indeed trace the detailed features of concrete cracking, the application of this approach has received limited acceptance due to two reasons:

1. difficulty in redefining the crack topology.

2. the excessive computational effort.

Thus, an alternative approach, the so-called *'smeared model'* has become more popular. This approach originally introduced by Rashid [62], has the advantage of permitting automatic crack propagation with a relatively small computation cost. Also it offers a complete generality in predicting the crack directions independent of mesh configuration and element type used in the analysis [63]. The smeared crack approach has nevertheless a drawback in its dependence on the finite element mesh size as pointed out by Bazant and Cedolin [64, 65]. Moreover, particularly in an element, the stress states at the Gauss integration points used for the evaluation of the stiffness matrix are more accurate compared with the discrete approach [66]. Barlow suggests that more reliable detection of cracks is possible with this model. Fig. 2.28 and 2.29 show the discrete and smeared representation of a single crack respectively.

For smeared cracking, two interrelated concepts *'tension stiffening'* and *'tension softening'* have been introduced [40, 56] and are explained in the next section briefly.

Post-cracked concrete

The simplest procedure for modelling the cracking of concrete is based on the tensile strength failure criterion in which the strength in the direction of maximum tensile stress is allowed to vanish suddenly at cracking. However, in this approach, as the finite elements are made smaller the tensile stress in the element ahead of the crack becomes larger, so that the crack grows at a lower level of applied load, hence the crack propagation has a fictitious dependence on mesh size as, pointed out by Bazant [63]. The post-cracked behaviour of plane concrete is modelled in literature by several methods such as: the *" fictitious crack model"* of Hillerborg et al. [67] and the *" crack band model "* of Bazant and Oh [65]. The latter is a two-parameter model, i.e. tensile strength and fracture energy, which is given by the area under the $\sigma - W$ curve where W is the crack width, and can be obtained

from test data as a material property, and the former is a three-parameter model (tensile strength, fracture energy and size of process zone) which are considered to be material parameters. A typical fracture process zone is shown in Fig. 2.30.

Non-linear fracture mechanics pioneered first by Hillerborg [67] is based on the initiation of crack at the maximum tensile strength which propagates with the formation of a fracture zone and its strength gradually decreases as shown typically in Fig. 2.31. In this approach, in addition to the tensile strength as a material property, the fracture energy which is the energy to be consumed per unit area should be evaluated experimentally which has been confirmed through an experimental observation by Ramoda et al. [68].

Concrete tension softening

Plain concrete if tested in tension under displacement control in a stiff testing apparatus exhibits a descending branch in the load displacement curve [59, 60, 68] which is called *"tension softening"* Fig. 2.32.

Based on the experimental data obtained from beams of width b, depth d, length L, and a notch of depth g, Nallathambi et al. [69] have suggested the following formula for evaluating fracture energy in the absence of exact test data.

$$G_f = 0.125[\frac{\acute{f}^2}{E}][\frac{g}{b}]^{0.173}[\frac{d}{L}]^{0.631+0.4(a/d)} \tag{2.31}$$

where $\acute{f}$ and E are the compressive strength and elastic modulus and g is the maximum size of the concrete aggregate and the parameter values are in N and M units. Bazant and Oh [65] have suggested use of the formula

$$G_f = (2.72 + 0.0214\acute{f}_t)\acute{F}_t^2 g/E \tag{2.32}$$

where, $\acute{F}_t$ is the tensile strength of the concrete and the parameters are in lb and inch units [50].

Based on a study on the effects of the shape of the descending branch of the tensile stress-strain curve carried out by Linda et al. [70] the performance of the linear, bilinear, discontinuous, and Dugdale tension softening representations were compared using a gird with 40 elements through the depth and a three-

element-wide non-linear zone. It was concluded that, both peak load and the corresponding displacement vary with the descending branch shape, typical examples of which are shown in Fig. 2.33. The discontinuous model is the most flexible for the ascending branch of the curve, while the bilinear, linear and Dugdale models are successively stiffer.

The approach to model post-cracked behaviour of concrete is called the *"fixed crack model"* if this direction is fixed (adopted in this study) and is called the *"rotating crack model"* if the principal material axes can be given a rotation to coincide with the principal stress and strain directions, and is explained in the nest section.

Concrete tension-stiffening

When reinforced concrete cracks, some of the tensile force is transferred to the reinforcement. The effect of tension retained in the concrete is called *"tension-stiffening"* [71, 72]. Considerable scatter is exhibited in test data on tension-stiffening as shown in Fig. 2.34 and 2.35 [71].

Tension-stiffening can be modeled in two ways:

- In the first method, it is assumed that the tensile strength in concrete reduces gradually to zero after tensile cracking is initiated [66], thus tension stiffening increases the fracture energy of the composite which is commonly used for simplicity.

- In the second method, a modified stress-strain curve for steel is used ("state-of-the-art" 1982 [74]).

Rotating crack model

Under loading the initial cracking directions in the reinforced concrete elements may shift and new cracks can develop. However, the reorientation of the initial cracking direction may also occur in orthogonally reinforced concrete elements subjected to proportional loading [71]. Under proportional loading, if the element

reinforcement is isotropic but is located at angles different from $\mp 45° or 90°$ with respect to the principal loading directions or when the reinforcement is skewed with respect to the principal loading directions additional non-orthogonal cracks may develop. Changing the crack direction has been shown both experimentally and analytically for example Steven and Collins [53].

2.5 Concrete in compression

Under low levels of compressive stress, the behaviour of concrete is linear elastic while for higher values of stress and under sustained loading it exhibits highly non-linear properties. However, this non-linearity decreases considerably under time-dependent loading such as impact or earthquake loading. Concrete exhibits higher strength under biaxial compressive loading than uniaxial loading.

The Youngs modulus of elasticity of concrete varies with strength. It also depends on the properties of aggregates and cement, the rate of loading and the type and size of specimen.

Since the curve in compression is non-linear, three definitions of the modulus of elasticity are commonly used

- Tangent Modulus.
- Secant Modulus.
- and Chord Modulus.

and are illustrated in Fig. 2.36. These three moduli have different strain-rate-dependent characteristics which will be explained in more detail in subsequent sections.

As the result of a statistical analysis of available data, the empirical formula

$$E = 33W^{1.5}\sqrt{f_c'} \tag{2.33}$$

can be used for calculating the initial modulus of elasticity with reasonable accuracy (ACI Code 318-77) where W is the unit weight of hardened concrete (between

90-155) in P/sf and $\acute{f}_c$ is the cylinder strength in Psi, E is the initial modulus of elasticity (GPa).

2.5.1 Mechanical properties of concrete in compression

Using normal testing speeds (quasi-static loading) the shape of the stress-strain curve is similar for low, normal and high strength concrete and a slightly higher strain at the peak stress is exhibited as is shown in Fig. 2.37. As can be seen, lower-strength concrete has greater ductility than higher-strength concrete. On the descending portion, higher strength concretes tend to behave in a more brittle manner with the stress dropping-off more sharply.

It is a well established fact that the failure of concrete under loads takes place through progressive internal cracking. In other words, the failure is the result of an essentially continuous material changing to an essentially discontinuous one [75]. Microcracks at the interface between coarse aggregate and mortar which are called *'bond cracks'* exist in concrete before it is subjected to any load [76] and seem to be chiefly a result of volume changes during hydration and drying [76]. Above approximately 30% of the ultimate compressive load these bond cracks begin to increase in length, width and number with increasing strain. At about 70% to 90% of the ultimate load cracks through the mortar begin to increase noticeably Fig. 2.38. The ultrasonic pulse velocity in the direction of loading has been observed to be constant until a fraction of 45% ultimate concrete strength [76]. It is deduced that the crack propagation in concrete starts at a fraction of ultimate loading. Fig. 2.39. shows the effects of microcracking on some concrete properties.

Biaxial behaviour oF concrete

Many important classes of structures can be approximated as being in a state of plane stress such as beams, panels and thin shells. In modelling such structures test results under different combinations of loading are required. Unfortunately,

there are insufficient experimental data available under such condition for reinforced concrete. It is postulated that the behaviour of concrete under biaxial loading differs from that of uniaxial [77, 78, 79]. Under compression-compression conditions, concrete exhibits an increased compressive strength of up to $1.25\acute{f}_c$ [80] which may be attributed to the Poisson's ratio effect, Fig. 2.40, while under biaxial tension concrete exhibits a constant [28, 29] or perhaps a slightly increased tensile strength [80].

In the absence of much experimental information for triaxial and biaxial stress-strain behaviour of concrete, most of the analytical expressions for the peak strength envelope have been developed using the test results of Kupfer and Grestle [28, 29]. The proposed failure function also has been obtained by fitting the parametric failure function with Kupfer's test results [28, 29], Fig. 2.41.

As can be seen, the peak strength envelope is constructed from three main portions, compression-compression, compression-tension and tension-tension portion.

Stress-degredation effect on concrete parallel to crack direction

After cracking has taken place, the concrete parallel to the crack direction is still capable of resisting compressive force.

Based on experimental observations [71] the principal compressive stress in concrete is found to be a function not only of the principal compressive strain but also of the co-existing principal tensile strain in the direction normal to the compression as shown in Figs. 2.42 A and B. The following relations were proposed

$$f_{c2} = f_{c_2 max}[2(\frac{\epsilon_2}{\epsilon_0}) - (\frac{\epsilon_2}{\epsilon_0})^2] \tag{2.34}$$

$$\frac{f_{c_2 max}}{\acute{f}_c} = \frac{1}{0.8 - 0.34\frac{\epsilon_1}{\epsilon_0}} \tag{2.35}$$

$$\frac{f_{c_2 max}}{\acute{f}_c} \leq 1.0 \tag{2.36}$$

where ϵ_0 is the strain corresponding to the maximum compressive stress so that increasing ϵ_0 will reduce $\frac{f_{c_2 max}}{f_c}$. ϵ_1 is the cracked concrete strain.

2.5.2 The constitutive law for concrete under uniaxial compression

For the rational analysis of the reinforced concrete structures under consideration analytical equations for the complete stress-strain curve are necessary. Kent and Park [81] have proposed the stress-strain relationship for confined and unconfined concrete shown in Fig. 2.43. A linear descending part was assumed which seems not to be very accurate. Sargin [82] has suggested the following equation:

$$Y = \frac{AX + (D-1)X^2}{1 + (A-2)X + DX^2} \tag{2.37}$$

in which $Y = \frac{\sigma}{\sigma_0}$, $X = \frac{\epsilon}{\epsilon_0}$ where σ and ϵ are the stress and strain σ_0 ϵ_0 are the peak stress and peak strain respectively. Equation (2.37) is plotted in Fig. 2.44, for confined and unconfined concrete. As can be seen, it describes the stress-strain curve of confined concrete quite accurately while it is not so accurate for unconfined concrete.

2.5.3 Proposed failure function

The failure function can be written in general form as

$$F(I_1, J_2) = \alpha I_1 + (\beta I_1^2 + 3\theta J_2)^{1/2} \tag{2.38}$$

in which α, β and θ are material constants which are evaluated by experimental data and I_1 J_2 are the first stress invariant and second deviatoric stress invariant.

Evaluation of material constants

α, β and θ can be evaluated from three stress tests using the analytical form proposed by Kupfer in the form

$$(\sigma(x)/\acute{f} + \sigma(y)/\acute{f}^2 - \sigma(y)/\acute{f} - 3.65\sigma(x)/\acute{f} = 0. \tag{2.39}$$

- uniaxial compression test ($\sigma_y = \sigma(z) = 0$, $\sigma(xy) = 0.$,and $\sigma_x = -\sigma_0$).

- biaxial compression test in which ($\sigma(x) = \sigma(y)$, $\sigma(z) = 0.$, and ($\sigma_{xy} = \sigma_{xz} = 0$). The values 0.5 and 1.2543 are obtained using the formula proposed by Kupfer as shown in Fig. 2.41.

- biaxial compression test in which ($\sigma_x = 0.5\sigma_y$, $\sigma(z) = 0$, $\sigma_y = 1.2543\sigma_(0)$, and ($\sigma_{xy} = \sigma_{xz} = 0$).

Substituting these conditions into Eq. (2.38) and solving the three equations the three unknowns are determined to be, $\alpha = -0.11749$, $\beta = -0.129287$, $\theta = 0.90811$.

The two-parametrical form of the proposed criteria is in a good agreement with those of Hinton's criteria and is compared in Table 2.1. The proposed failure surface and failure criteria in stress-space is plotted in Fig. 2.45 A and B respectively.

2.5.4 Crushing condition

In order to account for the limited load carrying capacity of concrete, the expansion of the loading surfaces is constrained such that beyond a certain point, perfect plastic flow occurs while the loading surface in stress space is fixed. This state continues until the ultimate deformation capacity of the concrete is reached and crushing occurs.

The crushing type of fracture as a strain controlled phenomenon has been used by many researchers [41].

Kaar, Hanson and Capell [83] have plotted the ultimate strain for high strength concrete in reinforced concrete beams. They recommended the following curve to fit the data

$$\epsilon_u = 0.00350 - 0.00003\acute{f_c} \tag{2.40}$$

where $\acute{f_c}$ is in kips.

Cope and Rao [84] assumed a complete loss of strength when $\epsilon > 0.0035$.

Another method to determine the ultimate carrying capacity of concrete is the *'energy dissipation approach'* which is an accumulated damage-based method [41].

Bicanic [41], employed a parameter k as the post-failure energy density in the form

$$k = W_p - W_P^* = \int_{t_f}^{t} \sigma^T \dot{\epsilon}_{vp} dt \tag{2.41}$$

$$W_p^* = \int_0^t \sigma^T \dot{\epsilon}_{vp} dt \tag{2.42}$$

where, W_p is the inelastic work density, W_p^* is the dissipated energy density evaluated from the moment when the stress point reaches the *' bounding failure surface'* and t_f is the time when failure occurs.

A failure surface in the strain space of the form

$$\alpha \acute{I}_1 + \beta \acute{J}_2 = \epsilon_u^2 \tag{2.43}$$

where $\acute{I}_1$ and $\acute{J}_2$ are the strain invariants and ϵ_u is the total strain value which can be extrapolated from uniaxial test. The concrete is assumed to lose its strength when reaches the crushing surface.

Biaxial tension and tension-compression

Within the smeared crack model adopted in this study, the initiation of a cracking process at any location occurs when the concrete stress reaches one of the failure surfaces either in biaxial tension or in the tension-compression region as shown in Fig. 2.46 A and B. Thereafter, concrete is treated as an orthotropic material with principal axes normal and parallel to the crack direction. However, a reasonable assumption for simplicity is commonly accepted so that the principal axes are coincident with the principal strain. The stress-strain relationships associated with the cracked coordinates then become

$$[D] = \begin{bmatrix} E_1 & 0 & 0 \\ 0 & E_2 & 0 \\ 0 & 0 & \beta G \end{bmatrix} \tag{2.44}$$

where E_1, E_2 are secant modulus β is the shear retention factor with $0 < \beta < 1$ and G is the shear modulus of the cracked concrete.

A reduced shear modulus βG is retained in the constitutive relation instead of dropping to zero due to aggregate interlock or shear friction and dowel action. Using a reduced shear modulus not only improves the realism of the cracking representation during the finite element analysis but also removes the numerical difficulties caused by the singularity of the composite material's constitutive matrix [85]. A constant value of $\beta = .25$ has been used.

Doubly cracked concrete

Upon further loading of singly cracked concrete, a second set of cracks can form in the direction normal to the first set of smeared cracks. Thereafter, the stresses in both principal directions follow the tension-stiffening process already mentioned.

2.5.5 Material modelling of reinforced steel

In developing a finite-element model of reinforced concrete members three alternative representation of reinforcement are commonly used.

1. Smeared-steel.
2. Embedded-steel.
3. Discrete-steel.

- In case (1) each layer of steel is distributed over the concrete element with a defined orientation angle and a composite concrete-reinforcement constitutive relation assuming perfect bond between steel and concrete is used.

- In case 2 which is usually used in higher order elements [86] the reinforcement bar is considered to be an axial member, built into the isoparametric element so that, its displacement is consistent with those of the element

and the bond also is assumed to be perfect. More information is given in [86].

- In case 3 a one-dimensional bar element or beam element is superimposed on the two dimensional concrete element. The advantage of this representation is that the bond slip can be taken into account. The disadvantage of the technique is that the total number of nodal points becomes large because the element mesh pattern has to follow the location of the reinforcement which is not economical in large-scale problems particularly dynamic analysis.

In contrast to concrete, the mechanical properties of steel are well-known especially the uniaxial response.

2.5.6 Constitutive equation for steel

Steel modulus of elasticity

The steel modulus of elasticity is generally taken as $2.1 \times 10^6 kg/cm^2$ [27]. Figs. 2.47 A and B, shows a typical stress-strain curve for a low-carbon steels.

Stress-strain idealization

For simplicity, the stress-strain relation of steel is idealized as shown in Fig. 2.48 A, B and C. The type of idealization depends upon the accuracy required. However, it is necessary to determine experimentally the values of the stress and strain at the onset of yield, strain hardening and ultimate strain.

A fully elastic-plastic response identical in tension and compression is assumed in the current study. Material unloading and reloading along a secant path are also permitted. This microcrack closing/reopening behaviour is shown in Fig. 2.49 for uniaxial tension and compression and an equivalent uniaxial compressive stress-strain model under unloading and reloading proposed by Darwin and Pecknold [87] is depicted in Fig. 2.50.

Matrix form of constitutive equation

In order to assess the efficiency of currently used reinforcing models, reinforcing has been modelled using both the smeared method in which steel is smeared out over the element and the embedded approach in which the reinforcing bar is considered to be an axial member built into the concrete element in such a way that its displacements are compatible with those of the surrounding concrete. The dowel action of the reinforcing is neglected and perfect bond between steel and concrete is assumed.

The material stiffness matrix for the steel in the material coordinates $\hat{x}$, $\hat{y}$ in the smeared model can be written as

$$[D_s] = \begin{bmatrix} \rho_i E_s & 0 & 0 \\ 0 & 0 & 0 \\ 0 & 0 & 0 \end{bmatrix} \tag{2.45}$$

where ρ_i and E_s are the steel percentage and the modulus of elasticity of the reinforcement in the ith layer respectively.

The total stiffness matrix is then determined by combining the component stiffness matrices using the appropriate transformation matrix

$$[T] = \begin{bmatrix} \cos^2\theta & \sin^2\theta & \sin\theta\cos\theta \\ \sin^2\theta & \cos^2\theta & -\sin^{\theta}\cos^2\theta \\ -2\sin\theta\cos\theta & 2\sin\theta\cos\theta & \cos^2\theta - \sin^2\theta \end{bmatrix} \tag{2.46}$$

Thus

$$[D] = [T]^T[D]_c[T] + \Sigma[T]^T[D]_{si}[T] \tag{2.47}$$

determines the reinforced concrete stiffness in the global system.

This type of reinforcing representation has been used successfully in much research work such as [73]. In the embedded representation of a reinforcement, the contribution of reinforcements to the element stiffness can be evaluated independently for each steel bar. The element stiffness matrix can be derived through the use of the virtual work principle based on the assumptions that

- Reinforcing bar has stiffness contribution only in the longitudinal direction.

- Reinforcing is straight and has a constant cross-section area.

The final expression of the element stiffness matrix has the following form

$$K = K_c + K_s \tag{2.48}$$

in which

$$K_s = A_s E_s \int_l B^T T^T B dl \tag{2.49}$$

and K, K_c and K_s are the stiffness matrices for overall composite, the concrete and the reinforcement respectively; A_s cross-section of the reinforcement $T = [cos^2\theta, sin^2\theta, cos\theta sin\theta]$, dl line segment along the reinforcement and B is strain-nodal displacement matrix. The integration of Eq. (2.49) is performed along the reinforcement between two points i and j as shown in Fig. 2.51.

Dynamic problems

Finite-element analysis of reinforced concrete structures subjected to transient force such as blast, impact, earthquake and nuclear accident loading has been studied extensively [41, 89-103]. It is worthwhile to mention here that most studies have been limited to uniaxial behaviour of concrete due to lack of experimental data.

The mechanical properties of cementitious composites have been observed to be sensitive to the rate of loading and this rate sensitivity has been attributed to the strain-rate effects on cracking.

In the following sections, the constitutive models for dynamic problems, the strain-rate parameters modelling will be discussed and those of which would be useful for developing the proposed model will be identified.

Before attempting dynamic analysis of concrete structures, it is important to determine to what extent the material properties are supposed to be strain-rate-dependent in the analysis under consideration. Although the experimental data in this field is scarce, most of laboratory experiments that have been undertaken to investigate the effects of strain-rate on the various properties of concrete were conducted at strain rates similar to those associated with earthquakes, wind and wave loading which are compatible with the aims of this study rather than blast and missile impact loadings .

2.5.7 Constitutive models

Visco-elastic-based model

Most of the constitutive formulations discussed previously are incapable of predicting the strain-rate effects observed in experimental investigations. However, long-term effects like creep or strain-rate-dependent description of material are predictable by a visco-elastic model.

Use of rheological models to predict hysteretic behaviour of metals was proposed by Timoshenko [104]. A model consisting of an elastic spring with a

Coulomb element in series was used. Iwan [105] used the same model with coulomb elements.

Generalizing the Maxwell model for a solid material, constitutive relations can be developed which model the strain-rate-dependent behaviour of material. In the classical form of linear visco-elasticity, the stress at a given instant depends not only on the strain at that instant but also on the previous strain history.

Bangash and England [106] have presented a three-dimensional formulation for creep which allows independent variation of irreversible and delayed recoverable strains with respect to temperature and time.

Recently, a one-dimensional response for concrete under tensile loading based on a rheological model has been developed by Oh [107]. The general equation used is

$$d\sigma_{ij} = D_{ijkm}(\epsilon, \sigma, \dot{\epsilon})d\epsilon_{km} \tag{2.50}$$

where $d\sigma_{ij}$ and $d\epsilon_{km}$ are the stress and strain increments D_{ijkm} is strain function, and $\dot{\epsilon}$ is strain-rate. The equation for predicting the dynamic uniaxial tensile strength of concrete is

$$F_{td} = [1.95 - \frac{3.32(1 - \dot{\epsilon}^{1.8})}{2.2 + 3.2\dot{\epsilon}^{1.8}}]F_{to} \tag{2.51}$$

where F_{td} and F_{to} are the dynamic and the static tensile strength respectively. It has been claimed that Eq. (2.51) is valid up to rates of 1/s.

Pozzo [108] proposed a rheological model for predicting the dynamic behaviour of concrete using linear visco-elasticity theory. It was demonstrated that visco-elasticity can not model the solid-friction type of dissipation that is prevalent in concrete. The rheological model which is useful in modelling the cyclic behaviour of concrete includes a frictional term of the form ;

$$\Gamma(\epsilon) = \sum_{i=1}^{n} \mu_i \epsilon_i \tag{2.52}$$

where μ_i is the friction constant and Γ is the dissipative stress. Pozzo's model [108] is illustrated in Fig. 2.52 Shah et al. [109, 110] have also proposed a rheological model for cyclic loading of concrete in which strain softening path-dependency, stiffness degradation and the concept of envelope curve are incorporated.

A rheological model may be employed in strain-rate-dependent problems to simulate the plastic deformation process. In this approach, the friction slider component develops a stress σ_p, becoming active only if $\sigma > y$ where σ is the total applied stress, y is some limiting yield value and the stress $\sigma_d = \sigma - \sigma_p$ is carried by a viscous dash pot.

A more elaborate material response can be modelled by the use of the so called *'overlay mechanical method'* [111] in which the solid to be analysed is assumed to be composed of several layers (or overlays), each of which undergoes the same deformation so that the total contribution of the overlays is equal to the applied stress. A family of rheological models such as visco-plastic, visco-elastic and visco-elastic -plastic may be modelled by this method. More detail is given in [111].

2.5.8 Visco-plasticity theory

It is well known that in many practical problems the actual behaviour of a material is governed by plastic as well as by rheological-effects. Recent research concerning the description of dynamic properties of materials has shown that the application of plasticity theory in which rheological effects are disregarded, leads to large discrepancies between the theoretical and experimental results. The advantages of visco-plasticity is the simultaneous description of the rheologic and plastic effects.

This theory was originally developed from static data for metals to model the slip associated with metal crystalline solids. By addition of flow rules that incorporate viscous constants, these models have been extended to include strain-rate-dependent problems.

Hinnerichs [112] developed a model based on the assumption that the elastic properties are constant, volumetric strains vary linearly or elastically below the limit surface and finally, the limit surface is pressure dependent. Using the incremental elastic-visco-plastic theory with the non-associated Drucker- Prager flow rule, the volumetric strains are controlled by a strain-hardening cap. The basic

equations are

$$\dot{\sigma_{ij}} = D(\dot{\epsilon_{kl}} - \dot{\epsilon_{kl}}^p) = D\dot{\epsilon_{kl}}^e \tag{2.53}$$

$$\dot{\epsilon_{ij}} = \lambda_d < \phi(F) > \frac{\partial Q}{\partial \sigma_{ij}} \tag{2.54}$$

where σ_{ij} is the stress, and the total strain is the sum of elastic strain with plastic strain

$$\epsilon_{ij} = \epsilon_{ij}^e + \epsilon_{ij}^p \tag{2.55}$$

In the above equations, D the material stiffness, $\dot{\epsilon}_{ij}^p$ the deviatoric strain-rate. $\dot{\epsilon}_{ii}^p$ the volumetric strain-rate, F a yield function, Q the plastic potential function and λ_d is the viscosity constants.

Hinnerichs showed that the model is suitable in cases where the dilatation is not important, which occurs during uniaxial strain conditions and under high confinement.

A strain-rate-dependent visco-plastic model has also been proposed by Rajendran et al. [113]. Internal state variables were used to model load histories of various metals at strain-rates of up to 100/s. In this model, the total strain-rate is decomposed into elastic and inelastic components

$$\dot{\epsilon_{ij}} = \dot{\epsilon_{ij}^e} + \dot{\epsilon_{ij}^P} \tag{2.56}$$

Stress rate and strain rate are related elastically, and inelastic strain rate is assumed to be a function of stress σ_{ij}. Following Prandtl-Reuss

$$\dot{\epsilon_{ij}^P} = \dot{e_{ij}^P} = \lambda S_{ij} \tag{2.57}$$

where $\dot{e_{ij}^P}$ is the deviatoric plastic strain rate, S_{ij} the stress and λ is the flow parameter. Inelastic strain rate is given by

$$\dot{\epsilon_{ij}^P} = D_0 exp(\frac{-(n+1)}{2n}\frac{[Z^2]^n}{3j_2})\frac{S_{ij}}{\sqrt{j_2}} \tag{2.58}$$

where D_0 limits the plastic strain rate in shear and n is a strain-rate sensitivity parameter. The state variable Z is a measure of overall material resistance to plastic flow and is loading history-dependent, which is given in the evolution form as

$$\dot{Z} = m(Z_1 - Z)\dot{W}_P \tag{2.59}$$

and

$$\dot{Z} = Z_1 - (Z_1 - Z_0)e^{-m\dot{W}_P} \tag{2.60}$$

where m an empirical parameter, $\dot{W}_P$ the plastic-flow rate, Z_0 the initial value of Z, and Z_1 is the maximum value attained by Z. It was concluded that this model, which contains five material parameters (D_0, Z_0, Z_1, m, and n) to be evaluated by high strain-rate experiments, is able to predict high strain-rate behaviour of metals in which the response is primarily governed by shear flow and slip along crystalline planes rather than concrete, where crack development is the predominant factor.

An adaptive technique for the solution of the dynamic elastic-visco-plastic problem has been developed by Bajer et al. [114], in which the mesh is modified by the use of *'space-time element'* method. The scheme appears not to be efficient in large scale problems due to refinement of the mesh. The use of the technique for the solution of two-dimensional non-linear problems of dynamic response has been examined by Sheu [115] in which the structure is divided into some sub-structures and a condensed stiffness matrix is used.

A pseudo-visco-plastic method for non-linear analysis of static problems has been proposed by Smith and Griffiths [116, 117]. A visco-plastic strain-rate has been in the form

$$\dot{\epsilon}^{vp} = F\frac{\partial Q}{\partial \sigma} \tag{2.61}$$

In this method, strain increment is approximated explicitly using a critical time-step as

$$(\Delta\epsilon^{vp})^i = (\Delta\epsilon^{vp})^{i-1} + \Delta t(dot\epsilon^{vp})^i \tag{2.62}$$

To ensure stability, the conditional time-step formulae derived by Cormeau [118] have been employed. It was shown through some examples that, a good agreement is obtained compared with Prandtl results.

2.5.9 Material elasto-visco-plasticity

As explained earlier, the theory of visco-plasticity emerges as an attempt to provide a realistic phenomenological approach to material behaviour combining plastic and creep effects in a unified model. A fundamental generalization of the theory has been produced by Naghdi and Murch [119] and has been modified by Perzyna [119, 120]. An alternative model has been proposed by Phillips [119].

This model has been adopted in the present study and is explained in the next section.

2.5.10 The yield criteria for a visco-plastic material

'Flow surface' was introduced by Naghdi and Murch [119]. in the form

$$f = f(\sigma_{ij}, \epsilon^p_{ij}, k, \beta) \tag{2.63}$$

The function f depends on the state of stress σ_{ij} and the state of plastic strain ϵ^p_{ij}. The parameters k and β represent the strain-hardening and the viscous effect respectively.

The time-variability of a flow surface can be written as

$$\dot{f} = \frac{\partial f}{\partial \sigma_{ij}}\dot{\sigma_{ij}} + \frac{\partial f}{\partial \epsilon^p_{kl}}\dot{\epsilon}^p_{kl} + \frac{\partial f}{\partial k}\dot{k} + \frac{\partial f}{\partial \beta}\dot{\beta} \tag{2.64}$$

If the instantaneous state under consideration at $t = \tau$ is denoted by σ^τ_{ij}, ϵ^τ_{kl}, k^τ and β^τ, the body is visco-elastic when

$$f(\sigma^\tau_{ij}, \epsilon^\tau_{kl}, k, \beta) \leq 0 \tag{2.65}$$

and visco-plastic when

$$f(\sigma^\tau_{ij}, \epsilon^\tau_{kl}, k, \beta) > 0 \tag{2.66}$$

Therefore the equation

$$f(\sigma^\tau_{ij}, \epsilon^\tau_{kl}, k, \beta) = 0 \tag{2.67}$$

represents the instantaneous *'loading surface'* corresponding to the state.

2.5.11 Perzyna's elasto-visco-plastic model

Perzyna [119, 120] has modified the constitutive equation proposed by Naghdi and Murch [119] based on the following assumptions

- The flow surface $f = 0$ in the nine-dimensional stress space is regular and convex.

- In isotropic materials, the flow vector is normal to what Perzyna called the *'subsequent dynamic loading surface'*. However, it is felt that the flow vector does not remain normal to the loading surface in orthotropic materials.

The onset of visco-plastic behaviour is governed by the positive values of a scalar yield function F, which for isotropic materials has the form

$$F(\sigma_{ij}, \epsilon_{vp}, k) = f(\sigma_{ij}, \epsilon_{vp}) - F_0 = 0 \tag{2.68}$$

in which F_0 is the uniaxial yield stress which may be a function of a hardening parameter k. A set of yield function forms is given in Table 2.2.

For an associated elasto-visco-plastic flow rule, the visco-plastic strain rate is related to the current stresses according to

$$\dot{\epsilon}_{ij}^{vp} = \gamma_P < \phi(F) > \frac{\partial f}{\partial \sigma} \tag{2.69}$$

in which γ_P is Perzyna's fluidity parameter i. e. a positive rate-dependent factor which depends on the temperature and the damage process [4, 5, 41]. The flow function $\phi(F)$ is a monotonically increasing function which for positive values $< \phi(F) >$ equal to ϕ and zero otherwise. Perzyna [119] proposed two types of flow functions

$$\phi(F) = (F/y)^N \tag{2.70}$$

and

$$\phi(F) = \exp(MF/y) - 1 \tag{2.71}$$

where the parameters N and M are evaluated from experimental data and y is the initiation yield stress.

In associated flow the flow vector, denoted by a, can be written as

$$a = \frac{\partial f}{\partial \sigma} \tag{2.72}$$

which implies that the visco-plastic strain rate vector is normal to the *'subsequent dynamic loading surface '* [119].

2.5.12 Continuous damage theory

Continuous damage theory is based on the assumption that, the evolution in a solid characterizes the energy dissipation mechanism.

Damage can be closely correlated to the amount of cracking and might be expressed as the degree of non-linearity of the stress-strain diagram.

Concrete behaviour under static and dynamic loading can be modelled by damage mechanics and many damage-based theoretical models have been developed [41, 122]. In the context of strain-rate-dependent problems each of the theoretical models proposed to characterize rate effects has concentrated on specific process. For instance, Suaris and Shah [121] used the variable ω as the damage parameter and developed the damage equation in the following form

$$\sigma = E(1 - \omega)\epsilon \tag{2.73}$$

in which E is the initial tangent modulus of elasticity of undamaged material and σ and ϵ are one-dimensional measures of stress and strain respectively. If ω is taken as a linear function of strain

$$\omega = A\epsilon \tag{2.74}$$

where A is a constant. By substituting (2.74) into (2.73), a quadratic equation in strain is obtained in the form of

$$\sigma = E(1 - A\epsilon)\epsilon \tag{2.75}$$

Equation (2.75) produces strain-softening model in which secant modulus is decreased as the strain is increased.

Hinton and Bicanic [41] have developed a history-dependent damage model. Two variable yield surfaces in stress space were defined. The onset of visco-plastic surface denoted by F_0 and the initiation of material degradation surface termed *'damage surface'* denoted by F_f are defined as

$$F_0(\sigma, \sigma_0) = 0 \tag{2.76}$$

$$F_f(\sigma, \sigma_f) = 0 \tag{2.77}$$

where, σ_f is a damage-dependent function which is defined as

$$\sigma_f(W_P) = \beta_0 \acute{f}_c(1 - \beta_1 W_p) \tag{2.78}$$

for $0 < W_p \leq W_p^f$ in which β_0 and β_1 are determined experimentally and $\beta_0 \acute{f}_c$ is the compressive strength obtained with infinite load rates and no inelastic strains and W_f is the visco-plastic work density defined as

$$W_p = \int_0^t \sigma^T \dot{\epsilon}_{vp} dt \tag{2.79}$$

Fig. 2.53, shows the variable damage surface together with the variable yield surface. As soon as the stress in the material lies outside the yield surface visco-plastic straining occurs and the two surfaces begin to change [41].

A continuous damage theory for quasi-static and dynamic behaviour of brittle material has been proposed by Suaris and Shah [122]. A vectorial representation of the damage variable was developed to predict the strain-rate-dependence of concrete in compression and tension. Assuming flat microcracks, the damage variable was vectorially represented and a free-energy function dependent on the coupled invariants of strain and damage was postulated. The constitutive relations and the damage evolution equations were derived consistent with the first and second laws of thermodynamics. A three-dimensional strain-rate-dependent constitutive relation for stress and strain was proposed of the form

$$\sigma_{11} = \sigma_{22} = E\nu^*[(1+\hat{\nu})\epsilon_{33} - \frac{C_1}{\sqrt{2}}(4\epsilon_{11} + \epsilon_{33}) + \frac{2C_3}{\sqrt{2}}\omega\epsilon_{11} + \frac{2^{n-1}}{\sqrt{2}}nC_2\omega^{n-1}\epsilon_{11}^{n-1}] = 0 \tag{2.80}$$

in which

$$\sigma_{33} = E\nu[2\hat{\nu}\epsilon_{11} + \epsilon_{33} - \frac{2C_1}{\sqrt{2}}\omega\epsilon_{11}] \tag{2.81}$$

and

$$\lambda + 2\mu = E\nu^* \tag{2.82}$$

$$\lambda = \hat{\nu}E\nu^* \tag{2.83}$$

$$\hat{\nu} = \frac{\nu}{1-\nu} \tag{2.84}$$

and

$$\hat{\nu} = \frac{(1-\nu)}{(1+\nu)(1-2\nu)} \tag{2.85}$$

$$C_i = \frac{\gamma_i}{E\hat{\nu}}(i = 1-3) \tag{2.86}$$

In the above equations E and ν are the modulus of elasticity and the Poisson's ratio, respectively. From the above relations, it is seen that the theory requires a large number of material parameters and involves difficulties in calculation which are the drawbacks of the method. More detail are given in [122].

Young et al. [123] have proposed a damage model to simulate the behaviour of reinforced concrete structures under several damaging load cycles such as those due to earthquakes. It was claimed that the predicted response of the model is in a good agreement with the experimental results.

2.5.13 Empirical models

Many empirical relations have been proposed to predict the influence of strain-rate on the dynamic response of concrete. Alhammad et al. [124] proposed a strain-rate-sensitive function of the form

$$F(\dot{\epsilon}) = A + Blog\dot{\epsilon} + C(log\dot{\epsilon})^2 \tag{2.87}$$

where, A, B, C are empirical constants, given in [124], F is either the dynamic strength of the concrete, modulus of elasticity or strain at maximum stress, which was claimed to be valid over a strain-rates range from static loading $(10^6/s)$ up to rates of 10/s. It was not explained why the formula is not valid for the rates above 10/s.

In the nest section, the traditional methods of modelling concrete strengthening and stiffening will be discussed.

2.5.14 Rate-sensitive function in tension

In order to develop a formula for modelling the response of concrete at higher rates, a basic static model is traditionally used [94] and the variations in response due to rate effects are added which will be explained in more detail in subsequent sections.

Various investigators have proposed formula to predict the strain-rate-dependent behaviour of concrete in tension [7, 9]. The proposed formulas are either very complicated or too approximate. An example of the latter is the formula proposed by Bazant and Oh [7] which is valid only for a strain rate range of $10^{-6}/S - 1/S$ and has the following form

$$\acute{f}_t^d / \acute{f}_t^s = 1.95 - 3.32(1 - \dot{\epsilon}^{0.125})(2.2 + 3.2\dot{\epsilon}^{0.125})^{-1} \tag{2.88}$$

A non-linear fracture mechanics model to predict the strain-rate effect on the fracture of concrete has been proposed by Shah et al. [125], based on experimental observations. The proposed model requires three material properties, i. e. critical stress intensity factor K_{IC}^S, Critical Crack Tip Opening displacement CTOD Fig. 2.54, and Young's Modulus. All the required parameters can be determined from static tests.

2.5.15 Strain-rate-sensitive function in compression

For predicting the dynamic ultimate compressive strength $\acute{f}_{cd}$, Bazant [90] proposed

$$\acute{f}_{cd} = \acute{f}_c(1.4 - 1.5f(\dot{\epsilon})) \tag{2.89}$$

in which the strain-rate-sensitive function $f(\dot{\epsilon})$ is given by

$$f(\dot{\epsilon}) = \frac{1 - \dot{\epsilon}^{1/8}}{1.84 + 3.2\dot{\epsilon}^{1/8}} \tag{2.90}$$

the peak strain ϵ_c^p is given by

$$\epsilon_0^P = \frac{P\acute{f}_{cd}}{E} \tag{2.91}$$

where P is given by

$$P = 2.09 - .00015\acute{f}_c + f(\dot{\epsilon}) \tag{2.92}$$

It was reported that these equations are valid for a strain-rate range of $10^{-5}/S$ to $1/S$. The parameters P and ϵ_0 are illustrated in Fig. 2.55.

Alternative rate sensitive functions established from experimental results have been suggested by Mander et al. [12], for peak compressive strength, initial modulus of elasticity and strain at peak stress. The equations are reported in [12] as follows:

Peak strength dynamic magnification factor

$$\acute{f}_c^d = D_f \acute{f}_c^s \tag{2.93}$$

where, $\acute{f}_c^s$ is the quasi-static compressive strength of concrete and

$$D_f = \frac{1 + [\frac{\dot{\epsilon}}{0.0035(\acute{f}_c)}]^{1/6}}{1 + [\frac{0.00001}{.035(\acute{f}_c)}]^{1/6}} \tag{2.94}$$

where, $\dot{\epsilon}$ is the strain rate and $\acute{f}_c^s$ is in MPa. The dynamic magnification factor D_f was found by regression analysis of the experimental results of Watstain [12] on plain concrete specimens of different strengths.

Dynamic stiffness magnification factor

$$E_c^d = D_e E_c^s \tag{2.95}$$

where, E_c^s is the quasi-static modulus of elasticity and

$$D_e = \frac{1 + [\frac{\dot{\epsilon}}{0.035(\acute{f}_c)^3}]^{1/6}}{1 + [\frac{0.00001}{0.035(\acute{f}_c)^3}]^{1/6}} \tag{2.96}$$

The Magnification factor against strain-rate is plotted in Figs. 2.56 A and B. The dynamic magnification factor D_e was also found by regression analysis of Watstein's experimental results [12].

Dynamic strain at peak stress

An equation based on the assumption that the work done on concrete to achieve its strength under different strain-rate is constant has been developed for the peak strain by Mandel et al. [12] in the form

$$\epsilon_c^d = D_\epsilon \epsilon_c^s \tag{2.97}$$

where, ϵ_c^s is the quasi-static strain at peak stress and

$$D_\epsilon = \frac{1}{3D_f}[1 + \sqrt{(1 + \frac{3D_f^2}{D_E})}] \tag{2.98}$$

In which D_f is determined by Eq. (2.94). They claimed that good agreement is obtained with observed results.

Strain-rate-sensitive function for steel

It is postulated that steel strength is also influenced by strain-rate and increases with increasing strain-rate [23, 24, 126], Fig. 2. 57. Various investigators have proposed strain-rate-sensitive function

2.6 Concrete stiffening and strengthening incorporation in the proposed model

Limited test results involving scattering data have been reported by experimental investigators [4-10]. Therefore, the existing formulae for predicting the strain-rate-dependent behaviour of concrete appear not to be efficient. Using a rheological model, the static strain reduction for a given stress due to strain-rate can be predicted by which the material stiffening and strengthening can be modelled.

A rheological model to describe strain-rate-sensitivity of concrete stiffness and strength has been proposed which will be discussed in the next section.

2.6.1 Proposed rheological model

In the proposed rheological model, increase in the concrete strength due to increased strain-rate both in tension and in compression is assumed to be attributable to the decrease in the visco-elastic and the visco-plastic deformations for a given stress and strain-rate when compared with those at the same stress and a lower strain-rate. Consequently the visco-plastic strain and hence the initial modulus of elasticity are influenced by strain-rate as has been confirmed by experimental evidence [9, 10, 12, 21]. The latter is attributed to elastic decrement which exhibits itself as an stiffened modulus of elasticity. Hence both the visco-elastic and visco-plastic strain decrease with increasing strain-rate and cause the material stiffening and strengthening. The proposed rheological model is illustrated in Fig. 2.58. As can be seen, the model is constructed from two series systems each of which involves a dash-pot.

When the rheological model is subjected to a stress $d\sigma$ within a time dt, the induced visco-elastic and visco-plastic stresses denoted by $\mu\frac{d\epsilon_e}{dt}$ and $\mu\frac{d\epsilon_{vp}}{dt}$ are in equilibrium with the external stress thus

$$\mu\frac{d^2\epsilon_e}{dt^2} + \mu\frac{d^2\epsilon_{vp}}{dt^2} + E_t\frac{d\epsilon}{dt} = \frac{d\sigma}{dt} = \dot{\sigma} \tag{2.99}$$

where E_t is the tangent modulus of elasticity, and μ the coefficient of viscosity which is assumed to have the same value for both elastic and visco-plastic deformations.

Introducing a fluidity parameter γ such that

$$\gamma = 1/\mu \tag{2.100}$$

and substituting into Eq. (2.99) leads to

$$\frac{d^2\epsilon}{dt^2} + \gamma E_t\frac{d\epsilon}{dt} = \gamma\dot{\sigma} \tag{2.101}$$

Since E_t, γ and $\dot{\sigma}$ are functions of time, Equation (2.101) is non-linear. The values of γ have been evaluated based on data from Hatano's tests [10] assuming a constant stress-rate. Hence the stress-rate at any point $\dot{\sigma}_i$ at $t = t_i$ is given by

$$\dot{\sigma}_i = \frac{\sigma_i}{t_i} \tag{2.102}$$

in which the time t_i can be obtained from

$$t_i = \frac{\sigma_i}{\sigma_{max}} t_f \tag{2.103}$$

where t_f is the failure time given by Hatano's test results [10].

If Eq. (2.101) is assumed to be linear in a small time-interval dt both E_t and γ will be constant in time-interval.

Solving Eq. (2.101) assuming a constant stress-rate in the time-interval dt gives

$$\frac{d\epsilon}{dt} = C_1 e^{-\gamma E_t t} + \frac{\dot{\sigma}}{E_t} \tag{2.104}$$

With the initial condition $\dot{\epsilon}(0) = \dot{\epsilon}_0$, then C_1 can be obtained as

$$C_1 = \dot{\epsilon}_0 - \frac{\dot{\sigma}_0}{E_t} \tag{2.105}$$

Denoting the increased modulus of elasticity by E_d then

$$C_1 = \frac{\dot{\sigma}_0}{E_d} - \frac{\dot{\sigma}_0}{E_t} = \alpha \frac{\dot{\sigma}_0}{E_t} \tag{2.106}$$

in which α is defined as

$$\alpha = \frac{E_t}{E_d} - 1 \tag{2.107}$$

Eq. (2.104) can be written as

$$\frac{d\epsilon}{dt} = \frac{\alpha \dot{\sigma}_0}{E_t} e^{-\gamma E_t t} + \frac{\dot{\sigma}}{E_t} \tag{2.108}$$

Integrating Eq. (2.108), strain at time t can be obtained as

$$\epsilon = \frac{\dot{\sigma}}{E_t} - \frac{\alpha \dot{\sigma}_0}{\gamma E_t^2} e^{-\gamma E_t t} + C_2 \tag{2.109}$$

Again by putting the initial condition $\epsilon(0) = 0$, C_2 can be obtained thus, equation (2.109) leads to

$$\epsilon = \frac{\dot{\sigma} t}{E_t} - \frac{\alpha \dot{\sigma}_0}{\gamma E_t^2}(1 - e^{-\gamma E_t t}) \tag{2.110}$$

Eqs. (2.108) and (2.110) are valid for $0 \leq t \leq dt$.

By putting $\dot{\sigma}_0 t = \sigma$ and $\sigma / E_t = \epsilon$ into (2.110), we have

$$\epsilon = \frac{\sigma}{E_t} - \frac{\alpha \dot{\sigma}}{\gamma E_t^2}(1 - e^{-\gamma E_t t}) \tag{2.111}$$

The first term of Eq. (2.111) is the static strain and the second term is the strain reduction due to strain-rate which not only depends upon strain-rate but also on fluidity parameter γ, time t, tangent modulus of elasticity E_t, the stress-level σ and initial conditions σ_0 and ϵ_0. Since E_t in the visco-plastic portion is less than that of visco-elastic, it is deduced that, the strain reduction in the visco-elastic stage is less than that in the visco-plastic stage. In other words, the visco-elastic range is less strain-rate-sensitive than the visco-plastic range which has been confirmed by experimental evidence.

Since the stiffening and strengthening fluidity parameter γ_T increases with increasing strain-rate Figs. 2.67-2.72, the irreversible visco-elastic strain and visco-plastic strain values depend on loading-rate and stress level. Hence the proposed model is a 'history' strain-rate dependent model.

Putting static strain ϵ_s as $\epsilon_s = \frac{\sigma}{E_t}$ in Eq. (2.111) gives

$$\epsilon_d = \epsilon_s[1 - \frac{\alpha}{\gamma E_t t}(1 - e^{-\gamma E t})] \tag{2.112}$$

where, ϵ_d is the reduced dynamic strain.

The characteristics of the proposed model

The main characteristics of the proposed history-strain-rate-sensitive model are summarized as:

- The Young's modulus of elasticity is a strain-rate-sensitive parameter.
- The visco-elastic-visco-plastic strain of concrete is history-strain-rate-dependent.
- The tangent modulus of elasticity is history-strain-rate-dependent.
- The secant modulus of elasticity is history-strain-rate-dependent.
- Only three parametric static tests i. e. the peak compressive strength and corresponding strain and the Young's modulus of elasticity are required.

In the case where the peak strain is not available, the formula proposed by Bazant [6] can be used for estimating the peak strain,

$$\epsilon_0 = 1.027 \times 10^{-7} \acute{f}_c + 0.00195 + 0.0296 \frac{f_r}{\acute{f}_c} \tag{2.113}$$

in which f_r is a confinement index and is zero in the current study. The Young modulus of elasticity can also be evaluated by Eq. (??).

Proposed formula for strain-rate-dependent modulus of elasticity

The stiffened initial modulus of elasticity E_d can be obtained using Eq. (2.112) at $t = dt$

$$\epsilon_d = \epsilon_s[1 - \frac{\alpha}{\gamma E_t t}(1 - e^{-\gamma E_t t})] \tag{2.114}$$

Denoting $\gamma_E = \frac{\gamma}{\alpha}$ as the fluidity parameter corresponding to initial modulus of elasticity, Eq. (2.112) changes to

$$\epsilon_d = \epsilon_s[1 - \frac{1}{\gamma_E E_t t}(1 - e^{-\gamma_E E_t t})] \tag{2.115}$$

where E_t is the static initial modulus of elasticity.

The equivalent dynamic modulus of elasticity E_d for a give strain ϵ_s is related to the static modulus of elasticity E_t by

$$\frac{E_d}{E_t} = \frac{\epsilon_s}{\epsilon_d} \tag{2.116}$$

Substituting Eq. (2.115) into (2.116) gives

$$E_d = E_t(\frac{\gamma_E E_t dt}{e^{-\gamma_E E_t dt} \gamma_E E_t dt - 1}) \tag{2.117}$$

where E_d is the stiffened modulus of elasticity. The term *'stiffened'* is used because as soon as the load is removed, it returns to its pre-loaded value.

As can be seen, the variation of the stiffened modulus of elasticity depends inversely on $\gamma_E E_t t$. Since $\gamma_E E_t t$ decreases with increasing strain-rate, E_d is also increased with increasing strain-rate.

Proposed formula for determining the fluidity parameter γ_E corresponding to dynamic modulus of elasticity

By fitting the experimental data reported in [10] and on the basis of constant stress-rate, the fluidity parameter γ_E for three types of concrete has been obtained which is assumed to be a function of the effective strain-rate $\dot{\epsilon}$ in a logarithmic form as

$$\gamma_E = \lambda_1 \dot{\epsilon}_{eff}^{\lambda_2} \tag{2.118}$$

The values of λ_1 and λ_2 for tension and compression are given in Tables 2.3, and 2.4. respectively. Figs. 2.59 - 2.61 illustrate variation of γ_E with strain-rate for three types of compressive concrete and Figs. 2.62 - 64 shown variation of γ_E with strain-rate for three types of concrete in tension.

Proposed history-strain-rate-dependent uniaxial stress-strain relation

In order to develop the stress-strain formula, it is necessary to rewrite Eq. (2.104)in the incremental form for time-steps n and n+1 as

$$(\frac{d\epsilon}{dt})n+1 = C_1 e^{-\gamma_{n+1} E_{n+1} t_{n+1}} + \frac{\dot{\sigma}_{n+1}}{E_{n+1}} \tag{2.119}$$

where $t_{n+1} \geq t \geq t_n$. C_1 can be determined by putting the initial condition at $t = t_n$ obtained from the previous time-step n which leads to

$$(\frac{d\epsilon}{dt})n+1 = \frac{\alpha\dot{\sigma}_0}{E_n} e^{-\gamma_{n+1} E_{n+1} t_{n+1}} + \frac{\dot{\sigma}_{n+1}}{E_{n+1}} \tag{2.120}$$

Integrating Eq. (2.120) for the time-step t_{n+1} yields

$$\epsilon_{n+1} = \frac{\alpha\dot{\sigma}_{n+1}}{\gamma_{n+1} E_{n+1} E_n} e^{-\gamma_{n+1} E_{n+1} t_{n+1}} + \frac{\dot{\sigma}_{n+1} t_{n+1}}{E_{n+1}} + C_2 \tag{2.121}$$

Again C_2 can be determined by putting the initial conditions at $t = t_n$ obtained from the previous time-step which leads to

$$\epsilon_{n+1} = \frac{\alpha\dot{\sigma}_n}{\gamma_n E_n^2} e^{-\gamma_{n+1} E_{n+1} t_{n+1}} + \frac{\dot{\sigma}_{n+1} t}{E_{n+1}} + \frac{\alpha\dot{\sigma}_n}{\gamma_n E_n^2} \tag{2.122}$$

Substituting $\sigma = \dot{\sigma} \quad t$ and rearranging Eq. (2.122) leads to

$$\epsilon_{n+1} = \frac{\sigma}{E_{n+1}} - \frac{\alpha\sigma}{\gamma_n E_n^2 t}(1 - e^{-\gamma_{n+1} E_{n+1} t_{n+1}}) \tag{2.123}$$

As can be seen, Eq. (2.123) gives the reduced strain due to strain-rate in each time-step.

In the case where the strain-rate is constant, Eq. (2.123) reduces to

$$\epsilon_{n+1} = \frac{\sigma_{n+1}}{E^s_{n+1}}[1 - exp(-\gamma_T E^s_{n+1} t_{n+1})] \tag{2.126}$$

where the fluidity parameter γ_T is constant and E_s is the secant modulus of elasticity corresponding to time-step $n+1$. Hatano et al. [10] and Ahmad et al. [21] test specimens have been analysed using the proposed model and the results were compared with the experimental data which will be discussed in Chapter 6.

Proposed model for multiaxial situation

In order to extend the proposed model to multiaxial situation, a uniaxial static stress-strain formula based on progressive damage of the form

$$\sigma_d = E_d \epsilon_s - (E_d \epsilon_0 - \sigma_0)(\frac{\epsilon_s}{\epsilon_0})^{\theta A} \tag{2.127}$$

where, σ_0 and ϵ_0 are the peak stress and peak strain respectively and

$$A = \frac{E\epsilon_0}{\sigma_0} \tag{2.128}$$

is proposed where θ is a parameter which varies between 1-3 and depends on the type of the concrete. and is assumed to be equal to 2.1 in the proposed model. The proposed uniaxial formula is graphically illustrated in Fig. 2.65.

Denoting $\gamma_T = \frac{\alpha}{\gamma}$ from Eq. (2.115) as the fluidity parameter corresponding to visco-plastic reduction strain, and replacing ϵ_d from Eq (2.112) by ϵ in Eq. (2.127), the proposed uniaxial strain-rate-sensitive stress-strain relation is obtained as

$$\sigma_d = E_d \epsilon_s - (E_d \epsilon_0 - \sigma_0)[\frac{\epsilon_s(1 - \frac{1}{\gamma_T E_t t})}{\epsilon_0}]^{\theta A} \tag{2.129}$$

in which E_t is the tangent modulus of elasticity corresponding to the quasi-static stress-strain relation and t is time. A typical uniaxial stiffened stress-strain curve is illustrated graphically in Fig. 2.66.

Due to lack of test results, extending the proposed model to a two-dimensional problem has been performed using *'effective strain '*. So, before deriving the fluidity parameter formula corresponding to the visco-elastic-visco-plastic strain reduction, the effective strain and stress will be discussed in the next section.

Effective stress and strain

When the uniaxial experimental results are to be used for multiaxial situation, some sort of stress and strain so called *'effective'* can be used. To this end, the loading function is used as a stress variable to define the effective stress of the form [2]

$$f(\sigma_{ij}) = C\sigma_{eff}^{n} \tag{2.130}$$

where C is some constant and is determined from the uniaxial parameters e. g. for Von-Mises material $n = 2$ and $C = 1/3$

Effective plastic strain is not quite simple. It is generally defined in incremental form by two approaches. The first one is in the form

$$dW^p = \sigma_{eff} d\epsilon_{eff}^p \tag{2.131}$$

in which W^p is the plastic work per unit volume. In the second method, the effective plastic-strain increment is defined as

$$d\epsilon_{eff}^p = C\sqrt{(d\epsilon_{ij}^p d\epsilon_{ij}^p)} \tag{2.132}$$

which for pressure-independent material which satisfies the plastic-incompressibility condition becomes [2]

$$d\epsilon_i^p = C\sqrt{([(d\epsilon_1^p)^2 + 1/2(d\epsilon_2^p)^2 + 1/2(d\epsilon_3^p)^2])} = C\sqrt{3}/2 d_i^p \tag{2.133}$$

from which C is determined as $C = \sqrt{\frac{3}{2}}$, thus

$$d\epsilon_{eff}^p = \sqrt{(\frac{2}{3} d\epsilon_{ij}^p d\epsilon_{ij}^p)} \tag{2.134}$$

The effective elastic strain can be defined either by the projection of the octahedral shear strain on x-axis in the form [41]

$$\epsilon^{e}_{eff} = (3\acute{J}_{2e}/(1+v)^2)^{1/2} \tag{2.135}$$

or by a combination of octahedral normal and shear strain as [2]

$$\epsilon^{e}_{eff} = \sqrt{(\epsilon^2_{oct} + 1/4\gamma^2_{oct})} \tag{2.136}$$

in which ϵ_{oct} and γ_{oct} are the octahedral normal and octahedral shear strain respectively.

Fluidity parameter

The flow vector a in the Perzyna's model Eq. (2.72) [120] is related to time by a fluidity parameter γ_P. (the subscript p has been used to avoid confusion with other fluidity parameters). Many relations have been proposed for determining γ_P in the literature.

Hinton et al. [41] proposed a logarithmic relation between γ_P and the effective elastic strain-rate in the form

$$\gamma_P(\dot{\epsilon}_e) = P_1(\dot{\epsilon}^{P_2}_e) \tag{2.137}$$

where, a_0 and a_1 are parameters which are be determined experimentally. Beshara [94] has proposed

$$\gamma_P = 10^{b_1}\,\dot{\epsilon}^{b_2}_{eff} \tag{2.138}$$

where, b_1 and b_2 are material parameters to be determined also by fitting test data.

Recently Famiyesin et al. [103] proposed a relation which relates the fluidity parameter to the total effective strain-rate.

2.6.2 Proposed fluidity parameter

In the proposed model, the fluidity parameter is related to the total effective strain-rate $\dot{\epsilon}_{eff}$ in logarithmic form as

$$\gamma_P = P_1\dot{\epsilon}^{P_2}_{eff} \tag{2.139}$$

where P_1 and P_2 are material parameters and have been evaluated by fitting the test results reported in [10] and are given in Table 2.5. Variation of fluidity parameter γ_P with total strain-rate for three types of concrete mix are illustrated in Figs. 2.67-69.

Fluidity parameter γ_T corresponding to material stiffening and strengthening

As discussed earlier, the material visco-elastic-visco-plastic strain decreases with increasing strain-rate. This decrement can be obtained using Eq. (2.113). The fluidity parameter γ_T corresponding to the material stiffening and strengthening has also been evaluated by fitting test results reported in [10]. A second order function in logarithmic scale in the form

$$\ln \gamma_T = T_3(\ln \dot{\epsilon}_{eff})^2 + T_2(\ln \dot{\epsilon}_{eff}) + \ln T_1 \tag{2.140}$$

was found to be a best fit to the data. This can be rewritten as

$$\gamma_T = T_1 \dot{\epsilon}_e^{T_2} e^{T_3 (ln \dot{\epsilon}_e)^2} \tag{2.141}$$

The constants parameters T_1, T_2 and T_3 are given in Table 2.6, and variation of γ_T with total strain-rate for three types of concrete mix are shown in Figs. 2.70-72.

2.7 Visco-plastic constitutive equation for steel

The visco-plastic model has been used to model strain-rate-sensitivity of reinforcing steel in this study. The stress-strain relation in the elastic range is governed by Hook's Law as

$$\sigma_s = E\epsilon_s \tag{2.142}$$

The constitutive relation for the stresses above yield point is given as

$$\sigma_s = E\epsilon_e = E(\epsilon - \epsilon_{vp}) \tag{2.143}$$

The visco-plastic strain-rate in the direction of the reinforcement is obtained by using the uniaxial form of Perzyna's model [120] as

$$\dot{\epsilon}_{vp} = \pm\gamma_s\langle\sigma - F_y\rangle/F_y \tag{2.144}$$

where σ_s is the current stress level in the steel and γ_s is the steel fluidity parameter. Finally, plastic strain is determined by the explicit form of the strain approximation as

$$\epsilon_{vp} = \int_t \dot{\epsilon}_{vp} dt \tag{2.145}$$

The fluidity parameter γ_s, has been related to the strain-rate by an exponential formula [127] as

$$\gamma_s(\dot{\epsilon}_s) = a_0(\dot{\epsilon}_s)^{a_1} \tag{2.146}$$

in which a_0 and a_1 were approximated by fitting experimental tests on steel bars. The values of $a_0 = 1.5386$ and $a_1 = 0.9705$ evaluated by [93] by using the test results carried out by Albertini and Montagnani [128] have been used in the proposed model. The test results reported in [128] have been performed at constant strain-rate while those reported in [10] were constant stress-rates.

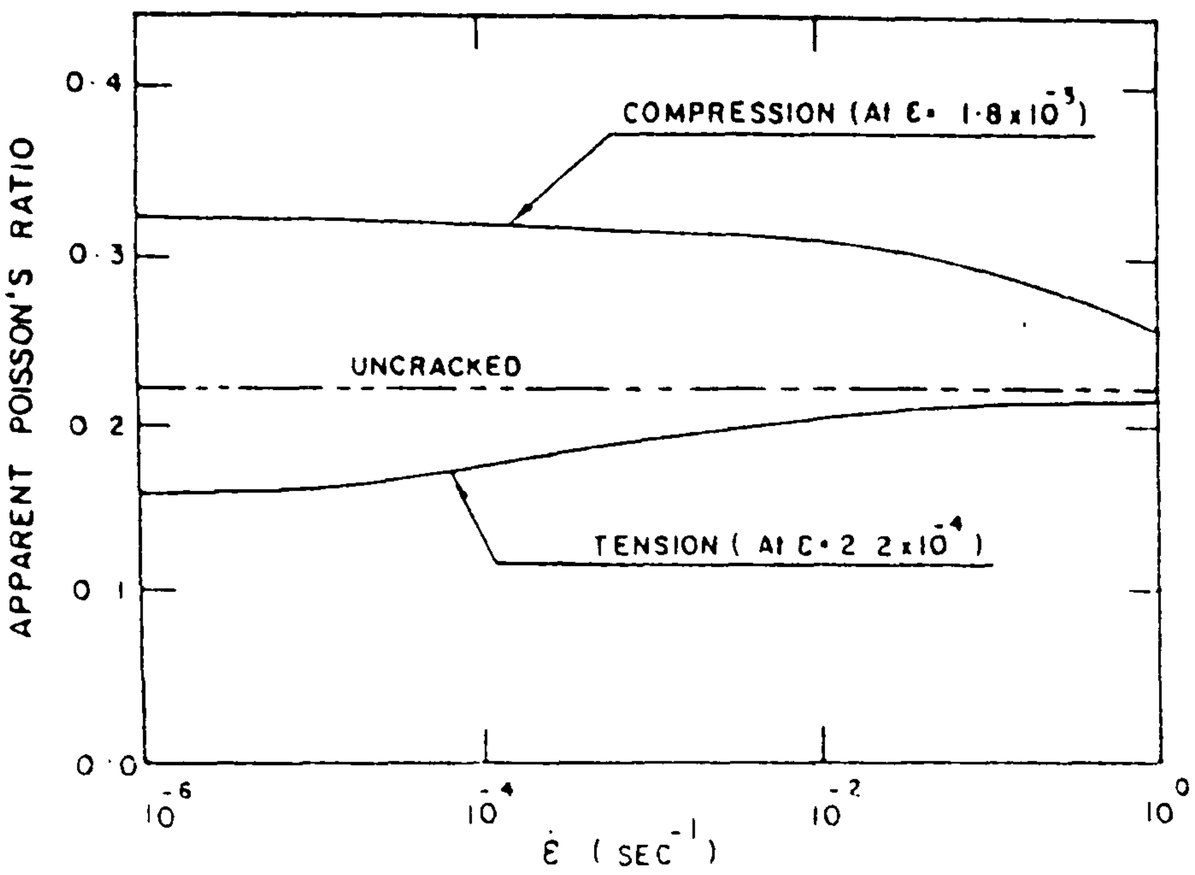

Fig. 2.1 A Effect of strain-rate on apparent Poisson's ratio,
(taken from [4])

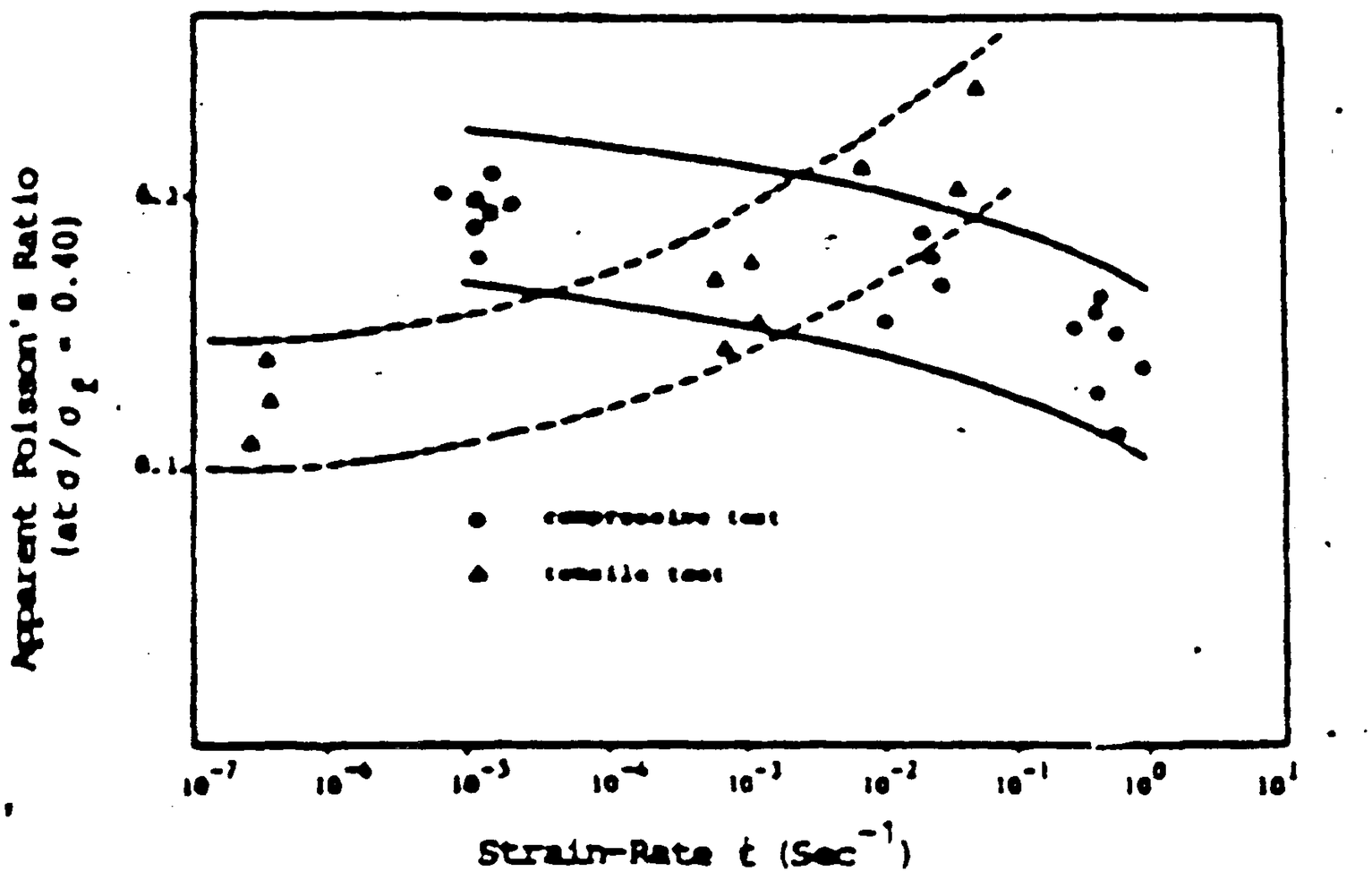

Fig. 2.1 B Effect of strain-rate on apparent Poisson's ratio,

(taken from [9])

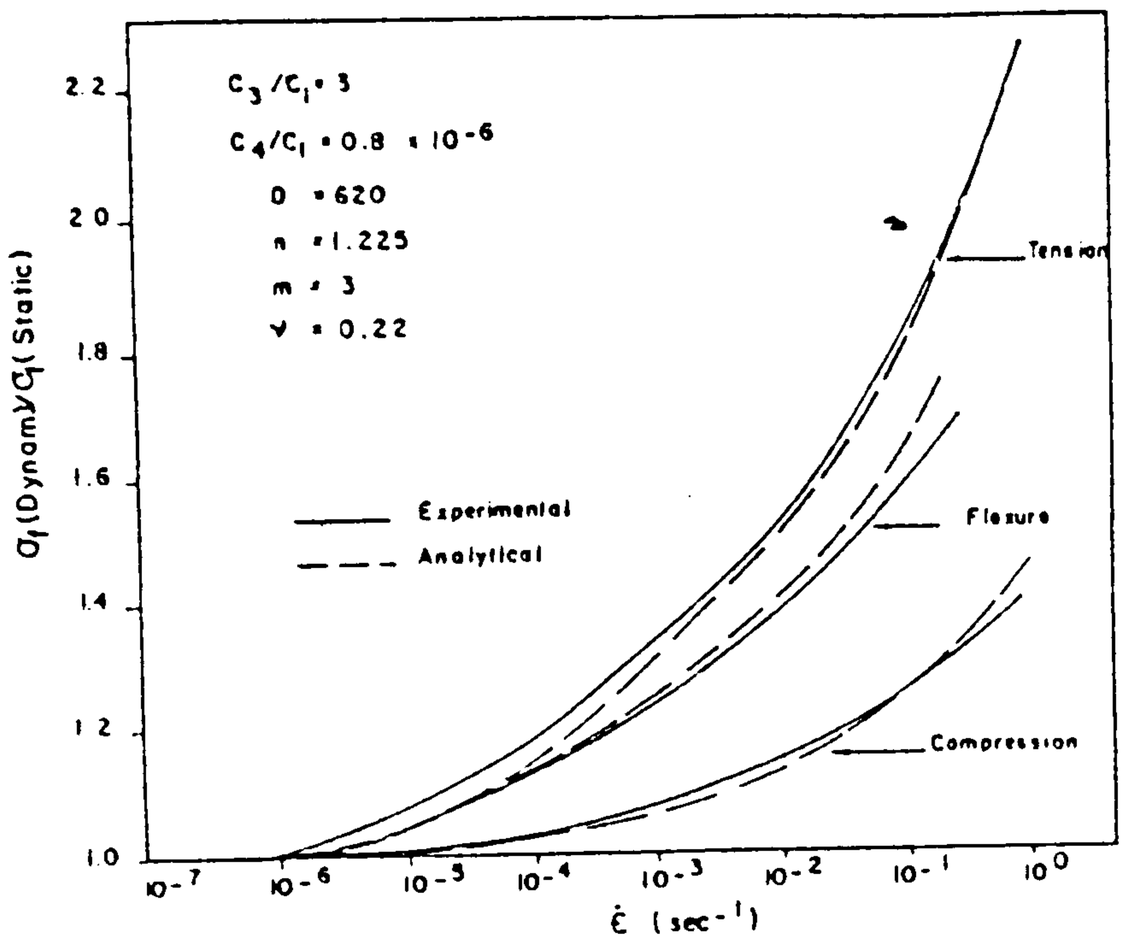

Fig. 2.2 Effect of strain-rate on ultimate strength of concrete,

(taken from [4]).

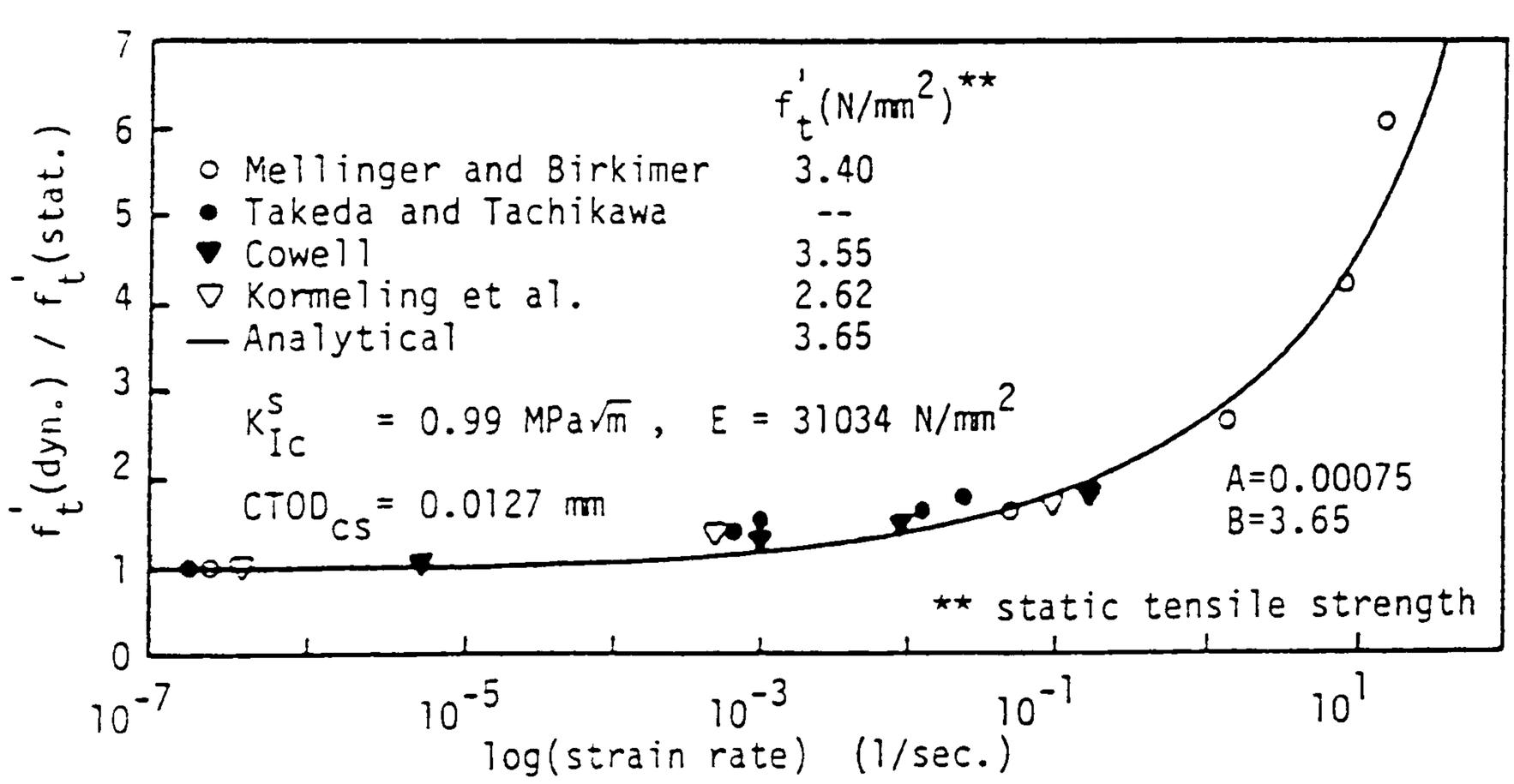

Fig. 2.3 Effect of strain-rate on tensile strength of concrete

(taken from [14])

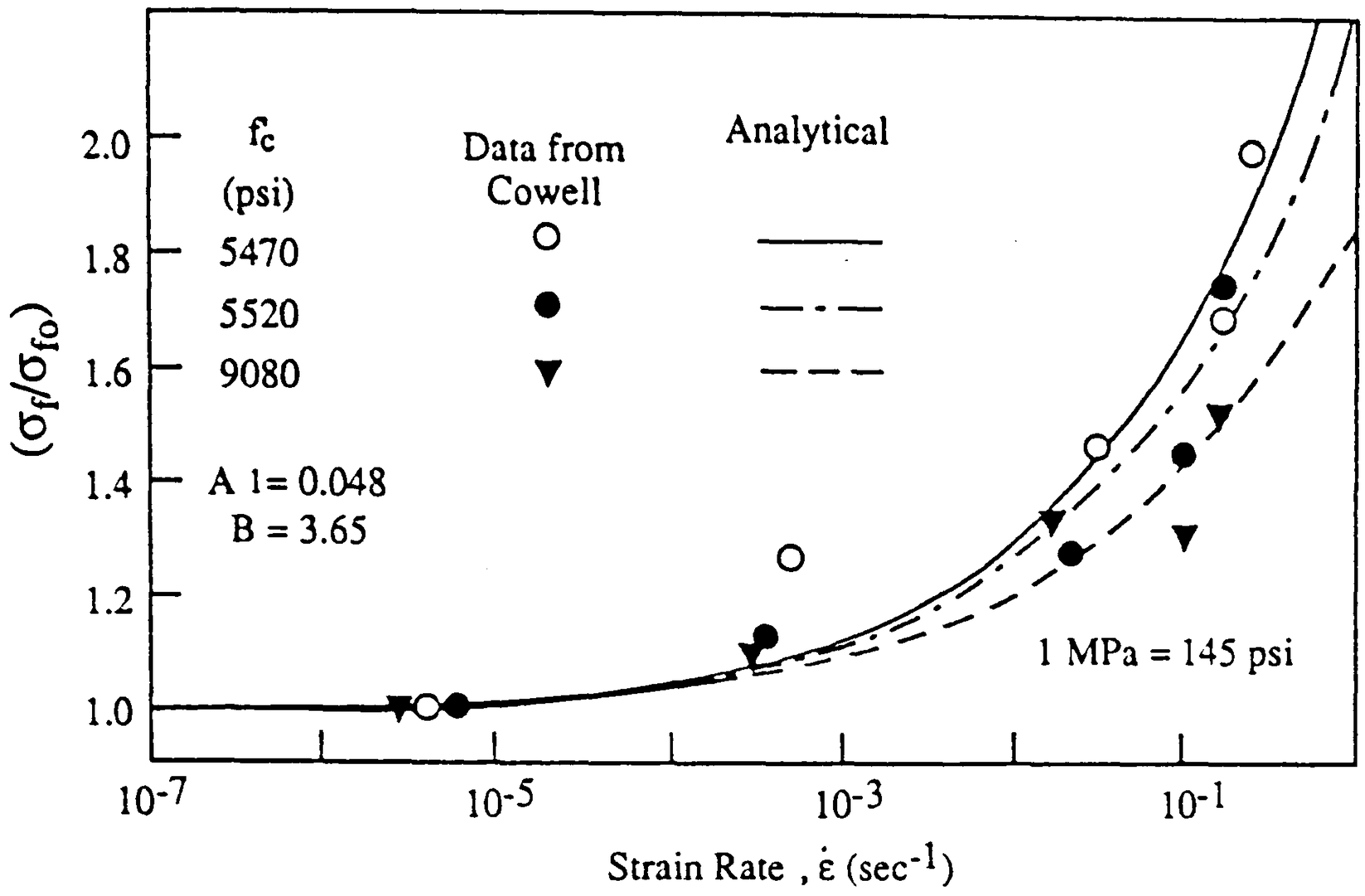

Fig. 2.4 Effect of strain-rate on tensile strength of concrete,

(taken from [14]).

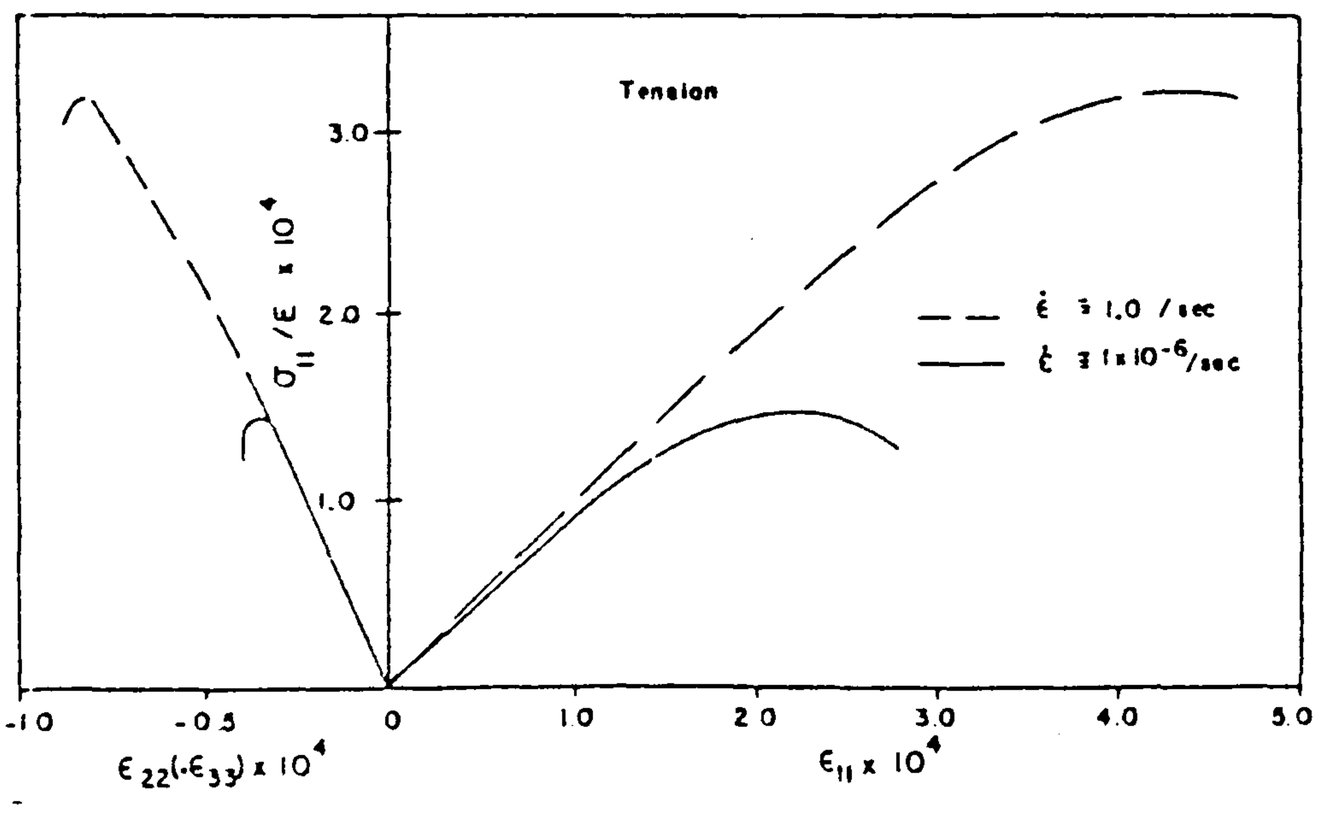

Fig. 2.5 Effect of strain-rate on tensile strength of concrete,

(taken from [4]).

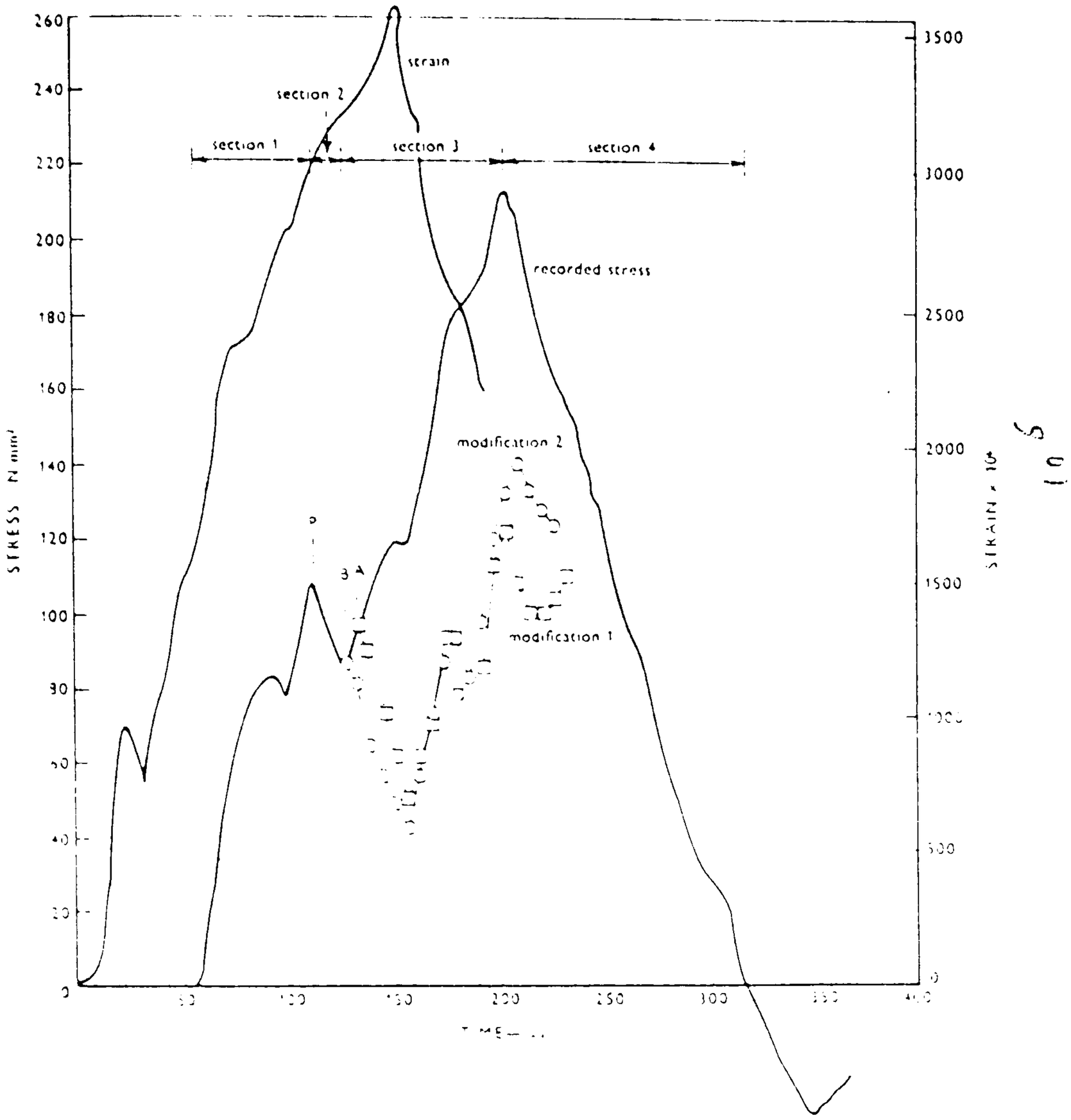

Fig. 2.6 Typical stress-time and strain-time for concrete under rate loading (taken from [5]).

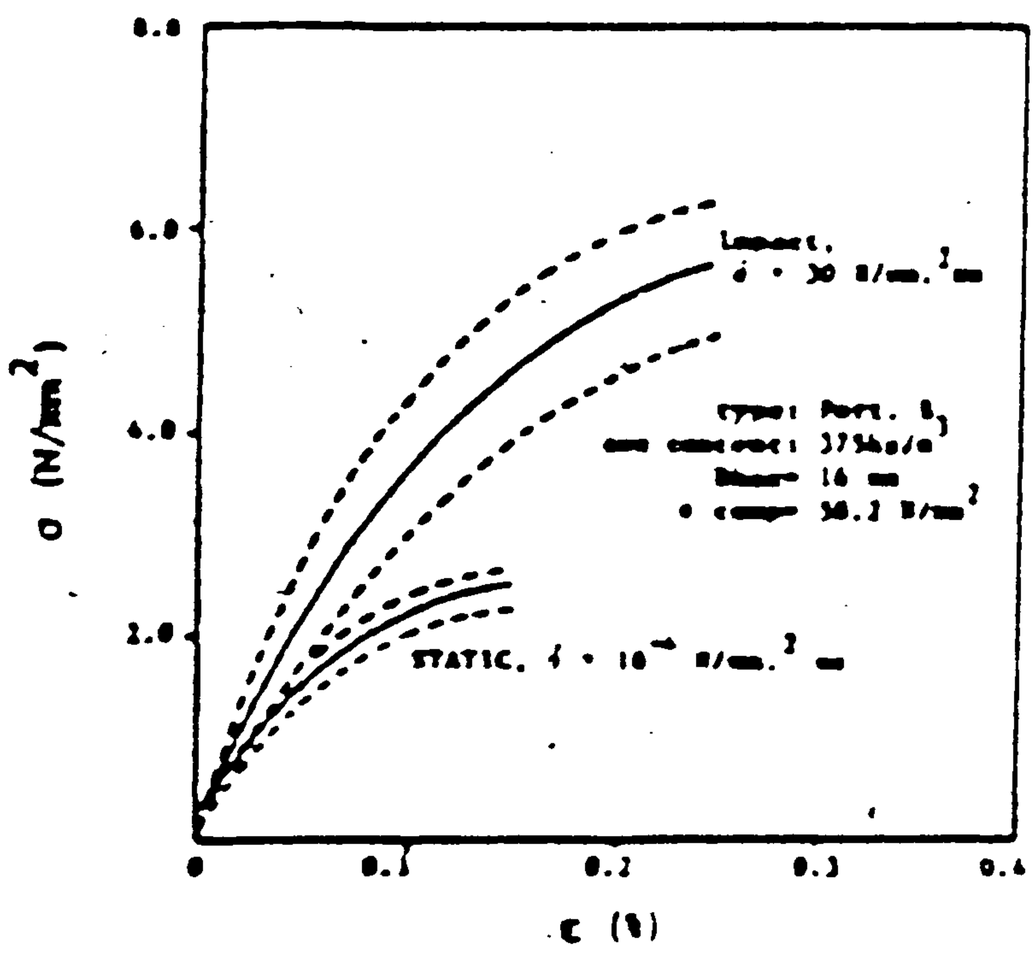

Fig. 2.7 Tensile stress-strain curves under static and impact loading (taken from [15]).

FIG 2-3 STRESS-STRAIN

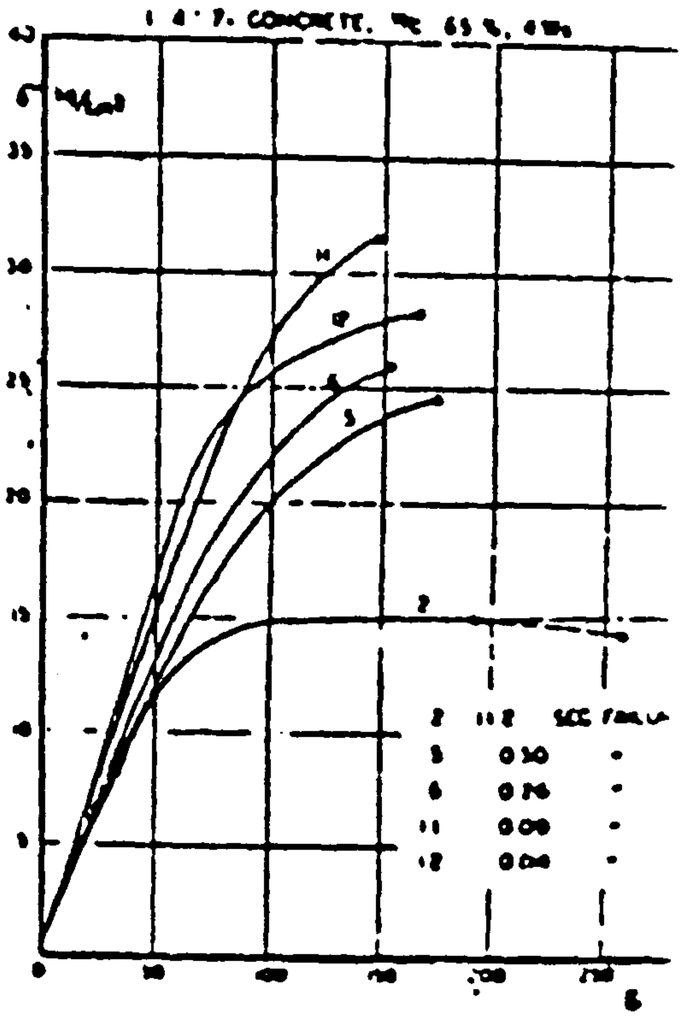

FIG 2-4 STRESS-STRAIN

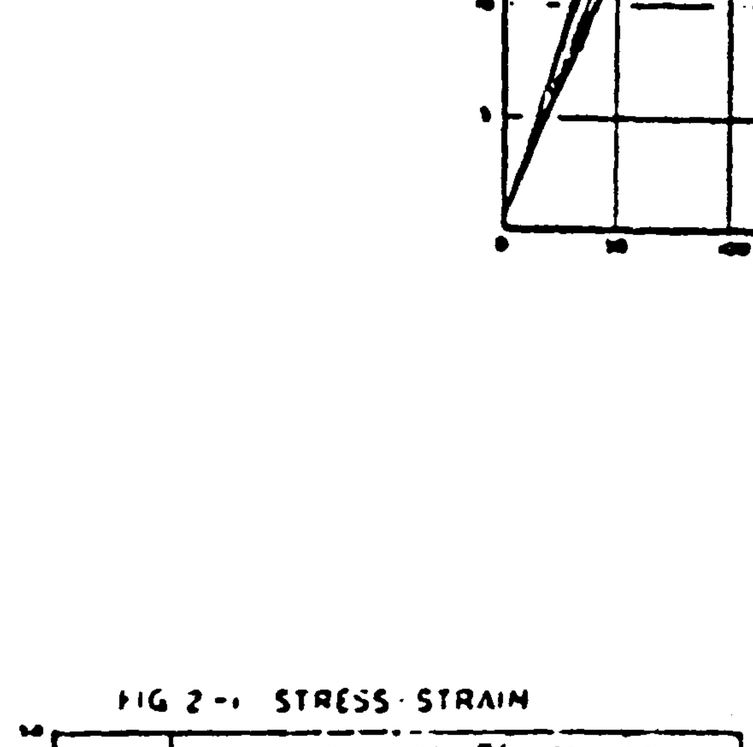

FIG 2-2 STRESS-STRAIN

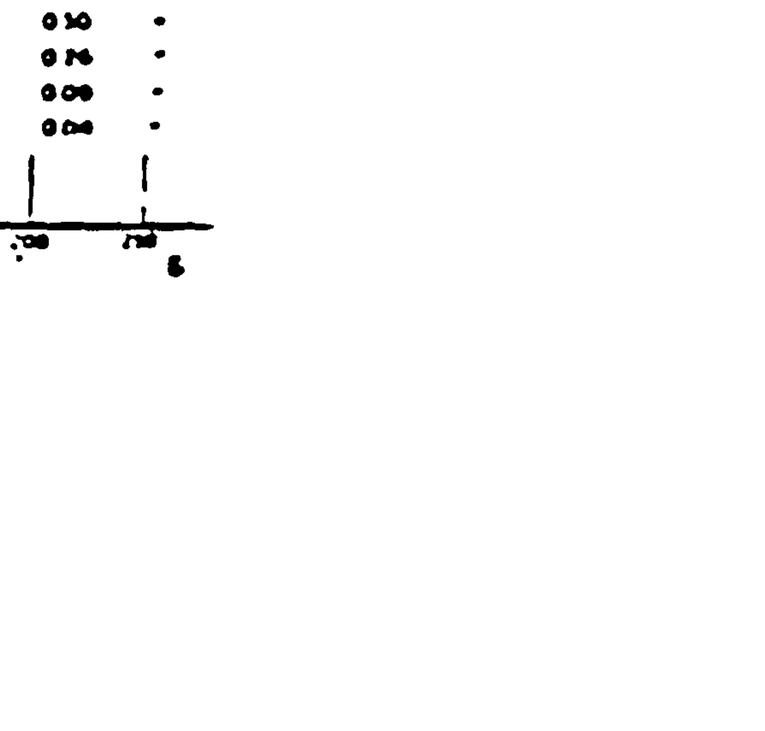

Fig. 2.8 Tensile stress-strain curves for three types of concrete mix (taken from [10]).

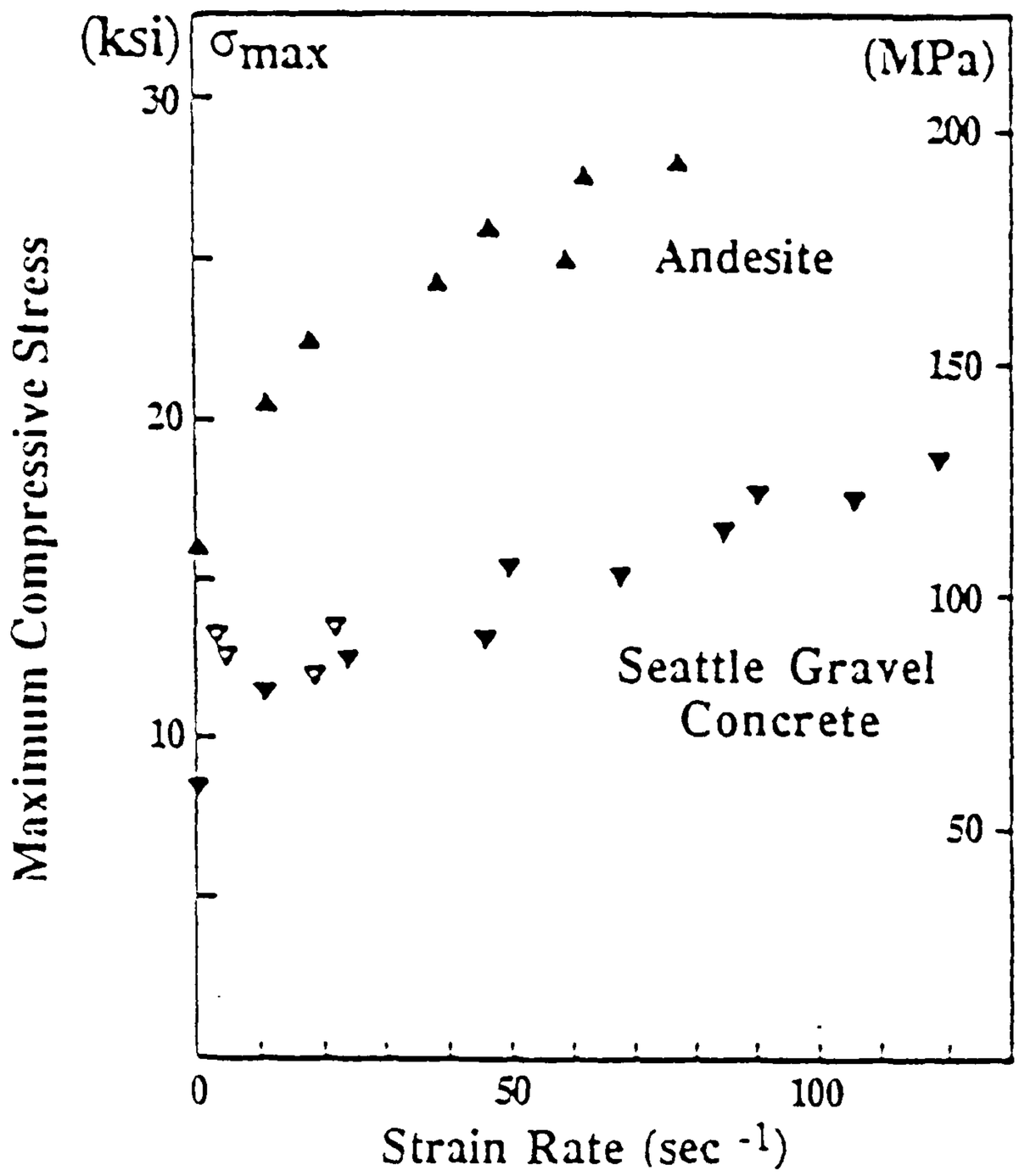

Fig. 2.9 A Maximum compressive stress versus strain-rate for two aggregate types (taken from [17]).

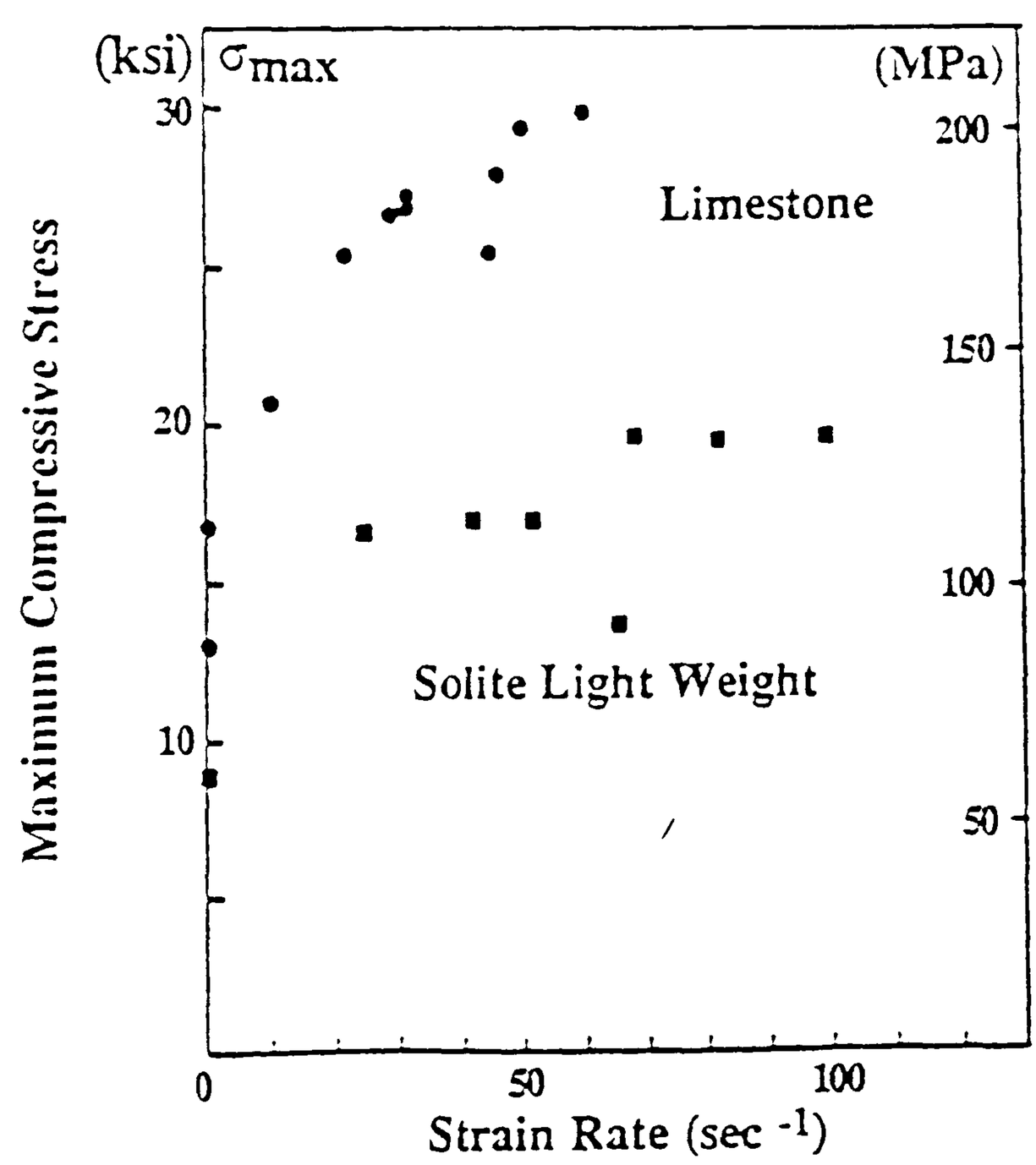

Fig. 2.9 B Maximum compressive stress versus strain-rate for two aggregate types (taken from [17]).

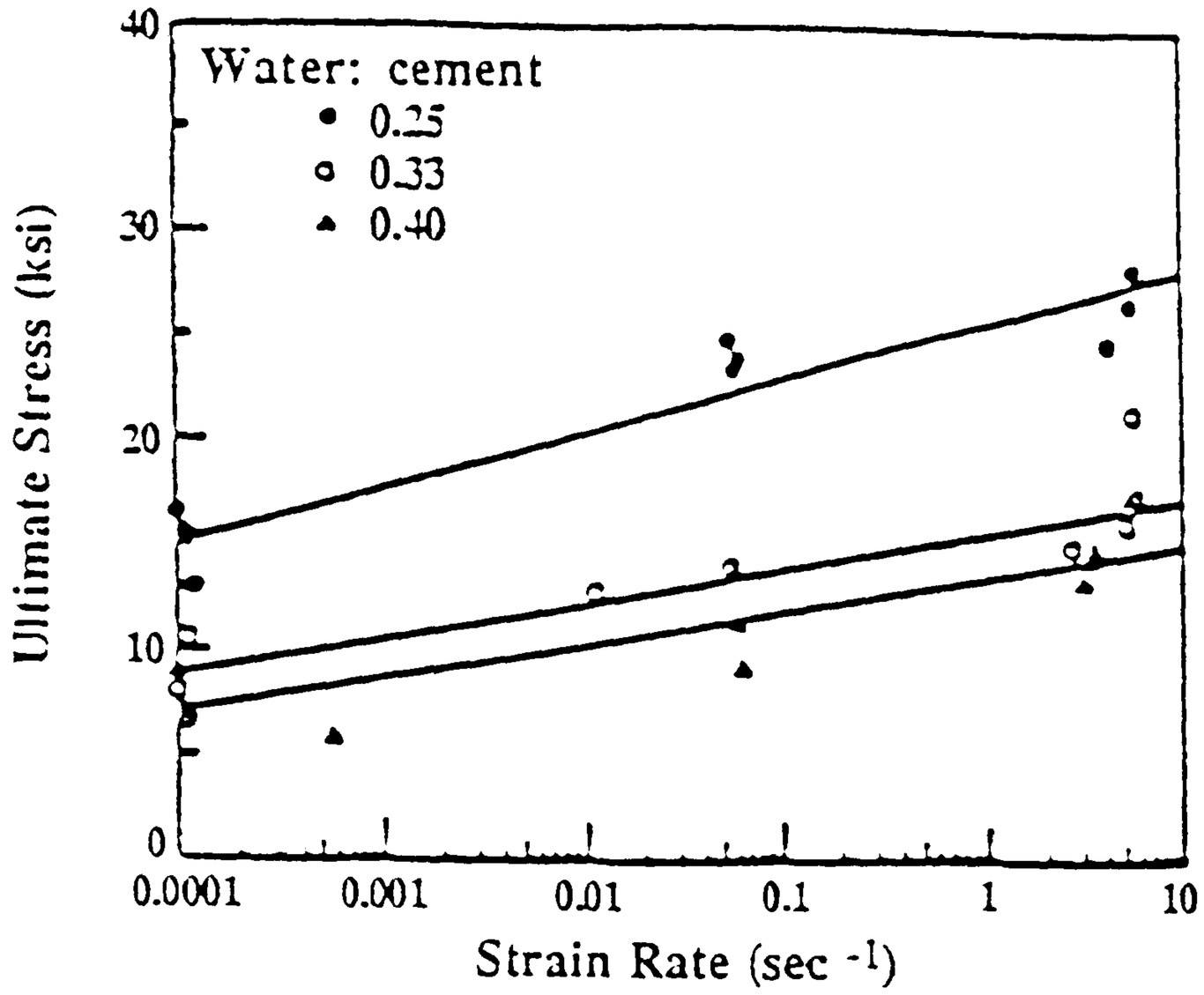

Fig. 2.10 Maximum compressive stress versus strain-rate for three w/c ratios, (taken from [18]).

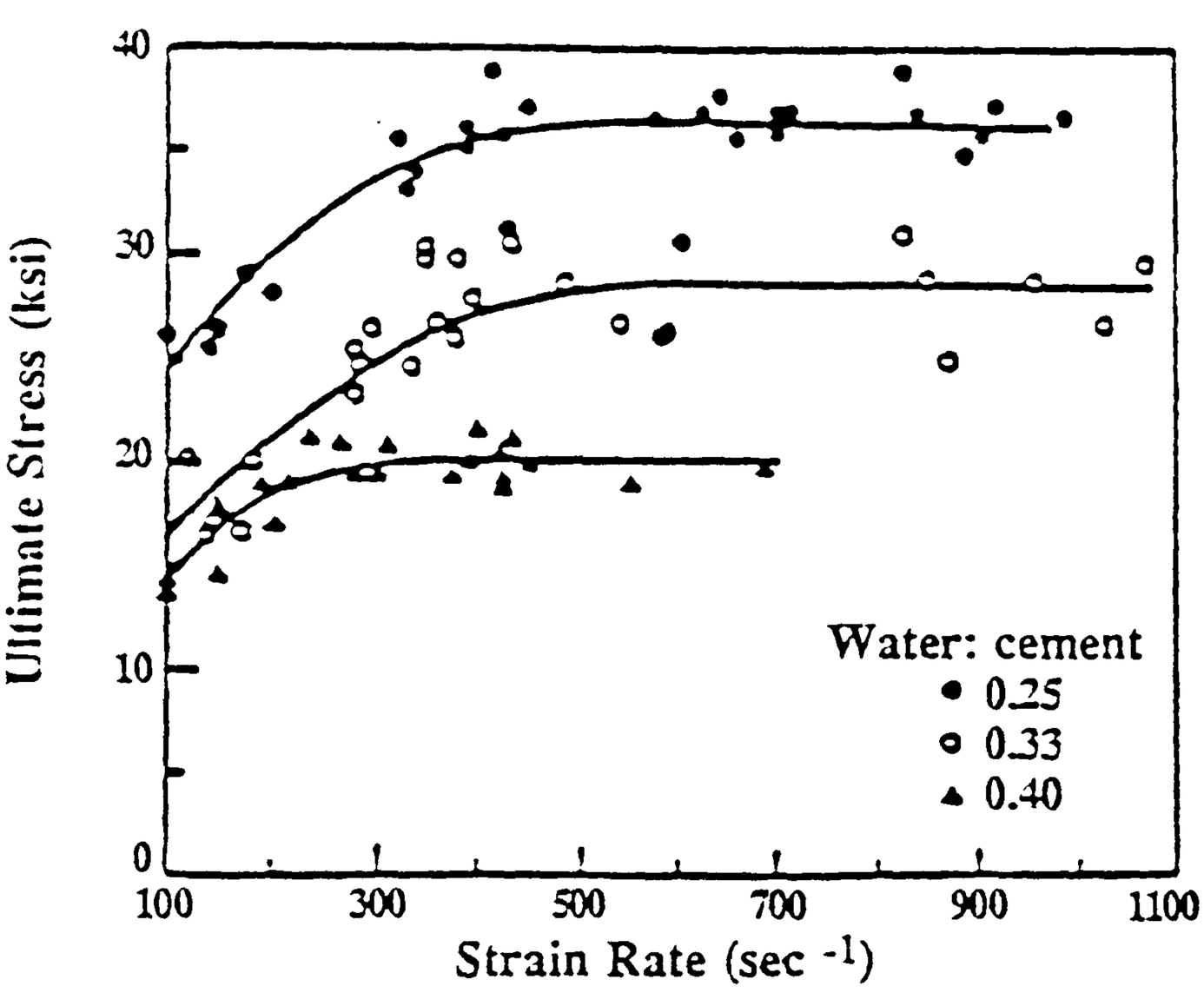

Fig. 2.11 Maximum compressive stress versus strain-rate for three w/c ratios, (taken from [18]).

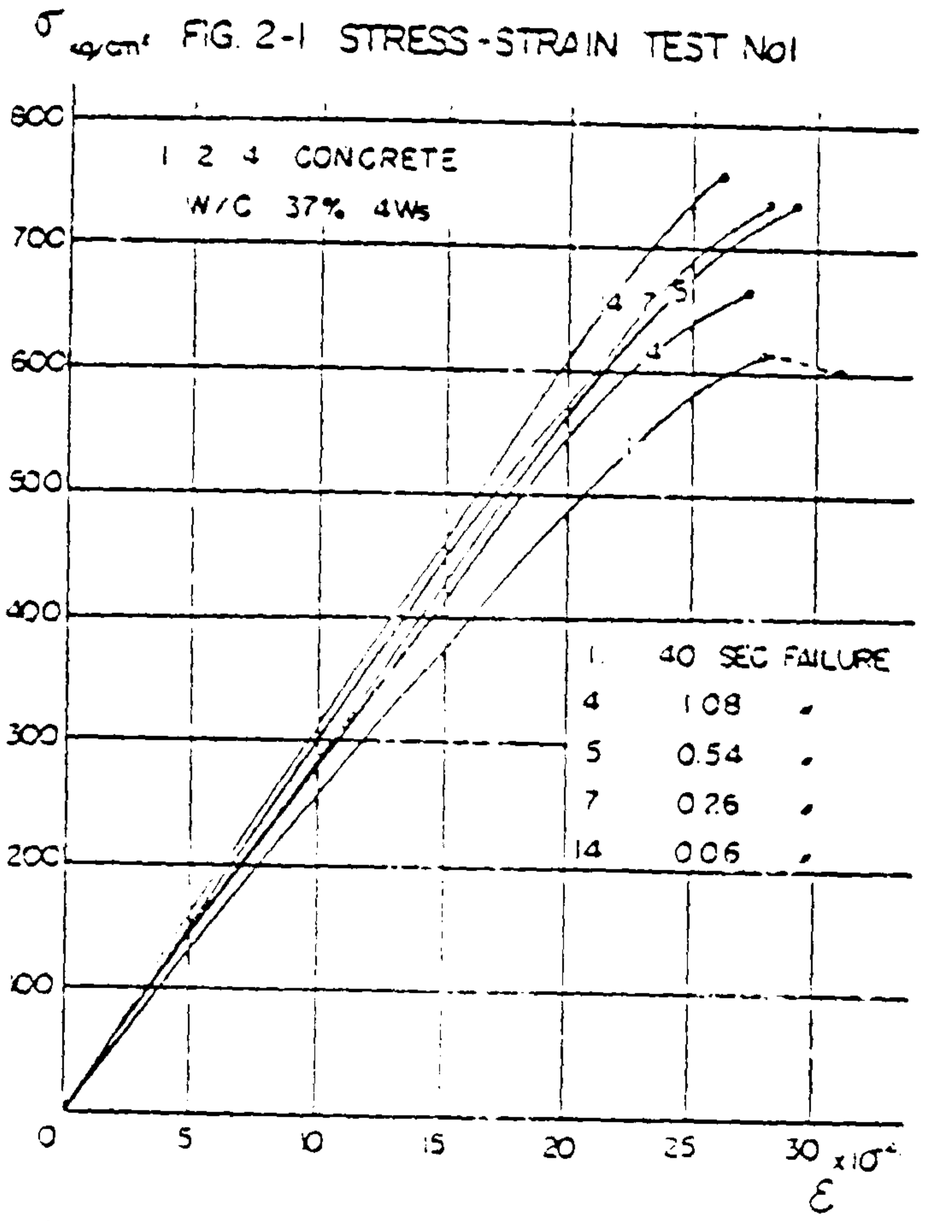

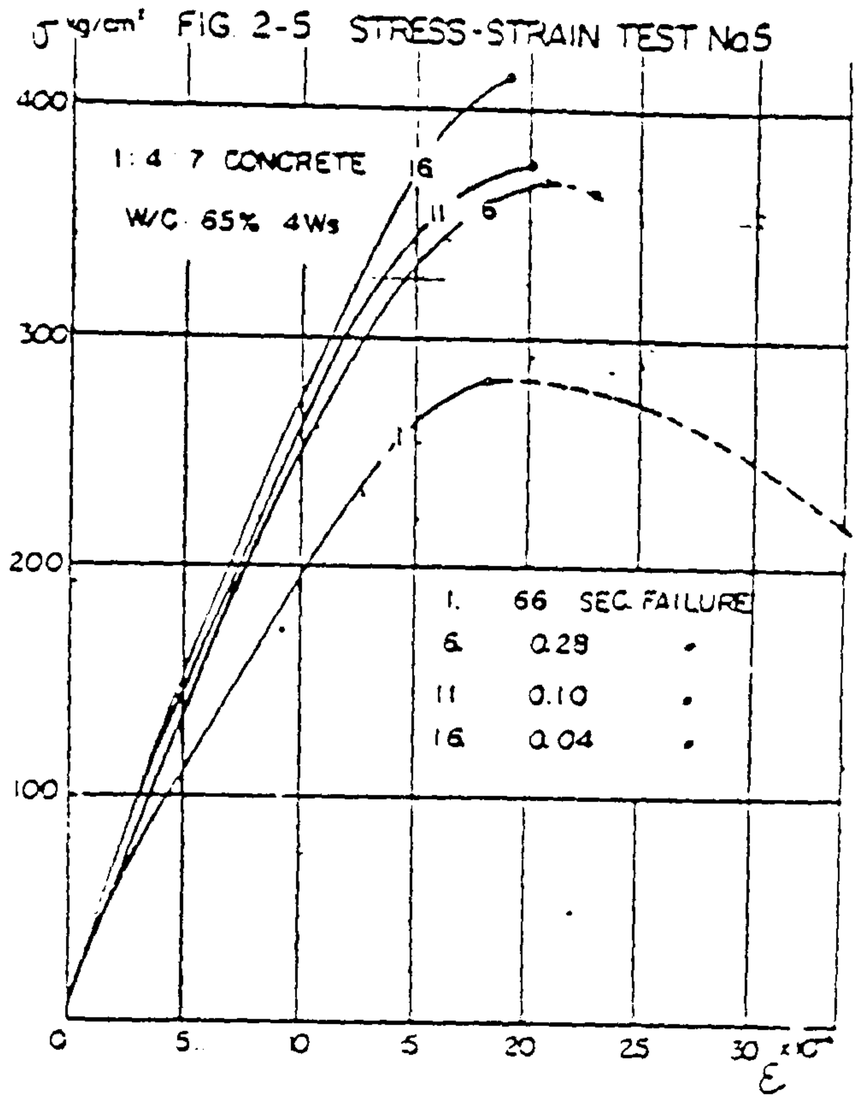

Fig. 2.12 Hatano's compressive tests for three types of concrete mix (taken from [10]).

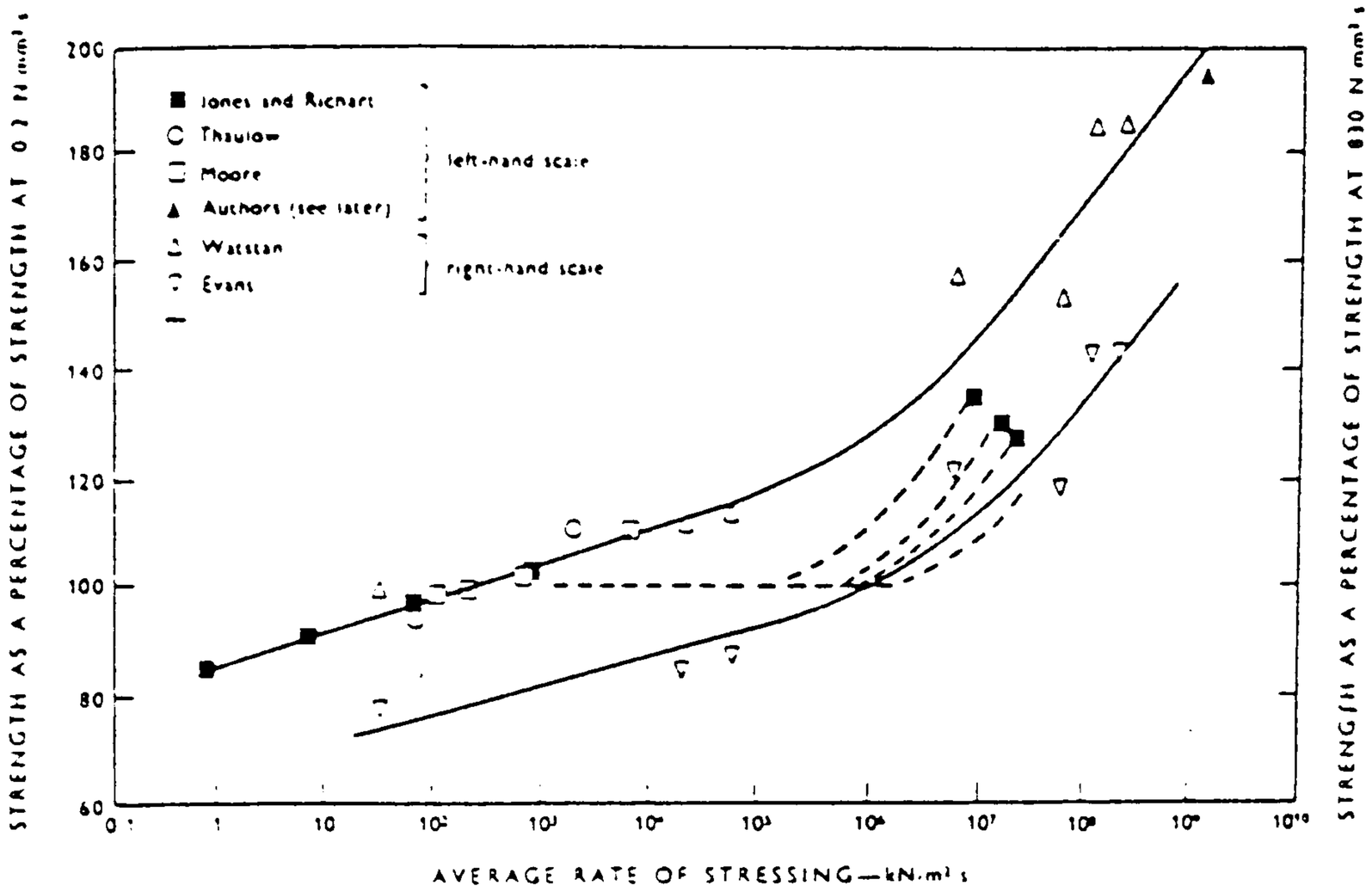

Fig. 2.13 Effect of strain-rate on the compressive strength of concrete (taken from [5]).

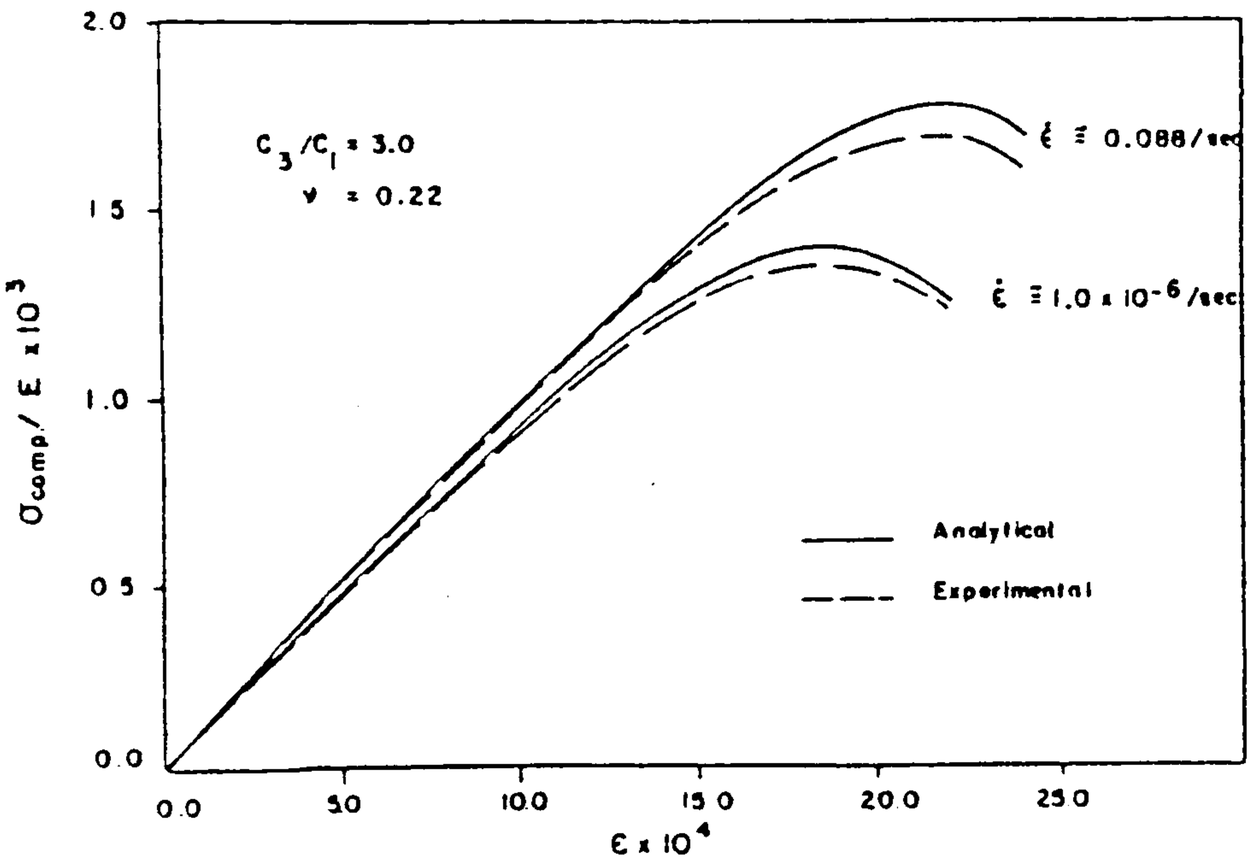

Fig. 2.14 Effect of strain-rate on the compressive strength of concrete (taken from [4]).

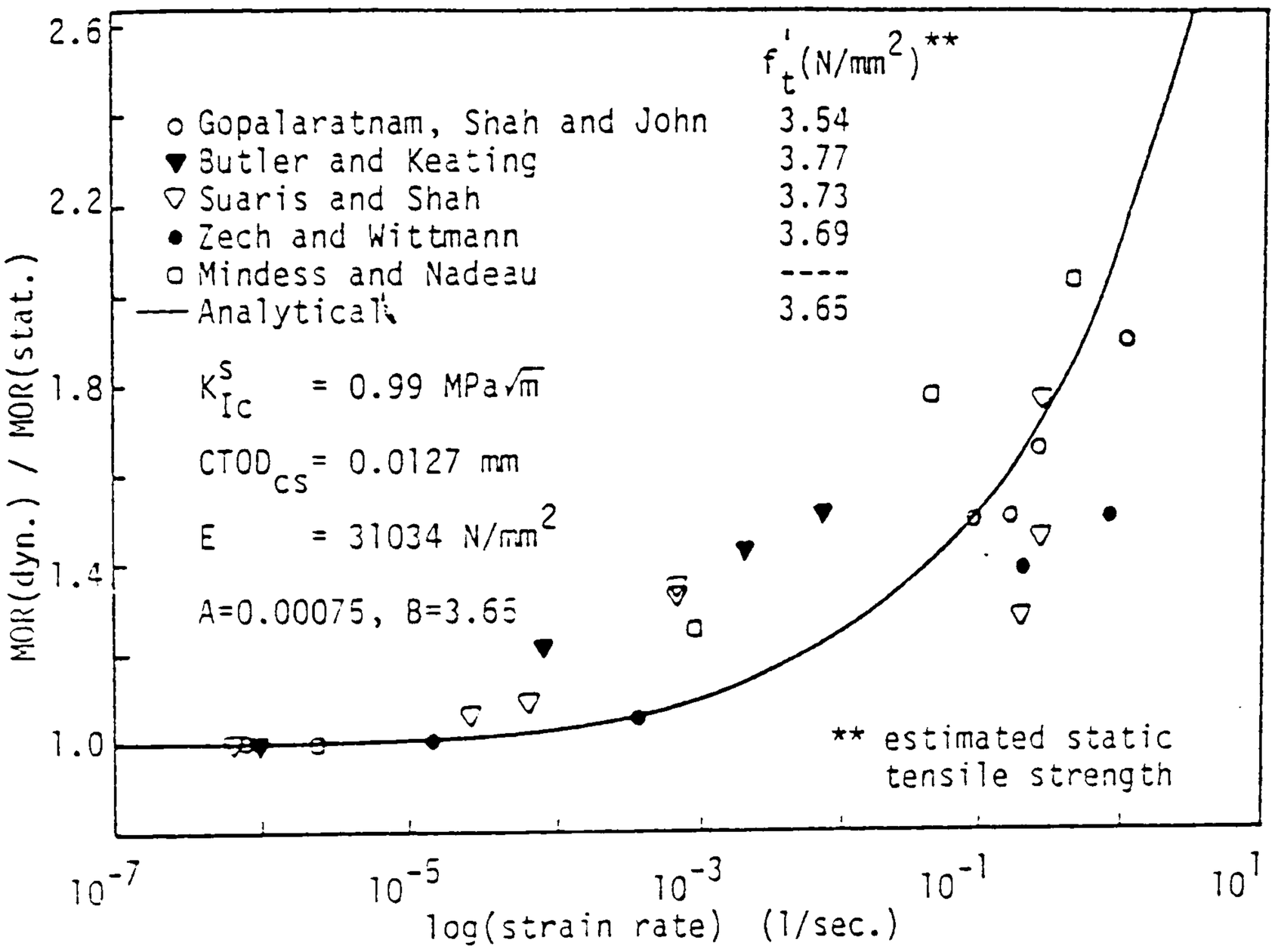

Fig. 2.15 Strain-rate on flexural strength of concrete

(taken from [14]).

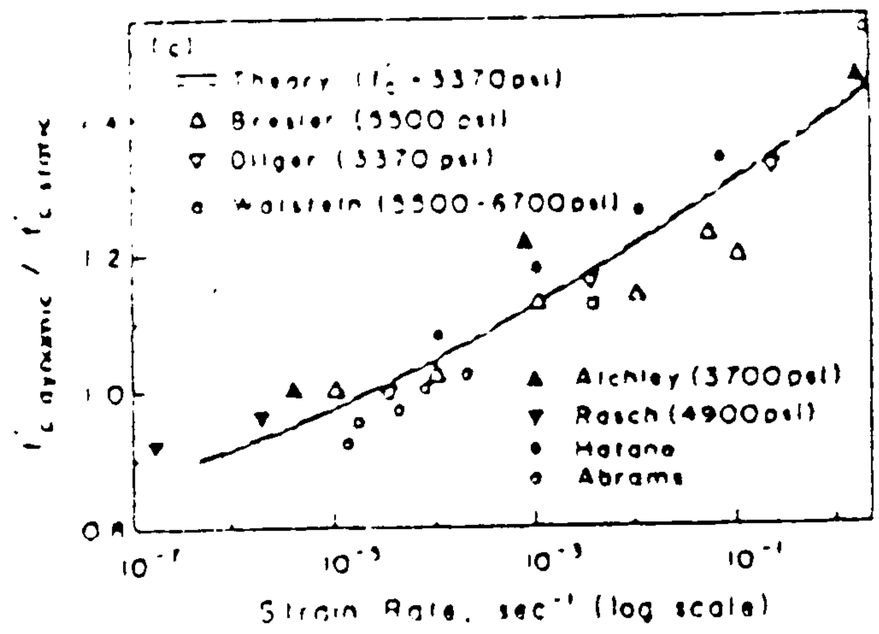

Fig. 2.16 Effect of strain-rate on the peak strength of concrete

(taken from [6]).

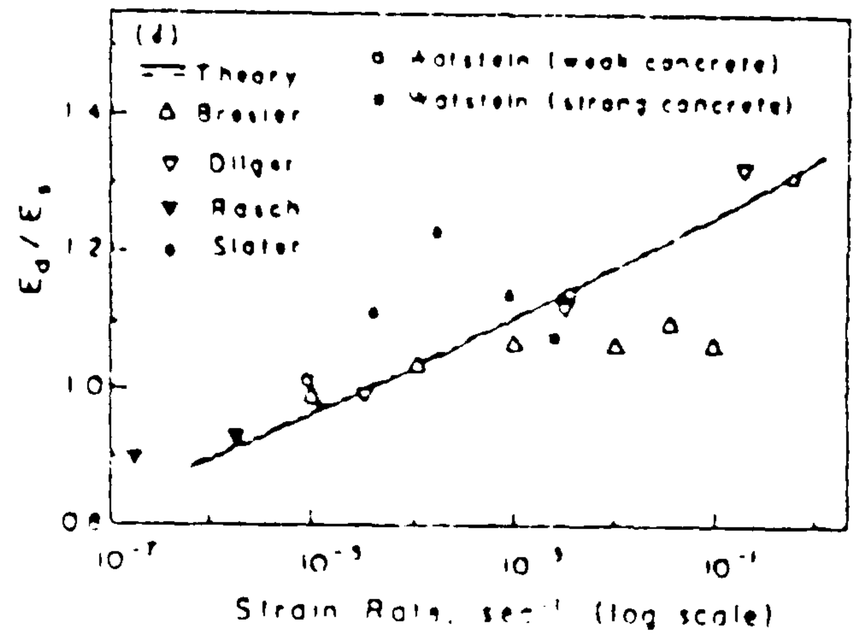

Fig. 2.17 Effect of strain-rate on secant modulus of elasticity (taken from [6]).

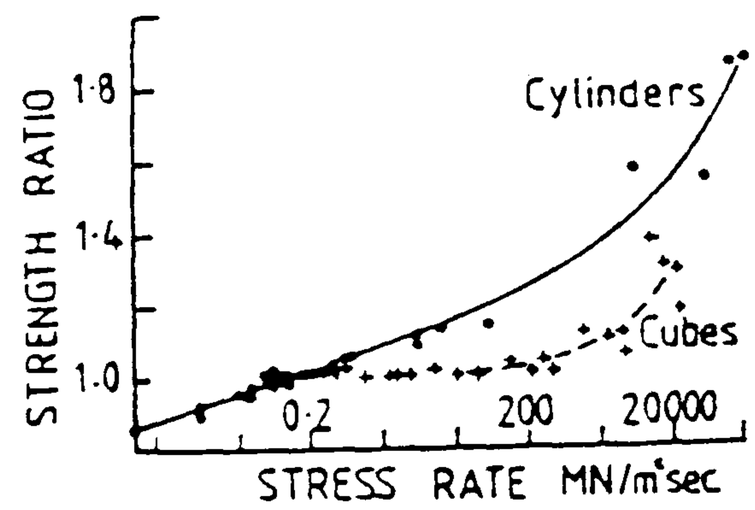

Fig. 2.18 Effect of loading-rate on compressive strength of concrete (taken from [19])

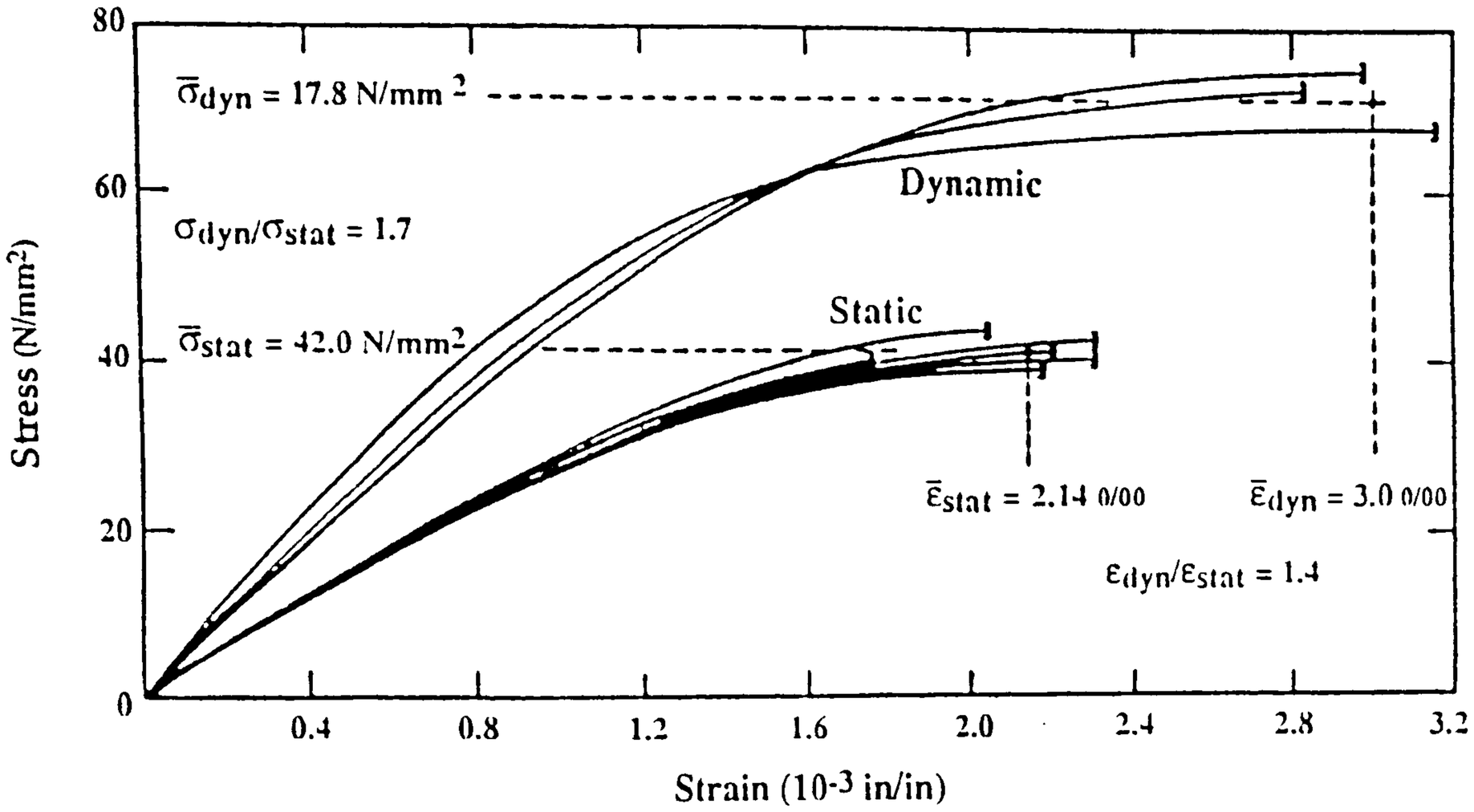

Fig. 2.19 Effect of loading-rate on compressive strength of concrete(taken from [20])

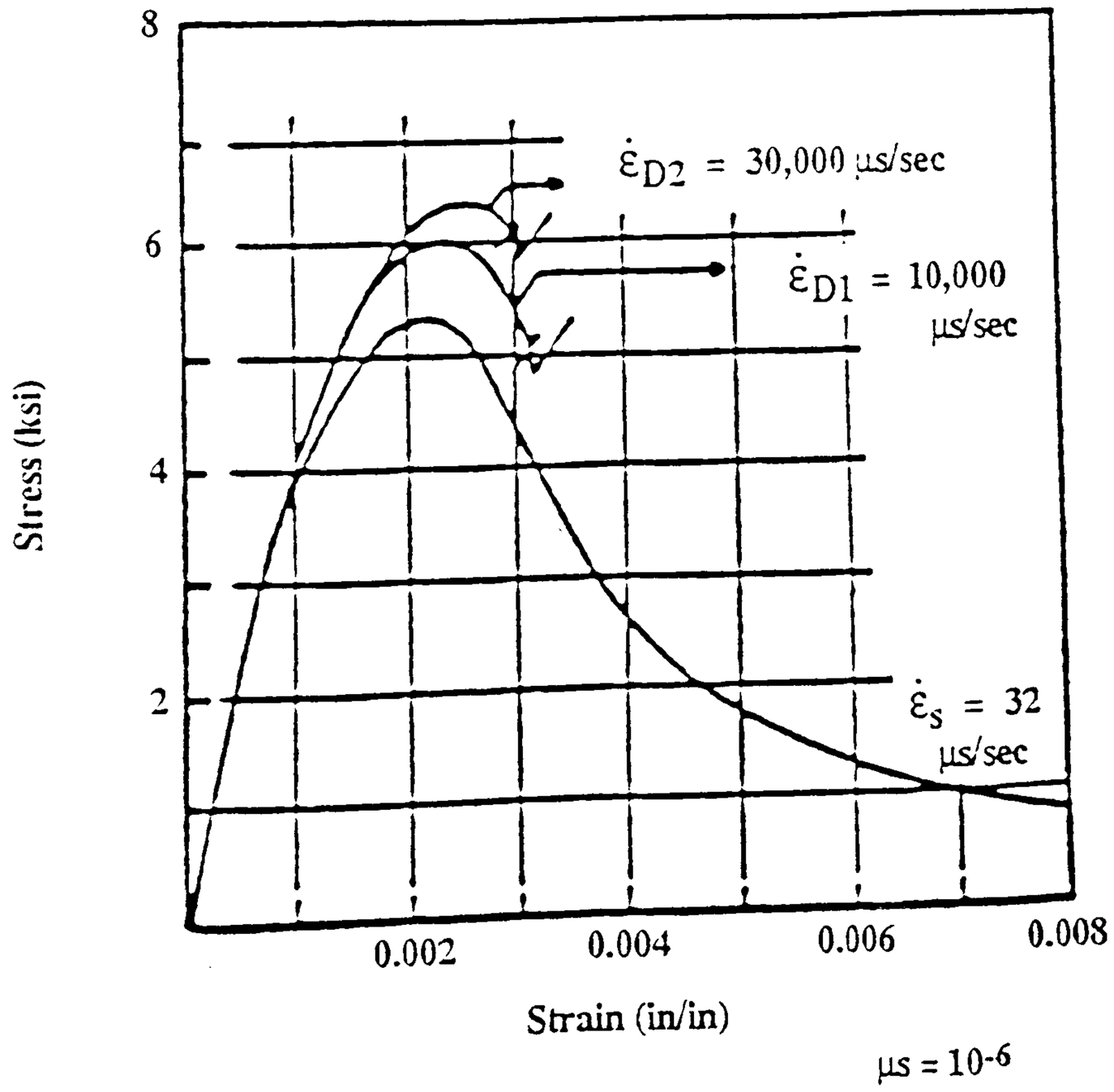

Fig. 2.20 Typical effect of strain-rate on compression stress-strain curve (taken from [21])

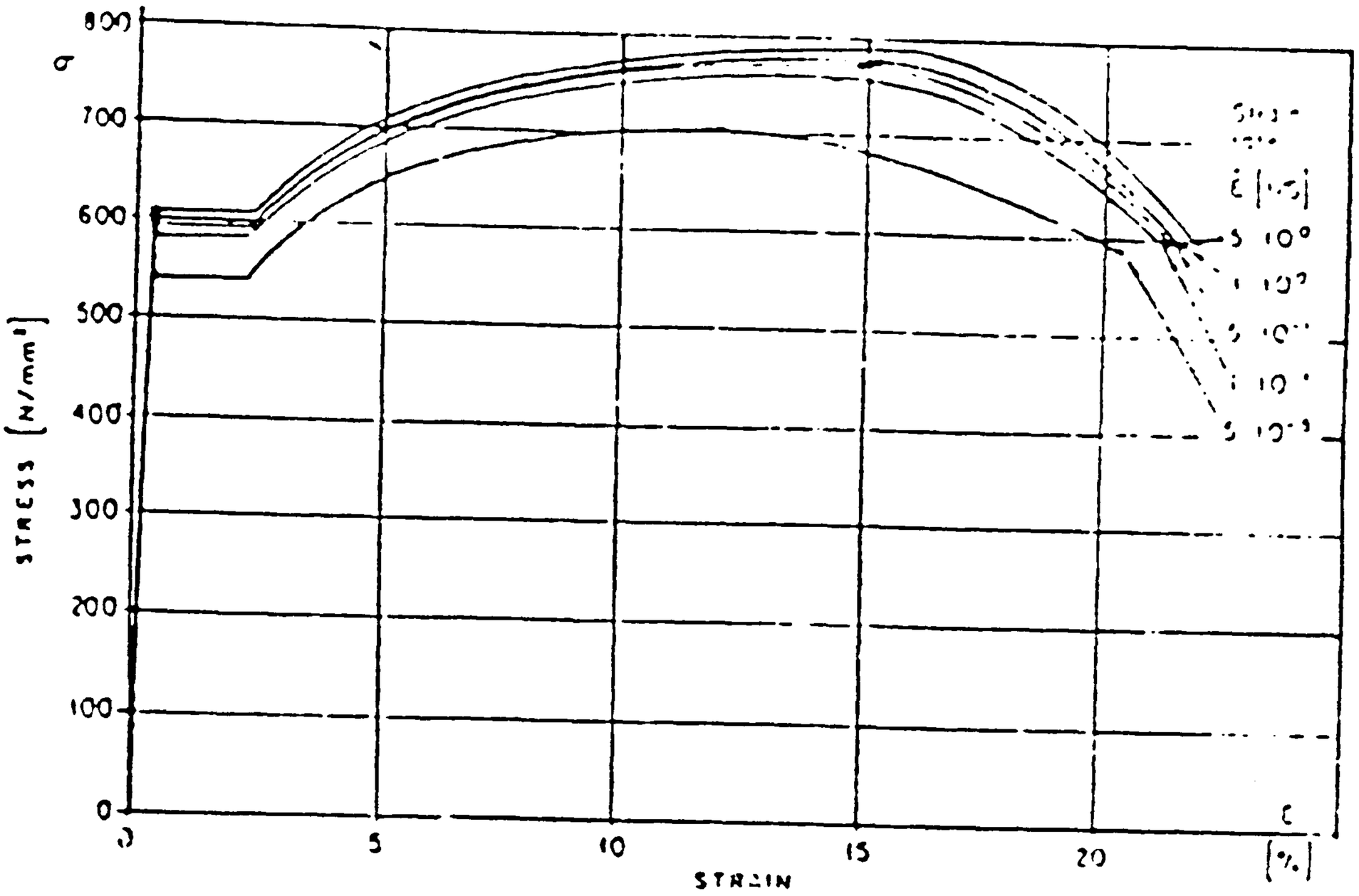

Fig. 2.21 Effect of strain-rate on compression stress-strain curve of steel (taken from [23])

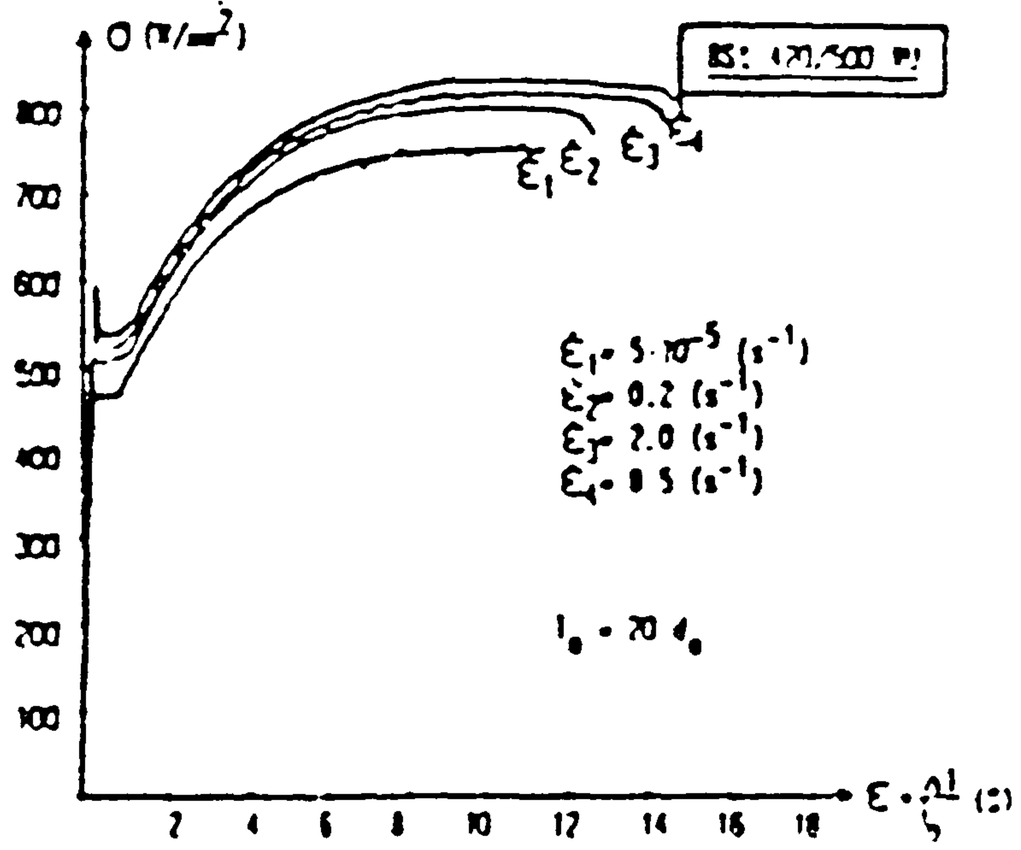

Fig. 2.22 Effect of strain-rate on compression stress-strain curve of steel (taken from [24])

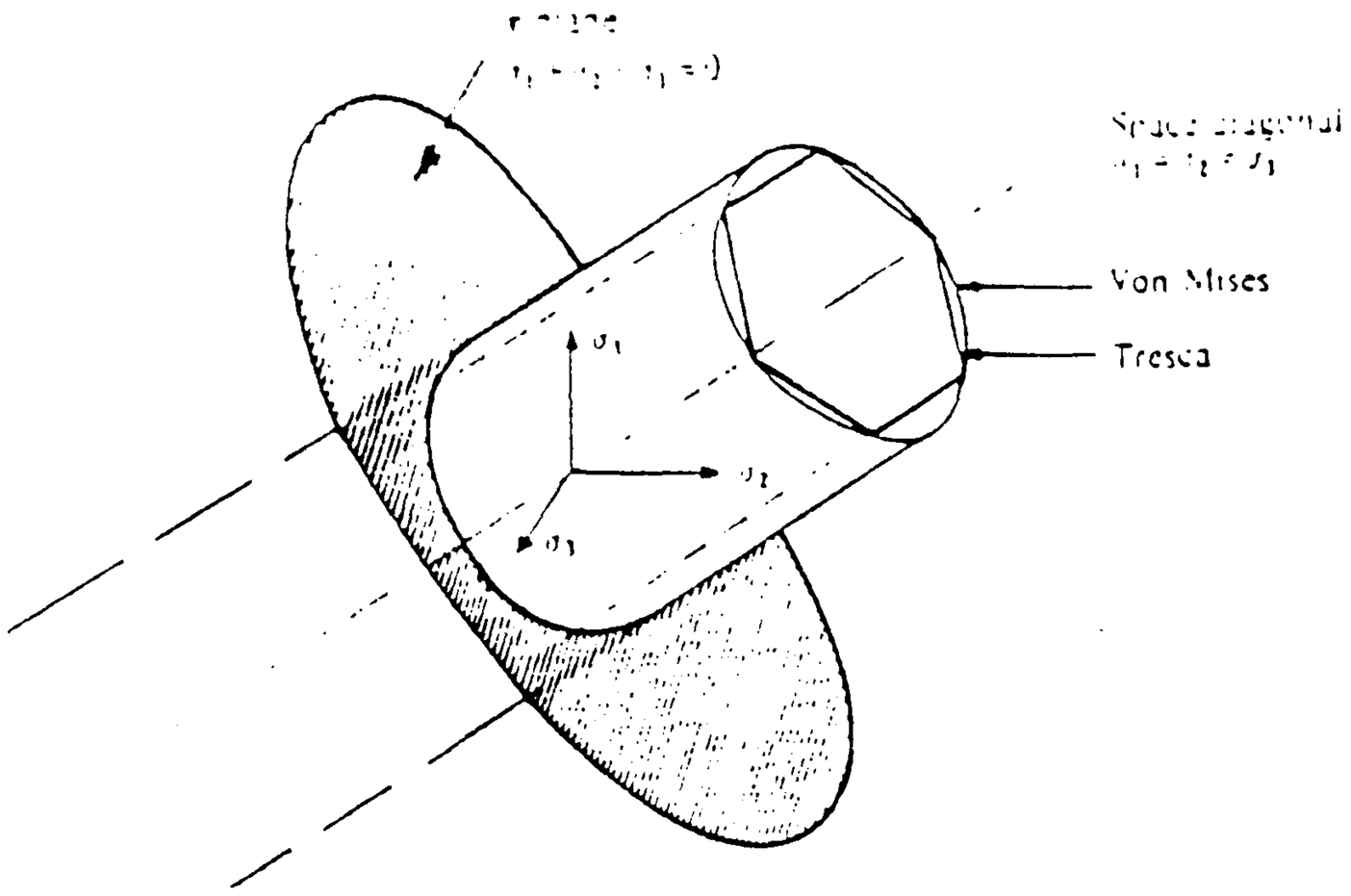

Fig. 2.23 Von-Mises and Tresca failure criteria

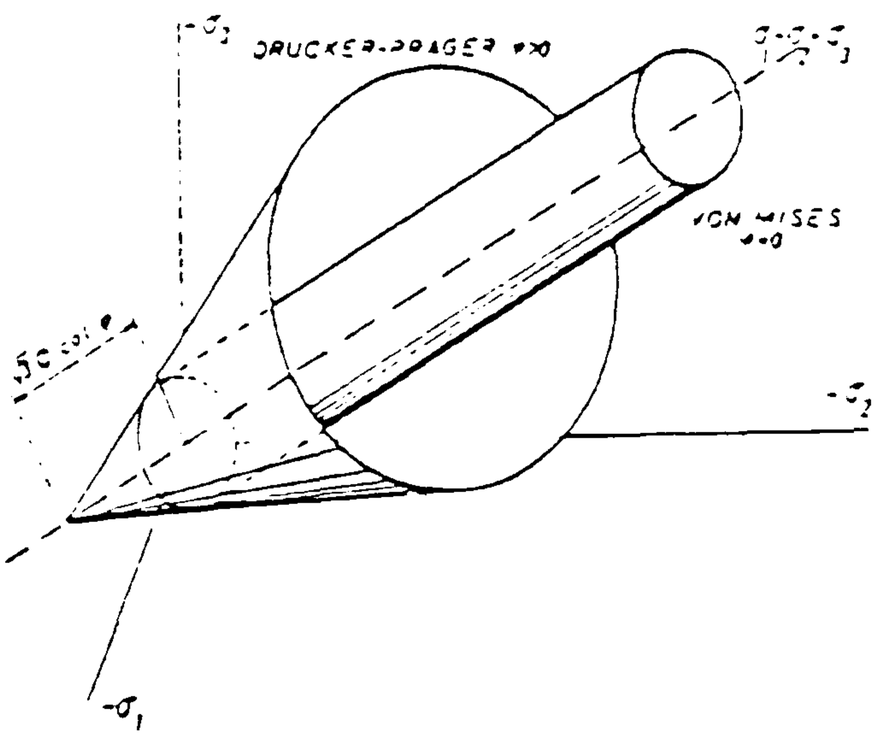

Fig. 2.24 Drucker-Prager failure criteria

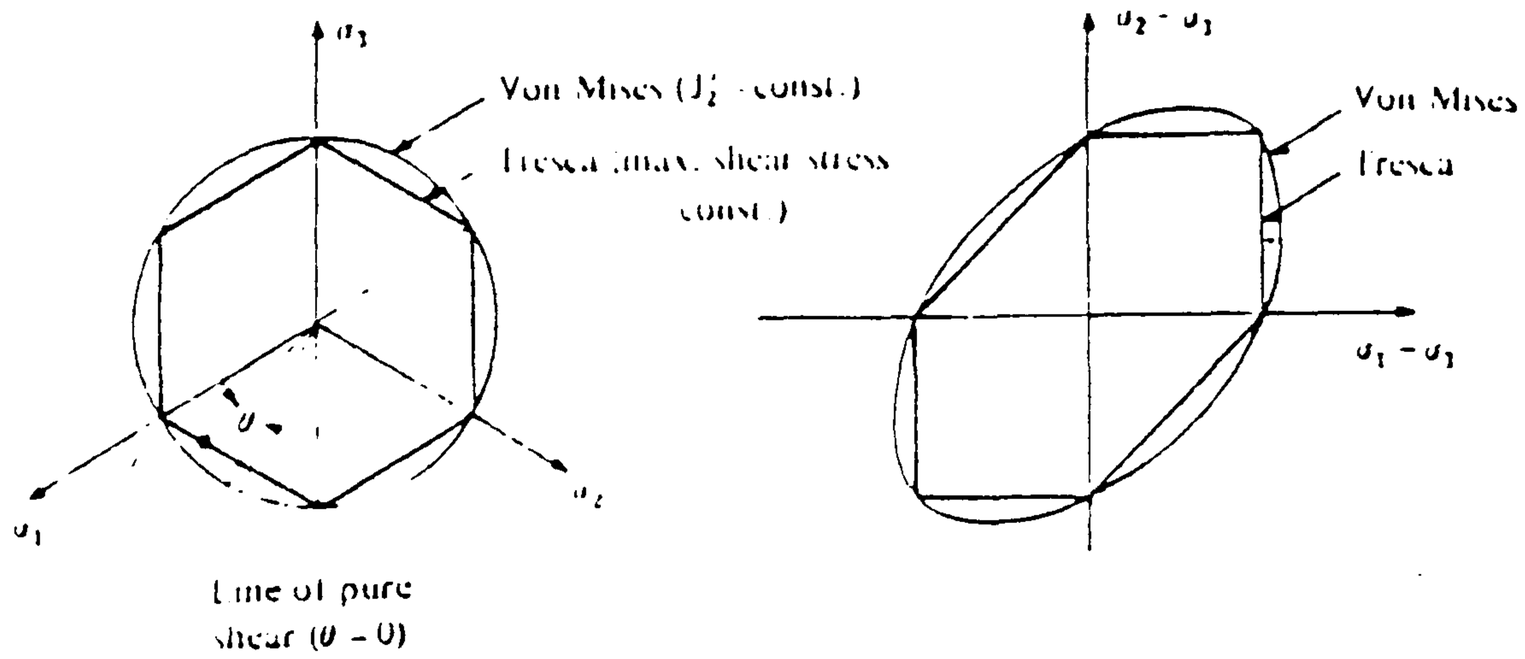

Fig. 2.25 Geometrical representation of the Tresca

and Von-Mises yield surface

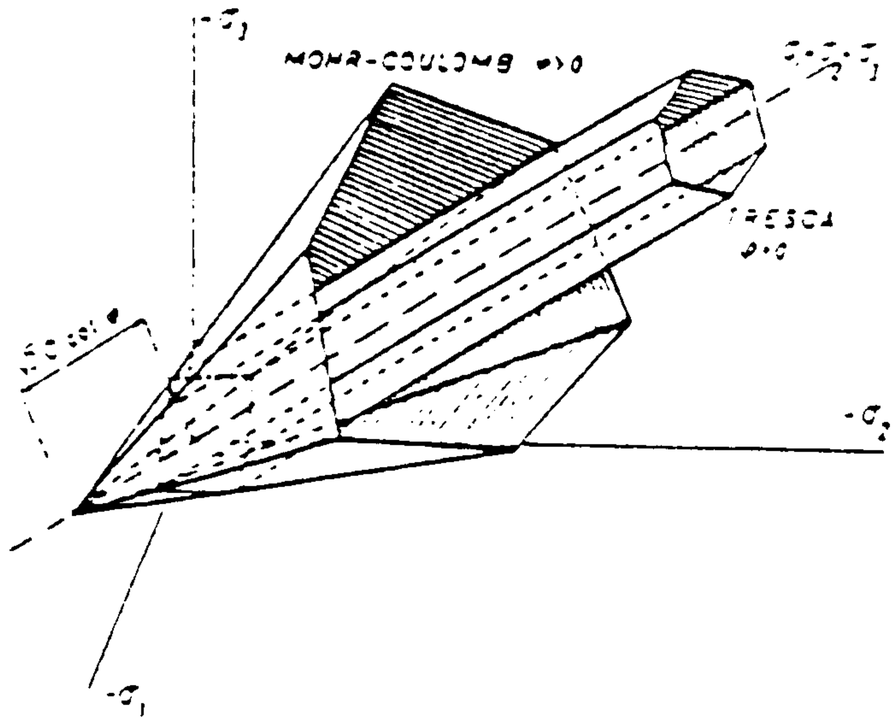

Fig. 2.26 Mohr-coulomb failure criteria.

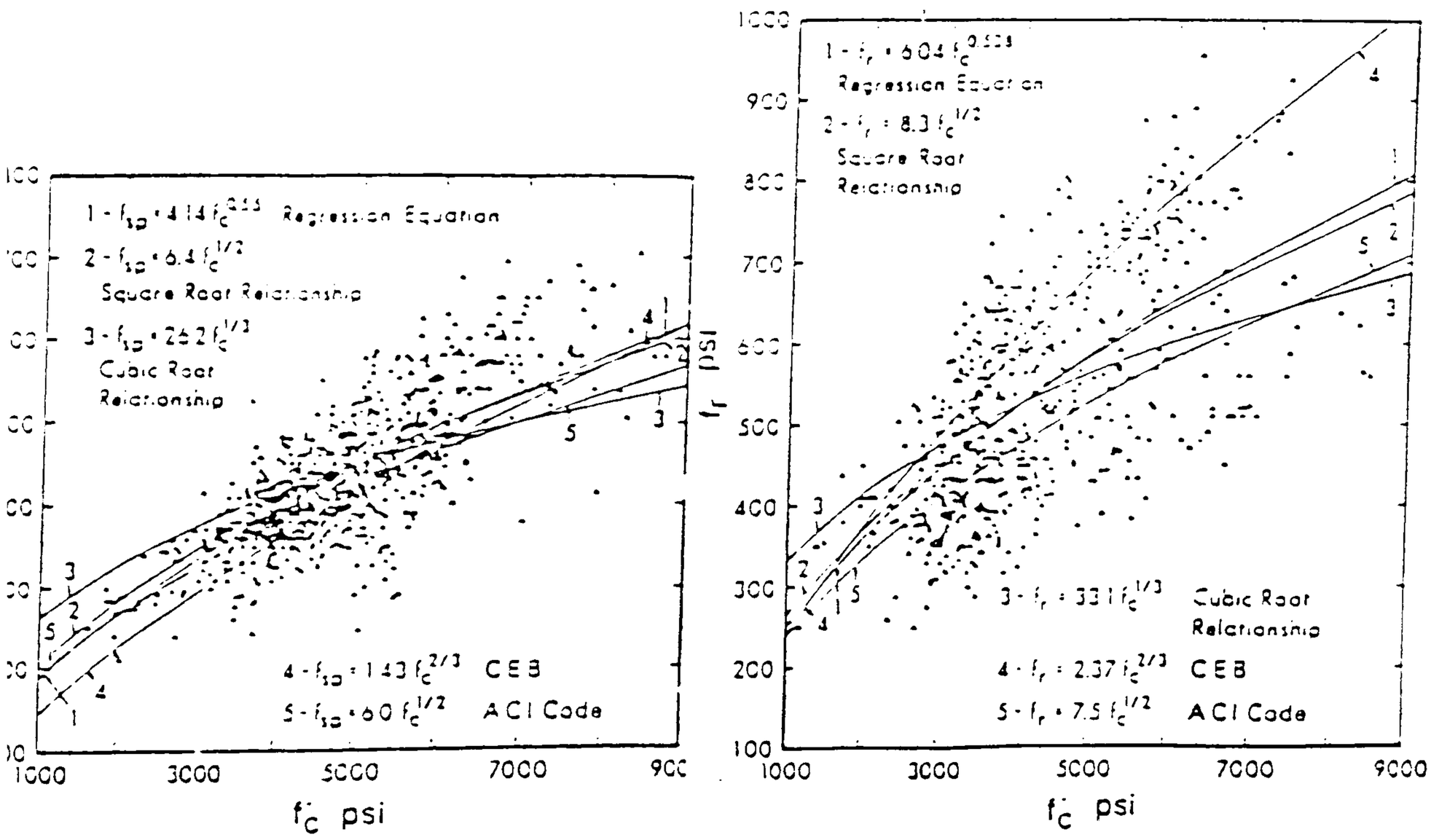

Fig. 2.27 Scatter in experimental results of the split cylinder strength and modulus rupture (taken from [52]).

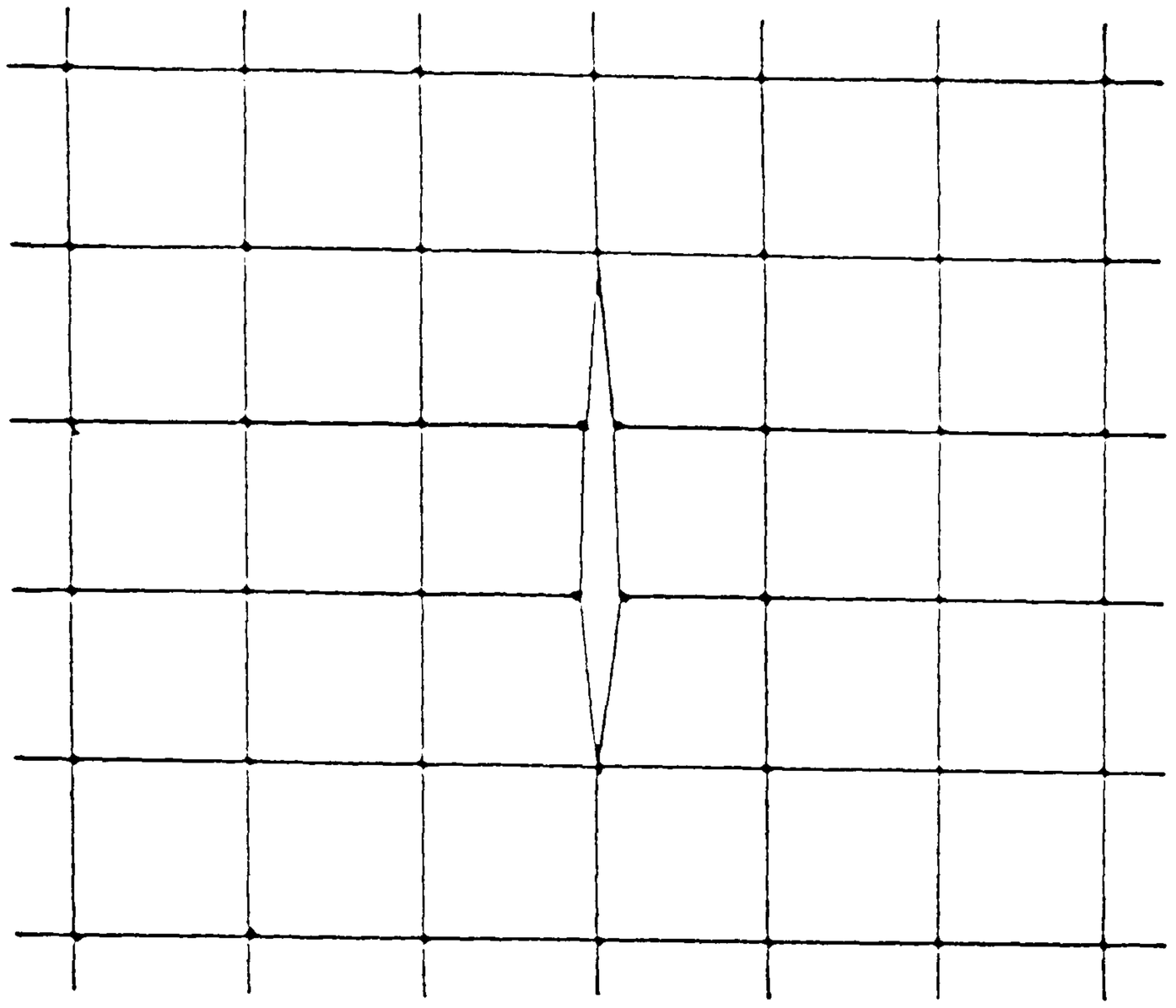

Fig. 2.28 Discrete representation of crack

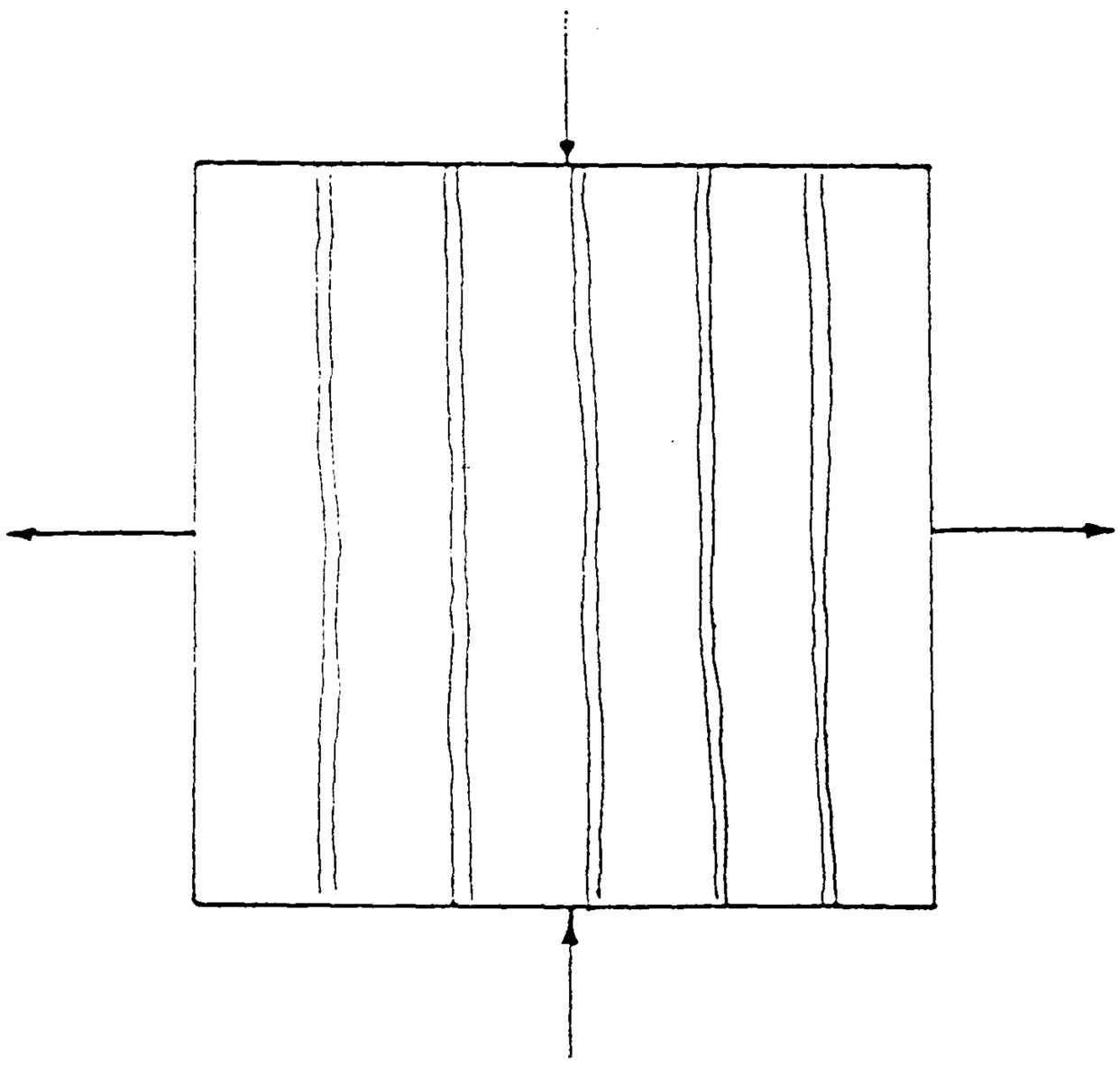

Fig. 2.29 Smeared representation of crack

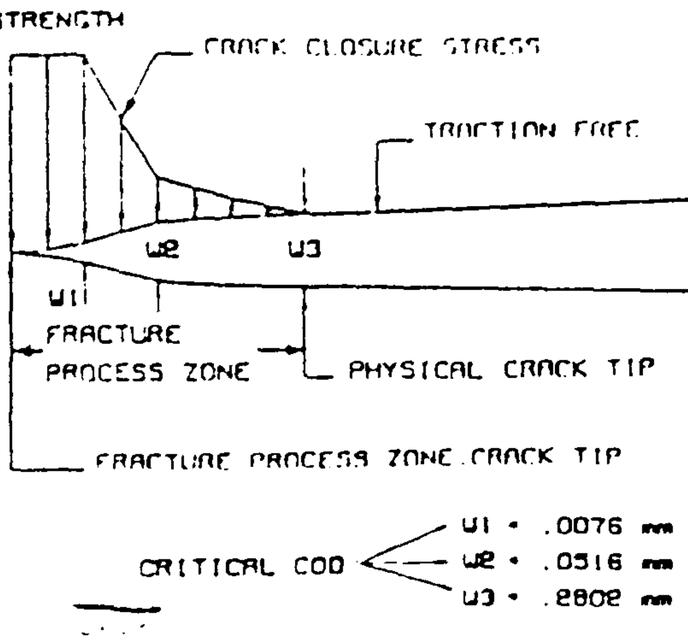

Fig. 2.30 Fracture process zone of concrete

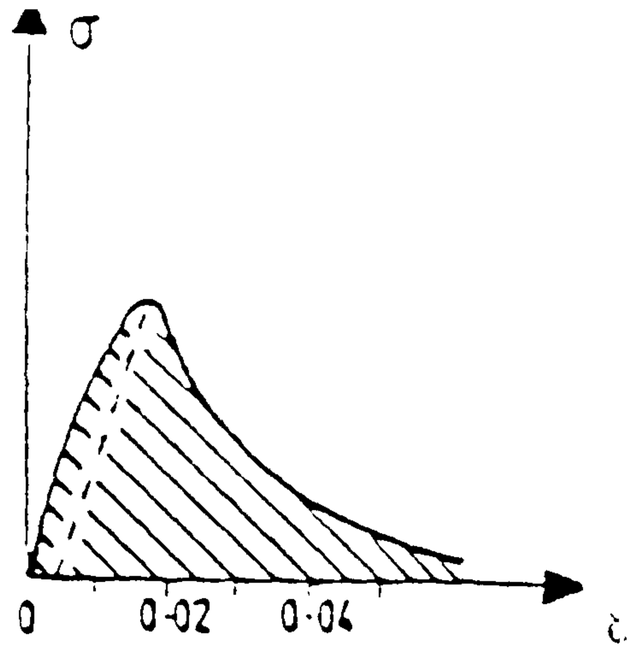

Fig. 2.31 Typical post-cracked behaviour of concrete

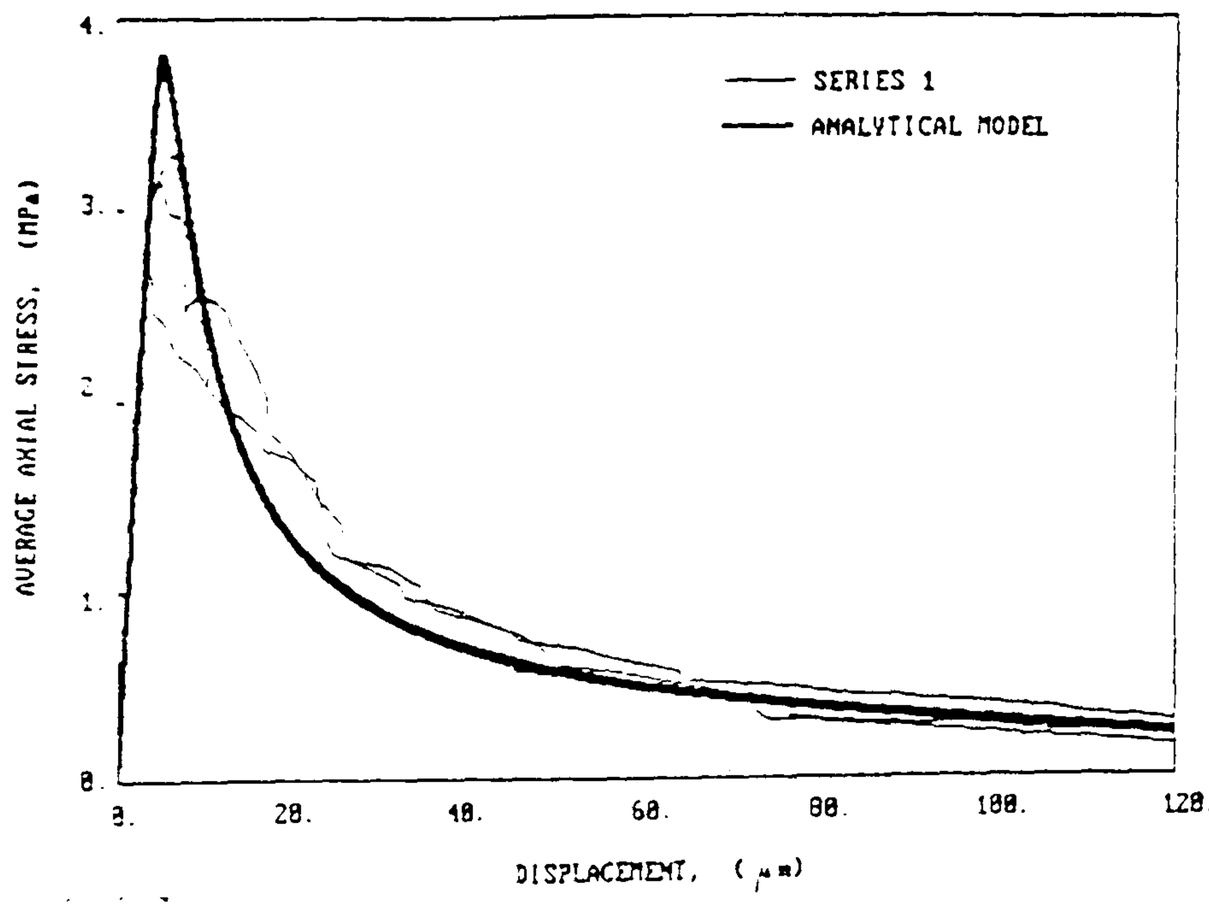

Fig. 2.32 Comparison of analytical envelope with experimental envelope (taken from [60]).

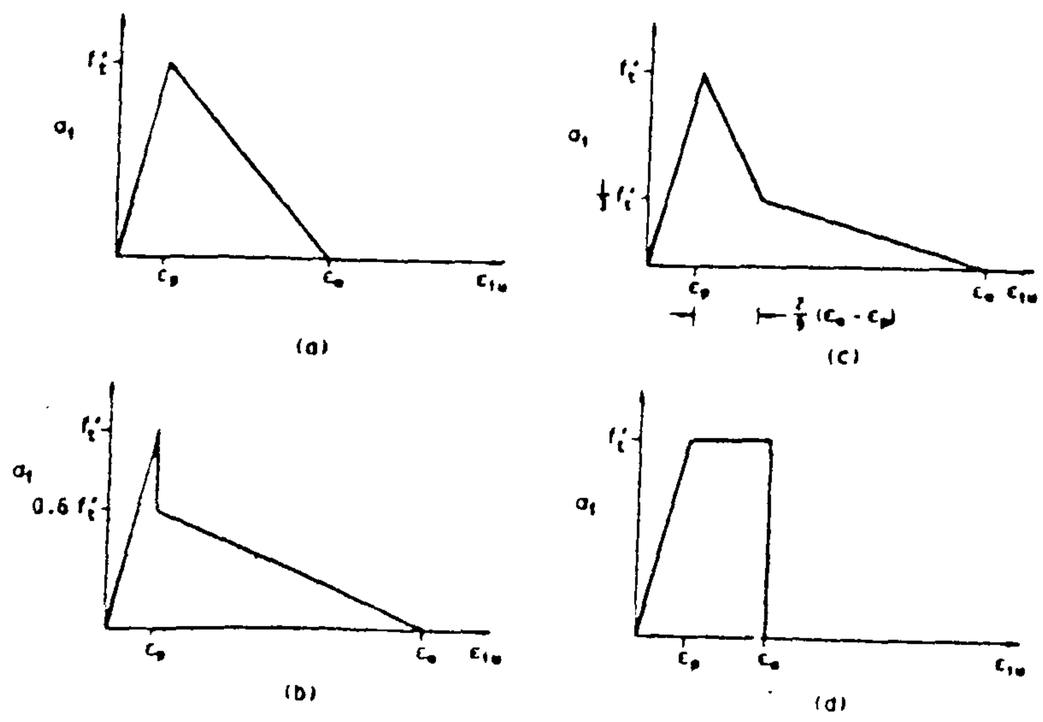

Fig. 2.33 Concrete models in tension: a)Linear softening, b)Discontinuous softening c)Bilinear softening, d) Dugdale softening

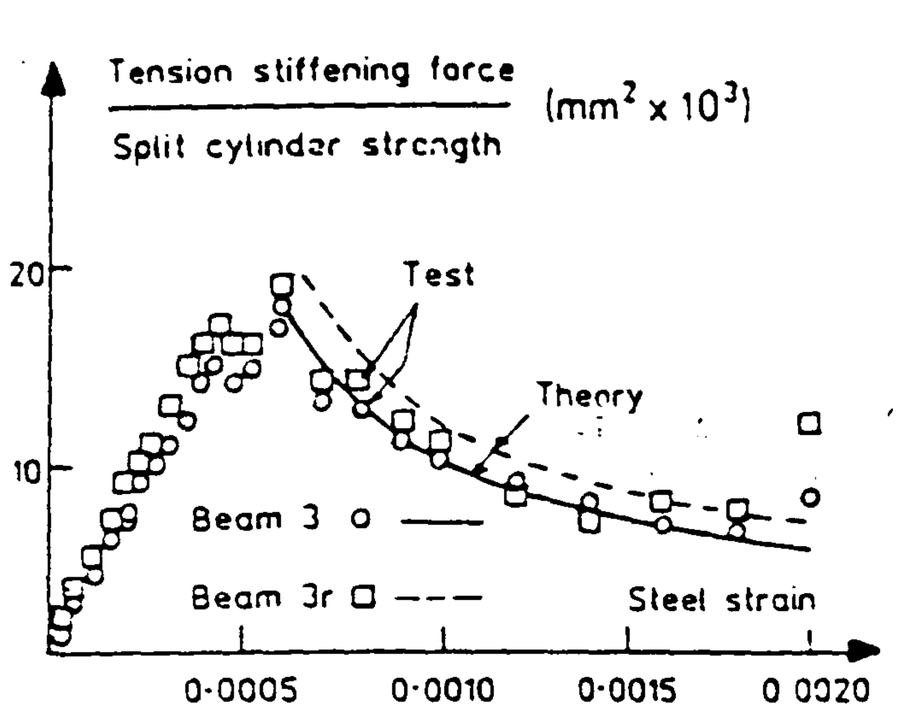

Fig. 2.34 Tension stiffening force-steel strain (taken from [71]).

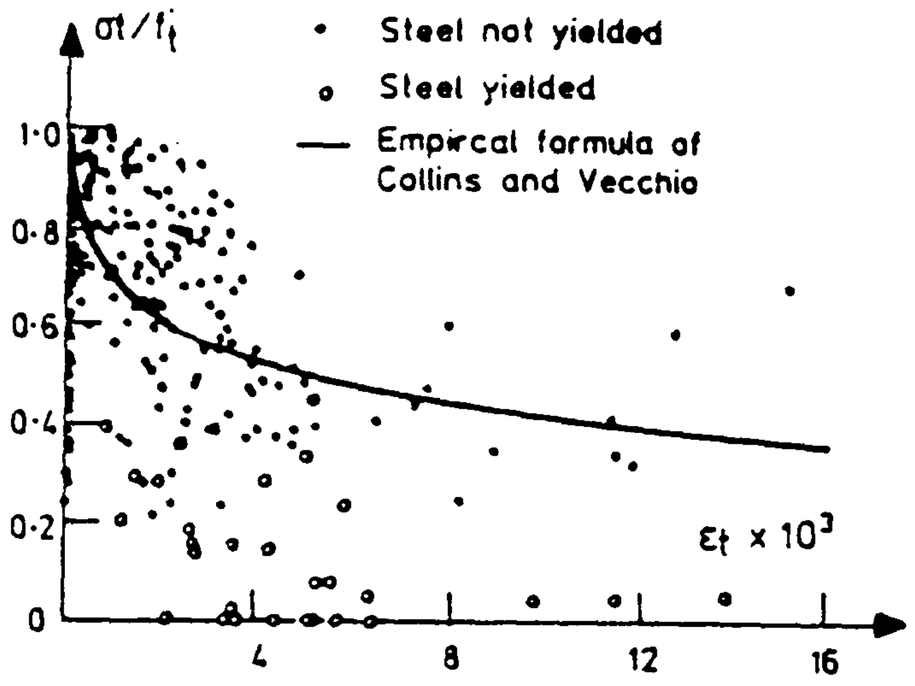

Fig. 2.35 Principal tensile stress data (taken from [71])

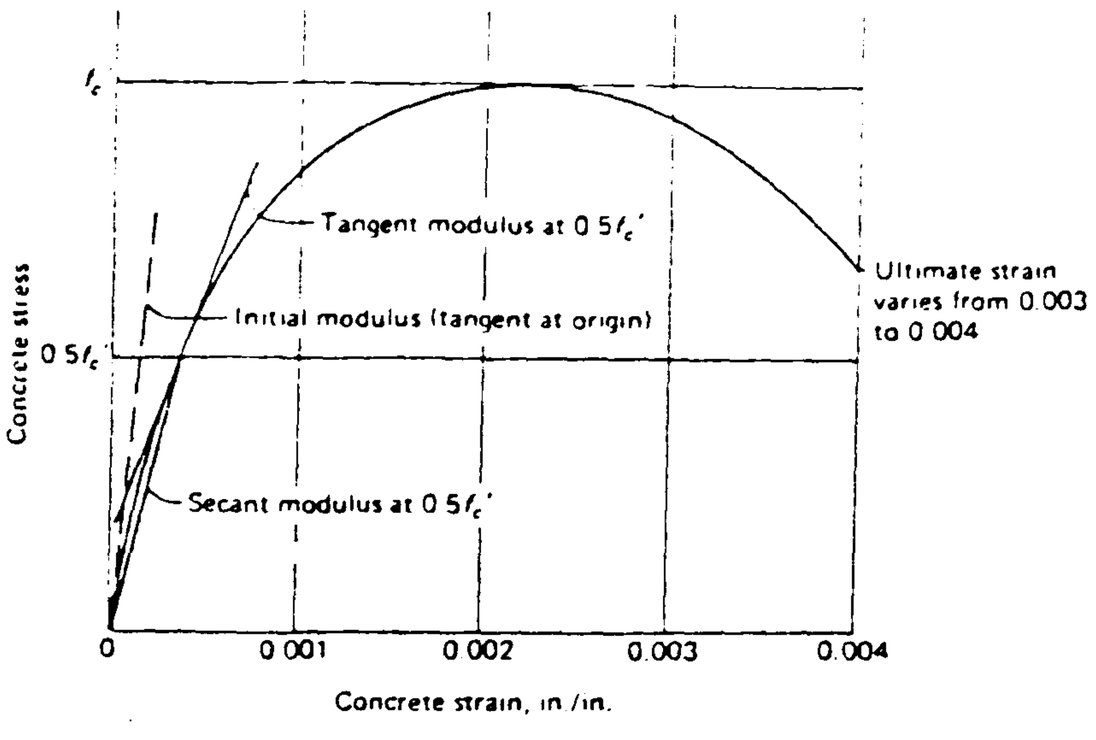

Fig. 2.36 Typical stress-strain curve for concrete taken from [11]).

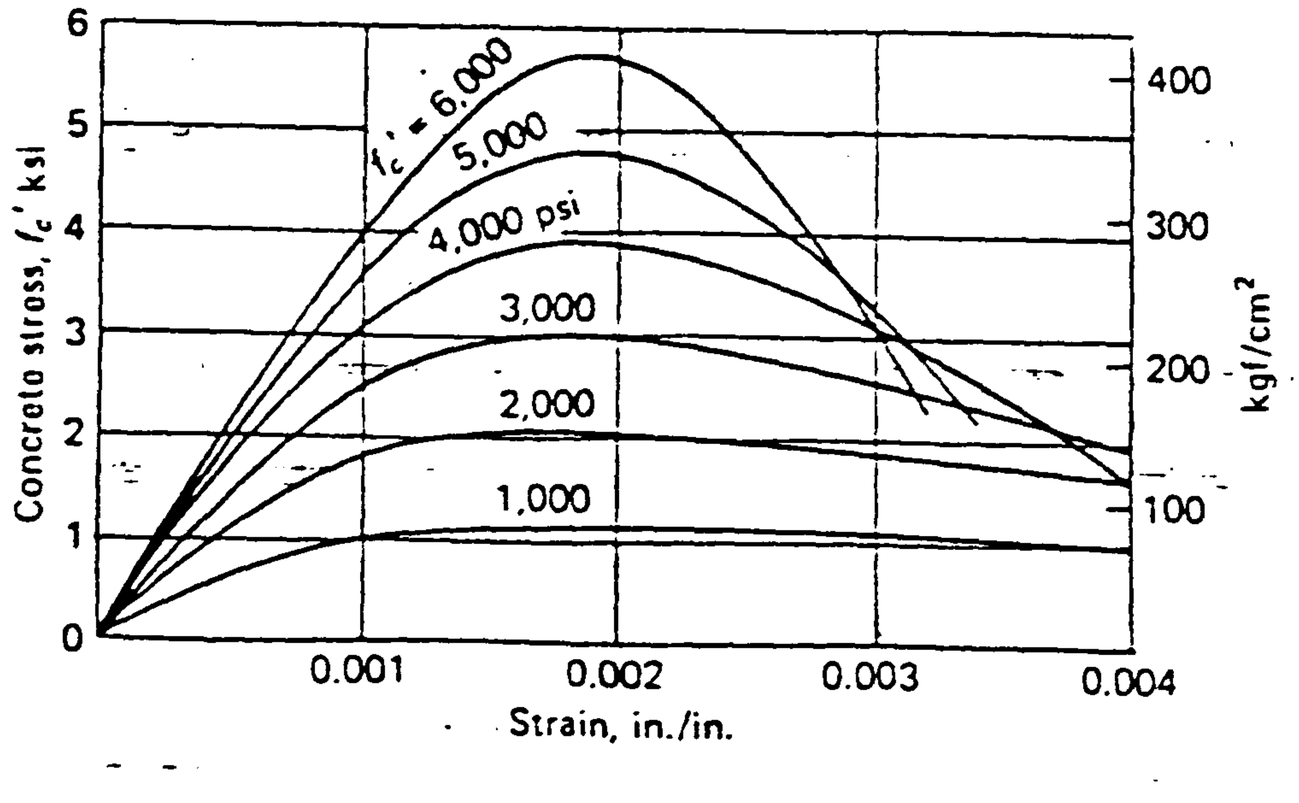

Fig. 2.37 Typical stress-strain curve for concrete (taken from [11]).

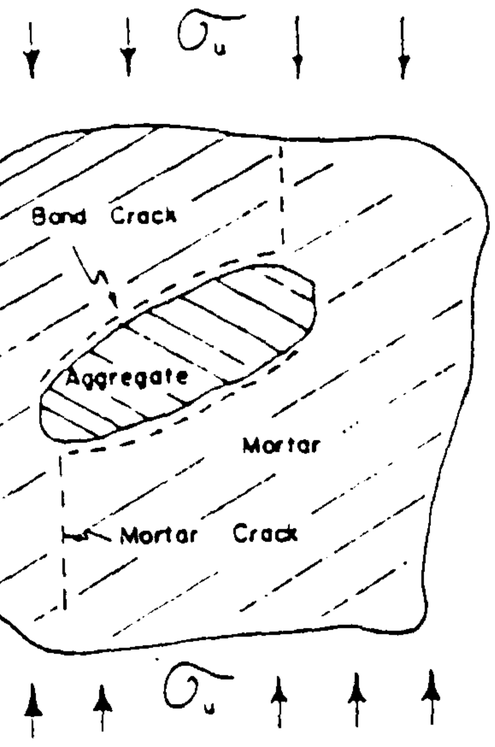

Fig. 2.38 Illustration of crack initiation and propagation in concrete (taken from [76]).

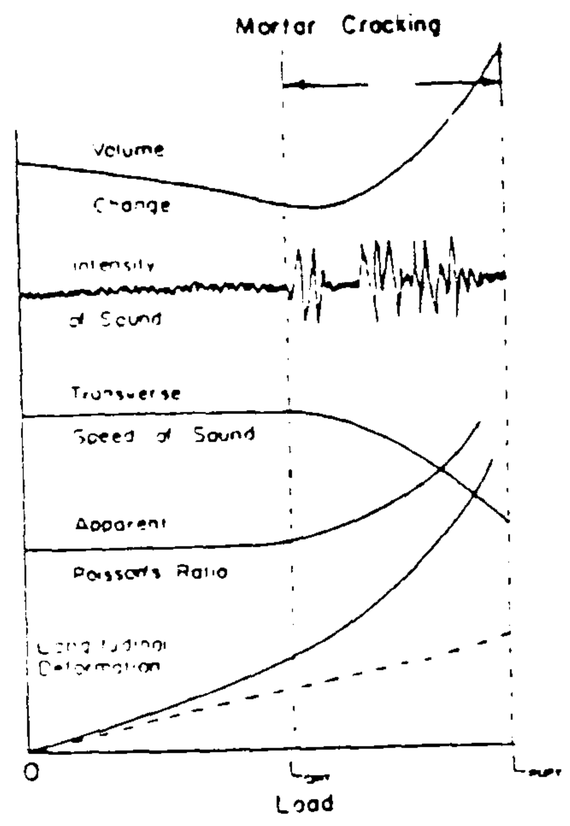

Fig. 2.39 Effects of microcracking under uniaxial compression on certatin properties of concrete (taken from [76]).

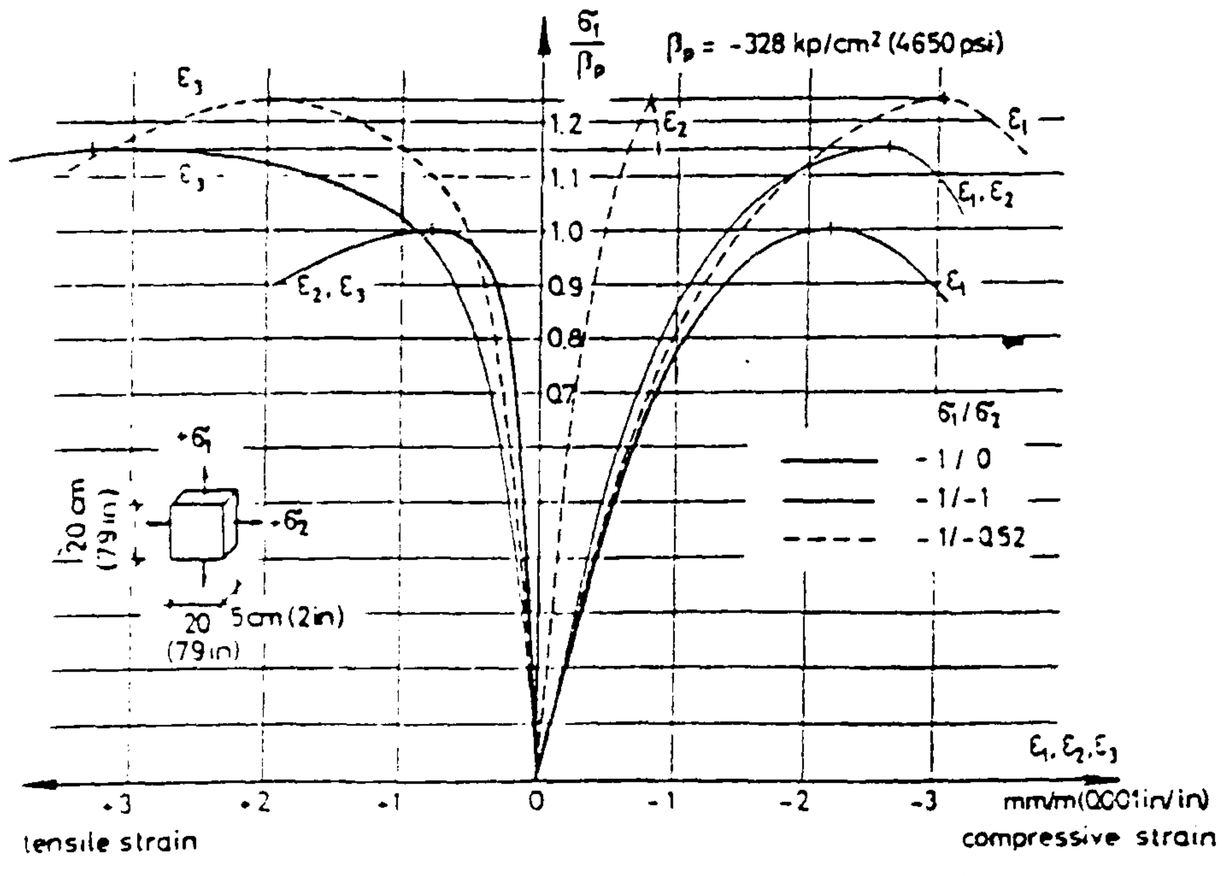

Fig. 2.40 Stress-strain relationship of concrete under biaxial compression (taken from [28]).

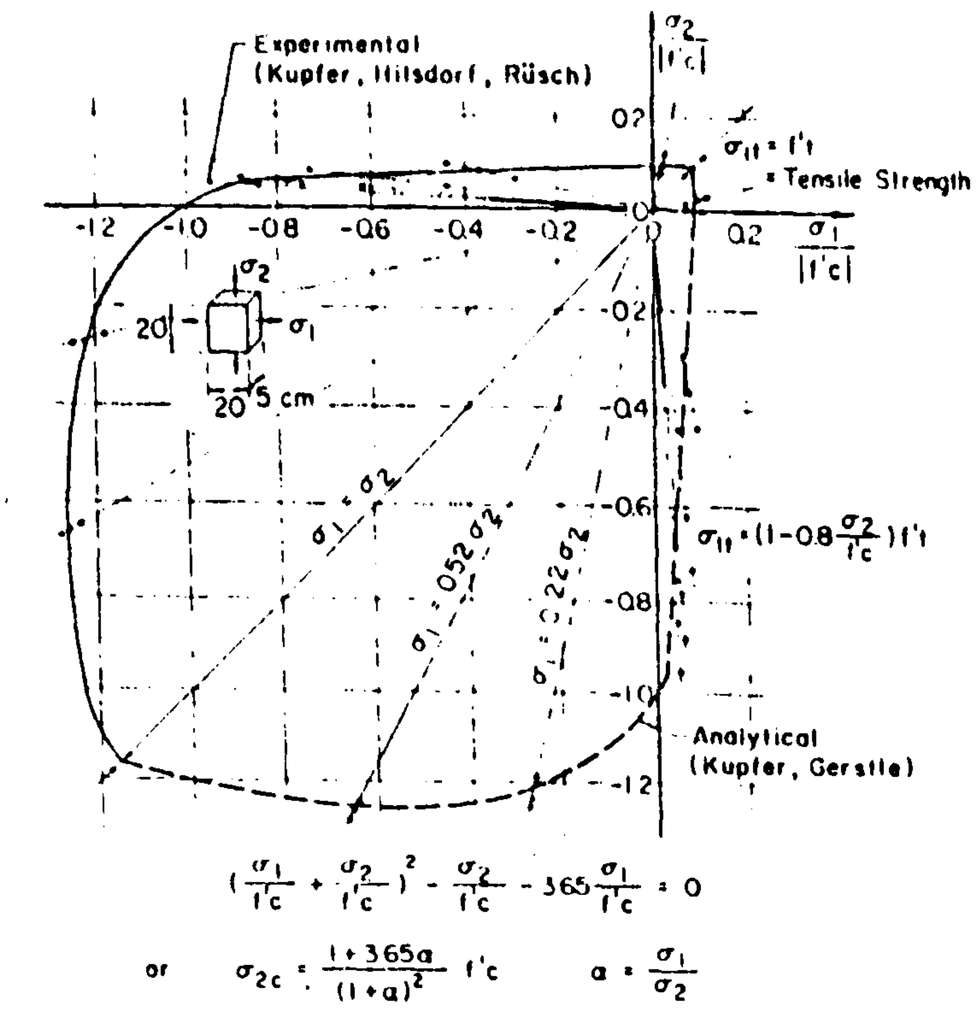

Fig. 2.41 Biaxial strength envelope for plain concrete

(taken from [29]).

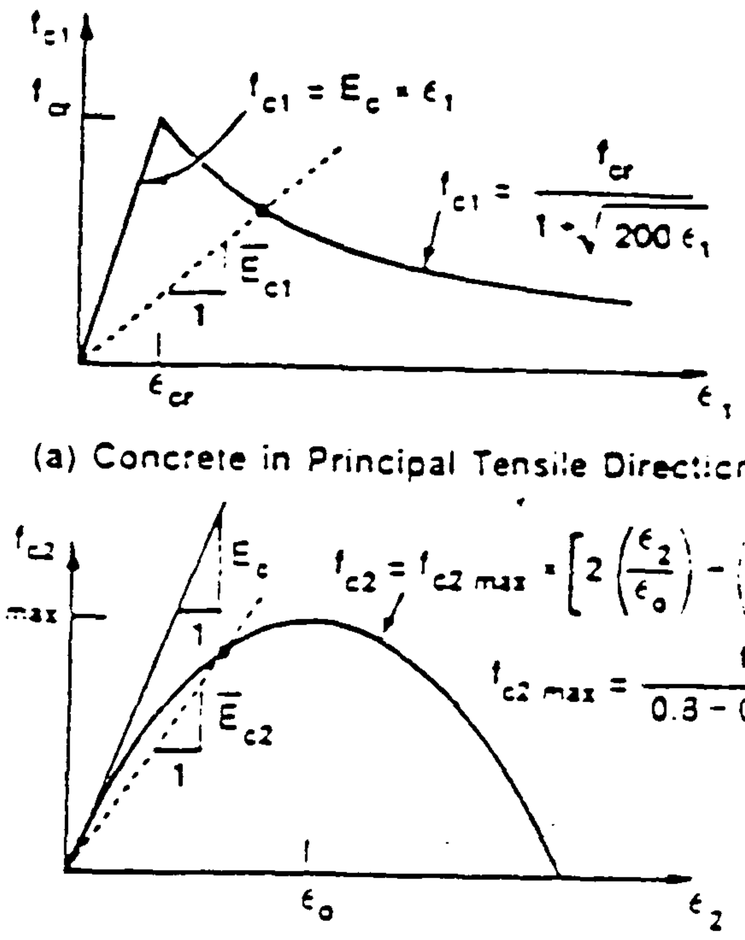

Fig. 2.42 A Concrete in principal compressive direction

(taken from [71]).

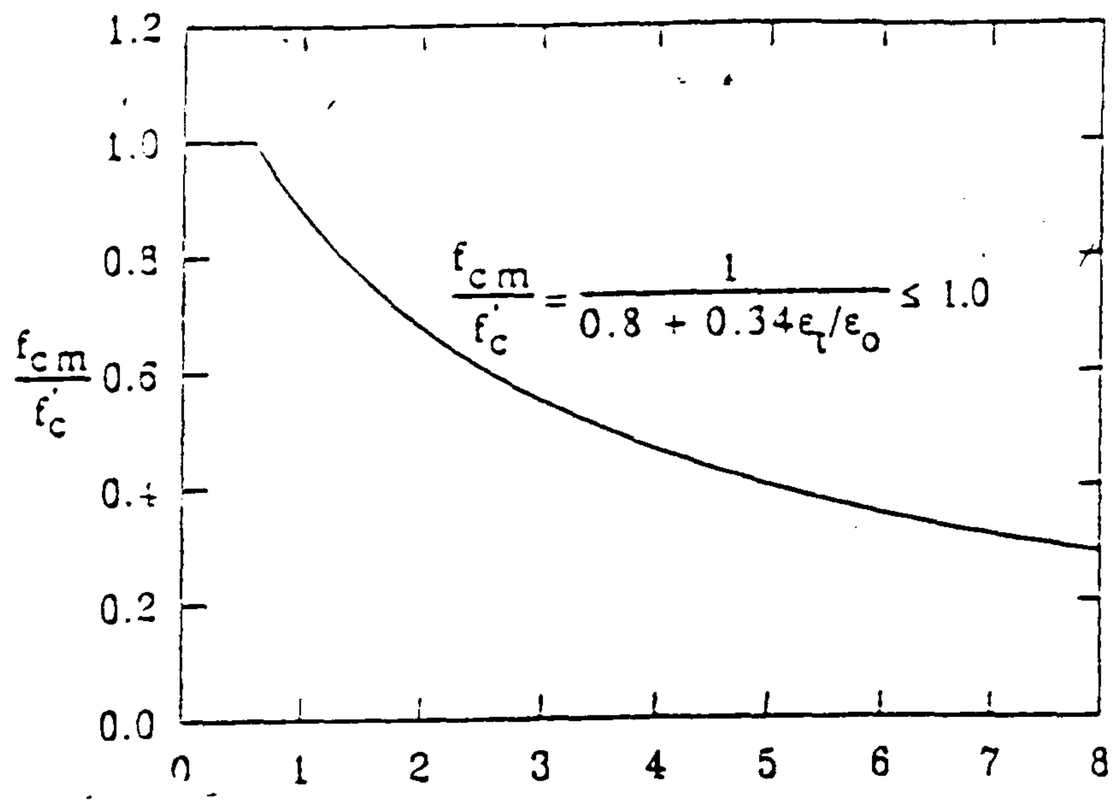

Fig. 2.42 B Degraded maximum compressive strength for cracked concrete (taken from [71]).

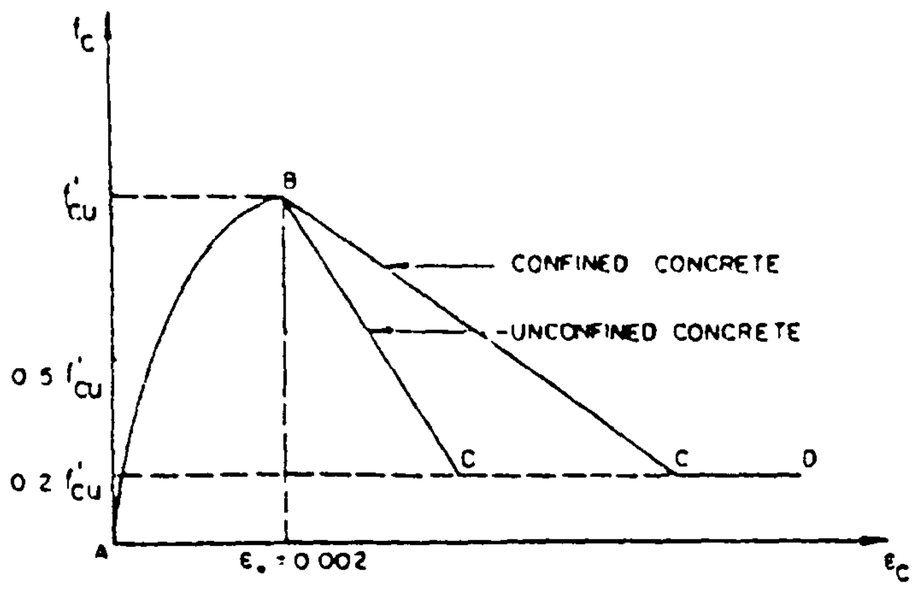

Fig. 2.43 Stress-strain relationship for unconfined and confined concrete (taken from [77]).

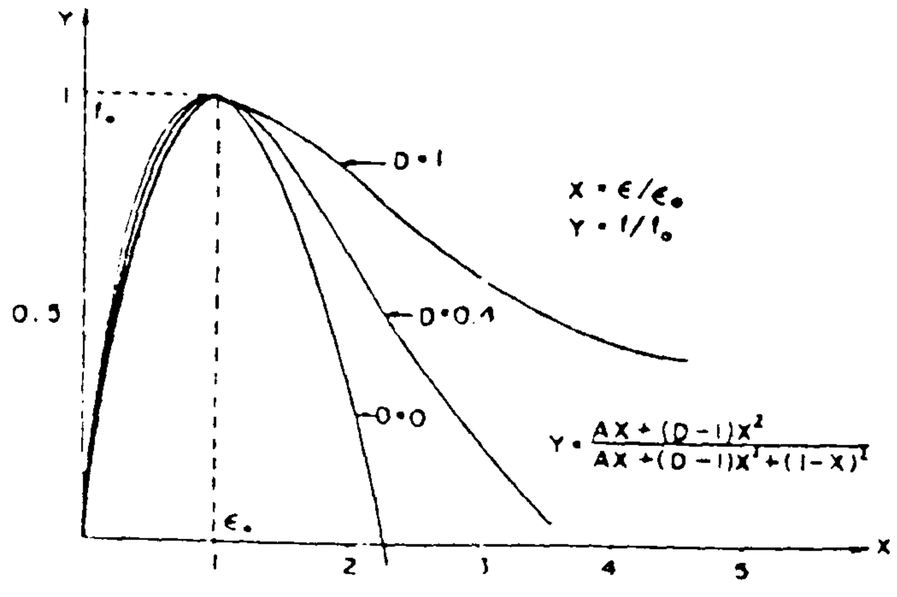

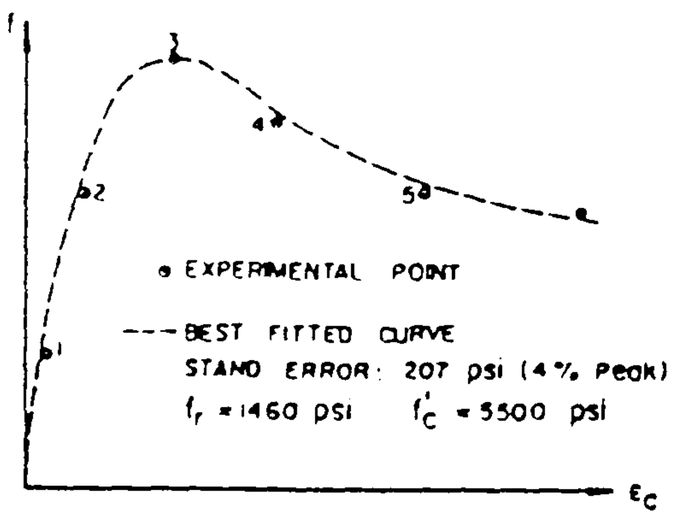

(a) CONFINED SPECIMEN

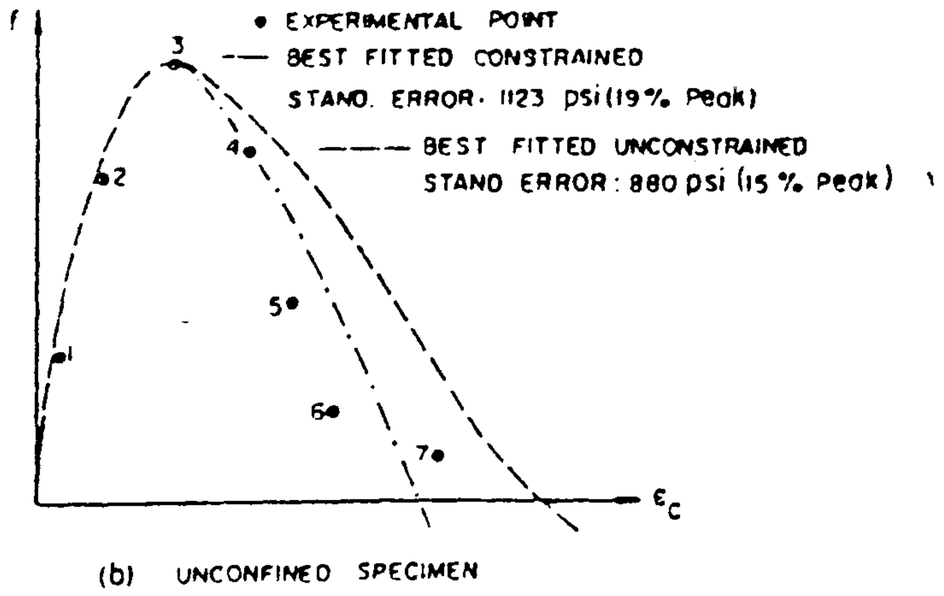

(b) UNCONFINED SPECIMEN

Fig. 2.44 Typical normalized curves of Sagin's equation (taken from [77]).

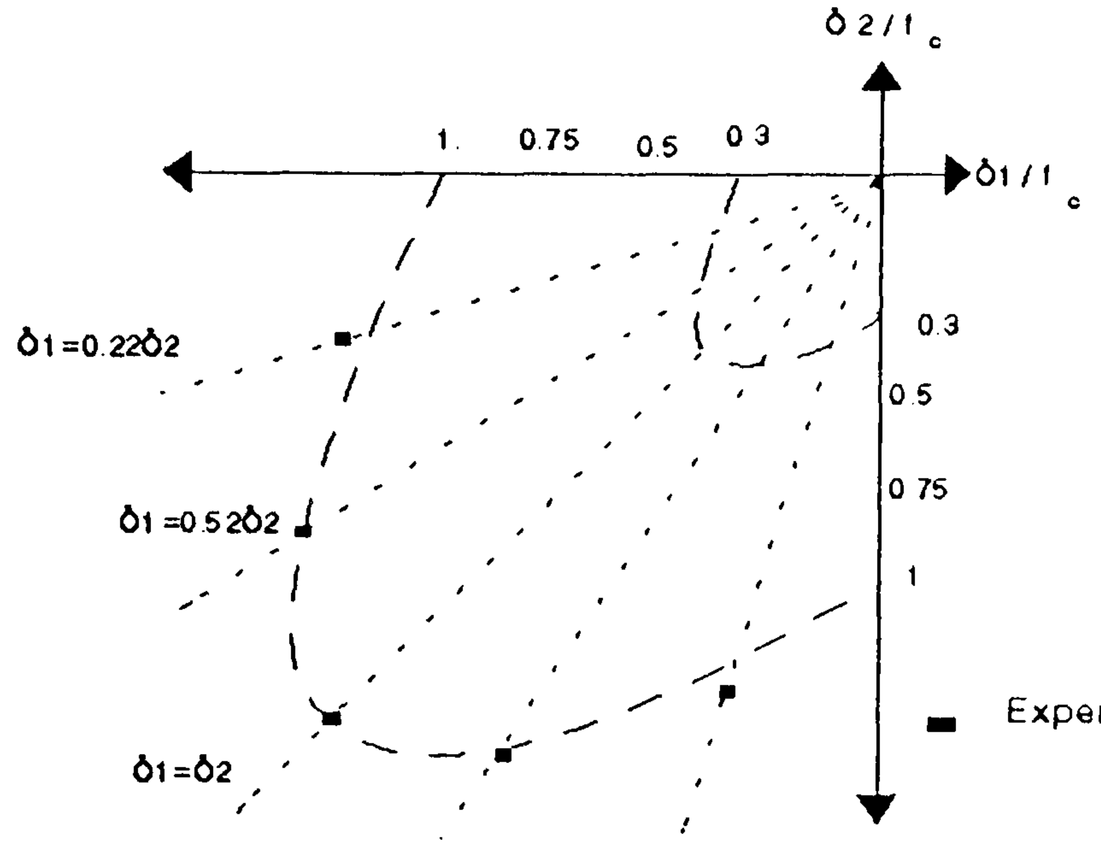

Fig. 2.45 A
Proposed failure surface

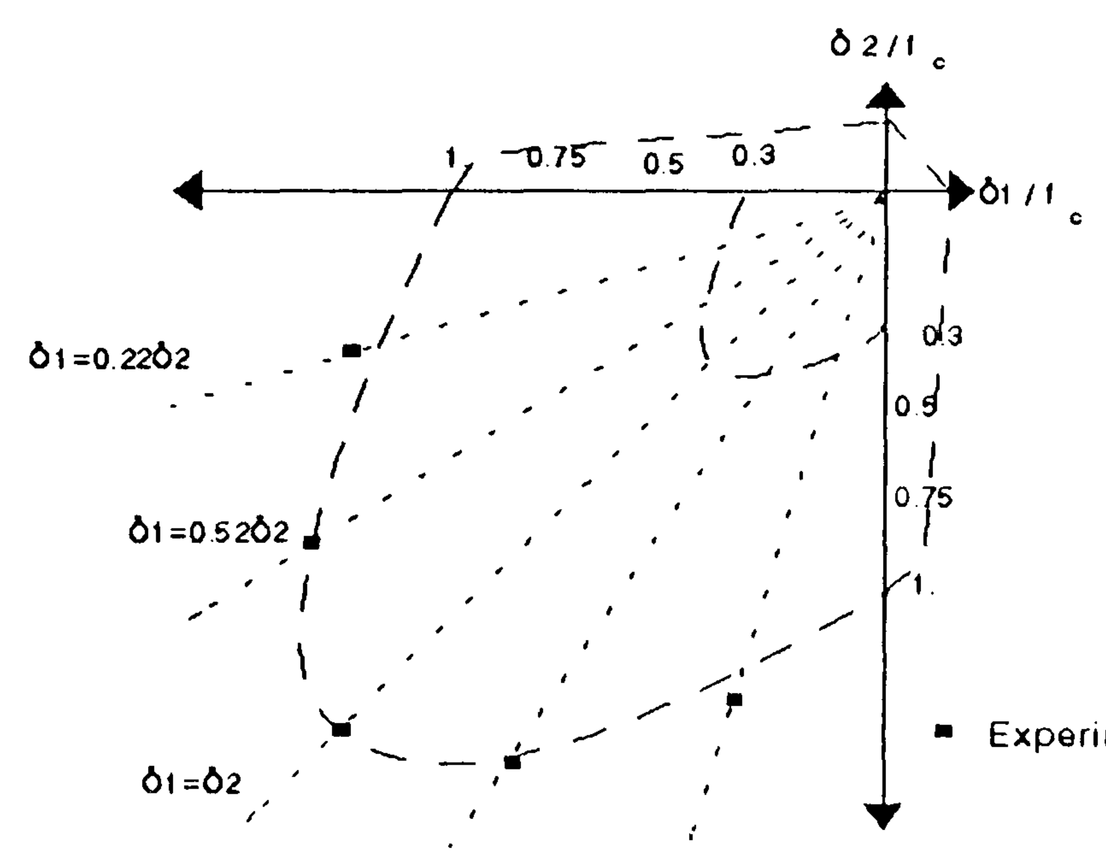

Fig. 2.45 B
Biaxial stress space representation of constitutive model

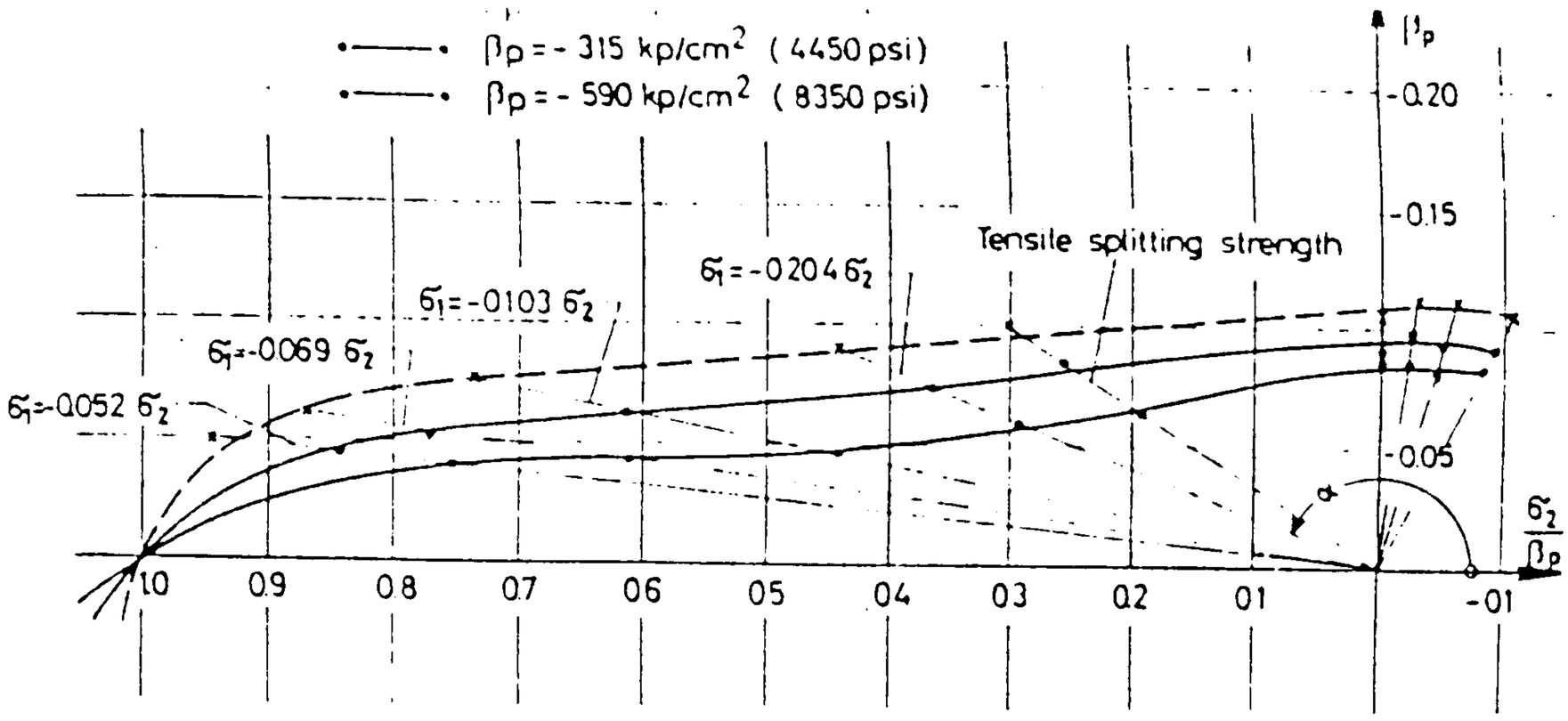

Fig. 2.46 A Strength of concrete under combined tension and compression and under biaxial tension (taken from [28]).

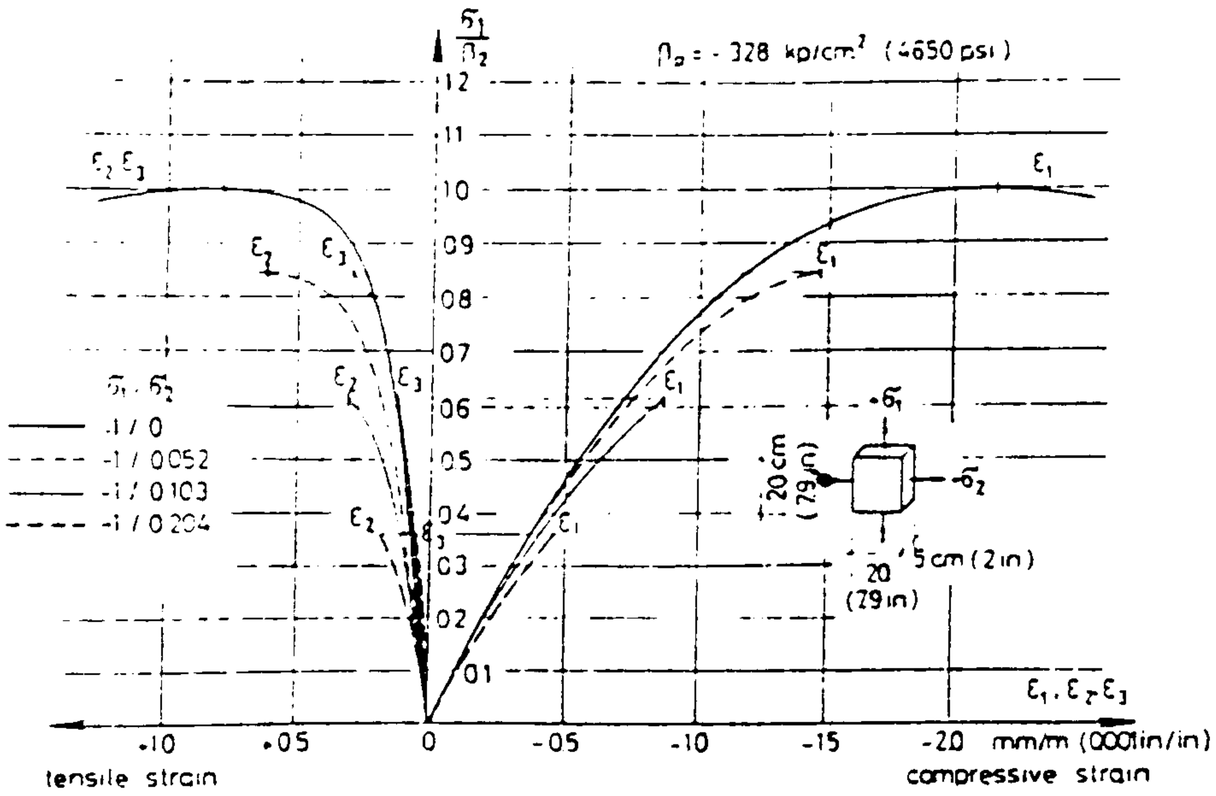

Fig. 2.46 B stress-strain relationship of concrete under combined tension and compression (taken from [28]).

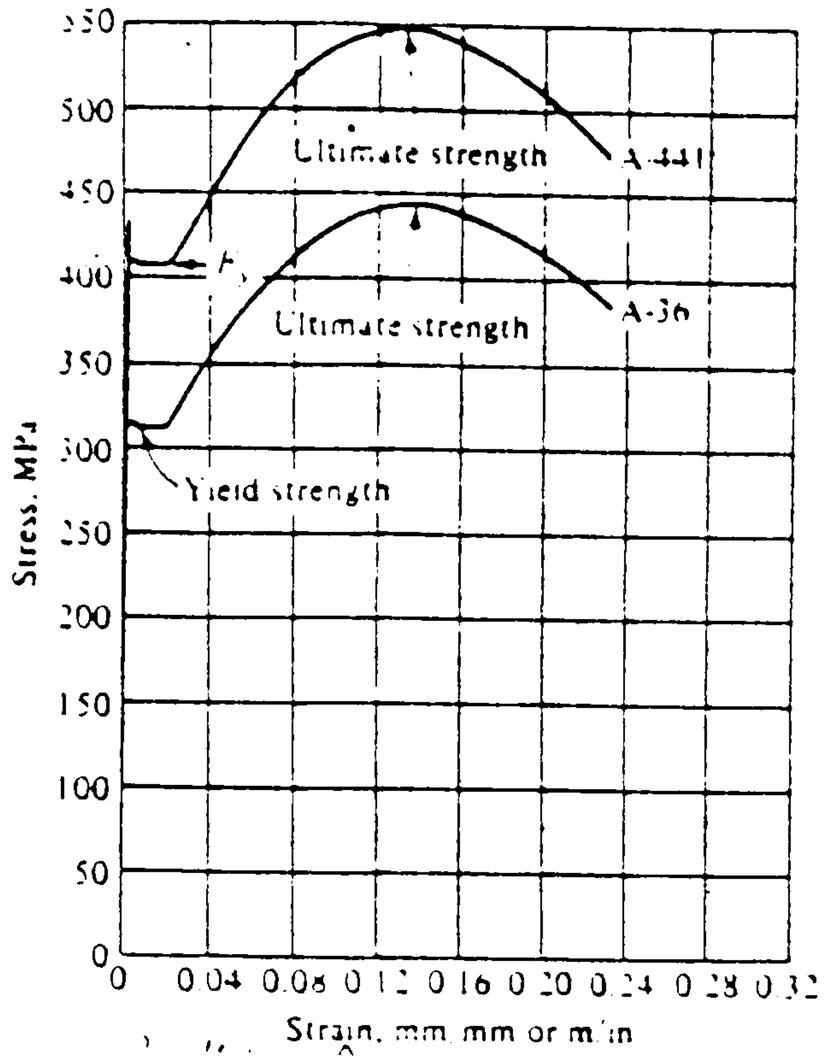

Fig. 2.47 A typical stress-strain curves for structural steel

(taken from [11]).

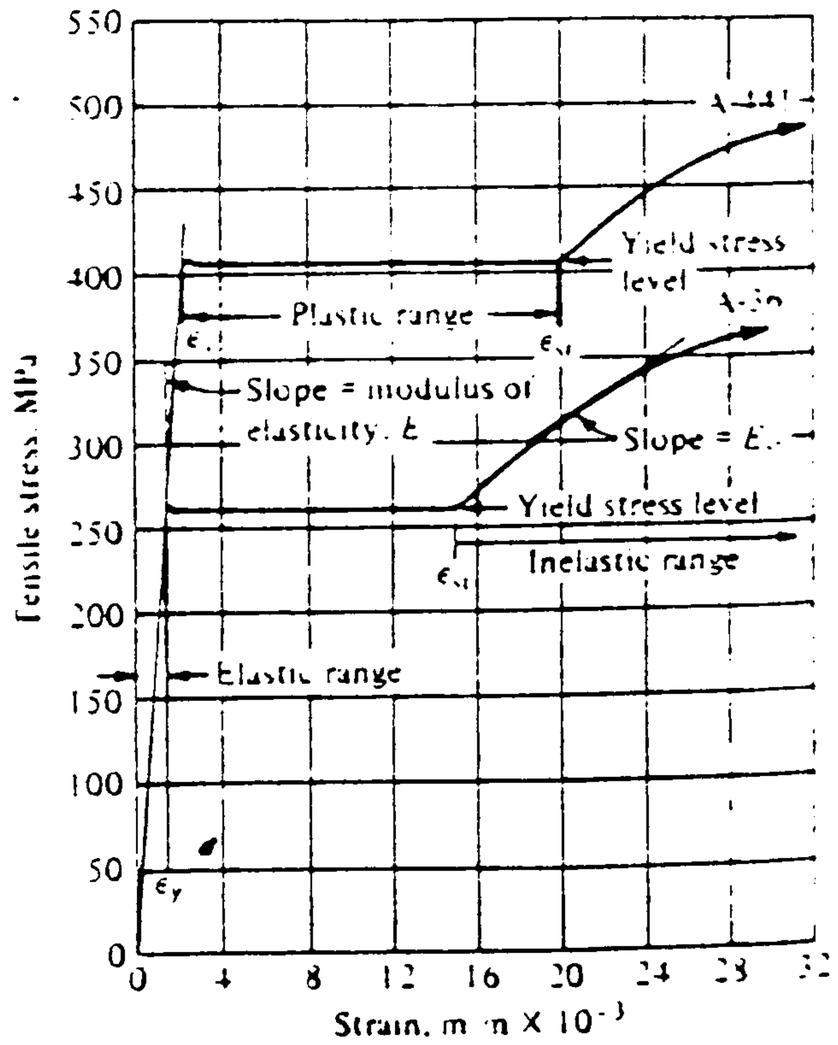

Fig. 2.47 B Stress-strain curves for two types of structural steel

(taken from [11]).

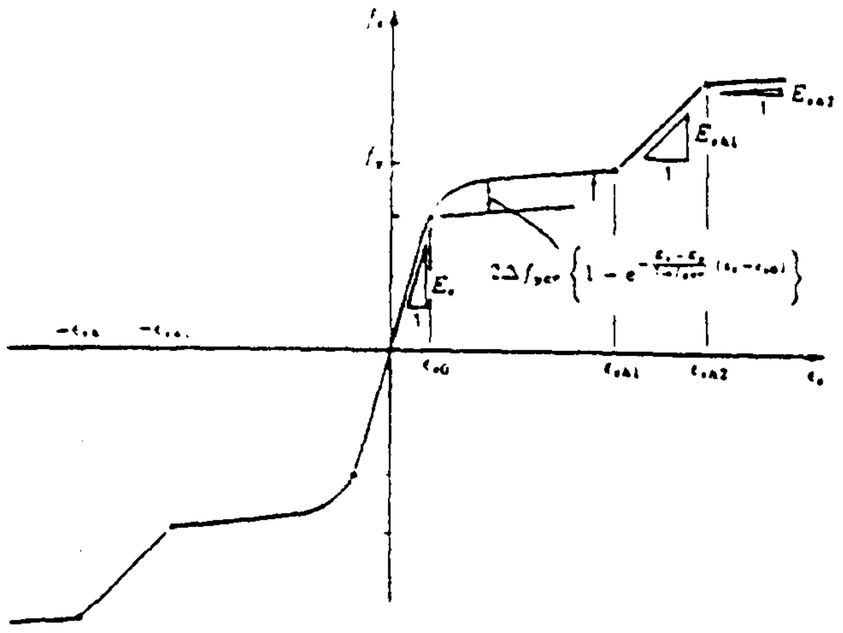

(B)

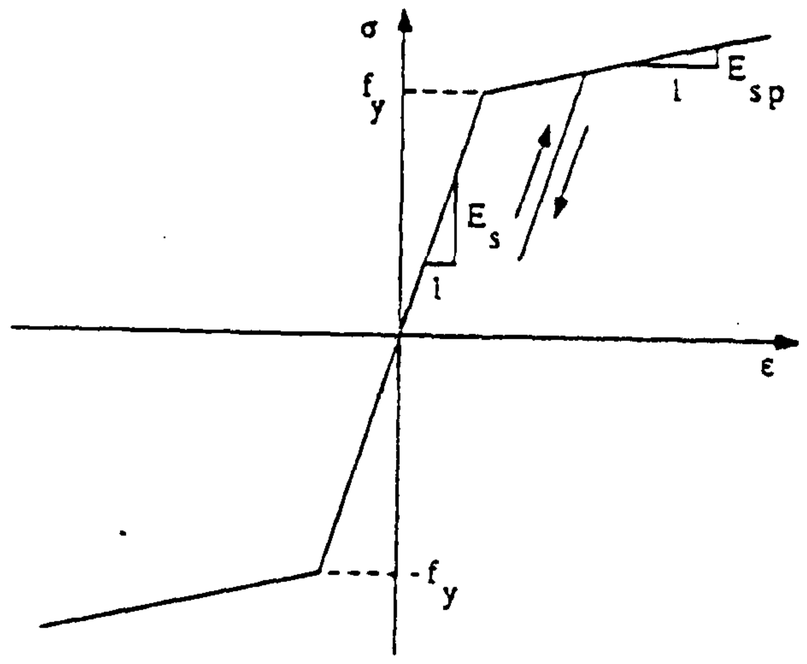

(A)

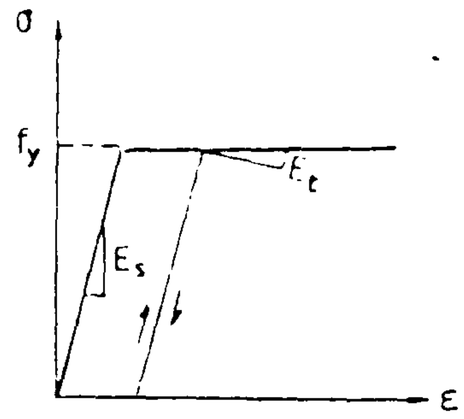

(C)

Fig. 2.48 Idealized stress-strain curves for steel (A), (B), (C)

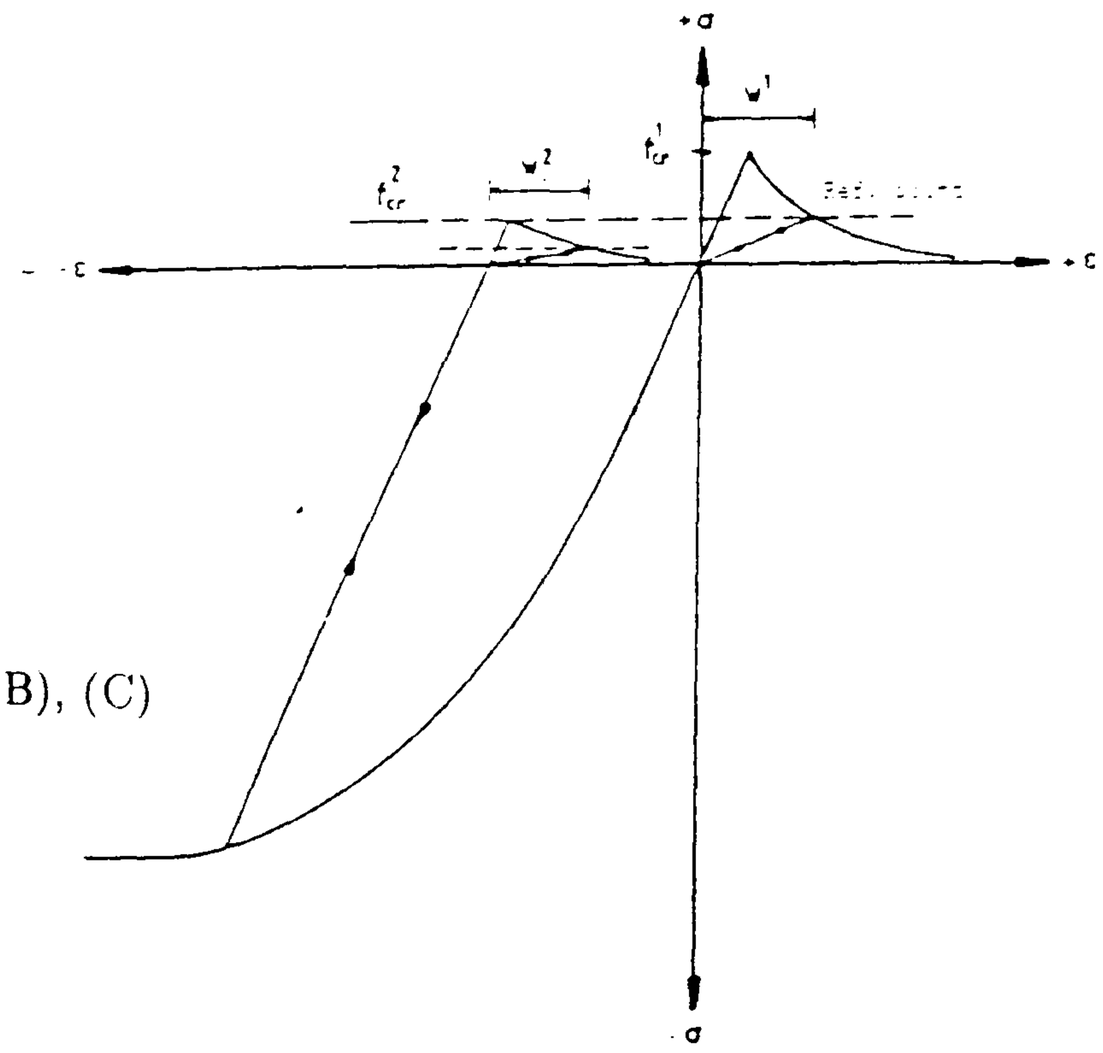

Fig. 2.49 Opening and closing of cracks

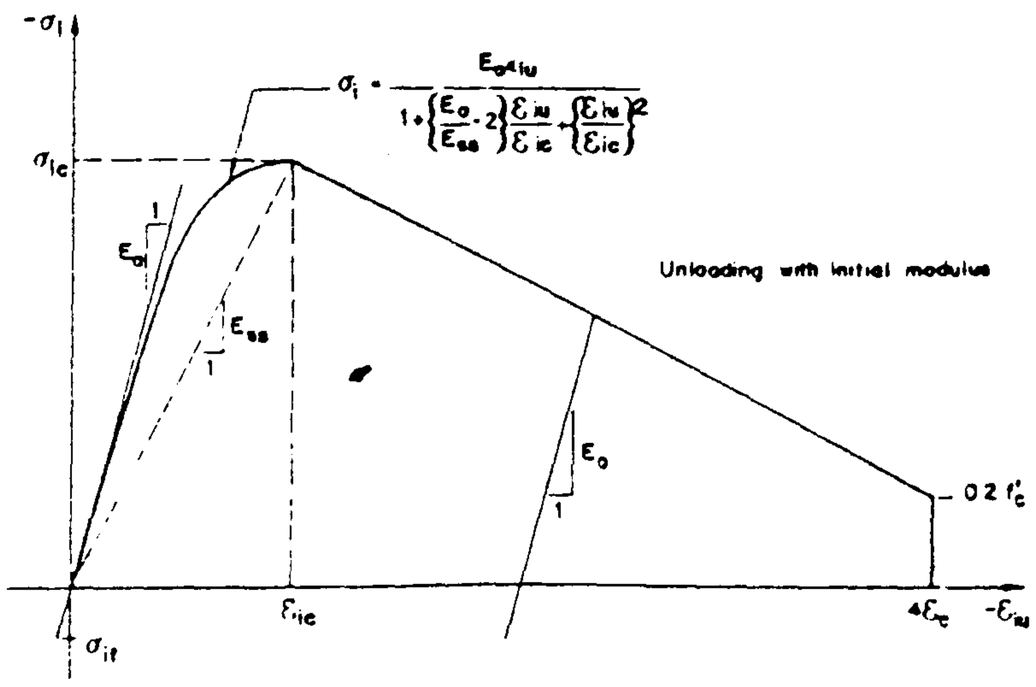

Fig. 2.50 Equivalent uniaxial stress-strain model for concrete proposed by Darwin and Pecknold. (taken from [87])

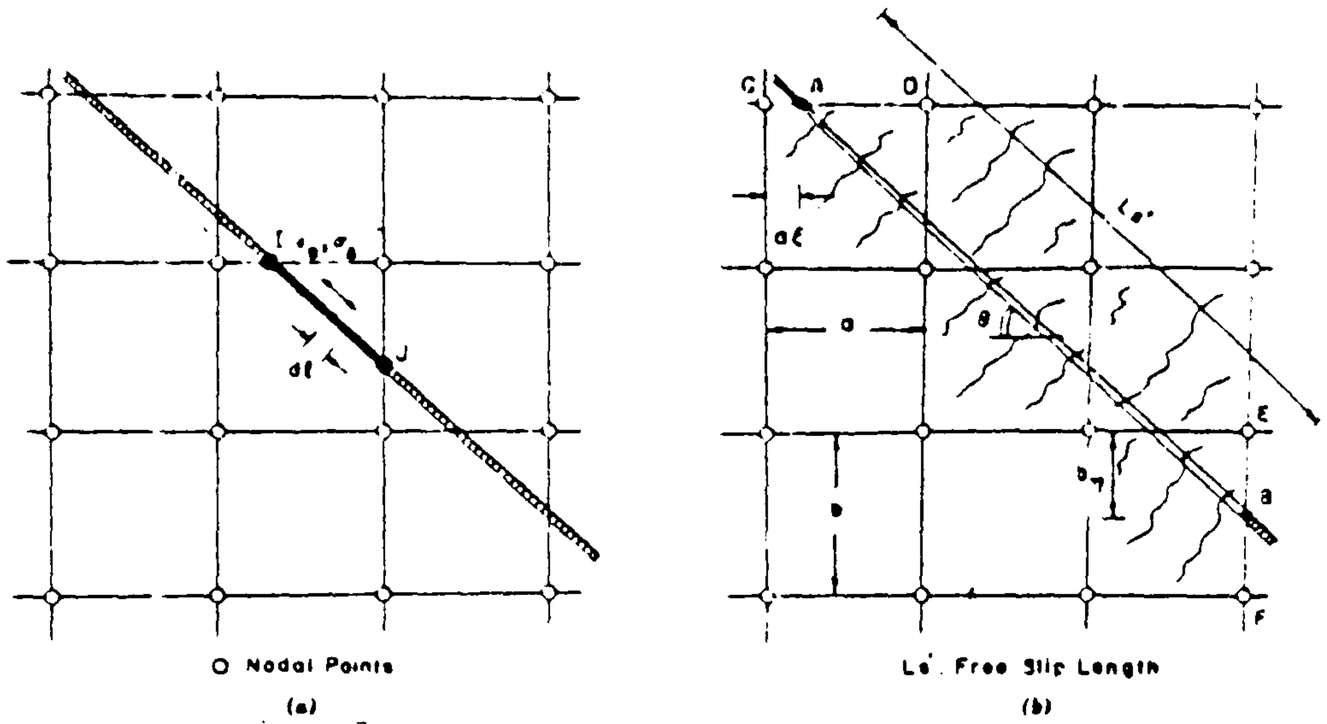

Fig. 2.51 Embedded representation of a reinforcement

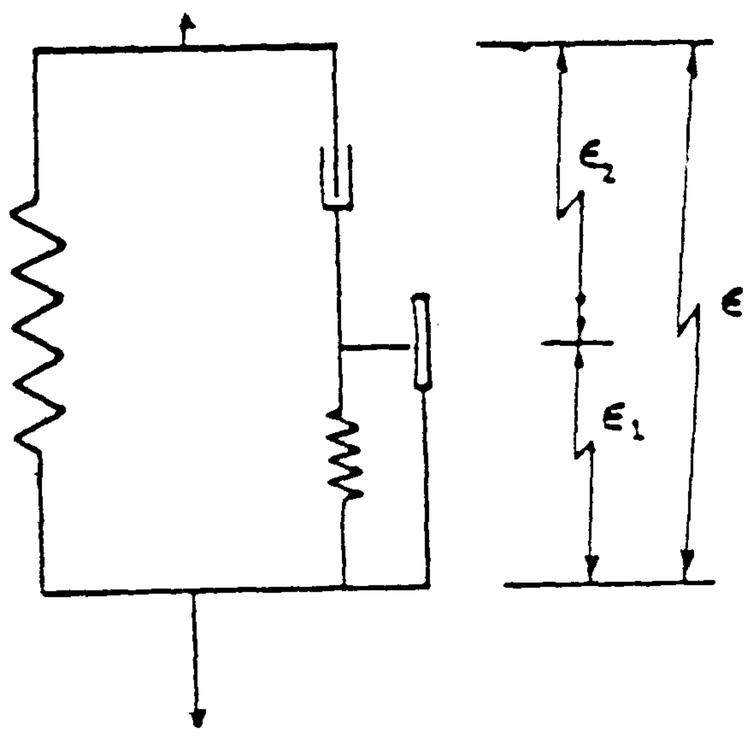

Fig. 2.52 Rheological model for concrete proposed by Pozzo (taken from [108]).

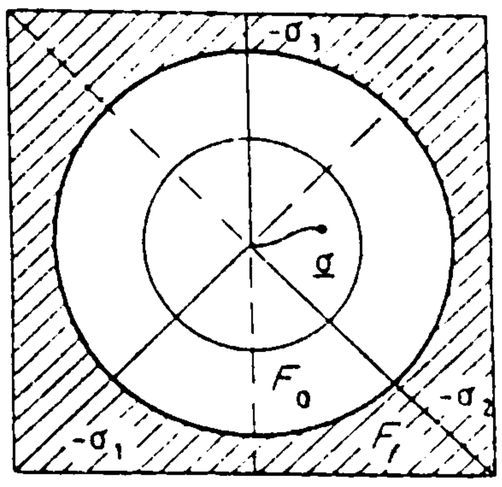

Linear elasticity
F_0 and F_f in initial positions

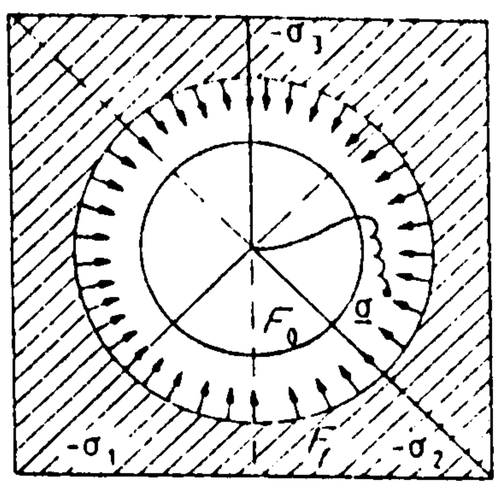

Elasto/Viscoplasticity
F_0 constant ; F_f shrinking

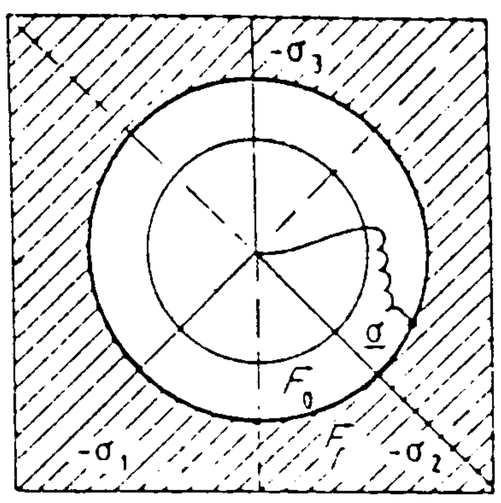

Failure

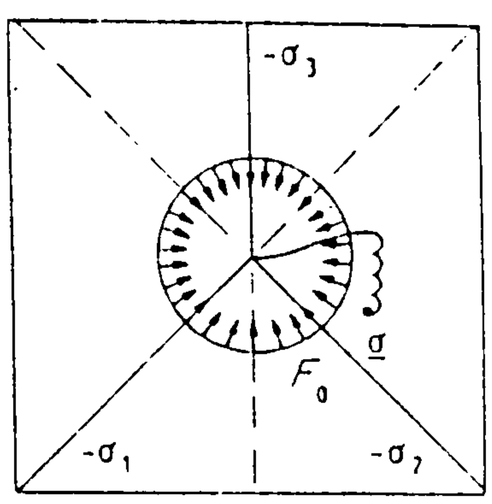

Postfailure
F_0 shrinking

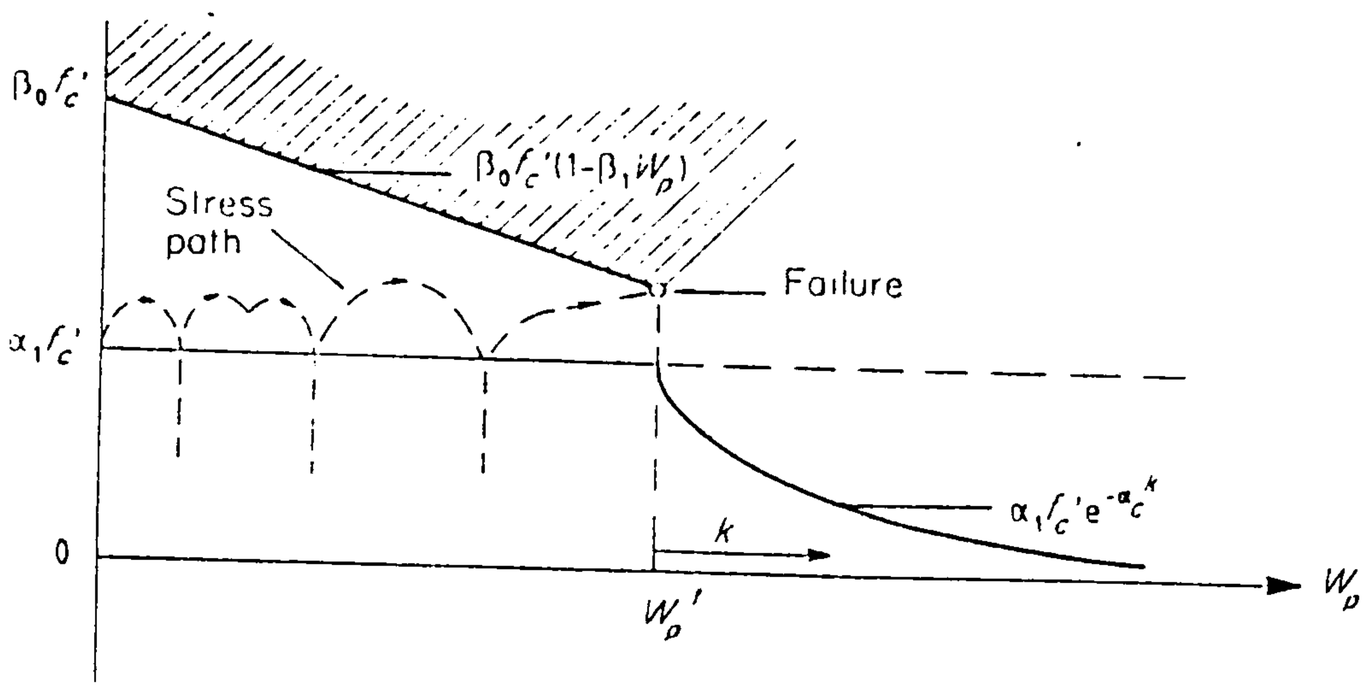

Fig. 2.53 Change of the yield and failure stresses with the plastic work (taken from [41]).

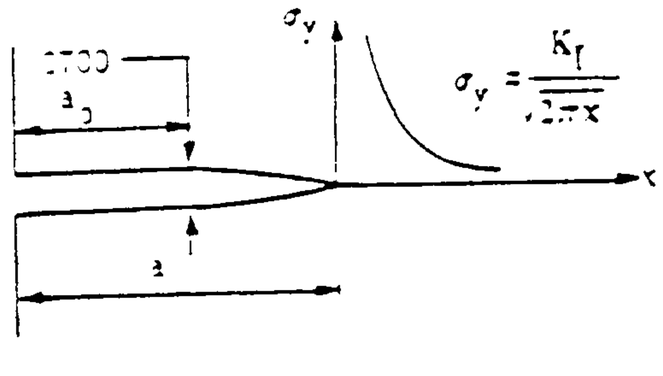

Fig. 2.54 Effective Griffith crack

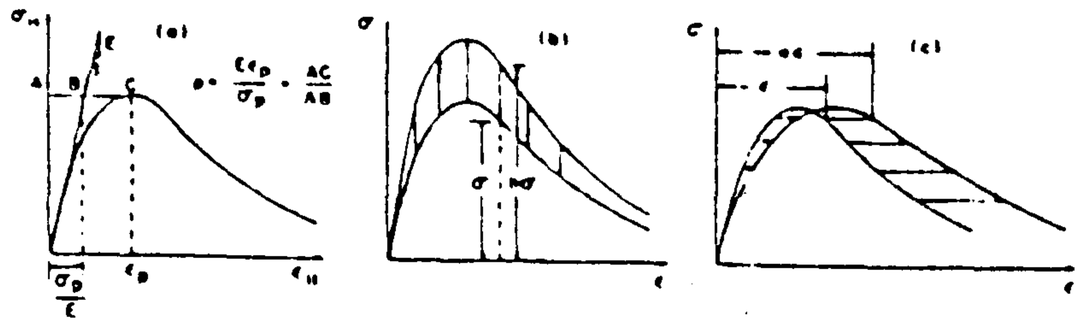

Fig. 2.55 Definition of coefficient P (taken from [6]).

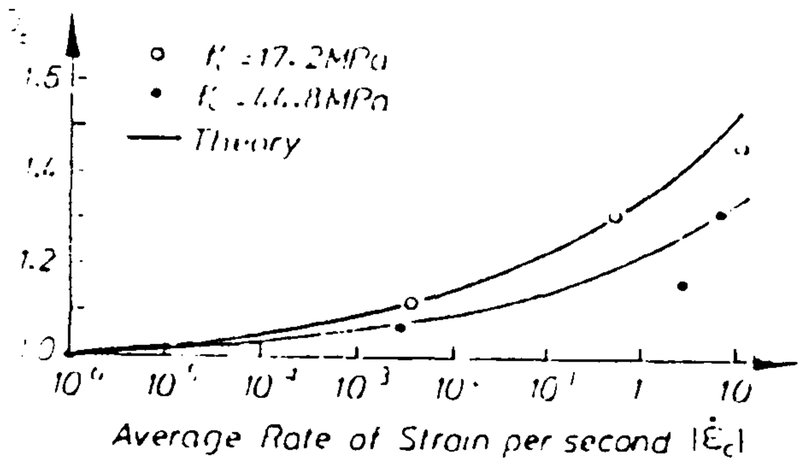

Fig. 2.56 A Magnification factor D_f to allow for strain-rate effects on stiffness (taken from [12]).

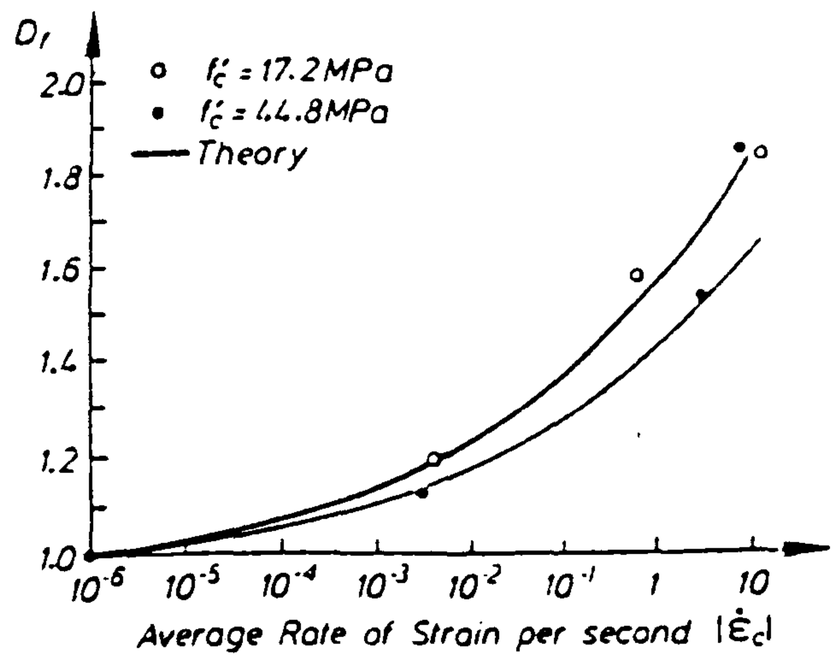

Fig. 2.56 B Magnification factor D_f to allow for strain-rate effects on strength (taken from [12]).

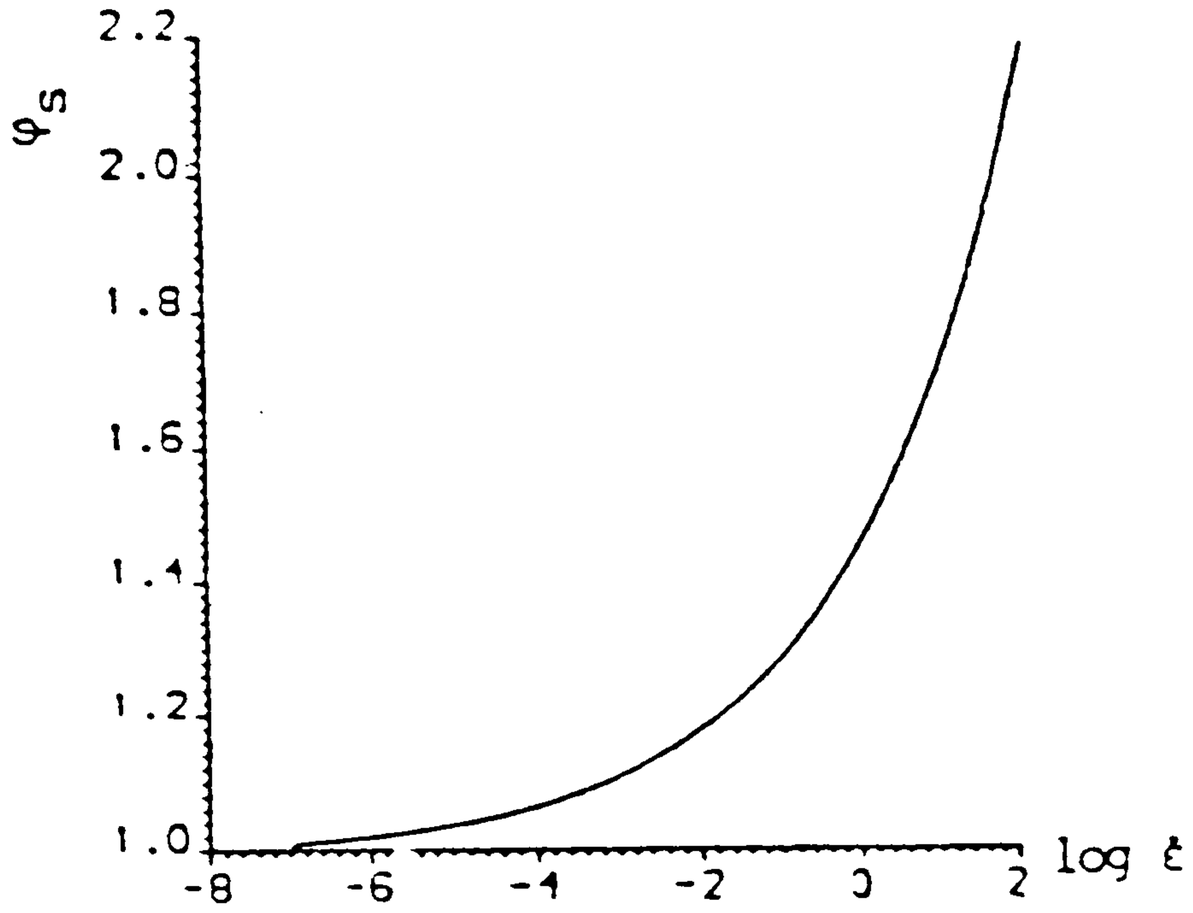

Fig. 2.57 Strain-rate sensitivity function of steel yield stress (taken from [94]).

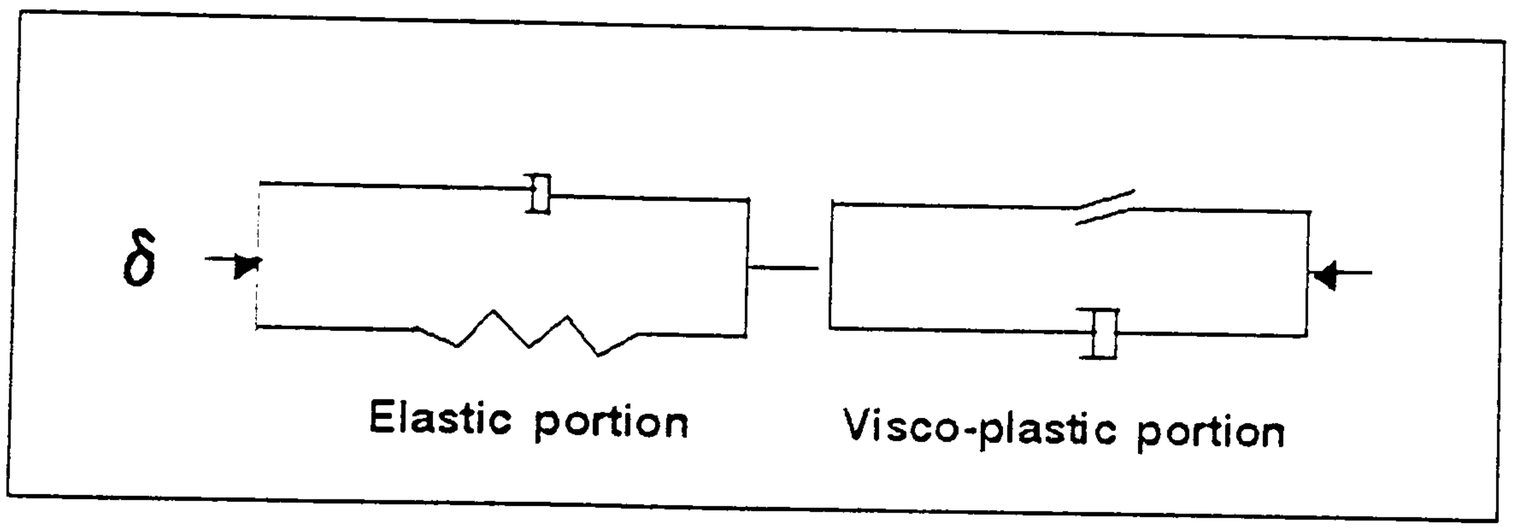

Fig. 2.58 Proposed rheological model

Fig. 2.59 Variation of fluidity parameter with strain-rate in compression
Concrete mix 1:4:7

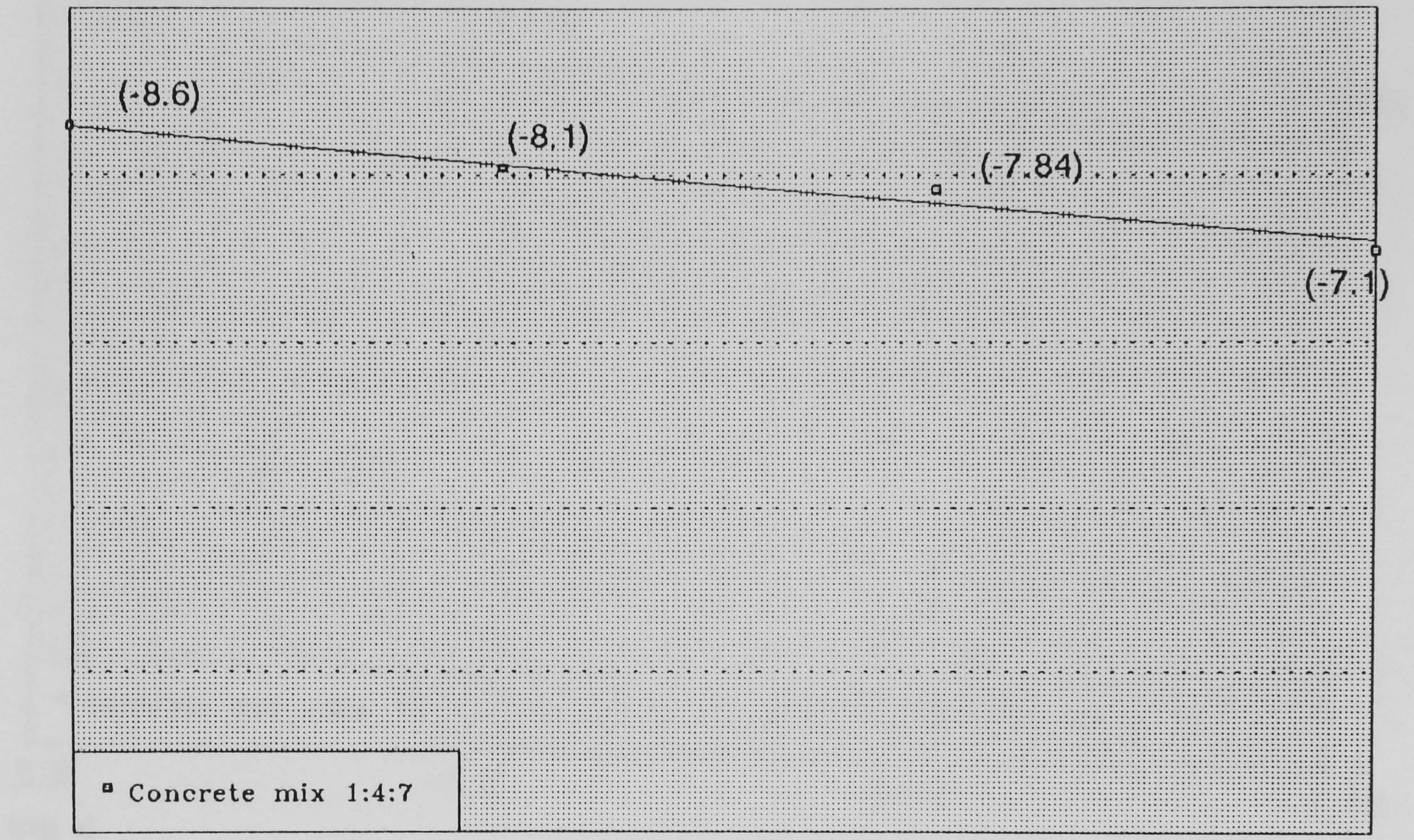

Fig. 2.60 Variation of fluidity parameter with strain-rate in compression
Concrete mix 1:3:5

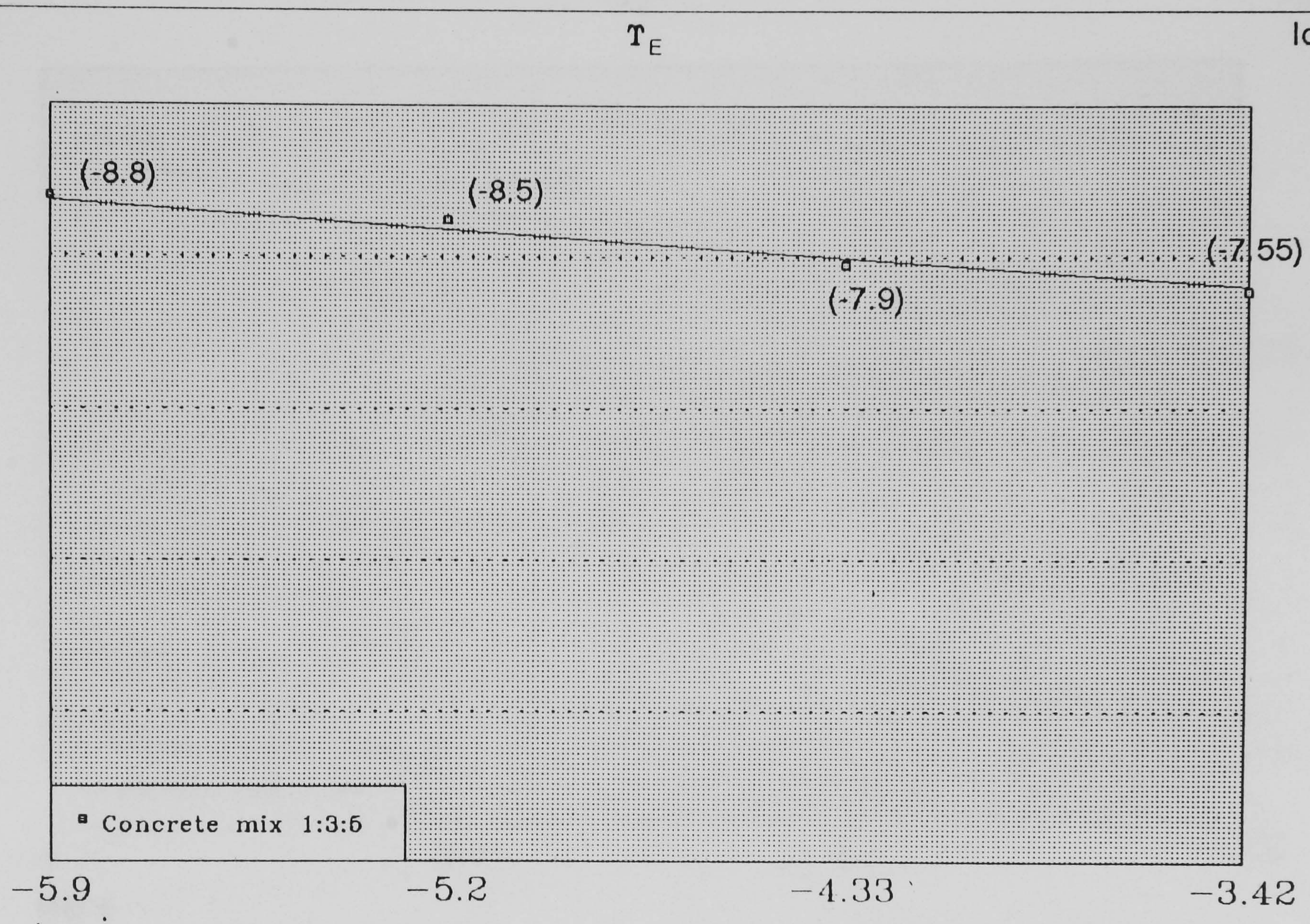

Fig. 2.61 Variation of fluidity parameter with strain-rate in compression
Concrete mix 1:2:4

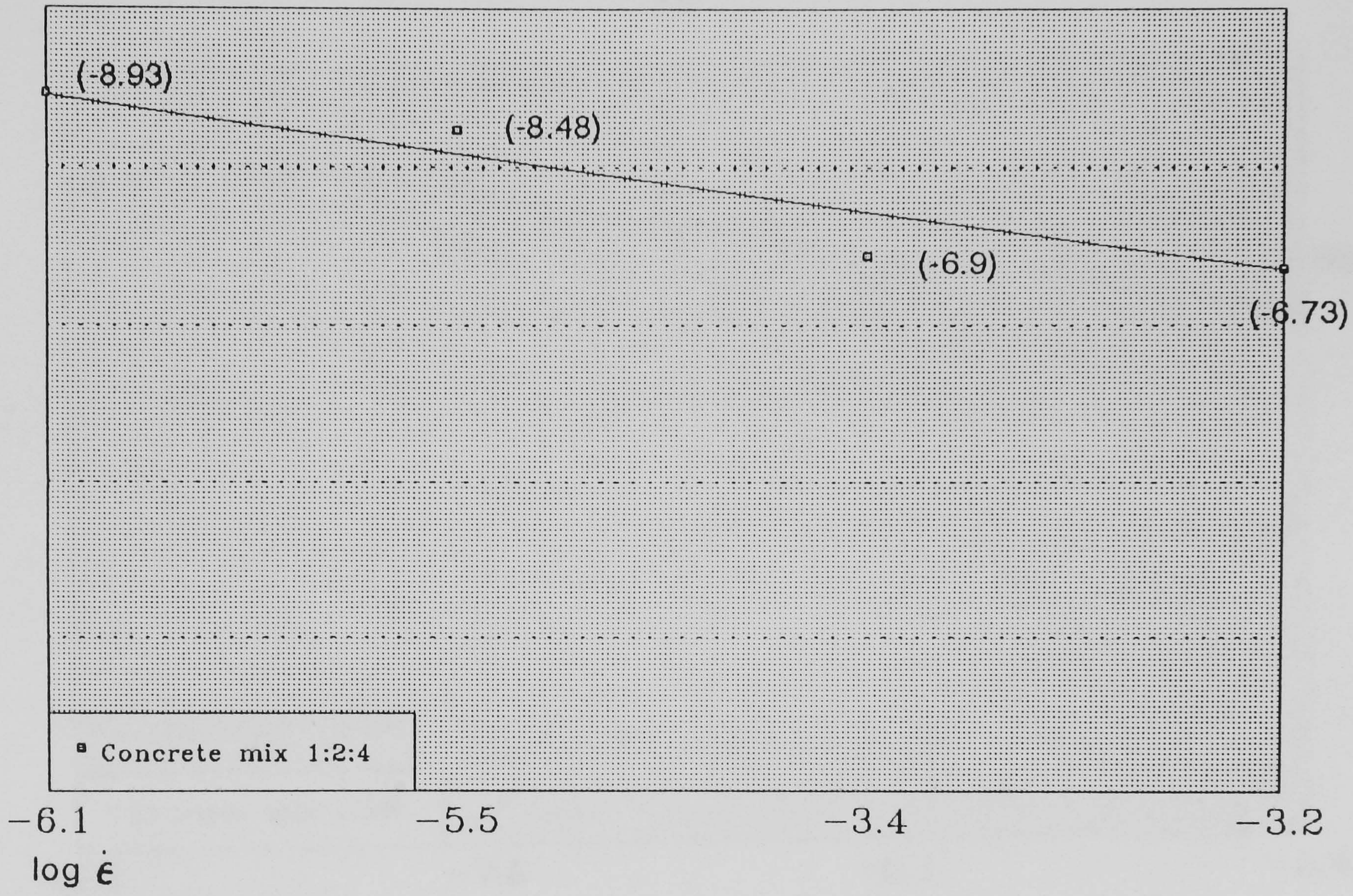

Fig. 2.62 Variation of fluidity parameter with strain-rate in tension
Concrete mix 1:3:5

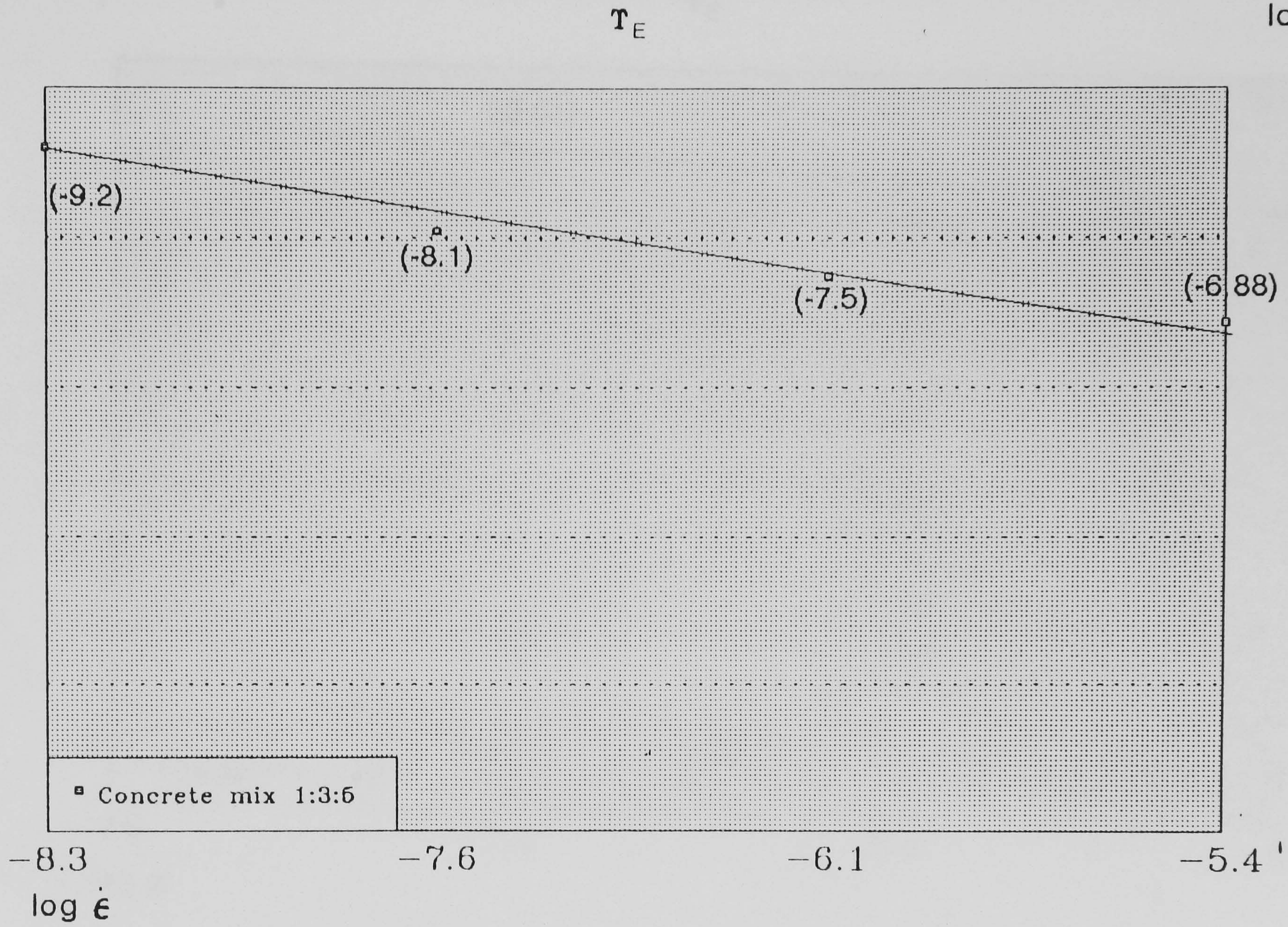

Fig. 2.63 Variation of fluidity parameter with strain-rate in tension
Concrete mix 1:2:4

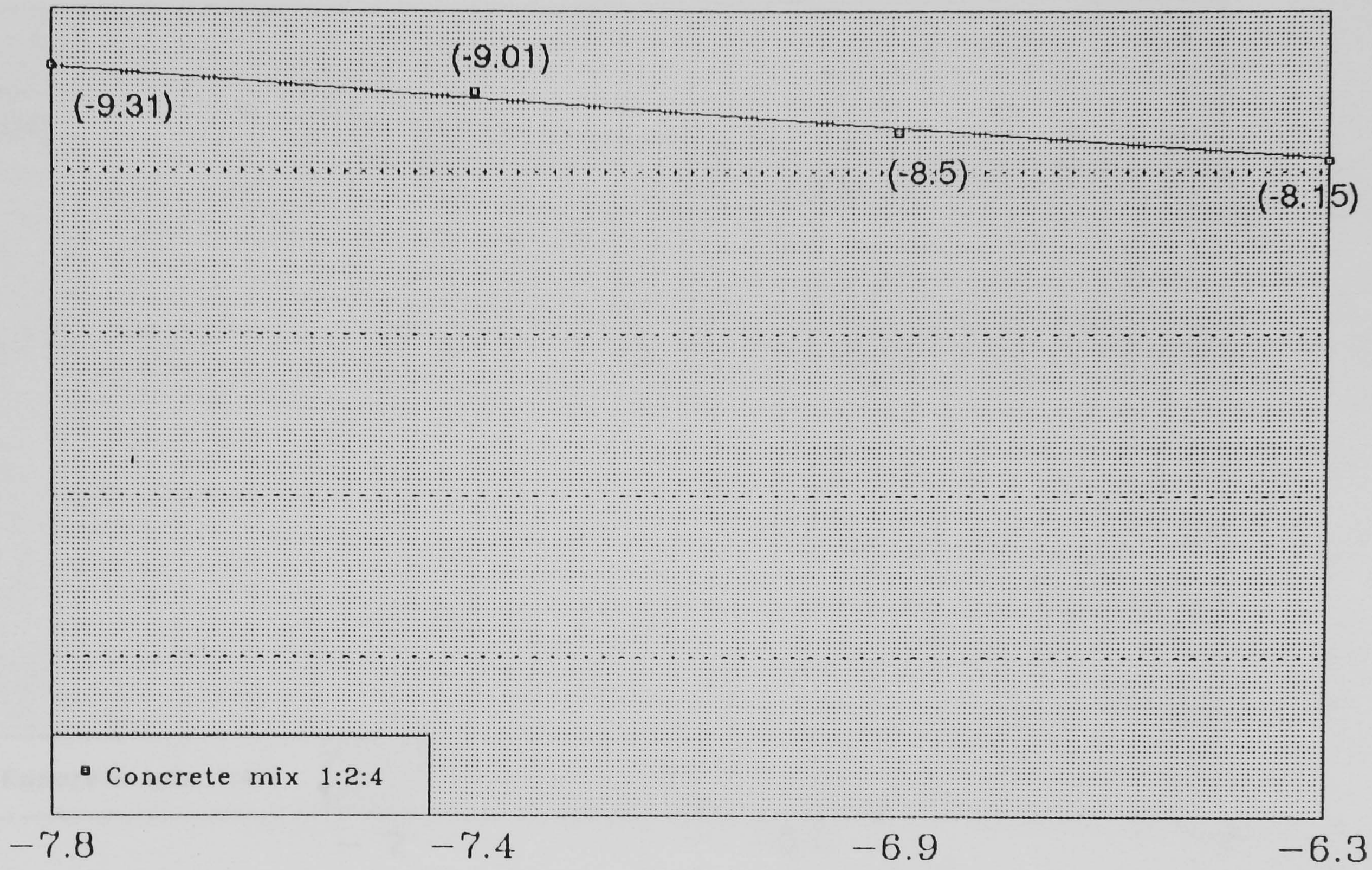

Fig 2.64 Variation of fluidity parameter with strain-rate in tension
Concrete mix 1:4:7

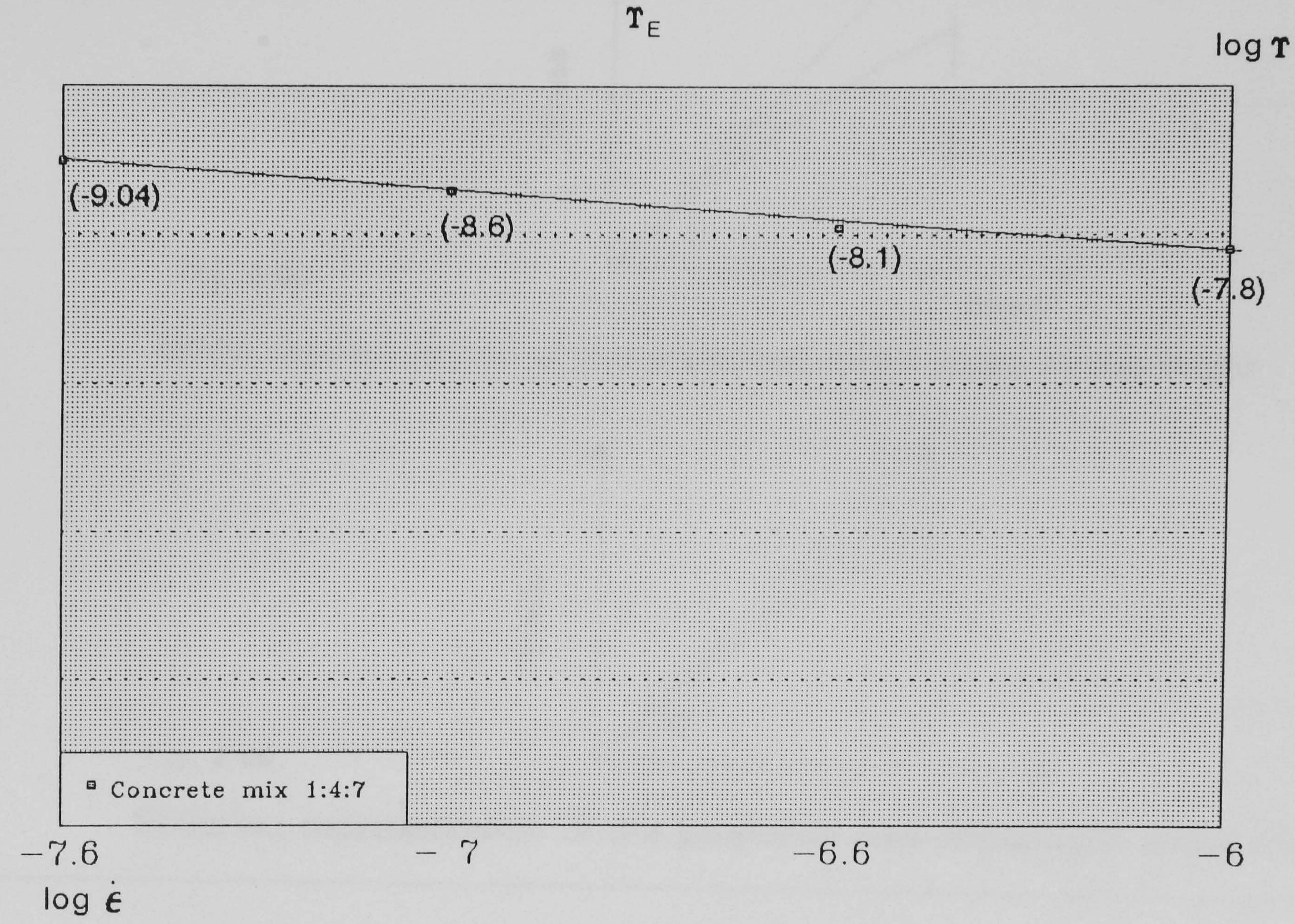

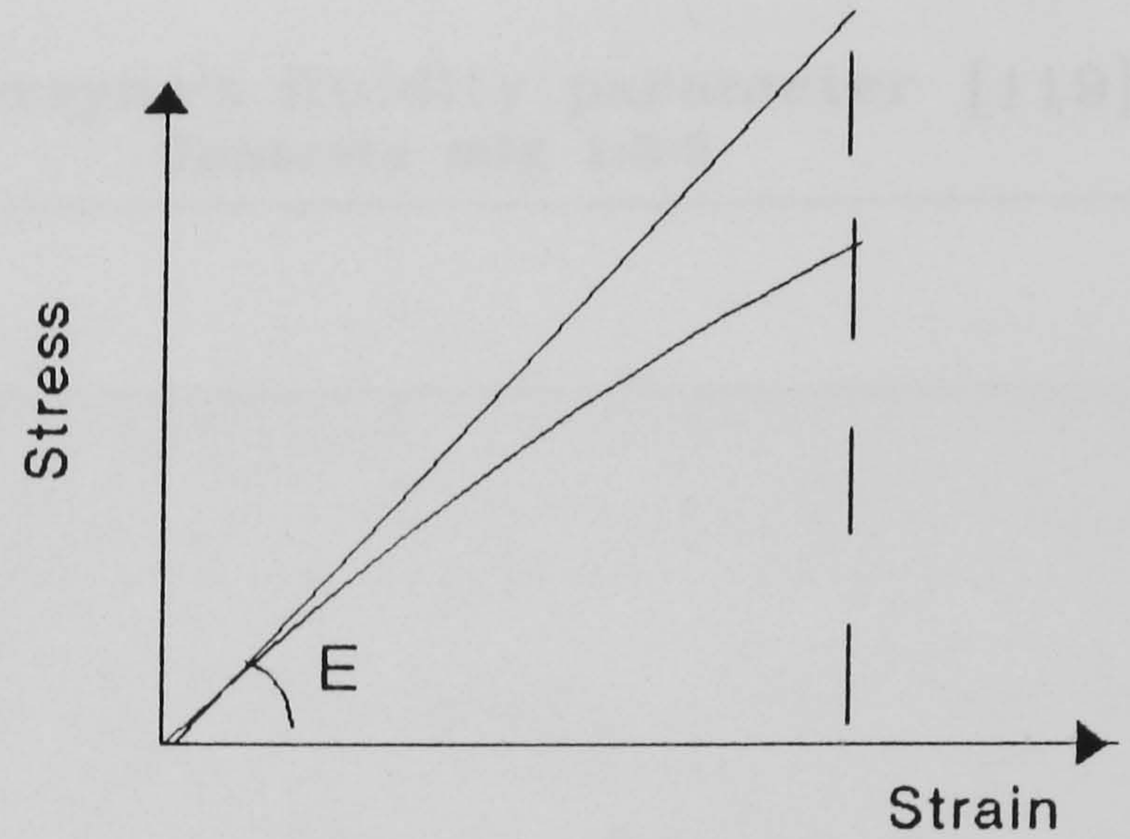

Fig. 2.65

Sratic representation of the proposed quasi-static stress-strain

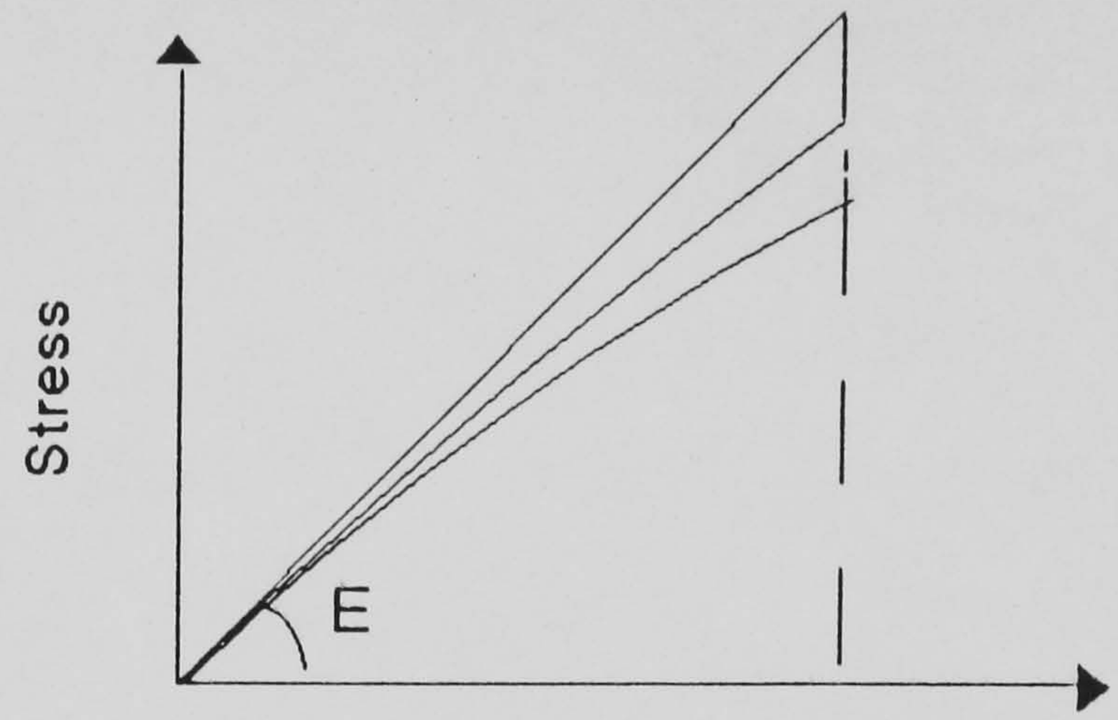

Fig. 2.66

Stiffened representation of the proposed rate-dependent stress-strain

Fig 2.67 Variation of Persyna's fluidity parameter [119] with strain-rate
Concrete mix 1:3:5

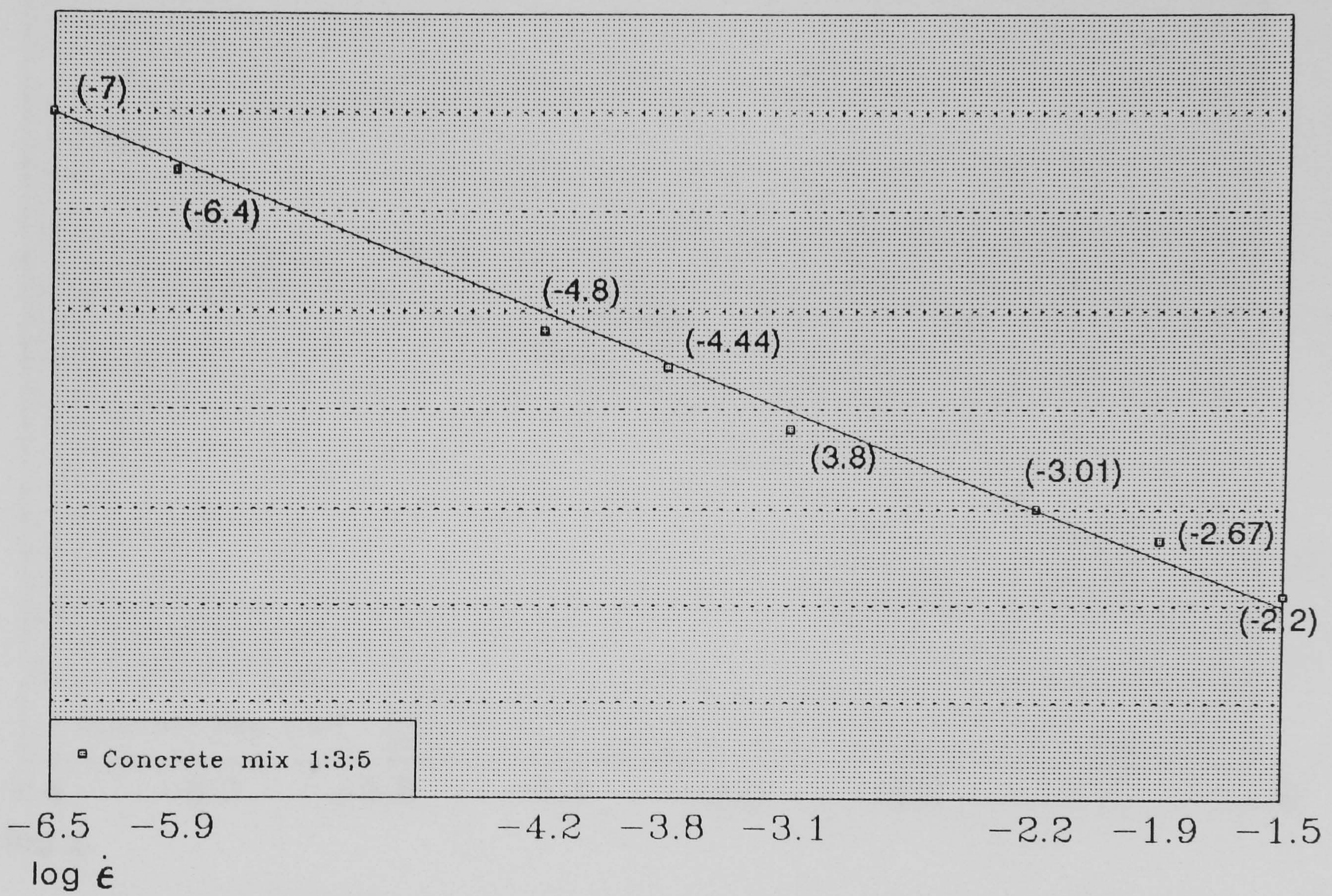

Fig 2.68 Variation of Persyna's fluidity parameter [119] with strain-rate
Concrete mix 1:4:7

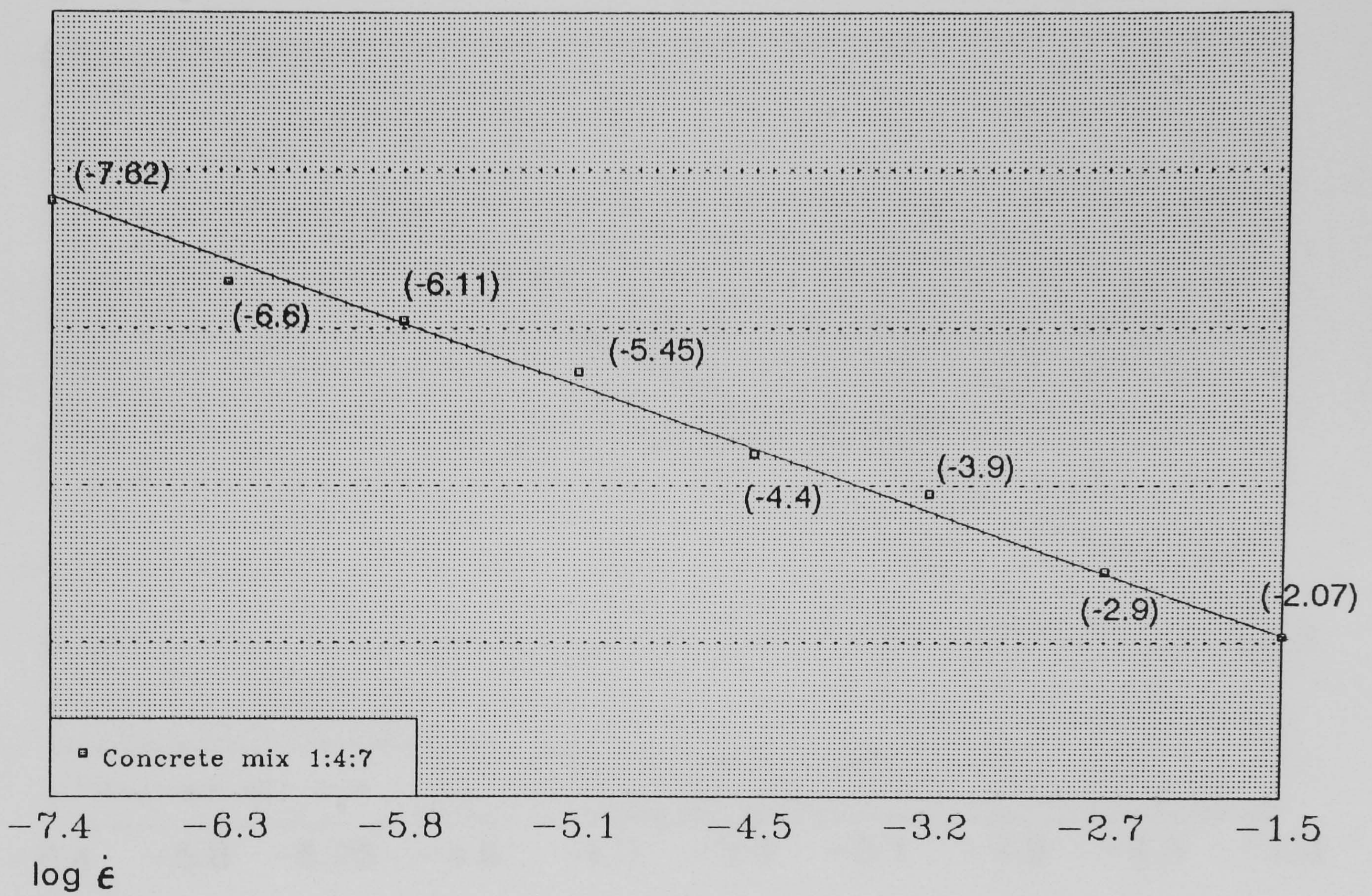

Fig. 2.69 Variation of Persyna's fluidity parameter [119] with strain-rate
Concrete mix 1:2:4

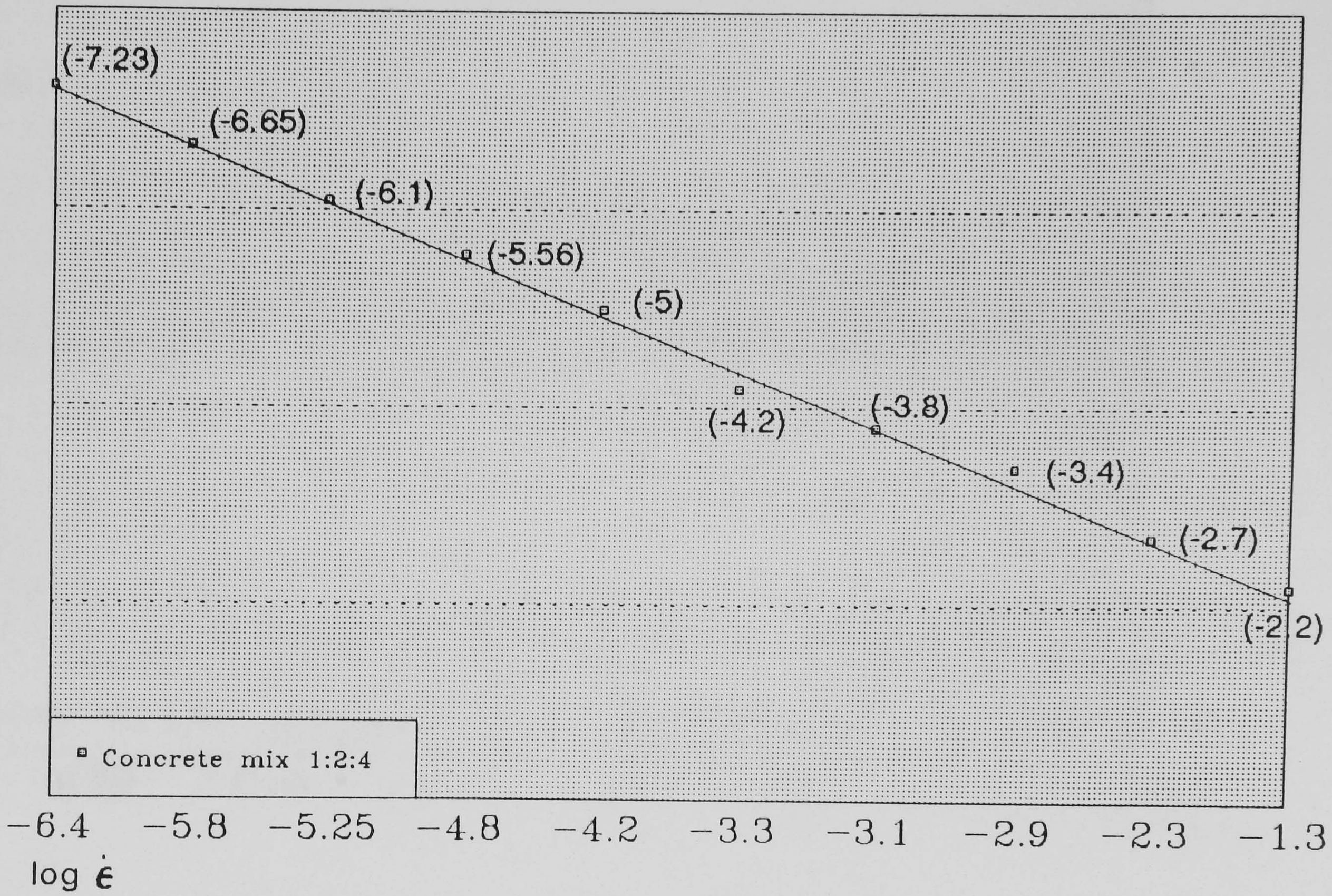

Fig 2.70 Variation of stiffening and strengthening fluidity parameter with strain-rate
Concrete mix 1:4:7

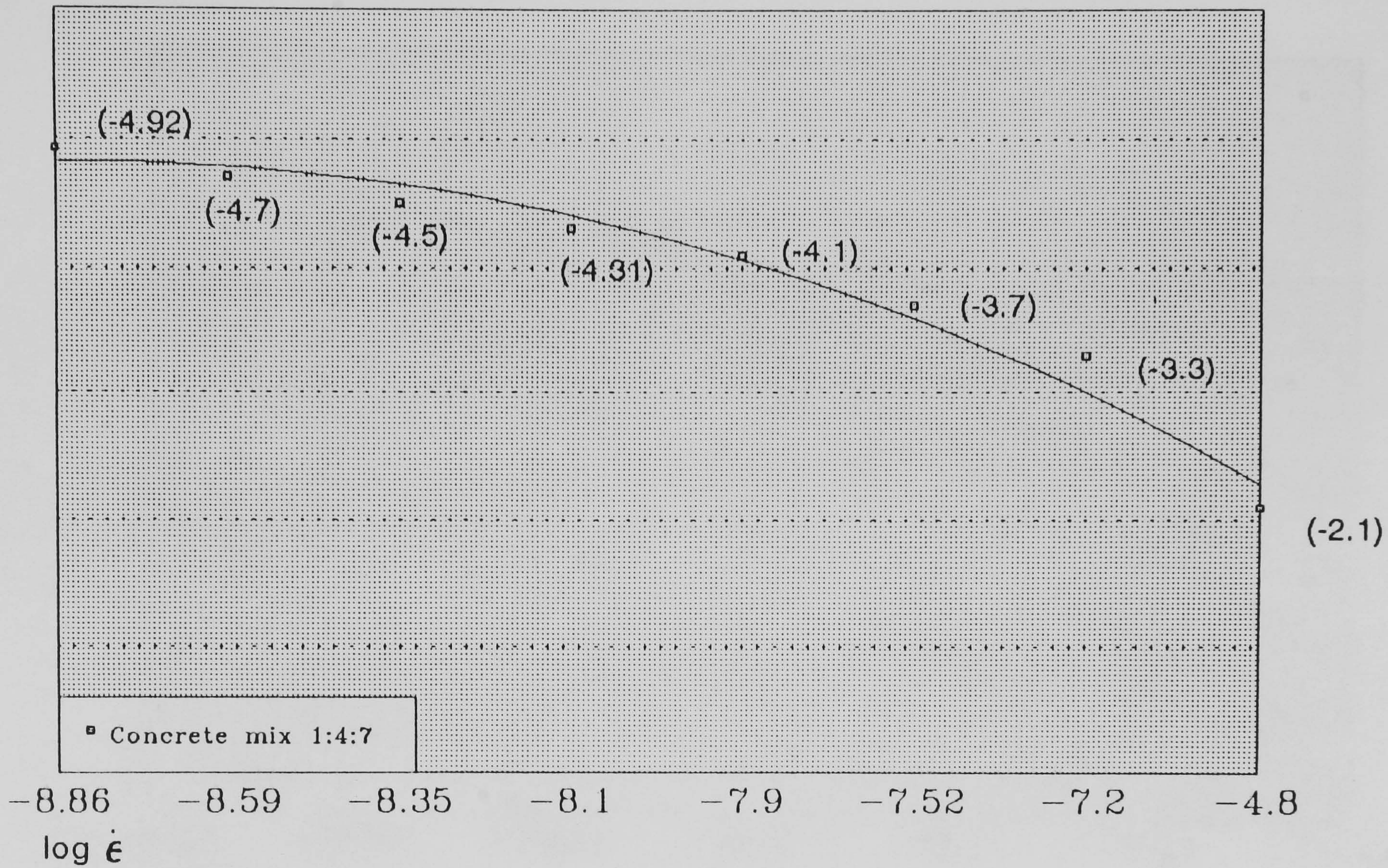

Fig 2.71 Variation of stiffening and strengtheninh fluidity parameter with strain-rate
Concrete mix 1:2:4

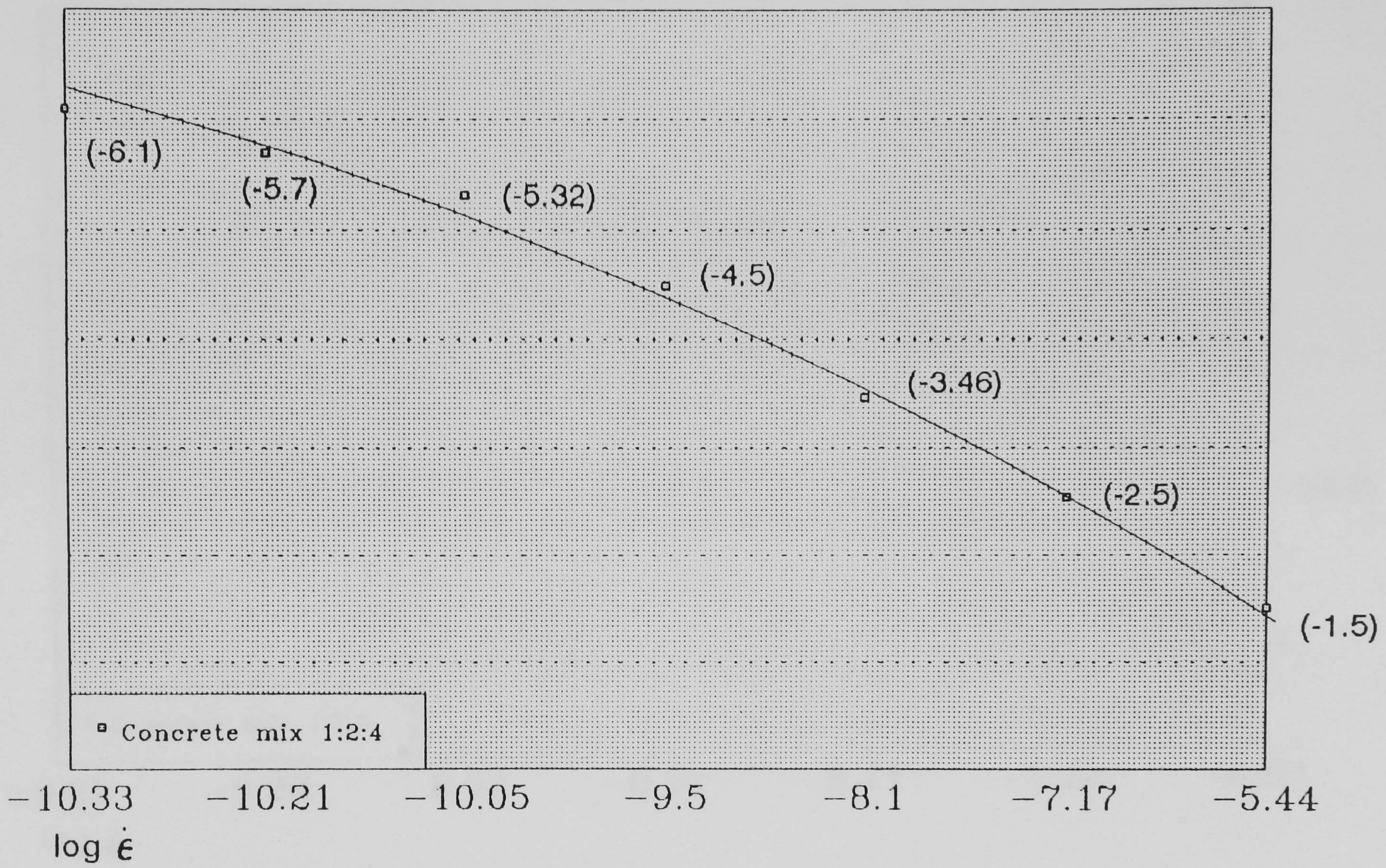

Fig 2.72 Variation of stiffening and strengthening fluidity parameter with strain-rate
Concrete mix 1:3:5

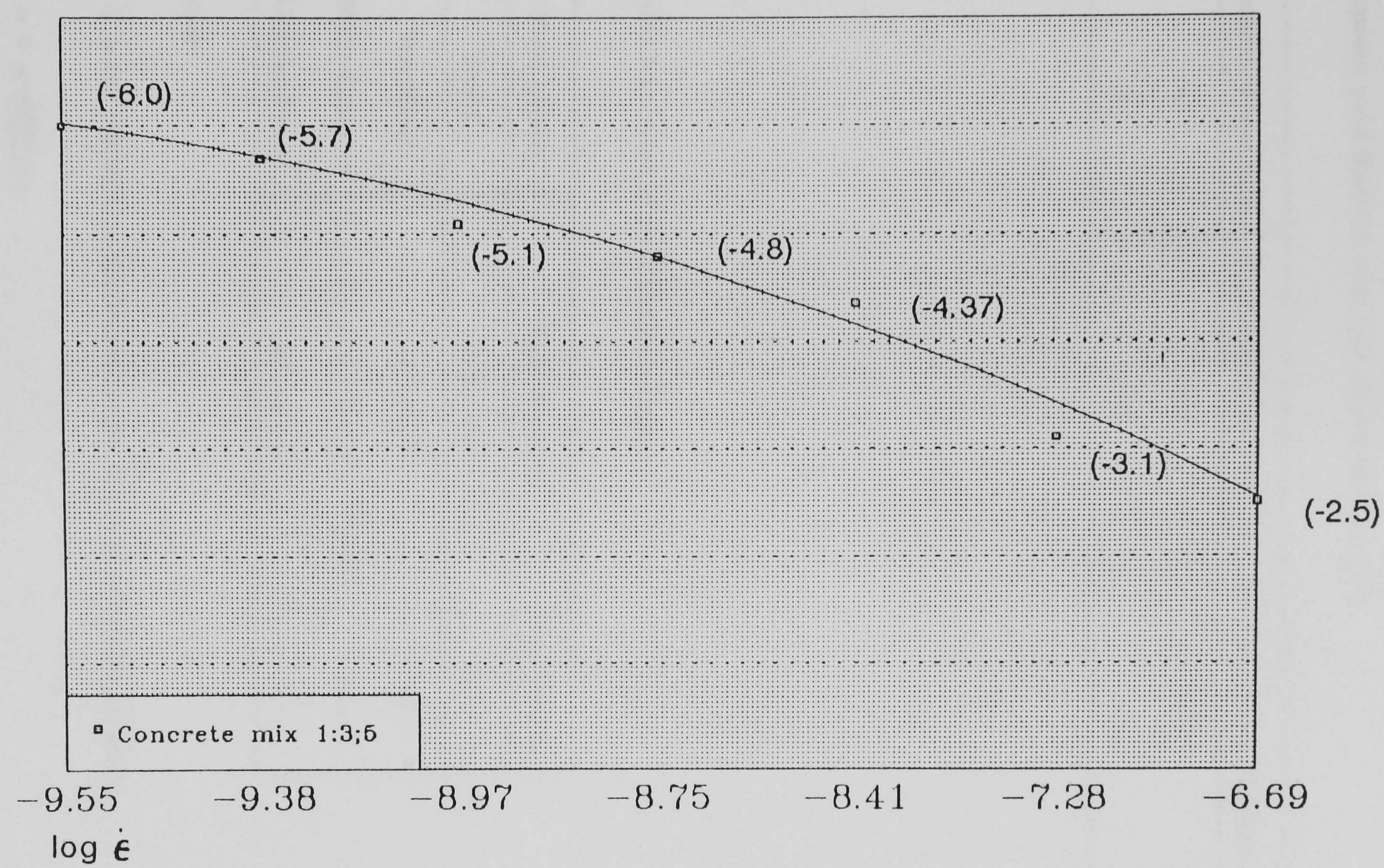

Table 2.1 Comparison of the two-parametric form of the proposed yield function with that of Hinton et al. [41].

Empirical constants	Proposed failure function	Hinton's failure function
a_1	0.18	0.177
b_1	1.36	1.35

Table 2.2 - A set of yield function forms.

Yield criteria	Yield function	Yield stress
Tresca	$2(\acute{J}_2)^{\frac{1}{2}} cos\theta$	Y(k)
Von Mises	$3^{.5}(\acute{J}_2)^{.5}$	Y(k)
Mohr-Coulomb	$\frac{1}{3}J_1 sin\varphi + (\acute{J}_2)^{.5}[cos\theta - \frac{sin\theta sin\varphi}{3^{.5}}]$	$Ccos\varphi$
Drucker-Prager	$\alpha J_1 + (\acute{J}_2)^{.5}$	$\acute{K}$

Notes:

- C is the cohesion, φ the friction angle, Y(k) the uniaxial yield stress
- $\alpha = \frac{2sin\varphi}{[3^{.5}(3 \pm sin\varphi)]}$
- $\acute{k} = \frac{6Ccos\varphi}{3^{.5}(3 \pm sin\varphi)}$

Table 2.3 -Empirical constants for the proposed fluidity parameter corresponding to dynamic modulus of elasticity in tension.

$$\gamma_E = \lambda_2 \dot{\epsilon}^{\lambda_1}$$

Empirical constants for concrete mix	λ_1	λ_2
1:4:7	0.75	0.0369
1:3:5	0.8	0.0773
1:2:4	0.77	0.0362

Table 2.4 -Empirical constants for the proposed fluidity parameter corresponding to dynamic modulus of elasticity in compression.

$$\gamma_E = \lambda_2 \dot{\epsilon}^{\lambda_1}$$

Empirical constants for concrete mix	λ_1	λ_2
1:4:7	0.82	0.013
1:3:5	0.48	0.0026
1:2:4	0.76	0.0137

Table 2.5 -Empirical constants for the proposed Perzyna's fluidity parameter γ_P [119] .

$$\gamma_P = P_2 \dot{\epsilon}^{P_1}$$

Empirical constants for concrete mix	P_1	P_2
1:4:7	0.946	0.52
1:3:5	0.930	0.41
1:2:4	0.968	0.4

Table 2.6 -Empirical constants for determining fluidity parameter γ_T corresponding to the concrete stiffening and strengthening.

$$\gamma_T = T_3 \dot{\epsilon}^{T_2} e^{T_1 (\ln \dot{\epsilon})^2}$$

Empirical constants for concrete mix	T_1	T_2	T_3
1:4:7	-0.22	-0.78	6.11×10^{-4}
1:3:5	0.066	1.38	0.026
1:2:4	0.184	2.461	0.07

Chapter 3

Finite Element Spatial Discretisation

3.1 Introduction

The finite element method is a numerical technique which can be used for the accurate solution of complex engineering problems. The method was first developed in 1956 for the analysis of aircraft structural problems [129]. Thereafter, the potential of the method for the solution of different types of applied sciences and engineering problems was recognized. Over the years, the finite element technique has become established such that today it is considered to be one of the best and most powerful methods for solving a wide variety of practical problems efficiently.

One of the main reasons for the popularity of the method in different fields of engineering is that, once a general computer program is written, it can be used for the solution of many problems simply by changing the input data. The finite element literature is very large and in a chapter this size it would scarcely be possible even to list the publications [129-133].

Application of the technique to reinforced concrete beams was first reported by Ngo [61]. Thereafter, it has been recognized as a powerful approach for linear and non-linear static and dynamic analysis of reinforced concrete structures which

may possess arbitrary geometry, loading and unloading, support conditions, irregular stiffening, and many other aspects of practical design. The complexity of time-dependent loadings such as those due to impulse or seismic effects, and the various types of concrete and steel, necessitates the use of finite elements in the analysis of impulsive resistant structures. This approach enables the response of such structures to be more accurately modelled.

The objectives of this chapter can be summarized as follows

- To introduce the finite element formulations necessary for the spatial and time discretisation of reinforced concrete structures under transient forces particularly earthquake loading.

- To assess the efficiency and accuracy of currently-used lumped matrix produced from a consistent mass matrix.

- To propose a method for determining lumped mass matrices for square and rectangular serendipity elements and to assess its accuracy.

- To discuss and assess the effect of classical damping on the response of reinforced concrete structures.

The chapter opens with a general description and the classification of dynamic problems and continues with a presentation of the formulation and numerical integration in finite element spatial discretisation. The equation of motion for the structures under transient and seismic loads is discussed. The chapter continues with a discussion of the various methods of producing lumped mass from consistent mass. The next section is devoted to a description of the proposed lumped mass scheme. Classical damping and non-classical damping are the subsequent subjects of discussion. The chapter closes with a description the Rayleigh Damping method.

3.2 Dynamic problems

The term *'dynamic '* implies that the *'inertia'* terms and the *'damping'* should be included in the equations of equilibrium. Among the many situations where dynamic action has to be incorporated in the analysis and design are:

- The impact loading of structures due to shock blast or explosive conditions in which the loading is applied in a short period with a high rate.
- Seismic action where the loading takes the form of a prescribed acceleration history,
- In the nuclear and chemical industries, where off-shore oil-drilling platforms and associated support equipment are subjected to undersea seismic action and wind-wave loading.

3.2.1 Classification of dynamic problems

In dynamic problems, the excitation load is usually defined in either a spectral form or as a given loading-time history. Generally linear or non-linear problems may be classified depending on the effect of the spectral characteristics of the excitation on the overall structural response as wave propagation problems and *'structural dynamics'* problems (or inertial).

Wave propagation problems

In problems involving shock-type excitations and wave propagation-type responses, the behaviour at the wave front is of engineering importance. It is the intermediate and high-frequency structural modes that dominate the response through the time span that are of interest. Explosive or impact loading and problems, in which wave effects such as focusing, reflections and diffractions are important, fall into this category.

Structural dynamic inertial problems

In these type of dynamic problems, the response is governed by a relatively small number of low-frequency modes. This class includes dynamic problems which are not wave-propagation type, such as structures under seismic loading. The dominant philosophy has been that the partial differential equations which represent the problem in space and time are first discretised in space. The result of space-discretisation of a structural dynamics problem is a system of second order ordinary differential equations in time.

3.2.2 Governing equations for structural dynamics.

To solve transient structural problems numerically, the governing partial differential equations are first discretised in space. This procedure is called *' semi-discretisation'*. The finite element method will be used to semi-discretise the governing equations. The equations then have to be integrated with respect to time to complete the solution process. In dynamic analysis of structures, the governing semi-discretise equations of motion are obtained by considering the static equilibrium at time t and including the effect of the acceleration-dependent inertia forces $F(t)^i$ in addition to damping nodal force $F(t)^d$, internal nodal forces $F(t)^{int}$ and externally applied descritised forces $F(t)^{ext}$. These may be written as

$$F(t)^i + F(t)^d + F(t)^{int} = F(t)^{ext} \tag{3.1}$$

where

$$F(t)^i = M\ddot{X} \tag{3.2}$$

is a vector of inertia forces

$$F(t)^d = C\dot{X} \tag{3.3}$$

is a vector of damping forces

$$F(t)^{int} = KX \tag{3.4}$$

is a vector of internal resisting forces, including forces due to initial stresses, and $F(t)^{ext}$ is a vector of external forces. The sign of $F(t)^{ext}$ is positive if the

external force is applied to the nodes, and negative if it is applied to the base of the structure e.g. earthquake loading. The subscript (t) denotes the time-dependence of the problem and the superscript (.) denotes time derivatives (e.g. $\ddot{X}$ is the acceleration vector). Thus Equation (4) may be written as

$$M\ddot{X} + C\dot{X} + KX = F(t)^{ext} \tag{3.5}$$

where M is the structural mass matrix and C is the structural damping matrix.

Equilibrium equation

The equation of static equilibrium governing the linear dynamic response of a semi-discrete structural system at time t is derived from either the Lagrange Equation or Hamilton's Principle [129].

The procedure involves deriving the finite element equations of motion by discretising the displacement model which for two dimensional problems is written as:

$$X(x, y, t) = [N(x, y)]^T Q^e(t) \tag{3.6}$$

where X is the vector of displacements, N is the matrix of shape functions and Q^e is the vector of nodal displacements which is also a function of time t.

The strain vector can be expressed as

$$\epsilon = BQ^e(t) \tag{3.7}$$

and the stress vector as

$$\sigma = D\epsilon = DBQ^e(t) \tag{3.8}$$

where B and D are the strain-displacement and material stiffness matrix, respectively.

Differentiating Eq. (3.6) with respect to time gives

$$\dot{X} = [N(x, y)]^T \dot{Q}^e(t) \tag{3.9}$$

where $\dot{Q}^e$ is the vector of nodal velocities.

The Lagrange equations are given by

$$\frac{d}{dt}[\frac{\partial L}{\partial \dot{Q}}] - \frac{\partial L}{\partial Q} + \frac{\partial R}{\partial \dot{Q}} = 0 \tag{3.10}$$

where

$$L = T - P_p \tag{3.11}$$

is called the Lagrangian Function. In Eq. (3.10) and Eq. (3.11), T is the kinetic energy, P_p is the potential energy, R is the dissipation function, and $\dot{Q}$ is the nodal velocity.

The kinetic and potential energies of an element 'e' can be expressed as:

$$T^e = \int\int_v \rho \dot{X}^T \dot{X}\, dv \tag{3.12}$$

$$P_p = 1/2 \int\int_v \epsilon^T \sigma\, dv - \int_v X^T \varphi\, dv - \int_s X^T \varphi\, ds \tag{3.13}$$

where v is the volume, ρ is the density and $\dot{X}$ is the vector of velocities of the element 'e', and s is that portion of the element surface on which the distributed force is applied. If the dissipative forces are assumed to be proportional to the relative velocities, the dissipation function of the element 'e' can be expressed as

$$R^e = 1/2 \int\int_v c\dot{X}^T \dot{X}\, dv \tag{3.14}$$

where c is called the damping coefficient, which will be explained in subsequent sections.

In Eqs. (3.12) to (3.14), the volume integration has to be taken over the volume of the element. The expressions for T, P_p and R can be obtained using Eqs. (3.10) to (3.14), as

$$T = \Sigma T^e = 1/2 \dot{Q}^T [\Sigma \int\int_v \rho N^T N\, dv] \dot{Q}^T] \tag{3.15}$$

$$P_p = \Sigma P_p^e = 1/2 \dot{Q}^T [\Sigma \int\int_v B^T D B]\, dv] Q - Q^T [\Sigma \int_s N^T \varphi(t)\, dS + \int\int_v N^T \varphi\, dv] - Q^T P_C(T)] \tag{3.16}$$

$$R = \Sigma R^e = 1/2 \dot{Q}^T [\Sigma \int\int_v cN^T N\, dv] \dot{Q}] \tag{3.17}$$

where Q and $\dot{Q}$ are the global nodal displacement vector and global nodal velocity respectively, and P_c is the vector of concentrated nodal forces of the structure.

Now, the matrices involving the integrals may be defined as

- Element mass matrix $M^e = \int\int_{V_e} \rho N^T N \, dv$
- Element stiffness matrix $K^e = \int\int_{V_e} B^T D B \, dv$
- Element damping matrix $C^e = \int\int_{V_e} c N^T N \, dv$
- Vector of element surface force $P_S^e = \int_{S_e} N^T \varphi \, ds$
- Vector of element body force $P_b^e = \int\int_{v_e} N T \varphi \, dv$

By writing Eqs. (3.12) to (3.14) in the form

$$T = 1/2 \dot{Q}^T M \dot{Q} \tag{3.18}$$

$$P_P = 1/2 Q^T K Q - Q^T P \tag{3.19}$$

$$R = 1/2 \dot{Q}^T C \dot{Q} \tag{3.20}$$

the following terms may be defined

- Total mass matrix of the structure. $M = \Sigma M^e$
- Total stiffness matrix of the structure $K = \Sigma K^e$
- Total damping matrix of the structure $C = \Sigma C^e$
- Total load vector $P(t) = \Sigma(P_s^e(t) + P_b^e(t) + P_c(t))$

By substituting Eqs.(3.16) to (3.18) into Eq. (3.5), the equation of motion is given by

$$M\ddot{X}(t) + C\dot{X}(t) + KX(t) = P(t) \tag{3.21}$$

where $\ddot{X}$ is the vector of nodal acceleration, $\dot{X}$ is the vector of nodal velocity and X is the vector of nodal displacement in the global system. In general, the mass matrix M is constant, positive definite and symmetric, the damping matrix C is positive semi-definite symmetric or non-symmetric, and is not constant for

non-linear behaviour of a structure. K is positive definite and $P = P(t)$ is a given external force which is a function of time t.

The equations of dynamic equilibrium for a seismic response analysis can be written as

$$M\ddot{X}(t) + C\dot{X}(t) + KX(t) = -MI\ddot{X}_g(t) \tag{3.22}$$

where I is a vector containing unit values for the degrees of freedom to be excited and $\ddot{X}_g$ is the specified ground acceleration. In the solution of equations (3.21) and (3.22), it would be extremely useful from a computational viewpoint if the matrices M and C could be made diagonal. This will be discussed in Chapter 4.

3.3 Finite-element spatial discretisation

In spatial discretisation the element geometry, element strain field and element volume are required to be defined.

Following the standard procedure [129-133], the spatial domain v is divided into N finite-elements interconnected at I nodal mesh points and a set of *"shape functions"* are employed to interpolate the field variables inside each element with respect to the set of nodal values. If a single function is employed for both the geometry and the field variable, the elements are known as *" isoparametric"* , which is one of the most popular approaches and has been adopted in this study.

3.3.1 Formulation and numerical integration

Due to ease of implementation of finite element analysis and its ability to account easily for curved boundaries, has been extensively used in many static and dynamic problems. The most popular finite element families used in static and dynamic problems are:

- Lagrangian Family
- Serendipity Family

Shape function and corresponding derivatives for some linear and quadratic 2D and 3D finite-elements are summarized in Tables 3.1 A, B and C. Some vectors and matrices used with the elements are presented in Table 3.2. The accuracy and efficiency of finite element programs depend on the shape of element and also on the number of sampling points used for the numerical integration to determine the stiffness and mass matrices. The commonly used Gauss-Legendre integration rule exactly integrates a polynomial of order $(2n-1)$ with only n function evaluations and is widely used in finite element schemes. The integration order will not only cause the cost of the analysis but also may affect the results significantly, so the optimum choice of integration order is very important.

The stiffness matrix of an element can be evaluated using one of the three integration schemes.

- Exact evaluation technique.
- Reduced integration technique.
- Selective integration technique.

The order for the exact solution of stiffness matrices of 2D elements are well established and are summarized in Table 3.3.

The displacement formulation, based on the exact order of the integration rule, overestimates the stiffness matrix [129]. Lower order integration rules soften the element stiffness and, when used, the error in estimating the stiffness is compensated, this is known as *"reduced integration technique"*.

The use of an integration rule of an order lower than required for the exact evaluation has led to improvement in the results [131, 134, 136].

This technique has been successfully used for 2D, 3D plate and shell elements, see for example Zienkiewicz et al. [131].

The selective integration technique in which the different strain terms are integrated with different Gauss-Legendre rules have been successfully applied to many static and dynamic problems [131] in which exact evaluation gives poor results.Only a level reduction of order has been recommended [134-136].

The 8-noded Serendipity isoparametric element has been adopted in this study due to its efficiency in simulating the stiffness and the mass of the system. A 2 by 2 integration points has been used for spatial discretisation and a 3 by 3 Gauss points for consistent mass discretisation.

Table 3.4 shows a recommended minimum Gauss-Legendre integration order for rectangular elements [136]. A discretised loading for distributed load is illustrated in Fig. 3.1.

3.3.2 Stiffness matrix formulation

For a 2D finite element,the stiffness matrix is given in general form as

$$K^e = \int_v B^T D B dx dy \tag{3.23}$$

where, v is the element volume, D and B are the material elastic modulus and strain-displacement matrices respectively. The strain-displacement matrix denoted by B is evaluated in the natural-coordinate system (ξ, η) and is transferred into the cartesian-coordinate by the Jacobian matrix as. then, the cartesian shape function derivatives are obtained using chain rule differentiation. The Jacobian matrix J is used to convert the local coordinate to the global coordinate.

$$\begin{bmatrix} \frac{\partial}{\partial \xi} \\ \frac{\partial}{\partial \eta} \end{bmatrix} = \begin{bmatrix} \frac{\partial x}{\partial \xi} & \frac{\partial y}{\partial \xi} \\ \frac{\partial x}{\partial \eta} & \frac{\partial y}{\partial \eta} \end{bmatrix} \begin{bmatrix} \frac{\partial}{\partial x} \\ \frac{\partial}{\partial y} \end{bmatrix} \tag{3.24}$$

The discretised elemental volume is given by

$$dv_e = detJ \times t_e \times d\xi d\eta \tag{3.25}$$

where det J is the determinant of the Jacobian matrix and t_e is the element thickness. The element characteristic matrix is evaluated numerically at the element level using the Gauss quadrature formula with desired sampling points, which leads to

$$\begin{aligned} \int_{v_e} F_{ij}(x,y) dv &= \int_{-1}^{+1} \int_{-1}^{+1} F_{ij}(\xi,\eta) \times t \times detJ d\xi d\eta \\ &= \sum_{P=1}^{m} \sum_{q=1}^{n} F_{ij}(\xi_p, \eta_q) \times t \times detJ W_p W_q \end{aligned} \tag{3.26}$$

where F_{ij} is the function to be numerically integrated, ξ_p, η_q are the natural coordinates of sampling points, with W_p, W_q as the corresponding weighting functions. Summing the stiffness on all of Gaussian points yields the element stiffness.

3.3.3 Mass matrix formulation

The mass matrix in Eqs. (3.21) and (3.22) is known as *'consistent'* because the same displacement function as is used for deriving the element stiffness matrix is used for the mass matrix. However, some investigators [137-139] have found that the use of consistent masses does not always lead to high accuracy while it always involves extensive computational work.

In some dynamic problems, an alternative mass matrix, produced from the consistent mass matrix known as *' lumped* , has been used for two reasons: simplicity and the requirement of less computational effort due to the possibility of decoupling the equations of motion. The lumped mass matrix is based on the assumption that concentrated masses, which refer to the translational and rotational inertia of the element, are calculated by assuming that the material within the mean locations on either side of the particular displacement behaves as a rigid body while the remainder of the element does not participate in the motion.

The rationale is that the product $\sum m_{i=1}^{N} \ddot{x}$ in any lumped mass matrices must yield the correct total inertial force on an element according to Newton's Law $F = M\ddot{X}$. This is easily obtainable with acceptable accuracy when only 'translational' displacements are included. Convergence to the correct results may not occur in cases when the elements are included in 'rotational' degrees-of-freedom.

In the next section, some lumped mass matrices produced from a consistent matrix are explained briefly.

3.3.4 Producing lumped matrix from consistent mass matrix

A very convenient simplification is achieved by lumping the element mass to the nodes. A lumped mass matrix is obtained by placing particle masses m_e^i at node i of an element such that M_e^i becomes the total element mass, i. e.

$$M_i^e = \sum_{i=1}^{N} m_i^e \tag{3.27}$$

HRZ lumping scheme

The HRZ scheme is an effective method for producing a diagonal mass matrix. The idea is to use only the diagonal terms of the consistent mass matrix but to scale them in such a way that the total mass of the element M is preserved. First, a number 'S' is computed by adding the diagonal coefficients m_{ii}, associated with translational d.o.f. (but not the rotational d.o.f., if any) that are mutually parallel and in the same direction. Then, all the diagonal coefficients are scaled by multiplying them by the ratio M_e/S, that is

$$m_{ii} = m_{ii}\frac{M_e}{S} \tag{3.28}$$

thus preserving the total mass of the element, as shown in Fig. 3.2.

Ad Hoc lumping scheme

Another scheme to produce a diagonal mass matrix which is widely used is the Ad Hoc method in which the particle mass m_{ii} is placed at node i of an element such that $\sum m_{ii}$ is the total element mass.

When the rotary inertia is included in the problem, producing a lumped mass matrix from a consistent mass matrix become more difficult. For example, the diagonal mass matrix in a beam element is obtained in the form

$$m = m/2[1, \alpha L^2/210, 1, \alpha L^2/210] \tag{3.29}$$

where the second and fourth terms define the rotary inertia. The rotary inertia can be selected as the mass moment of inertia I_R of a uniform slender bar of

length L/2 and mass m/2 spinning about one end, that is, $I_R = (m/2)(l/2)l/3$ to be preserved from which $\frac{4ml^2}{420} \times \alpha = \frac{1}{6}ml^2$ leads to $\alpha = 17.5$.

Optimal lumping scheme

In this approach, the element nodes are chosen as the sampling points of the quadrature rule used for integrating the consistent mass $\int \rho N^T N \, dv$. Since the integration points are coincident with the nodal locations of the element having translational degrees-of-freedom only, then no off-diagonal terms are generated. In this approach, some of the terms may be negative or zero, which is the weakness of the method and can lead to imaginary frequencies.

3.3.5 Proposed lumped mass method

Hinton et al. [138, 139] have proposed a lumped mass scheme which was tested using examples of the vibration of a simply supported, square, thick plate with a 4×2 mesh for half of the plate. It was concluded that, in general, the proposed lumping scheme was at least as good as the use of a consistent mass matrix for the lower modes while better results were obtained for higher modes. The recommended lumping scheme, was based on assigning of areas of influence for two-dimensional parabolic elements as shown in Fig. 3.3. The lumping mass scheme proposed by Hinton et al. [139] has been obtained from a square mesh of a thick plate.

An alternative mass lumping scheme for rectangular elements based on the optimal lumped mass approach is proposed. The two-dimensional form of the Newton-Cotes formula has been chosen to determine an approximate solution to the consistent mass integral $\int_v N^T \rho N dv$. For the rectangular element shown in Fig. 3.4. This can be written as

$$\int_a^b \int_c^d f(x,y)dxdy = \frac{(d-c)(b-a)}{36}\{f(c,a) + 4f(\frac{c+d}{2},a) + f(d,a)$$
$$+4f(c,\frac{a+b}{2}) + 16f(\frac{c+d}{2},\frac{a+b}{2}) + 4f(d,\frac{a+b}{2}) + f(c,b)$$
$$+4f(\frac{c+d}{2},b) + f(d,b)\} \quad (3.30)$$

where (a, d), (b, d), (b, c), (a, c) are the coordinates of the corner nodes in global coordinate system.

The consistent mass matrix for a rectangular element is given by

$$M = \rho \int_a^b \int_c^d N_i^T N_j dxdy$$
$$= \rho J \int_{-1}^{+1} \int_{-1}^{+1} N_i^T N_j d\xi d\eta \quad (3.31)$$

in which the Jacobian J is $\frac{(d-c)(b-a)}{4}$. The mass associated with the first term of the lumped mass matrix in the proposed lumped mass scheme has been approximated by the first term of Eq. (3.30) which can be determined by substituting ($\xi = -1$, $\eta = -1$) into Eq. (3.31) such that

$$m_{11} = \rho J \int_{-1}^{+1} \int_{-1}^{+1} N_j(-1)N_i(-1)d\xi d\eta \quad (3.32)$$

According to the Sturm theorem [141] which will be discussed in more detail in chapter 5, the natural frequencies of a system decrease and tend to the correct values as the numbers of degrees-of-freedom of the system is increased. The fundamental natural frequency of the rectangular 8-noded element can also be achieved by increasing the lumped mass at each corner nodes while the total element mass is preserved. A cantilever has been analysed using consistent mass matrices. The number of elements increased until the fundamental natural frequency had converged. This was then used as a reference.

Since the terms of the lumped mass of an 8-noded element is to be determined, the ninth term of Eq. (3.30) which correspondents to a central node has to be distributed between the nodes with the weighting to the mid-nodes twice that of the corner nodes.

Integrating Eq. (3.30) and distributing the weight of center node to the edge-nodes with that of ninth-term and evaluating the first eight natural frequencies to be closest to those of the consistent mass leads to

$$m_{11} = 0.0735M \tag{3.33}$$

for a square element. For a rectangular element with aspect ratio $R = \frac{h}{L}$ Fig. 3.4

$$m_{11} = \frac{0.0958}{1 + 0.2946R}M \tag{3.34}$$

The natural frequencies obtained from the proposed method for a square and rectangular element are compared with those of Hinton et al. [138] and Smith et al. [116]. As can be seen, the proposed lumped mass scheme is more accurate than those of the other investigators.

Remarks

- Since the kinetic energy is positive, that is, $\dot{X}^T M\dot{X}/2 > 0$ for all $\dot{X} \neq 0$, then the consistent mass matrices are positive definite.

- The consistent mass matrix determination is similar to the standard stiffness matrix determination. Mass coefficients are computed for individual elements of the structure and combined by simple superposition to obtain the mass matrix for the complete system.

- Lumped mass matrices are simpler to form, occupy less storage space, and consequently require less computational effort.

EXAMPLE

The proposed lumped mass scheme has been examined by determining the natural frequencies of a cantilever beam.

The has been spatially discretised using 8-noded square and rectangular serendipity isoparametric elements Figs. 3.5 A and B. The proposed formula for producing a lumped mass matrix form a consistent mass matrix has been used. In order to compare the accuracy of the proposed lumped scheme, the beam mesh has

been refined until convergence of natural frequencies were obtained by using consistent mass. The natural frequencies obtained from the proposed lumped mass for square and rectangular elements with span-ratio R are compared with those obtained by Hinton et al. [138, 139] and Smith et al. [116] Tables 3.5 and 3.6. It can be seen that, the proposed lumped scheme results in the natural frequencies close to those of using a consistent mass matrix.

Table 3.5 Comparison of the first 8 natural frequencies of a cantilevere beam obtained from different approaches using the Lumped Mass Matrix.

Mode number	N. F. of a square mesh	N. F. using lumped mass and elements with $R = 1$		
	Consistent mass	Smith method	Hinton method	Proposed method
1	25.4410	0.9801	1.0047	0.9993
2	130.6980	0.9690	0.9718	0.9770
3	164.6241	0.9202	0.9611	0.9661
4	303.1368	0.8912	0.9596	0.9601
5	492.9398	0.8560	0.9324	0.9547
6	495.5648	0.8410	0.8870	0.9255
7	702.5973	0.8005	0.8800	0.8730
8	817.2678	0.7876	0.8120	0.8026

Table 3.6 Comparison of the first 8 natural frequencies of a cantilevered beam obtained from different approaches using the Lumped Mass Matrix.

Node number	N. F. of a square mesh consistent mass	N. F. using lumped mass and elements with $R = 1.34$		
		Smith Method	Hinton Method	Proposed Method
1	25.4410	0.9716	0.9740	0.9862
2	130.6980	0.9426	0.9444	0.9530
3	164.6241	0.9301	0.9303	0.9391
4	303.1368	0.9106	0.9118	0.9187
5	492.9398	0.8598	0.8606	0.8664
6	495.5648	0.8321	0.8342	0.8397
7	702.5973	0.8001	0.8072	0.8448
8	817.2678	0.7902	0.7940	0.8277

3.4 Damping matrix formulation

In practical structures, the damping force in equations (3.21) and (3.22), is not solely a viscous mechanism but is also due to dissipative mechanisms such as friction in the structural joints, elastic-plastic hysteretic loss, and material micro-cracking, none of which are well understood. The selection of realistic damping values for a particular structure should be based on experimental evidence from other structures of similar geometry and material. Due to the complexity of the damping mechanism in structures, the damping is customarily introduced as a fraction of the critical damping $c_c = 2 \times \omega m$, denoted by ξ called *'the damping ratio'* i. e., the damping for which the oscillatory response of a structure under free vibration transmits to non-oscillatory response. If the damping is less than the critical value, i. e. $\xi < 1$, the amplitude of free vibration experiences a logarithmic decay [140-144]

$$A_D = A_F e^{-2\omega\xi} \tag{3.35}$$

where A_F and A_D are the defections due to free-vibration and damped-vibration of the system. The magnitude of the frictional force depends on the texture of the contact surfaces and the normal force value applied on the surface. Coulomb and viscous damping have very different energy-dissipation characteristics. The influence of Coulomb damping always diminishes as the displacement amplitude increases, while that of viscous damping remains unchanged. More details are given in [142]. Hysteretic damping which is another form of energy dissipation, is associated with the inelastic behaviour of structural materials. However, if the damping effect is small, the characteristics of hysteretic and viscous damping are very similar.

3.4.1 Classical damping

If there is a reasonable degree of homogeneity in the energy loss mechanisms throughout the structure, the independent modal assumption may be valid. In this case, the diagonal damping matrix can be simply obtained by transforming

into normal coordinates [140, 142, 143].

The proportional damping method, so-called *"classical damping"*, is traditionally used for two reasons;

1. The response of most concrete structures is not significantly influenced by coupled damping, and non-proportional damping introduces approximations which may lead to unacceptable errors [140]. However, the basic assumption in this approach is the homogeneity in the energy-loss mechanisms through the structure, otherwise it might not be an accurate method [140].
2. The simplicity and the less computational effort required in using methods with no off-diagonal terms.

A discussion of the advantages and disadvantages of these procedures was given by Clough and Mojtehedi [140]. They proposed a new method of analysis of non-classically damped systems, a method that makes effective use of undamped mode-shapes. Clough and Mojtehedi [140] proposed integration of the transformed coupled equations of motion where the transformation matrix consists of a truncated set of mode-shapes.

Based on the above, it is concluded that the damping properties of a structure are difficult to define in terms of any single mechanism. Hence structural damping is measured in terms of an equivalent viscous damping ratio, ξ , which is sufficiently accurate for most dynamic problems. The damping properties are frequency-dependent and a range of $5\%-10\%$ for the damping ratio ξ is commonly approximated in practice for various types of reinforced concrete structures.

It is worth mentioning here that there is another type of damping which is known as *'artificial algorithmic damping* which exists even if none of the aforementioned types of dampings are included, further details are given in Chapter 5.

3.4.2 Rayleigh damping scheme

It is difficult, if not impossible, in practice to determine for general finite element assemblages the element damping parameters because of its frequency-dependency. For this reason, and to avoid more computational effort, the damping matrix C, in general, is not assembled from element damping matrices but is constructed using the mass matrix M and stiffness matrix K of the complete element assemblage.

If the damping matrix is assumed to possess the same orthogonality property as do with respect to mass and stiffness matrices, i. e.

$$\varphi_i^T C \varphi_j = 0.0 \tag{3.36}$$

which is equivalent to assuming that the normal modes of the damped system are identical to those of the system (this approximation is acceptable for low values of damping), Equations (3.21) and (3.22) can be decoupled into N independent equations. If C is defined as a linear combination of orthogonal mass and stiffness matrices, it can be easily shown that C is also orthogonal [143]. A damping matrix of the form:

$$C = M \sum_b a_b \{M^{-1} K\}^b \tag{3.37}$$

where a_0, b are damping constants satisfies the orthogonality condition given by Eq. (3.36). Any desired number of terms in the Caughey series can be used to establish the damping matrix. However, since the damping only can be controlled by the modes, one would never use more than N terms, thus Equation (3.37) can be written as

$$C = M \sum_{b=1}^{N-1} a_b \{M^{-1} K\}^b \tag{3.38}$$

which can be controlled in all modes by proper selection of the damping constants $a_b (b = 0, 1, 2..., N-1)$. The damping ratio ξ at the n^{th} normal mode can be expressed as [143]

$$\xi_n = \frac{1}{2\omega_n} \sum_{b=1} a_b \omega_n^{2b} \tag{3.39}$$

For example, with $b = 0$ and $n = 1$ we have

$$C = a_0 M \tag{3.40}$$

where $a_0 = \frac{4\pi\xi_1}{T_1}$, (T is the fundamental period of the structure).

Rayleigh proposed a linear combination of the mass and the stiffness matrix in the form

$$C = \alpha K + \beta M \tag{3.41}$$

where α and β are the stiffness and mass proportional damping constants, respectively, or given Rayleigh constants.

In fact, Rayleigh used the first two terms of Eq. (3.37) with $b = 0, 1$, $n = 1, 2$, which can be written as

$$C = a_0 M + a_1 K \tag{3.42}$$

where

$$a_0 = \frac{4\pi(\xi_1 T_1 - \xi_2 T_2)}{T_1^2 - T_2^2} \tag{3.43}$$

in which T_2 is the second period of the structure. A disadvantage of Rayleigh damping is that the higher modes are considerably more damped than the lower modes for which the Rayleigh constants have been selected.

Two methods for the numerical evaluation of orthogonal damping matrices have been developed by Wilson and Penzien [143]. The first relates the modal damping ratios to the coefficients of a Caushey series and the second is a direct approach which expresses the damping matrix as the sum of a series of matrices each of which produces damping in a particular mode. The direct approach has been found to be more convenient to apply and is less numerically sensitive than the series approach.

In many dynamic problems, the assumption of proportional damping is adequate. However, in the analysis of structures with widely varying material properties, non-proportional damping may be needed. An example of a system in which non-proportional damping may be expected is a nuclear reactor containment vessel founded on soft soil. When such a system is subjected to earthquake motion, the response of the stiff massive containment structures will be modified considerably by the dynamic deformation of the soil. During this dynamic soil-structure interaction, the relatively high damping forces in the soil will induce modal coupling in the combined system. Similar behaviour may be expected in

any structure-foundation system in which significant interaction is developed and where the damping properties of the structure and the foundation medium are quite different.[144].

A time-integration procedure for dynamic analysis of so-called *'non-classical'* damped systems, has been proposed by Shrikrishna and co-workers [225] in which, owing to the presence of off-diagonal terms in the transformed damped matrix, high-frequency modes play a significant role. This procedure is an extension of the method of Clough and Mogtahedi [140]. Clough and Mojtahedi suggested integration of the transformed coupled equations of motion where the transformation is done using a truncated set of mode-shapes.

From the above discussion and since the higher modes in earthquake loading problems do not have a significant role in the structural response, which will be discussed in chapter 4, it can be deduced that a classical damping method,such as Rayleigh damping can be appropriate for dynamic analysis of reinforced concrete structures.

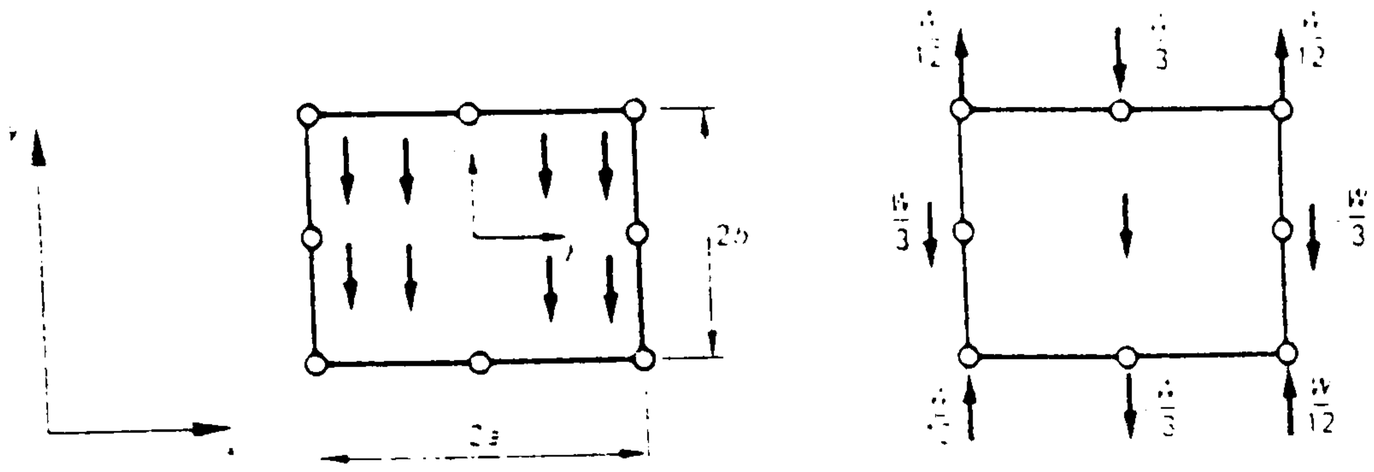

Edge loading and equivalent nodal forces.

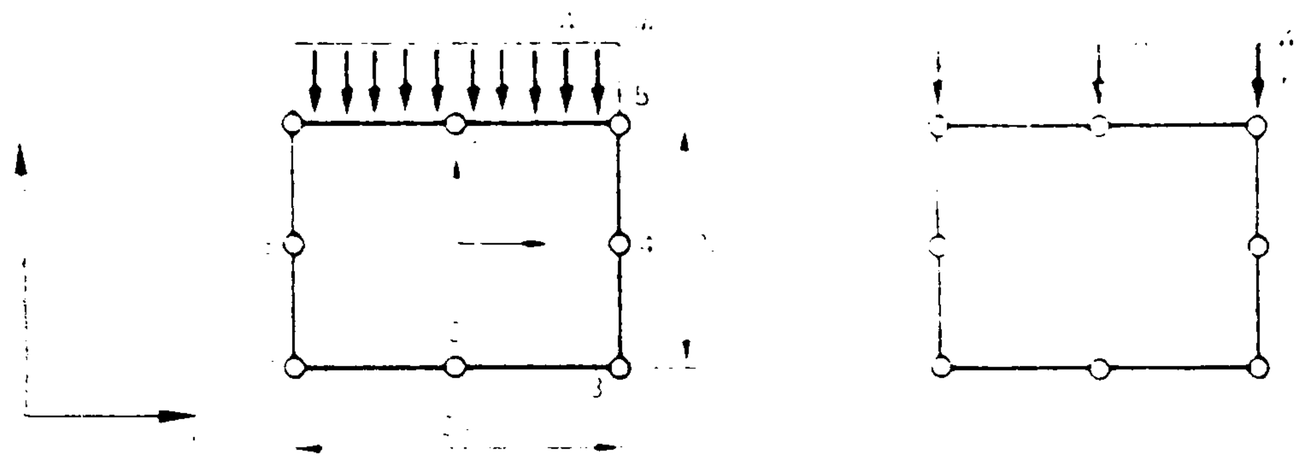

Gravity loading and equivalent nodal forces.

Fig. 3.1 A typical load discretisation

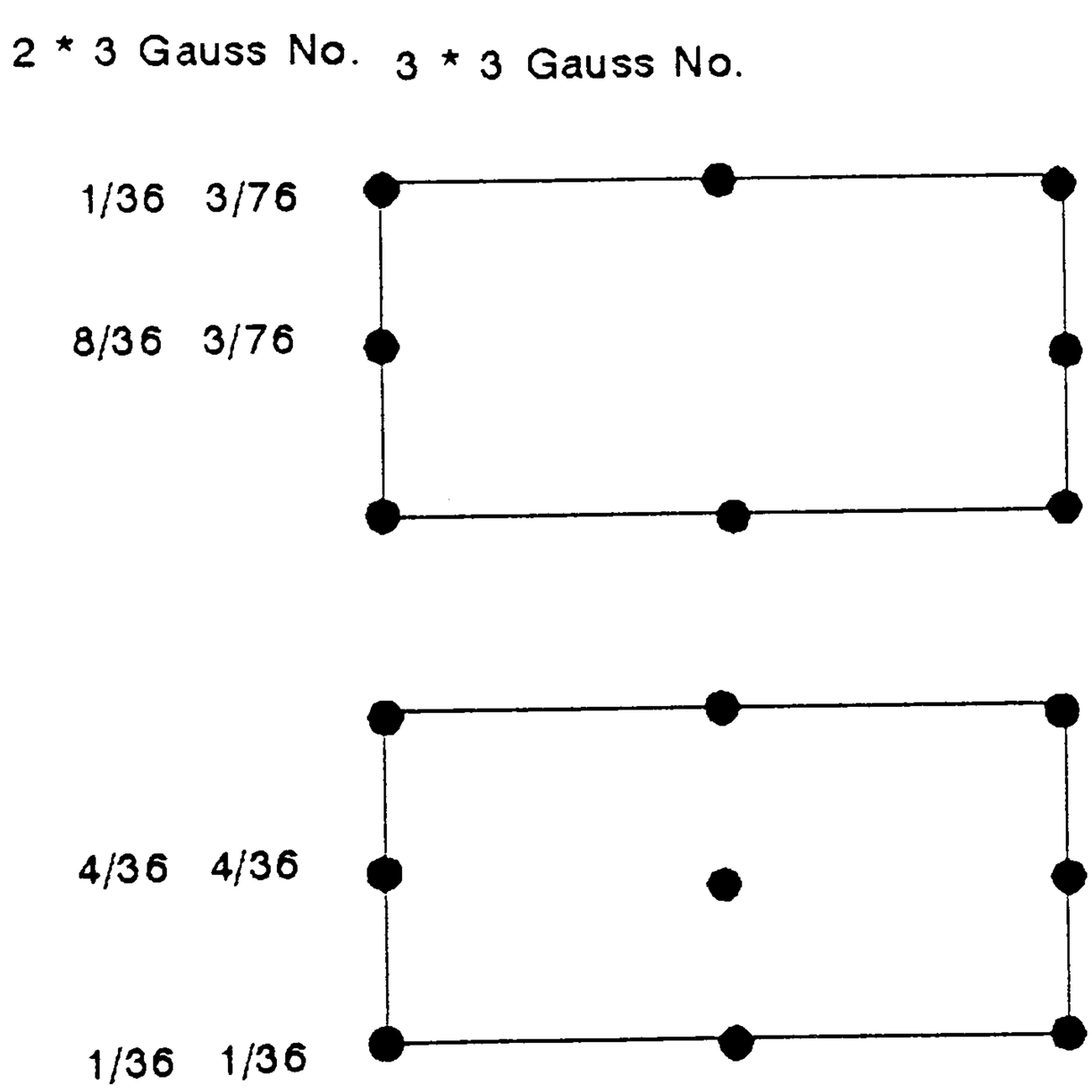

Fig. 3.2 HRZ scheme

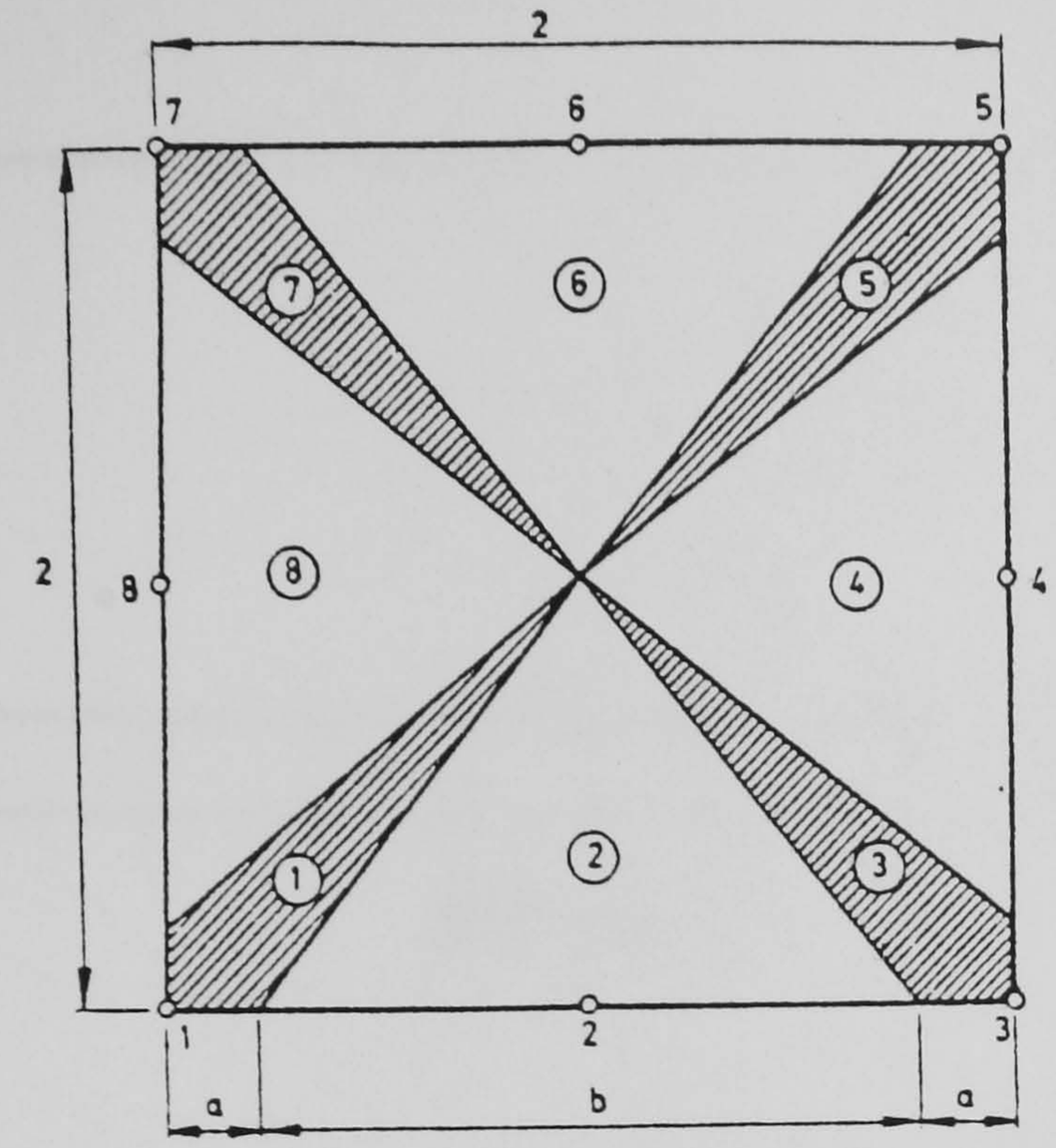

a = 0·111 (2 x 2 GAUSS) 0·158 (3 x 3 GAUSS)
b = 1·777 (2 x 2 GAUSS) 1·684 (3 x 3 GAUSS)

Fig. 3.3 Equivalent influenced area in lumped mass scheme

(taken from [138])

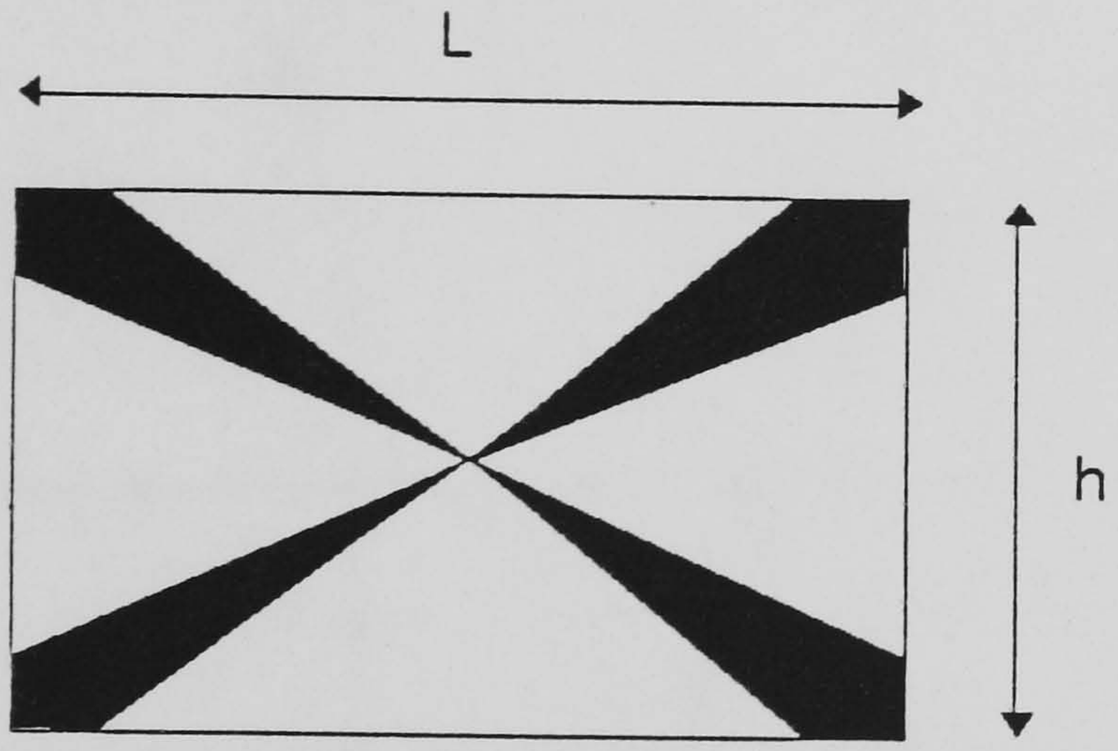

R = h / L

Fig. 3.4 Equivalent influenced area in the proposed lumped mass method.

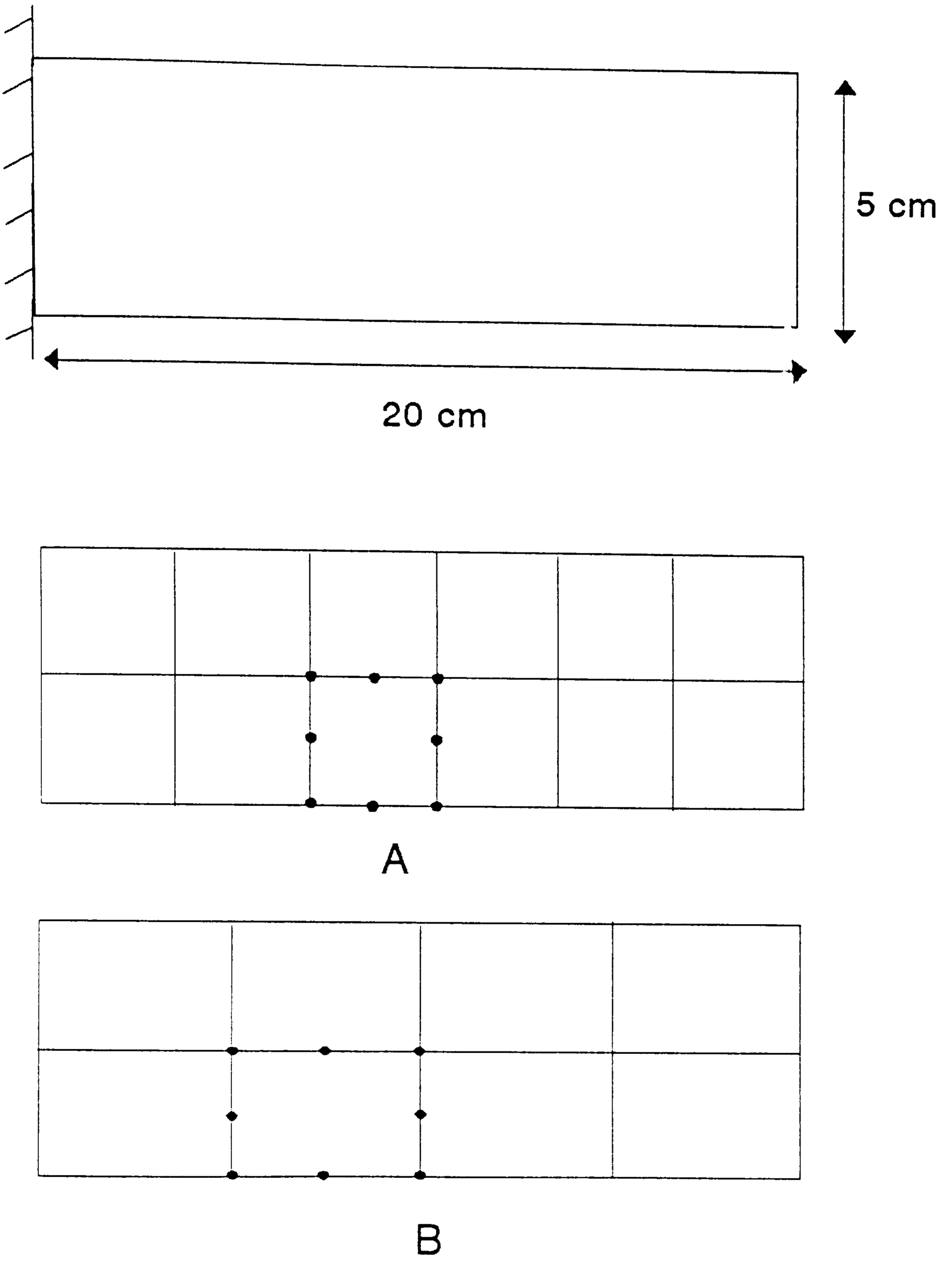

Fig. 3.5 Geometry and spatial discretisation of cantilever beam, A square, B rectangular

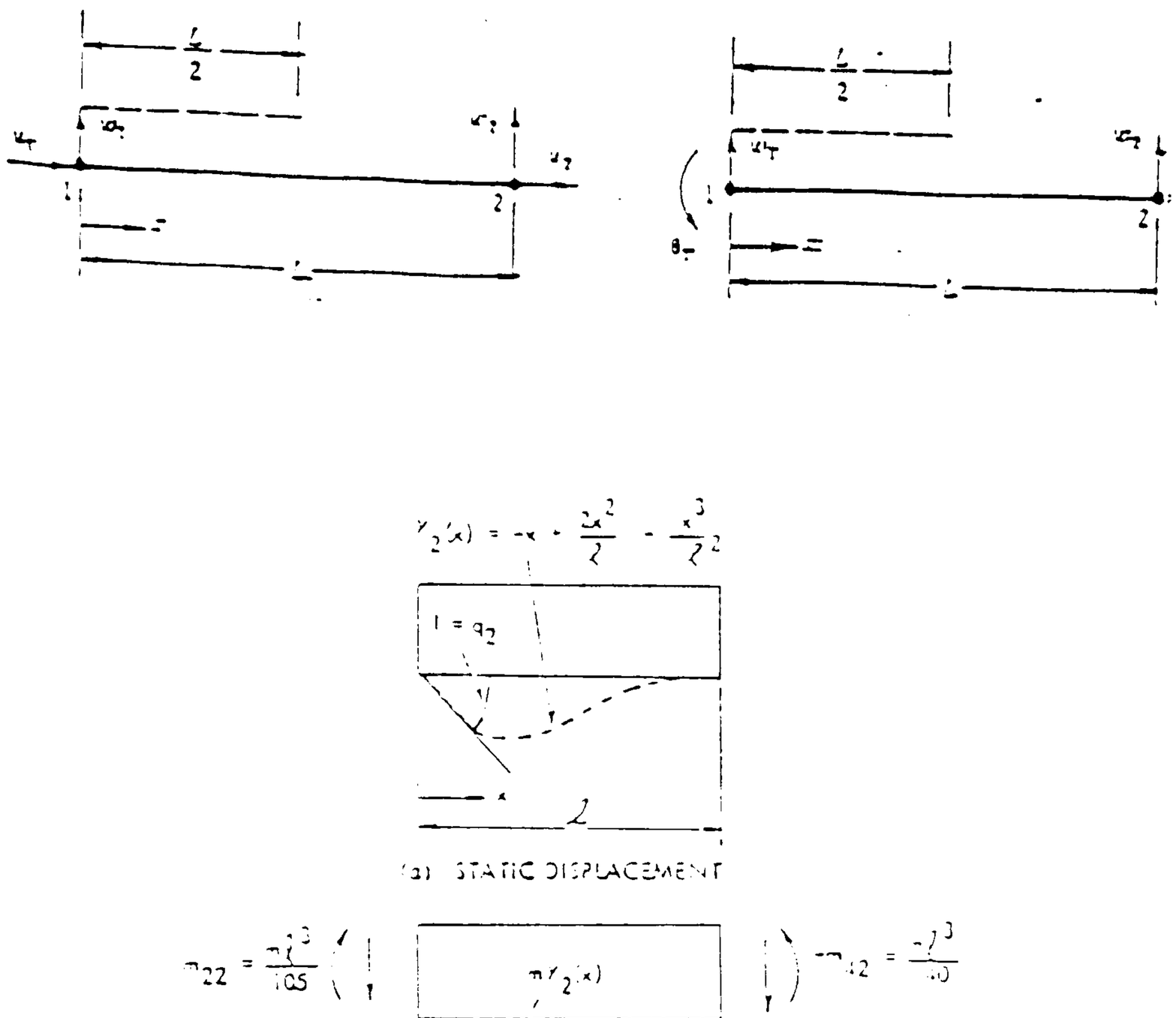

Displacements and internal loads

for rotation coordinate of uniform beam segment.

$$\begin{Bmatrix} Q_1 \\ Q_2 \\ Q_3 \\ Q_4 \end{Bmatrix} = \frac{ml}{420} \begin{bmatrix} 156 & -22l & 54 & 13l \\ -22l & 4l^2 & -13l & -3l^2 \\ 54 & -13l & 156 & 22l \\ 13l & -3l^2 & 22l & 4l^2 \end{bmatrix} \begin{Bmatrix} \ddot{q}_1 \\ \ddot{q}_2 \\ \ddot{q}_3 \\ \ddot{q}_4 \end{Bmatrix}$$

Fig. 3.6 Representation of consistent mass matrix.

Table 3.1 A Twenty noded solid element

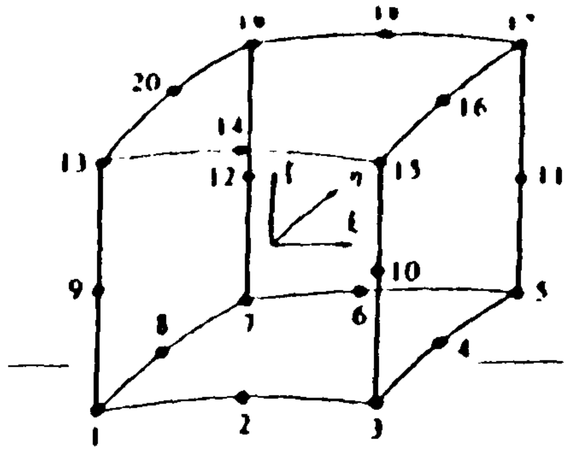

Node i	*Shape functions* $N_i(\xi,\eta,\zeta)$	*Derivatives* $\frac{\partial N_i}{\partial \xi}$	$\frac{\partial N_i}{\partial \eta}$	$\frac{\partial N_i}{\partial \zeta}$
1	$\frac{1}{8}(1-\xi)(1-\eta)(1-\zeta)(-\xi-\eta-\zeta-2)$	$\frac{1}{8}(1-\eta)(1-\zeta)(2\xi+\eta+\zeta+1)$	$\frac{1}{8}(1-\xi)(1-\zeta)(2\eta+\xi+\zeta+1)$	$\frac{1}{8}(1-\xi)(1-\eta)(2\zeta+\eta+\xi+1)$
2	$\frac{1}{4}(1-\xi^2)(1-\eta)(1-\zeta)$	$-\frac{1}{4}(1-\eta)(1-\zeta)\xi$	$-\frac{1}{4}(1-\xi^2)(1-\zeta)$	$-\frac{1}{4}(1-\xi^2)(1-\eta)$
3	$\frac{1}{8}(1+\xi)(1-\eta)(1-\zeta)(\xi-\eta-\zeta-2)$	$\frac{1}{8}(1-\eta)(1-\zeta)(2\xi-\eta-\zeta-1)$	$\frac{1}{8}(1+\xi)(1-\zeta)(2\eta-\xi+\zeta+1)$	$\frac{1}{8}(1+\xi)(1-\eta)(2\zeta-\xi+\eta+1)$
4	$\frac{1}{4}(1+\xi)(1-\eta^2)(1-\zeta)$	$\frac{1}{4}(1-\eta^2)(1-\zeta)$	$\frac{1}{4}(1+\xi)(1-\zeta)\eta$	$-\frac{1}{4}(1-\eta^2)(1+\xi)$
5	$\frac{1}{8}(1+\xi)(1+\eta)(1-\zeta)(\xi+\eta-\zeta-2)$	$\frac{1}{8}(1+\eta)(1-\zeta)(2\xi+\eta-\zeta-1)$	$\frac{1}{8}(1+\xi)(1-\zeta)(2\eta+\xi-\zeta-1)$	$\frac{1}{8}(1+\xi)(1+\eta)(2\zeta-\xi-\eta+1)$
6	$\frac{1}{4}(1-\xi^2)(1+\eta)(1-\zeta)$	$-\frac{1}{4}(1+\eta)(1-\zeta)\xi$	$\frac{1}{4}(1-\xi^2)(1-\zeta)$	$-\frac{1}{4}(1-\xi^2)(1+\eta)$
7	$\frac{1}{8}(1-\xi)(1+\eta)(1-\zeta)(-\xi+\eta-\zeta-2)$	$\frac{1}{8}(1+\eta)(1-\zeta)(2\xi-\eta+\zeta+1)$	$\frac{1}{8}(1-\xi)(1-\zeta)(2\eta-\xi-\zeta-1)$	$-\frac{1}{8}(1-\xi)(1+\eta)(2\zeta-\eta+\xi+1)$
8	$\frac{1}{4}(1-\xi)(1-\eta^2)(1-\zeta)$	$-\frac{1}{4}(1-\eta^2)(1-\zeta)$	$-\frac{1}{4}(1-\xi)(1-\zeta)$	$-\frac{1}{4}(1-\xi)(1-\eta^2)$
9	$\frac{1}{4}(1-\xi)(1-\eta)(1-\zeta^2)$	$-\frac{1}{4}(1-\zeta^2)(1-\eta)$	$-\frac{1}{4}(1-\xi)(1-\zeta^2)$	$-\frac{1}{4}(1-\xi)(1-\eta)\zeta$
10	$\frac{1}{4}(1+\xi)(1-\eta)(1-\zeta^2)$	$\frac{1}{4}(1-\eta)(1-\zeta^2)$	$-\frac{1}{4}(1+\xi)(1-\zeta^2)$	$-\frac{1}{4}(1+\xi)(1-\eta)\zeta$
11	$\frac{1}{4}(1+\xi)(1+\eta)(1-\zeta^2)$	$\frac{1}{4}(1+\eta)(1-\zeta^2)$	$\frac{1}{4}(1+\xi)(1-\zeta^2)$	$-\frac{1}{4}(1+\xi)(1+\eta)\zeta$
12	$\frac{1}{4}(1-\xi)(1+\eta)(1-\zeta^2)$	$-\frac{1}{4}(1+\eta)(1-\zeta^2)$	$\frac{1}{4}(1-\xi)(1-\zeta^2)$	$-\frac{1}{4}(1-\xi)(1+\eta)\zeta$
13	$\frac{1}{8}(1-\xi)(1-\eta)(1+\zeta)(-\xi-\eta+\zeta-2)$	$\frac{1}{8}(1-\eta)(1+\zeta)(2\xi+\eta-\zeta+1)$	$\frac{1}{8}(1-\xi)(1+\zeta)(2\eta+\xi-\zeta+1)$	$\frac{1}{8}(1-\xi)(1-\eta)(2\zeta-\eta-\xi-1)$
14	$\frac{1}{4}(1-\xi^2)(1-\eta)(1+\zeta)$	$-\frac{1}{4}(1-\eta)(1+\zeta)\xi$	$-\frac{1}{4}(1-\xi^2)(1+\zeta)$	$\frac{1}{4}(1-\xi^2)(1-\eta)$
15	$\frac{1}{8}(1+\xi)(1-\eta)(1+\zeta)(\xi-\eta+\zeta-2)$	$\frac{1}{8}(1-\eta)(1+\zeta)(2\xi-\eta+\zeta-1)$	$\frac{1}{8}(1+\xi)(1+\zeta)(2\eta-\xi-\zeta+1)$	$\frac{1}{8}(1-\eta)(1+\zeta)(2\zeta+\xi-\eta-1)$
16	$\frac{1}{4}(1+\xi)(1-\eta^2)(1+\zeta)$	$\frac{1}{4}(1-\eta^2)(1+\zeta)$	$-\frac{1}{4}(1+\xi)(1+\zeta)\eta$	$\frac{1}{4}(1+\xi)(1-\eta^2)$
17	$\frac{1}{8}(1+\xi)(1+\eta)(1+\zeta)(\xi+\eta+\zeta-2)$	$\frac{1}{8}(1+\eta)(1+\zeta)(2\xi+\eta+\zeta-1)$	$\frac{1}{8}(1+\xi)(1+\zeta)(2\eta+\xi+\zeta-1)$	$\frac{1}{8}(1+\xi)(1+\eta)(2\zeta+\eta+\xi-1)$
18	$\frac{1}{4}(1-\xi^2)(1+\eta)(1+\zeta)$	$-\frac{1}{4}(1+\eta)(1+\zeta)\xi$	$\frac{1}{4}(1-\xi^2)(1+\zeta)$	$\frac{1}{4}(1-\xi^2)(1+\eta)$
19	$\frac{1}{8}(1-\xi)(1+\eta)(1+\zeta)(-\xi+\eta+\zeta-2)$	$\frac{1}{8}(1+\eta)(1+\zeta)(2\xi-\eta-\zeta-1)$	$\frac{1}{8}(1-\xi)(1+\zeta)(2\eta-\xi+\zeta-1)$	$\frac{1}{8}(1-\xi)(1+\eta)(2\zeta-\xi+\eta-1)$
20	$\frac{1}{4}(1-\xi)(1-\eta^2)(1+\zeta)$	$-\frac{1}{4}(1-\eta^2)(1+\zeta)$	$-\frac{1}{4}(1-\xi)(1+\zeta)\eta$	$\frac{1}{4}(1-\xi)(1-\eta^2)$

EIGHT-NODED

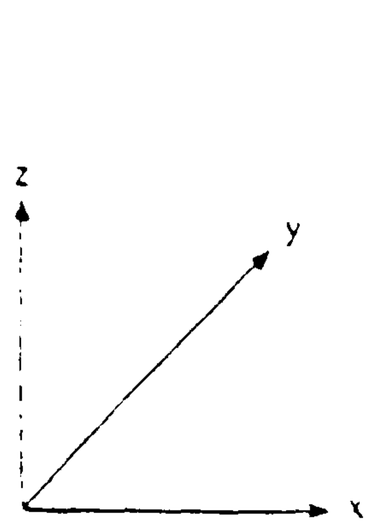

Global axes

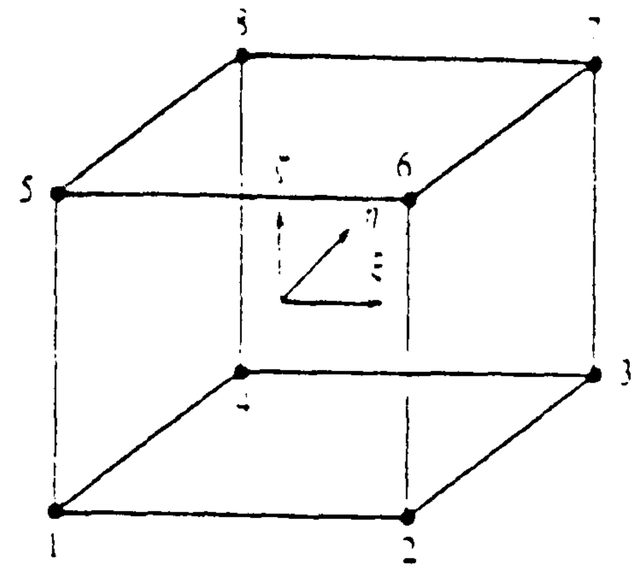

Table 3.1 B

Node i	*Shape functions* $N_i(\xi, \eta, \zeta)$	*Derivatives*		
		$\frac{\partial N_i}{\partial \xi}$	$\frac{\partial N_i}{\partial \eta}$	$\frac{\partial N_i}{\partial \zeta}$
1	$\frac{1}{8}(1-\xi)(1-\eta)(1-\zeta)$	$-\frac{1}{8}(1-\eta)(1-\zeta)$	$-\frac{1}{8}(1-\xi)(1-\zeta)$	$-\frac{1}{8}(1-\eta)(1-\xi)$
2	$\frac{1}{8}(1+\xi)(1-\eta)(1-\zeta)$	$\frac{1}{8}(1-\eta)(1-\zeta)$	$-\frac{1}{8}(1+\xi)(1-\zeta)$	$-\frac{1}{8}(1+\xi)(1-\eta)$
3	$\frac{1}{8}(1+\xi)(1+\eta)(1-\zeta)$	$\frac{1}{8}(1+\eta)(1-\zeta)$	$\frac{1}{8}(1+\xi)(1-\zeta)$	$-\frac{1}{8}(1+\xi)(1+\eta)$
4	$\frac{1}{8}(1-\xi)(1+\eta)(1-\zeta)$	$-\frac{1}{8}(1+\eta)(1-\zeta)$	$\frac{1}{8}(1-\xi)(1-\zeta)$	$-\frac{1}{8}(1-\xi)(1+\eta)$
5	$\frac{1}{8}(1-\xi)(1-\eta)(1+\zeta)$	$-\frac{1}{8}(1-\eta)(1+\zeta)$	$-\frac{1}{8}(1-\xi)(1+\xi)$	$\frac{1}{8}(1-\xi)(1-\eta)$
6	$\frac{1}{8}(1+\xi)(1-\eta)(1+\zeta)$	$\frac{1}{8}(1-\eta)(1+\zeta)$	$-\frac{1}{8}(1+\xi)(1+\zeta)$	$\frac{1}{8}(1+\xi)(1-\eta)$
7	$\frac{1}{8}(1+\xi)(1+\eta)(1+\zeta)$	$\frac{1}{8}(1+\eta)(1+\zeta)$	$\frac{1}{8}(1+\xi)(1+\zeta)$	$\frac{1}{8}(1+\xi)(1+\eta)$
8	$\frac{1}{8}(1-\xi)(1+\eta)(1+\zeta)$	$-\frac{1}{8}(1+\eta)(1+\zeta)$	$\frac{1}{8}(1-\xi)(1+\zeta)$	$\frac{1}{8}(1-\xi)(1+\eta)$

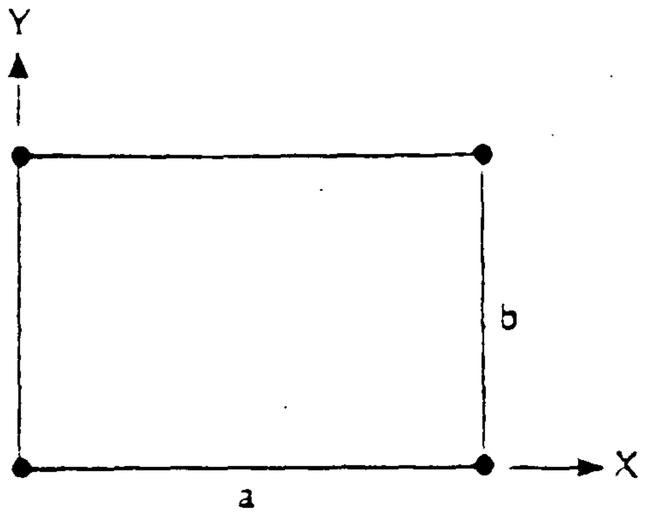

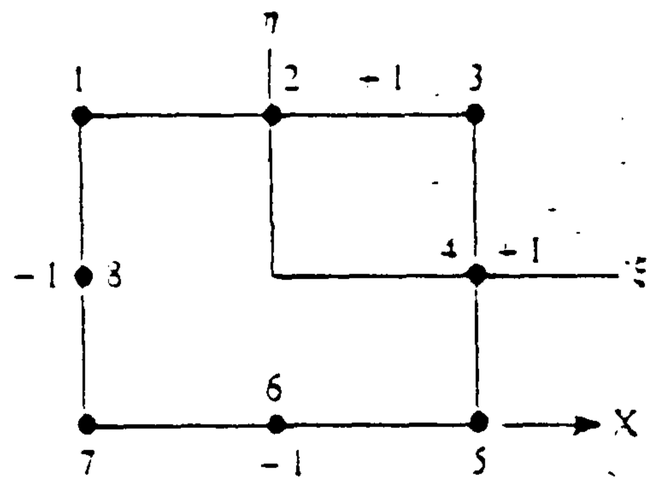

Linear shape functions:

$N_1 = \frac{1}{4}(1-\xi)(1+\eta)$ mid-side nodes 2.6 $(\xi_r = 0)$
$N_2 = \frac{1}{4}(1+\xi)(1+\eta)$ $N_r = \frac{1}{2}(1-\xi^2)(1+\eta_0)$
$N_3 = \frac{1}{4}(1+\xi)(1-\eta)$ mid-side nodes 4, 8 $(\eta_r = 0)$
$N_4 = \frac{1}{4}(1-\xi)(1-\eta)$

} Quadratic

Quadratic general shape function for the corner nodes:

$$N_r = \tfrac{1}{4}(1+\xi_0)(1+\eta_0)(\xi_0+\eta_0+1) \qquad (\xi_0 = \xi\xi_r,\ \eta_0 = \eta\eta_r)$$

$$[B] = \sum_{r=1}^{4}[B]_r = \sum_{r=1}^{4}\begin{bmatrix} \frac{\partial N_r}{\partial y} & 0 \\ 0 & \frac{\partial N_r}{\partial x} \\ \frac{\partial N_r}{\partial y} & \frac{\partial N_r}{\partial x} \end{bmatrix}$$

Table 3.1 C

	PLANE STRESS	PLANE STRAIN	AXISYMMETRIC	THREE DIMENSIONAL
STRAIN VECTOR	$[\varepsilon_x \ \varepsilon_y \ \gamma_{xy}]^T$	$[\varepsilon_x \ \varepsilon_y \ \gamma_{xy} \ \varepsilon_z]^T$	$[\varepsilon_r \ \varepsilon_z \ \gamma_{rz} \ \varepsilon_\theta]^T$	$[\varepsilon_x \ \varepsilon_y \ \varepsilon_z \ \gamma_{yz} \ \gamma_{zx} \ \gamma_{xy}]^T$
STRESS VECTOR	$[\sigma_x \ \sigma_y \ \tau_{xy}]^T$	$[\sigma_x \ \sigma_y \ \tau_{xy} \ \sigma_z]^T$	$[\sigma_r \ \sigma_z \ \tau_{rz} \ \sigma_\theta]^T$	$[\sigma_x \ \sigma_y \ \sigma_z \ \tau_{yz} \ \tau_{zx} \ \tau_{xy}]^T$
STRAIN DISPLACEMENT SUBMATRIX, $\underline{B}_i$	$\begin{bmatrix} \partial N_i/\partial x & 0 \\ 0 & \partial N_i/\partial y \\ \partial N_i/\partial y & \partial N_i/\partial x \end{bmatrix}$		$\begin{bmatrix} \partial N_i/\partial r & 0 \\ 0 & \partial N_i/\partial z \\ \partial N_i/\partial z & \partial N_i/\partial r \\ N_i/r & 0 \end{bmatrix}$	$\begin{bmatrix} \partial N_i/\partial x & 0 & 0 \\ 0 & \partial N_i/\partial y & 0 \\ 0 & 0 & \partial N_i/\partial z \\ 0 & \partial N_i/\partial z & \partial N_i/\partial y \\ \partial N_i/\partial z & 0 & \partial N_i/\partial x \\ \partial N_i/\partial y & \partial N_i/\partial x & 0 \end{bmatrix}$
ELASTIC STRESS-STRAIN MATRIX, $\underline{D}$	$\frac{E}{1-\nu^2}\begin{bmatrix} 1 & \nu & 0 \\ & 1 & 0 \\ & & \frac{1-\nu}{2} \end{bmatrix}$	$\frac{E}{(1+\nu)(1-2\nu)}\begin{bmatrix} 1-\nu & \nu & 0 & \nu \\ & 1-\nu & 0 & \nu \\ & & \frac{1-2\nu}{2} & 0 \\ & & & 1-\nu \end{bmatrix}$		$\frac{E}{(1+\nu)(1-2\nu)}\begin{bmatrix} 1-\nu & \nu & \nu & 0 & 0 & 0 \\ & 1-\nu & \nu & 0 & 0 & 0 \\ & & 1-\nu & 0 & 0 & 0 \\ & & & \frac{1-2\nu}{2} & 0 & 0 \\ & & & & \frac{1-2\nu}{2} & 0 \\ & & & & & \frac{1-2\nu}{2} \end{bmatrix}$

Table 3.2 Some vectors and matrices for 2D and 3D problems

Table 3.3 The orders of Gauss-Legendre integration for exact evalution of stiffness matrix (parallelogramic elements) [128].

Isoparametric element	Gauss-Legendre integration order for exact evaluating stiffness matrix
Bilinear 4-noded	2×2
Biquadratic 8-noded Serendipity	3×3
Biquadratic 9-noded Lagrangian	3×3
Bicubic 16-noded Lagrangian	4×4

Table 3.4 - Recommended minimum Gauss-Legendre integration order for evaluating stiffness matrix (Parallelogramic elements) [128].

Isoparametric element	Minimum Gauss-Legendre integration order for evaluating stiffness matrix.
Bilinear 4-noded	2×2
Biquadratic 8-noded Serendipity	2×2
Biquadratic 9-noded Lagrangian	3×3
Bicubic 12-noded Serendipity	3×3
Bicubic 16-noded Lagrangian	4×4

Chapter 4

Finite Difference and Dynamic Solution Techniques

4.1 Introduction

Finite element methods were first applied to transient analysis of structures by Costantino [145]. Subsequently, the method was extended to non-linear and visco-elastic media by incorporating the pseudo or fictitious force technique in which the non-linearity is accounted for by an equivalent force. A finite element program was subsequently reported by Wilson [146] and Farhoomand and Wilson [147] in which the nodal displacement at the end of each time-step was found by solving the equations with force equivalent to inertia and internal forces on the right hand side. A tangential stiffness approach was used with the internal force resulting from previous deformations treated as pseudo-force in the non-linear solution technique.

As discussed in chapter 3, in dynamic problems, finite elements are used for spatial discretisation and time is discretised by finite difference. In spite of many achievements to date, time discretisation still remains a costly step in non-linear analysis of structures. This chapter is dedicated to the description and assessment of the more reliable, accurate and efficient linear and non-linear solution schemes currently available for dynamic problems. The aim of the chapter can

be summarized as

- To assess the strengths and weakness of numerical methods in which time is not discretised.

- To discuss the contribution of higher modes which have a significant role in structural response.

- To discuss the formulation of the currently used numerical methods for solving dynamic problems.

- To assess the efficiency of mixed explicit-implicit methods in which the predictor-corrector approach is employed.

- To assess the efficiency of numerical algorithms suitable for dynamic analysis of structures subjected to seismic loading.

The chapter opens with solution techniques of dynamic problems, and continues with the modal superposition method and eigenvalue problems. The next section is devoted to the contribution of modes in structural response.

A discussion of the direct integration methods is given in two parts. In the first part different implicit algorithms currently used such as; the Newmark family of methods, the Wilson-θ method and the Houbolt method are discussed. In the second part, some of the widely-used explicit forms of integrators such as the central difference method as a one-step method and the Runge Kutta method as a multi-step approach are described. The strength and weakness of each method are discussed and assessed. The chapter closes with a description of the mixed explicit-implicit and predictor-corrector approaches. The stability and accuracy of above-mentioned methods will be discussed in Chapter 5.

4.2 Solution techniques for dynamic problems

The three most popular techniques for solving the equation of dynamic equilibrium are :

1. Modal superposition method.
2. Direct integration methods.
3. Complex response methods.

4.3 Modal superposition method

A solution technique that is available for solving most dynamic problems involves finding the structures natural frequencies and mode shapes (eigenvalues and eigenvectors) [148-151]. If the structure has n degrees of freedom then it has n eigenvalues and n corresponding eigenvectors. Eigenvalue problems are therefore discussed first.

4.3.1 Eigenvalue and eigenvectors

Recalling the general form of the equilibrium equation

$$M\ddot{X} + C\dot{X} + KX = P(t) \tag{4.1}$$

neglecting damping C and loading P(t) leads to the free undamped equation of motion

$$M\ddot{X} + KX = 0 \tag{4.2}$$

Premultiplying the above equation by M^{-1}, the following eigenvalue problem is obtained:

$$I\ddot{X} + AX = 0 \tag{4.3}$$

in which I is a unit matrix. The matrix A is referred to as the system matrix, since the dynamic properties of the system are defined by this matrix.

Assuming harmonic motion of the form

$$X = e^{i\sqrt{\lambda}t}X(x) \tag{4.4}$$

where $\lambda = \omega^2$.

Then substituting (4.4) into (4.3), leads to

$$(A - \lambda)X = 0 \tag{4.5}$$

The characteristic equation of the system is

$$A - \lambda I = 0 \tag{4.6}$$

The roots of the characteristic equation are the eigenvalues, λ_i and the circular natural frequencies are given by

$$\omega_i = \sqrt{\lambda_i} \tag{4.7}$$

The corresponding mode shapes denoted by the eigenvectors φ_i can be obtained by substituting λ_i into (4.3). For an n-degree of freedom system, there will be n eigenvalues and n eigenvectors.

4.3.2 Standard modal superposition analysis

In order to determine the forced vibration of a system, it is usually assumed that the mode shapes are normalized so that the modal matrix φ whose columns are the mode shapes arranged in ascending order of frequencies satisfies the following orthogonality conditions

$$\varphi_i^T M \varphi_j = \delta_{ij} \tag{4.8}$$

$$\varphi_i^T K \varphi_j = \Omega_i \delta_{ij} \tag{4.9}$$

where δ_{ij} is the Kronecker delta and Ω denotes a diagonal matrix containing the diagonal terms $\omega_i^2 (i = 1, 2, 3...3n)$. Assuming proportional damping then

$$\varphi_i^T C \varphi_j = 2\xi\omega \tag{4.10}$$

where, $2\xi\omega$ is a diagonal matrix containing the diagonal terms of $2\xi_i\omega_i (i = 1, 2, ...3n)$.

The dynamic response X may be approximated as a linear combination of modes shapes as

$$X = \varphi Y \tag{4.11}$$

where Y is a vector of modal amplitudes.

Substituting Eq. (4.11) into (4.1), by φ^T then the following set of decoupled equations of motion in terms of normal co-ordinates are obtained

$$\ddot{Y}_i + 2\xi\omega\dot{Y}_i + \Omega Y_i = \varphi^T P(t) = \sum_{i=1}^{3n} \varphi^i P^i(t), n = 1, 2...3n \tag{4.12}$$

Each equation may be solved separately using the Duhamel integral thus

$$Y_i(t) = \frac{1}{\bar{\omega}} \int_0^t P_i(\tau) e^{-\bar{\xi}\omega_i(t-\tau)} \sin \bar{\omega}_i(t-\tau) d\tau \tag{4.13}$$

The total response is obtained by summing each of the modal responses using Equation (4.11) [148, 152]. This method is advantageous for problems in which a limited number of lower modes are sufficient for accurate dynamic responses. Since in structures under earthquake loading the structural response is dominated by a few lower modes, the superposition process can be suitable for such problems [153]. Maddox [153] has proposed a dynamic Truncation Method by which a limited number of lower modes is considered to approximate the displacements of the dynamic problems and has claimed that very good predictions can be obtained for both displacements and forces.

If the structure is not proportionally damped, the generalized damping matrix is not diagonal thus its off-diagonal coefficients cause coupling of the equation of motion and the above-mentioned procedure of decoupling the system is not permitted [153].

For seismic response analysis Eq. (4.12) has the following form:

$$\ddot{Y} + 2\xi\omega\dot{Y} + \Omega Y = -\varphi^T M I \ddot{X}_g(t) \tag{4.14}$$

where $\ddot{X}_g(t)$ is the base acceleration. The Duhamel integral for the solution of

each equation is of the form

$$Y_N(t) = \frac{1}{\bar{\omega}} \int_0^t \ddot{X}_g(t)(\tau) e^{-\bar{\xi}\omega_N(t-\tau)} \sin \bar{\omega_N}(t-\tau) d\tau \tag{4.15}$$

It is worthwhile noting that this method can be used in non-linear analysis of dynamic problems by using the tangent damping matrix and the tangent eigen-problem at each time-step during non-linear behaviour [154-156].

4.3.3 Contribution of modes in structural response

Since earthquake loadings comprise low to medium frequencies, only a small number of mode responses are required to obtain sufficiently accurate results for the analysis of structures. However, the minimum sufficient number of modes depends on the type of structure.

The contribution of the higher modes for a hinged-ends uniform beam under arbitrary initial conditions of motion has been determined by McDonald [155].

Fig. 4.1 illustrates the role of the first, third and fifth modes on the mid-span displacement.

Shing et al. [157] compared the a response of discretised cantilevered beam using beam elements with a continuous system to show how the accuracy of the value of the frequency for different modes was influenced by the increased number of degrees-of-freedom.

In order to discuss the contribution of the higher modes in the structural response, an undamped system under harmonic loading has been analysed using the modal superposition method. The equation of motion is

$$M\ddot{X} + KX = P_0 \sin \bar{\omega} t \tag{4.16}$$

where, P_0 and $\bar{\omega}$ are the amplitude and frequency of the external force respectively. Eq. (4.16) can be decoupled by transforming the system to normal coordinate in which each degree-of-freedom can be treated as a single degree-of -freedom problem. Hence, Eq.(4.16) become

$$\ddot{Y}_i + \Omega Y_i = \varphi_i^T P_0 \sin \bar{\omega} t \tag{4.17}$$

where, $\omega_i = \sqrt{\Omega_i}$ is the free-vibration frequency in the normal coordinate and φ is the mode shape matrix.

The general solution of Eq.(4.17) is given as a combination of the complementary solution and the particular solution as

$$Y(t) = Y_c(t) + Y_p(t) = A\sin\omega t + B\cos\omega t + \frac{P_0}{\Omega_i}\frac{1}{1-\beta^2}\sin\bar{\omega}t \qquad (4.18)$$

in which $\beta = \frac{\bar{\omega}}{\omega}$ is the ratio of applied load frequency to the natural vibration frequency.

Substituting $d_{st} = \frac{\bar{P}_0}{\Omega}$ and assuming $Y(t) = \dot{Y(t)} = 0$ the response given by (4.18) is

$$Y(t) = d_{st}\frac{1}{1-\beta^2}(\sin\bar{\omega}t - \beta\sin\omega t) \qquad (4.19)$$

Fig. 4.2 shows a typical response of a single degree-of-freedom system under a harmonic loading.

From Eq. (4.19) it can be deduced that: the contribution of each degree-of-freedom, in other words, the contribution of each mode, depends on $\bar{\omega}$ and hence β.

- For $\beta \ll 1$ then the effect of higher modes is negligible.
- In undamped problems, as β tends to 1, the structural deformation increases so that, for $\beta = 1$, resonance occurs and causes the displacement to grow infinitely.
- The response of the structure is sensitive to the frequencies not far from the frequency of the applied load.

The contribution of the higher modes is examined by an example in the next section.

EXAMPLE 4.1

In order to assess the contribution of higher modes to the structural response, a cantilever beam under a harmonic loading $P = A\cos\omega t$ has been analysed. The first and second natural frequencies of the system are 13.7 and 82.7/sec and

a value of ω between the first and the second natural frequencies equal to 30/sec was chosen.

The beam has been spatially discretised using 8-noded isoparametric element and the consistent mass has been used for mass discretisation. The geometry and the spatial discretisation of the beam are shown in Fig. 4.3 and the material properties are listed in Table 4.1.

Table 4.1 Material properties for cantilever beam (kip, in).

Youngs Modulus	$E_c = 6100.0$
Poisson's ratio	$\nu = .20$
Mass density	$\rho = 0.217E - 06$

The beam is loaded with a harmonic load of the form

$$P_n = A \cos \omega t \tag{4.20}$$

The beam has been analysed using meshes with 6×3, 4×2, 4×1, 2×1, and one element. The tip-displacement of the beam has been calculated including the contribution of different number of higher modes. To this end, the shape modes were calculated and superposed using Eq. (4.11). It is concluded that,

- The frequency corresponding to each mode increases rapidly for subsequent modes Table 4.2. Hence, the role the modes with a higher natural frequency compared with that of the applied load reduces rapidly.

- In this example, which includes 64 degrees-of-freedom only up to the tenth modes was found to have a significant contribution Fig. 4.4.

- The maximum tip-deformation of the beam depends on β Eq. (4.19).

- changing the lumped mass distribution in this example did not significantly affect the mode shapes.

Table 4.2 Natural frequencies of the modes for different meshes of a cantilever beam

Mode number	N. F. with 6 × 3 elements	N. F. with 4 × 2 elements	N. F. with 4 × 1 elements	N. F. with 2 × 1 elements	N. F. with 1 × 1 elements
1	25.44107	25.5401	25.7122	25.8932	26.6444
2	130.6982	131.7975	140.157	139.3345	164.6845
3	164.6240	160.8275	160.9475	163.4586	161.2852
4	303.1367	310.1420	316.1711	353.1635	591.1245
5	492.9397	494.1224	494.4258	501.8125	911.9458
6	495.5647	526.8421	531.7521	713.6228	1027.3195
7	702.5972	731.4128	757.4896	902.8326	1117.1258
8	817.2677	817.8475	822.3345	955.3925	1487.4312
9	870.2709	907.7122	966.01185	1012.1228	2166.9742
10	974.7750	1038.1325	1044.5715	11216.8427	3314.2115
11	1032.459	1115.1524	1087.2215	1342.2514	
12	1114.044	1129.63	1163.0515	1397.1225	
13	1157.827	1241.1915	1191.4151	1435.7112	
14	1193.802	1286.9225	1325.1248	1492.2521	
15	1269.096	1304.6312	1408.7512	1573.6812	
16	1290.171	1322.4219	1419.1912	1580.5121	
17	1307.447	1330.9811	1469.5712	2118.1215	
18	1321.474	1362.4425	1493.2714	2246.5224	
19	1346.663	1450.3625	1516.3525	3312.8125	
20	1374.579	1505.1921	1644.0112	3325.1625	

Table 4.2 (continued)

Mode number	N. F. with 6×3 elements	N. F. with 4×2 elements	N. F. with 4×1 elements
21	1472.3065	1.0680	1.1596
22	1478.9487	1.1069	1.2219
23	1571.1315	1.0961	1.1941
24	1571.6720	1.1521	1.1980
25	1683.8560	1.1159	1.1990
26	1721.2656	1.1063	1.2156
27	1781.1402	1.0950	1.1881
28	1857.1439	1.0991	1.1632
29	1891.1807	1.1079	1.1618
30	1914.1590	1.1196	1.1917
31	1979.5785	1.1122	1.1930
32	1996.9917	1.1338	1.3287
33	2047.7331	1.1334	1.3429
34	2171.2522	1.1312	1.2883
35	2214.7471	1.1743	1.4304
36	2289.4969	1.1485	1.4155
37	2290.8765	1.1681	1.4472
38	2355.9598	1.1617	1.4085
39	2381.4442	1.1755	1.3956
40	2483.9296	1.1321	1.3834

Table 4.2 (continued)

Mode number	N. F. with 6×3 elements	N. F. with 4×2 elements
41	2558.4741	1.1415
42	2571.8600	1.1385
43	2574.3197	1.1570
44	2578.9177	1.1846
45	2617.7935	1.1685
46	2646.1086	1.1859
47	2672.6297	1.2073
48	2708.8029	1.1935
49	2731.0088	1.1955
50	2806.8827	1.1818
51	2853.2999	1.1947
52	2869.3881	1.2747
53	2947.9099	1.4104
54	2973.6149	1.4060
55	2984.4000	1.4035
56	2990.0379	1.4164
57	3003.9173	1.6160
58	3066.4938	1.5907
59	3104.1695	1.5802
60	3119.2387	1.5960
61	3181.3661	2.0833
62	3187.3890	2.080
63	3233.2845	2.050
64	3315.8425	2.001

Fig. 4.4 illustrates the contribution of the modes to the maximum deflection of the cantilevered beam.

- a) with 8×4 elements.
- b) with 4×2 elements.

4.4 Direct integration methods

The numerical methods used for integration are generally a difference equation involving a number of consecutive approximations $X_{n+j}, j = 0, 1, ...k$ from which it will be possible to compute sequentially the sequence $[X_n | n = 0, 1, ...n]$. The integer k is called the step number of the method; if k = 1, it is called a one-step method while if $k > 1$ it is called a linear multi-step method (LMM) or a k-step method [158].

The ease of implementation of direct integration methods, along with their usefulness for non-linear analysis as compared with superposition methods, has tended to enhance rapidly the popularity of these approaches [159, 160]. In the direct integration method, the governing ordinary second order differential equation (4.1) is integrated directly using a numerical step-by-step procedure. The term *'direct'* means that no transformation of the equations into a different form is carried out prior to the numerical integration process.

In these methods, the dynamic equilibrium equation (4.1) is satisfied at a discrete time interval,which subsequently is called the time-step, denoted by Δt. Equilibrium including inertia, damping, body force and external load effects is sought at discrete time points within each time-step solution. A variation of displacements, velocities and accelerations within each time-step is assumed. The different direct integration algorithms make different assumptions for such variations. Each of these algorithms has different stability, accuracy and cost in computing time; these will be explained in more detail later on.

4.5 Implicit time integration methods

In these approaches, the equations for the displacement at the current time-step involve the velocities and accelerations at the same time-step. The calculation of displacements at t_{n+1} involves the solution of a set of simultaneous equations at each time-step. In large problems, the solution of these equations leads to the factorization of the effective stiffness matrix $\hat{K}$ which is a combination of mass, damping and stiffness matrices and may be computationally expensive. This is the most important weakness of these methods.

Many of the implicit methods are unconditionally stable for linear and non-linear system and are the most effective for structural dynamic problems in which the response is controlled by a relatively small number of low frequency modes. The maximum allowable time-step that can be employed in these algorithms is governed by the required accuracy rather than stability. It is worthwhile noting that, unfortunately, the implicit approaches suffer from one major drawback in non-linear procedure; the material state during the time-step t_{n+1} must be estimated for the next step prior to the solution. This may cause some problems when the estimation of material behaviour is not possible. An example of this problem occurs when the transition between elastic and plastic material behaviour is not gradual. Abrupt transitions of material from plastic to elastic states can also produce numerical instability.

In the next sections, the conventional implicit time-integration procedures, such as the Newmark method, the Wilson-θ algorithm and The Houbolt methods for linear problems are described.

The Newmark family of methods

Newmark [161] originally proposed an unconditionally stable scheme with constant accelerations at the ends of the time-step in which $\gamma = 1/2$ and $\beta = 1/4$.

The linear acceleration method can be obtained by putting $\gamma = 1/2$ and $\beta = 1/6$ in the standard Newmark family. Three types of linear variation of acceleration within a time-step are illustrated in Fig. 4.5. To calculate the

displacements, velocities and accelerations at time$t+\Delta t$, the equilibrium equation of motion is considered at time $t + \Delta t$ so that

$$M\ddot{X}_{n+1} + C\dot{X}_{n+1} + KX_{n+1} = P_{n+1} \tag{4.21}$$

$$X_{t+\Delta t} = X_t + \Delta t\dot{X} + (\Delta t)^2[(1/2 - \beta)\ddot{X}_t + \beta\ddot{X}_{t+\Delta t}] \tag{4.22}$$

$$\dot{X}_{t+\Delta t} = \dot{X}_t + \Delta t[(1 - \gamma)\ddot{X}_t + \gamma\ddot{X}_{t+\Delta t}] \tag{4.23}$$

solving Equation (4.22) for $\ddot{X}_{t+\Delta t}$ in terms of $X_{t+\Delta t}$ and substituting in equation (4.23) we obtain equations for $\ddot{X}_{t+\Delta t}$ and $\dot{X}_{t+\Delta t}$ in terms of the unknown displacements $X_{t+\Delta t}$. Substituting these two relations into (4.21) gives a system of simultaneous equations in the form

$$[K + \frac{\gamma}{\beta\Delta t}C + \frac{1}{\beta\Delta t^2}M]X_{t+\Delta t} = P_{t+\Delta t} + C[\frac{\gamma}{\beta\Delta t} + (\frac{\gamma}{\beta} - 1)\dot{X}_t + \Delta t(\frac{\gamma}{2\beta} - 1)\ddot{X}_t]$$
$$-M[\frac{1}{\beta\Delta t^2}X_t + \frac{1}{\beta\Delta t}\dot{X}_t + (\frac{1}{2\beta} - 1)\ddot{X}_t] \tag{4.24}$$

where $(K + \frac{\gamma}{\beta\Delta t}C + \frac{1}{\beta\Delta t^2}M)$ is called *effective stiffness matrix* denoted by $\hat{K}$ and the right-hand side of Eq. (4.24) *effective stiffness matrix* denoted by $\hat{P}$.

The algorithm is not self-starting but it can be started at time t = 0 by using the initial conditions prescribed as X_0 and $\dot{X}_0$ from which $\ddot{X}_0$ is obtained using Eq. (4.21). Then equations (4.21) , (4.23) and (4.22) are solved for $X_{\Delta t}$, $\dot{X}_{\Delta t}$ and $\ddot{X}_{\Delta t}$, respectively and so on. Warburton [162] has suggested a direct approach in which the effective load vector depends only on the displacements at t and $t + \Delta t$ thus additional computation of velocity and acceleration components at time t are eliminated.

Chan et al. [163] have proposed the same relation in the form of a three-point finite difference formula.

An implicit algorithm has been proposed by Zienkiewicz et al. [164] in which the second order differential equation of motion has been written as the pair of equations

$$M\dot{v} + Cv + Kx = F \tag{4.25}$$

$$v - \dot{x} = 0 \tag{4.26}$$

and the weighted residual method has been used to obtain the difference equations

$$M(v_{n+1-v_n}) + \Delta t C[\theta v_{n+1} + (1-\theta)v_n] + \Delta t K[\theta x_{n+1} + (1-\theta)x_n]$$
$$= \Delta t[\theta F_{n+1} + (1-\theta)F_n] \qquad (4.27)$$

and

$$\Delta t[\alpha v_{n+1} + (-1\alpha)v_n] - [x_{n+1} - x_n] = 0 \qquad (4.28)$$

Finally, the method leads to the condition

$$1 = \theta + 1/2 = \alpha + \theta \qquad (4.29)$$

for the local truncation error to be of $O(\Delta t^2)$ and the stability condition as

$$4 + 2C\Delta t(2\theta - 1) + \omega^2 \Delta t^2 (2\theta - 1)(2\alpha - 1) > 0 \qquad (4.30)$$

$$C\Delta t + \omega^2 \Delta t^2 (\alpha + \theta - 1) \geq 0, \omega^2 \Delta t^2 \qquad (4.31)$$

Weighted residual methods have been used to derive a general family of four-time-level schemes, from which a third and fourth-order accuracy may be obtained by Zienkiewicz [164] and Thomas et al. [165].

Wood [166] has proposed a modification of the Newmark method which replaces the general equation by the following equation

$$(1-\alpha_B)\ddot{Y}_{n+1} + \alpha_B \ddot{Y} + C\dot{Y}_{n+1} + \omega^2 Y_{n+1} = P_{n+1} \qquad (4.32)$$

Reducing this method to a difference equation in the displacements gives a four-time-level scheme from which the unconditional stability is obtainable with second order accuracy but not more.

Wood [166] suggested the use of

$$\ddot{Y} + C\dot{Y} + \omega^2 Y = Pe^{ist} \qquad (4.33)$$

instead of

$$\ddot{Y} + \omega^2 Y = 0 \qquad (4.34)$$

in order to gain some insight into the effect with natural damping and/or a period forcing term, and has been introduced in some useful three-and four-time-level schemes.

Wilson- θ-method

In the Wilson-θ method the acceleration is assumed to vary linearly from time t, to time $t + \Delta t$. Hence, this method is essentially an extension of the linear acceleration method. If $\theta = 0$, the method reduces to the linear acceleration variation the Newmarks family of methods. The method is unconditionally stable if $\theta \geq 1.37$ and $\theta = 1.4$ The method can be derived as follows.

The acceleration for anytime within a time-step i. e. $0 \leq \tau \leq \theta\Delta t$, can be written as

$$\ddot{X}_{t+\tau} = \ddot{X}_t + \frac{\tau}{\theta\Delta t}(\ddot{X}_{t+\theta\Delta t} - \ddot{X}_t) \tag{4.35}$$

If Equation (4.35) is integrated and initial conditions are applied then

$$\dot{X}_{t+\tau} = \dot{X}_t + \tau\dot{X}_t + \frac{\tau^2}{2\theta\Delta t}(\ddot{X}_{t+\theta\Delta t} - \ddot{X}_t) \tag{4.36}$$

By integrating Equation (4.36) then

$$X_{t+\tau} = X_t + \tau\dot{X} + \frac{1}{2}\tau^2\ddot{X}_t + \frac{\tau^3}{6\theta\Delta t}(\ddot{X}_{t+\theta\Delta t} - \ddot{X}_t) \tag{4.37}$$

Equations (4.36) and (4.37) at time $t + \theta\Delta t$ become

$$\dot{X}_{t+\theta\Delta t} = \dot{X}_t + \frac{1}{2}\theta\Delta t(\ddot{X}_{t+\theta\Delta t} + \ddot{X}_t) \tag{4.38}$$

$$X_{t+\theta\Delta t} = X_t + \theta\Delta t\dot{X}_t + 1/6\theta^2\Delta t^2(\ddot{X}_{t+\theta\Delta t} + 2\ddot{X}_t) \tag{4.39}$$

from which $\ddot{X}_{t+\theta\Delta t}$ and$\dot{X}_{t+\theta\Delta t}$ can be solved in terms of$X_{t+\theta\Delta t}$.

The applied load vector is projected to time $t+\theta\Delta t$ which is performed linearly as

$$P_{t+\theta\Delta t} = P_t + \theta(P_{t+\Delta t} - P_t) \tag{4.40}$$

The equation of motion at time $t + \theta\Delta t$ can be written as

$$M\ddot{X}_{t+\theta\Delta t} + C\dot{X}_{t+\theta\Delta t} + KX_{t+\theta\Delta t} = P_{t+\theta\Delta t} \tag{4.41}$$

No special starting procedures are required in this method, because the displacements ,velocities and accelerations are all expressed at the same time.

The Houbolt method

This method [167] is based on the backward difference formulation in which the accelerations and velocities are obtained in terms of three successive backward displacement component as

$$\ddot{X}_{t+\Delta t} = \frac{1}{\Delta t^2}[2X_{t+\Delta t} - 5X_t + 4X_{t-\Delta t} - X_{t-2\Delta t}] \tag{4.42}$$

$$\dot{X}_{t+\Delta t} = \frac{1}{6\Delta t}[11X_{t+\Delta t} - 18X_t + 9X_{t-\Delta t} - 2X_{t-2\Delta t}] \tag{4.43}$$

The equilibrium equation is considered at time $t + \Delta t$. In this approach, a special starting procedure is necessary which is more accurate if another explicit or central difference method with a time-step equal to a fraction of the original time-step is used.

Since the effective mass in these methods includes a stiffness matrix, a full simultaneous equation solution is required for each time-step. The Houbolt method which is implicit is unconditionally stable and the required accuracy usually restricts the time-length. The stability of the method is discussed in [164]. The most significant weak point of this method is its artificial damping when a large time-step is used.

Implicit methods with numerical dissipation property

A α-Dissipation Family of Methods by which the artificial algorithmic errors due to higher modes are relatively damped out has been proposed by Hilber et al. [168] in which the dissipation in lower modes is parametrically controlled. The method uses the Newmark formulas with the modified equation of motion

$$M\ddot{X}_{n+1} + (1+\alpha)C\dot{X}_{n+1} - \alpha C\dot{X}_n + (1+\alpha)KX_{n+1} - \alpha KX_n = (1+\alpha)F^{ext}_{n+1} - \alpha F^{ext}_n \tag{4.44}$$

The algorithm is unconditionally stable and has second order accuracy if the parameters are selected so that $-1/3 \leq \alpha \leq 0$, $\gamma = \frac{1-2\alpha}{2}$ and $\beta = \frac{(1-\alpha)^2}{4}$. With $\alpha = 0$, the method reduces to the trapezoidal rule which has no dissipation. Numerical artificial damping increases when α is decreased. An implicit method

with numerical dissipation has been developed by Pohl [169] for dynamic problems but the higher mode errors can not be damped out properly.

4.6 Explicit time integration methods

This approach is based on time-integration techniques in which the solution at time $t + \Delta t$ is obtained by considering the information calculated at the previous time t.

These methods require no factorization of the effective stiffness matrix in the step-by-step solution so less storage of matrices is required.

All the explicit algorithms are *'conditionally stable'* so require a small time-step which is inversely proportional to the highest natural frequency of the discrete system.

The time-step restriction of these methods make them to be well suited for short-duration dynamic problems or wave propagation problems such as structures subjected to blast on high velocity impact. However, this restriction limits the effectiveness of the approach when used to study dynamic problems of long-duration, for example earthquake response problems.

It is worth noticing that, these methods enable new material properties to be used at the next step, so complex material models can be easily incorporated.

Among the currently used explicit approaches, the central difference method, the explicit form of the Newmark methods as a forward scheme and the Rung-Kutta method as a k-step approach are explained in the next sections.

4.6.1 Central difference method

One of the most widely used methods of explicit numerical integration in large-scale structural dynamic problems is the second order *' central difference Technique '*. It is said to have the maximum stability and highest accuracy of any explicit method of order two [170]. This method is based or the following central

difference formulae

$$\dot{X}_{t+1/2\Delta t} = \frac{(X_{t+\Delta t} - X_t)}{\Delta t} \tag{4.45}$$

$$\dot{X}_{t-1/2\Delta t} = \frac{(X_t - X_{t-\Delta t})}{\Delta t} \tag{4.46}$$

$$\dot{X}_t = \frac{(X_{t+1/2\Delta t} - X_{t-1/2\Delta t}}{)}\Delta t \tag{4.47}$$

$$\ddot{X}_t = \frac{(\dot{X}_{t+1/2\Delta t} - \dot{X}_{t-1/2\Delta t})}{\Delta T} \tag{4.48}$$

$$X_{t+1/2\Delta t} = 1/2(X_{t+\Delta t} + X_t) \tag{4.49}$$

and

$$X_{t-1/2\Delta t} = 1/2(X_t + X_{t-\Delta t}) \tag{4.50}$$

where $X_{t-\Delta t}$, X_t, and $X_{t+\Delta t}$ are displacements at three successive times. For calculating velocity and acceleration, Equations (4.49) and (4.50) are substituted in (4.47) and Equations (4.45) and (4.46) in (4.48) respectively, then we have:

$$\dot{X}_t = (\frac{1}{2\Delta t})(X_{t+\Delta t} - X_{t-\Delta t}) \tag{4.51}$$

$$\ddot{X}_t = \frac{1}{\Delta t^2}(X_{t+\Delta t} - 2X_t + X_{t-\Delta t}) \tag{4.52}$$

Using the Taylor Series Rule, it can be shown that, errors in Equations (4.49) and (4.50) are of order two, $O(\Delta t^2)$ which means that the error in displacement is quartered when Δt is halved. Substituting Equations (4.51) and (4.52) into (4.21) at time-step n and rearranging terms, a fully discrete temporal system for linear problems is obtained:

$$(\frac{1}{\Delta t^2}M + \frac{1}{2\Delta t}C)X_{t+\Delta t} = P(t) - (K - \frac{2}{\Delta t^2}M)X_t - (\frac{1}{\Delta t^2}M - \frac{1}{2\Delta t}C)X_{t-\Delta t} \tag{4.53}$$

from which displacement at time $t + \Delta t$ is obtained using displacements at time $t - \Delta t$ and t. In fact, these schemes, are based on the equilibrium condition at time t and that is why these algorithms are called *' explicit '*. The term $\frac{1}{\Delta t^2}M + \frac{1}{2\Delta t}C$ is called the *'effective stiffness'* denoted by $\hat{M}$ and the term on the right hand-side is called the ' effective force ' denoted by $\hat{P}$. Thus

$$\hat{M}X_{t+\Delta t} = \hat{P(t)} \tag{4.54}$$

The method is not self starting and a special starting procedure must be employed. Using Equation (4.21) with the two known values X_0 and $\dot{X}_0$, the acceleration $\ddot{X}_0$ is obtained. From Equations (4.51) and (4.52)

$$X_{t-\Delta t} = X_t - \Delta t \dot{X}_t + 1/2 \Delta t^2 \ddot{X}_t \tag{4.55}$$

from which $X_{-\Delta t}$ can be obtained.

It should be noted that, in cases in which only diagonal damping terms are included, the factorization of the effective mass matrix can be avoided and only mass matrix multiplication is then required to solve the equations which results in computational saving. Hence the effectiveness of this method depends on the use of an appropriate diagonal mass matrix. On the other hand, if non-diagonal damping terms are introduced, the solution requires the factorization of the effective mass matrix. This and the time-step restriction due to stability problem are shortcomings of this method. If diagonal mass is used, the effective stiffness does not need to be factorized the displacement components are obtained using

$$X_{t+\Delta t_i} = (\frac{\Delta_t^2}{m_{ii}})(P_t^i - \sum_{j=1}^{N} K_{ij} X_t^j) + 2X_t^i - X_{t-\Delta t}^i \tag{4.56}$$

where N is the number of degrees-of-freedom of the system, m_{ii} denotes the i th element of the diagonal mass matrix, and $X_{t+\Delta t}^i$ and P_t^i denote the i th component of $X_{t+\Delta t}$ and P_t respectively. Warburton [171] has suggested a backward difference approximation explicit method in which damping may be included. Alternative schemes of explicit integration procedures using a central difference method have been proposed by Belytschko and Noor for undamped structural systems [172].

There are many other types of explicit direct integration methods [173], some of the widely used schemes are explained in the subsequent sections.

4.6.2 Explicit form of Newmark family method

By letting β equal zero in the Newmarks methods Eqs. (4.21) , (4.22) and (4.23), the algorithm becomes explicit and displacement at $t + \Delta t$ can be evaluated from the displacement, velocity and acceleration at t.

4.6.3 Fourth-order Runge-Kutta method

One of the most popular explicit methods with high accuracy is the Runge-Kutta method which is recommended in most numerical references [174-176]. In this algorithm, the accuracy is increased by subdividing the time in each time-step (hence tending the numerical method to the exact solution). The accuracy of the Runge-Kutta method can be graphically illustrated when compared with that of the the Euler rule method and the the trapezoidal rule method Fig. 4.6 A and B.

The governing equations may be written as

$$X_{t+\Delta t} = X_t + \Delta t\dot{X} + \Delta t^2/6[A_0 + A_1 + A_2] + O(\Delta t^5) \tag{4.57}$$

$$\dot{X}_{t+1} = \dot{X}_t + 1/6\Delta t^2[A_0 + 2A_1 + 2A_2 + A_3] + O(\Delta t^5) \tag{4.58}$$

where

$$A_0 = \ddot{X}(t, X_t) \tag{4.59}$$

$$A_1 = \ddot{X}(t + 1/2\Delta t, X + 1/2\Delta t\dot{X}_t) \tag{4.60}$$

$$A_2 = \ddot{X}(t + 1/2\Delta t, 1/2\Delta t\dot{X} + 1/4(\Delta t^2)A_0) \tag{4.61}$$

$$A_3 = \ddot{X}(t + \Delta t, X_t + \Delta t\dot{X}_t + 1/2(\Delta t^2)A_1) \tag{4.62}$$

The desirable features of this one-step algorithm are

- The algorithm is self-starting and the time-step can be changed easily.
- The method possesses a high order of accuracy.
- The algorithm has all the merits of an explicit method such as negating the need for iteration in a non-linear procedure.

The disadvantage of the algorithm is the computational time required which may be relatively large compared with the other numerical integration methods.

The Advantages and disadvantages of the explicit methods

As already mentioned, since in these methods factorization of the effective mass matrix is not required, the number of computations depend principally on the number and complexity of the elements regardless of node numbering and hence, the bandwidth of the mesh. The only disadvantage of these procedures is the restriction of the time-step due to the stability problem. In the cases where these methods are used for dynamic problems with very rapid load variations or for non-linear path-dependent materials such as elasto-plastic materials in which the required time-step to follow the material stress history is often not much more than the stability limit, the time-length restriction should not be considered as a disadvantage. On the contrary, with long duration loads with low load variation particularly in large scale systems in which the time-step stability limits are often far below the time-step required for accuracy, following the material stress history costs expensive computational time. On the other hand, reduction in time-step causes the round-off error to be increased. For this reason in such dynamic problems more accurate procedures such as fourth order Runge-Kutta methods are more appropriate.

Explicit-implicit methods

As mentioned in previous sections, both explicit and implicit algorithms have advantages and disadvantages. Explicit methods possess a lower order of accuracy, require a small critical time-step particularly in stiff systems and round-off error can have significant error while, the factorization of the effective mass matrix is the most significant problem in implicit algorithms. However, the merits of the two algorithms may be incorporated by combining them in an explicit-implicit method. In this method different parts of the overall system are treated by either an implicit or explicit algorithm. Thus the mesh is partitioned into two sets: explicit and implicit.

The time-step is restricted by the explicit part and this is the main shortcoming of such algorithms. However, the accuracy of these methods can not be

compared with explicit methods.

Two techniques of merging implicit and explicit methods for linear and non-linear finite element transient analysis, namely *'implicit-explicit mesh partition'*, and *'implicit-explicit operator splitting'*, have been proposed by Hughes and Taylor [177]. The stability and accuracy properties of the methods were discussed and techniques for improving implicit-explicit *' operator splitting* methods, which enable the treatment of kinematic constraints (e. g. incompressibility) in transient analysis were also discussed. In these mixed integration approaches, the critical time-step of explicit elements governs the system.

A family of implicit-explicit algorithms for transient finite-element analysis of dynamic problems has been proposed by Hughes and Liu [178]. The Newmark family of methods was used to define the implicit method and a predictor-corrector constructed from the Newmark family defined the explicit method. The implementation and the stability aspects of the proposed method were discussed. The critical time-step was found to be governed by the explicit elements.

The explicit-implicit methods are suitable for the dynamic problems in which the value of the highest natural frequency of the system is much greater than the lowest. This will be discussed in the next section.

Stiff systems

The equations of motion of large scale structural dynamic systems are often characterized by widely varying frequency components. Such structural dynamic equations whose highest frequencies are much greater than the lowest, are termed *' stiff system'* and the corresponding structure is called *' stiff structure'*. A statement which define the concept of stiffness is quoted from [158],

' stiffness occurs when stability requirements rather than those of accuracy constrain the time-length of a numerical integration method.'

The accuracy of the above mentioned numerical methods can be increased using predictor-corrector approach which will be discussed in the next section.

4.6.4 Predictor-corrector

Since error in a numerical analysis procedure is accumulative, the role of initial value accuracy through each time-step is of significant importance. In other words, if as good an initial guess as possible for the value of the displacement, velocity and acceleration at each time-step is used, the values at the end of corresponding time-step will have a better accuracy. This is conveniently done by using a predictor such as a separate explicit algorithm to provide the initial guess for a corrector which can be either an explicit or implicit method. Hence, the two algorithms together construct a method, the so called *' predictor- corrector method (PC)'*.

Many types of predictor-corrector algorithm can be described based on the number of predictions evaluations and corrections in the procedure. Single point PC methods use only information from the previous time-step while multi-point PC methods make use of information from more than one previous time-step. In PC methods, the corrector is used iteratively while in PEC methods (predictor-evaluate-corrector) or PECE (predictor -evaluate-corrector-evaluate), the corrector is used only once.

In the next section the non-linear solution techniques for static and dynamic problems will be discussed.

4.7 Non-linear solution techniques

Soon after the expression *'finite element method'* was pioneered [179] the method was extended to material [180] and geometric [181] non-linearity.

The increasing sophistication of theoretical models and the expansion of computer power have enabled the finite element analyst to predict more and more accurately the non-linear stress-strain relations of reinforced concrete.

The solution processes for non-linear finite element problems are in general computationally expensive, hence any steps that can be taken to significantly reduce these cost are of practical importance.

In static problems, the external forces are applied gradually in proportional steps until the desired final level is reached and the structural behaviour is simultaneously linearized. The so-called *' self correcting '* approaches emerge which are the basis of widely adopted incremental-iterative methods in which a number of iterations are performed during each load step until a convergence criterion either some norm of the residual or out-of-balance is satisfied.

The accurate solution of the equilibrium equations at each time step is even more important in dynamic than in static analyses as was pointed out by Bathe [180] namely, *any error introduced in step-by-step algorithms will accumulate which can not be compensated for later as in many static geometrically nonlinear analyses.*

In this section some of the more reliable accurate and efficient non-linear solution algorithms currently available are reviewed, more details are given in references [182-184].

4.7.1 Standard Newton-Raphson method (NR)

The finite element equilibrium equations of structural problems formulated in terms of displacements may be written as

$$KX = F \tag{4.63}$$

where X is the vector of unknown displacements, K is the global stiffness matrix in static and effective stiffness matrix in dynamic problems and F is the vector of nodal applied forces in static and effective force in dynamic problems.

The direct solution of Eq.(4.63) is readily obtained as

$$X = K^{-1}F \tag{4.64}$$

While any source of nonlinearity causes the dependence of the stiffness matrix /load vector, or both, on the displacements or their derivatives, direct solution becomes generally impossible and an incremental/iteration scheme appears to be inevitable [181].

Due to the nonlinearity, the equilibrium between internal and external force will generally not be satisfied and the procedure demands the simultaneous satisfaction of Eq. (4.63) and the residual force in the form

$$\phi = \int_{\Omega} B^T \sigma d\Omega - f = 0 \tag{4.65}$$

where f is the vector of body forces and surface traction.

The Taylor series expansion of residual force at $X_i + \Delta X_i$ gives

$$\phi_i(X_i + \delta X_i) = \phi_i(X_i) + \frac{\partial \phi}{\partial X}\Delta X_i = 0 \tag{4.66}$$

where the residual Jacobian matrix coincides with the tangential stiffness matrix K_t corresponding to displacement state X_i. Thus, the incremental displacements can be obtained as

$$\Delta X_i = P_i = -K_t^{-1}\phi_i \tag{4.67}$$

The solution of a non-linear problem almost invariably involves an increment/iterative process in which a number of iterative cycles are performed for each increment of applied load until the residual force ϕ vanishes. Therefore, a non-linear solution algorithm requires a means of determining successive *'search direction'* P_i, so that ultimately on the (i+1)th iteration the displacements

$$X_{i+1} = X_i + P_i \tag{4.68}$$

result in a stress field σ_i satisfying Eq. (4.65).

Equations (4.65) and (4.68) constitute the standard or full Newton-Raphson method.

In non-linear dynamic problems, the internal forces are predicted using the effective stiffness matrix

$$N(X)_{t+\Delta t} = \int_V N(X)_t + K_t(X)\Delta X \tag{4.69}$$

where $K_t(X)$ is the tangential matrix calculated at time t and

$$\Delta X = X_{t+\Delta t} - X_t \tag{4.70}$$

It should be mentioned that, the tangent matrix needs to be reformed for each time-step and the effective load vector also has to be reformed at each equilibrium iteration until convergence with desirable tolerance is achieved. Since a large computational effort is required in factorization and reformation of these matrices it is essential to seek a strategy to minimize these operations.

Chen [185] proposed an algorithm based on a relaxation of the response increments obtained by the Modified Newton Raphson scheme. It was reported in [185] that the algorithm is stable even if large load sizes are adopted for the analysis.

The accelerated constant stiffness iteration proposed by Chen is shown in Fig. 4.7. More detail can be found in [185]. The computational aspects and numerical evaluation of the mixed-time implicit-explicit methods for structural dynamics have been presented by Liu et al. [286]. Two numerical examples were shown to examine the efficiency of the scheme.

The currently available techniques for the iterative dissipation of the residuals may be categorized as:

4.7.2 Modified Newton-Raphson method (MNR)

In several variations of the standard non-linear solution procedures the tangent stiffness is only updated occasionally such as Initial Stiffness and Modified NR, which will be explained here briefly.

Initial stiffness methods (IS)

In this approach, the internal forces are predicted by

$$N(X)_{t+\Delta t} = \int_v K X_{t+\Delta t} + P(X)_t \tag{4.71}$$

where K is the initial stiffness matrix and $P(X)_t$ is the pseudo-force.

The IS method seeks to reduce the computation costs associated with the NR method by employing the original structural stiffness matrix K_0 at all times when determining the search direction, Eq. (72). In this way, after the first increment of the first iteration, only Equation resolution needs to be performed. This approach has been shown to be unconditionally stable [187]. However, whereas the NR method possesses a quadratic rate of convergence, the Initial Stress approach has only a linear rate, and convergence can be slow if the structure exhibits a high degree of nonlinearity. Therefore, an efficient algorithm can be found by combining the two approaches and the stiffness matrix needs to be factorized only once during a load increment thus is termed the *Modified Newton method (MN).*

The Standard and Modified Newton-Raphson methods are depicted schematically in Figs. 4.8 A and B.

Non-linear solution techniques in direct integration methods

4.7.3 Implicit algorithms in non-linear problems

In this section the solution algorithms for linear problems already described are extended to account for non-linear behaviour. Two basic modifications are required to be made.

1. The equivalent nodal elastic resisting forces (internal forces) of the structure i. e. KX, must be replaced by its non-linear counterpart KX given by Eq. (4.1)

2. The displacements and the corresponding stress should satisfy the non-linear stress-strain relationship of the structure's material.

The equilibrium condition is

$$M\ddot{X}_{t+\delta t} + C\dot{X}_{t+\delta t} + N(X)_{t+\delta t} = P^{ext}_{t+\delta t} \tag{4.72}$$

where the equivalent internal force vector $N(X)_{t+\Delta t}$ is given by

$$N(X)_{t+\delta t} = \int_V B_{t+\delta t}\sigma(\epsilon)_{t+\delta t}\, dV \tag{4.73}$$

In the above Equation, $N(X)_{t+\delta t}$, is the nodal plastic/elasto-plastic resisting force, B is the strain-displacement matrix and σ is a non-linear function of ϵ depending on the constitutive material low defined as

$$\sigma = F(\epsilon) \tag{4.74}$$

The integral is taken over the element volume at time $t + \Delta t$.

A formula is required to predict the internal forces at time $t + \Delta t$, in terms of the internal forces at time t, which may be made by two approaches, tangent stiffness and initial stiffness methods.

4.8 Explicit algorithms in non-linear problems

For non-linear analysis the displacement at time $t+\Delta t$ is calculated by considering the equilibrium equation of the discrete structural system at time t. In this case the equilibrium of motion can be written as

$$M\ddot{X} + C\dot{X} + P^{int} = P^{ext} \tag{4.75}$$

where, P^{int} is the nodal visco-elastic or visco-elasto-plastic resisting forces which is evaluated by

$$P^{int} = \sum_{i=1}^{N} \int_v B^T \sigma(\epsilon_e)\, dV \tag{4.76}$$

where B is the strain-displacement matrix and σ depends on the non-linear behaviour of the material. The integral is taken over the element in which one or

more Gauss points have reached their yielding point according to the proposed failure criterion. For example, for the central difference method Equation (4.53) becomes

$$(\frac{1}{\Delta t^2}M+\frac{1}{2\Delta t}C)X_{t+\Delta t}=P^{ext}(t)-(N(X_t)-\frac{2}{\Delta t^2}M)X_t-(\frac{1}{\Delta t^2}M-\frac{1}{2\Delta t)}C)X_{t-\Delta t} \tag{4.77}$$

In each time-step, the excess stress vector is evaluated using the proposed failure criterion. The visco-plastic strain is evaluated and is subtracted from the total strain to obtain the elastic strain. The internal force $N(X_t)X_t$ is determined using Eq. (4.76), The residual force vector ϕ is evaluated using

$$\phi = P^{ext}_{n+1} - [M\ddot{X}_{n+1} + P^{int}_{n+1}] \tag{4.78}$$

The unknown vector Δd is evaluated using $K_{eff}\Delta d = \phi$ and the displacement vector is modified through iterations until the residual force is converged. The convergence criterion used for the examples is in the form

$$\frac{\phi^i_{n+1}}{\phi^I_{n+1}} \leq tol \tag{4.79}$$

where ϕ^i_{n+1} and ϕ^I_{n+1} are the residual force vectors for the ith and first iteration respectively and the tolerance tol is equal to 0.05.

It is worth noting that all terms in the right hand side (effective force $\hat{F}$) of Eq. (4.77) are determined at time t and $t-\Delta t$ so that the displacement at time $t+\Delta t$ is obtainable explicitly.

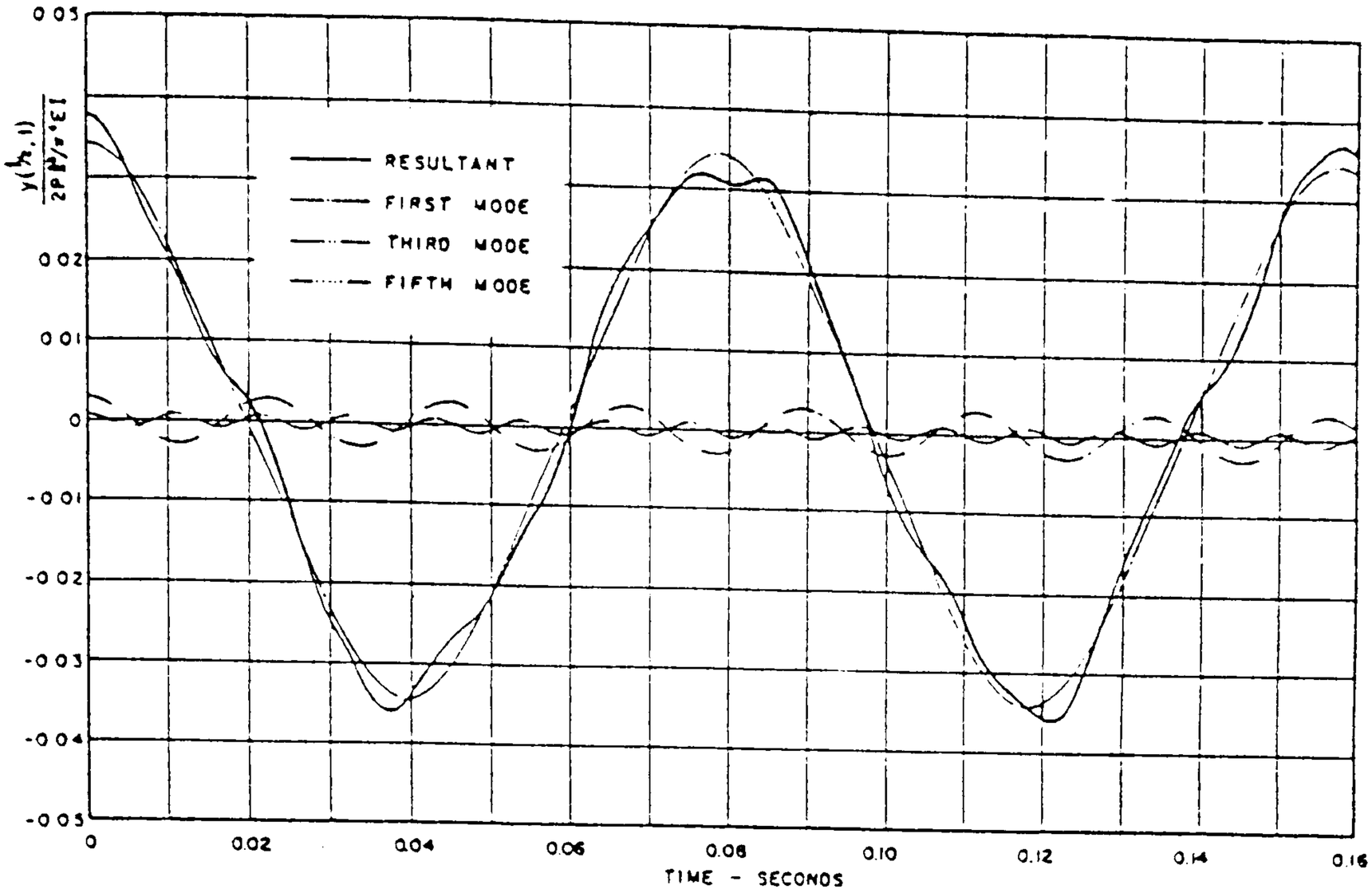

Fig. 4.1 Representation of the first fifth modes of a beam

(taken from [157]).

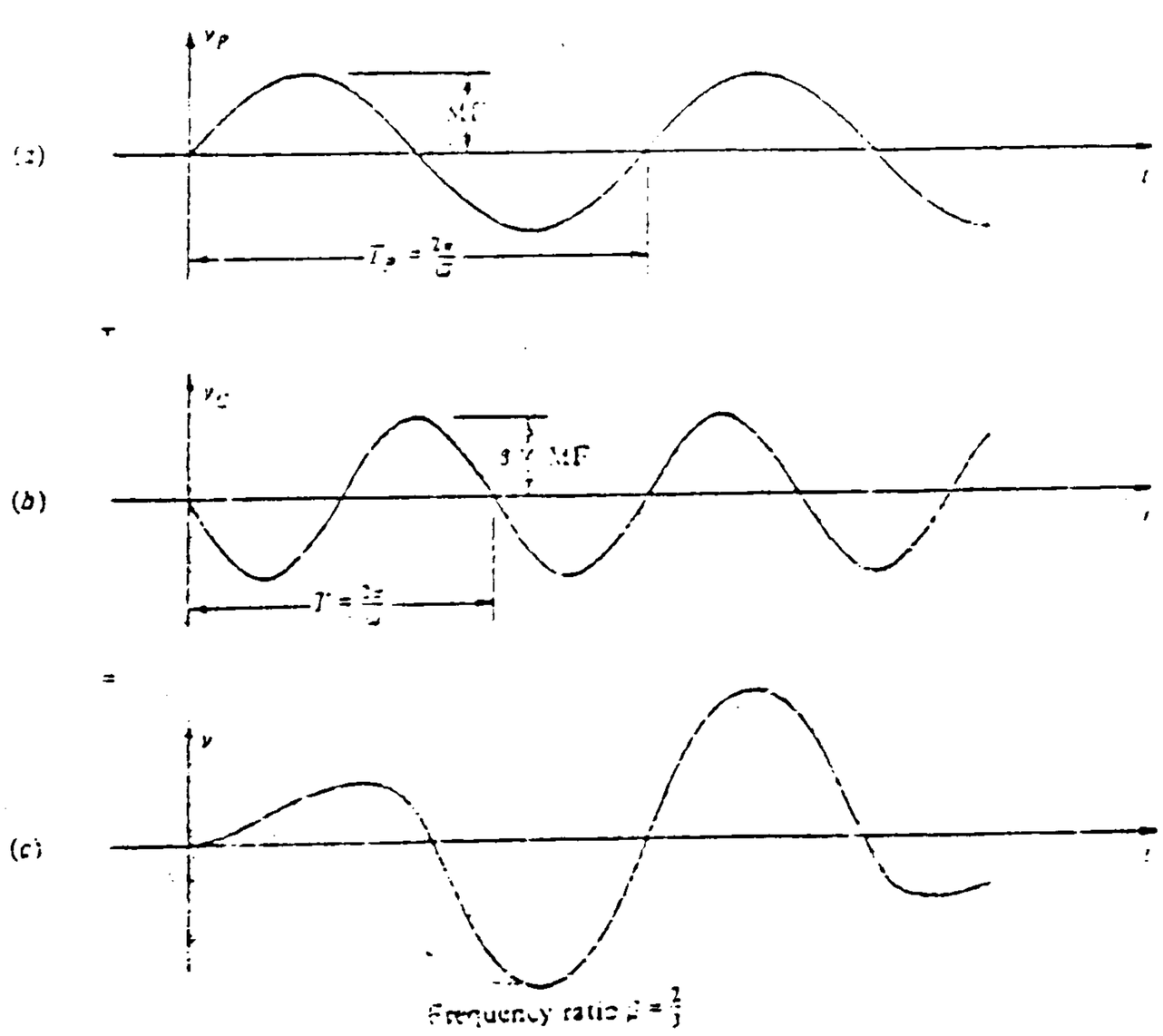

Fig. 4.2 Response to harmonic load from at-rest initial condition,

a) steady state, b) transient, c) total response.

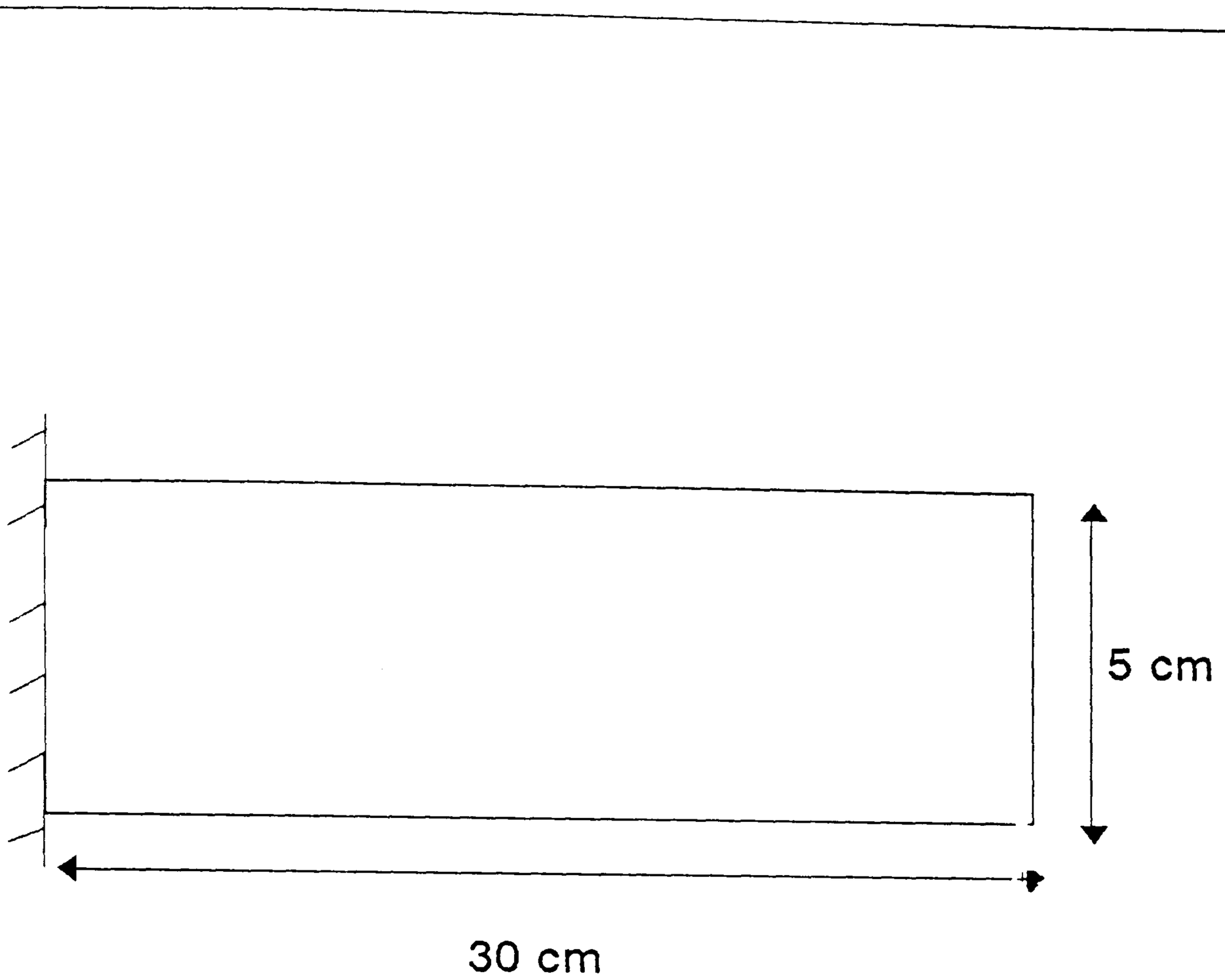

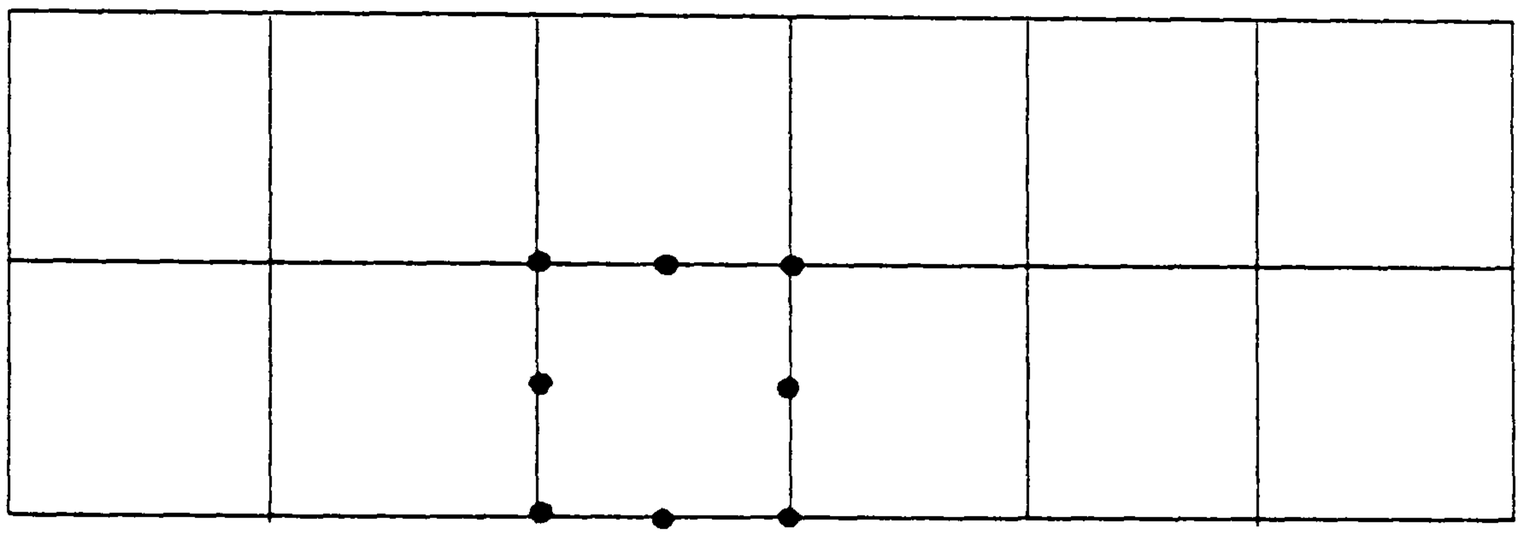

Fig. 4.3 Geometry and spatial discretisation of cantilever beam.

Fig. 4.4 Tip-deformation of the cantilever beam
with different degrees-of-freedom

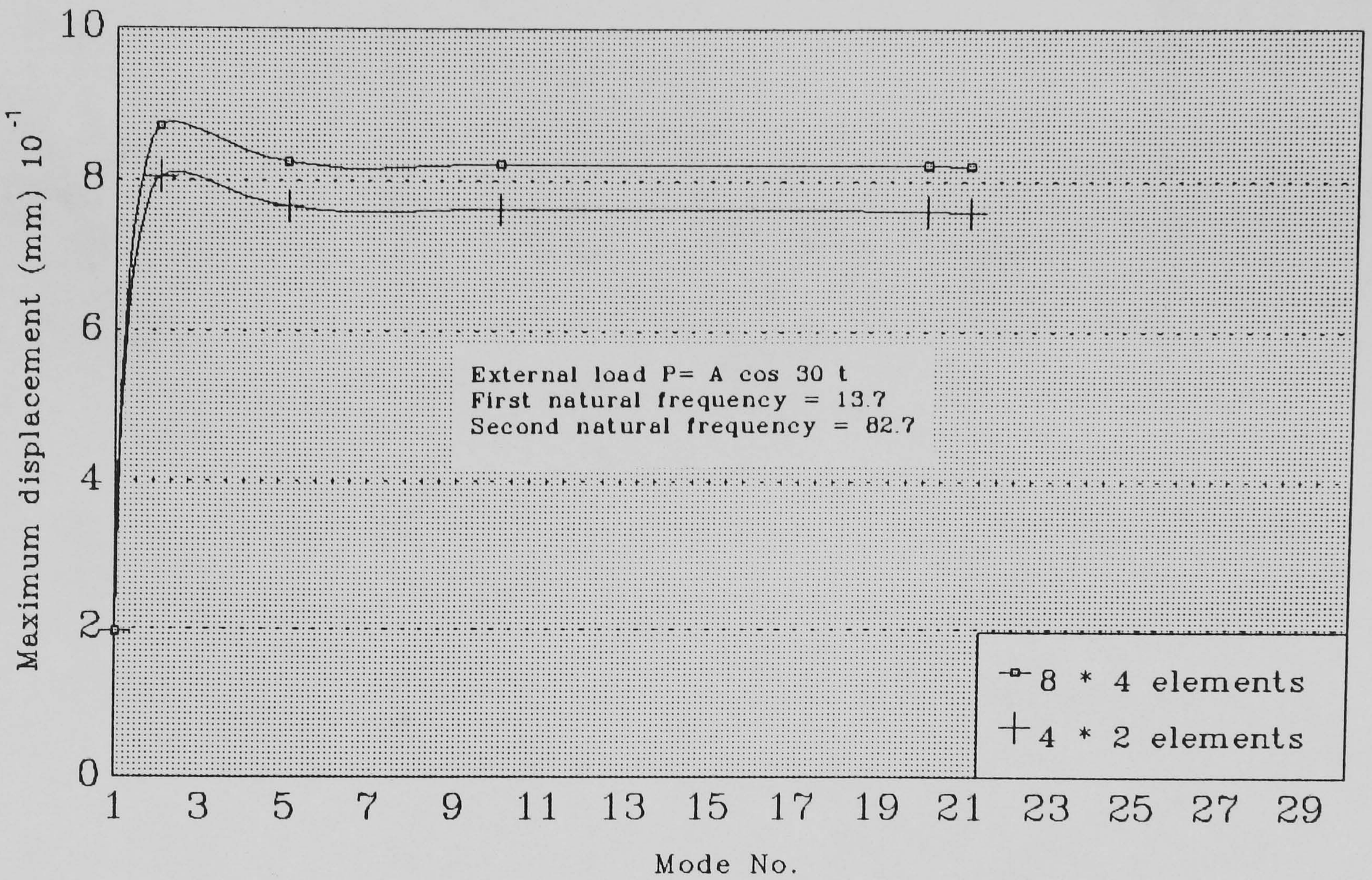

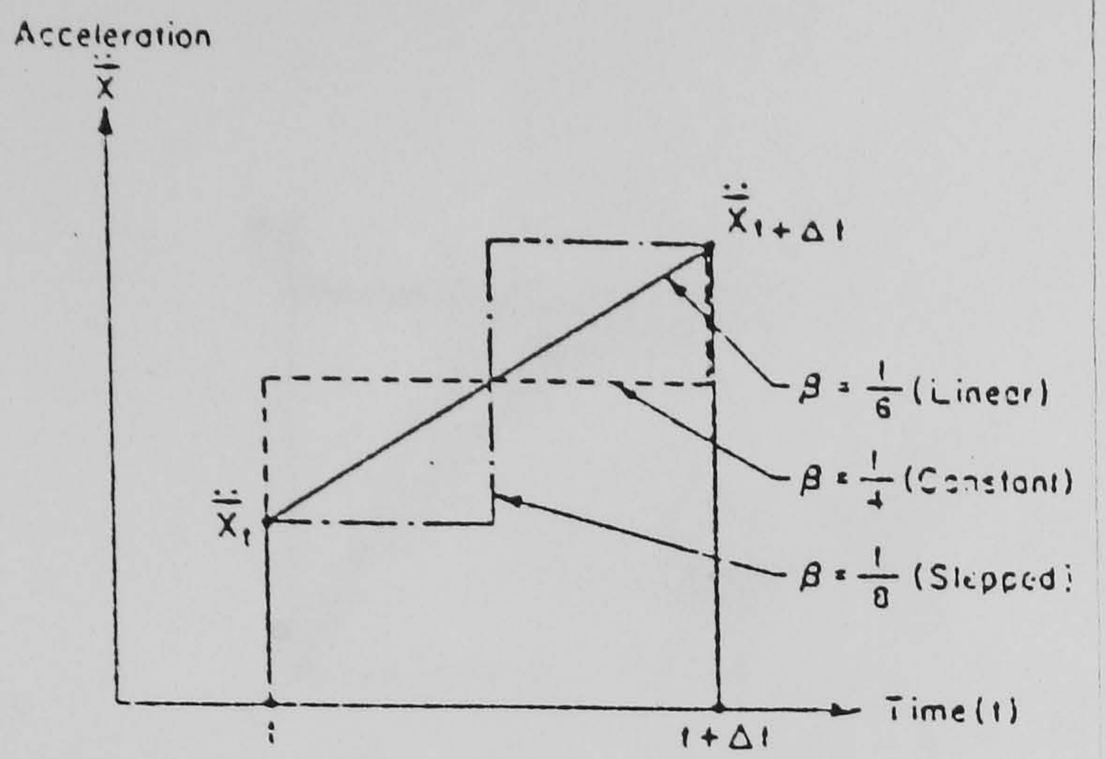

Fig. 4.5 Three types of linear variation of acceleration.

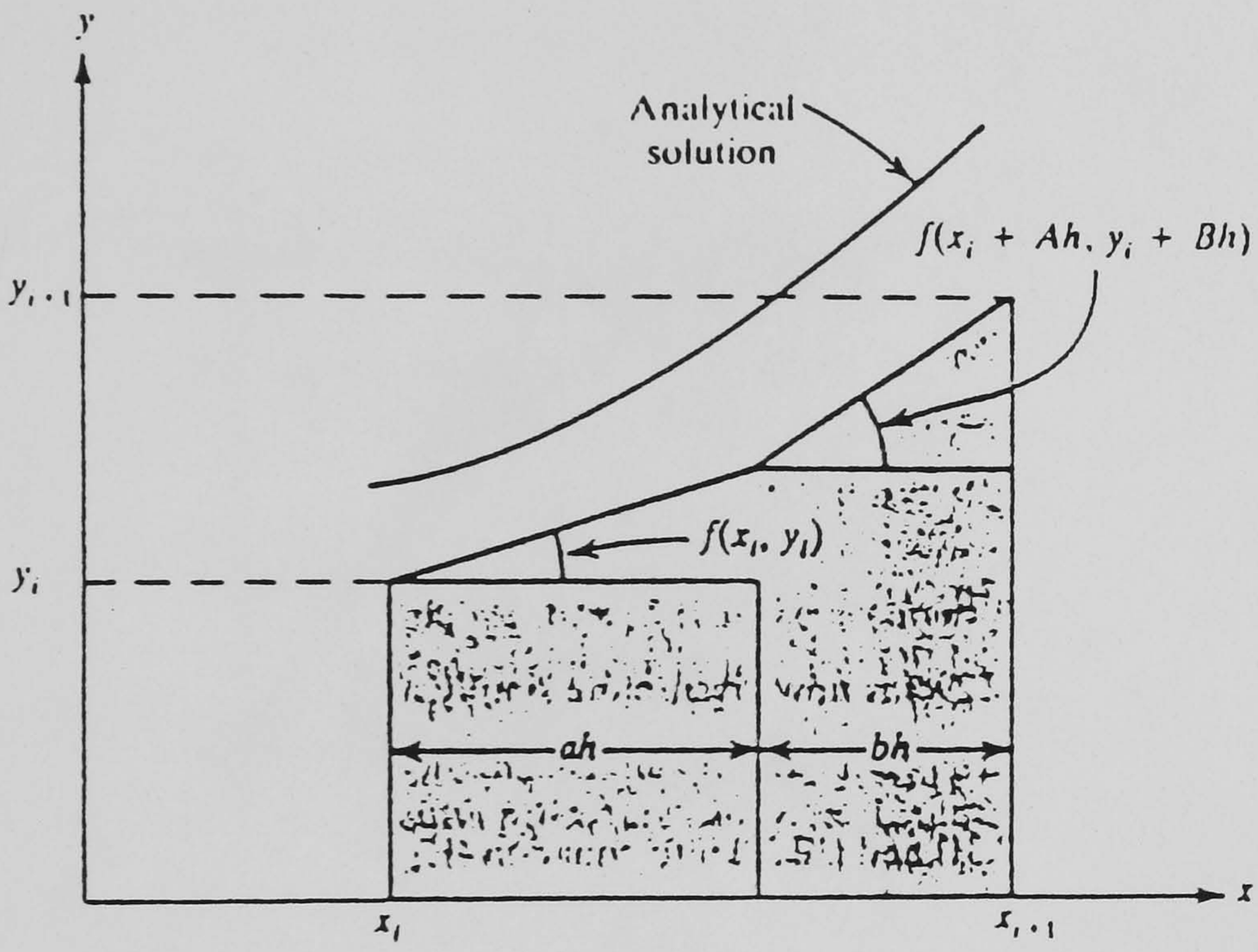

Fig. 4.6 A Graphical representation of second-order

Runge-Kutta method

Fig. 4.6 B Graphical representation of the relationship

between X and t

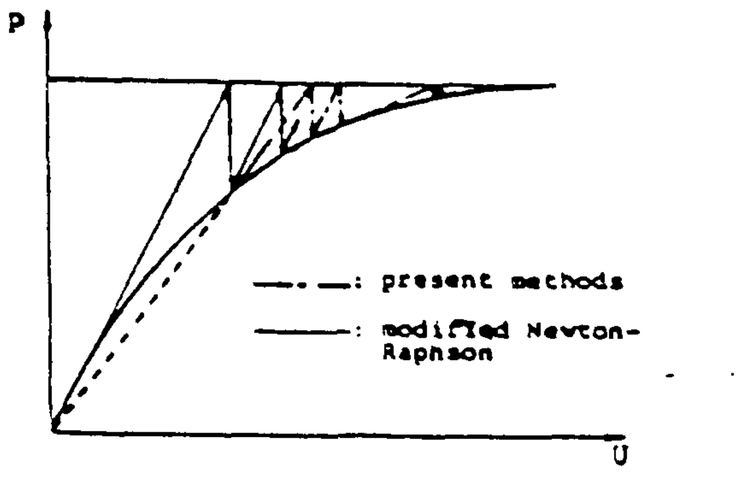

Fig. 4.7 Accelerated constant stiffness iteration. (taken from [185])

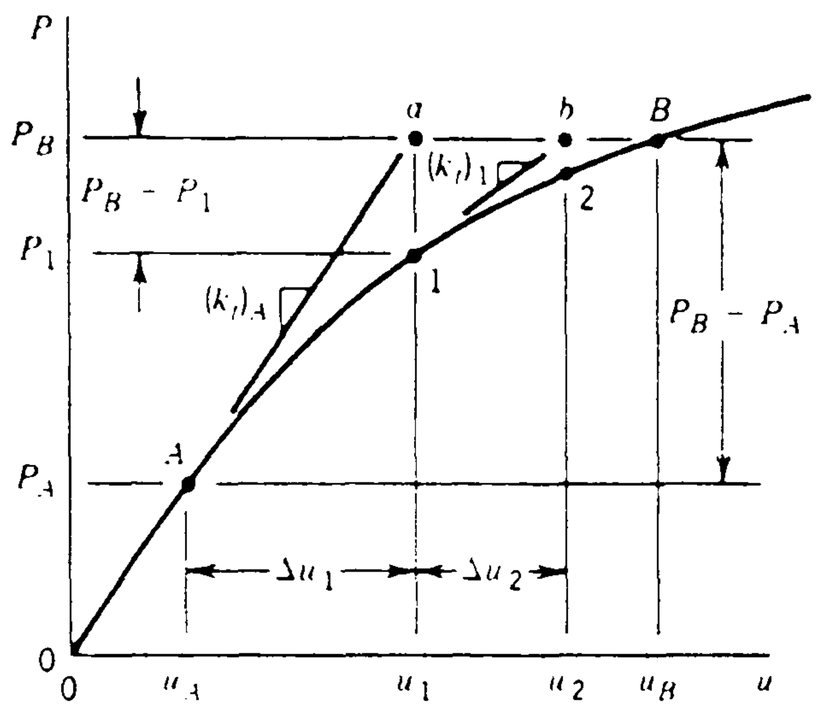

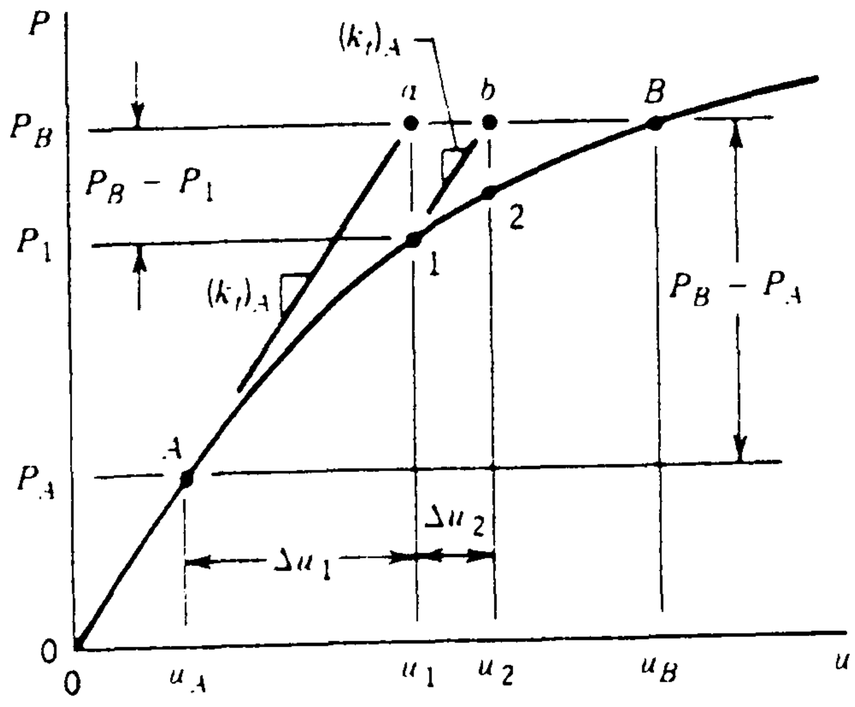

Fig. 4.8 and B, Newton-Raphson and modified Newton-Raphson.

Chapter 5

Stability and Accuracy Criteria for Numerical Algorithms

5.1 Introduction

The term stability refers to the study of errors made at one stage of the computations and how they may affect subsequent computations. The differential equation to be solved has a solution which remains bounded as time t increases and it is required that the numerical solution should have the same property which if so, means that a stable solution has been obtained.

As previously stated, most of the implicit integration methods for the solution of discretised equations of structural dynamics are *'stable'* algorithms, but have problems associated with *'accuracy'*. On the other hand the explicit methods have the advantage of *'accuracy'* but are only *'conditionally stable '*. Therefore, a comprehensive study of *stability* and of the various algorithms available is necessary.

The aims of this chapter are summarized as follows

- To review the mathematical forms of various types of errors arising from numerical analysis of dynamic problems .
- To assess the accuracy and stability of currently used methods of integrators.

- To assess the inaccuracies arising from the time-discretisation used in direct methods.

- To compare the numerical stability of the direct integration methods discussed in Chapter 4.

- To discuss and assess the instability due to visco-plastic strain approximation in visco-plastic problems.

The Chapter starts with the definitions of some of the terms used in dynamic problems and continues with an explanation of the accuracy of some currently used methods. The next section is devoted to a discussion of the accuracy of the Newmark family of methods, and a discussion of the methods for deriving the stability conditions of implicit and explicit algorithms. The artificial algorithmic errors, numerical dissipation and dispersion, are the subject of the next sections.

In the next section the effect of numerical damping on the structural responses using the currently used integration methods is discussed and assessed.

The chapter closes with a description of the stability criteria in non-linear analysis of static and dynamic problems.

5.2 Errors in numerical analysis of dynamic problems

Local and global truncation error

In the numerical analysis literature two measures of error of the Linear Multistep Method (LMM) are usually defined. These are the local truncation error (LTE) and the global truncation error (GTE) [174-176, 188, 189].

The local truncation error (LTE)

The local truncation error is the error that occurs during a time step assuming that there are no previous errors, thus all of the back values are exact. The local

truncation error can be defined by the associated linear difference expression [158]

$$LTE = \sum_{J=0}^{k} [\alpha_j X_{t+j\Delta t} - \Delta t^q \beta_j X^q_{t+j\Delta t}] \tag{5.1}$$

where X(t) is a continuously differentiable function in the interval of integration and q takes values 1 or 2 according to whether (5.1) is a first or second order ordinary differential equation. By expanding as a Taylor series it can be shown that the expression is equivalent to a principal local truncation error (PLTE) of the form

$$T_{n+k} = C_{p+1} \Delta t^{p+1} X_n^{p+1} + O(\Delta t^{p+2}) \tag{5.2}$$

where p, a positive integer is the order of the method and C_{p+1} is the error constant.

The term $C_{p+1} \Delta t^{p+1} X_n^{p+1}$ is referred to as *'Principal local truncation error'* or PTLE. Relation (5.2) can be used for both explicit and implicit methods. The global truncation error (GTE) is the actual accumulated error at a given time t_n, thus the global error is defined by

$$E_{n+k} = X(n+k) - X_{n+k} \tag{5.3}$$

where $X(n+k)$ X_{n+k} and are the exact and the numerical values respectively. It can be shown that, while the local truncation error is of order p+1 the global truncation error is of order p due to accumulation [158]. Therefore, the error associated with each increment (LTE) in the Euler Rule is of order $O(\Delta t^2)$ and the global truncation error (GTE) is of order $O(\Delta t^1)$, hence, the Euler Rule methods are more suitable for *'predicting'* the unknown value in each time-step. In fact, the Modified Euler Rule can be categorized as a simple predictor corrector rule Fig. 5.1.

Round-off Error

When working with a limited number of digits to represent a number as on a computer, rounding error is inevitable for most arithmetic calculations. Its value is dependent upon the precision of the computational accuracy chosen for

example, single-precision, double-precision or triple-precision. In the numerical solution of differential equations, computers can retain only a finite number of significant figures. Hence rounding errors increase as time-length decreases.

Users usually choose to work in single-, double-,or triple-precision and have no further control over the level of round-off errors which is a fixed value for a specified computer. The point is that as Δt tends to zero, the rounding-off tends to infinity, thus what common sense tells us is corroborated that, in general, convergence to the accurate solution can never be achieved in practice with a computer that works in finite arithmetic.

Starting Error

Since initial value problems are being solved numerically, a further numerical error the so called *'starting error '* is likely to occur [188, 189].

It is worth noting that [158]

Contrary to the effect of truncation error on the order of GTE, there is no loss of order in the starting errors due to accumulation. In other words, one can afford to take starting error equal to $O(\Delta t^p)$ without altering the order of GTE.

5.3 Accuracy

The accuracy of numerical integration methods is affected by many parameters. Apart from the expected acceptable tolerance usually defined in engineering problems and the round-off error due to the capability of the computer, the accuracy of a numerical algorithms, can be categorized as follows:

- *'Spatial discretisation'* accuracy.
- *Accuracy due to the order of the integrator* used in the method.
- *'Time discretisation'* accuracy.
- Accuracy due to *numerical damping.*

5.3.1 Spatial discretisation accuracy

According to the Sturm separation theorem [141], the values of the natural frequencies of a system decrease as the number of degrees of freedom increase. In other words, if A_r denotes a symmetric $r \times r$ matrix and $\lambda_i(A_r)$ denotes the ith eigenvalue of the matrix A_r then

$$\lambda_i(A_{r+1}) \leq \lambda_i(A_r) \leq \lambda_{i+1}(A_{r+1}) \tag{5.4}$$

It can be deduced that, the error due to spatial discretisation increases as the number of elements in the mesh is decreased [157].

The influence of spatial discretisation on the natural frequencies of structures has been studied and is discussed in the next section.

5.3.2 The effect of spatial discretisation on the natural frequency

As previously mentioned, in the finite element method the stiffness of the system is influenced by the number of degrees-of-freedom, the number of nodes per element, the type of shape function and the number of integration points in an element. Assuming the shape function and Gaussian points are defined, the natural frequencies of a system decrease as the number of elements in mesh is increased. This will be shown by an example in the following section.

Example 5.1

In order to assess the effect of spatial discretisation on the structural natural frequencies, a cantilever beam has been analysed using different number of isoparametric elements. The beam has been spatially discretised using 8-noded isoparametric element. The consistent mass matrix has been evaluated using a 3 by 3 integration points. A program originally developed by Smith et al. [116] has been used for evaluating the natural frequencies.

The natural frequencies of the cantilever beam for different numbers of elements have been evaluated and the effect of spatial discretisation on the natural

frequencies has been studied.

The influence of spatial discretisation on the natural frequency is shown in Tables 5.1 A, B and C. It can be seen that as the number of elements in mesh increases, the natural frequencies are decreased, hence *the natural frequencies of the system tend to real structure as the number of elements become infinit.*

Table 5.1 A The effect of spatial discretisation on the natural frequencies in a cantilever beam. The natural frequencies are given as the ratio of the natural frequencies with respect to those of the finest mesh which are given in the first column.

Node number	N. F. with 6 × 3 elements	N. F. with 4 × 2 elements	N. F. with 4 × 1 elements	N. F. with 2 × 1 elements	N. F. with 1 × 1 elements
1	25.44107	1.0039	1.0106	1.0177	1.0471
2	130.6982	1.0084	1.0252	1.0660	1.2600
3	164.6240	1.0013	1.0020	1.0176	1.4101
4	303.1367	1.0232	1.0430	1.1650	1.9504
5	492.9397	1.0024	1.0030	1.0183	1.8496
6	495.5647	1.0628	1.0730	1.4384	2.0730
7	702.5972	1.0413	1.0783	1.2850	1.5869
8	817.2677	1.0007	1.0062	1.1689	1.8164
9	870.2709	1.0437	1.1103	1.1632	2.4494
10	974.7750	1.0647	1.0062	1.1560	3.4035
11	1032.459	1.0795	1.0530	1.3013	
12	1114.044	1.0144	1.0440	1.2540	
13	1157.827	1.0121	1.0290	1.2385	
14	1193.802	1.0780	1.1098	1.2540	
15	1269.096	1.0284	1.1056	1.2411	
16	1290.171	1.0248	1.1031	1.2248	
17	1307.447	1.0176	1.1239	1.6190	
18	1321.474	1.0310	1.1302	1.7040	
19	1346.663	1.0773	1.1263	2.4621	
20	1374.579	1.0946	1.1929	2.4185	

Table 5.1 B

Node number	N. F. with 6×3 elements	N. F. with 4×2 elements	N. F. with 4×1 elements
21	1472.3065	1.0680	1.1596
22	1478.9487	1.1069	1.2219
23	1571.1315	1.0961	1.1941
24	1571.6720	1.1521	1.1980
25	1683.8560	1.1159	1.1990
26	1721.2656	1.1063	1.2156
27	1781.1402	1.0950	1.1881
28	1857.1439	1.0991	1.1632
29	1891.1807	1.1079	1.1618
30	1914.1590	1.1196	1.1917
31	1979.5785	1.1122	1.1930
32	1996.9917	1.1338	1.3287
33	2047.7331	1.1334	1.3429
34	2171.2522	1.1312	1.2883
35	2214.7471	1.1743	1.4304
36	2289.4969	1.1485	1.4155
37	2290.8765	1.1681	1.4472
38	2355.9598	1.1617	1.4085
39	2381.4442	1.1755	1.3956
40	2483.9296	1.1321	1.3834

Table 5.1 C

Node number	N. F. with 6 × 3 elements	N. F. with 4 × 2 elements
41	2558.4741	1.1415
42	2571.8600	1.1385
43	2574.3197	1.1570
44	2578.9177	1.1846
45	2617.7935	1.1685
46	2646.1086	1.1859
47	2672.6297	1.2073
48	2708.8029	1.1935
49	2731.0088	1.1955
50	2806.8827	1.1818
51	2853.2999	1.1947
52	2869.3881	1.2747
53	2947.9099	1.4104
54	2973.6149	1.4060
55	2984.4000	1.4035
56	2990.0379	1.4164
57	3003.9173	1.6160
58	3066.4938	1.5907
59	3104.1695	1.5802
60	3119.2387	1.5960
61	3181.3661	2.0833
62	3187.3890	2.080
63	3233.2845	2.050
64	3315.8425	2.001

5.3.3 Accuracy due to the order of the method

In order to assess the accuracy of methods currently used, a number of methods are discussed in the next sections.

Basic Euler and modified Euler method

A number of direct integration approaches are based on the *' Euler Rule '* and are normally expressed in the form

$$y_{n+1} = y_n + \Delta t \dot{y}_n + (O)\Delta t^2 \tag{5.5}$$

where $\dot{y}_n = f(y_n, t_n)$. y_{n+1} is the approximated functional value and y_n is the given initial condition. Since the local truncation error associated with each time-step Δt is of the order $(O)\Delta t^2$, and the global truncation error over many intervals is of order $(O)\Delta t$ [158], this method can be inaccurate.

The Modified Euler method uses a truncated Taylor series in which the first and second derivative terms are retained, that is

$$y_{n+1} = y_n + \Delta t \dot{y}_n + \frac{\Delta t^2}{2} \ddot{y}_n \tag{5.6}$$

Substituting

$$\ddot{y}_n = \frac{\dot{y}_{n+1} - \dot{y}_n}{\Delta t} \tag{5.7}$$

into Eq. (5.6) and rearranging gives

$$y_{n+1} = y_n + \frac{\Delta t}{2}(\dot{y}_n + \dot{y}_{n+1}) + (O)\Delta t^3 \tag{5.8}$$

where

$$\dot{y}_n = f(y_n, t_n) \tag{5.9}$$

$$\dot{y}_{n+1} = f(y_{n+1}, t_{n+1}) \tag{5.10}$$

Clearly, the local truncation error is now of order three and the global truncation error is of order two consequently, the Modified Euler method is one order more accurate than the Basic Euler method. The Euler method is demonstrated graphically in Fig. 5.2.

5.3.4 Accuracy of the Newmark family of methods

Order of the method [161]

The Newmark method can be expressed as

$$M\ddot{X}_{n+1} + C\dot{X}_{n+1} + KX_{n+1} = F_{n+1} \tag{5.11}$$

$$X_{t+\Delta t} = X_t + \Delta t\dot{X} + (\Delta t)^2[(1/2-\beta)\ddot{X}_t + \beta\ddot{X}_{t+\Delta t}] \tag{5.12}$$

$$\dot{X}_{t+\Delta t} = \dot{X}_{t+\Delta t}[(1-\gamma)\ddot{X}_t + \gamma\ddot{X}_{t+\Delta t}] \tag{5.13}$$

As previously described, the parameter γ determines the order of the accuracy of the method. The Newmark method is a single-step in the vectors $[\ddot{X}_n, \dot{X}_n, X_n]$ whereas it is equivalent to the two-step (three-time-level) if written as a difference scheme in the displacements. The condition under which the local truncation error of the Newmark method is of order $O(\Delta t^2)$ can be obtained using Eq. (5.2) and the required consistency conditions from which with $\gamma = 1/2$ the accuracy of the method id of order $O(\Delta t^2)$ and is the same as when $C = 0$.

Period Elongation Error (numerical dispersion property) and Artificial Algorithmic Damping Error (numerical dissipation property) of the currently used numerical integrators will be discussed and assessed later on. In the next section, the theoretical stability conditions under which the critical time step is obtained will be discussed.

5.4 Stability problem

5.4.1 Theoretical stability conditions

In order to assess the stability of an algorithm, it is necessary to investigate the eigenvalues of the system [150, 151]. The equilibrium equations of motion are cast in normal coordinates which together with the prediction relation for the displacement and velocity enables the construction of a 3 by3 matrix in the form

$$X_{n+1} = AX_n + r_{n+1} \tag{5.14}$$

where X_n the so-called *state vector* is

$$X_n = [d_n, \Delta t v_n, \Delta t^2 a_n]^T \tag{5.15}$$

A is the *' amplification matrix '* and r_{n+1} is the *'load vector'* which is independent of the state.

The stability conditions for the parametric Newmark Family of Methods will be developed here, more details are given in [189].

The Newmark integration scheme in normal coordinate can be written as

$$\ddot{X}_{t+\Delta t} + 2\xi\omega\dot{X}_{t+\Delta t} + \omega^2 X_{t+\Delta t} = r_{t+\Delta t} \tag{5.16}$$

and the parametric relations for the displacement and velocity are expressed as

$$\dot{X}_{t+\Delta t} = \dot{X}_t + [(1-\delta)\ddot{X}_t + \delta\ddot{X}_{t+\Delta t}]\Delta t \tag{5.17}$$

$$X_{t+\Delta t} = X_t + \Delta t\dot{X}_t + [(1/2-\alpha) + \alpha\ddot{X}_{t+\Delta t}]\Delta t^2 \tag{5.18}$$

The above equations can be arranged in the following form

$$\mid \ddot{X}_{t+\Delta t}, \dot{X}_{t+\Delta t}, X_{t+\Delta t} \mid^T = A \mid \ddot{X}_t, \dot{X}_t, X_t \mid + L^r_{t+\Delta t} \tag{5.19}$$

where

$$A = \begin{bmatrix} -(1/2-\beta)\theta - 2(1-\gamma)k & \frac{1}{\Delta t}(-\theta - 2k) & \frac{1}{\Delta t^2}(-\theta) \\ \Delta t[1-\gamma-(1/2-\beta)\gamma\theta - 2(1-\gamma)\gamma k] & 1-\theta\gamma-2\gamma k & \frac{1}{\Delta t}(-\theta\gamma) \\ \Delta t^2[1/2-\beta-(1/2-\beta)\beta\theta - 2(1-\gamma)\beta k] & \Delta t(1-\beta\theta-2\beta k) & (1-\beta\theta) \end{bmatrix} \tag{5.20}$$

and

$$\theta = \mid \frac{1}{\omega^2\Delta t^2} + \frac{2\xi\gamma}{\omega\Delta t} + \alpha \mid^{-1}, k = \frac{\xi\theta}{\omega\Delta t} \tag{5.21}$$

$$L^T = \mid \frac{\theta}{\omega^2\Delta t^2}, \frac{\theta\gamma}{\omega^2\Delta t}, \frac{\beta\theta}{\omega^2} \mid \tag{5.22}$$

Stability and accuracy of an algorithm can be shown to depend on the eigenvalues of the amplification matrix A.

For deriving the accuracy and stability conditions, two points should be taken into account:

- If a method is stable then the free-vibration response is stable. Considering the free-vibration response, Equation (5.14) becomes

$$X_{n+1} = AX_n \tag{5.23}$$

- Since viscous damping causes an increase in the critical time-step, the undamped response of the desired approach will be considered.

The eigenvalues of A are determined by the characteristic Equation

$$det(A_{ii} - \lambda) = \lambda^3 - 2A_1\lambda^2 + A_2\lambda - A_3 = 0 \tag{5.24}$$

in which A_1, A_2, A_3 depend on the numerical algorithm . The maximum absolute value of the eigenvalues (λ_1, λ_2, λ_3) of A is called the *' spectral radius '* denoted by $\rho(A)$, thus

$$\rho(A) = \max[\lambda_1, \lambda_2, \lambda_3] \tag{5.25}$$

By repeated use of (5.23), the velocities and accelerations can be eliminated; then the difference Equation in terms of displacements can be obtained as

$$d_{n+1} - 2A_1 d_n + A_2 d_{n-1} - A_3 d_{n-2} = 0, \in (2, 3...N-1) \tag{5.26}$$

The discrete solution for d_n has the form

$$d_n = C_1\lambda_1 + C_2\lambda_2 + C_3\lambda_3 \tag{5.27}$$

in which C_1, C_2 and C_3 are determined from initial data.

Only two sets of eigenvalues will be obtained either

1. Two complex-conjugate roots (principal roots) i. e.

$$\lambda_{1,2} = A \pm iB \tag{5.28}$$

and one so-called *'spurious'* root

$$\lambda_3 \leq \lambda_{1,2} \tag{5.29}$$

which satisfy $\mid \lambda_3 \mid < \mid \lambda_{1,2} \mid < 1$

or

2. Three real roots λ_1, λ_2, λ_3.

The first case is desirable because substituting (5.27), into (5.26), leads to displacements d_n

$$d_n = \rho^n(C_1 \cos \Omega_D n + C_2 \sin \Omega_D n) + C_3\lambda_3 \tag{5.30}$$

in which

$$\rho = \sqrt{A^2 + B^2} \tag{5.31}$$

is the spectral radius. Comparing (5.30) with the exact solution for a viscously under-damped free-vibration, which in general has the form [168]

$$U_n = \exp -\xi_n \Omega n[d_0 \cos \Omega_D n + C_2 \sin \Omega_D n] \tag{5.32}$$

in which

$$C_2 = \frac{1}{\omega_D}(\xi_n \omega_D d_0 + v_0) \tag{5.33}$$

where, d_0 and v_0 are the initial displacement and velocity, ω_D and Ω_D are physically damped frequency and sampling frequency, respectively, and

$$\omega_D = \omega\sqrt{1 - \xi^2} \tag{5.34}$$

The terms in Eq. (5.30) can be specified as

- Artificial (numerical) frequency

$$\hat{\omega} = \omega_a\sqrt{1 - \hat{\xi}^2} \tag{5.35}$$

  in which ω_a is the artificial (numerical) undamped frequency.

- Numerical Sampling frequency

$$\hat{\Omega} = \hat{\omega}\Delta t \tag{5.36}$$

$$\hat{\Omega} = \arctan(\frac{B}{A}) \tag{5.37}$$

- The artificial (numerical) period can be related to artificial (numerical) frequency by

$$\hat{T} = 2\frac{\pi}{\hat{\omega}} \tag{5.38}$$

Therefore a numerical error known as the *'relative period error'* or *'dispersion'* can be defined as

$$e_r = \frac{\hat{T} - T}{T} \tag{5.39}$$

- Algorithmic (artificial) damping ratio due to numerical induced energy dissipation can be determined by

$$\hat{\xi} = -\frac{\ln(A^2 + B^2)}{2\hat{\Omega}} \tag{5.40}$$

in which

$$\hat{\Omega} = \frac{\omega_a \Delta t}{\sqrt{1 - \hat{\xi}^2}} \tag{5.41}$$

The spectral radius, the algorithmic damping and the relative period error are commonly used as criteria for assessment of a numerical algorithm.

For completeness, it is noticed that, the logarithmic decrement $\hat{\delta} = \ln[\frac{d(t_n)}{d(t_{n+\hat{T}})}]$, and amplitude decay function $AD = 1 - \frac{d(t_n+\hat{T})}{d(t_n)}$, are also measures of algorithmic dissipation. Either of these measures determines the other since

$$AD = 1 - \exp(-\hat{\delta}) \tag{5.42}$$

Remarks

- The first two roots of the characteristic Equation (5.24) must be complex-conjugate. Beyond the bifurcation point where the roots of the characteristic equation Eq. (5.24) change from complex-conjugate to real values so that the comparison is not longer valid.

- From Equation (5.30), it can be deduced that, the spurious roots λ_3, must be much smaller that the complex-conjugate roots and a large spurious root may causes significant errors in the numerical solution.

- In numerical analysis of dynamic problems, more attention must be focused on the effects of numerical dissipation and dispersion induced by higher modes.

5.5 Stability conditions for explicit algorithms

As mentioned previously, the most significant shortcoming of explicit methods is their conditional stability. In these procedures the time-step is bounded by a critical time-step obtained from the stability condition. Since the central difference methods are mathematically equivalent to the explicit form of the Newmark family of methods with $\gamma = 0.5$, the stability formulations of the former will be derived first after which those of the latter can be obtained easily.

For simplicity, a linear elastic single-degree-of-freedom system based on the modal superposition concept will be developed.

The response of a free-vibration system is bounded if the spectral radius determined from the eigenvalues of the amplification matrix of the method if

$$\rho(A) \leq 1 \tag{5.43}$$

In other words, the algorithm is stable if $\rho(A)$ lies in or on the unit circle in the Argand Diagram, otherwise the response growth infinitely.

Using the implicit form of the Newmark Family of Methods with $\beta = 0.$ which is the case for explicit algorithms, the Amplification Matrix A for the explicit algorithms can be written as

$$A = \begin{bmatrix} -1/2\theta - 2(1-\gamma)k & \frac{1}{\Delta t}(\theta - 2k) & \frac{1}{\Delta t^2}(-\theta) \\ \Delta t[1-\gamma-1/2\gamma\theta - 2(1-\gamma)\gamma k] & 1-\theta\gamma - 2\gamma k & \frac{1}{\Delta t}(-\theta\gamma) \\ 1/2\Delta t^2 & \Delta t & 1 \end{bmatrix} \tag{5.44}$$

with the third eigenvalue $\lambda_3 = 0$.

The values A and B Eq. (5.28) is obtained as

$$A = 1 - \frac{\Omega}{2}(\gamma + 1/2) \tag{5.45}$$

$$B = \Omega\sqrt{1 - \frac{\Omega^2}{4}(\gamma + 1/2)^2} \tag{5.46}$$

The spectral radius of A is traditionally plotted against $\omega\Delta t$ Fig. 5.3, for various values of γ. As is shown, the explicit Newmark method is stable if $\rho(A) \leq 1$ which is possible under the condition that:

$$\gamma \geq 1/2 \tag{5.47}$$

$$\Omega \leq \sqrt{\frac{2}{\gamma}} \tag{5.48}$$

From (5.46) it can be easily determined that, the requirement for a stable oscillatory response is

$$\Omega \leq \frac{2}{\gamma + 1/2} \tag{5.49}$$

and the eigenvalues are real if

$$\frac{2}{\gamma + 1/2} < \Omega < (\frac{2}{\gamma})^{1/2} \tag{5.50}$$

Hence

$$\Omega = \frac{2}{\gamma + 1/2} \tag{5.51}$$

is a bifurcation point beyond which $\rho(A)$ increases rapidly. Fig. 5.3.

The conditional spectral stability for explicit algorithms can be obtained by substituting $\gamma = 1/2$, in Equation (5.51) from which the maximum stability limit leads to

$$\Omega = \omega\Delta t \leq 2 \tag{5.52}$$

and the time-step restriction for each frequency is

$$\Delta t \leq \frac{2}{\omega} \tag{5.53}$$

It is a simple exercise to verify that the maximum frequency of the system satisfies the bound [177]

$$\omega_{max} \leq \max \omega^e_{max} \tag{5.54}$$

Where ω^e_{max}, is the maximum frequency of the unrestrained ith element then

$$\Delta t_{cr} \leq \frac{2}{\omega^e_{max}} \tag{5.55}$$

for undamped system.

The following should be noted:

- In cases in which viscous damping is included in the system , Equation (5.48) changes to [177].

$$\Omega < \frac{\sqrt{(\xi^2 + 2\gamma)} - \xi}{\gamma} \tag{5.56}$$

where ξ, is the viscous damping coefficient. Therefore the effect of damping is to increase the critical time-step of conditionally stable schemes and the undamped critical sampling frequency specified by Equation (5.56) serves a conservative value.

- When viscous damping is absent, the maximum value of Ω occurs for $\gamma = 1/2$ that is, $\Omega = 2$ which is the same result as for the central difference method.

- The critical time-step Δt_{cr} can be expressed alternatively as the time required for an acoustic wave to transverse the element with the least transversal time. For homogeneous strain elements, this condition can be rewritten as

$$\Delta t_{cr} \leq \frac{l}{C} \tag{5.57}$$

where l and C are the element length and acoustic wave speed [190, 191].

- The stability and accuracy of a non-linear system is based on the fact that a non-linear system can be considered as piece-wise linear, where the tangent stiffness will represent the properties of the material at each time-step. This implies that for a hardening system as well as softening, the selected time-step will remain conservative if it is based on the initial linear stiffness of the system.

The artificial algorithmic damping $\bar{\xi}$ in the explicit Newmark method is plotted against sampling frequency $\omega\Delta t$ for different γ in Fig. 5.4. It can be seen that the explicit Newmark algorithm with $\gamma = 1/2$ exhibits zero damping and also has

the minimum numerical period distortion/shift phase Fig. 5.5. Therefore, it is deduced that the algorithm is most accurate when $\gamma = 1/2$. Fig. 5.6 illustrates the relative period elongation of free-vibration response obtained with $\gamma = 1/2$. The numerical instability caused by the time step can also be seen in the figure.

The round-off error effects on the free-vibration response of a linear single-degree-of-freedom system using the basic central difference method and the explicit Newmark method are plotted versus time in Fig. 5.7. This demonstrates the greater accuracy of the Newmark method compared with the central difference algorithm.

In the next section, the accuracy due to artificial algorithmic damping is discussed.

5.5.1 Accuracy due to artificial algorithmic damping

Numerical dissipation or period elongation (PE)

Period Error or Period Elongation (PE), is a measure of accuracy which can be used for comparing the efficiency of an algorithm, particularly when the higher modes are to be taken into account. Fig. 5.8 illustrates the the relative period elongation for some implicit algorithms. It can be seen that, the Houbolt method results in the maximum errors and the trapezoidal rule gives the minimum.

Numerical dispersion or amplitude decay (AD)

Since, as previously discussed the higher modes are likely to contain more numerical errors a desirable property for an algorithm which is to be used in structural dynamic problems, in which the role of the higher modes is not expected to contribute to the response of the system, is to filter the high frequency contributions out of the solution and to ensure simultaneously that the lower modes are not affected significantly. The mode number after which the effects of higher modes are to be damped depends upon the desired accuracy and the frequency of the applied load. Figs. 5.9 A, B, demonstrate the numerical dissipation property versus relative period (higher mode period/fundamental period) of some algorithms

and the corresponding spectral radii are illustrated in Figs. 5.10 A and B. These results confirm that, the Wilson θ Method exhibits appreciable (AD) error whilst the Trapezoidal Rule exhibits no dissipation property. It can be seen that, for the α-dissipation method and the Newmark algorithm with $\beta = 0.3025$ and $\gamma = 0.6$, the spectral radii are less than one as Δt tends to infinity which ensures that the response of higher modes is likely to be damped-out.

The bifurcation point at which the complex conjugate principal roots tends to real roots in the Wilson-θ Method, i. e. $\frac{\Delta t}{T} \approx .3$, is shown in Fig. 5.10 B.

The effect of Amplitude Decay Error ADE on the first and second modes of the tip-displacement of a cantilever beam under harmonic loading using the Wilson-θ Method with $\theta = 1.4$ is demonstrated in Fig. 5.11. This ensures that, for $\frac{\Delta t}{T_1}$, the algorithm has no numerical dissipation property, while for $\frac{\Delta t}{T_2}$ the response amplitude is damped-out strongly, (see Fig. 5.10 A). The effect of the variation of θ in the Wilson Method is plotted in Fig. 5.13 showing how the spectral radius changes with varying θ.

5.6 Implicit algorithm stability conditions

In contrast with the explicit algorithms in which stability limits restrict the time-step, implicit methods are mostly unconditionally stable and it is the accuracy requirement and computational cost that dominates the choice of time-step for non-linear problems. However, the slow convergence in iterative procedures, or errors introduced due to approximating the non-linear effects usually dictate the maximum acceptable time-step [169, 170, 189, 192-195]. The same procedure as used for explicit algorithms, can be used to determine the conditions under which implicit methods are stable, as follows.

5.6.1 Stability conditions

By evaluating the roots of the characteristic polynomial Eq. (5.24) the conditions under which the algorithm is stable are obtained as:

$$4 + C\Delta t(4\gamma - 2) + \omega^2 \Delta t^2 (4\beta - 2\gamma) > 0 \tag{5.58}$$

$$C\Delta t + \omega^2 \Delta t^2 (\gamma - 1/2) \geq 0 \tag{5.59}$$

$$\omega^2 \Delta t^2 \geq 0 \tag{5.60}$$

The algorithm has

- Unconditional stability, if

$$2\beta \geq \gamma \geq \frac{1}{2} \tag{5.61}$$

- Conditional stability, if

$$\gamma \geq \frac{1}{2}, \beta < \frac{1}{2} \tag{5.62}$$

and

$$\Delta t \leq \frac{\xi(\gamma - \frac{1}{2}) + \sqrt{\gamma/2 - \beta + \xi^2(\gamma - 1/2)^2}}{\omega_{max}(\frac{\gamma}{2} - \beta)} \tag{5.63}$$

The same results are obtained as with $C = 0$. However, for $C > 0$ can have $\gamma = 1/2$ to give a second order method and the roots of the characteristic polynomial will of course, still have a spectral radius less than unity [190, 191].

A variety of useful techniques obtained from the Newmark Family of Methods is listed in Table 5.2. It can be seen that the methods have no algorithmic damping and are second-order accurate when $\gamma = \frac{1}{2}$.

5.6.2 Stability conditions for the k-step algorithms

The k-step numerical algorithms such as the fourth-order Runge-Kutta scheme are k-step for the displacements and give the following recurrence relations when applied to the forced equation of motion,

$$\sum_{j=0}^{k} [\alpha_j M + \gamma_j \Delta t C + \beta_j \Delta t^2 K] X_{n+j} = F(t) \tag{5.64}$$

where F(t) are weighted values of the forcing function.

If the vector

$$X_{n+j} = r^{n+j}U \tag{5.65}$$

is assumed to be the general solution of the homogeneous equation

$$\sum_{j=0}^{k}[\alpha_j M + \gamma_j \Delta t C + \beta_j \Delta t^2 K]X_{n+j} = 0 \tag{5.66}$$

then the above equation has a non-trivial solution if

$$det \mid \sum_{j=o}^{k}[\alpha_i M + \gamma_j \Delta t C + \beta_j \Delta t^2 K]r^j \mid = 0 \tag{5.67}$$

If ϕ_n is assumed to be a particular solution, then the solution of Equation (5.65) is

$$X_{n+j} = r^{n+j}U + \phi_n \tag{5.68}$$

Substituting (5.68) into (5.67), gives the characteristic polynomial of the form

$$\sum_{j=0}^{k}[\alpha_j M + \gamma_j \Delta t C + \beta_j \Delta t^2 K]r^j = 0 \tag{5.69}$$

The numerical solution given by Equation (5.69) is *' stable'* if all the roots of the characteristic polynomial (5.67) lie in or on the unit circle in the Argrand diagram [192, 193].

There are different kinds of stability depending on the eigenvalues of the A matrix, which are given by det $P(\lambda) = 0$:

- A_0 -stable algorithms are those which give stability for differential equations with real negative eigenvalues [192]. In other words, for any value of $\lambda_j \Delta t$ on the negative real axis in Fig. 5.14, these algorithms which would apply to the dynamic equation with all overdamped modes, are stable.

- A-stable algorithms are those with stable solutions for values of $\lambda_j \Delta t$ anywhere in the left-hand half plane in Fig. 5.14 [193].

- Conditionally stable are algorithms if it is stable only for values of $\lambda_j \Delta t$ on one side of a stability boundary Fig. 5.14.

- A further result of Lambert [158] may be added as

  The A-stable method with second order accuracy and the smallest error constant is given by the Trapezium Rule.

5.7 Stability criteria in non-linear analysis

The stability conditions discussed earlier are based on linear material behaviour. In this section the stability conditions required in the nonlinear analysis of structures under transient force are discussed.

If the explicit form of visco-plastic strain approximation is used in non-linear analysis of dynamic problems, another stability criterion is added to the problem.

The implicit form of visco-plastic strain approximation for the displacement increments, discussed in Chapter 4, has the form

$$K\Delta X_n = \Delta f_n + (1-\theta)\Delta t_n \int_\Omega B^T D\dot{\epsilon}_n^P d\Omega + \theta\Delta t \int_\Omega B^T D\dot{\epsilon}_{n+1}^P d\Omega \qquad (5.70)$$

in which $\Delta f_n(t)$ is the effects of applied (body and boundary) loads, thermal strains, etc. By taking the time discretisation parameter $\theta = 0$, an explicit form of the above equation is obtained in the form:

$$K\Delta X_n = \Delta f_n + \Delta t_n \int_\Omega B^T D\dot{\epsilon}_n^p d\Omega \qquad (5.71)$$

in which D is the material stiffness. The stress increments can be determined by

$$\Delta\sigma_n = DB\Delta X_n - \Delta t_n D\dot{\epsilon}_n^{vp} \qquad (5.72)$$

Substituting ΔX from (5.71) into (5.72) leads to

$$\Delta\sigma_n = DBK^{-1}(\Delta t \int_\Omega B^T D\dot{\epsilon}_n^{vp} d\Omega + \Delta f_n) - \Delta t_n D\dot{\epsilon}_n^{vp} \qquad (5.73)$$

The explicit form of visco-plastic strain increment in a time-interval Δt can be expressed as

$$\Delta\epsilon_n^{vp} = \Delta t\dot{\epsilon}_n^{vp} = \Delta t\Gamma_n(\sigma_n)\sigma_n \qquad (5.74)$$

in which Γ_n is the *'visco-plastic strain-stress matrix'*, which is a local symmetric stress-dependent matrix whose specific form depends upon the yield criteria

employed. For isotropic situations with an associated visco-plastic law, Γ_n is symmetric and its order is that of the number of stress components in the constitutive relations i. e. 6, 4, 3 for three-dimensional, plane strain/axisymmetric and plane stress situations respectively. Matrix Γ_n is positive definite/semi-definite because the irrecoverable dissipation energy due to visco-plastic flow has the form

$$\sigma^T \dot{\epsilon}_{vp} \Delta t = \sigma^T \Gamma \sigma \Delta t \geq 0 \tag{5.75}$$

Putting (5.74) into (5.72) gives

$$\Delta\sigma_n = DBK^{-1}(\Delta t \int_\Omega B^T D\Gamma_n \sigma_n d\Omega + \Delta f_n) - \Delta t D\Gamma_n \sigma_n \tag{5.76}$$

Dividing both sides by Δt leads to

$$\dot{\sigma} = DBK^{-1} \int_\Omega B^T D\Gamma_n \sigma d\Omega - D\Gamma_n \sigma + DBK^{-1} \dot{f}_n \tag{5.77}$$

which is equivalent to the first order ordinary differential equations of the form

$$\frac{d}{dt} Y = AY + B \tag{5.78}$$

As previously stated, the eigenvalues of the A restrict the maximum time-step of the system.

The Jacobian matrix of the system Equation (5.77) can be written as

$$J = \frac{\partial \dot{\sigma}}{\partial \sigma} = A = DBK^{-1} \int_\Omega B^T DH d\Omega - DH \tag{5.79}$$

in which $H = \frac{\partial \dot{\epsilon}^{vp}}{\partial \sigma}$ is the form in which the stability conditions are determined.

Cormeau [118] proposed the stability criteria for Von Mises, Drucker-Prager, Tresca and Mohr-Coulomb by ignoring the first term of (5.79) to obtain an upper bound for the shared eigenvalues of H_n and D matrices. Cormeau's formula which is an under estimate of the critical time-step may result in serious problem in long duration problems due to round-off error and *evaluating the eigenvalues of DH seems to give a more reasonable critical time-step.*

5.7.1 Conclusions

The assessment of a numerical algorithm should be based on

- firstly, the required computational effort and
- secondly, the required accuracy.

As mentioned previously, in general, structural dynamic problems can be placed into one of two categories. The first are those which comprise the loading of low to medium frequencies, e. g. earthquake loading, while those under the loading consisting of high frequencies, e. g. impulsive loading, fall into the second category, each of which has its own problems associated with predicting the structural response. These are summarized below:

- Since earthquake loading possesses low to medium frequencies, structures are designed to possess a fundamental mode frequency range beyond that of the applied load, hence the structural response is influenced by only a limited numbers of modes and the higher modes no longer play an important role. In this circumstance, the mode-superposition method is efficient for solving the problem.
- In the second type of problem in which the higher modes should be taken into account, or for the first type as described above but in which a large problem is be analysed, a direct integration scheme is preferable. The criteria for selecting the suitable method depends on several factors such as; the scale of the problem, the required accuracy, and the type and duration of the applied dynamic load. These are.
  - In small-scale problems, attention should be focused on the order of integrator, critical time-step and the convergence properties of the method in non-linear analysis procedure.
  - The algorithm should possess numerical dissipation properties to damp out the numerical errors due to higher modes. The required amount of such numerical properties depends mainly on the nature and duration of the applied load.

    Since impulsive loadings are of short duration, the structural response is not affected seriously by the period elongation error (PEE), while the

amplitude decay error (ADE) may cause serious problems hence the method to be chosen should have the numerical dissipation property. In this context, the α-method proposed by Hilber et al. [168] was found to be efficient. In long-duration problems, ADE (sometimes called the Shift-Phase Error), might cause a fictitious response history, which may lead to unacceptable response.

- The mixed explicit-implicit method proposed by Hughes et al. [177] could be suitable for such problems. However, the stability condition of the method is governed by the critical time-step corresponding to the explicit elements. The order of accuracy of the mixed methods can be increased by using an explicit algorithm as the predictor and an implicit method as the corrector. The effect of ADE and EPE still remain as biggest difficulty of the method.

The chapter has also attempted to assess the critical time-step in non-linear dynamic problems comprising long-duration loading. It was concluded that,

- since the time-step proposed by Cormeau [118] has been derived based on an upper bound of the shared eigenvalues of the D and H matrices, it is conservative nature i. e. is less than the critical time-step. This may cause serious difficulties in problems with large number of time steps due to round-off error. A more accurate formula is required for determining the critical time-step if neither the eigenvalues of the DH matrix nor the implicit form of strain approximation are to be used for each Gaussian point due to computational cost.

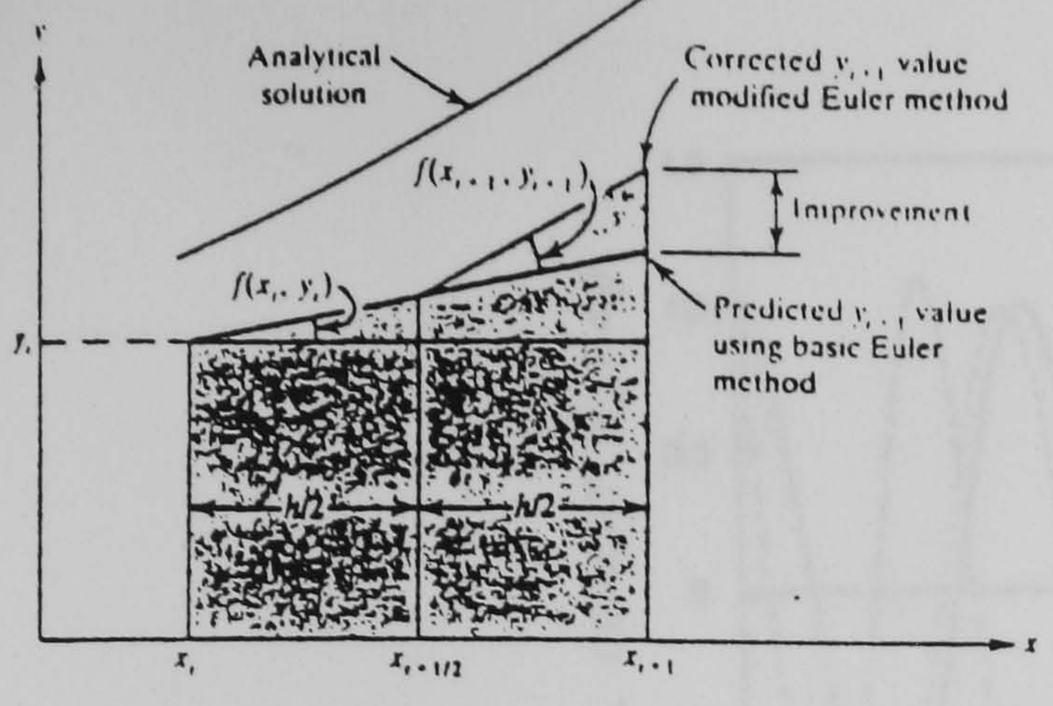

. 5.1 Garphical illustration of the modified Euler's method.

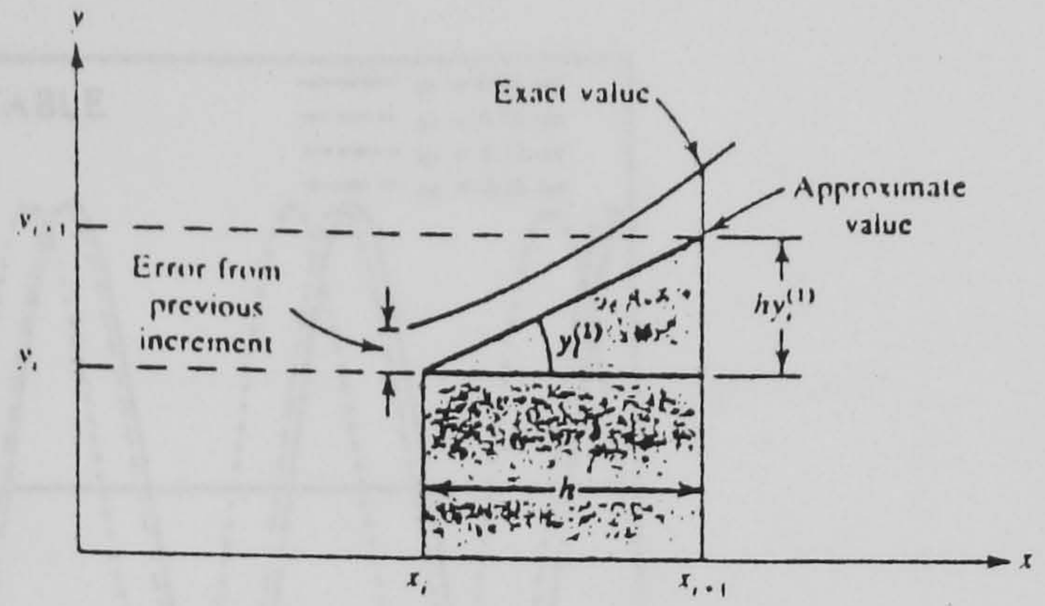

Fig. 5.2 Garphical illustration of the Euler's met

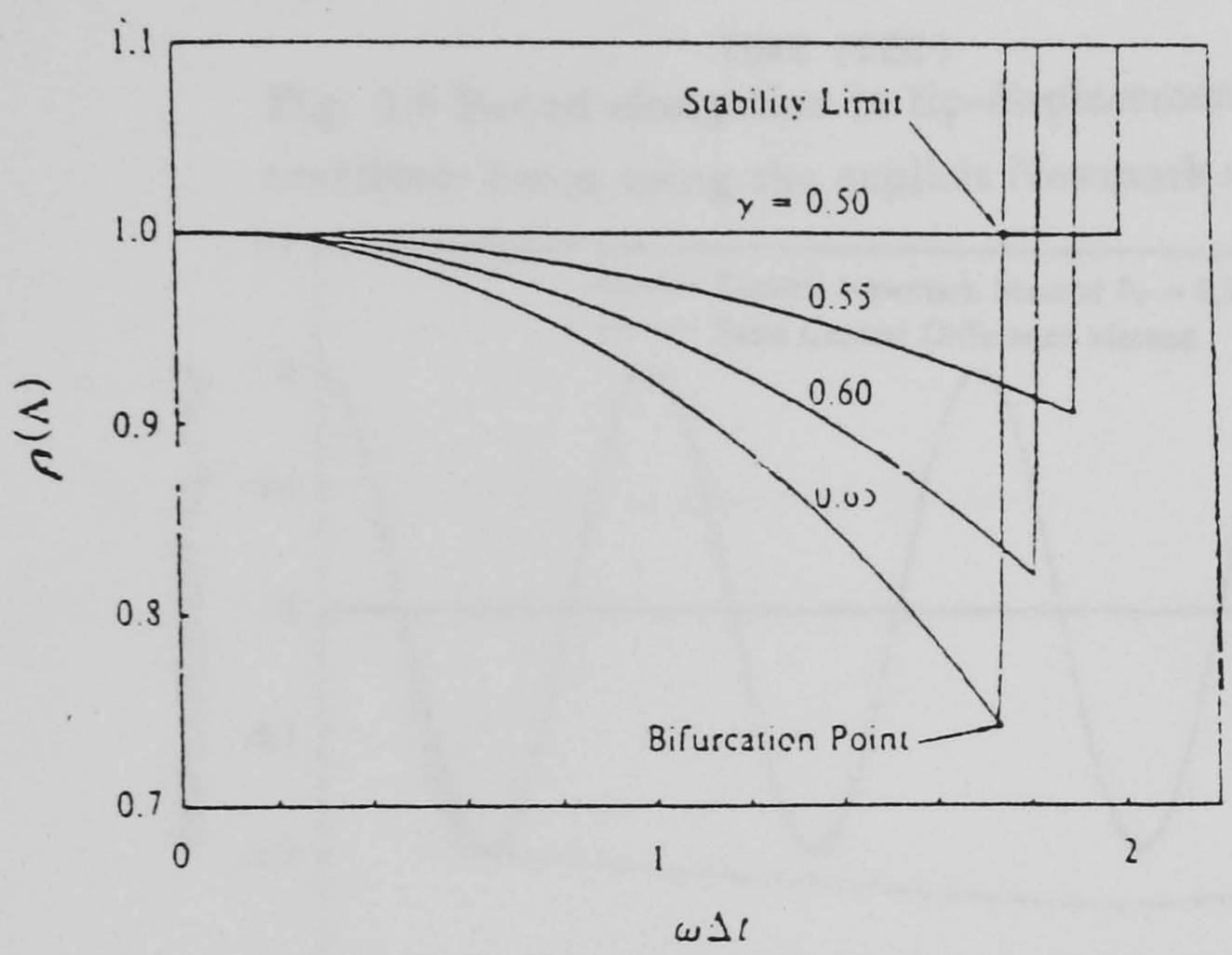

Fig. 5.3 Spectral radii of the amplification matrix for the explicit Newmark method.

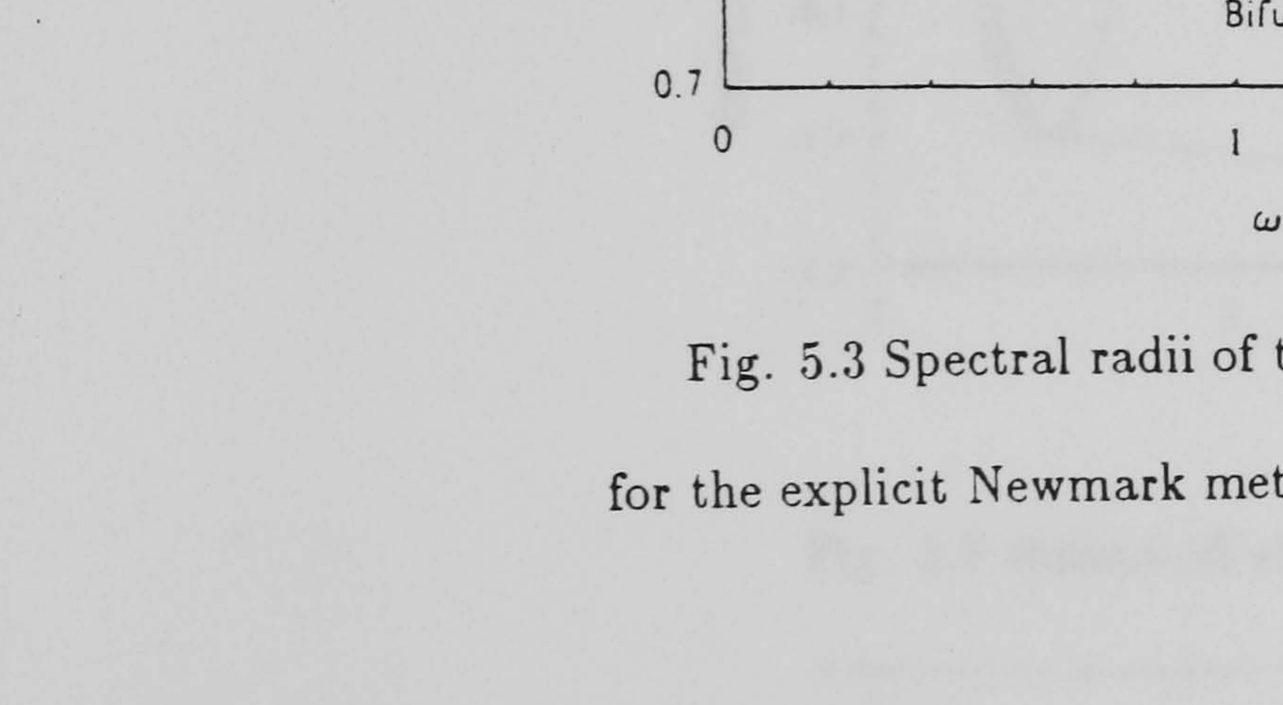

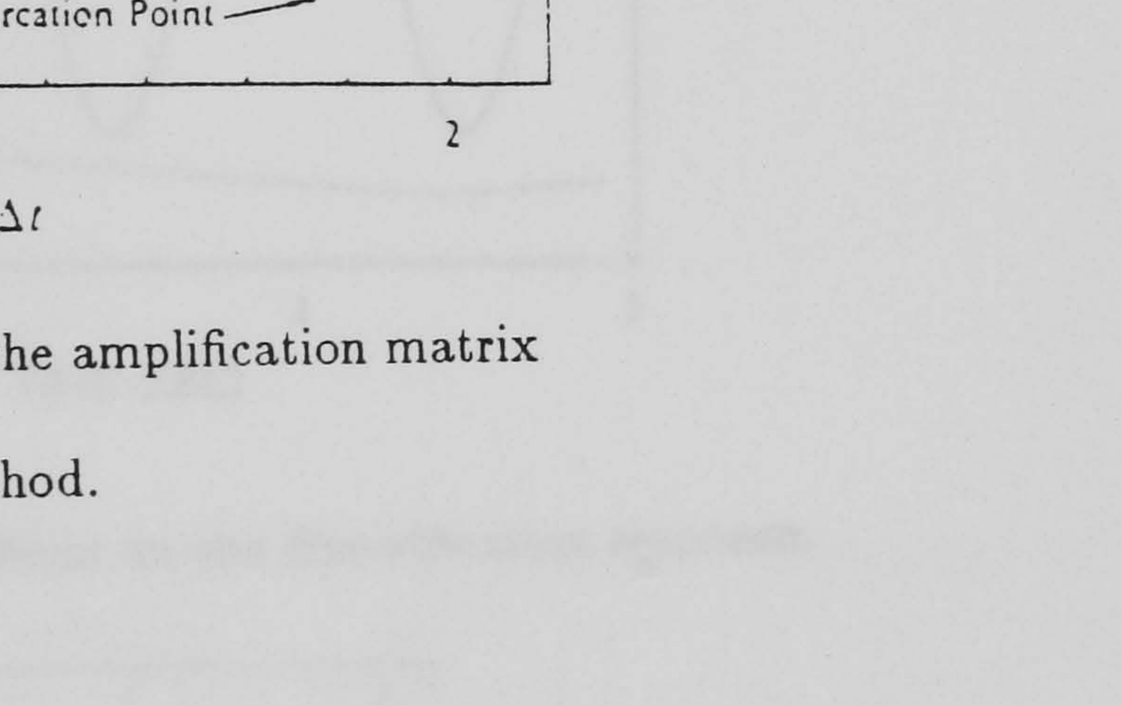

Fig. 5.5 Period shrinkage for the explicit Newmark met

5.4 Numerical damping for the explicit Newmark method

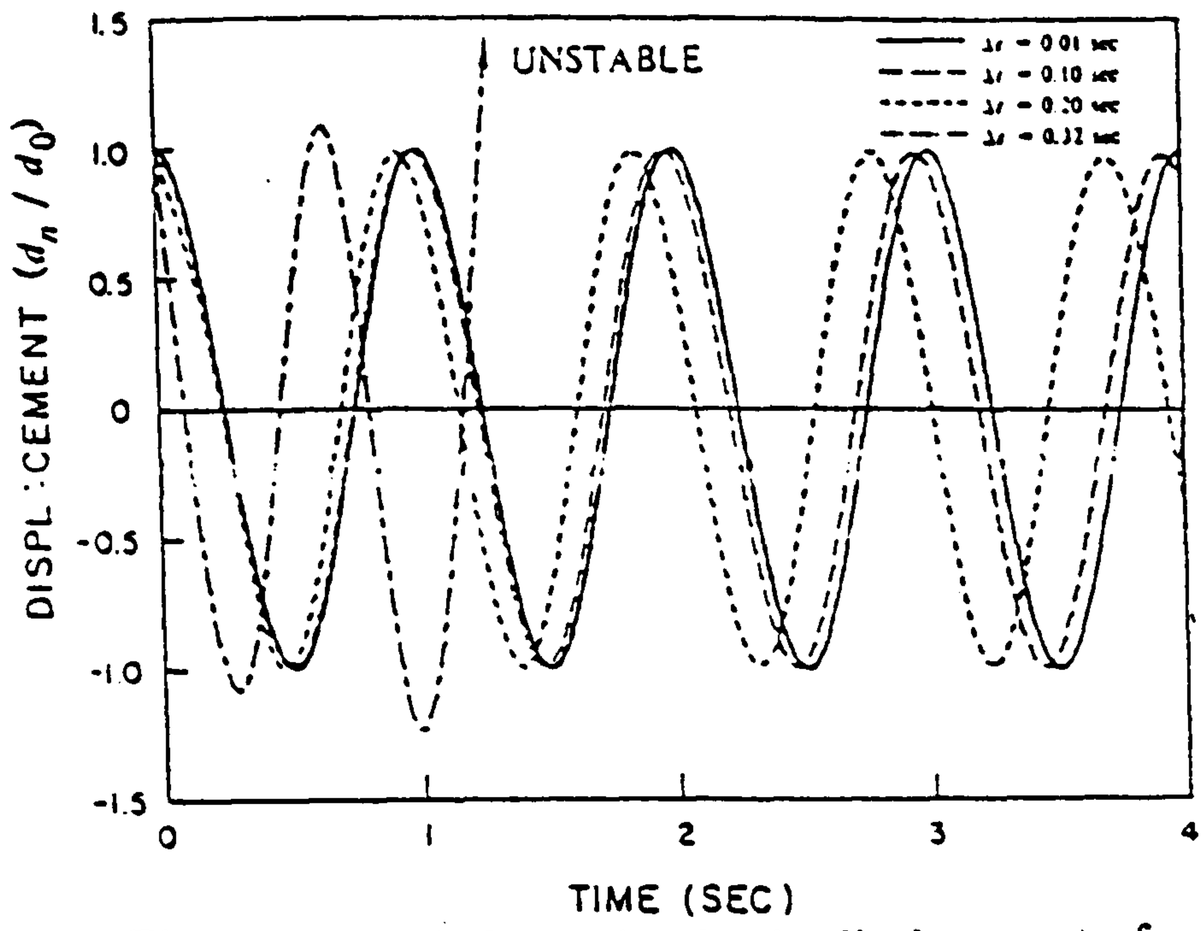

Fig. 5.6 Period elongation in tip-displacement of a cantilever beam using the explicit Newmark method.

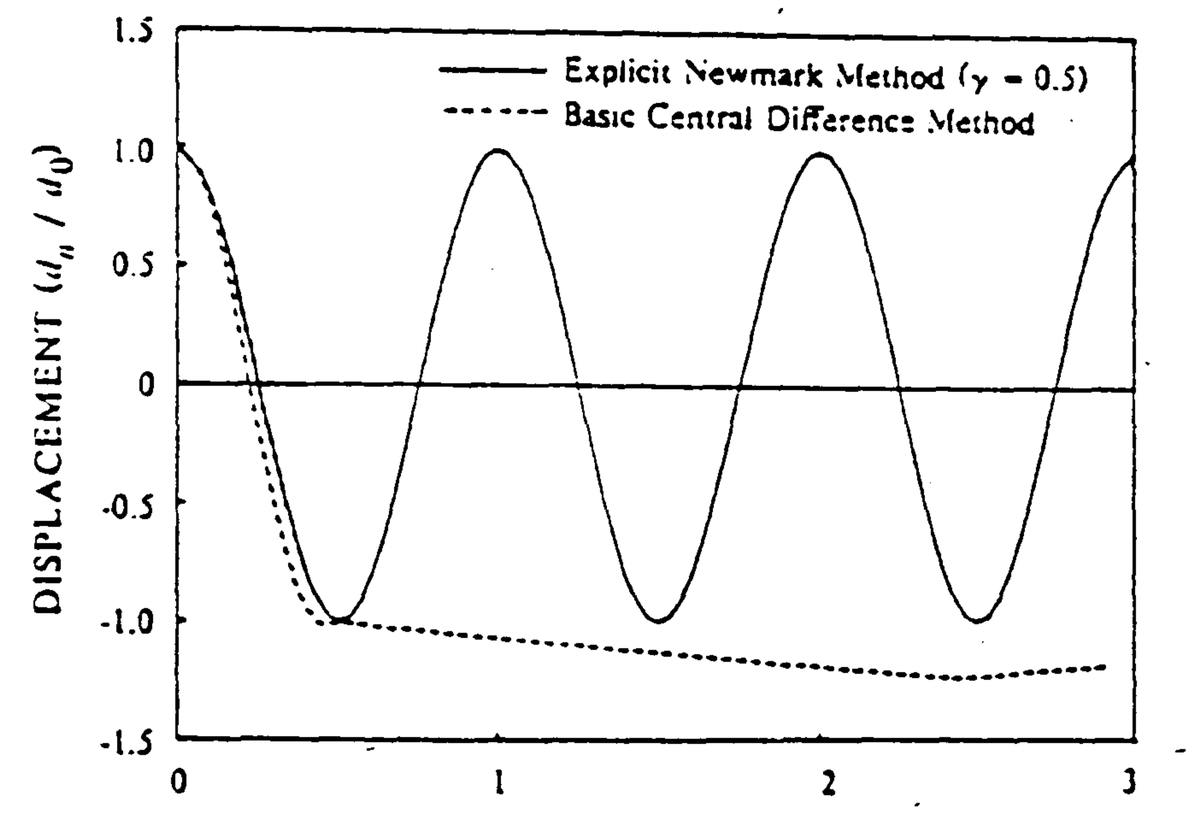

Fig. 5.7 Round-off effects on the free-vibration response.

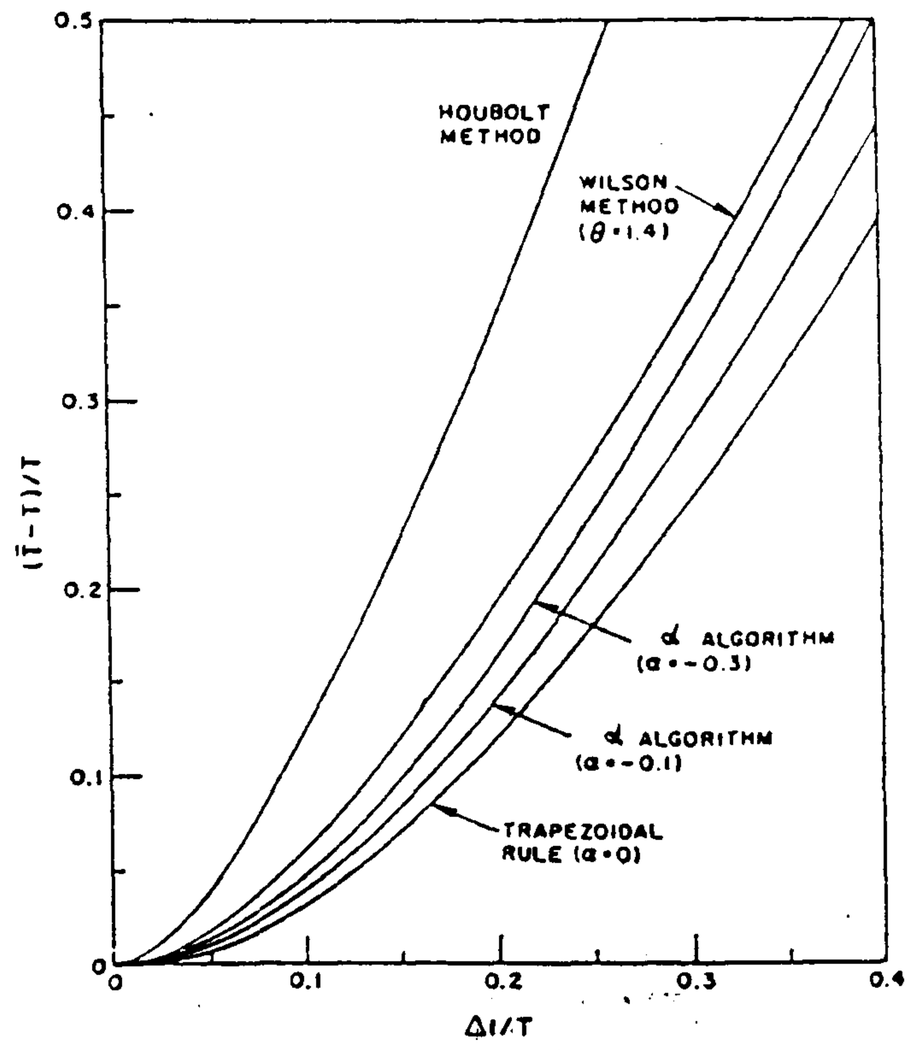

Fig. 5.8 Relative period error vs $\frac{\Delta t}{T}$ for some algorithms.

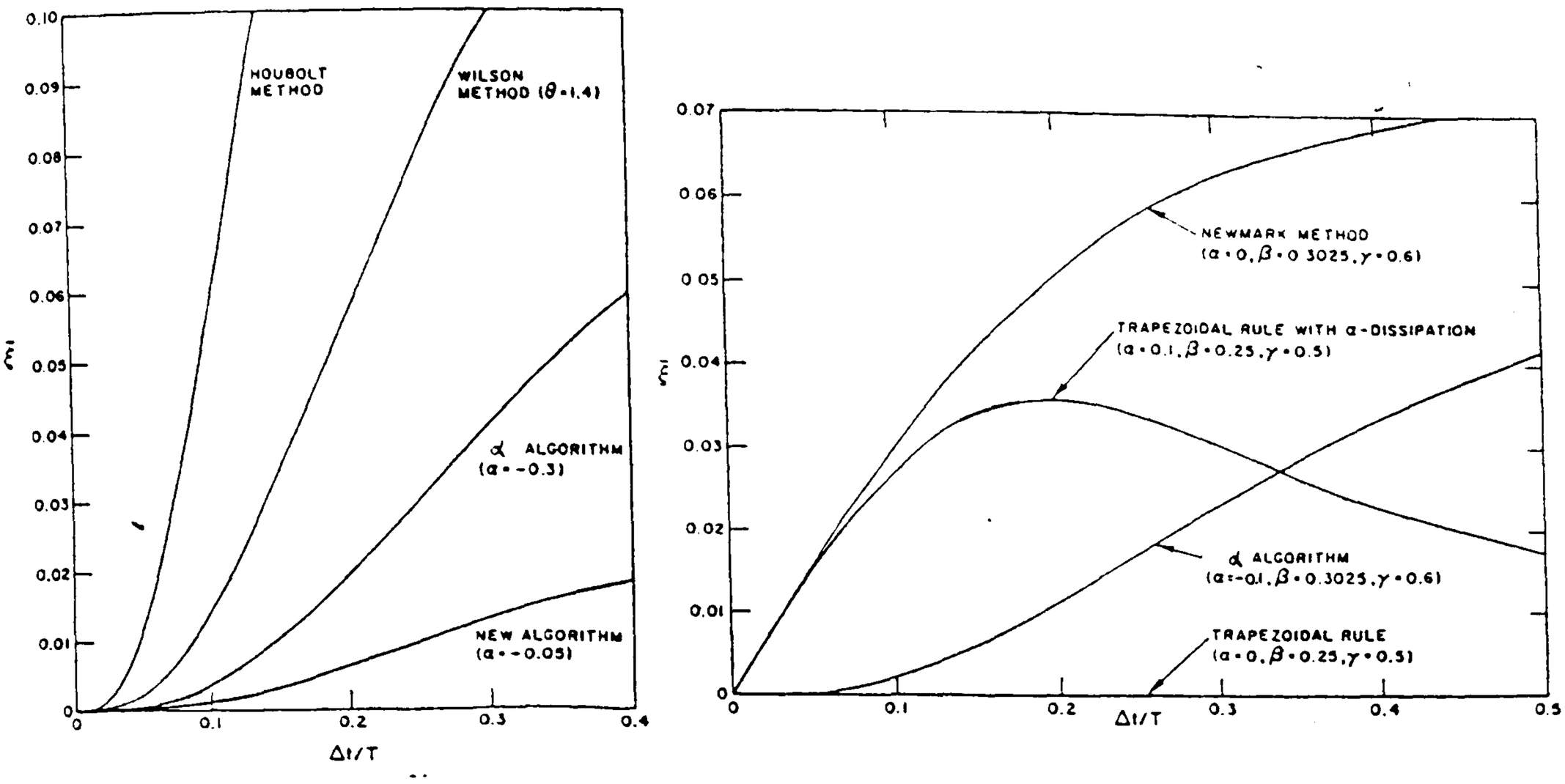

Fig. 5.9 A and B Damping ratios vs $\frac{\Delta t}{T}$ for some algorithms.

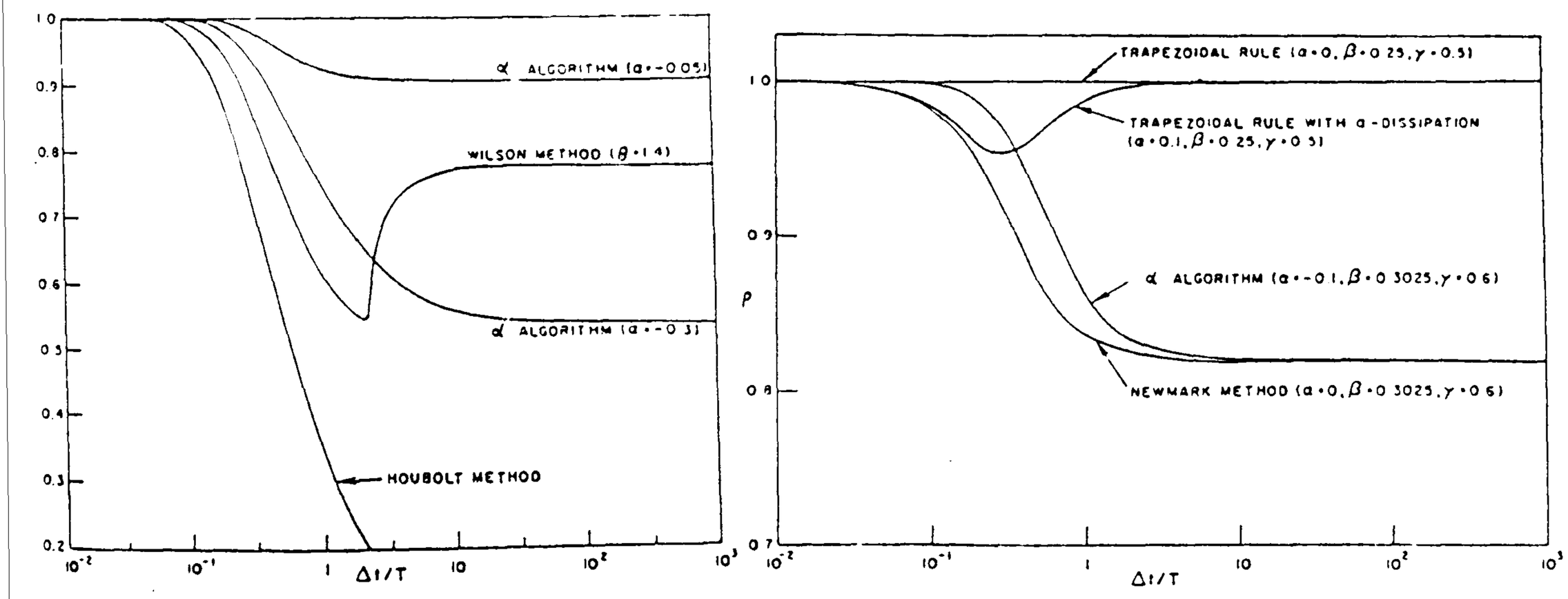

Fig. 5.10 A and B Spectral radii vs $\frac{\Delta t}{T}$ for some algorithms.

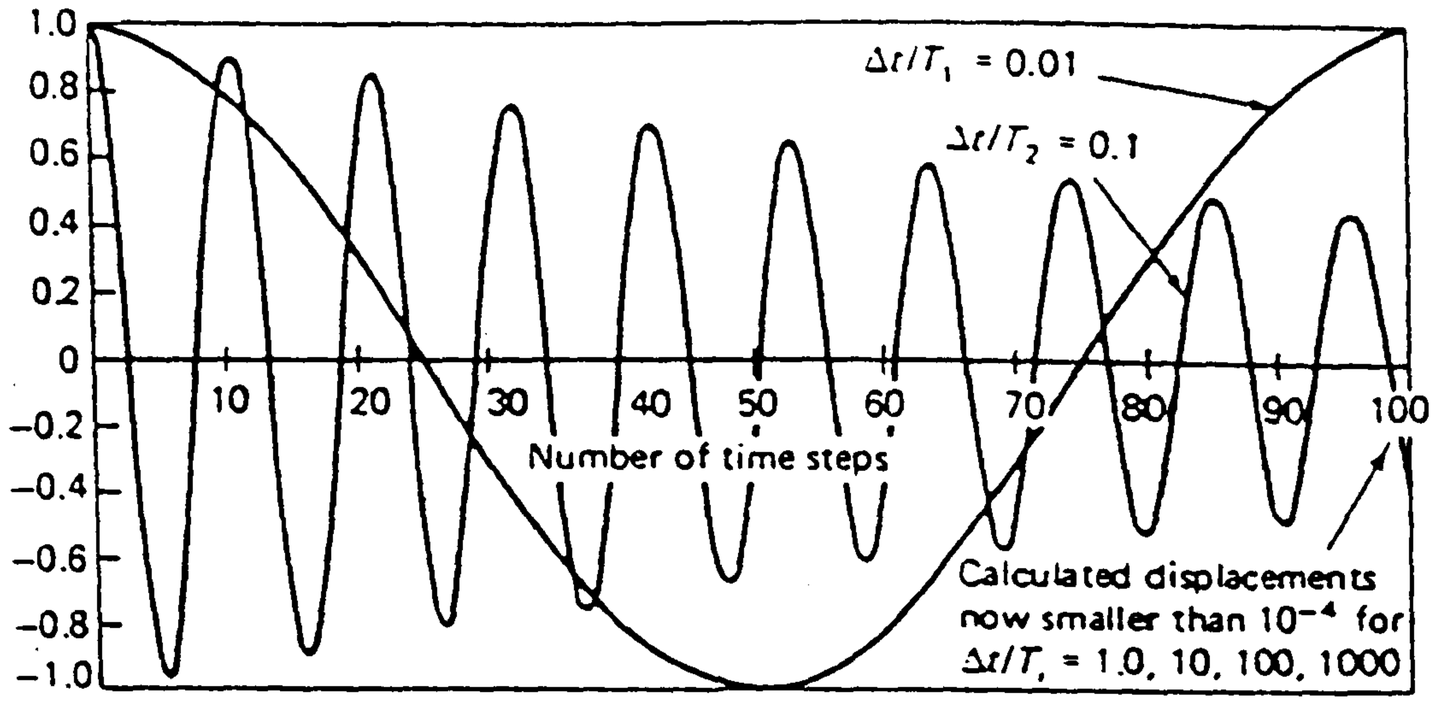

Fig. 5.11 Displacement response predicted with increasing $\frac{\Delta t}{T}$ ratio in Wilson-θ method with $\theta = 1.4$.

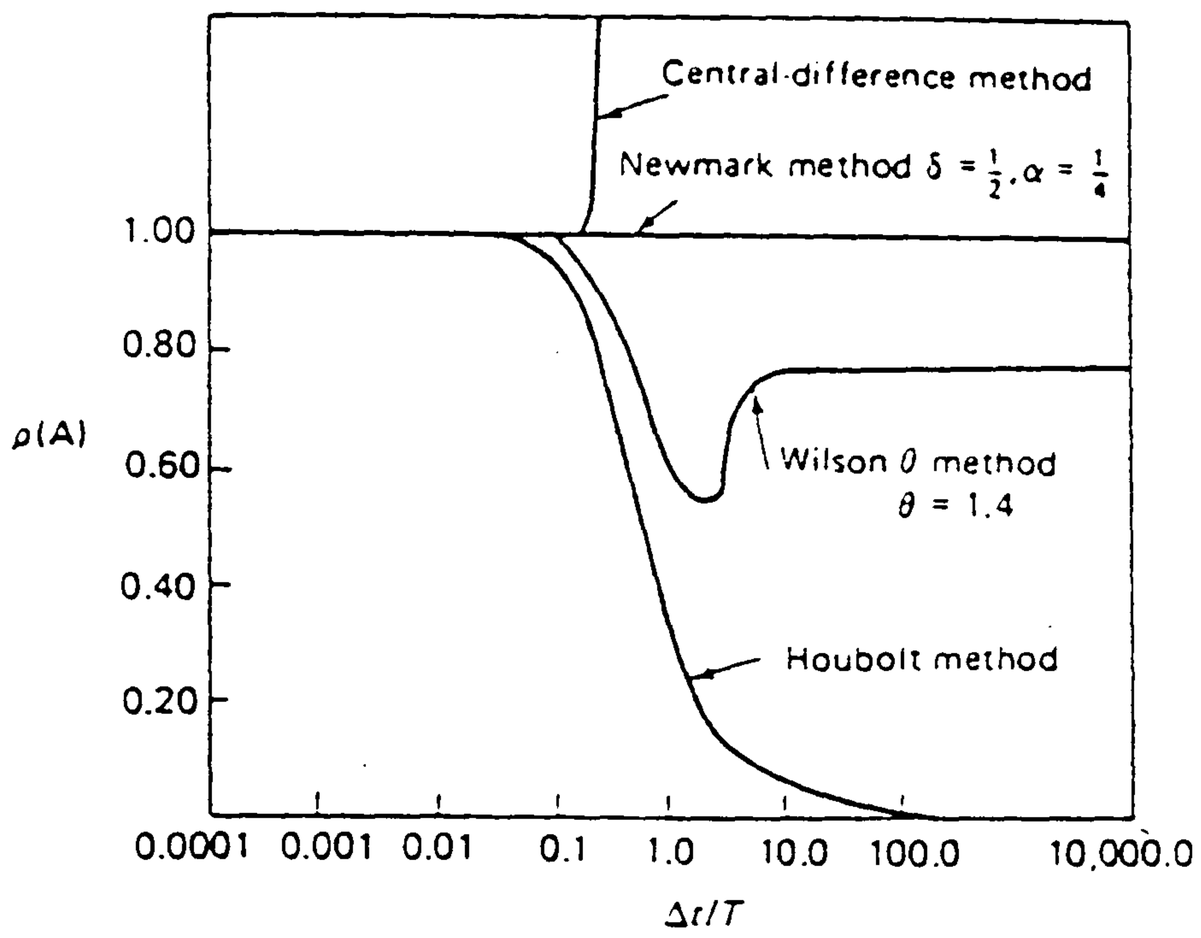

Fig. 5.12 Spectral radii for four types of algorithms (taken from [168]).

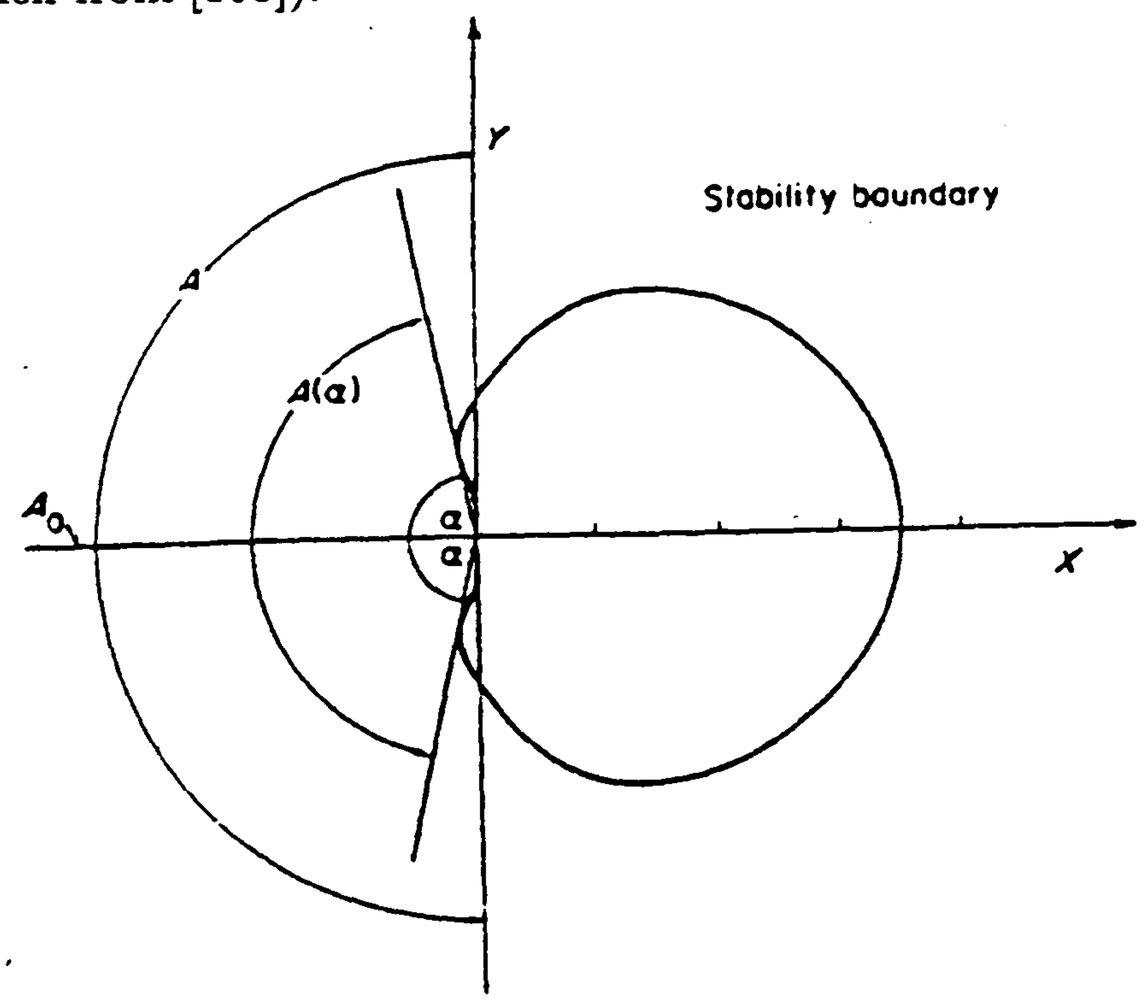

Fig. 5.13 Graphical illustration of stability conditions.

Table 5.2 Properties of well-known members of the Newmark family of methods.

	Method	β	γ	Ω_{crit}	Accuracy
Implicit	Artificially damped	$> \gamma/2$	$> 1/2$	[illegible]	$O(\Delta t)$
	Average acceleration (trapezoidal rule)	1/4	1/2	[illegible]	$O(\Delta t^2)$
	Linear acceleration	1/6	1/2	$2\sqrt{3} \approx 3.464$ [illegible]	$O(\Delta t^2)$
				Eq. (A) [illegible]	
	Fox–Goodwin (royal road)	1/12	1/2	$\sqrt{6} \approx 2.449$ [illegible]	$O(\Delta t^4)$ [illegible]
				Eq. (A) [illegible]	$O(\Delta t^2)$ [illegible]
Explicit	Central difference [M], [C] diagonal	0	1/2	2 [illegible]	$O(\Delta t^2)$
				Eq. (A) [illegible]	
	Artifically damped [M], [C] diagonal	0	$> 1/2$	Eq. (A) [illegible]	$O(\Delta t)$

Chapter 6

Implementation and Examples

6.1 Introduction

In tests it has been observed that concrete exhibits more strength and stiffness as the strain-rate is increased and that this strengthening and stiffening is more rate-sensitive in tension than in compression, Chapter 3. Poisson's ratio has also been observed to be influenced by strain-rate, decreasing in compression and increasing in tension [4, 9].

A number of analytical models for the prediction of concrete stiffening and strengthening due to increasing strain-rate are described in the literature and can be categorized as:

- Strain-rate-sensitive, damage based models [16, 41, 121, 123].
- Models in which static stress-strain relation associated with a rate-sensitive function is used [6, 90, 94, 125].
- Rheological-based models.

The aim of this chapter is to demonstrate:

a) The effect of increasing loading-rate on the reinforced concrete structures response.

b) Material strengthening and stiffening due to increasing loading-rate and

the effect of such phenomenon on the structural response. To this end, a strain-rate-sensitive model based on a rheological model has been developed and a uniaxial static stress-strain formula has been proposed to relate the uniaxial strain-rate-sensitivity loading surfaces to the multiaxial situation. The above-mentioned are demonstrated with some examples of reinforced concrete structures under time-dependent loading with and without incorporating the strain-rate-sensitive parameters and the results are compared and assessed. Also in this chapter is described a computer program written in Fortran for the nonlinear analysis of reinforced concrete structures subjected to transient forces particularly earthquake loading, which uses the model described above to predict the history-strain-rate sensitive behaviour of reinforced concrete structures under transient forces.

The chapter starts with a brief explanation of the formulation of numerical algorithm used in the proposed model and continues with a description of the formulae used for the elastic-viscoelastic and visco-elastic-visco-plastic analysis of reinforced concrete structures. The next section is devoted to a brief explanation of the program structure. Four series of dynamic analysis of plain concrete and reinforced concrete structures, Hatano's concrete specimens [10], Ahmad's specimen [21], a simply supported reinforced concrete beam and a reinforced concrete circular slab under transient force are the subject of the next sections. These structures are dynamically analysed excluding and including the effect of the strain-rate parameters on the structural response. The chapter closes with the comparison of the results with those previously carried out by other investigators and a discussion of the results.

6.2 Dynamic analysis of reinforced concrete structures

Reinforced concrete structures can be dynamically analysed using different types of numerical techniques depending on the type of the problem and the desired accuracy as discussed in Chapter 4 and 5. An explicit algorithm, the Central

Difference Method, which has the maximum time-step, has been used in the study described in this chapter. As discussed in chapter 4, the governing equations for dynamic analysis can be summarized as

$$M\ddot{X}_t + C\dot{X}_t + KX_t = P_t^{ext} \tag{6.1}$$

$$(\frac{1}{\Delta t^2}M + \frac{1}{2\Delta t}C)X_{t+\Delta t} = P(t)^{ext} - (K - \frac{2}{\Delta t^2}M)X_{t-\Delta t} - (\frac{1}{\Delta t^2}M - \frac{1}{2\Delta t}C)X_{t-\Delta t} \tag{6.2}$$

$$\dot{X}_t = (\frac{1}{2\Delta t})(X_{t+\Delta t} - X_{t-\Delta t}) \tag{6.3}$$

$$\ddot{X}_t = \frac{1}{\Delta t^2}(X_{t+\Delta t} - 2X_t + X_{t-\Delta t}) \tag{6.4}$$

The acceleration vector at time $t = 0$ $\ddot{X}(0)$, can be evaluated by solving Eq. (6.1) at $t = 0$.

$$\ddot{X}(0) = M^{-1}[P(0) - KX(0)] \tag{6.5}$$

$$X_{t-\Delta t} = X_0 - \Delta t\dot{X}_0 + 1/2\Delta t^2\ddot{X}_0 \tag{6.6}$$

The critical time-step is a function of the maximum natural frequency of the system and is approximated by

$$\Delta t \leq \frac{2}{\omega_e^{max}} \tag{6.7}$$

in which ω_e^{max} is the maximum natural frequency of smallest element in the mesh.

For non-linear analysis the displacement vector $X_{t+\Delta t}$ is determined by

$$(\frac{1}{\Delta t^2}M+\frac{1}{2\Delta t}C)X_{t+\Delta t} = P^{ext}(t)-(N(X_t)-\frac{2}{\Delta t^2}M)X_{t-\Delta t}-(\frac{1}{\Delta t^2}M-\frac{1}{2\Delta t)}C)X_{t-\Delta t} \tag{6.8}$$

in which the internal nodal force is given by

$$P^{int} = \sum_i^N \int_v B^T\sigma(\epsilon)dV \tag{6.9}$$

where B is the strain-displacement matrix and $\sigma(\epsilon)$ is a non-linear function of strain which is based on the material model. For a material with associated viscoplasticity, a linear flow function $\varphi(F)$ and Von Mises yield criterion, the

computational time-step for the explicit visco-plastic strain approximation proposed by Cormeau [118] of the form

$$\Delta t = \frac{4(1+\nu)\sigma_0}{3\gamma_P E} \tag{6.10}$$

has been used in non-linear analysis of the problems. In Eq. (6.10) v is Poisson's ratio, σ_0 is the visco-plastic initiation stress, E is the modulus of elasticity and γ_P is the fluidity parameter.

6.2.1 Pre-cracked concrete

Concrete is assumed to behave elastically before cracking. The proposed formula for determining the increased initial modulus of elasticity E_d is

$$E_d = E_s(\frac{\gamma_E E_s t - 1}{\gamma_E E_s t}) \tag{6.11}$$

which is valid for $0 < t \leq dt$.

The elasticity matrix D matrix for plane stress problems is given by

$$D = \frac{E_d}{1-v^2}\begin{bmatrix} 1 & v & 0 \\ v & 1 & 0 \\ 0 & 0 & \frac{1-v}{2} \end{bmatrix} \tag{6.12}$$

and for axisymmetric problems

$$D = \frac{E_d(1-v)}{(1+v)(1-2v)}\begin{bmatrix} 1 & \frac{v}{1-v} & 0 \\ \frac{v}{1-v} & 1 & 0 \\ 0 & 0 & \frac{1-2v}{2(1-v)} \end{bmatrix} \tag{6.13}$$

6.2.2 Post-cracked concrete

As explained in chapter 2, the maximum tensile strain criterion has been adopted. The principal strains and corresponding directions are evaluated. The Gauss point is assumed to be cracked if the maximum principal strain exceeds a defined value, then a crack is formed in a plane orthogonal to the offending strain. The fixed cracked approach is adopted as discussed in chapter 2. The fracture

energy approach is adopted for post-cracked behaviour of concrete. The tension-stiffening effect has been simulated using an exponential curve of the form

$$\sigma = \acute{f}_t exp[-\frac{\epsilon - \epsilon_0}{\alpha}] \tag{6.14}$$

$$\alpha = \frac{G_f}{l_c \acute{f}_t} \tag{6.15}$$

where, l_c is the characteristic length associated with the sampling point. $l_c$is evaluated from

$$l_c = (dV)^{1/3} \tag{6.16}$$

in which dV is the volume of concrete represented by the sampling point.

Compressive behaviour of cracked concrete

The cracking of concrete is assumed to be a partial failure and it does not affect the stiffness in the direction parallel to the cracking plane as discussed in chapter 2. A secondary cracking may occur and viscoplastic yielding may occur if compressive stress is present one of the directions.

6.2.3 Viscoplastic analysis of concrete

The compression behaviour of concrete is modelled using the visco-elastic visco-plastic model described in chapter 2. In this section the equations used in the proposed model are summarized.

Perzyna's visco-plastic strain-rate is given by [119]

$$\dot{\epsilon}_{ij}^{vp} = \gamma_P < \phi(F) > \frac{\partial f}{\partial \sigma_{ij}} \tag{6.17}$$

The proposed formula for determining fluidity parameter γ_P of the form

$$\gamma_P = P_2 \dot{\epsilon}_e^{P_1} \tag{6.18}$$

has been used. The values of P_1 and P_2 are given in Table 2.5. The effective strain ϵ_{eff} is given by [2]

$$\epsilon_{eff}^e = \sqrt{(\epsilon_{oct}^2 + 1/4\gamma_{oct}^2)} \tag{6.19}$$

where ϵ_{oct} and γ_{oct} are the octahedral normal and octahedral shear strain respectively.

The exponential form of the flow function is given by

$$\phi(F) = (F/y)^N \tag{6.20}$$

where y is the initial yield stress. A value of $N = 1$ has been used.

The fluidity parameter γ_E corresponding to dynamic modulus of elasticity is evaluated by

$$\gamma_E = \lambda_2 \dot{\epsilon}^{\lambda_1} \tag{6.21}$$

The values of I_1 and I_2 are given in Table. 2.3.

The proposed uniaxial stress-strain formula including strain-rate parameters has the form

$$\sigma_d^n = E_d \epsilon_s^n - (E_d \epsilon_0 - \sigma_0)[\frac{\epsilon_s^n(1 - \frac{1}{\gamma_T E_t t})}{\epsilon_0}]^{\theta A} \tag{6.22}$$

in which E_t is the tangent modulus of elasticity corresponding to the quasi-static stress-strain relation, t is the time corresponding to time-step n, $A = \frac{E_s \epsilon_0}{\sigma_0}$, and $\theta = 2.1$. σ_0 and ϵ_0 are peak stress and corresponding strain σ_0 and ϵ_0 are peak stress and corresponding strain. Eq. (6.22) is valid for $dt \geq t > 0$

The analyses carried out in this study are under the assumption of constant load-rate and the analyses stopped when the strain corresponding to the maximum stress reached.

The tangent modulus of elasticity E_t in the proposed uniaxial static stress-strain formula is given by

$$E_t = \frac{\partial \sigma_s}{\partial \epsilon_s} = E_s[1 - \theta A(\frac{\epsilon_s}{\epsilon_0})^{\theta A - 1}] \tag{6.23}$$

where E_s is the quasi-static initial modulus of elasticity.

The proposed formula for evaluating fluidity parameter γ_T corresponding to the material stiffening and strengthening has the form

$$\gamma_T = T_3 \dot{\epsilon}^{T_2} e^{T_1 (\ln \dot{\epsilon})^2} \tag{6.24}$$

The values of T_1, T_2, and T_3 are given in Table 2.5.

6.2.4 Viscoplastic analysis of steel

Perzyna's uniaxial model for steel in tension and compression has been used where

$$\dot{\epsilon}_{vp} = \pm\gamma_s(\sigma_s - F_y)/F_y \tag{6.25}$$

where σ_s is the current stress level and F_y is the static yield strength has been used. The fluidity parameter γ_s for steel is given by

$$\gamma_s(\dot{\epsilon}) = a_0 \dot{\epsilon_s}^{a_1} \tag{6.26}$$

in which $a_0 = 1.5386$ and $a_1 = 0.9605$ [90].

Energy balance check

In order to guard against the artificial errors discussed in chapter 5, an energy balance check is used for checking the stability problem discussed in chapter 5. Denoting W^{kin}_{n+1}, W^{int}_{n+1}, W^{ext}_{n+1} as kinetic, internal and external energies of the system respectively, the energy balance check is given as

$$\frac{W^{kin}_{n+1} + W^{int}_{n+1} - W^{ext}_{n+1}}{W^{kin}_{n+1} + W^{int}_{n+1}} \leq tol \tag{6.27}$$

where the tolerance $tol \leq 0.03$ is usually used.

6.3 Numerical Examples

Four dynamically loaded reinforced concrete structures have been analysed using the program described above. The results of the analyses are compared with the results of analyses carried out by other investigators. The problems analysed are,

- Hatano's compressive and tensile specimen tests under a uniform time-dependent loading [10].
- Ahmad's compressive test specimen under two loading-rates [21].
- A simply supported reinforced concrete beam under two suddenly applied loads.
- A reinforced concrete circular slab under a uniform distributed ramp-loading.

6.3.1 Program structure and a brief explanation

Program DYNICK2D

The proposed history-strain-rate sensitive visco-elastic-visco-plastic model has been implemented in a two dimensional program.

A computer program DYNICK2D has been developed for the dynamic analysis of reinforced concrete structures. A flow chart is given in Fig. 6.1. The strain-rate sensitive parameters incorporated in the material used in the analysis are

- The initial modulus of elasticity E.
- The secant modulus of elasticity.
- The tangent modulus of elasticity E_t.
- The peak-strength of the concrete σ_P.

The effect of the afore-mentioned strain-rate-sensitive parameters on the structural response will be shown in the examples in the next sections.

The structure of the program in which subroutines developed by Smith et al. [116] have been used are summarized as follows

1. Read the input data, geometry, material property and loading.
2. Calculate the element lumped mass matrix and the global mass matrix.
3. Time-step marching
   - Evaluate total strain components at each Gauss point.
   - Check for primary or secondary cracking with respect to the strain states of each Gauss point.
   - Update the stress components if the Gauss point is cracked.
   - Check for visco-plasticity, if yielding occurs then calculate the stiffened loading surface.
   - Calculate the viscoplastic strain-rate components viscoplastic strain components.

- Determine the residual forces.
- Evaluate the residual force vector ϕ Eq. (4.78)
- Check the convergence criterion Eq. (4.79). if the residual force is converged then update the strain and stress components.

4. Check for the crushing using the ultimate crushing surface as discussed in chapter 2. The stresses sustained by the concrete are released if crushing occurs.
5. Write the displacement, velocity and acceleration vectors as output data and go to time-step marching for the next time-step.
6. Calculate the external work done and the internal work and the kinematic energies of the system and check the energy balance.

6.3.2 Hatano's dynamic tests [10]

Hatano's compressive and tensile specimens have been chosen as the first series of analyses. However, since the analyses are based on the uniaxial tests, the validation of the proposed model in predicting the dynamic behaviour of the reinforced concrete structures can not be assessed properly based on these results and the problem can be analysed without using finite element procedure.

6.3.3 Example 6.1 Hatano's compressive tests [10]

A total of 14 experiments on concrete and mortar specimens have been carried out. The mix proportions of the specimens are shown in Table 6.1. The compressive test specimens [10] were concrete cylinders of 10 cm diameter and 20 cm height which had been cured in the water at a temperature of 20 degree C until testing. Twenty specimens were used for each test series. The stress-strain curves have been drawn up on the basis of test records. The failure time t_f, which is the time from the beginning of loading to failure, is given in the figure. It was concluded that as the failure time is decreased, the stress-strain curves becomes steeper. The weaker the concrete the more convex the curve that is obtained.

6.3.4 Dynamic analysis of Hatano's tests

The analysis of Hatano's specimens have been performed in three parts and the analytical and experimental stress-strain curves have been compared. Three test series of Hatano et al. [10] have been used in identifying relevant rate-sensitive parameters. The quasi-static analytical tests are discussed first and the compressive and tensile tests will be described in subsequent sections.

6.3.5 Quasi-static compressive tests

In this example the concrete compressive specimens have been numerically analysed under quasi-static loading i. e. the material is assumed to have a very low fluidity parameter.

The geometry of the compressive, tensile specimens, and a typical ramp loading are illustrated in Figs. 6.2 A, B and C.

The specimen has been spatially discretised using isoparametric serendipity 8-noded elements Fig. 6.3. The stiffness matrix has been evaluated using 3 by 3 Gauss points and the proposed method Eq. (3.34) for producing a lumped mass matrix from a consistent mass has been used. Only half of the structure has been analysed using axisymmetric finite element. The central difference method has been used for time integration with a computational time step equal to .000004. The details of compressive test are summarized in Table 6.2.

Table 6.2 Details of compressive tests simulated.

Concrete mix	Test No.	Failure time (sec.)	Ultimate strain
1:2:4	A4	1.08	28.5×10^{-4}
	A7	0.26	28.5×10^{-4}
	A14	0.06	28.5×10^{-4}
1:4:7	A6	0.28	18.2×10^{-4}
	A11	0.10	18.2×10^{-4}
	A16	0.04	18.2×10^{-4}
1:3:5	A5	0.84	23.65×10^{-4}
	A10	0.165	23.65×10^{-4}
	A15	0.045	23.65×10^{-4}

The material properties of the compressive specimens are shown in Table 6.3.

Table 6.3 Material properties of compressive tests.

Material properties	Concrete mix		
	1: 2: 4	1: 3: 5	1: 4: 7
Young Modulus of elasticity (Kg/cm^2)	32.1×10^4	27.5×10^4	27.2×10^4
Poisson's ratio	0.2	0.2	0.2
Compressive strength (Kg/cm^2)	605	445	265
Tensile strength (Kg/cm^2)	31	25	20
Cracking strain	0.75E-4	0.75E-4	0.75E-4
Fracture energy $Kgcm/cm^2$	75	70	60
Mass density $Krsec^2/cm^4$	2.45×10^{-6}	2.45×10^{-6}	2.45×10^{-6}
Fluidity parameters			
P_1	0.358	0.93	1.01
P_2	6.1E-3	0.61	0.115
Empirical coefficients			
λ_1	0.77	0.8	.75
λ_2	0.362	0.0773	0.0369
T_1	0.184	0.066	-0.22
T_2	2.461	1.38	-0.78
T_3	0.07	0.026	6.11E-4

6.3.6 Loading

In Hatano's tests, the load was applied to the specimen by a rotating fly wheel. The relationship between time and loading was approximated by

$$f(t) = 1 - cos\omega t \tag{6.28}$$

where $0 \leq f(t) \leq 1$, for $0 \leq t \leq t_f$, in which t_f is the failure time and ω is the angular velocity. The loading function used in dynamic analysis of the compressive specimens is approximated by a time dependent function in the form

$$f(t) = \frac{1}{t_f} \tag{6.29}$$

Numerical analysis of compressive specimens under quasi-static loading and results

Three numerical analyses on the compressive specimens have been carried out using the lowest stress-rate (quasi-static) reported in [10]. The strain-rate-sensitive parameters have been simulated in the analytical tests. The plots of the quasi-static analytical results for the three types of concrete in compression are compared with those reported in [10] in Figs. 6.4 to 12. The rate effects on the compressive strength of specimens are also shown in the figure which will be explained later on. As can be seen, the analytical quasi-static results are in a good agreement with those of experimental observation.

6.3.7 Dynamic compressive tests

The proposed rate-sensitive model in which increasing the material strength and stiffness are included have been used in the dynamic analysis of the Hatano's compressive specimens. Three analytical tests have been carried out for each concrete mix under different loading rates (see Table 6.2).

The analytical results are compared with the experimental observation Figs. 6.4 to 12. Good agreement can be seen which confirms that the model is able to simulate the material strengthening and stiffening under strain-rate loading

condition. However, the problem can be analysed without using finite element method.

Benchmark 1 - Comparison of the results with other investigators

In order to compare the proposed model with other investigators, compressive test No. A10 on a cylinder concrete mix 1:3:5 has been analysed including all the strain-rate parameters. The same analytical test has been carried out by Bicanic [41] and Famiyesin [103]. Results of analyse are compared in Fig. 6.13. Since in the proposed model the peak dynamic strain and static strain is assumed to be constant while in both Bicanic and Famiyesin models the peak strain decreases with increasing strain-rate , the dynamic analysis of the specimen resulted in different peak strains.

6.3.8 Example - 6.2 Dynamic tensile tests

The tensile test specimens used by Hatano [10], had a cylindrical configuration of 15 cm diameter and were 30 cm long. In order to localize the failure in the middle-section, the middle third section was beveled down to achieve a diameter of 11 cm at the mid-section, Fig 6.2 B. Three types of experimental data for three concrete mixes have been used for identifying the empirical constants. Three tensile specimens in which increasing the modulus of elasticity due to strain-rate has been included have been analysed. Because the structure is symmetry only half the specimen has been modelled using axisymmetric finite elements.

The tensile test details reported in [10] are shown in Table 6.4, and the material properties are listed in Table. 6.5.

Table 6.4 Details of tensile simulated.

Concrete mix	Test No.	Failure time (sec.)	Peak strain
1:2:4	A4	0.27	18.1×10^{-5}
	A7	0.10	18.1×10^{-5}
	A10	0.035	17.5×10^{-4}
1:4:7	A5	0.50	17.5×10^{-5}
	A6	0.26	15.5×10^{-5}
	A11	0.09	14.5×10^{-5}
1:3:5	A5	0.51	$20. \times 10^{-5}$
	A7	0.29	18×10^{-5}
	A12	0.03	16.5×10^{-5}

Table 6.5 Material properties of tensile tests.

Material properties	Concrete mix		
	1: 2: 4	1: 3: 5	1: 4: 7
Young Modulus of elasticity (Kg/cm^2)	44.7×10^4	32.5×10^4	28.8×10^4
Poisson's ratio	0.18	0.18	0.18
Tensile strength (Kg/cm^2)	32.	27.0	20.0
Cracking strain	0.75E-4	0.75E-4	0.75E-4
Compressive strength (Kg/cm^2)	550	445	215.
Fracture energy $Kgcm/cm^2$	10	7	6
Mass density $Kgsec^2/cm^4$	2.45E-6	2.45E-6	2.45E-6
Empirical coefficients			
λ_1	0.77	0.8	0.75
λ_2	0.362	0.0773	0.0369

The concrete has been assumed to behave linearly elastic in tension and only increase in the initial modulus of elasticity was included. An ultimate strain criteria has been used for crack initiation.

The analytical results for the three types of concrete mix are compared with the experimental data reported in [10]. The plots of the tensile stress with strain for different strain-rates are shown in Figs. 6.14 to 21. As can be seen, the peak tensile strength is more than the experimental data which is due to the assumption made in the model that the peak strain remain constant under rate loading.

6.3.9 Example 6.3 - Ahmad's dynamic compressive tests

An experimental investigation to establish the response of concrete when subjected to high strain-rates under short-term compressive loading carried out by Ahmad and Shah [21] has been analysed. The strain-rates used for the tests varied between 10 000 to 30 000 microstrains/sec. Cylindrical 3×3 in specimens were used. Table 6.6 shows the mix proportion of the specimens and the material properties are listed in Table 6.7.

The Ahmad's cylindrical specimen has been analysed under constant strain-rates of 10 000 and 30 000 microstrains/sec. The procedure of analysis was the same as Hatano's tests. The peak-strain was assumed to be the same as the quasi-static test. The stress-strain curves of the specimen under two different strain-rates are plotted in Fig. 6.22 As can be seen, the concrete stiffness and strength are increased as the strain-rate is increased.

Table 6.7 Material properties for Ahmad's tests [21].

Concrete (ksi)	
Concrete Young Modulus	$E_c = 4.11E + 3$
Poisson's ratio	$\nu = .20$
Peak compressive stress	$\acute{f} = 6.98$
Peak compressive strain	$\epsilon_0 = .0024$
Mass density	$\rho = 0.217E - 06$
Cracking tensile strain	$\epsilon_{cr} = .75E - 04$
Fracture energy	$G_f = .6E - 3$
Fluidity parameters	
P_1	0.93
P_2	0.61
Empirical coefficients	
λ_1	0.8
λ_2	0.0773
T_1	0.066
T_2	1.38
T_3	0.026

Discussion of the results

Three dynamic analyses of tensile specimens with different water/cement ratio and concrete mix and three dynamic analyses of compressive specimens with different water/cement ratio and concrete mix have been carried out. Rate effect of rate-dependent parameters have been incorporated in the model. The plots of stress-strain curves were compared with those reported in [10]. The conclusions made are,

- As expected, the analytical strains in compression and tension were found to be less that the experimental observations. The reason may be due to the constant stress-rate assumption made in the model.

- The peak strain in tension tests were found to be more than the experimental results. The reason may be due to the assumption of linear elastic behaviour of concrete in tension.

- The peak strains in compression tests were found to be less than experimental results which is due to the assumption that peak strain remains constant under rate loading and constant rate loading assumption used in the model.

- Although the results of the above analytical tests on the concrete specimens do not confirm the validation of the model properly, the effect of strain-rate on strain-rate parameters are confirmed.

- More experimental data is required for obtaining the empirical coefficients.

6.3.10 Example 6.4 - Simply supported reinforced concrete beam under suddenly applied concentrated load

A simply supported reinforced concrete beam subjected to two concentrated suddenly applied loads has been analysed as the third series of the tests. The problem

has also been solved by other investigators such as those reported in [41]. Damping has been neglected in the analysis.

6.3.11 Material properties, geometry and loading

Fig. 6.23 shows the geometry and loading of the reinforced concrete beam under consideration. As can be seen, the reinforcement is placed in the lower half of the beam section in the tension region. Table 6.8 gives the material properties of the concrete and steel as used by Hinton et al. [41]. These values have been used for comparing the dynamic response of the beam with those reported in [41].

Table 6.8 Material properties for simply supported reinforced concrete beam

Concrete (ksi)	
Concrete Young Modulus	$E_c = 6100.0$
Poisson's ratio	$\nu = .20$
Ultimate compressive stress	$\acute{f} = 3.74$
Ultimate compressive strain	$\epsilon_{cu} = .0035$
Mass density	$\rho = 0.217E - 06$
Cracking tensile strain	$\epsilon_{cr} = .75E - 04$
Fracture energy	$G_f = .6E - 3$
Fluidity parameters	
P_1	0.93
P_2	0.61
Empirical coefficients	
λ_1	0.8
λ_2	0.0773
T_1	0.066
T_2	1.38
T_3	0.026
Steel (ksi)	
Steel Young Modulus of elasticity	$E_s = 30000.0$
Yield stress	$f_y = 44.$
Fluidity parameters	
a_0	1.5386
a_1	0.9705

6.3.12 Spatial discretisation

Concrete has been modelled using rectangular 8-noded serendipity isoparametric elements with two displacement degrees of freedom per node. The size of elements varies horizontally and vertically.

In order to assess the effect of the spatial discretisation on the fundamental frequency of the beam, the natural frequencies of the beam have been determined using different meshes of elements to obtain the converged fundamental frequency. For this purpose, a computer program originally developed by Smith et al. [116] was used for determining the natural frequencies.

The mesh and node numbering of the simply supported beam is illustrated in Fig. 6.24. Due to the symmetry of the structure and loading, only half of the structure is analysed.

Reinforcing bars have been modelled using embedded elements in which the steel is smeared as a one-dimensional element placed in concrete so that the natural coordinate perpendicular to steel bar is constant, and is idealised using elastic-perfectly plastic model. Perfect bond is assumed between the steel reinforcement and the concrete.

Reduced integration with 2×2 Gaussian points as discussed in Chapter 3 has been adopted for determining the stiffness of the structure and 3×3 Gaussian points have been used for determining the consistent mass matrix.

6.3.13 Time discretisation

The central difference method given by Eqs. (6.2), (6.3) and (6.4) which has a maximum time-step in explicit methods has been used as the time integrator.

The initial conditions are determined using Eqs. (6.5) and (6.6).

Critical time-step

Based on the conclusions discussed in Chapter 5, two different time-steps have been used in the analysis of the reinforced concrete beam. The first one which has been used for the elastic analysis, which was based on the maximum natural

frequency of the beam using Eq. (6.7), was found to be .000006 sec. Since an explicit form for the determination of the strain has been used in the viscoplastic analysis, the computational time-step for viscoplastic analysis proposed by Cormeau [118] Eq. (6.10), which equals to .000002 s has been used.

6.3.14 Mass discretisation

The proposed method for producing a lumped mass matrix from a consistent mass matrix discussed in chapter 3 has been used.

6.3.15 Dynamic analysis of the problem

Two sets of analyses have been carried out. In the first set, the material strain-rate-sensitive parameters have not been included in order to compare the results with [41]. They have been included in the second set of the analyses. The analyses carried out can be summarized as follows

- Elastic analysis excluding the strain-rate-sensitive parameters.
- Viscoplastic analysis with no cracking.
- Viscoplastic analysis cracking is included.
- Elastic analysis including the strain-rate-sensitive parameters.
- Viscoplastic analysis with no cracking.
- Viscoplastic analysis with no cracking.

These will be discussed in the following sections.

Elastic analysis

An elastic analysis has been carried out. The variation of mid-span displacement with time is plotted in Fig. 6.25. As can be seen , the elastic response is in good agreement with those of Hinton et al. [41] and Famiyesin [103].

6.3.16 Dynamic analysis including cracking and results

In the proposed material model, a maximum principal tensile strain criterion has been adopted as the crack initiation criteria. The initiation of cracks starts when the tensile strain at any Gauss-point reaches a defined value normally obtained from experimental evidence. For comparison purposes, the maximum strain has been chosen to be the same as that used by Hinton et al. [41]. The fracture energy approach discussed in Chapter 2 has been used to model the post-cracked behaviour of concrete. The variation of mid-span displacement with time is plotted in Fig. 6.25. Figs 6.26 shows the crack initiation and propagation and the corresponding time. Cracking starts from the central portion of the beam at the tension side and propagates through the two ends of the beam.

6.3.17 Viscoplastic analysis with no cracking

An elasto-viscoplastic analysis of the beam has been carried out assuming that viscoplatic behaviour initiates at $\sigma_0 = \acute{f}_c$. In this analysis, however no viscoplastic behaviour occurred. Hence, the nonlinear effect is due to the cracking of concrete only. The variation of mid-span displacement of the beam is plotted in Fig. 6.25.

6.3.18 Viscoplastic analysis including cracking

In this example, an elasto-viscoplastic analysis has been carried out assuming viscoplasticity is initiated at $\alpha\acute{f}_c$. with $\alpha = .3$. Perzyna's model Eq. (6.17) has been used to determine the strain-rate in each time-step. The exponential form of the flow function Eq. (6.20) with $N = 1$ has been used.

Perzyna's fluidity parameter γ_P has been evaluated using Eq. (6.18). In Eq. (6.19) the total effective strain-rate ϵ_{effec} which is a function of the octahedral normal ϵ_{oct} and the shear strain γ_{shear} [2], has been used to relate the multiaxial strains to an equivalent uniaxial strain. The variation of mid-span displacement of the beam is plotted in Fig. 6.25.

6.3.19 Dynamic analysis including strain-rate-sensitive parameters

In the second set of analyses of the beam, all the rate-sensitive parameters were included in the material model. The proposed fluidity parameter γ_I for evaluating the increase in the initial modulus of elasticity with strain-rate Eq. (6.21) has been used and the increased modulus of elasticity E_d has been determined using Eq: (6.11). In order to simulate the increase in the secant and tangent modulii of elasticity with strain-rate, the proposed fluidity parameter γ_T has been used, Eq. (6.24).

The proposed uniaxial strain-rate-sensitive stress-strain formula Eq. (6.22) has been used to relate the uniaxial problem to multiaxial situation.

Elastic analysis including strain-rate-sensitive parameters

An elastic analysis including all material rate-sensitive parameters has been carried out. As expected, the response was found to be influenced by the strain-rate. The variation of mid-span displacement of the beam with time is illustrated in Fig. 6.27. As expected, the maximum mid-span displacement of the beam has been decreased due to the effect of strain-rate on the material strength and stiffness.

Non-linear analysis excluding cracking

A non-linear analysis of the reinforced concrete beam has been carried out assuming that visco-plasticity is initiated at $\sigma_0 = \acute{f}_c$. No viscoplastic behaviour occurred, which confirm that the non-linear behaviour is due to cracking Fig. 6.27. As can be seen, the results are in good agreement with previous work reported in references [41] and [103].

Non-linear analysis including cracking

The beam has been analysed including cracking and all material strain-rate-sensitive parameters. The nonlinearity was found to be influenced by the increase

in the material strength due to strain-rate. Fig. 6.27. illustrates the variation of mid-span displacement with time. A reduction in the maximum displacement can be seen when compared with the analysis excluding the strain-rate-sensitive parameters. The results are in good agreement with the that reported in references [41] and [103].

Discussion of the results

From the analyses of the beam described above, the following conclusions can be made.

- That the maximum mid-span displacement predicted by the analyses including cracking are increased by almost 50 percent compared with the linear elastic response.

- That the fundamental period of the beam is increased by about 25 percent in the analyses including cracking when compared with the predicted linear elastic fundamental period.

- That the non-linear effects were due mainly to cracking as can be seen form Fig. 6.25.

- That the viscoplasticity was found to occur in the top portion of the beam starting from the mid-span and spreading to the two ends of the beam.

- That as expected, because the increase in the modulus of elasticity, the strengthening and stiffening of the concrete have been simulated, the maximum displacement of the beam was found to decrease. The plots of the mid-span displacement of the beam with time shows such effect Fig. 6.27, and describe increasing the material stiffness and strength due to increasing strain-rate which is the objective of the model.

6.3.20 Example 6.5 - Clamped circular reinforced concrete slab

A circular reinforced concrete slab subjected to a distributed load of intensity 1.4 kg/cm^2 applied with a rise-time equal to half of the elastic fundamental period (T=0.06 s), has been analysed. The geometry of the slab and loading are shown in Fig. 6.28. The reinforced concrete slab which has a radius of 10 m and thickness of 1 m is reinforced in both the radial and tangential directions at the top and lower surfaces with a reinforcement ratio of 1%. The material properties for the slab are shown in Table 6.9. Damping has been considered. The reinforced concrete slab is spatially discretised using 8-noded rectangular serendipity isoparametric axisymmetric finite element. The proposed lumped mass scheme has been used for producing a lumped mass matrix from a consistent mass matrix. Due to symmetry only half of the structure has been analysed .

The central difference method has been used for time integration with a computational time-step equal to 0.000005 s. It is worth noting that the time-step determined from stability conditions is rounded down to obtain the computational time-step.

Table 6.9 Material properties of reinforced concrete slab.

Material properties	Concrete	Steel
Young Modulus E	30×10^4 (Kg/cm^2)	2.1×10^6 (Kg/cm^2)
Poisson's Ratio v	.19	
Compressive strength $\acute{f}$	350. (Kg/cm^2)	4600.0 (Kg/cm^2)
Tensile strength	31.5 (Kg/cm^2)	
Cracking strain	0.75E-4	
Ultimate compressive strain ϵ_u	0.0035	
Mass density ρ	2.45×10^{-6}, $(Kgsec^2/cm)$	
Fracture energy Gf	250. $Kgcm/cm^2$	
Fluidity parameters		
P_1	1.01	
P_2	0.115	
Empirical coefficients		
λ_1	0.75	
λ_2	0.0369	
T_1	-0.22	
T_2	-0.78	
T_3	6.11E-4	
a_0		1.5386
a_1		0.9605

The analyses carried out were as follows.

- Elastic analysis excluding the strain-rate-sensitive parameters.
- Viscoplastic analysis with no cracking.
- Viscoplastic analysis cracking is included.
- Elastic analysis including the strain-rate-sensitive parameters.
- Viscoplastic analysis with no cracking.
- Viscoplastic analysis with no cracking.

These will be discussed in the following sections.

6.3.21 Elastic analysis

A linear elastic dynamic analysis has been carried out in which the material strain-rate-sensitive parameters were not included.

The variation of the central-point deflection with time is plotted in Fig. 6.29. As can be seen, the elastic analysis response is in good agreement with those reported in references [41] and [103].

6.3.22 Visco-plastic analysis with no cracking

An analysis of the reinforced concrete circular slab has been carried out in which the cracking is not included. In this test the viscoplastic behaviour was assumed to initiate at $\sigma_0 = \acute{f}_c$. No viscoplastic behaviour occurred. The plots of the variation of the central displacement of the slab with time is given in Fig. 6.29.

As can be seen, only a slight amplitude increase with approximately the same period compared with that of the elastic analysis occurs if crack is not considered.

6.3.23 Viscoplastic analysis including cracking

An analyses has been carried out in which cracking is included. For the purpose of comparison of the structural response with that of previous work, the material

strain-rate-sensitive parameters have not been included. Cracking was assumed to initiate when the maximum strain exceeds a defined value in principal direction.

The plots of variation of the central point displacement for this and the preceeding two analyses with time are given in Fig. 6.29. It can be concluded that major nonlinearity is due to cracking.

Fig. 6.30 shows the crack patterns on plan and section. The tangential cracks were formed at the upper portion of the clamped edge and spread to the centre of the slab.

6.3.24 Elastic analysis with strain-rate sensitive parameters

An elastic analysis including the material strain-rate-sensitive parameters has been carried out. The plot of variation of the central point displacement with time is illustrated in Fig. 6.31. As can be seen, the maximum displacement decreases which indicates the increase of the structural stiffness and validation of the proposed mode.

6.3.25 Visco-elastic-visco-plastic analysis, with no cracking

The reinforced concrete slab has been analysed with no cracking. The plot of variation of central point displacement with time is given in Fig. 6.31. As can be seen the visco problem is influenced by the material stiffening and strengthening due to strain-rate effect which confirm the validation of the proposed model. As can be seen, the elastic analysis response is in good agreement with those reported in references [41] and [103].

6.3.26 Visco-elastic-visco-plastic analysis, cracking is considered

In the final analyses, the structure has been analysed with cracking considered. Significant nonlinearity was found to occur. Fig. 6.31 illustrates the time-history central point displacement of the slab which is influenced by the material strengthening and stiffening. The results are in good agreement with the that reported in references [41] and [103].

Discussion of the results

Three different time-dependent loading, boundary conditions and geometries were used. The analytical results have been compared with experimental and analytical results obtained from other sources. The same conclusions as for the reinforced concrete beam can be made for reinforced concrete slab. In addition to the specific conclusions made for each example the following general conclusions can be drawn.

- The tangential cracks are formed first at the upper section of the clamped edge, radial and tangential cracks spread from the center Fig. 6.30.

- The proposed history-strain-rate model is able to predict the dynamic behaviour of concrete and reinforced concrete structures under transient forces with and without simulating the material stiffening and strengthening. However, the accuracy of the model depends mainly on the availability of experimental data for determining the empirical values.

- The explicit form of strain approximation is suitable for predicting the strain increment in non-linear analysis in each time-step.

- The major non-linearity in the examples was cracking which caused elongation of the fundamental period and increase in the maximum displacement.

Fig. 6.1 Structure chart for Program DYNICK2D

Fig. 6.1 Flow chart (continued, page 2)

Calculate excess stress F

Check if the point is viscoplastic

If yes

IF NO

Calculate the reduced strain

Calculate the excess stress F

Calculate viscoplastic strain
DEVP
Datails are given on Page 4

Add DEVP to total viscoplastic strain EVPT

Subtract the total viscoplastic strain from total strain

Calculate flow function

Calculate flow vector

Calculate strain-rate

Calculate viscoplastic strain vector

Add to total viscoplastic strain vector

Calculate element bodyload, global bodyload

Read external loads

Calculate effective force, solve equilibrium equation

output data
Calculate X1, D1X1, D2X2

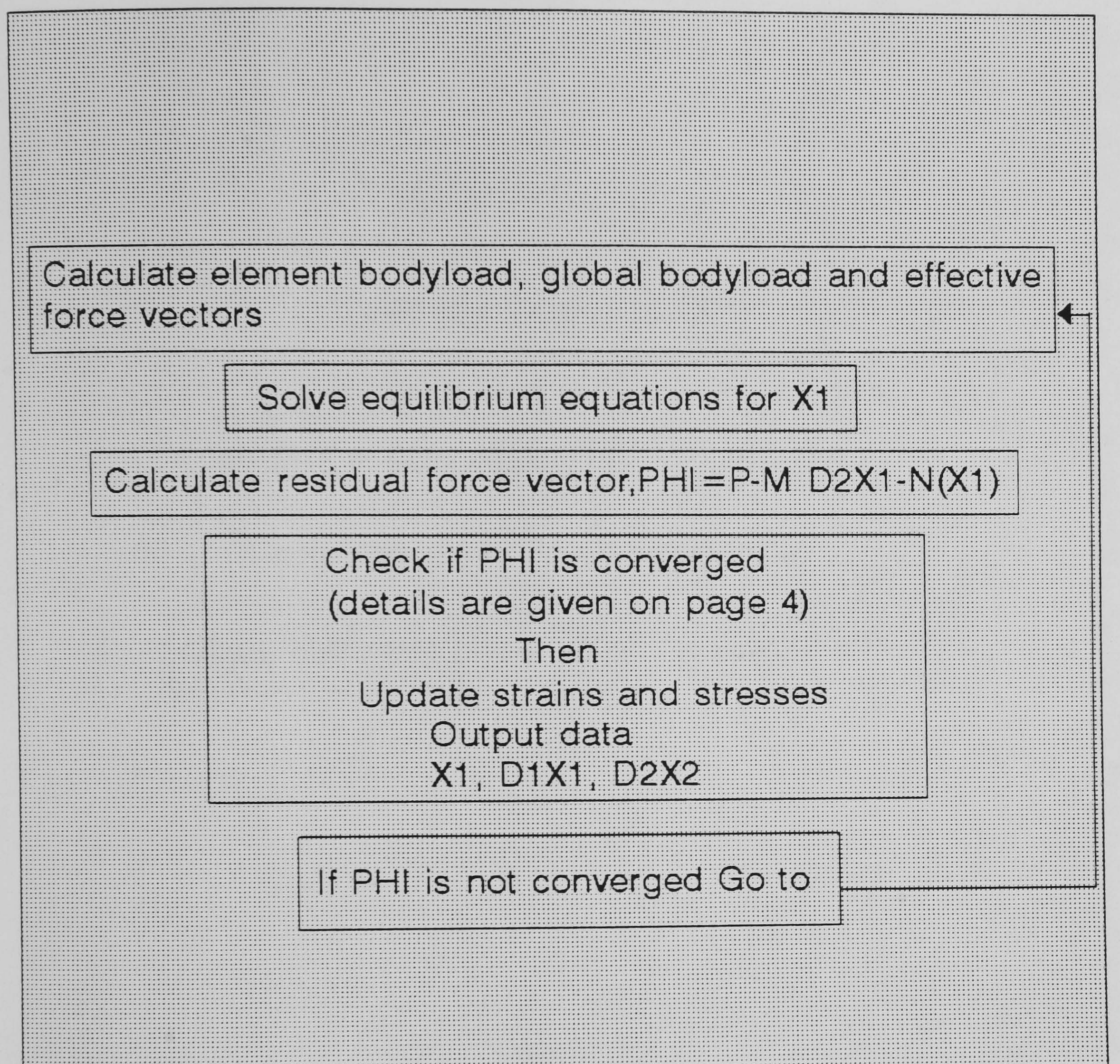
Calculate element bodyload, global bodyload and effective force vectors
Solve equilibrium equations for X1
Calculate residual force vector,PHI=P-M D2X1-N(X1)
Check if PHI is converged
(details are given on page 4)
Then
Update strains and stresses
Output data
X1, D1X1, D2X2
If PHI is not converged Go to

Fig. 6.1 Structure chart for Program DYNICK2D

Page 4 Viscoplastic strain evaluation

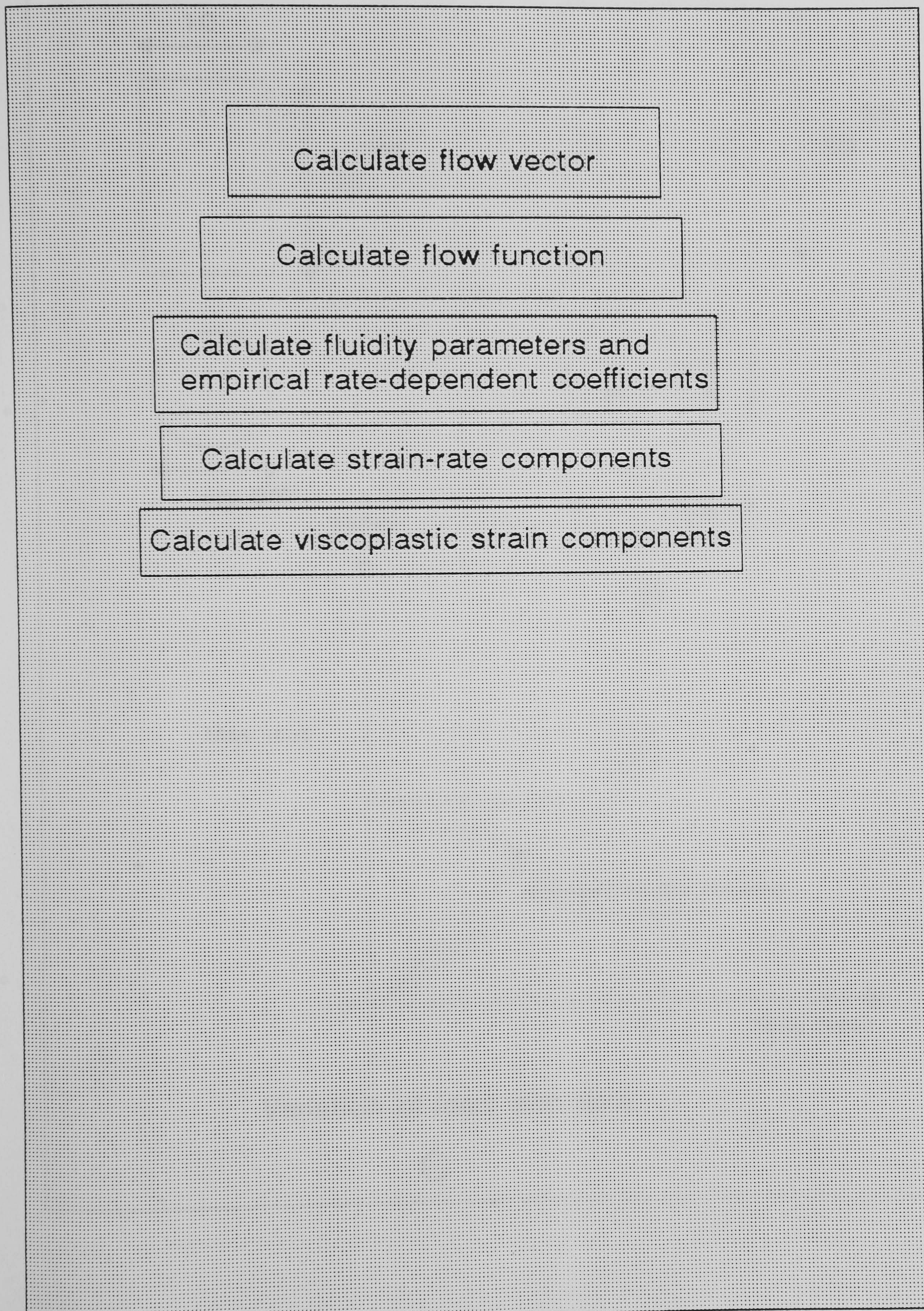

g. 6.2 Geometry of compressive and tensile Hatano's specimen and loading
A - Compressive, B - Tensile, C - Loading

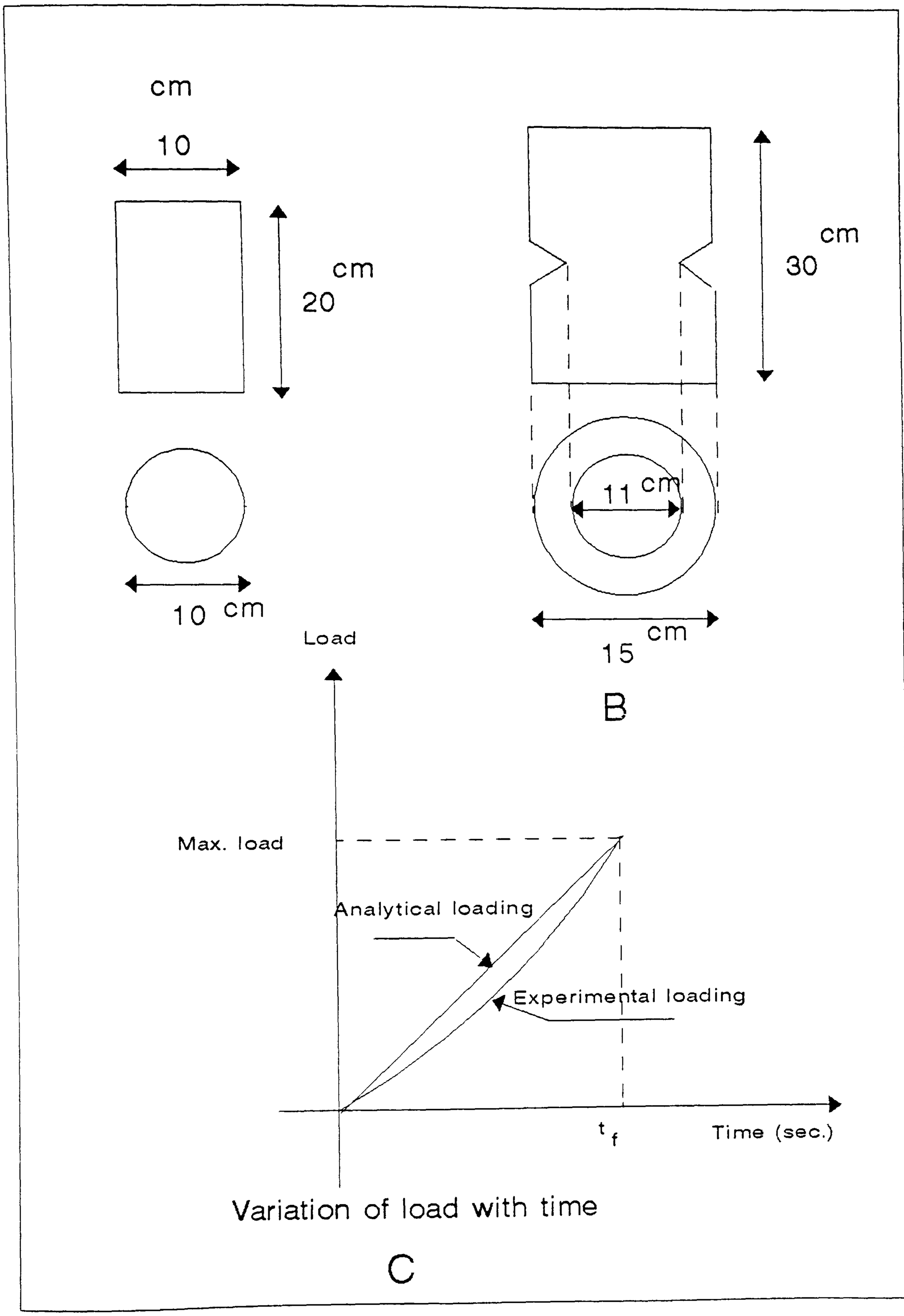

Fig. 6.3

Spatial discretisation, node numbering, restrained nodes and load discretisation of the compressive Hatano's specimen [10].

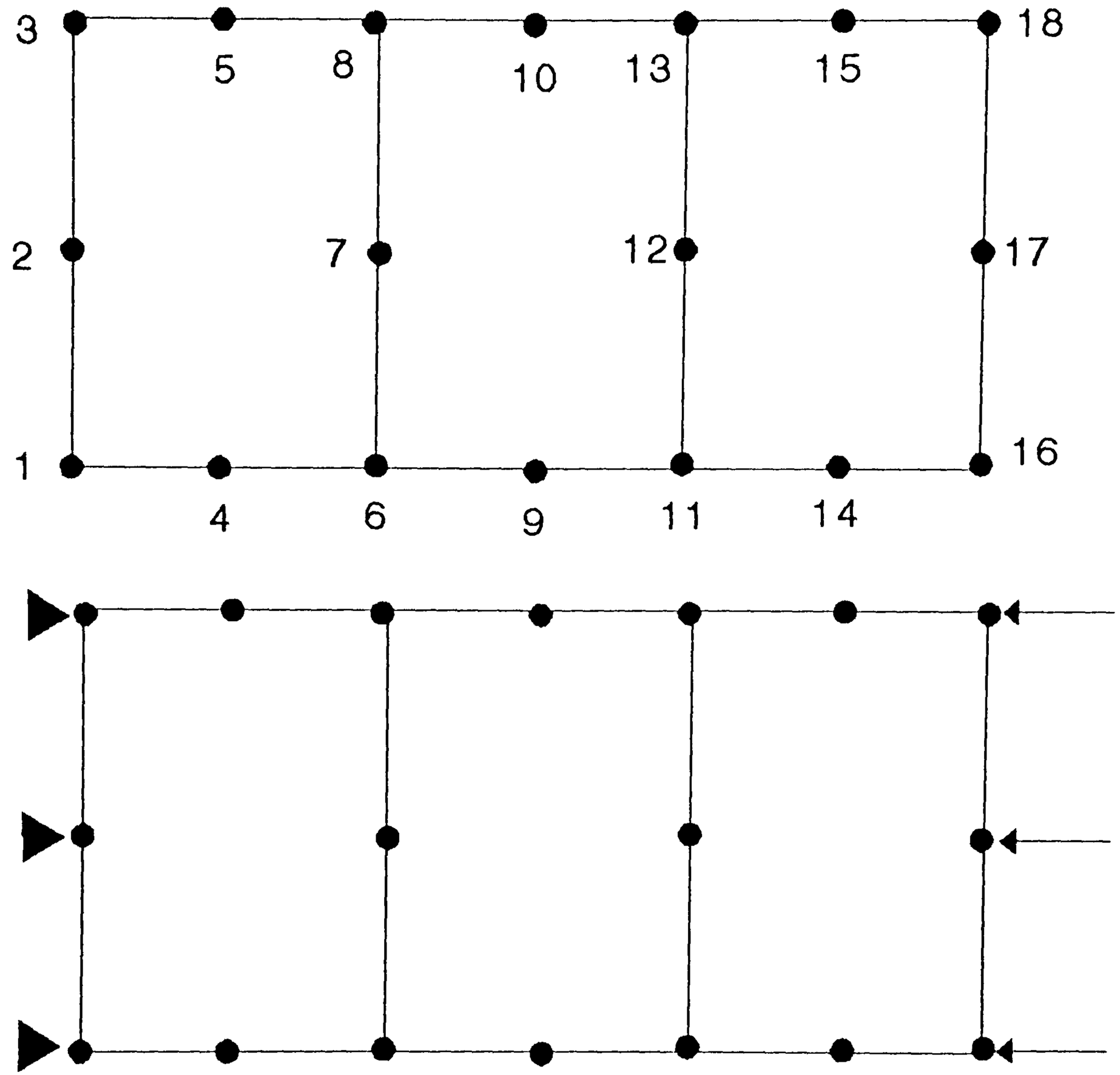

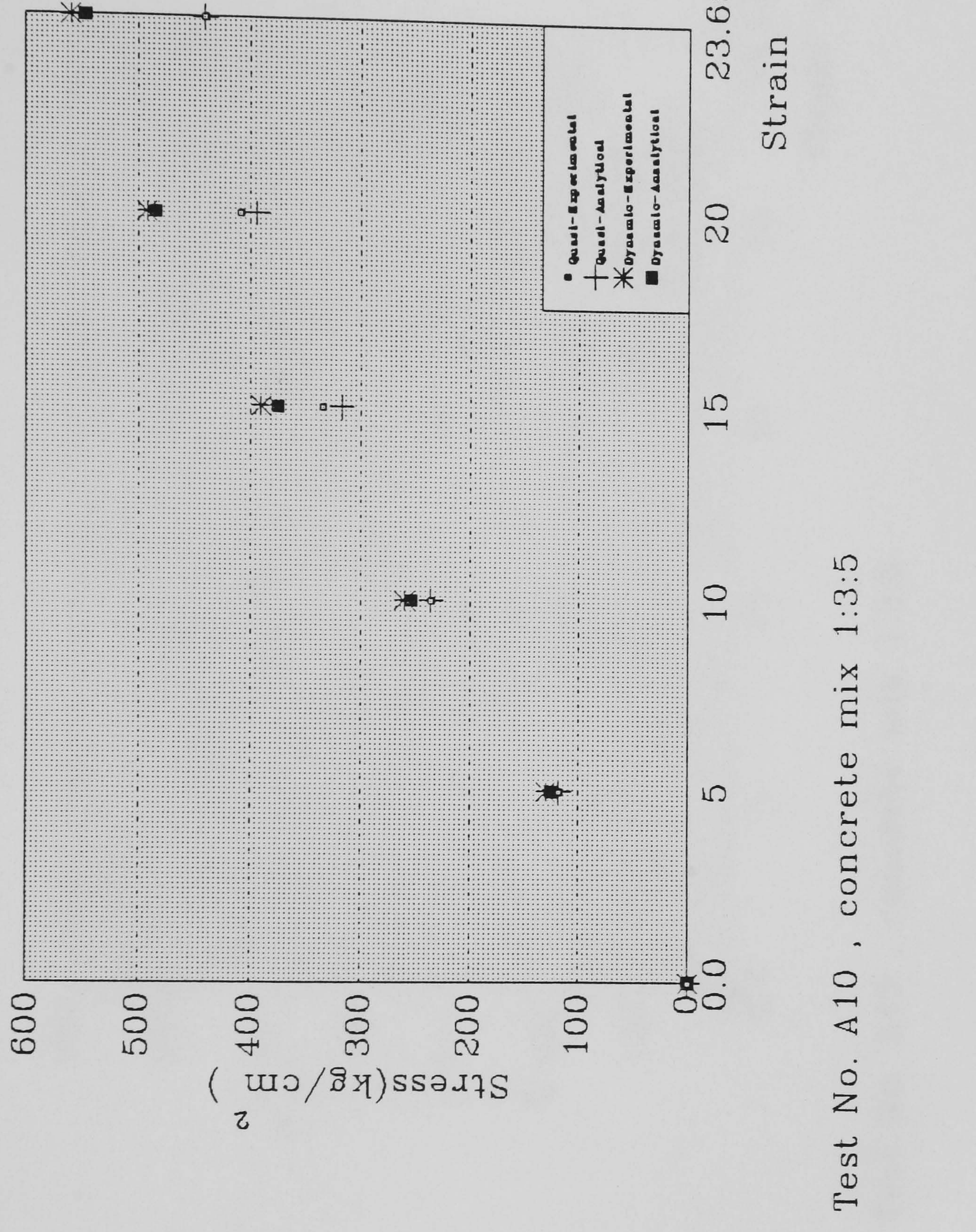

Fig. 6.4 Compression test ressults
Comparison of results with Hatano's test

Test No. A10 , concrete mix 1:3:5

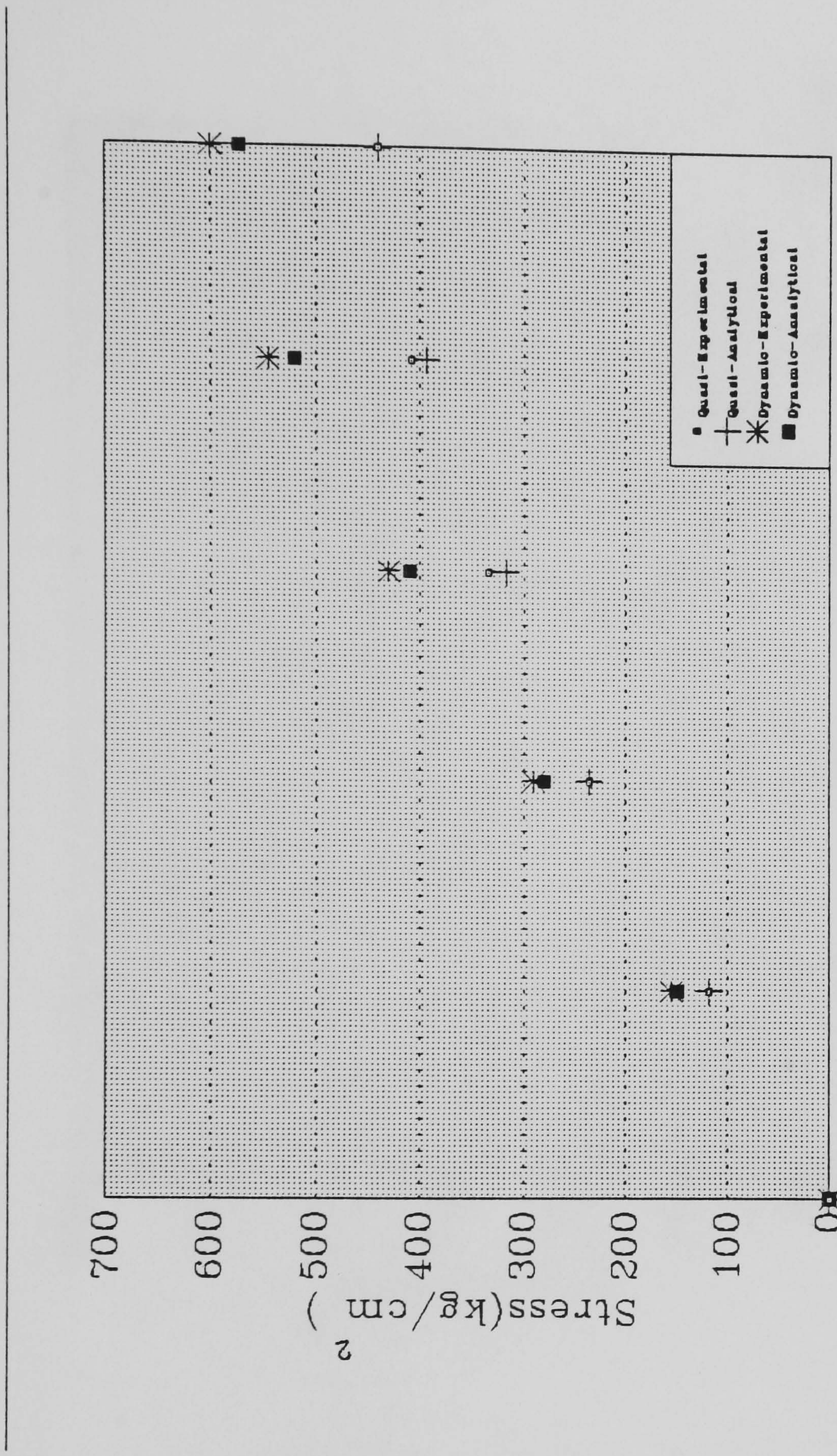

Fig. 6.5 Compression test results

Comparison of results with Hatano's tests

Test No. A15 , concrete mix 1:3:5

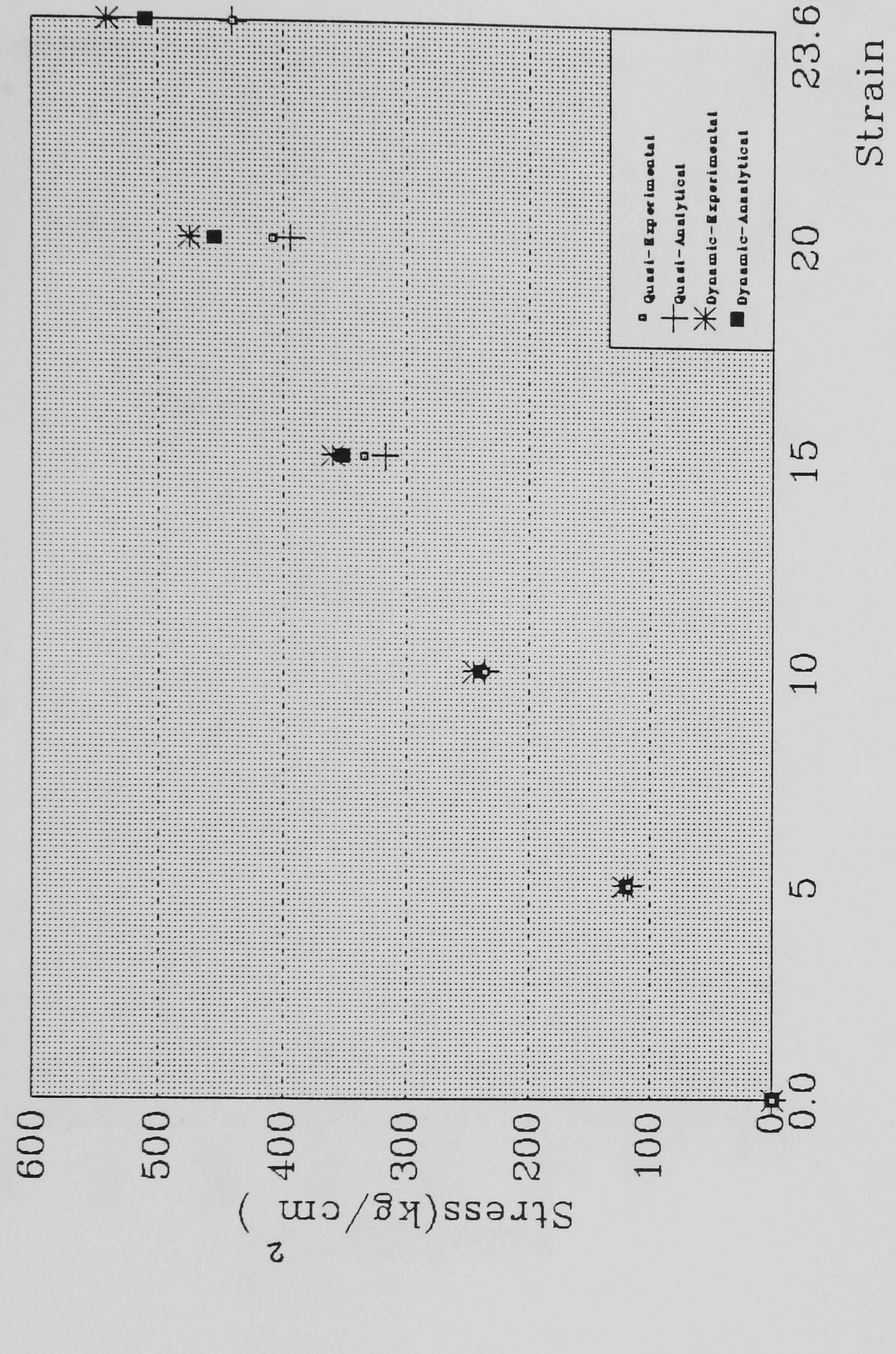

Fig. 6.6 Comparison the proposed quasi static model with Hatano test results

Fig. 6.7 –Compression test results

Comparison of results with Hatano's tests

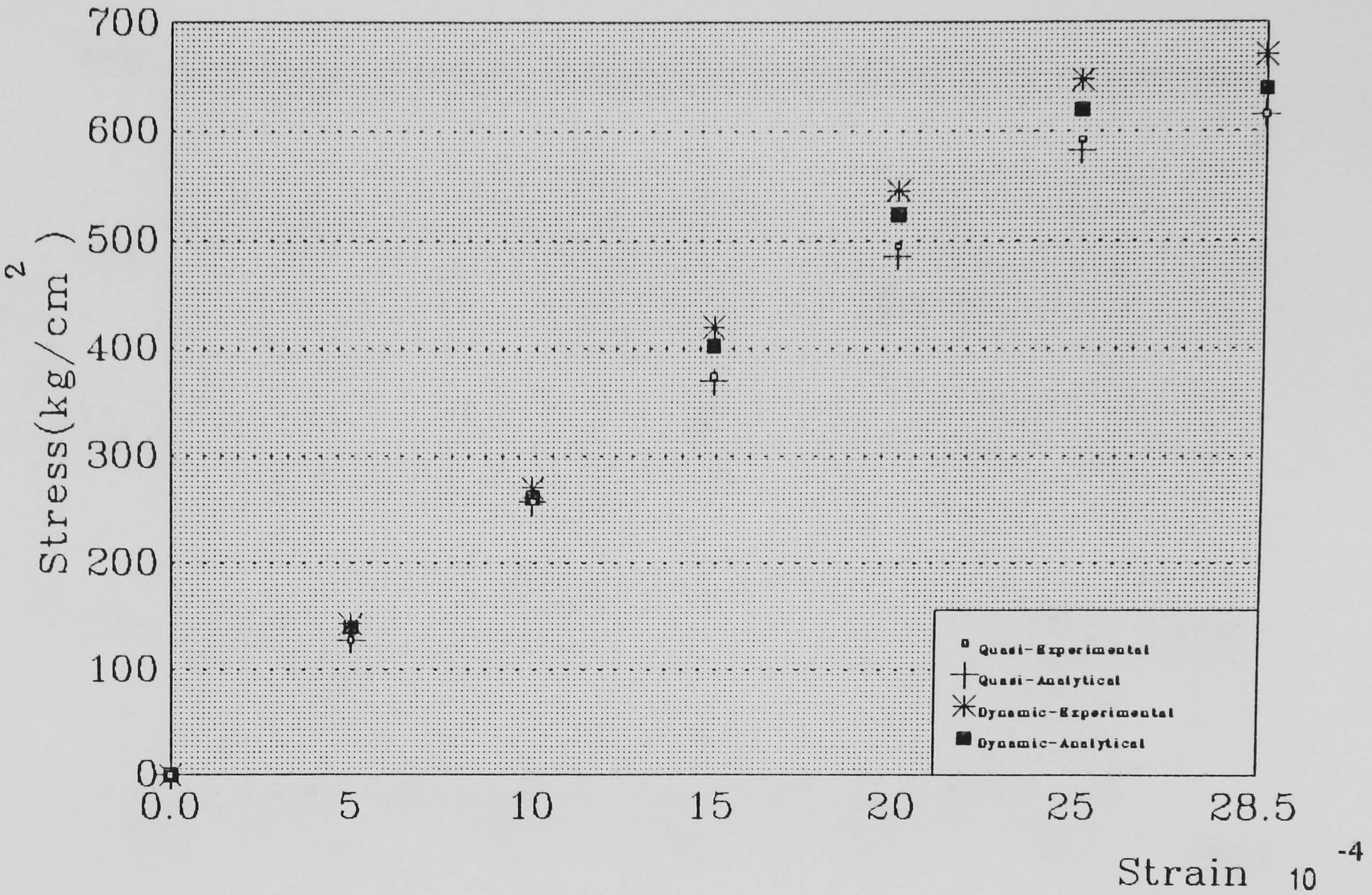

Test No. A4 , concrete mix 1:2:4

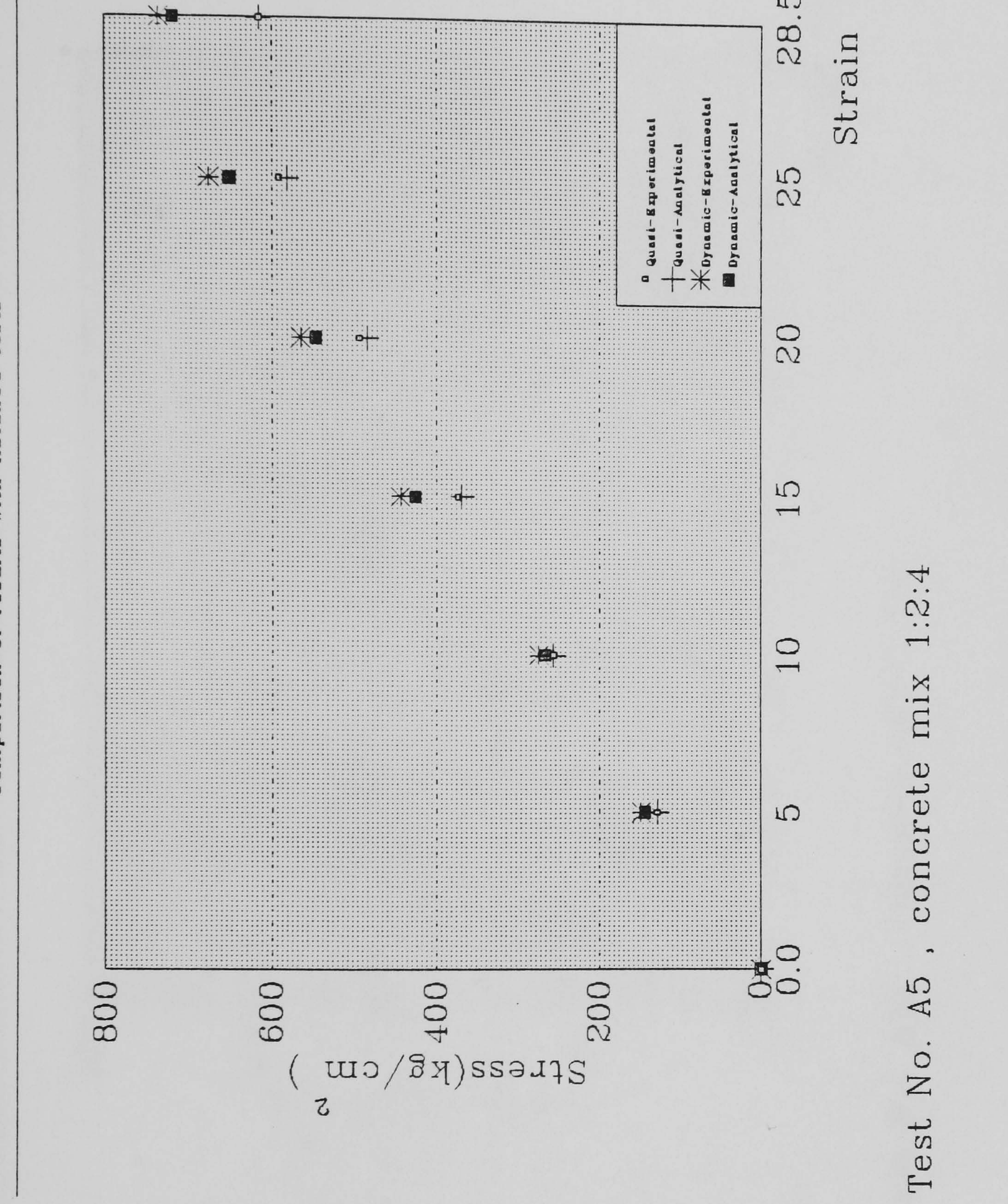

Fig. 6.8 -Compression test results
Comparison of results with Hatano's tests

Test No. A5 , concrete mix 1:2:4

Fig. 6.9 –Compression test results
Comparison of results with Hatano's tests

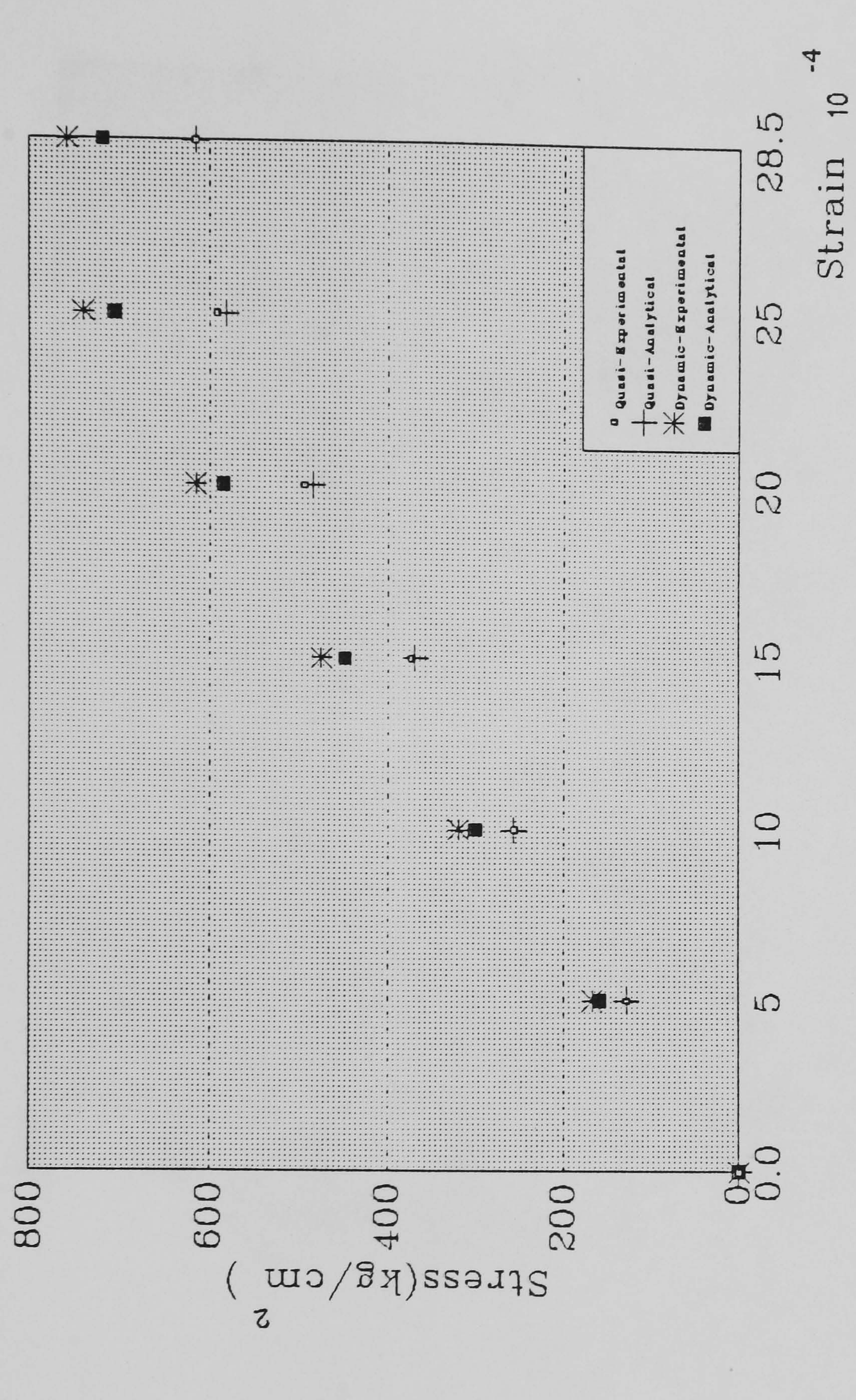

Test No. A14 , concrete mix 1:2:4

Fig. 6.10 –Compression test results

Comparison of results with Hatano's tests

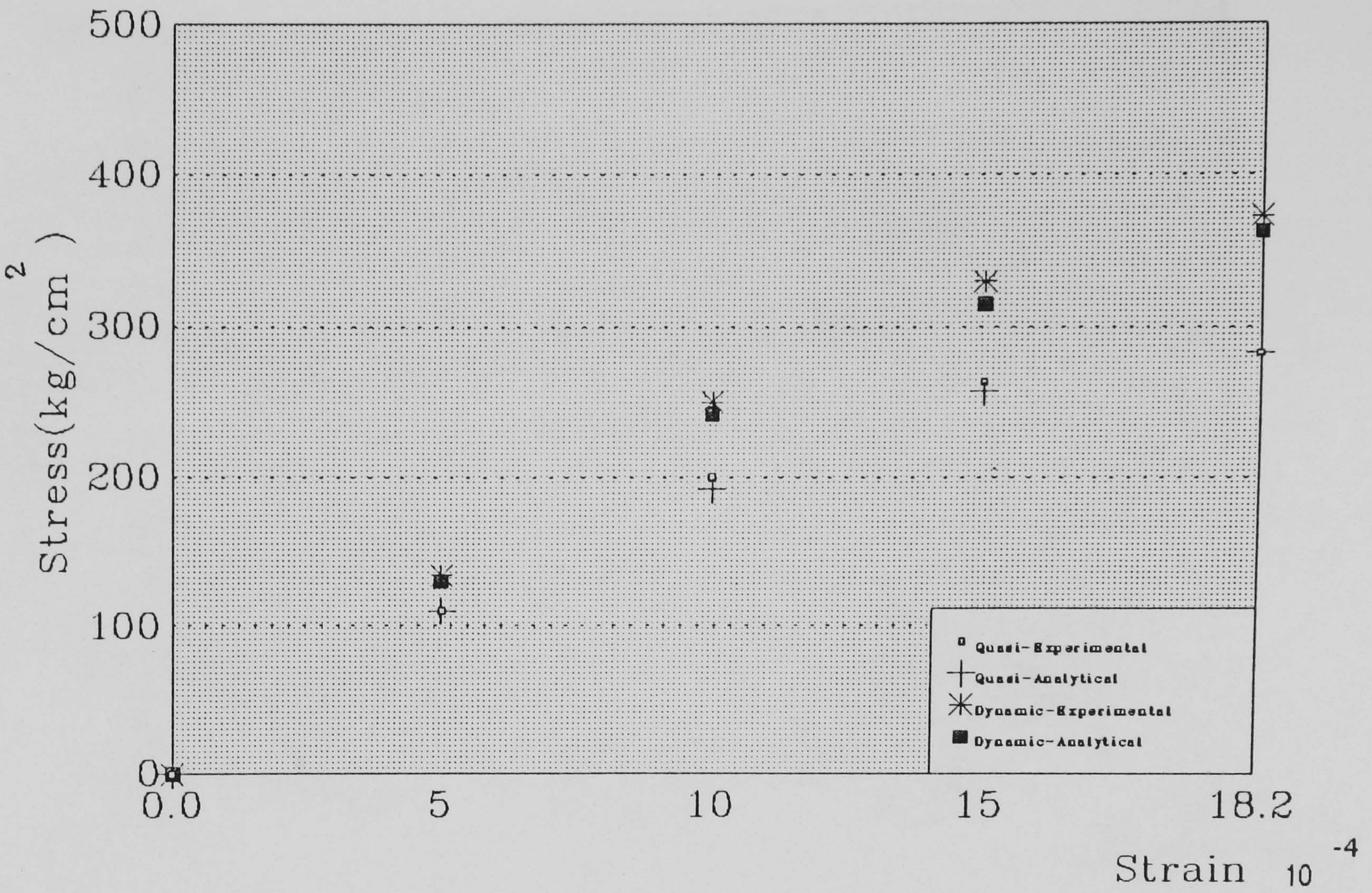

Test No. A6 , concrete mix 1:4:7

Fig. 6.11 –Compression test results

Comparison of results with Hatano's tests

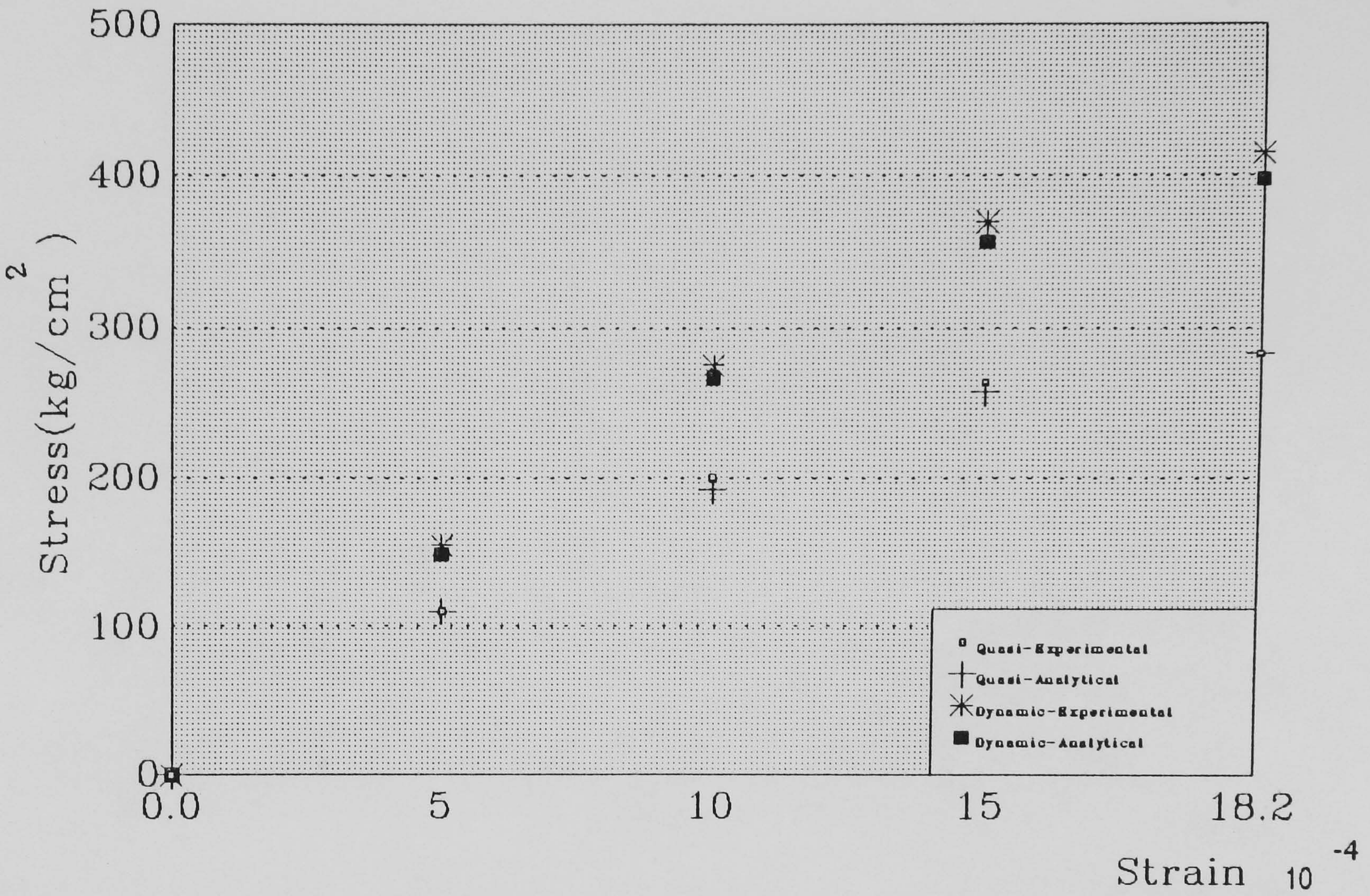

Test No. A11 , concrete mix 1:4:7

Fig. 6.12 –Compression test results

Comparison of results with Hatano's tests

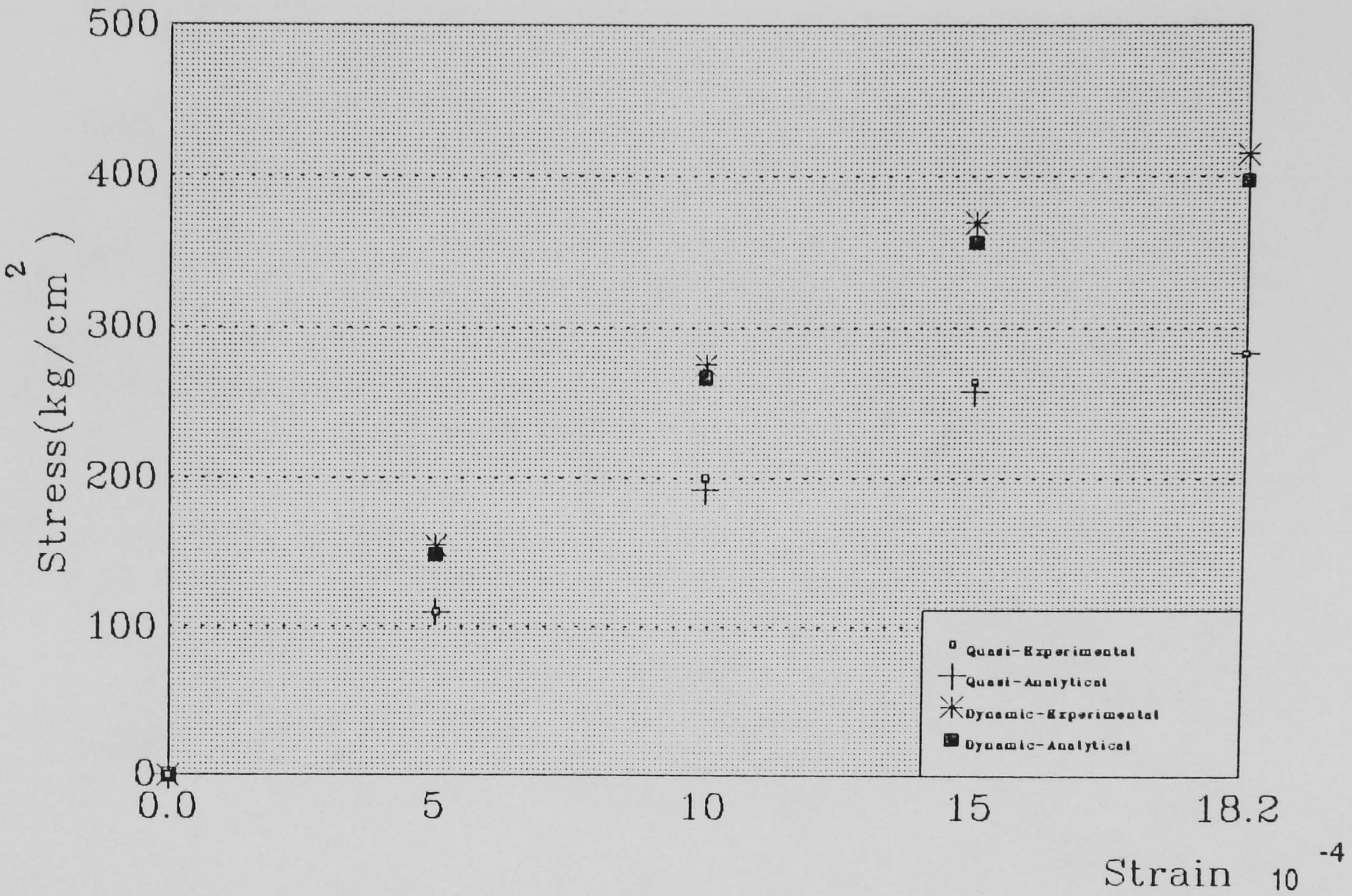

Test No. A1b , concrete mix 1:4:7

Fig. 6.13 Compression test results

Comparison of analytical results with Hatano's test [10] and other investigators.

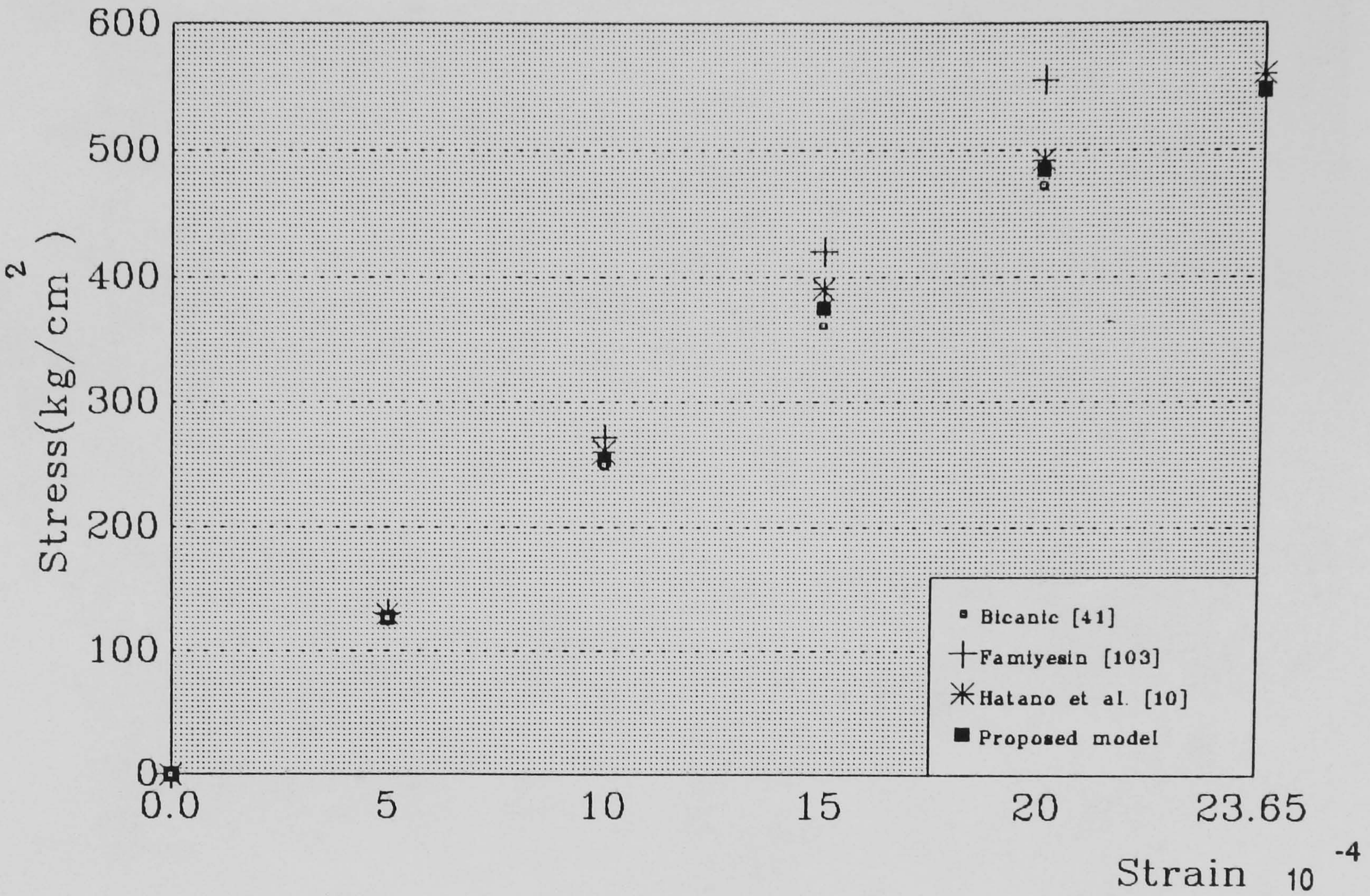

Test No. A10 , concrete mix 1:3:5

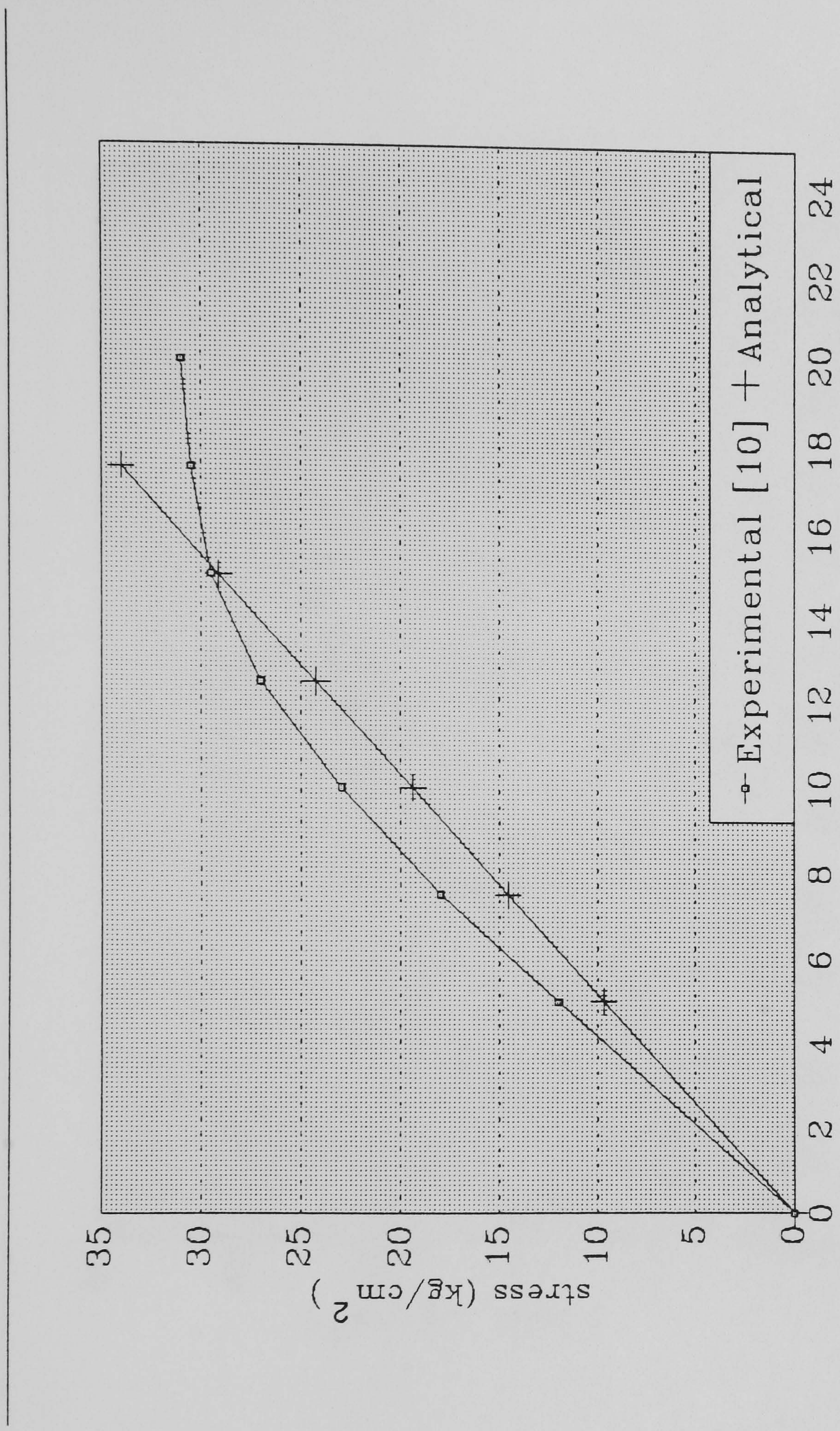

Fig. 6.14 –Comparison of tensile Hatano's tests
Concrete mix 1:3:5, test No. A5

Fig. 6.15 –Comparison of tensile Hatano's tests
Concrete mix 1:3:5, test No. A7

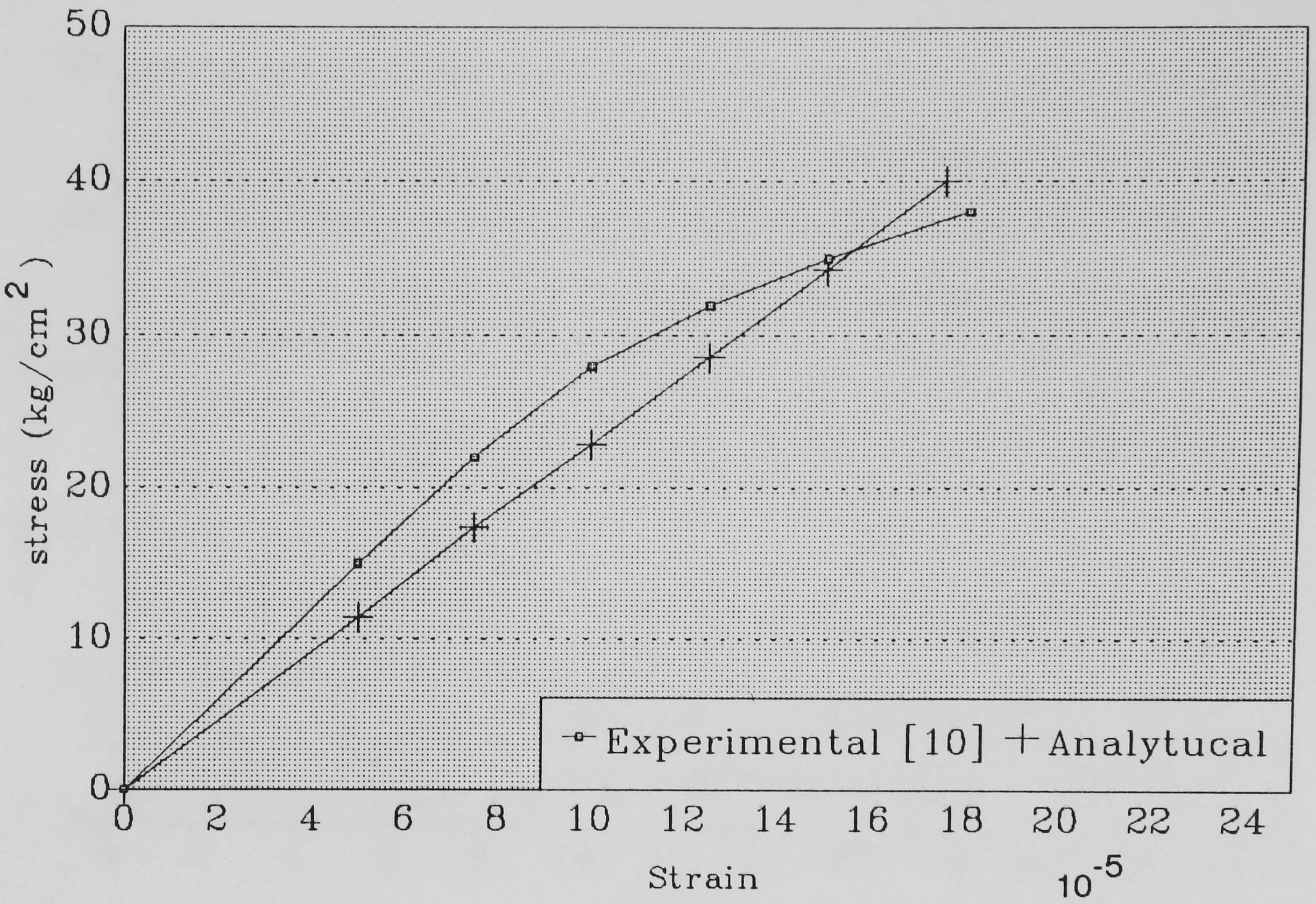

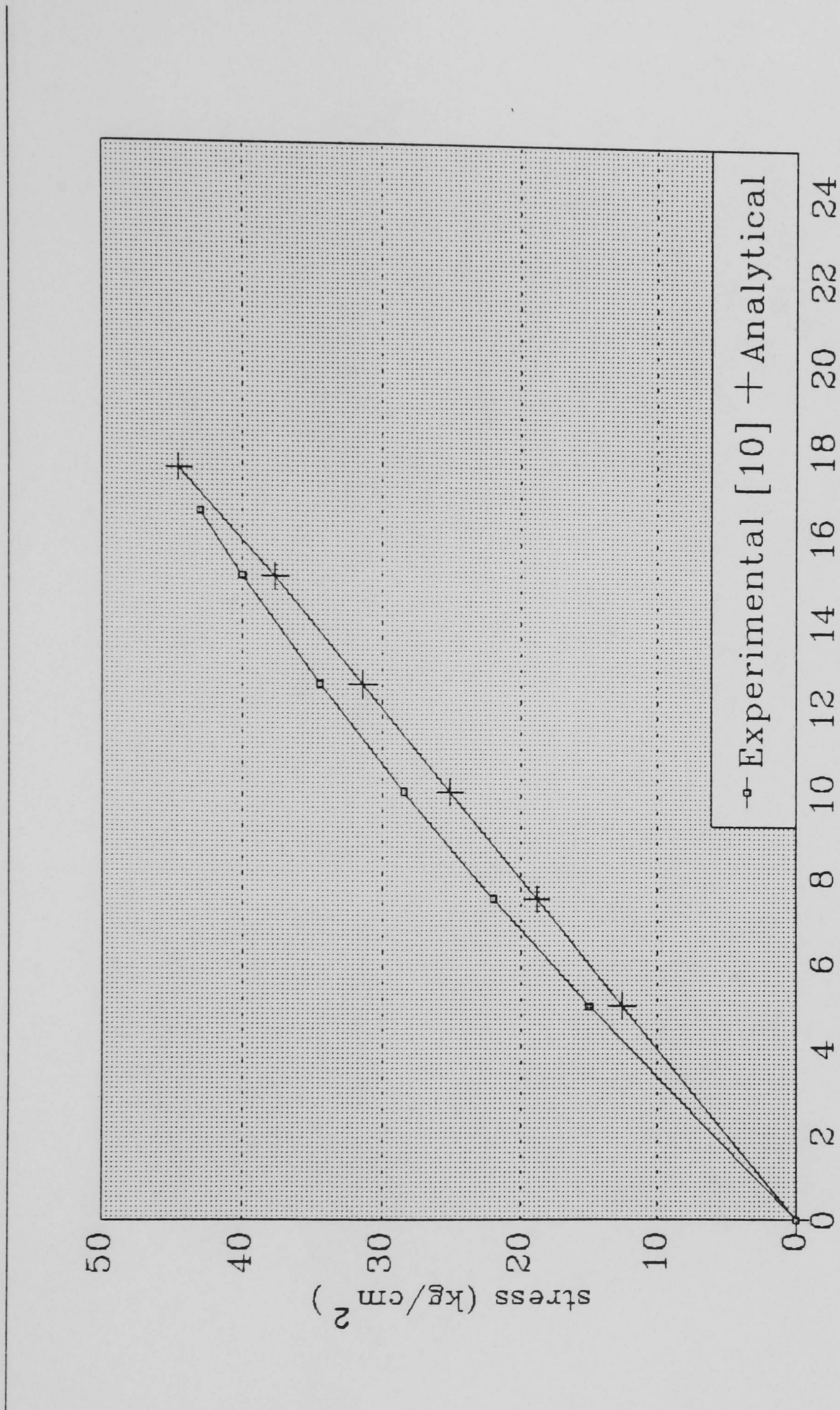

Fig. 6.16 –Comparison of tensile Hatano's tests
Concrete mix 1:3:5, test No. A12

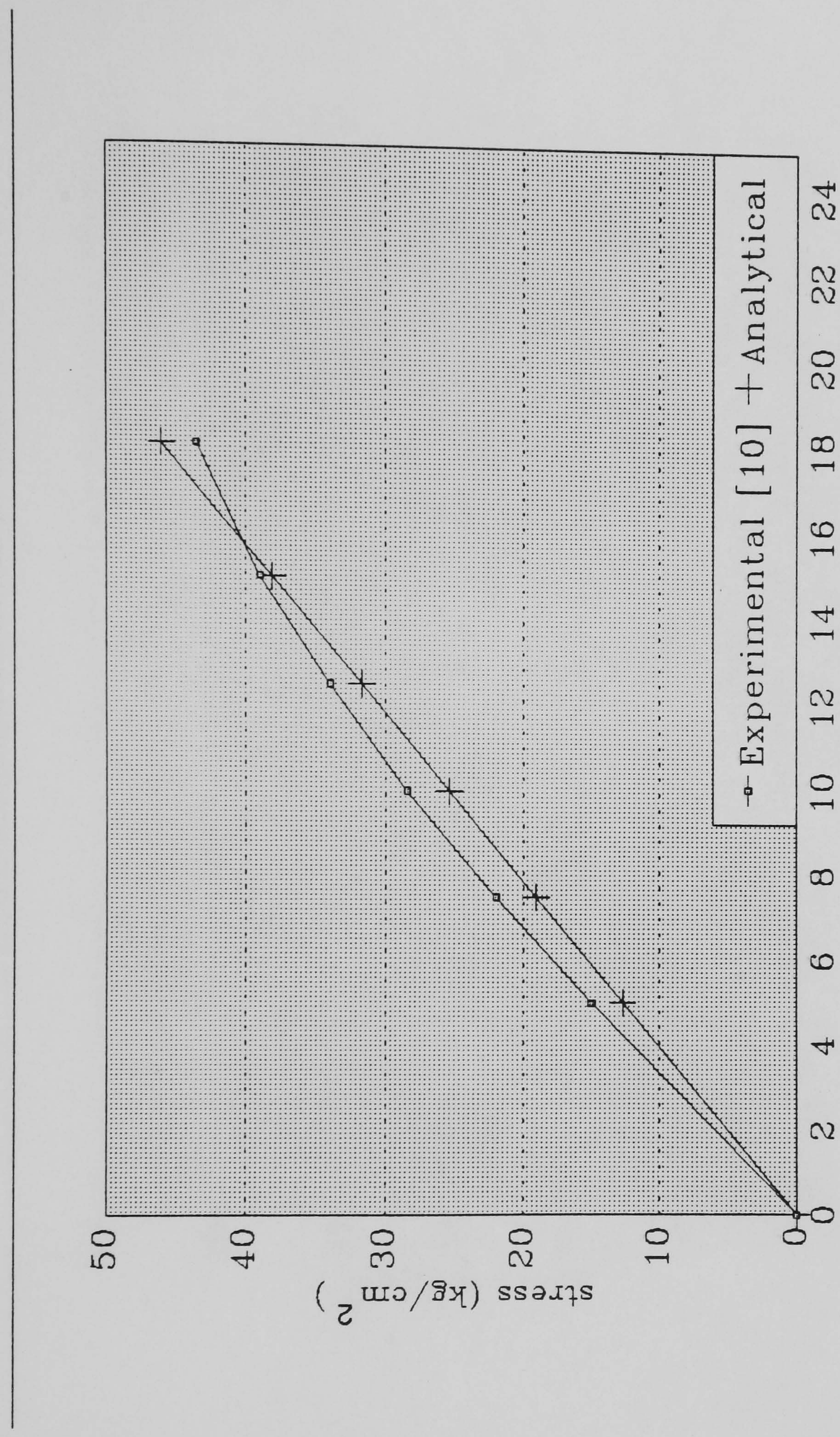

Fig. 6.17 –Comparison of tensile Hatano's tests
Concrete mix 1:2:4, test No. A4

Fig. 6.18 –Comparison of tensile Hatano's tests
Concrete mix 1:2:4, test No. A10

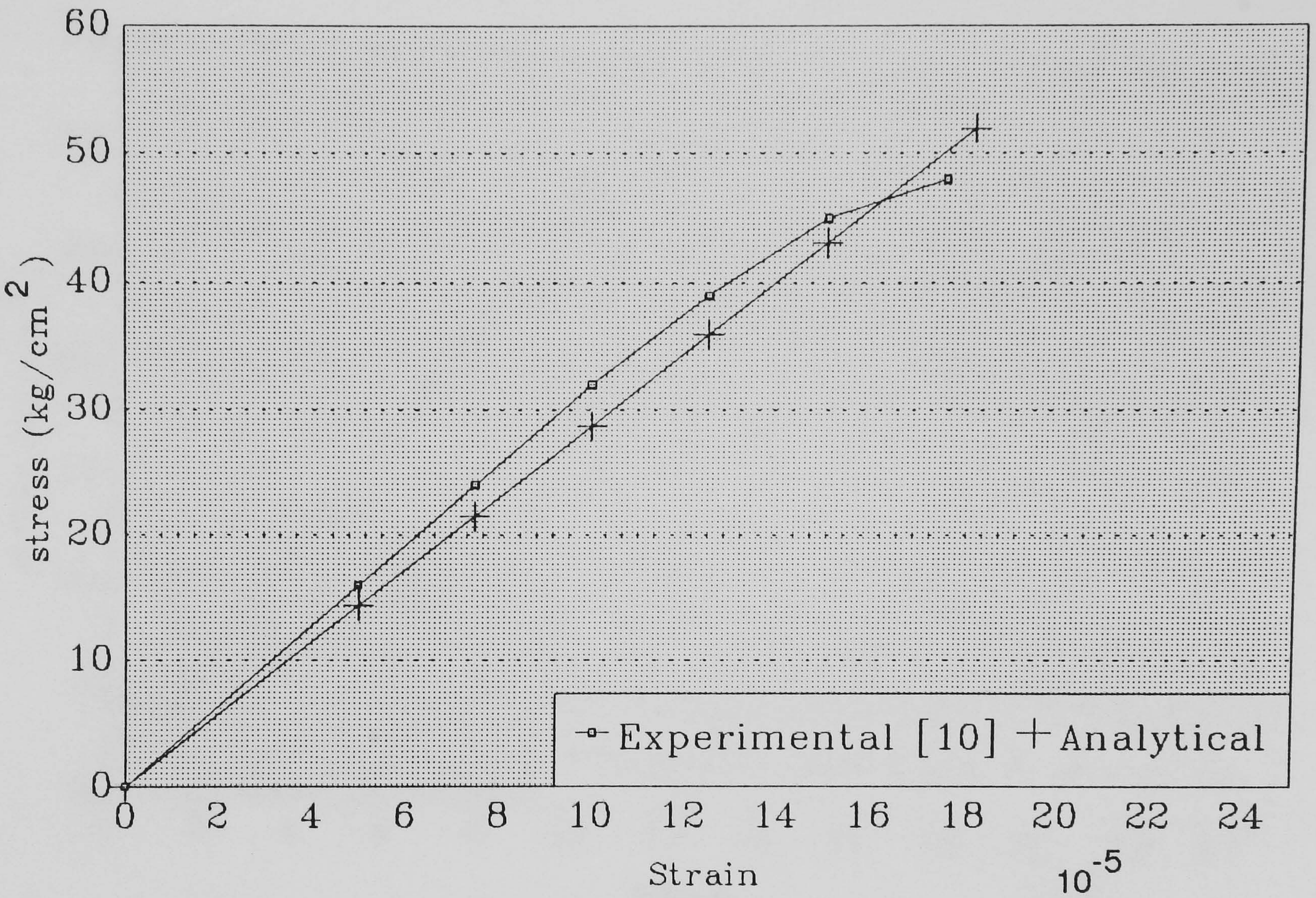

Fig. 6.19 –Comparison of tensile Hatano's tests
Concrete mix 1:4:7 Test No. A11

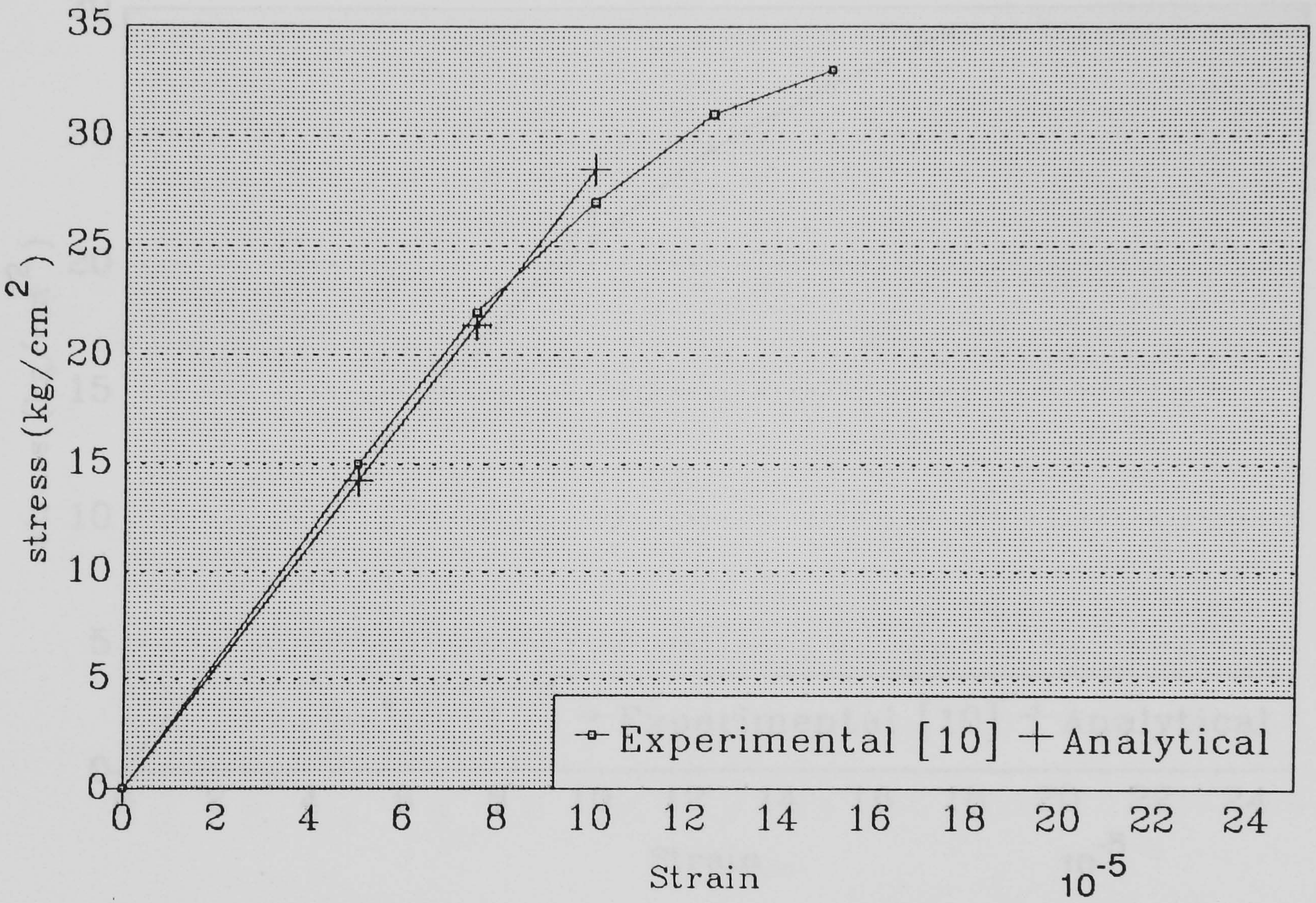

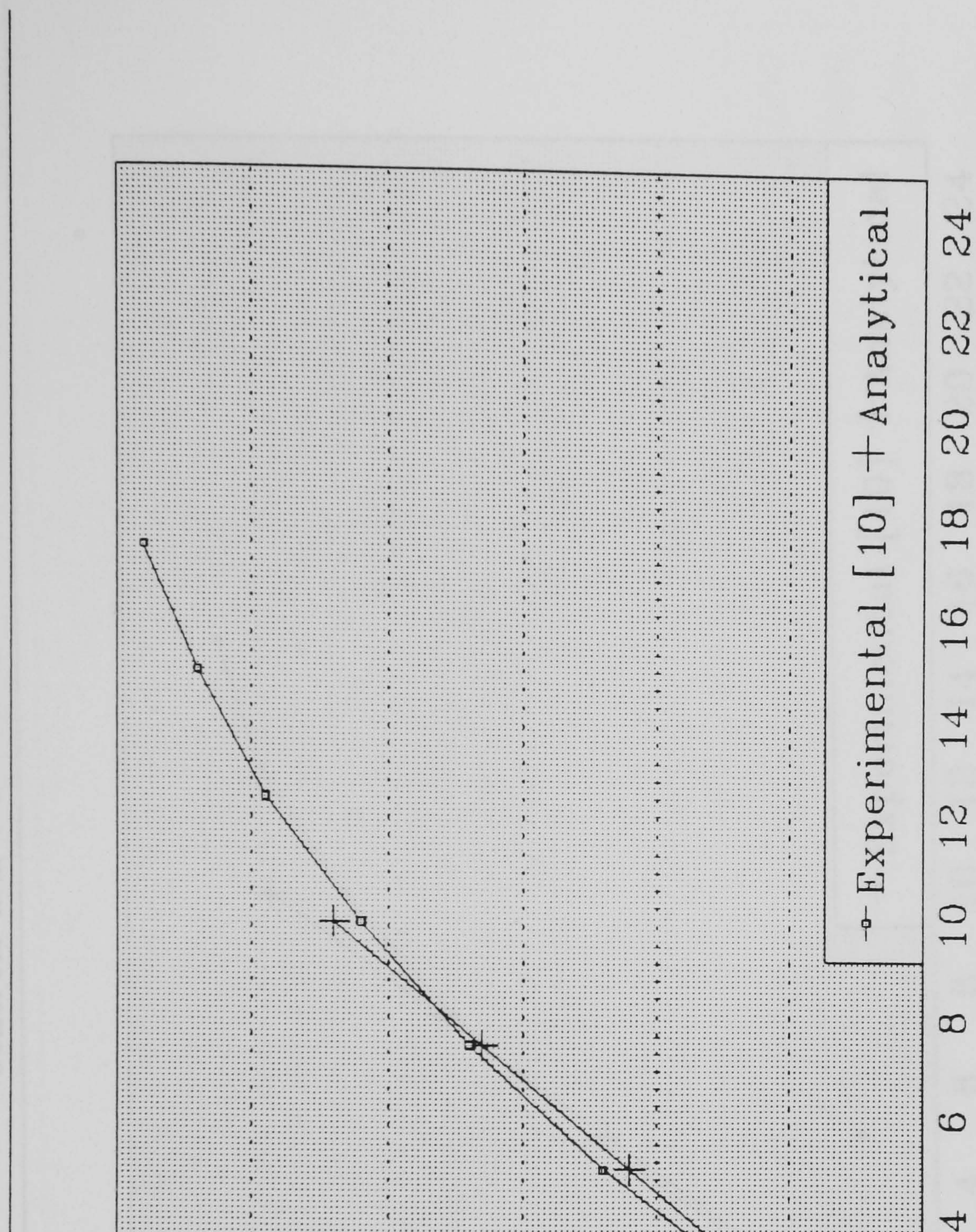

Fig. 6.20 –Comparison of tensile Hatano's tests
Concrete mix 1:4:7 Test No. A5

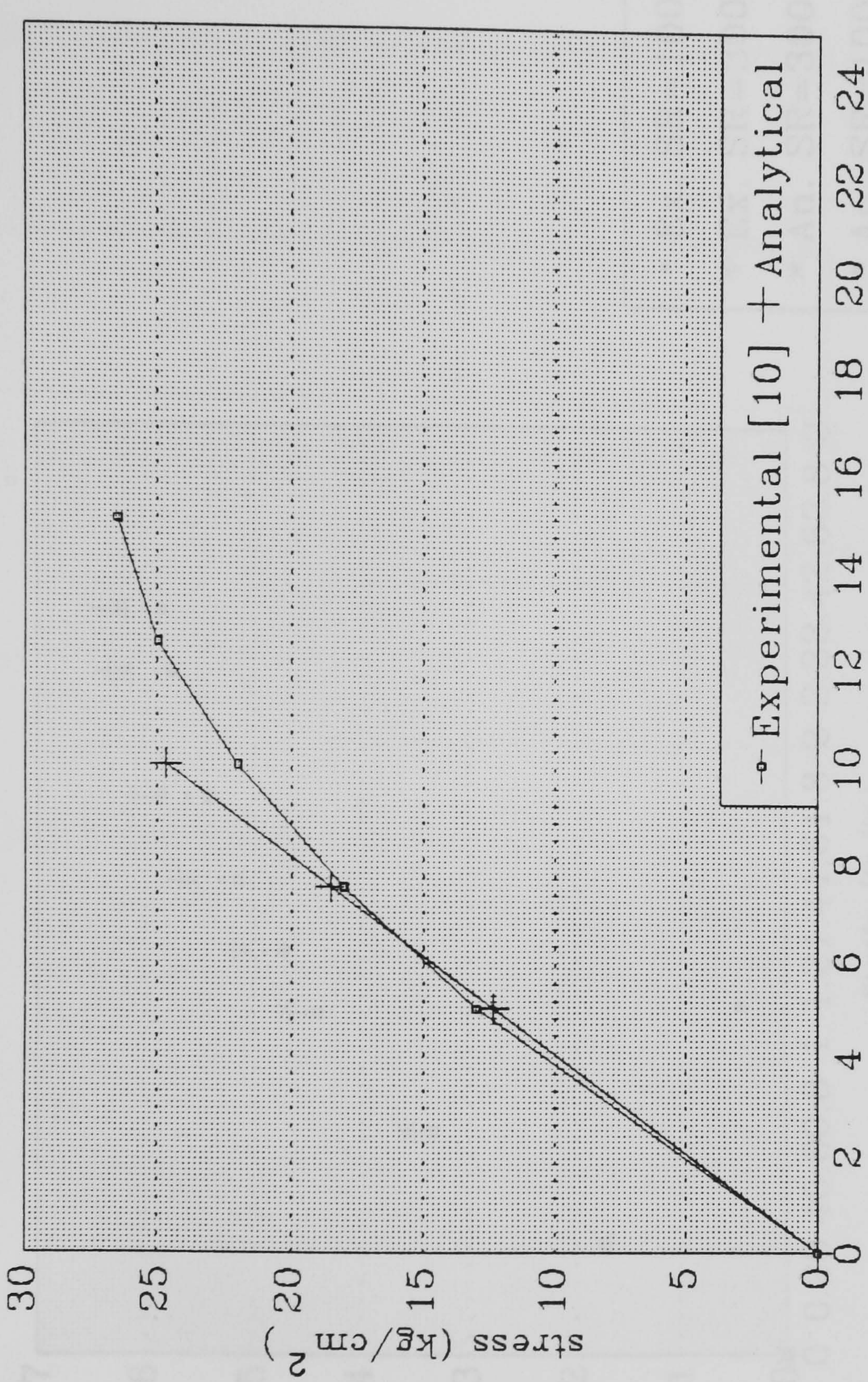

Fig. 6.21 –Comparison of tensile Hatano's tests
Concrete mix 1:4:7 Test No. A6

Fig. 6.22 -Strain rate effect on the compression stress-strain curve of concrete
Comparison with Ahmad's test

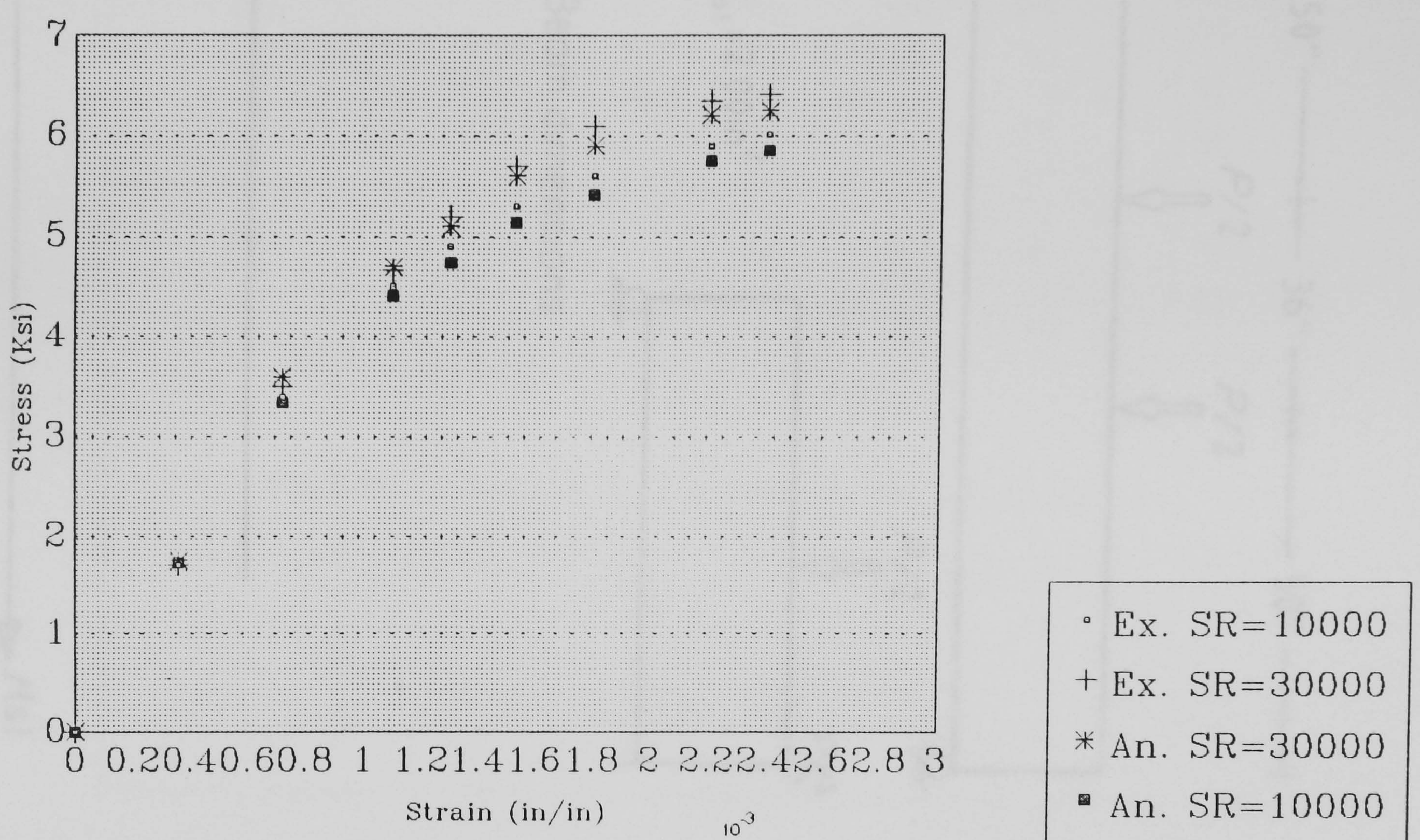

SR=strain-rate (microstraina/sec)
Ex.=experimental, An.=analytical

Microstrains/sec= 10^{-6}

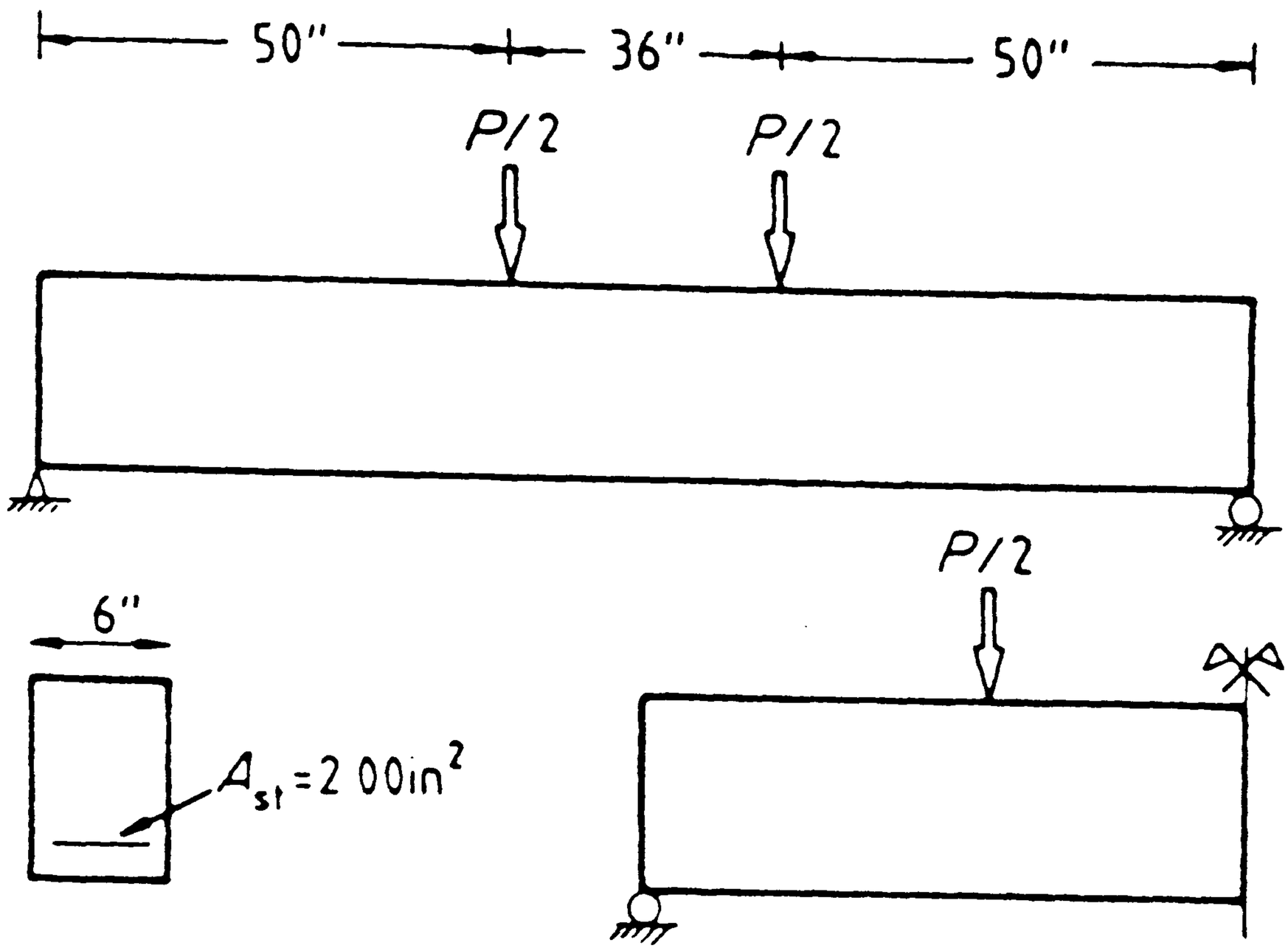

Beam dimensions

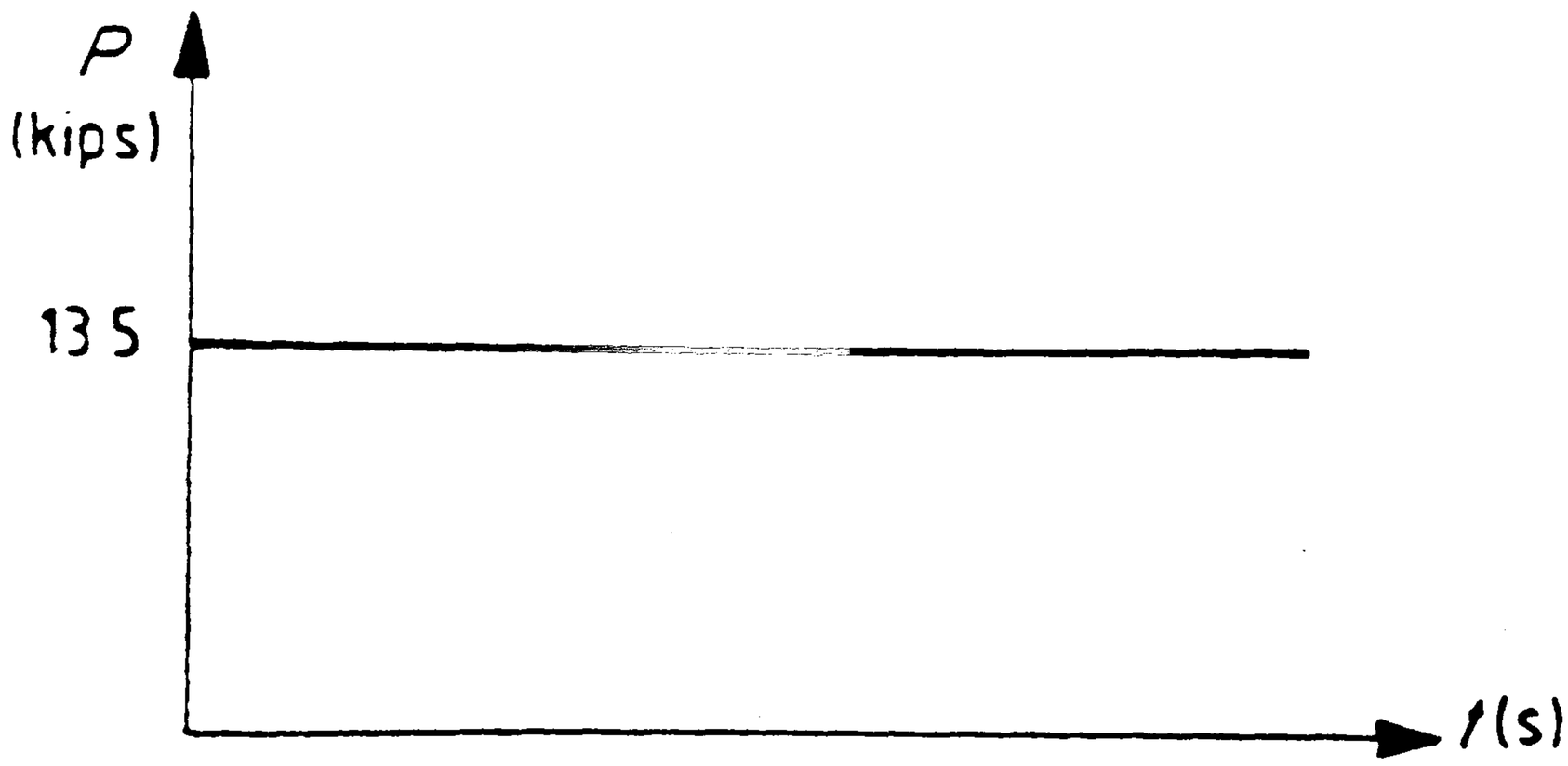

Fig. 6.23 Geometry and Loading of simply supported beam.

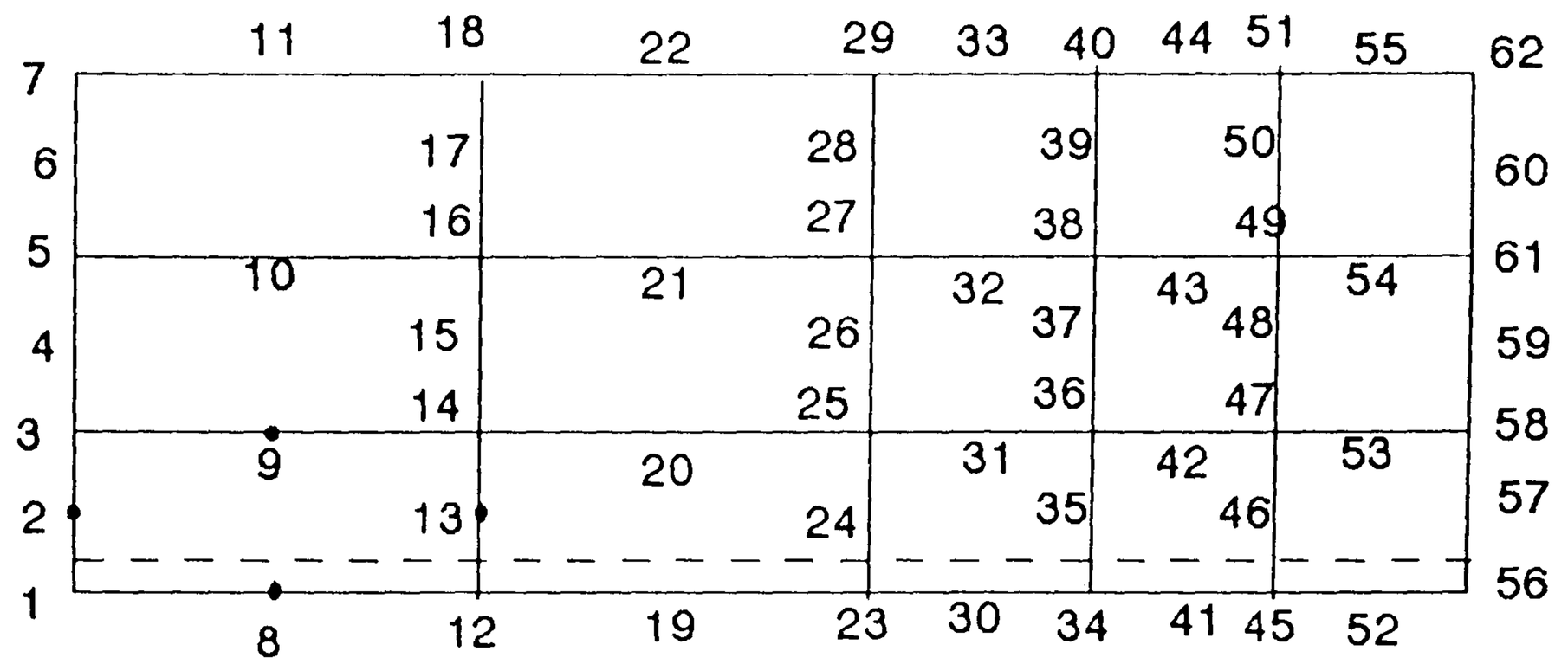

Fig. 6.24 SPATIAL DISCRETISATION OF THE BEAM

Fig. 6.25 Non-linear dynamic response of Reinforced Concrete Beam
Material stiffening and strengthening is not considered

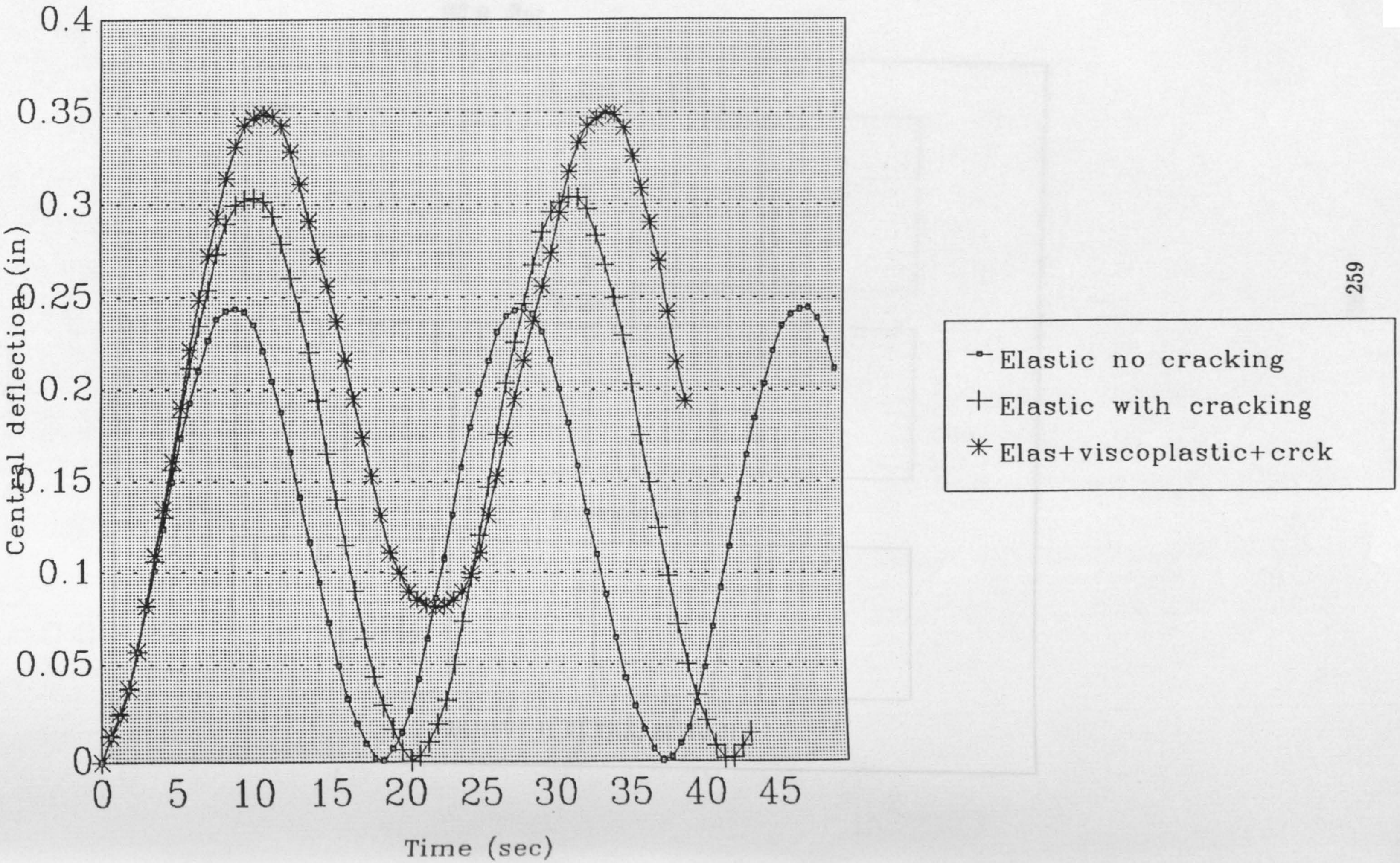

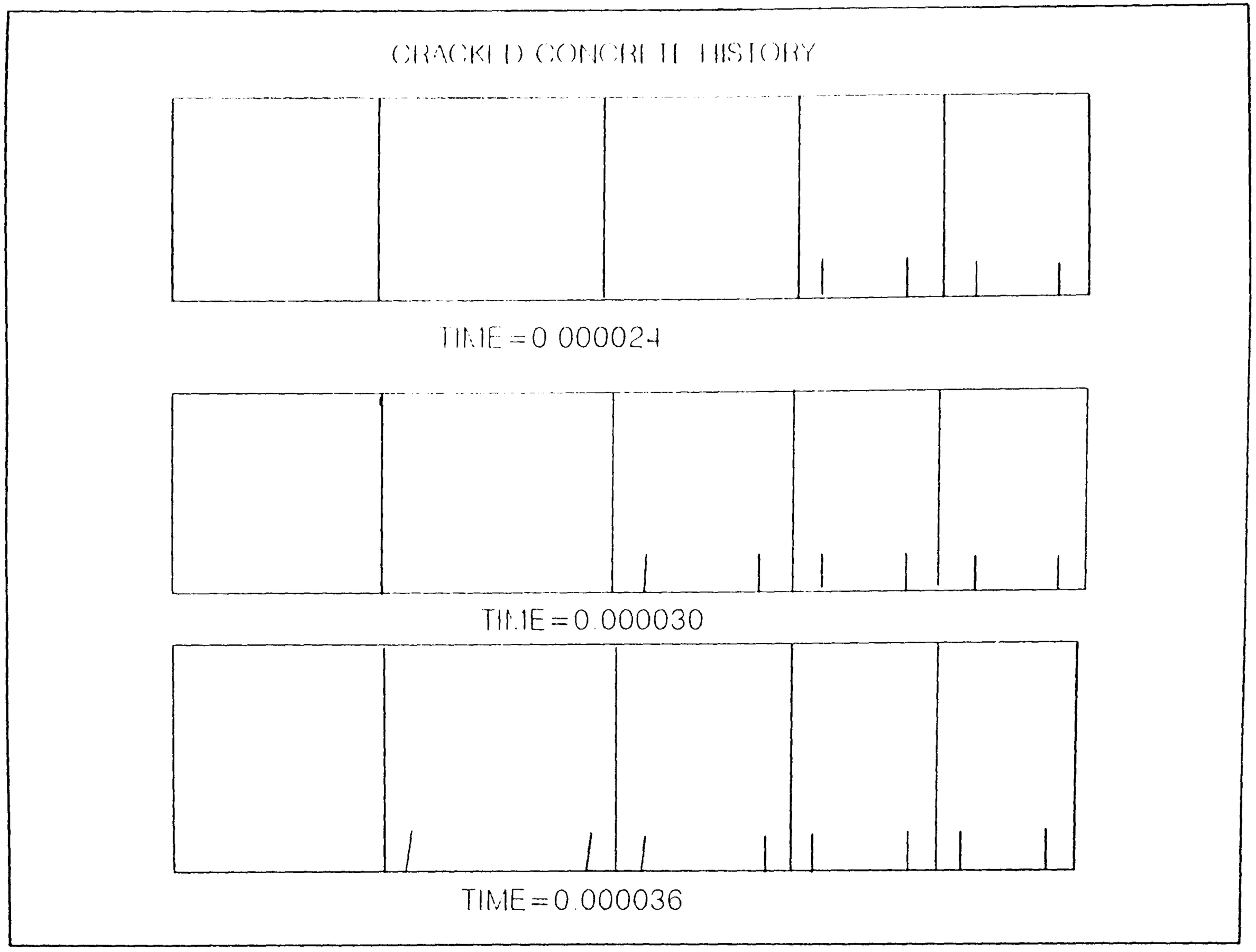
CRACKED CONCRETE HISTORY
TIME=0.000024
TIME=0.000030
TIME=0.000036

Fig. 6.26

Fig. 6.27– Non–linear dynamic response of Reinforced Concrete Beam
Material stiffening and strengthening is considered

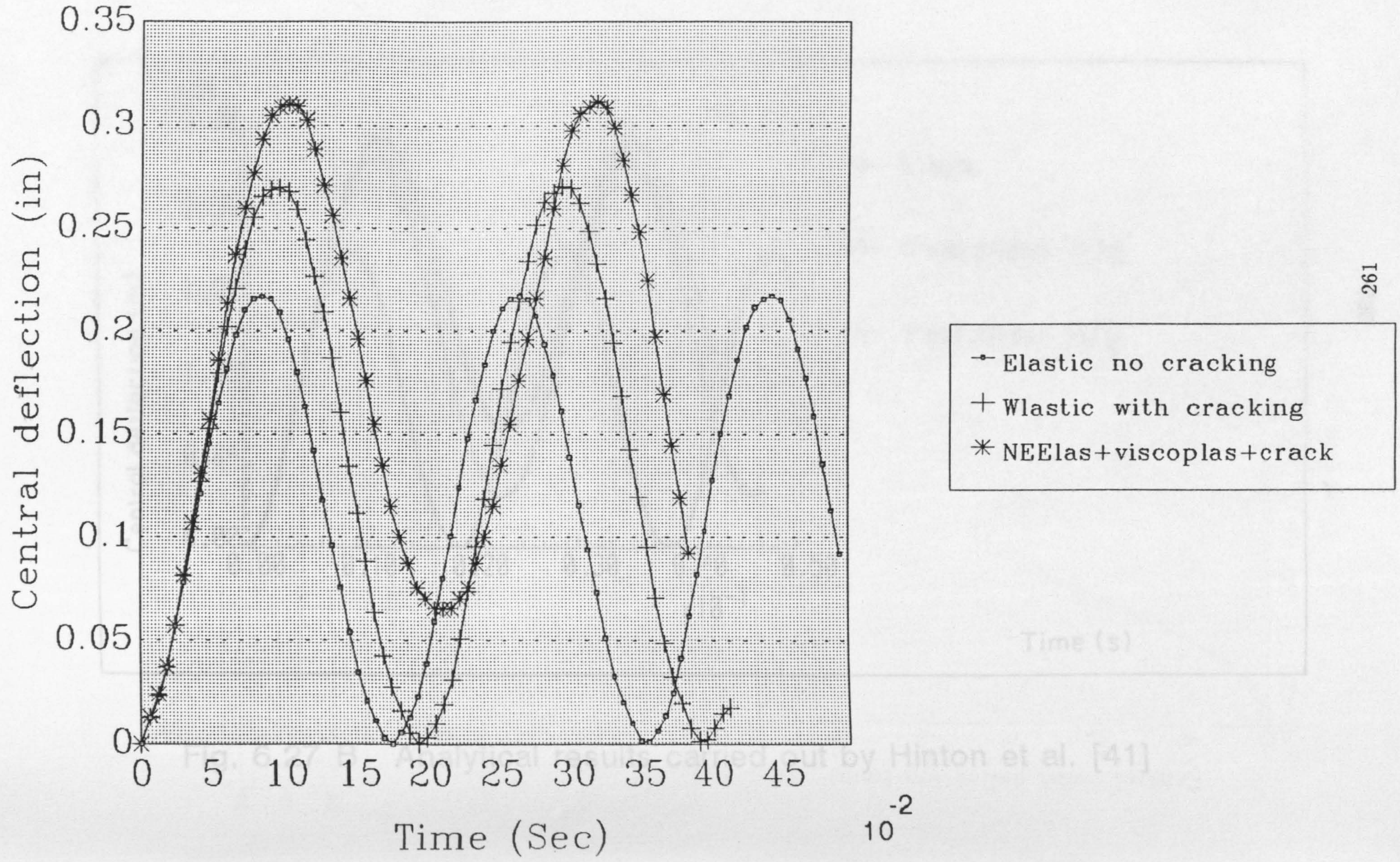

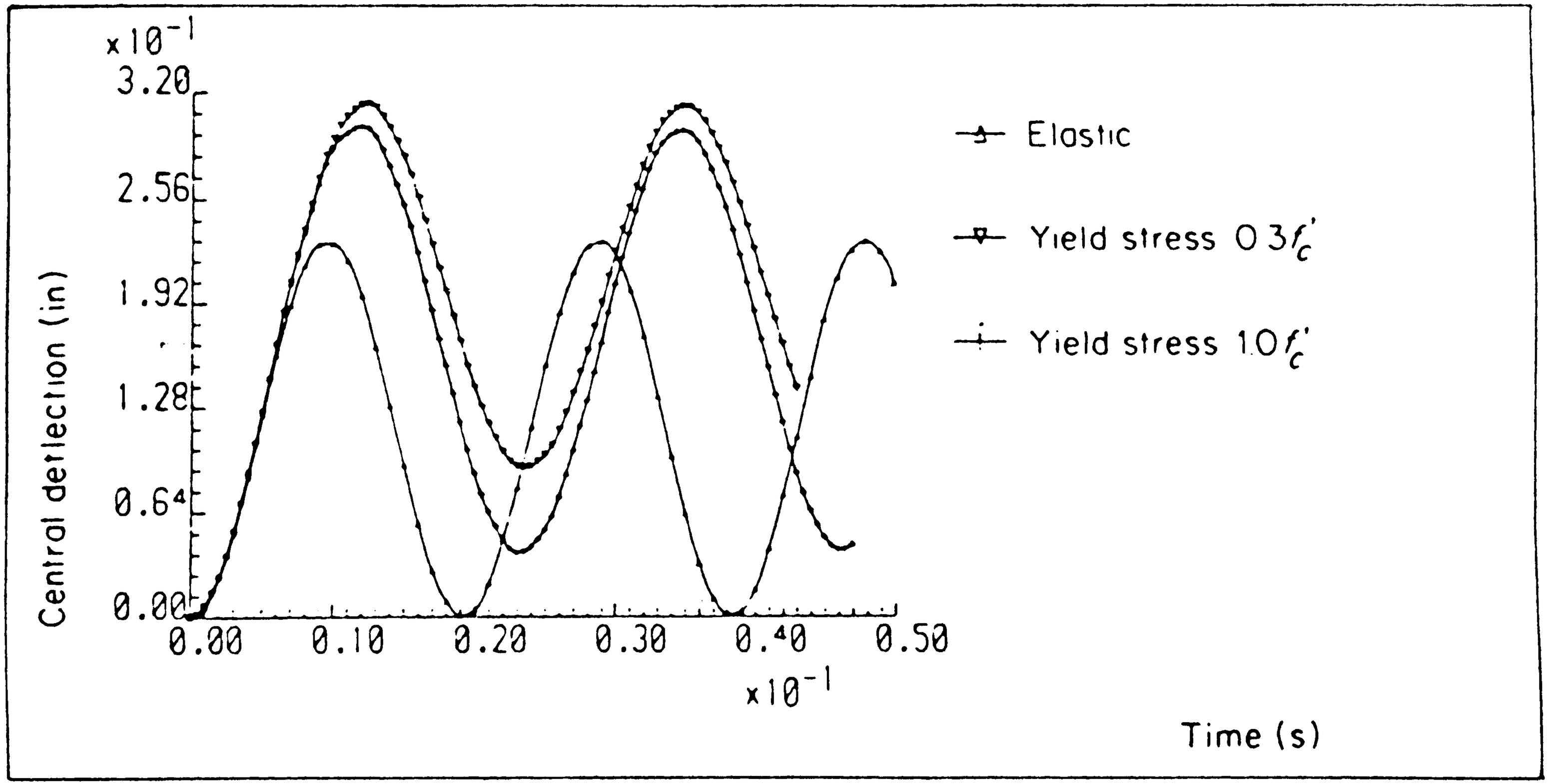

Fig. 6.27 B Analytical results carried out by Hinton et al. [41]

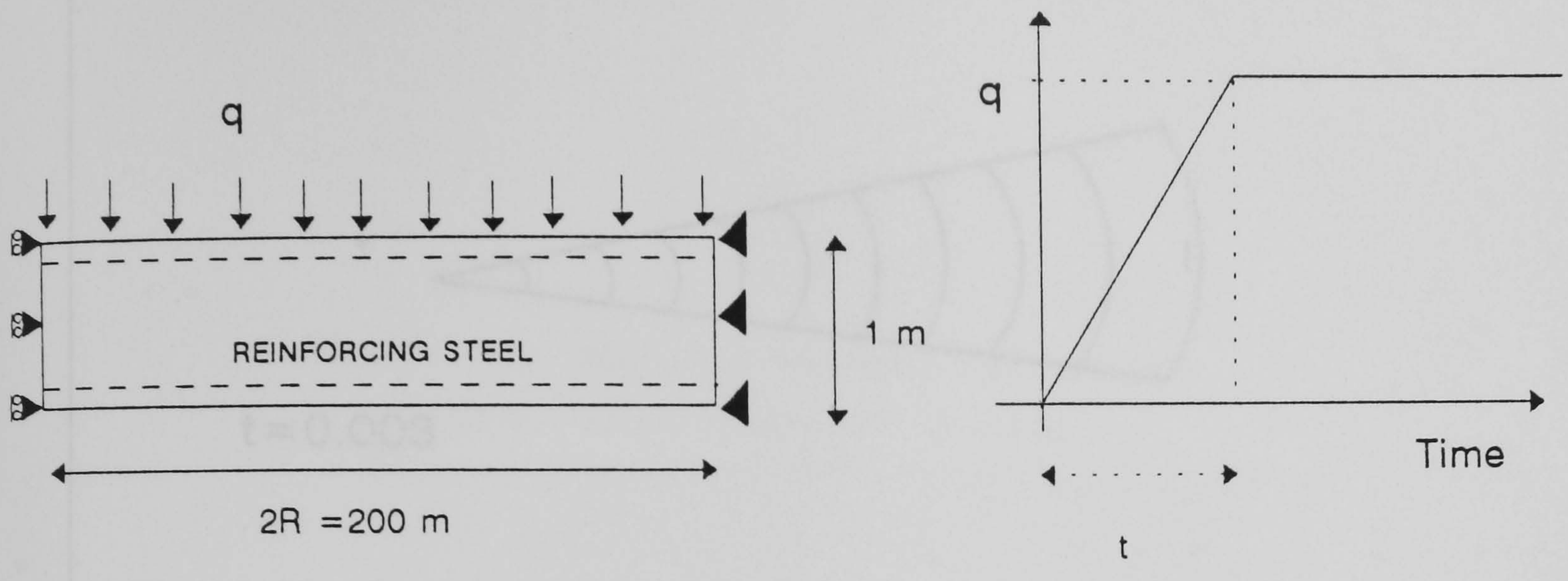

Fig. 6.28 Geometry and loading of circular plate

Fig. 6.31 – Central–point deflection of reinforced concrete slab
Strain–rate parameters are not included

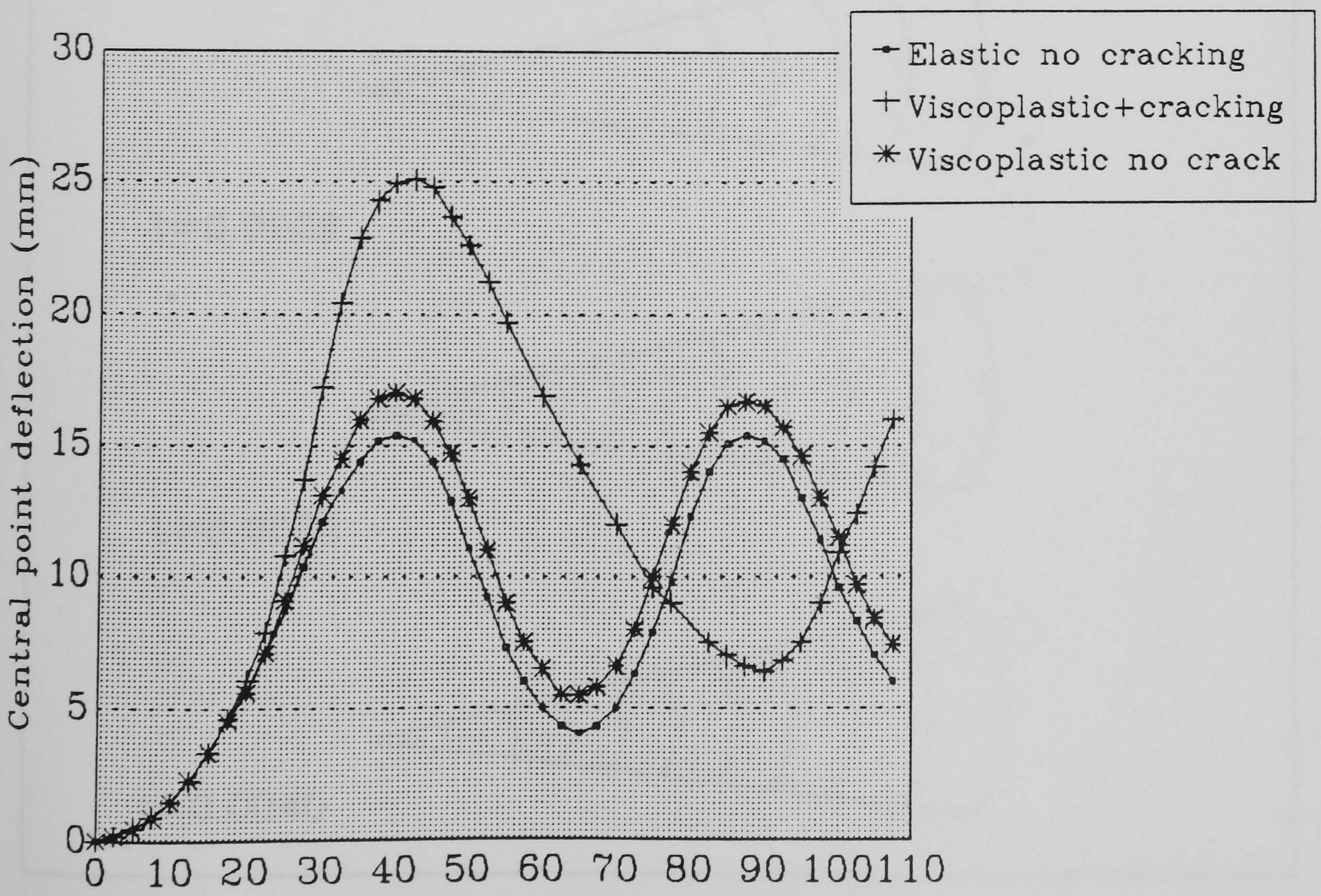

Fig. 6.30 Crack pattern in reinforced concrete slab

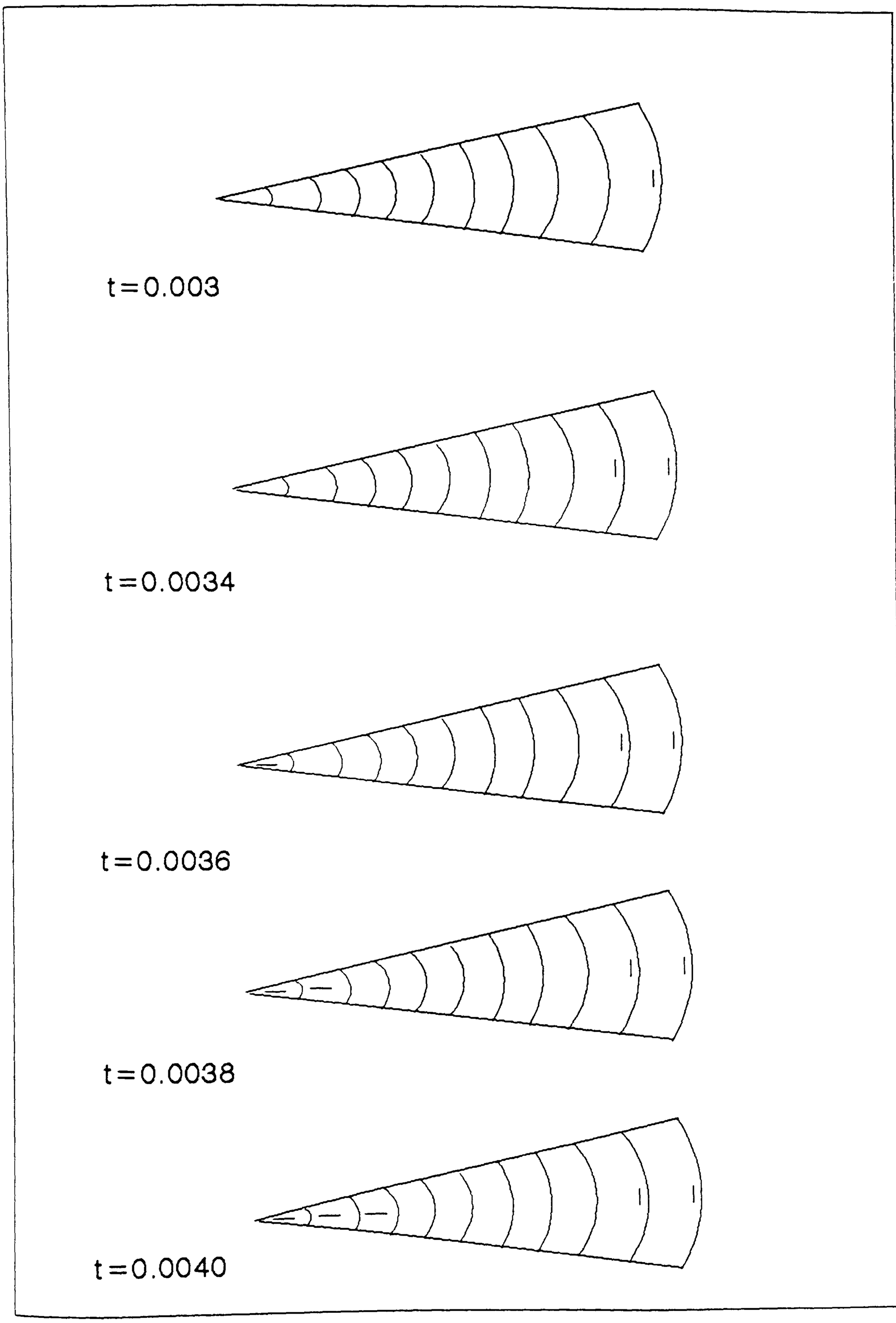

Fig. 6.31 – Non-Linear response of circular plate

Strain-rate parameters are not included

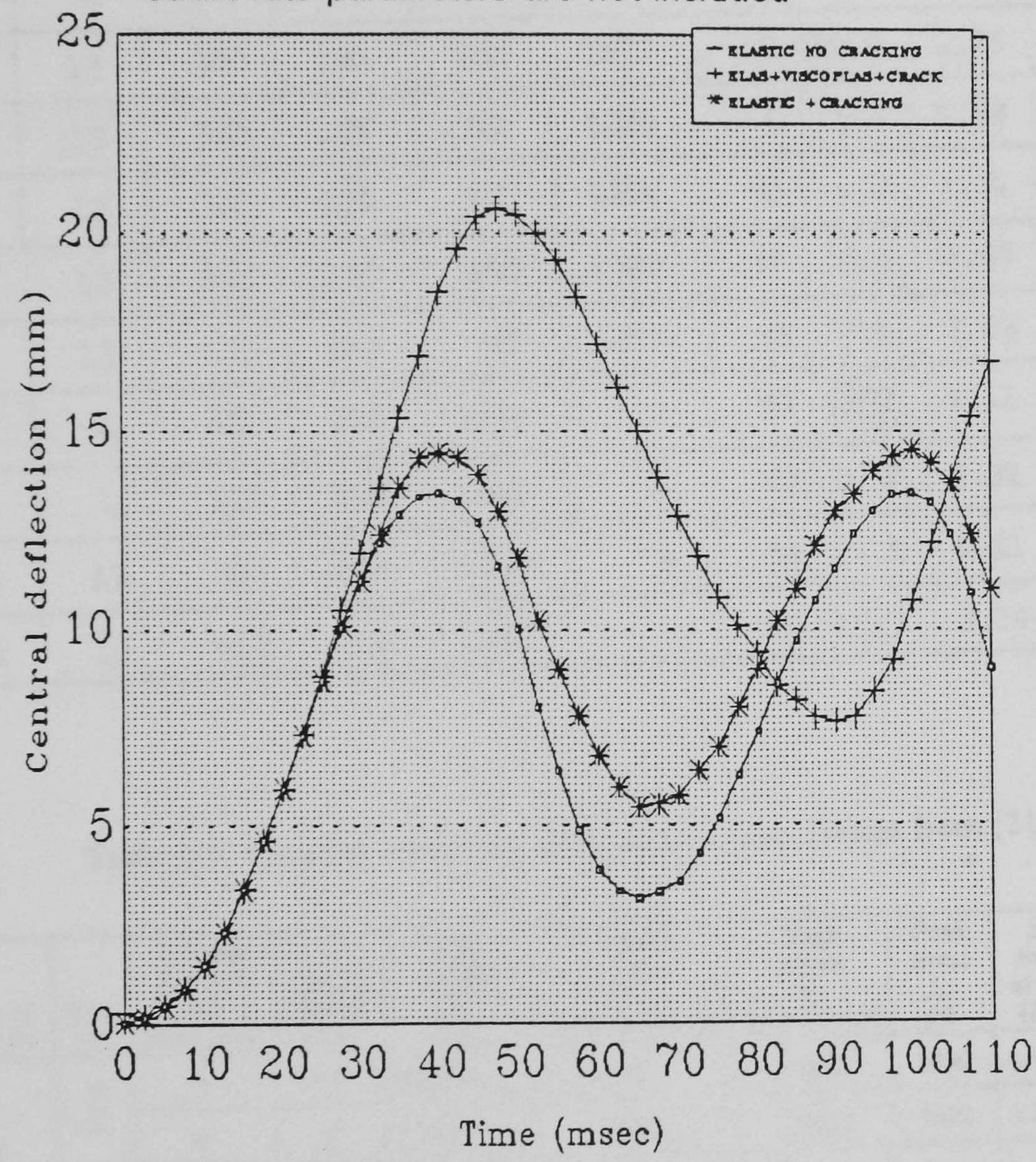

Table 6.1 Mix proportion of Hatano's compressive tests (taken from [10])

Test No.	Age in Weeks	Mix proportion					Slump & air		
		Cement (kg/m³)	Water (kg/m³)	Sand (kg/m³)	Gravel (kg/m³)	W/c (%)	Slump (cm)	Air(%)	cement void ratio C/V
1	4	380	140	698	1296	37	0.6	1.69	0.757
2	4	380	160	658	1222	42	10.0	0.98	0.700
3	4	300	150	710	1264	50	10.3	1.18	0.580
4	4	220	125	800	1300	57	0.5	2.20	0.467
5	4	220	143	781	1276	65	3.5	1.64	0.431
6	13	380	160	653	1222	42	10.0	1.25	0.685
7	13	300	135	724	1288	45	1.5	1.68	0.618
8	13	300	150	710	1264	50	4.3	1.34	0.574
9	13	220	130	800	1300	57	0.5	2.80	0.435
10	13	220	143	781	1276	65	3.4	2.03	0.421
11	4	511	256	1533	-	50	flow 17.0	4.41	0.528
12	4	410	246	1640	-	60	16.2	5.81	0.421
13	13	511	256	1533	-	50	17.1	4.11	0.538
14	13	410	246	1640	-	60	15.3	5.79	0.422

Table 6.6 Material properties of Ahmad's tests (taken from [21]).

Type of concrete	Size, in.	Average number of specimens	Age at testing, days	Unit weight w, lb/ft³	Strain rate $\dot{\epsilon}$, microstrain/sec	Peak strain ϵ_o, microstrain	Peak stress f_o, psi	Secant modulus at 0.45 f_o, $(E_c)_s$, psi
Unconfined concrete	3 x 6	4	55	148.88	32	0.0026	6980	4.11×10^6
		4	55	150.10	10,000	0.0029	7620	4.23×10^6
	6 x 12	2*	28	148.60 wet 147.90 dry				
		2*	28				5176	
		2*	28					4.75×10^6
		2*	28				$f_1' = 442$	
Confined concrete spiral spacing = 1 in.	3 x 6			w, lb/ft³	$\dot{\epsilon}$	ϵ_∞	f_∞	$(E_c)_s$, psi
		4	55	156	32	0.0037	7250	4.00×10^6
		4	55	154.95	10,000	0.0043	8020	4.35×10^6
		4	55	154.70	30,000	0.0051	7970	4.50×10^6

*6 x 12 in. cylinders tested at Material Service Laboratory, Chicago, Ill. Secant modulus calculated from deformations measured by the mechanical compressometer.

Chapter 7

Proposed Algorithm For Structures Under Transient Force

7.1 Introduction

There are two general classes of solution techniques for dynamic problems, the modal superposition method and direct integration methods as discussed in chapters 4 and 5. In the modal superposition method, in which time is not discretised, the equations of motion are converted to a normal system of coordinates which gives a system of independent equations. Each equation is solved independently and the unknown displacements due to an applied loading can be obtained by summing the contributions from each of the modes.

In direct integration methods the governing second order ordinary differential equations in time are integrated using either an explicit or an implicit step-by-step method. In implicit methods the system of equations is solved once, or more step per time to advance the solution, which is computationally expensive. Implicit methods tend to be numerically stable but storage requirements tend to increase dramatically, particularly in non-linear problems discussed in Chapter 4. In explicit algorithms the solution is advanced without the need to store or solve

the system of equations. However, a small time-step has to be employed to give numerical stability. The implicit methods have a higher order of accuracy than the explicit schemes.

Recently mixed explicit-implicit methods, in which some of the elements are integrated implicitly, while an explicit form of integrator is used for the other elements have been used for solving dynamic problems. In these algorithms, it is necessary to define which of the elements will be explicit and which will be implicit as input data.

The maximum permitted time-step is determined from that required for the explicit elements to ensure stability. The accuracy of the method depends on the type of the integrator and the number of explicit elements used and decreases with any increase in the number of explicit elements.

In long-duration dynamic problems, errors in the explicit elements, for example local truncation error i. e. the difference between the numerical and the exact values, and round-off error can cause serious problems. The traditional mixed explicit-implicit algorithms may not be suitable for such problems because of the need to define the explicit elements at the beginning of the analysis. The elements designated as explicit remain explicit through out the analysis.

The aim of this chapter is therefore to present a mixed explicit-implicit algorithm for long-duration dynamic problems with an accuracy higher than that of the traditional explicit-implicit methods.

In the proposed algorithm the minimum number of explicit elements are used at any time-step therefore these errors tend to be reduced.

The accuracy of the methods mentioned above are compared using as an example the analysis of a structure with a long-duration loading.

The chapter starts with a brief explanation and formulation of the modal superposition method and continues with a description of the Newmark implicit, explicit and the mixed explicit-implicit algorithms. The next section is devoted to a discussion of the proposed variable explicit-implicit algorithm and a brief explanation of the computer program. A comparison of the accuracy of the

methods through an example is the subject of the next section. The chapter closes with a discussion of a dynamic analysis of a shear wall under a seismic loading.

7.2 Numerical techniques for solving dynamic problems

In order to assess the accuracy of the proposed numerical algorithm, a beam has been analysed using the modal superposition method discussed in Chapter 4. The results are compared with those of the implicit, the explicit, the traditional mixed explicit-implicit and the proposed variable mixed explicit-implicit algorithms.

A brief explanation of each of the above-mentioned methods is given first.

7.2.1 Modal superposition method

As discussed in chapter 4, this method is based on transforming the system to normal coordinates after which each of the equations of motion can be solved independently.

If a structure is loaded by a harmonic force $A_i cos\theta t$, then the governing equations for determining the displacement vector X can be written as

$$X = \varphi Y \tag{7.30}$$

and

$$\ddot{Y} + 2\xi\omega\dot{Y} + \Omega Y = \varphi^T A cos\theta t \tag{7.31}$$

thus

$$Y_i = \frac{\varphi^T A_i(\omega_i^2 - \theta^2)}{(\omega_i^2 - \theta^2) + 4\xi^2\omega^2\theta^2}\cos\theta t + \frac{2\varphi^T A_i\xi\omega_i\theta}{(\omega_i^2 - \theta^2)^2 + 4\xi^2\omega_i^2\theta^2}\sin\theta t \tag{7.32}$$

and where Y is a vector of modal amplitudes and is determined by solving Eq. (7.30) and φ is the matrix of eigenvectors.

7.2.2 The Newmark implicit method

This method was discussed in chapter 4. Because the method is unconditionally stable, the time-step is governed by the desired accuracy.

The implicit form of the Newmark method is used:

$$X_{t+\Delta t} = X_t + \Delta t\dot{X}_t + (\Delta t)^2[(1/2-\beta)\ddot{X}_t + \beta\ddot{X}_{t+\Delta t}] \tag{7.33}$$

The equations for determining the displacement velocity and acceleration vectors are

$$[K + \frac{\gamma}{\beta\Delta t}C + \frac{1}{\beta\Delta t^2}M]X_{t+\Delta t} = P_{t+\Delta t}$$
$$-M[\frac{1}{\beta\Delta t^2}X_t + \frac{1}{\beta\Delta t}\dot{X}_t + (\frac{1}{2\beta}-1)\ddot{X}_t] \tag{7.34}$$

$$\dot{X}_{t+\Delta t} = \dot{X}_t + \Delta t[(1-\gamma)\ddot{X}_t + \gamma\ddot{X}_{t+\Delta t}] \tag{7.35}$$

$$\ddot{X}_{t+\Delta t} = \frac{X_{t+\Delta t} - \bar{X}_{t+\Delta t}}{\Delta t^2\beta} \tag{7.36}$$

in which $X_{t+\Delta t}$ is a predictor and is given by

$$\bar{X}_{t+\Delta t} = X_t + \Delta t\dot{X}_t + 1/2\ddot{X}_t\Delta t^2 \tag{7.37}$$

A value of $\gamma = 0.5$ in Eq. (7.35) is used which results in accuracy of order $O(\Delta t)^2$, as discussed in chapter 5 and a value of $\beta = 0.25$ is used.

As discussed in Chapter 4, this method does not have numerical dissipation and therefore in problems with loadings of long-duration serious problems, due to the effect of errors produced by the higher modes, can occur.

The Newmark explicit method

This method which is conditionally stable also does not have numerical dissipation to damp out the errors due to higher modes, the method also possesses considerable round-off error, as discussed in Chapter 5. The critical time-step which is governed by the maximum natural frequency of the element in a mesh, is given by

$$\Delta t \leq \frac{2}{\omega_e^{max}} \tag{7.38}$$

The displacement vector is predicted by

$$\bar{X}_{t+\Delta t} = X_t + \Delta t \dot{X}_t + 1/2 \Delta t^2 \ddot{X}_t \tag{7.39}$$

and is corrected by

$$(\frac{2}{\Delta t^2} M) X_{t+\Delta t} = P_t - K X_t + \frac{2}{\Delta t^2} M (X_t + \Delta t \dot{X}_t) \tag{7.40}$$

The equations for determining the velocity and the acceleration vectors are

$$\dot{X}_{t+\Delta t} = \dot{X}_t + \Delta t \ddot{X}_t \tag{7.41}$$

$$\ddot{X}_{t+\Delta t} = \frac{X_{t+\Delta t} - X_t}{\Delta t^2} \tag{7.42}$$

The effective stiffness matrix does not require to be factorized in this method.

7.2.3 Advantages and disadvantages of the implicit and the explicit methods

The advantages and the disadvantages of the implicit and the explicit methods have been discussed in chapter 4 and 5 and will be reviewed here briefly.

The implicit methods

The advantages of the implicit algorithms in elastic analysis are

- High accuracy

  The local truncation error of the algorithm is of order $O(\Delta t^3)$, hence the method possesses a high accuracy.

- Stability

  The algorithm is unconditionally stable if in Eqs. (7.33) and (7.35)

$$2\beta \geq \gamma \geq 1/2 \tag{7.43}$$

The disadvantages of the method are that

- The algorithm is computationally expensive particularly for large problems.

- The method suffers from algorithmic artificial errors such as amplitude decay error and elongation error if the Newmark methods are used.

In analyses of visco-plastic materials, two methods may be used for determining the visco-plastic strain.

Visco-plastic analysis

a) The implicit form of the visco-plastic strain approximation

$$\epsilon_{n+1} = \epsilon_n + \Delta t[(1-\theta)\dot{\epsilon}_n + H_n \Delta\sigma_n] \tag{7.44}$$

where $1 > \theta > 0$ and

$$H_n = \frac{\partial \dot{\epsilon}_n}{\partial \sigma} \tag{7.45}$$

The advantages of the approximation are that it is

- Stable
- Has high accuracy which is determined by the choice of

time-step.

The disadvantages of the method are

- Using the implicit form of visco-plastic strain approximation requires that the matrix H is calculated for each Gauss point for each iteration within the time-step which causes the analysis to be computationally expensive.

- The time-step needs to be small enough to follow the material stress-strain relationship, particularly when the material behaviour changes abruptly.

b) The explicit form of the visco-plastic strain approximation is obtained by substituting $\theta = 0$ in Eq. (7.44) thus

$$\epsilon_{n+1} = \epsilon_n + \Delta t \dot{\epsilon}_n \tag{7.46}$$

The advantage of this method is that

- Since the time step is very small the method is very accurate.

The disadvantages of the method are that

- Since the time-step is determined from the stability condition, as discussed in chapter 5, the time-step is dependent on the shared eigenvalues of the D and H matrices. This causes the method to be very expensive particularly in long-duration problems.

  Cormeau [118] has proposed formulae for determining the critical time-step, when the explicit form of the strain approximation is used, which are conservative and assume a linear flow function and pure relaxation.

- Although the algorithmic artificial errors of the method are less than the implicit analysis, they may be serious in long-duration problems.

The explicit methods

The advantage of the explicit method for elastic and visco-plastic analyses are that it is

- Simple because the effective stiffness does not need to be determined and factorized, which causes the method to be relatively cheap.

In visco-plastic analyses the explicit form of strain approximation is usually used because the time-step of the method is small. Hence the material stress-strain relation can be followed properly.

The disadvantages of an explicit method are

- The method is conditionally stable and the critical time-step is restricted by the highest natural frequency of the elements in the mesh, as discussed earlier.

- The local truncation error of the method is of order $O(\Delta t^2)$, hence the method is less accurate.

- The round-off error which is a serious problem in the explicit schemes particularly in the central difference method as discussed in Chapter 4.

- The artificial algorithmic errors such as the amplitude decay error and the period elongation error can result in serious problems.

It is worth noting that, the accumulated global error and algorithmic artificial errors might cause the predicted response of the structure to be elastic when it should behave visco-plastically.

7.2.4 Conclusions

- From the above it can be concluded that, the ideal solution for elastic analyses of dynamic problem is to use an implicit method particularly in long-duration problems.

- For visco-plastic analyses the explicit methods are more suitable.

- The above analyses can be combined in a mixed explicit-implicit method in which the visco-plastic elements are explicit and the elastic elements are implicit.

- Since the number of visco-plastic elements can not be predicted before the start of the analysis, in the traditional explicit-implicit method more explicit elements that can cause inaccurate results.

7.2.5 Proposed algorithm

In the proposed to be described in this section, all the elements are assumed to be implicit when the material is elastic. As soon as any Gauss point goes visco-plastic, then the element corresponding that Gauss point is automatically changed to explicit . Hence the method has the maximum possible accuracy, particularly in long-duration problems.

Computational algorithm

As explained previously, all the elements are initially assumed to be implicit.

To start the time-step procedure, the initial values of displacements $X(0)$, velocity $\dot{X}(0)$ should be given and the initial acceleration $\ddot{X}(0)$ is obtained using the dynamic equilibrium equation at $t = 0$,

$$\ddot{X}(0) = M^{-1}[P^{ext}(0) - KX(0)] \tag{7.47}$$

In order to increase the accuracy of the proposed algorithm, the explicit Newmark method in the form

$$\bar{X}_{t+\Delta t} = X_t + \Delta t\dot{X}_t + 1/2\Delta t^2(1 - 2\beta)\ddot{X}_t \tag{7.48}$$

is used as the predictor of the integrator and the implicit form of the Newmark as the corrector. However, any type of predictor-corrector method, as discussed in Chapter 4 depending on the type of the problem and required accuracy may be employed. The time-step may be dominated either by the required accuracy or by the applied load frequencies, e. g. the frequencies in seismic problem. It is worth noticing that, the numerical dissipation property of this implicit integrator for damping the higher modes error is of importance.

Eqs. (7.39) to (7.42) are used to calculate the displacement, velocity and acceleration vectors in each time-step.

In each time-step, a failure criteria is used to calculate the excess stress F for example,

$$F = f(I_1, J_2) - \sigma_0 \tag{7.49}$$

where I_1 is the first stress invariant and J_2 is the second deviatoric stress and σ_0 is the stress corresponding to visco-plastic initiation.

If F is negative then the algorithm remains in implicit method while in the case where F at any Gauss point becomes positive then the corresponding element changes to explicit i. e., the algorithm becomes explicit-implicit. Then after different time integrators for different parts of the system is used. The elements in which any Gauss point goes to visco-plastic stage are partitioned as explicit elements while another elements remain as implicit element.

Governing equation in explicit-implicit method

An explicit Newmark method is used as the predictor

$$\bar{X}_{t+\Delta t} = X_t + \Delta t \dot{X}_t + 1/2\Delta t^2(1-2\beta)\ddot{X}_t \tag{7.50}$$

The governing equations for the explicit and the implicit method is cast in a slightly different form to derive the governing equations for the mixed explicit-implicit algorithm of the form

$$[\frac{1}{\beta\Delta t^2}M + K]X_{t+\Delta t} = P_{t+\Delta t} + \frac{1}{\beta\Delta t^2}M\bar{X}_{t+\Delta t} \tag{7.51}$$

for implicit elements and

$$(\frac{1}{\Delta t^2\beta}M)X_{t+\Delta t} = P_{t+\Delta t} + (\frac{1}{\Delta t^2\beta}M - K)\bar{X}_{t+\Delta t} \tag{7.52}$$

for explicit elements.

The velocity and the acceleration vectors are given by

$$\ddot{X}_{t+\Delta t} = \frac{X_{t+\Delta t} - X_{t+\Delta t}}{\Delta t^2\beta} \tag{7.53}$$

$$\dot{X}_{t+\Delta t} = \dot{X}_t + \Delta t(1-\gamma)\ddot{X}_t + \Delta t\gamma\ddot{X}_{t+\Delta t} \tag{7.54}$$

The equilibrium equation, the effective stiffness and the effectives force matrices in mixed explicit-implicit methods are graphically illustrated in Fig. 7.1.

The visco-plastic strains are determined using Perzyna's's model [119] as discussed in Chapter 2. The fluidity parameter γ_p is determined Eq. () and the explicit form for determining visco-plastic strain is used.

Since in the analysis procedure the Gauss points of the implicit elements remain elastic , the effective stiffness $\hat{K}$ remain constant and only the effective force $\hat{P}$ is required to be determined according to the material stress level which is the advantage of the algorithm. This can be seen in Fig. 7.1 and Eqs. (7.51) and (7.52).

The velocities and the acceleration vectors of the total system are evaluated using Eqs. (7.54) and (7.53) respectively.

0.0.1 Description of the proposed algorithm

In the proposed algorithm there are essentially two different iteration procedures. The equilibrium equation is solved in the time-stepping procedure which forms the outer loop. The evolution equation by which the visco-plastic strain is evaluated forms the inner loop which is solved explicitly in each time-step i. e.

$$\epsilon_{n+1}^{vp} = \epsilon_n^{vp} + \Delta t \dot{\epsilon}_n^{vp}$$

In elastic analysis of dynamic problems the proposed method is completely implicit and all of the degrees-of-freedom in the effective stiffness matrix have off-diagonal terms. However, in non-linear analysis the elements in which any Gauss points has entered into the visco-plastic stage are changed to explicit elements and the element stiffness appear as diagonal term in the effective stiffness matrix Fig. 7.1. The effective stiffness matrix will be factorized in each time-step hence the algorithm may be termed as an "Implicit method".

It is worth noting that the non-linear solution procedure in the proposed algorithm differs from traditional implicit methods because the stiffness of the elements in which a Gauss point has become the visco-plastic does not appear in effective stiffness matrix.

7.2.6 Description of computer program

DYNICK2T Program

A computer program ' DYNICK2T ' has been developed in Fortran using the proposed variable explicit-implicit elements. The program structure is shown in Fig. 7.2. The structure of the program can be summarized as follows

1. Input the geometry, material properties and loading data.
2. Calculate the element consistent mass matrices and the global mass matrix.
3. Calculate the element stiffness matrices and the global stiffness matrix.
4. Assume the elements to be implicit.
5. Calculate the effective stiffness matrix.
6. Calculate the effective force matrix.
7. Evaluate the displacement vector Eq. (7.50).
8. Evaluate the stresses and strains at each Gauss point.
9. If the Gauss point is failed then update the strains and stresses.
10. Determine the velocity and acceleration vectors.
11. If the Gauss point is not failed then change the corresponding element to explicit type.
12. Calculate the partitioned effective stiffness matrix.
    The explicit nodes in the effective stiffness matrix are stored as a diagonal matrix and the implicit nodes as an upper triangular matrix.
13. Calculate the effective force for both the implicit and explicit elements.
14. Calculate the displacement vector.
15. Calculate the total strains, visco-plastic strains and the elastic strains.
16. Calculate the stresses at each Gauss point.
17. Calculate the displacement, velocity and acceleration vectors.
18. update the stresses and strains and go for the next time-step

7.3 Numerical examples

7.3.1 Dynamical analysis of a simply supported beam using different methods

Since in direct methods most of the numerical errors such as local truncation error, global truncation error and artificial algorithmic error are due to the time integration, the accuracy of the proposed method is demonstrated by solving a relatively long-duration problem using different types of the dynamic solution techniques.

A simply supported beam under a harmonic loading has been dynamically analysed for a duration of 1.2 second using the following methods

1. Modal superposition method.
2. Implicit method.
3. Explicit method.
4. The traditional mixed explicit-implicit method.
5. The proposed variable mixed explicit-implicit algorithm.

7.3.2 Example 7.1 - Modal superposition method

A computer program originally developed by Smith et al. [116], has been used.

The results of the analysis of a simply supported beam with a variable loading given by $P = 1000 \cos 200t$ using the superposition method are discussed in this section.

The geometry of the structure and the loads are illustrated in Fig. 7.3. The beam is spatially discretised using 8-noded serendipity elements Fig. 7.4., 2 by 2 Gauss Points are used for evaluating the element stiffness. The consistent mass is evaluated using 3 by 3 Gauss points which results in a more accurate estimation of natural frequencies, as discussed in chapter 3. Due to symmetry of the structure, only half of the beam has been analysed, no damping is considered. The plots of

variation spectral mid-span displacement of the beam with time is shown in Fig. 7.5.

7.3.3 Analysis using implicit method

Program verification

The simply supported beam under two-suddenly applied loads has been analysed. Fig. 7.6 illustrates the variation of mid-span deflection of the beam with time, and the result is in good agreement with those reported by Hinton et al. [41].

The simply supported beam under the applied harmonic loading $P = 1000cos200t$ has been analysed using the implicit Newmark method. The plots of the spectral mid-span displacement of the beam is illustrated in Fig. 7.5.

7.3.4 Analysis using explicit method

The beam has also been analysed using the explicit Newmark algorithm. The spatial discretisation is the same as used for the implicit analysis above. The proposed method, discussed in Chapter 3, for producing a lumped mass matrix from a consistent mass matrix has been used. The critical time-step is governed by the maximum natural frequency of the elements in the mesh, as discussed in chapter 5, and was found to be 0.000005 sec.

Fig. 7.7 illustrates the variation of mid-span displacement of the beam under two suddenly applied loads with time. and Fig. 7.5 shows the spectral mid-span deflection of the beam under the harmonic $P = 1000cos200t$ loading and will be discussed later on.

Comparing the two solution techniques, it is deduced that the implicit algorithm is more accurate than the explicit method due to its higher integrator as discussed in chapter 5.

7.3.5 Example 7.2 - Traditional mixed explicit-implicit method

The traditional mixed implicit-explicit method has been used to analyse the beam. Both the implicit and explicit methods used in the mixed algorithm are Newmarks methods. In other words, the two algorithms used in the analysis demonstrated above are mixed in this example. A graphical illustration of the mixed explicit-implicit elements is presented in Fig. 7.1. The explicit and implicit elements, in the mesh, are shown in Fig. 7.8.

The effective stiffness is formed using the sky-line storage method as shown in Fig. 7.1. The spectral mid-span displacement of the beam under a harmonic load $P = 1000cos200t$ is shown in Fig. 7.5.

7.3.6 The Proposed variable mixed explicit-implicit algorithm

Program verification

Dynamic analysis of the simply supported beam under harmonic loading

For the purpose of verification of the method, the beam under two suddenly applied loads has been analysed using the proposed variable mixed explicit-implicit method. Fig. 7.9 illustrates the explicit and implicit elements used in the mesh and the plots of variation mid-span displacement of the beam is shown in Fig. 7.10. As can be seen, the result is in good agreement with that reported in [41]. The number of explicit elements can be seen in the figure.

Results of analysing the beam under a harmonic loading $P = 1000cos200t$ are plotted in Fig. 7.11 and is compared with that of the traditional analysis. As can be seen, the results from proposed algorithm lie between those from the implicit and explicit methods with a tendency to be closer to those the implicit algorithm.

7.3.7 Example 7.3 - A shear wall Subjected to a seismic loading

In this example, a shear wall has been subjected to the action of the horizontal components of an acceleration of an artificial earthquake loading. The geometry, spatial discretisation of the shear wall and the artificial ground acceleration are illustrated in Fig. 7.12.

The Johnson-Epstein sinesweep artificial earthquake with a maximum acceleration level of $0.33g$ [194, 195], will be used as a prescribed acceleration history. The sinesweep is given by

$$\ddot{d}_g(t) = \ddot{d}_g^{max}(\bar{\omega}) sin\theta(t) \tag{7.55}$$

where

$$\bar{\omega} = \frac{\dot{\theta}(t)}{2\pi} \tag{7.56}$$

$$\theta(t) = At + Bt^N \tag{7.57}$$

For $\bar{\omega} < 1.5$

$$\ddot{d}_g^{max} = 0.22\bar{\omega}g \tag{7.58}$$

and for $1.5 < \bar{\omega} < < 3.5$

$$\ddot{d}_g^{max} = 0.33g \tag{7.59}$$

where $\ddot{d}_g(t)$ is the acceleration time-history, $\ddot{d}_g^{max}$ is the maximum ground acceleration defined as a function of the forcing frequency $\bar{\omega}$ and $\sin(t)$ is a variable frequency sinusoidal signal. With $A = 1$, $B = 3$ and $N = 3$, the artificial accelelogram is equivalent to EL Centro NS , Fig. 7.13.

The material properties of the shear wall are shown in Table 7.1.

Table 7.1-Material properties of shear wall.

Young's modulus	$E = 6 \times 10^6$ psi
Poisson's ratio	v=.2
Mass density	$\rho = 0.217 \times 10^{-3}\ lbsec/in^2$

A plane stress analysis of half of the structure is performed due to the symmetry of the structure. The 8-noded isoparametric finite elements are used. The variation of tip-deformation of the shear wall with time is shown in Fig. 7.14. As can be seen, two different time-steps are used for the first and second part of the analysis procedure. The number of explicit elements can be in the figure.

7.3.8 Discussion of the results

- The plots of the spectral displacements of a simply supported beam under two suddenly applied loads are given in Figs. 7.5. and 7.14.

  As expected, since the local truncation error in the explicit method is one order lower than the implicit method, as discussed in chapter 5, the mid-displacement of the beam in long-duration loading results in considerable global error. The mid-displacement of the beam obtained from the mixed explicit-implicit method is bounded by the explicit and implicit methods as shown in Fig. 7.5.

  It is worth noting that, since both the implicit and explicit methods used in the problem do not have numerical dissipation and dispersion properties to damp out the higher modes error as discussed in chapter 5, the difference between the spectral mid-span displacement of the explicit and the implicit methods are not included in artificial algorithmic error.

- In the traditional mixed explicit-implicit algorithm, the type of the elements, i. e., explicit or implicit should be defined as an input data. Since the elements which might behave visco-plastically in the analysis can not be predicted before solving the problem, all those elements which are likely to be explicit should be explicit initially.

- In the proposed algorithm all of the mesh elements are initially implicit. As soon as any sampling point enters the visco-plastic stage, the corresponding element is changed to be explicit automatically. Hence, the minimum

number of elements change to explicit in the proposed algorithm and this results in a more accurate response.

- The proposed variable mixed explicit-implicit algorithm has the advantages of the implicit and the explicit methods hence is suitable for long-duration problems which will be discussed in the next sections.

- A comparison of the spectral mid-span displacement of the simply supported beam obtained from the modal superposition method, the traditional explicit-implicit method Fig. 6.11 shows that decreasing the number of the explicit elements in the mesh results in more accurate structural response.

- Since the nodal points in a structure are linked by the stiffness of the system and the nodes in the implicit elements possess more accuracy, *'some part of the explicit element response inaccuracies are compensated'*. The term *'some'* is used because when the number of explicit elements increases, *'some'* of the nodes in explicit elements become independent of implicit elements Fig. 7.1. It can be seen that, some of the explicit nodes deformation can be determined irrelevant to the implicit nodes.

Since in many large problems, the failure modes are dominated by a limited number of failed sampling points, most of the elements will remain in the implicit form of integrator up to the failure mode. This causes the explicit nodes inaccuracy to be mostly compensated by the implicit nodes. In other words, the proposed algorithm is between implicit and explicit method with more tendency to implicit methods.

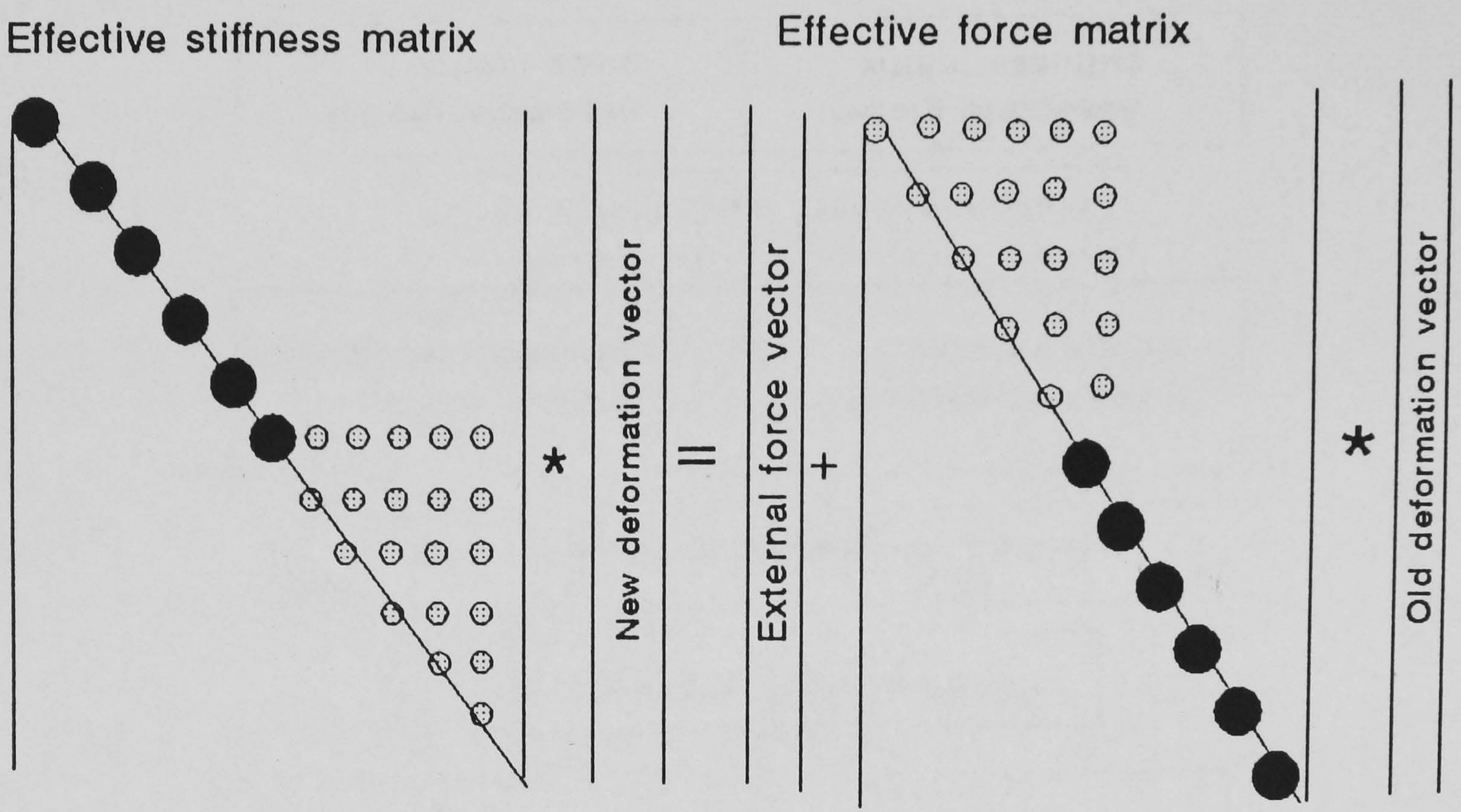

Fig. 7.1 Presentation the independency of Lumped Nodes from Consistent Nodes

Input data

Geometry, loading and material properties.

Put all element types ' implicit '

Calculate integration constant $C1=1/\beta\Delta t^2$

Calculate element stiffness matrix	Calculate element consistent mass matrix

Muliply element mass matrix by C1

Assemble global stiffness matrix	Assemble global mass matrix

Assemble effective stiffness matrix

Put initioal condition

Fig.7.2 - Structure chart for proposed variable explicit-implicit algorithm.

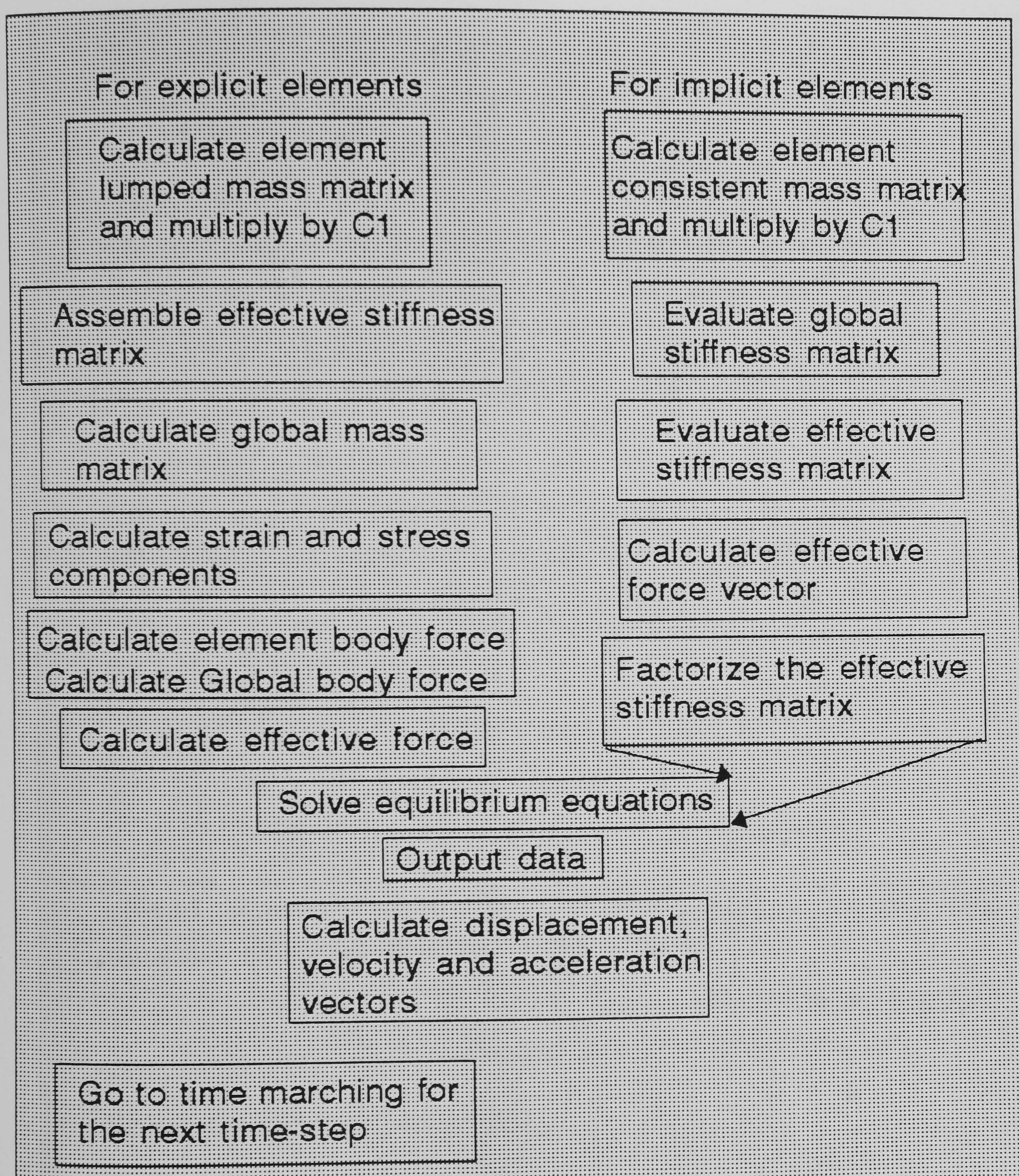

(continued 3/3)

Fig. 7.2 Structure chart for proposed variable explicit–implicit algorithm

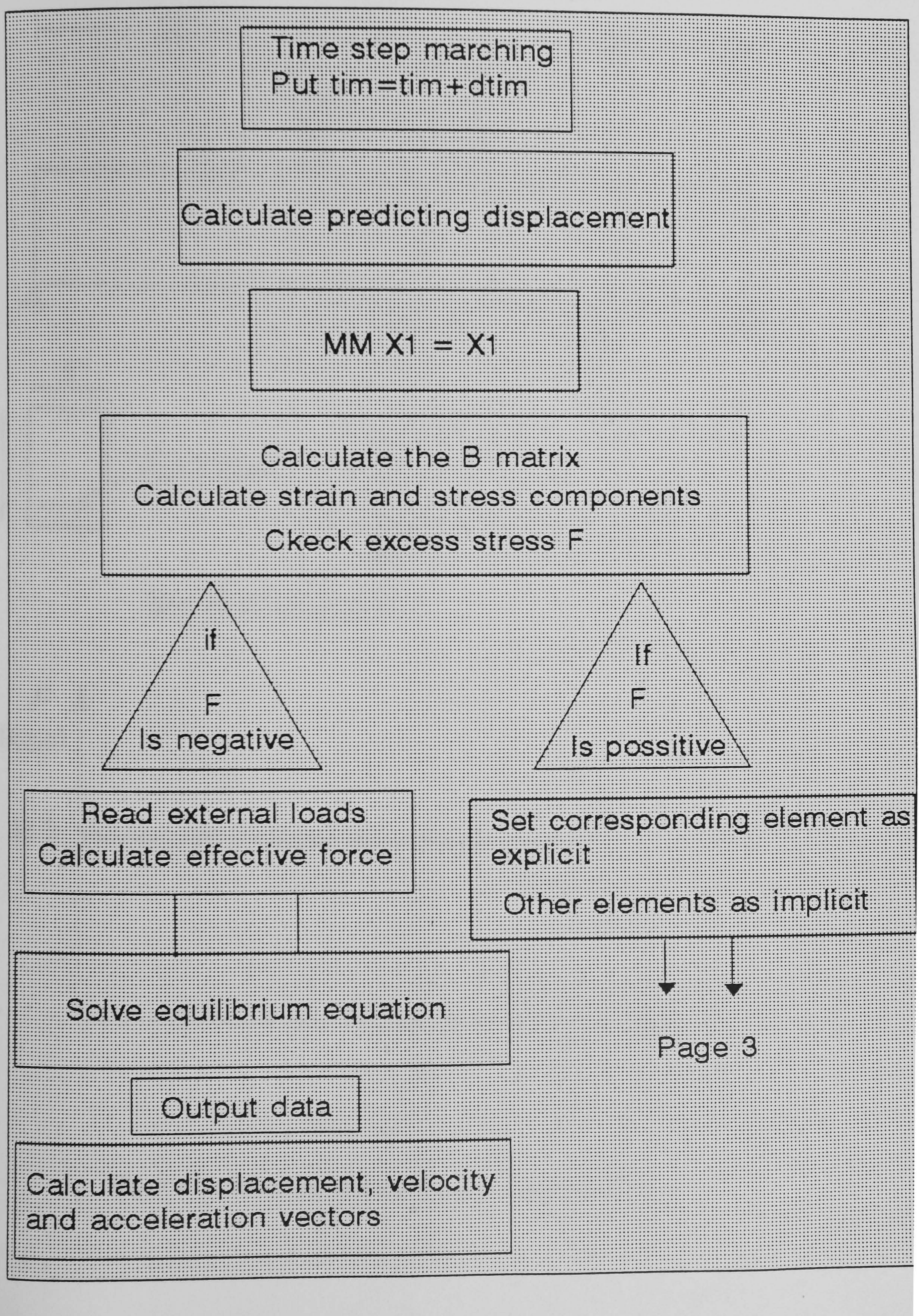

contunued 2/3)

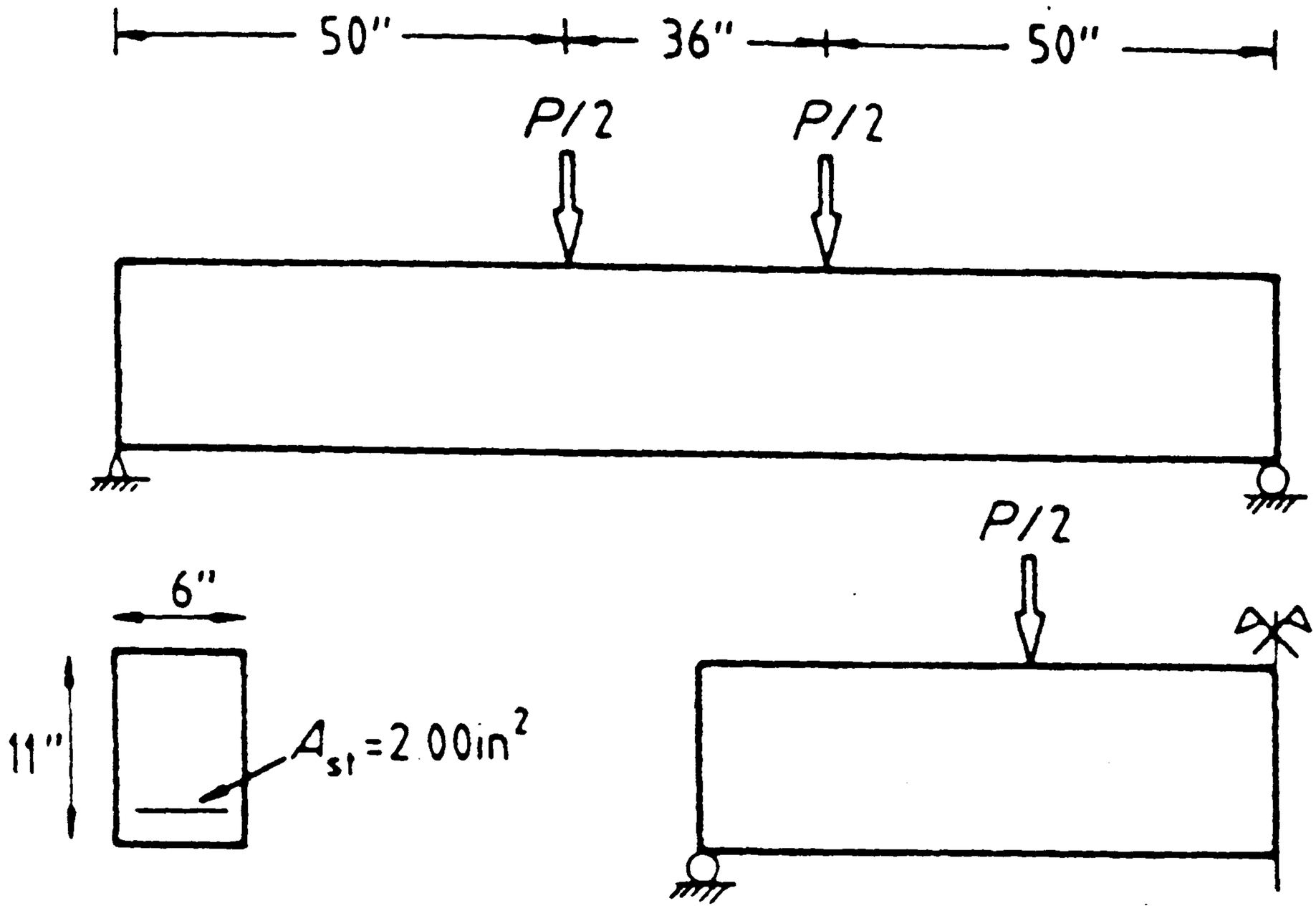

Beam dimensions

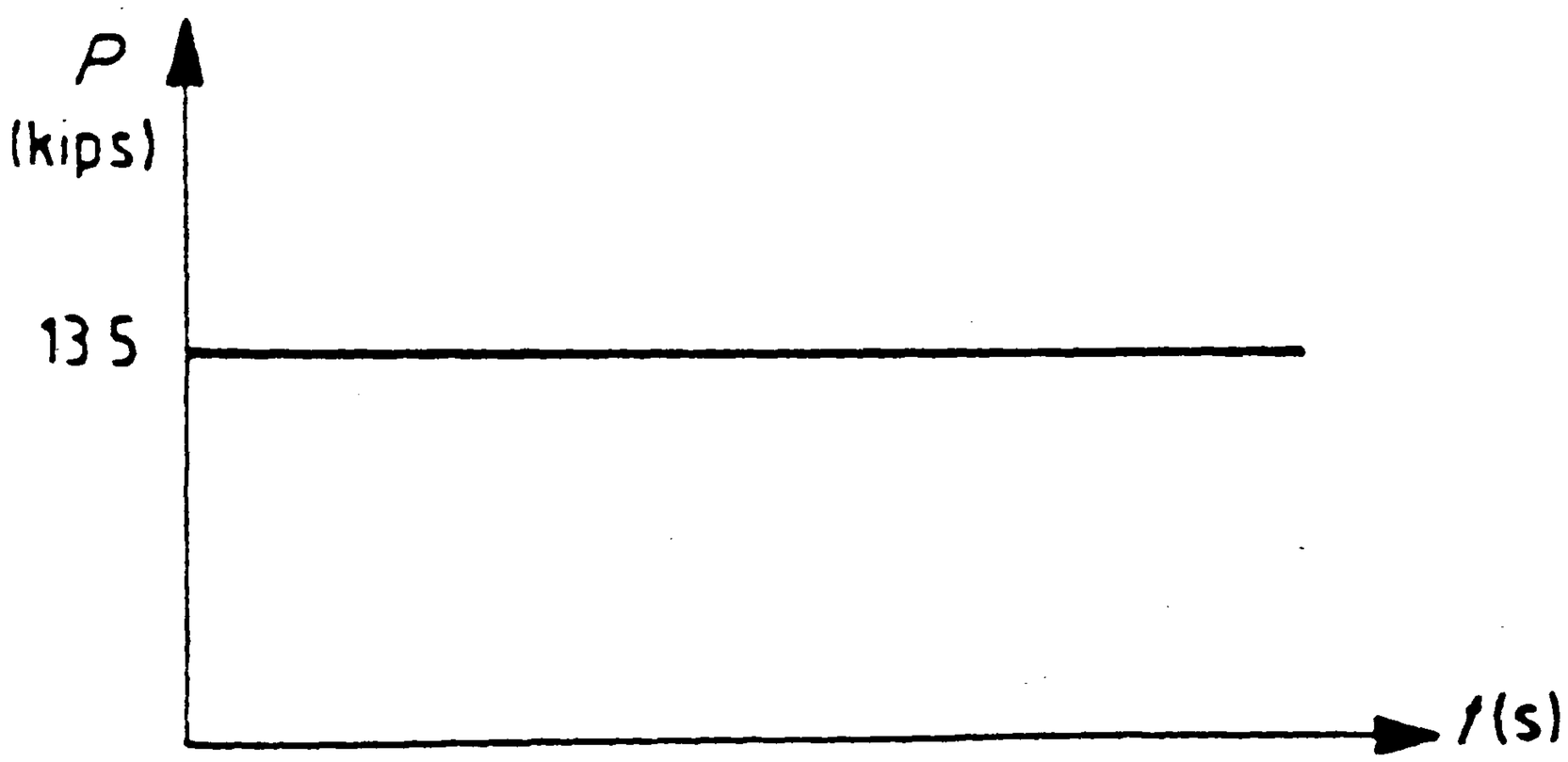

Fig. 7.3 Geometry and Loading of simply supported beam.

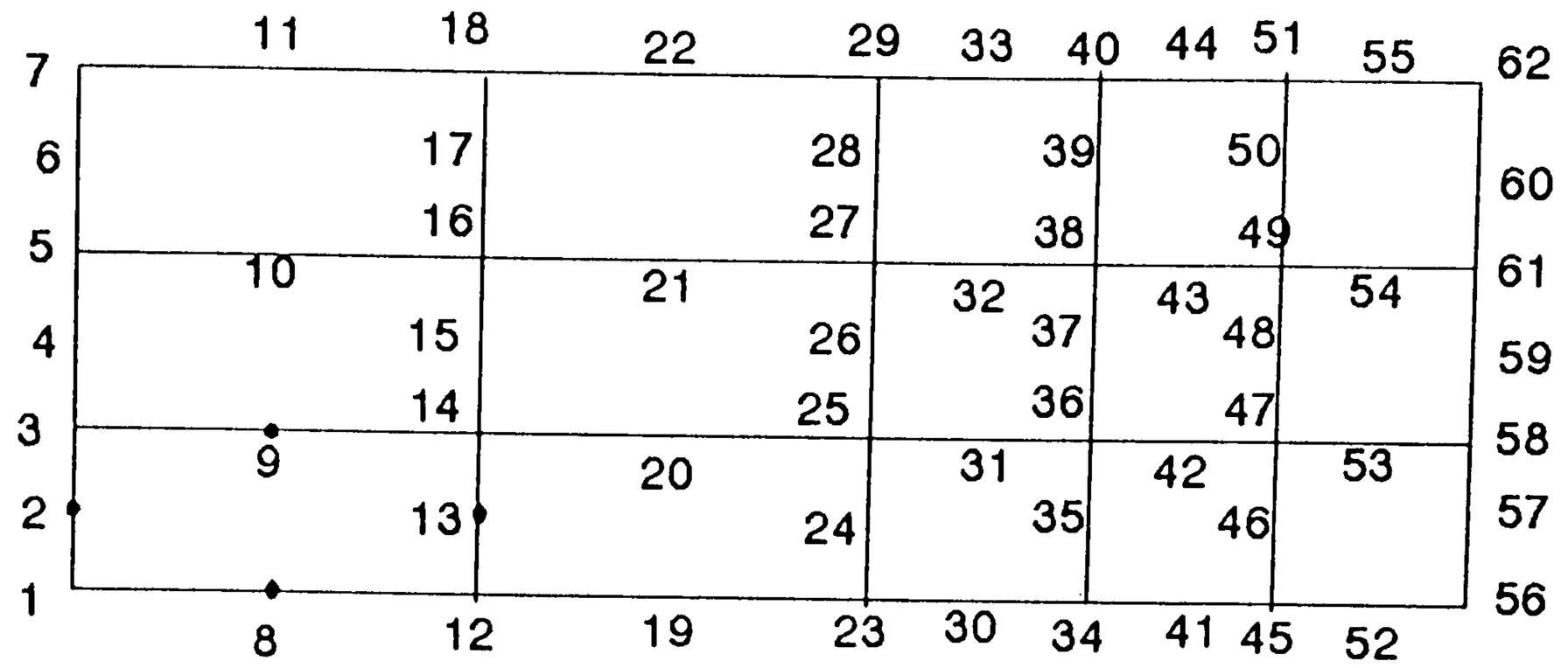

Fig. 7.4 SPATIAL DISCRETISATION OF THE BEAM

Fig. 7.5 Spectral mid-span displacement of simply supported beam
Obtained from diffrrent solution techniques

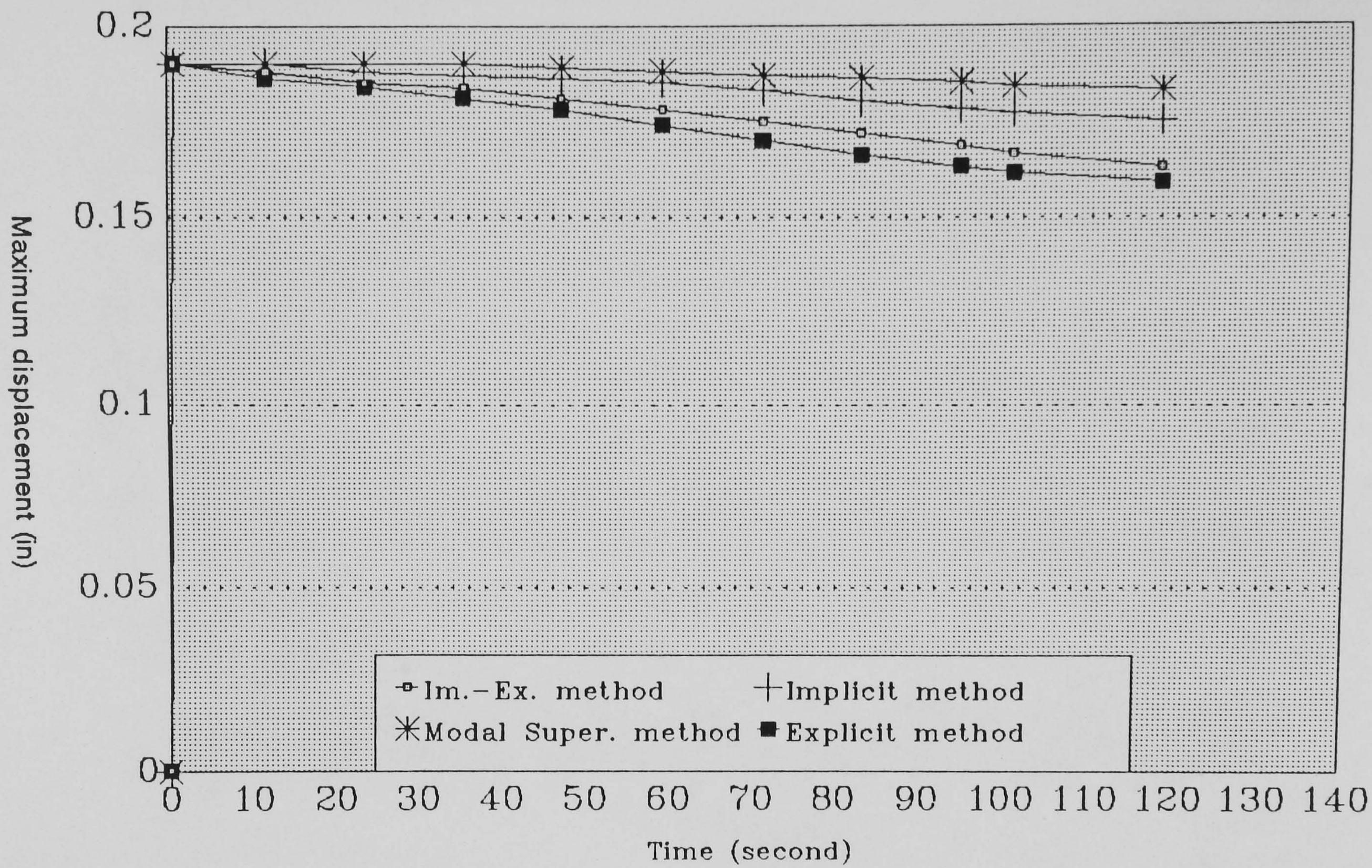

Fig. 7.6 Time-history mid-span displacement of beam using the Implicit method
Under suddenly two applied load

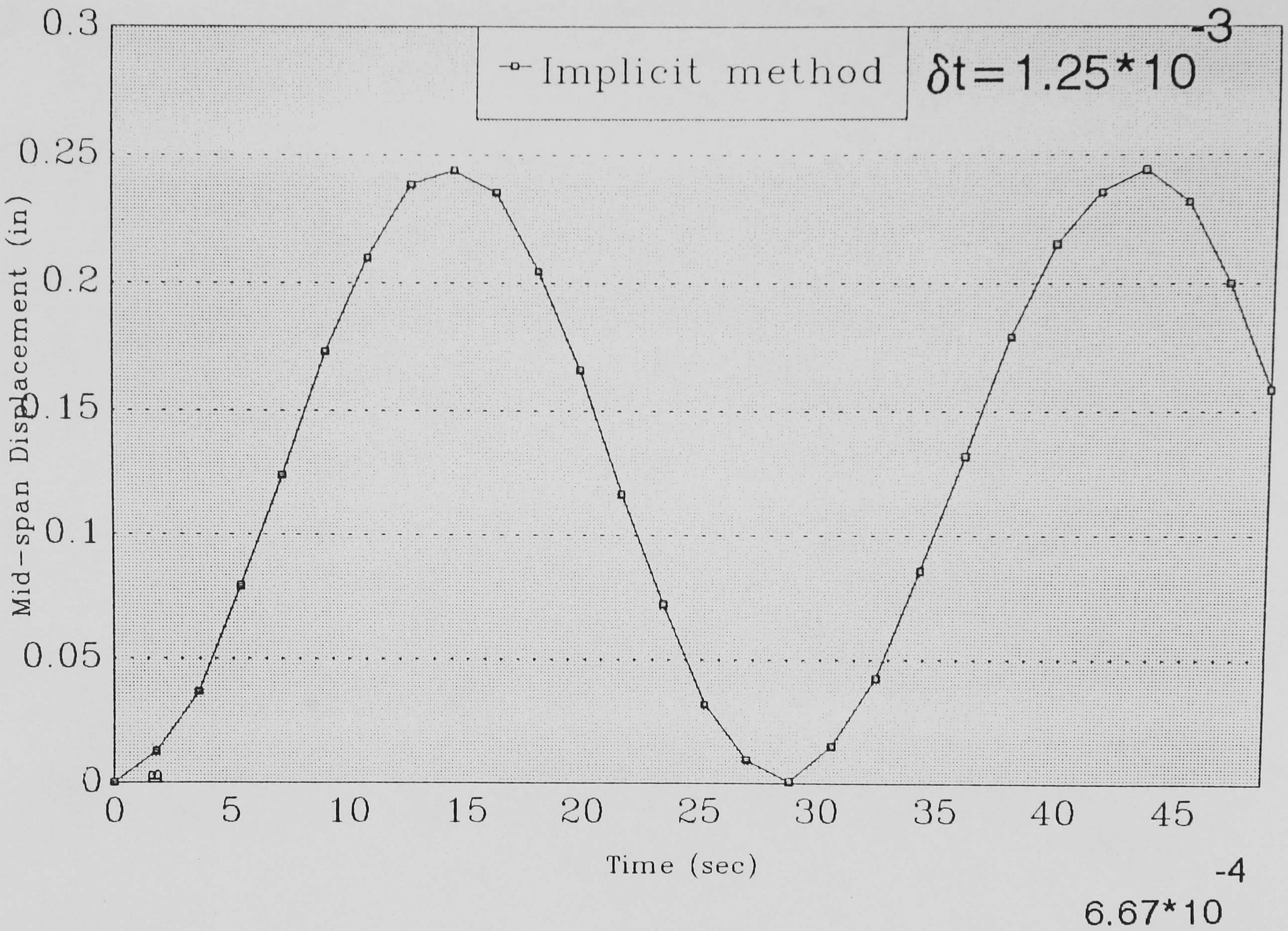

Fig. 7.7 Time-history mid-span displacement of the simply supported beam.
Under two suddenly applied load.

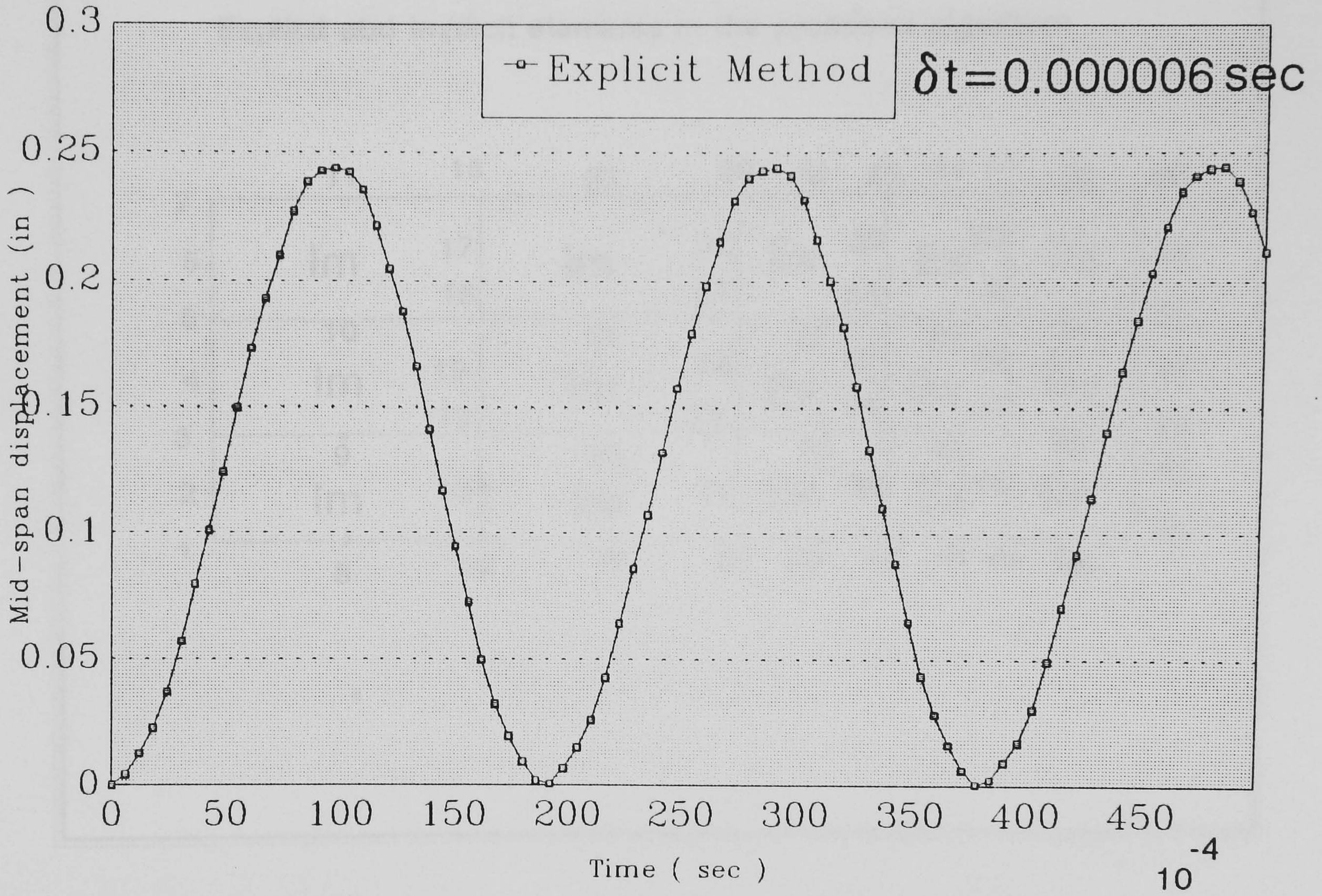

Fig. 7.8 SPATIAL DISCRETISATION OF THE BEAM

Explicit abd Implicit elements in the proposed algorithm

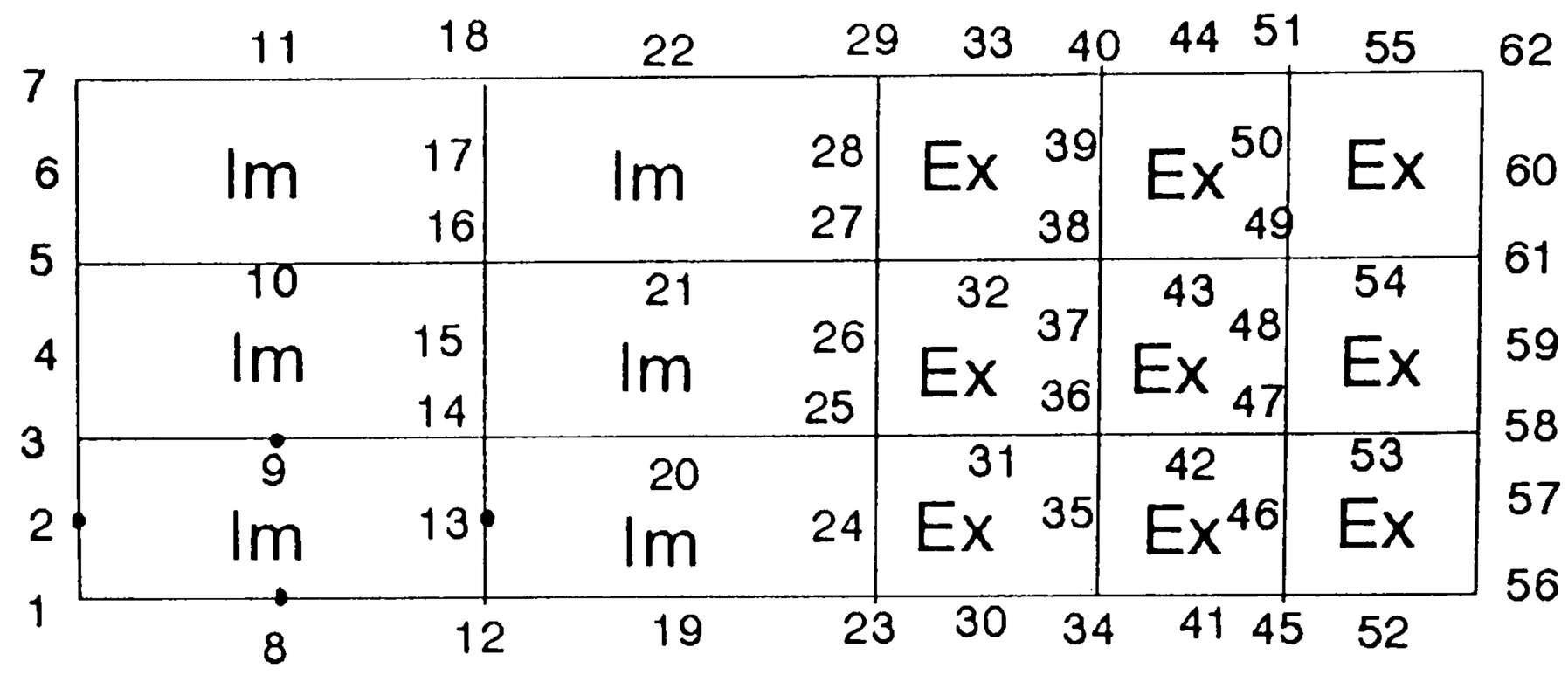

Fig. 7.9 SPATIAL DISCRETISATION OF THE BEAM

Explicit abd Implicit elements in the proposed algorithm

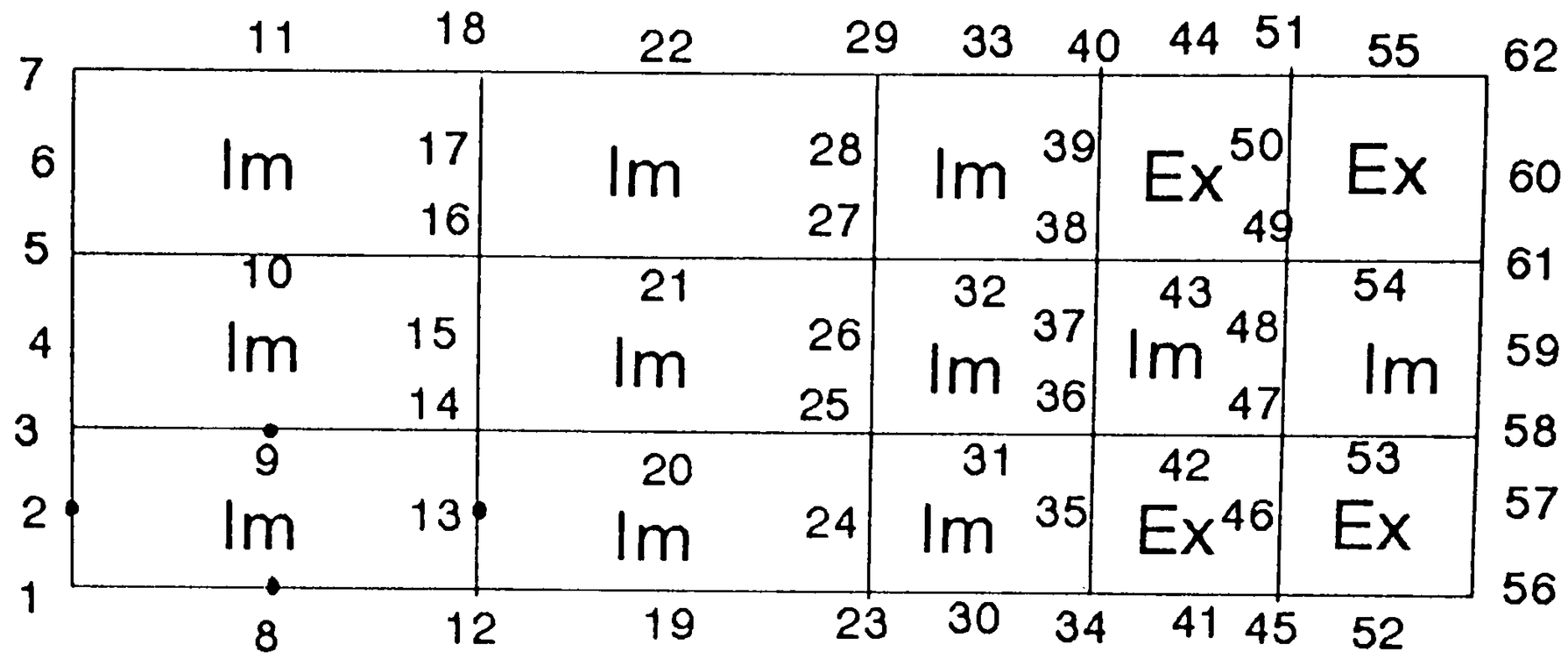

Fig. 7.10 Mid-deflection of a simply supported beam
Variable explicit-implicit method

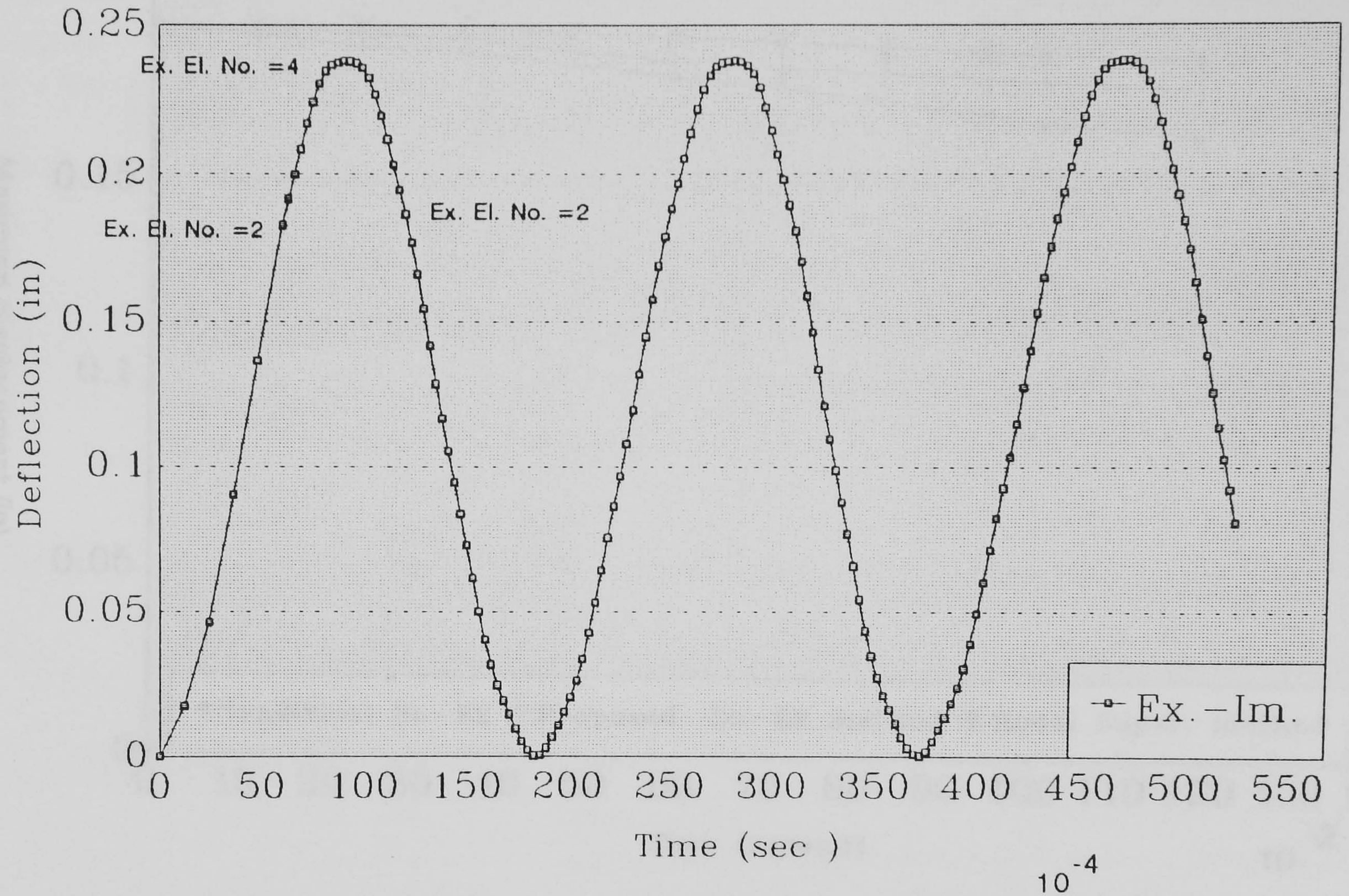

Ex. El. No., number of explicit elements

Fig. 7.11 Spectral mid-span displacement of simply supported beam
Comparison of the proposed algorithm with the traditional
efexplicit-implicit method

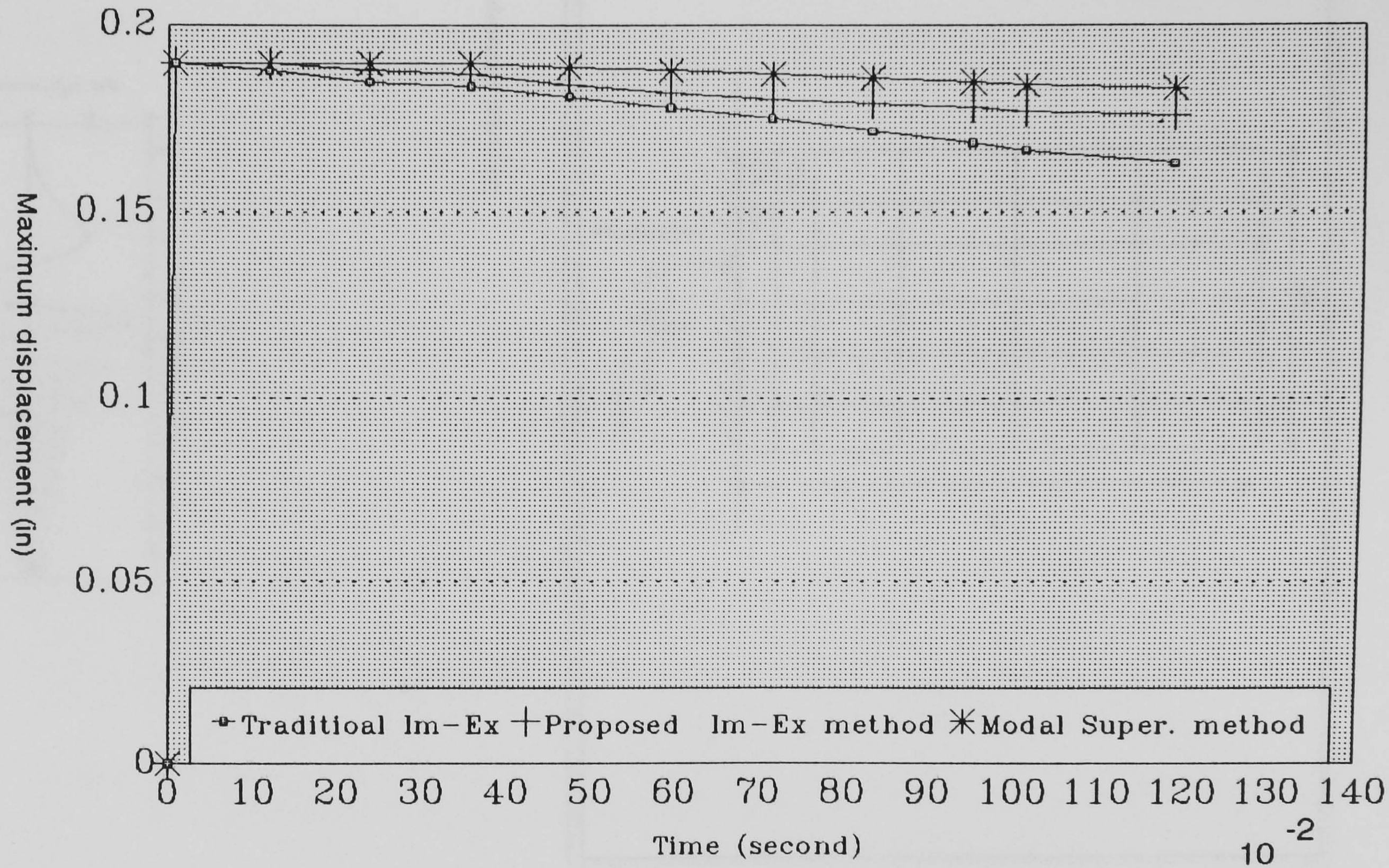

Fig. 7.12 Geometry, spatial discretisation of shear wall and ground acceleration

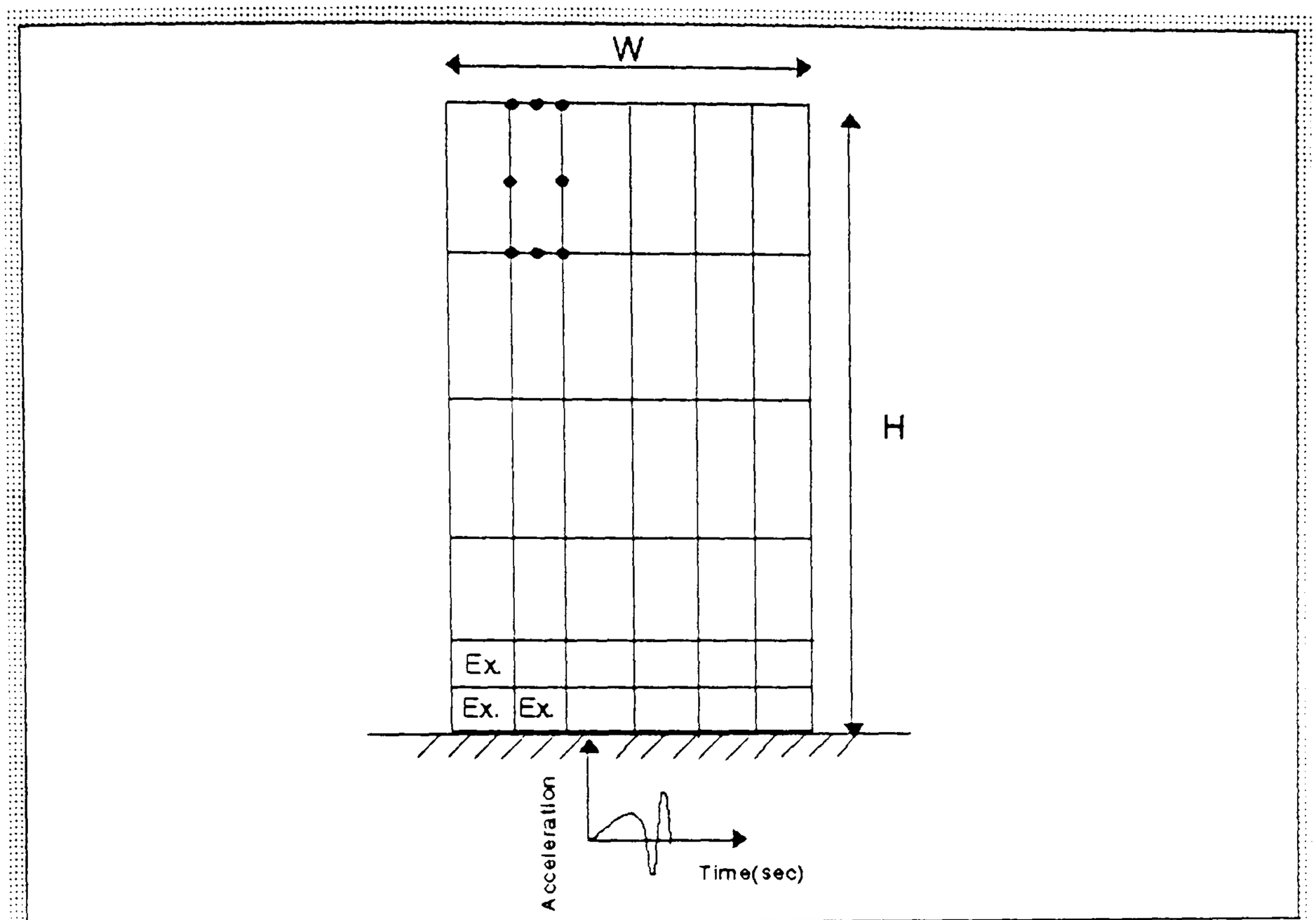

Ex. = Explicit element number

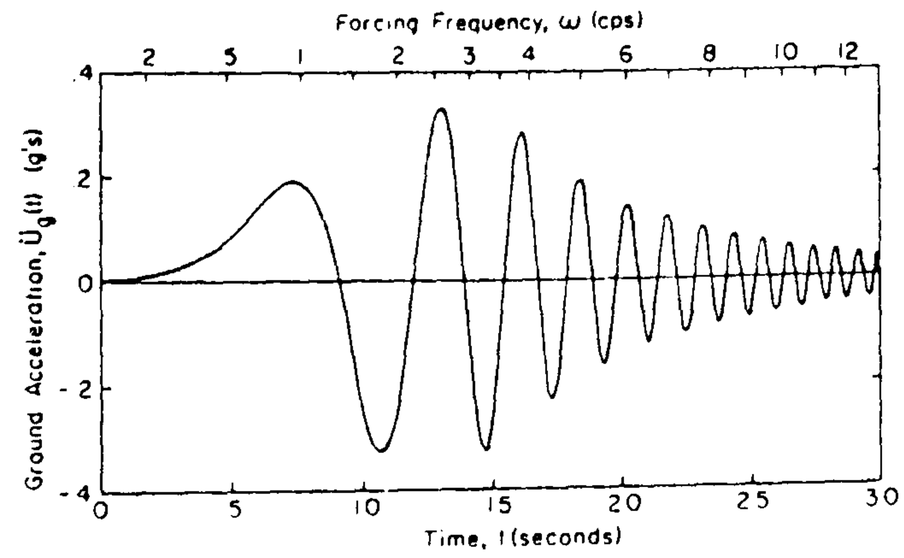

Fig. 7.13 Sine sweep earthquake (taken from [194])

Fig. 7.14 Tip-deformation of a shear wall under seismic load.

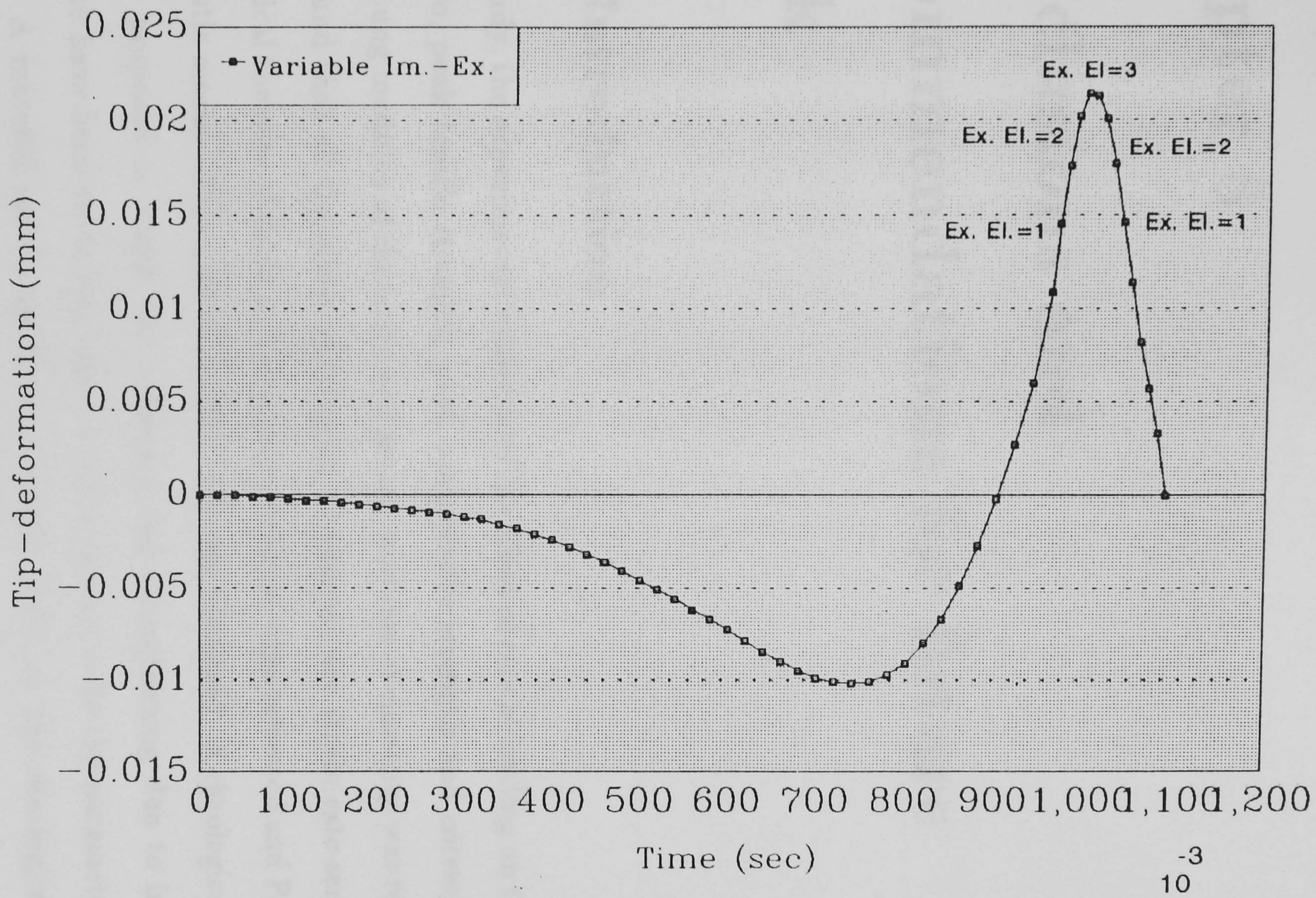

Ex. El. No. = Explicit element number

Chapter 8

Conclusions and recommendations for future work

8.1 Introduction

In this study, the experimental evidence of the effect of rate of loading on the Poisson's ratio, peak tensile strength, peak compressive strength and corresponding strain, Young modulus of elasticity and secant modulus of elasticity was reviewed. It was found that all the above-mentioned parameters are strain-rate-sensitive. The classical theories of static and dynamic problems were reviewed and Perzyna's visco-plastic model [119] adopted in this study was discussed. A rheological model has been proposed in which the stiffening and strengthening due to increased strain-rate have been modelled, because these appear to be the parameters most affected. A material model has been proposed based on the rheological model by which the material stiffening and strengthening due to increasing strain-rate were modelled.

The currently used spatial, time and mass discretisation methods have been reviewed and the advantages and disadvantages of the existing methods have been assessed. The plane and axisymmetric reinforced concrete structures used

in this study, have been spatially discretised using finite element method. It was found that the quadrilateral serendipity 8-noded element is appropriate in plane and axisymmetric dynamic problems. Finite difference schemes have been used for time discretisation. The type of integrator employed in dynamic problems was found to be dominated by the size of the problem, the required the accuracy, frequency of the applied loading and duration of loading.

The chapter starts with the conclusions made in discretisation problems. The next sections are devoted to the conclusion made in the dynamic solution techniques such as modal superposition, direct integration methods and material nonlinearity. The chapter closes with recommendations for further research.

8.2 Discretisation problems

The conclusions made regarding the spatial discretisation are summarized below.

- Using full integration scheme for determining the consistent mass matrix and preserving the total mass gives better mass distribution compared with reduced integration method and results in more accurate natural frequencies of the system.

- Since the eigenvalues of a system with a defined mesh are constant, using a 3×3 Gauss points for determining the consistent mass matrix compared with a 2×2 Gauss points, results in more discretised mass and less frequencies which is more compatible with the real natural frequencies of the system.

- Although theoretically the mass matrix should be consistent, an equivalent lumped mass matrix can be produced from the consistent mass matrix. The proposed lumped mass scheme was found to give natural frequencies more close to those given by the consistent mass matrix compared with the existing methods.

- In dynamic problems in which the frequency of the applied load is higher than the fundamental natural frequency, for example earthquake loading, the contribution of the higher modes are not significant. For example, in a cantilevered beam under a harmonic loading the contribution of the modes above 15% of the total mode number was found to be significant.

- In dynamic problems more accurate response is obtained using embedded steel modelling than with smeared steel modelling, this is because for an accurate response with smeared steel, small elements are required but small elements can cause stability problems. Such problem is not included in embedded steel modelling hence ends up with more accurate results.

- As the mesh is refined, the inaccuracy involved in the prediction of the frequencies of the higher modes decreases appreciably.

8.3 Dynamic Problems

8.3.1 Modal Superposition Method

The modal superposition method was found to suffer from one major drawback because in non-linear problems the eigenvalues and the mode shapes should be evaluated in each time-step. This procedure is computationally expensive.

8.3.2 Direct Integration Methods

A number of direct integration schemes for the dynamic analysis of structures have been reviewed and the efficiency, advantages and disadvantages of the currently used methods were assessed. Attention was focussed on the accuracy, stability and algorithmic error aspects of the methods particularly those suitable for dynamic analysis of structures subjected to seismic loading. The conclusions are

- The local truncation error (LTE), the global truncation error (GTE) and the round-off error in the explicit methods can lead to unacceptable results in long duration problems.

- Using an appropriate explicit form of integrator as the predictor and an implicit method as the corrector increases the accuracy of the method, however higher order integrators or k-step methods can also increase the response accuracy .

- Both the explicit and the implicit types of integrators suffer from algorithmic errors such as amplitude decay (AD) and period elongation (PE).

- Although the currently used implicit methods for dynamic analysis of structures under earthquake loading such as the Wilson-θ method or the Houbolt method possess numerical dissipation property, they do not have sufficient accuracy. Among the currently used numerical algorithms, the α-method is expected to be more efficient, provided that an appropriate α which depends on the type of structure and loading, is chosen.

- The central difference method possesses the maximum critical time step in the currently used explicit algorithms.

- Although the implicit methods do not suffer from the problem of stability, the structural response using such algorithms can be greatly influenced by the error due to higher modes thus may lead to serious problems. Hence, in dynamic problems of a long-duration, such as those due to earthquake loadings, emphasise should be concentrated on damping out the artificial frequencies due to higher modes.

- The proposed variable explicit-implicit method using an appropriate explicit form of integrator as predictor and an implicit form possessing suitable numerical dissipation properties as a corrector is expected to be more efficient in large problems particularly those involved in earthquake loading. This algorithm has the advantages of both the explicit and implicit methods particularly in non-linear analysis.

- Since the failure mode in large problems is often expected to be dominated by a small number of elements, in the proposed algorithm, the local truncation error (LTE) and round-off error produced by the explicit elements is compensated by the implicit elements through the system stiffness. In fact, the accuracy of the proposed method lies between the implicit and the explicit methods with a tendency to the implicit method. In the proposed algorithm, attention has been focussed on increasing the accuracy and minimizing the computational effort.

8.3.3 Pre-Cracked and Post-Cracked Concrete Problems

The assumption of elastic behaviour of concrete in tension prior to cracking was found to be an appropriate assumption for dynamic problems. It is felt that concrete exhibits appreciable non-linearity which increases with increasing strain-rate. This problem remained unsolved in this study due to lack of experimental results. However increasing in the Young modulus of elasticity due to strain-rate was simulated in the proposed model.

The post-cracked modelling of concrete has been reviewed. It was concluded that,

- In dynamic problems, use of smeared crack model with the use of fracture energy can simulate the behaviour of post-cracked concrete, however fracture energy is felt to be strain-rate-sensitive. The effect of fracture energy rate-sensitivity remained unsolved due to lack of experimental data.

8.3.4 Rate dependency problems

The effect of rate dependency on the following parameters for concrete has been reviewed

- The initial modulus of elasticity.
- The tangent modulus of elasticity.

- Poisson's ratio in both compression and tension.

- The maximum compressive strength and corresponding strain.

A material model has been proposed by which the material stiffening and strengthening due to increasing strain-rate are simulated. A formula has been developed for Perzyna's fluidity parameter [119]. A formula for determining the equilibrium dynamic initial modulus elasticity and a formula for determining the increased stiffness and strength of concrete have been proposed. however, developing the above mentioned formulae in three dimensional problems remained unanswered due to lack of experimental data in this study.

Based on the proposed rheological model, the rate-dependency of the following parameters has been incorporated into the proposed model.

- The modulus of elasticity.

- The tangent modulus of elasticity.

- The concrete compressive peak strength and corresponding strain.

- The tensile strength of the concrete.

It was concluded that,

- The strain-rate-dependent parameters of concrete can be modelled appropriately which end up with the concrete stiffening and strengthening simulation, and results in increasing the ultimate load capacity of the structure.

- In the proposed model, both variable stress-rate and strain-rate have been simulated.

8.3.5 Material non-linearity problems

- The material non-linearity, either due to crack propagation or material viscoplasticity causes the fundamental period to be elongated. This elongation might causes serious problem such as resonance phenomenon and should be taken into account in structural design.

- In reinforced concrete structures with high ductility property, more energy is expected to be absorbed when are loaded by a transient force.

8.4 Recommendations for further research

- The available formulae for producing a lumped mass matrix from consistent mass are applicable when only translational degrees-of-freedoms are included. A formula is required for the case when translational and rotational degrees-of-freedom are included in the problem.

- An algorithm possessing adequate accuracy and numerical dissipation property so that can damp out any defined number of higher modes is required in dynamic problems particularly those under earthquake loading.

- More experimental results for concrete under rate loading are required to enable the following parameters to be determined

  - multiaxial rate-dependent failure criteria.
  - the strain-rate effect on the initial modulus of elasticity, tangent modulus of elasticity, Poisson's ratio, peak compressive strength and corresponding strain, peak tensile strength and corresponding strain and ultimate compressive and tension strain.
  - The cracking processes under strain-rate which are not well understood.

- A more accurate formula is required for determining the critical stability-dependent time-step for the explicit form of visco-plastic strain approximation.

- The results described in this thesis suggest that, the proposed rheological model could be extended to two and three dimensional situations by assuming different fluidity parameters for different directions which needs test results.

- The computer programs DYNICK2D, DYNICK2T could be modified to be used for the three dimensional analysis of reinforced concrete structures.

References

[1] Timoshenko S. and Goodier, "Theory of Elasticity", McGraw-Hill New York, 1953.

[2] Chen W. F., "Plasticity in Reinforced Concrete", McGraw-Hill Book Company, 1982.

[3] Yang, B. L., Dafalias, Y. F. and Herrman, L. R., "A bounding Surface Plasticity Model for Concrete", Journal of Engineering Mechanics Division, ASCE, Vol. 111(3), pp. 359-381, March 1985.

[4] Wimal Suaris, "Dynamic Behaviour of Concrete; A Phenomonegical Theory and Instrumented Impact Testing", Thesis, Department of Civil Engineering, Northwestern University, Evanston, Illinois, 60201.

[5] Hughes, B. P. and George R., "Concrete Subjected to High Rates of Loading in Compression", Magazine of Concrete Research, Vol. 24, No. 78, March 1972, pp. 25-36.

[6] Zdenek P. Bazant and H. Oh, "Strain-Rate Effect in Rapid Triaxial Loading of Concrete", Journal of Engineering Mechanics Division, Vol. 108, No. EM5, October 1982, pp. 764-783.

[7] Dougill J. W., "The Response of Concrete to Short term Loading", Dams and Concrete, TTL, London, pp. 113-123, 1981. " Mchenry D., and Schideler J. J., 'Revise of Data on the Effect of Speed in Mechanical Testing of Concrete' Symposium on Speed of Testing Non-Metallic Materials. Phyladelphia.

[8] Ban S. and Muguruma H., "Behaviour of Plain Concrete Under dynamic Loading With Straining Rate Comparable To Earthquake Loading", Kyota University, Kyota, Japan.

[9] Takeda, J., and Tachikawa, H., "Deformation and Fracture of Concrete Subjected to Dynamic Load", International Conference on Mechanical Behaviour of Materials, Vol. 4, pp. 267-277.

[10] Hatano, T., Tsutsumi, and H., "Dynamic Compressive Deformation and Failure of Concrete Under Earthquake Load", Procs. 2nd, WCEE, Vol. 3, pp.

1963-1978 Tokyo, 1960.

[11] George Winter and Arthur H. Nilson, "Design of Concrete Structures", McGraw-Hill Book Company 1985.

[12] Mander J. Priestly N. and Park, Fellow, "Observed Stress-Strain Behaviour of Confined Concrete", Journal of Structural Engineering, Vol. 114, No. 8, August 1988, pp. 1827-1849. "Watstain, D., 'Effect of Strain Rate on the Compressive Strength and Elastic Properties of Concrete'.

[13] Wimal Suaris, and Surendra P. Shah, 'Constitutive Model for Dynamic Loading of Concrete', Journal of Structural Engineering, Vol. 111, No. 3, March 1985, pp. 563-577.

[14] John, R. and Shah S. P., "Constitutive Modeling of Concrete Under Impact Loading", in Procs. of SMIRT-9 Post Conference Seminar; Impact, Lauanne, Switzerland, August 1987.

[15] Kormelling, H. A., "The Rate Theory and The Impact Tensile Behaviour of Plain Concrete, Fracture Toughness and Fracture Energy of Concrete", F. H. Wittmann, The Netherlands, Elsevier Science, pp. 467-477.

[16] Wimal Suaris, and Surendra P. Shah, 'Rate-Sensitive Damage Theory For Britle Solids', Journal of Engineering Mechanics, Vol. 110, No. 6, June, pp. 985-997, 1984.

[17] Malvern, L., E., Jenkins, D. A., Tang T. and Ross, C. A. "Dynamic Compressive Testing of Concrete", Procs. of 2nd Symp. on The Interaction Non-Nuclear Munitions With Structures, Panama City Beach, FL, pp. 194-199, 15-18 April 1985.

[18] Jed, I., "High Strain Rate Behaviour of Hydrated Cement Paste", Cement and Concrete Research, Vol. 17, No. 3, PP. 433-440, 1987.

[19] McHenry D. and Schideler J. J. "Revise of data on the effect of speed in mechanical testing of concrete", Symposium on speed of testing non-metallic materials. Philadolphia, ASTM Special Technical Publication STP185, PP. 72-82, 1956.

[20] Curbash, M. and Eibl, J., "Non-Linear Behaviour of Concrete Under High Compressive Loading Rates", Int. Conf. on Recent Developments in Fracture of Concrete and Rock, University. of Wales, College of Cardiff, Uk, Elsevier Applied Science Press, London and New York, 20-22 Sept. 1989.

[21] Ahmad, S. and Shah, S. P., "Behaviour of Hoop Confined Concrete Under High Strain-Rate", Journal of American Concrete Institute, PP. 634-647, september-October 1985. In ACI Committee 446 Chapter 4, Dynamic Fracture, May 1992.

[22] Riad, Hany Labib, "Finite Element Analysis of Reinforced Concrete Structures under Impact Loading", PhD thesis, Pennsylvania State University. 1991.

[23] Amman, W., Mohlematter, M., and Bachmann, J., "Stress Strain Behaviour of Non-Prestressed and Pre-Stressed Reinforced Steel at High Strain Rates", Procs. RILEM/CEB/IABSE/AISS Symposium on concrete structures under impact and impulsive loading, Berlin, (West), pp. 146-156, 1982.

[24] Limberger E., Brandes, K. and Herter, J., "Influence of Mechanical Properties of Reinforcing Steel on The Ductility of Reinforced Concrete Beams With respect to High Strain Rates", Procs of RILEM/CEB/IABSE/AISS Symposium on concrete structures under impact and impulsive loading, Berlin, (West), pp. 134-145, 1982.

[25] Zienkiewicz, O. C., Valliappan, S. and King, I. P., "Elasto-plastic Solutions of Engineering Problems; "initial stress", Finite Element Approach", International Journal of Numerical and Mechanical Engineering, vol. 1, pp. 75-100, 1969.

[26] Cedolin, L., Curtzen, Y.R.J., and Poli, S.D., 'Triaxial stress- strain Relationship for Concrete', ASCE, Journal of the engineering Mechanic Division, Vol. 103, No. EM3, pp. 423-439. 1977.

[27] Coon, M. D., and Evans, R.J., 'Incremental Constitutive Laws and their Associated Failure Criteria with Application to plain concrete', International Journal of Solids and Structures, Vol. 8, pp. 1169-1183. 1972.

[28] Kupfer, H. B., and Gerstle, K. H., 'Behaviour of Concrete under Biaxial Stresses', ASCE, Journal of the Engineering Mechanics Division, Vol. 99, No. EM4, pp. 853-867, 1973.

[29] Kupfer, H. B., and Gerstle, K. H., "Behaviour of Concrete Under Biaxial Stresses", Journal of ACI, Vol. 66, No. 8, pp. 656-666, 1969

[30] Palaniswamy, R., and Shah, S.P., 'Fracture and stress-strain Relationship of Concrete under Triaxial Compression', ASCE, Journal of the Structural Division, Vol. 100, No. ST5, pp. 901-915, 1974.

[31] Mendelson, A. and Hanson, S. S., "Practical Solution of Plastic Deformation Problems in the Elastic-plastic Range", NASA TR-R-28, 1959.

[32] Mander J. B., Priestly M. J. N. and Park R., "Theoretical Stress-Strain Model for Confined Concrete", Journal of Structural Engineering, Vol. 114. No. 8, pp. 1804-1826, August 1988.

[33] Lee J. H., "Some Exact and Approximate Solutions for The Modified Von Mises Yield Criterion ", Journal of Applied Mechanics, ASME, Applied Mechanic Division, V. 55, pp. 260-266, June 1988.

[34] Bhattachar V. S. and Weisgerber F. E., "Dynamic Analysis Using A linearized Failure Surfaces", Computers and Structures, Vol. 37, No. 1, pp. 95-102, 1990.

[35] William, K.J. and Warnke, E.P., 'Constitutive Model for the Triaxial Behaviour of Concrete', International Association of Bridge and Structural Engineers, Seminar on Concrete Structures Subjected to Triaxial Stresses, Paper III-1, ISMES, Bergamo, Italy, May 17-19, 1974.

[36] Green, S.J. and Swanson, S.R., 'Static Constitutive for Concrete', Air Force Weapons Laboratory, Technical Report No. AFWL-TR-72-2, Kirtland Air Force Base, 1973.

[37] Nilsson, L., 'Impact Loading of Concrete Structures', Publication No. 79, Department of Structural Mechanics, Chalmers University of Technology 1979.

[38] Poul V. Lade and Richard B. Nelson, "Incrementalisation Procedure for Elasto-plastic Constitutive Model With Multiple, Intersecting Yield Surface",

International Journal for Numerical and Analytical Methods In Geomechanics. Vol. 8, PP. 311-323, 1984.

[39] Barros H. F., Marques C. M. S. and Martin R. A. F., "A Symmetric Formulation in Non-Associated Plasticity", Computers and Structures, V. 38, No. 1, pp. 25-29, 1991.

[40] Samanaidu Balakrishnan and Murray, David W., "Prediction of R/C Panel and Deep Beam Behaviour By NLEFA", Journal Of Structural Engineering, Vol. 114, No. 10, pp. 2323-2343, October 1988.

[41] Cervera, M. Hinton, E. and Bicanic, N., "Non-linear Transient Dynamic Analysis of Three-dimensional Reinforced Concrete Structures Using a Three-Dimensional Approach", Numerical Methods for Transient and Coupled Problems, Edited by Lewis, R. W. Hinton, E., Bettes, P. and Scherefler, B. A., John Willey and Sons Ltd., 1987.

[42] Pope, G. G., "A Discrete Element Method for Analysis of Plane Elasto-plastic Strain Problems", R. A. E., Farnborough, TR 65028, 1965.

[43] Bangash M. Y. H., "Concrete and Concrete Structures: Numerical Modelling and Applications", Middlesex Polytechnic, Faculty of Engineering, Science and Mechanics, London, U.K., 1989.

[44] Frank J. Vecchio, "Nonlinear Finite Element Analysis of Reinforced Concrete Membranes", ACI Structural Journal, January-February 1989.

[45] Crisfield M. A., "Incremental/Iterative Procedures For Non-Linear Structural Analysis In Numerical Methods For Non-Linear Problems", in Taylor C., et al (Eds.), Pineridge Press, Swansea, pp. 261-290, 1980.

[46] Samanaidu Balakrishnan, Elwi Alaa E. and Murray, David W., "Effect of Modelling on NLFE of Concrete Structures", Journal Of Structural Engineering, Vol. 114, No. 7, pp. 1467-1486, July 1988.

[47] Steven N. J., Uzumeri S. M., Collin M. P., and Will G. T., "Constitutive Model For Reinforced Concrete Finite Element Analysis", ACI structural Journal, November-December 1991.

[48] Hsuan-Teh Hu and William C. Schnobrich, "Non-linear Analysis of Reinforced Concrete", ACI Structural Journal, pp.199-207, March-April 1990.

[49] Valanis K. C., "A Theory of Viscoplasticity Without A yield surface", Archiwum Mechaniki Stossowanej, V. 23, pp.517-551. 1971.

[50] Bazant Z. P. and Bhat P., "Endochronic Theory of Inelasticity and Failure of Concrete", Journal of The Engineering Mechanics Division, ASCE, V. 102, No. EM4, pp. 701-722, Aug. 1976.

[51] Dougill J. W. Lau J. C. and Burt N. J., "Towards a Theoretical Model for Progressive Failure and Softening in Rock, Concrete and Similar Materials ", Mechanics in Engineering (Eds. Dubey R. N. and Lind N. C.), University of Waterloo Press, Waterloo, pp. 335-355, 1977.

[52] Mirza, S. A., Hatzinikdas, M. Macgregor, J. G., "Statistical Descriptions of Strength in Concrete", Journal of the Structural Dvision Procs. ASCE, ST6, June, pp. 1021-1037, 1979.

[53] Stevens N. J., Uzumeri S. M., and Collins M. P., "Analytical Modelling of Reinforced Concrete Subjected to Monotonic and Reversed Loadings", University of Toronto, Department of Civil Engineering, Publication No. 87-1 ISBN 0-7727-7088-3, 1987.

[54] Gerstle, K. H., "Material behaviour under various types of loading", in High Strength Concrete, University. of Illinois at Chicago Circle, pp. 43-78, 1979.

[55] Johnson, R. D., " Structural Concrete ". McGraw-Hill Publishing Company Limited. London, 1967.

[56] Samanaidu Balakrishnan and Murray, David W., "Concrete Constitutive Model for NLFE Analysis of Structures", Journal Structural Engineering., ASCE, 114(7),pp. 1449-1465 December 1988a.

[57] Samanaidu Balakrishnan and Murray, David W., "Concrete Constitutive Model for NLFE Analysis of Structures", Journal of Structural Engineering, ASCE, 114(7), pp. 1449-1465, December 1988b .

[58] Eiki Yamaguchi and Chen, Wai-Fah, "Cracking Model for Finite Element Analysis of Concrete Materials", Journal of Engineering Mechanics, Vol. 116,

No. 6, pp. 1242-1259, June 1990.

[59] Robert H. Dodds, and Darwin, David, "Stressed Controlled Smeared Cracking In R/C Beams.", Journal of Structural Engeering, Vol. 110, No. 9, pp. 1959-1976, September 1984.

[60] David Z. Yankelevsky and Reinhardt, Hans W., "Response of Plain Concrete to Cyclic Tension", ACI Material Journal, PP. 365-373. September-October 1987.

[61] Ngo, D., and Scordelis, A. C., "Finite Element Analysis of Reinforced Concrete Beams", ACI Journal, 64(3), pp. 152-163, 1967.

[62] Rashid Y. R., "Ultimate Strength Analysis of Prestressed Concrete Pressure Vessels", Nuclear Engeering and Design, 7(4), pp. 334-344, 1968.

[63] Zdenek P. Bazant, "Instability, Ductility, and Size Effect in Strain-Softening Concrete", Journal of the Engineering Mechanics Division, Vol. 102, No. EM2, PP. 331-345, April 1976.

[64] Bazant Z. P. and Cedolin L., "Blunt Crackband Propagation in Finite Element Analysis", Journal of Engeering Mechanical Division ASCE, V. 105, pp. 297-315, 1979.

[65] Bazant, Z. P., and Oh, B. H., "Crack Band Theory for Fracture of Concrete", Material and Structures, RILEM, Paris, 16, pp. 155-177, 1983.

[66] Barlow, J., "Optimal stress location in finite element model", International Journal of Numerical Methods in Engineering.. 10(2), pp. 243-251, 1976.

[67] Hillerborg, A., Monder, M., and Peterson, P. E., "Analysis of Crack Fomation and Crack Growth in Concrete by Means of Fracture Mechanics and Finite Elements", Cem. Concr. Res. 6(6), pp. 773-782, 1976.

[68] Ramoda A. and Maso J. C., "The Effect of Loading History on Fracture Mechanics Properties of Concrete: Effects of Low-Frequency Loading", ACI Material Journal pp. 341-346, September-October 1988.

[69] Nallathambi, P., Karihaloo, B. L. and Heaton, B. S., "Effect of specimen and crack sizes, water/cement ratio and course aggregate texture upon fracture

toughness of concrete", Mag. of Concrete Research, Vol. 36, No. 129, pp. 227-236, 1984.

[70] Linda, D. Leibengood, and Darwin David and Robert H. Dodds, 'Parameters Affecting FE Analysis of Concrete Structures', Journal of Structural Engineering, Vol. 112, No. 2, pp. 326-341, February 1986.

[71] Vecchio, F., and Collins, M. P., "The Modified Compression-Field Theory for Reinforced Concrete Elements Subjected to Shear", ACI Journal, Mar-Apr. 1986

[72] Clerk, L. A. and Speirs, D. M., "Tension Stiffening in Reinforced Concrete Beams and Slabs Under Short Term Loads", Tech. Report. 42.521, Cement and Concrete Ass., London, 1987.

[73] Chang T. Y., Taniguchi H. and Chen W. F., "Nonlinear Finite element Analysis of Reinforced Concrete Panels", Journal of Structural Engineering, Vol. 113, No. 1, pp. 122-140, January, 1987.

[74] State-of-The Art Report, "Finite element analysis of reinforced concrete", Published by the American Society of Civil Engineers, 345 East 47th Street, New York, York 10017, 1982.

[75] Neville, A. M., "Properties of Concrete", 2nd Edition, John Wiley and Sons, New York 1973.

[76] Sandor Popovics, "Fracture Mechanism in Concrete: How much do we know?", Journal of American Society of Civil Engieering, Vol. 95, No. EM3, pp. 531-543, 1969.

[77] Fafitis and Shah, S. P., "Constitutive Model for Biaxial Cyclic Loading of Concrete", Journal of Engineering Mechanics, Vol. 112, No. 8, August 1986.

[78] Oral Buyukozturk and Tsi-Ming Tseng, "Concrete In Biaxial Compression", Journal of Structural Engineering, Vol. 110, No. 3, March 1984.

[79] Bresler, B. and Pister, K.S.C., 'Strength of Concrete under Combined Stresses', ACI Journal, pp. 321-345, September. 1958.

[80] Tasuji, M. E., Slate, F. O., and NIlson, A. H., "Stress-Strain Response and Fracture of Concrete in Biaxial Loading", Journal of the American Concrete

Institute, Vol. 75, No. 7, pp. 306-312, July 1978.

[81] Kent D. C. and Park, R., "Flexural Members With Confined Concrete", Journal of the Structural Division, Vol. 97, No. ST7, pp. 1969-1990, July 1971.

[82] Sargin, M., "Stress-Strain Relationships for Concrete and the Analysis of Structural Concrete Sections" , Solid Mechanics Division, University of Waterloo, Waterloo, Ontario, Canada, 1971.

[83] Kaar P. H., Hanson, N. W., and Capell, H. T., "Stress-Strain Characteristics of High Strength Concrete", ACI, SP 55-7, December 1978.

[84] Cope, R. J. and Rao, P. V., "Moment Redistribution in Skewed Slab Bridges", Procs. Inst. of Civil Engineers, Vol. 75, pp. 419-452, 1983.

[85] American Society of Civil Engineers, "Finite Element Analysis of Reinforced Concrete", New York, 1982.

[86] Pillips, D. V. and Zienkiewicz, O. C., "Finite Element Non-Linear Analysis of Concrete Structures", Procs. Inst. Civil Engineering., Part 2 Vol. 61, pp. 59-88, 1976.

[87] David Darwin and David A. Pecknold, "Analysis of R/C Shear Panels Under Cyclic Loading", Journal of Structural Division, Vol.102, No. ST2, February 1976.

[88] 10th Conference in, "Finite Element Analysis of Reinforced Concrete ", Civil Engineering of Tokyo University, Tokyo, Japan, July 1990.

[89] Scott B. D., Park R. and Priestly J. N., "Stress-Strain Behaviour of Concrete Confined by Overlapping Hoops at Low and High Strain Rates", ACI Journal pp. 13-27, January-February 1982

[90] Bazant, Z. P., and Oh, B., 'Strain Rate Effect in Rapid Nonlinear Triaxial Deformation of Concrete', Report No. 80-8/640s, Dept. of Civil Engineering, Northwestern University, Evanston, I11., August 1980.

[91] Galloway, R. G., "Strain-rate Effect in Plane Concrete Modelling", PhD. Thesis, University. of New Mexico, 1989.

[92] Narques, J. M. M. C., "Finite and Infinite Elements in Static and Dynamic Structural Analysis", PhD. Thesis, University. of Swansea, 1984.

[93] Liu, G. Q., "Non-Linear and Transient Finite Element Analysis of General Reinforced Concrete Plates and Shells.", Ph.D. Thesis, University of Wales, Swansea, C/Ph/84/85, 1985.

[94] Beshara, F. B. A., "Non-Linear Finite Element Analysis of Reinforced Concrete Structures Subjected to Blast Loading", PhD. Thesis, University. of London, 1991.

[95] Riad, H. L., "Finite Element Analysis of Reinforced Concrete Structures under Impact Loading", PhD. Thesis, Pensylvania State University. 1991.

[96] Nilsson, L., "Impact Loading on Concrete Structures. A Constitutive Modelling Finite Element Analysis and Experimental Study of Non-Linear wave Propagation", University. of Chalmers, Tech., 1979.

[97] Anil, K. Chopra and Chakrabarti, P., "The Earthquake Experience at Koyna Dam and Stresses in Concrete Gravity Dams", Earthquake Engineering and Structural Dynamics, Vol. 1, pp.151-164, 1972.

[98] Bicanic N. and Zienkiewicz O. C., "Constitutive Model for Concrete Under Dynamic Loading", Earthquake Engineering and Structural Dynamics, Vol. 11, pp. 689-710, 1983.

[99] Zienkiewicz, O. C., Hinton, E., Bicanic, N. and Fejzo, P., "Computational Models for The Transient Dynamic analysis of Concrete Dams", Dams and Earthquake, TTL, London, pp. 171-178, 1981.

[100] Liu, M. C. M. and Krempl, E., "A uniaxial Viscoplastic Model Based on Total Strain and Overstress", Journal of Mechanics and Physics of Solids, Vol. 27, pp.377-391, 1979.

[101] Damjanic F. B., "Reinforced Concrete Failure Prediction under both Static and Transient Conditions", PhD. Thesis, University. of Wales, Swabsea, 1983.

[102] liu, G. Q., "Non-Linear and Transient Finite Element Analysis of General Reinforced Concrete Plates and Shells.", PhD. Thesis, University. of Wales, Swansea, 1985.

[103] Famiyesin, O., O., "Modelling and Computational Aspects of the Non-Linear Finite Element Analysis of General Concrete Structures", PhD., Thesis, University of Wales, Swansea, 1990.

[104] Timoshenko, S. P., "Strength of Material", part 2, D. van Nostrand Co. 1966'

[105] Iwan, W. D., "On A Class of Models for the Yield Behaviour of Continuous and Composite Systems", ASME, pp. 612-617, December 1966.

[106] Bangash, Y., and England, G. L., 'The Influence of Thermal Creep on the Operational Behaviour of Complex Structures', Procs. International Conference on Fundamental Research on Creep and Shrinkage, Lausanne, Martinus Nijhoff, The Hague, 1982.

[107] Oh, B. H., 'Behaviour of Concrete Under Dynamic Tensile Loads', American Concrete Institute, Vol. 84, No. 7, Jan-Feb. 1987.

[108] Pozzo, E., 'Rheological Model of Concrete in the Dynamic Field', Mecca nica, pp. 143-158, June 1970.

[109] Surendra P. Shah, and Apostolos Fafitis, "Cyclic Loading of Spirally Reinforced Concrete", Journal of Structural Engineering, Vol. 109, NO. 7, July, 1983.

[110] Apostolos Fafitis and Surendra P. Shah, "Rheological Model for Cyclic Loading of Concrete", Journal of Structural Engineering, Vol. 110, N0. 9, PP. 2085-2101, September, 1984.

[111] Hinton E. and Owen D. R. J., "Finite Element Software For Plates and Shells", Pineridge Press, Swansea, U.K., 1984.

[112] Hinnerichs, T.D., 'Viscoplastic and Creep Crack Growth Analysis by the Finite Element Method', AWFAL-TR-80-4140, July 1981.

[113] Rajendran A. M., Bless S. J. and Dawicke D. S., "Determination of Tensile Flow Stress Beyond Necking At Very High Strain Rate", Experimental Mechanics, Aug. 1985.

[114] Bajer C., Bogacz R. and Bonthoux C. " Adaptive Space-Time Element in the Dynamic Elastic-Viscoplastic Problem", Computers and Structures, V. 39,

No. 5, pp. 415-423, 1991.

[115] Sheu C. H., Roeck G. De. Van Laethem M. and Geyskens P., "Application of The Substructuring Technique to Non-linea Dynamic Structural Analysis", Computers and Structures, V. 35, No. 5, pp. 593-601, 1990.

[116] Smith I. M. and Grifiths D. V., "Programming The Finite Element Method", Second edition, John Wiley and Sons 1988.

[117] Griffits, D. V., "Finite Element Analysis of Walls, Footings and Slopes", PhD. Thesis, University. of Manchester, 1980.

[118] Cormeau, I. C., "Numerical Stability in Quasi-Static Elasto/Visco-plasticity", International Journal for Numerical Methods In Engineering, Vol. 9, PP. 109-127, 1975.

[119] Perzyna P., "Fundamental Problems in Viscoplasticity", Institute of Basic Technical Research, Polish Academy of Science Warsaw, Poland. pp. 243-377, 1966.

[120] Perzyna, P., "The Constitutive Equations for Rate Sensitive Plastic Materials", Quarterly Journal of Applied Mathematics, Vol. 20, pp. 321-332, 1963.

[121] Wimal Suaris, and Chengsheng Ouyang and Viraj M. Fernando, 'Damage Model for Cyclic Loading of Concrete', Journal of Engineering Mechanics, Vol. 116, 5, pp. 1020-1035, May, 1990.

[122] Wimal Suaris and Surendra P. Shah, "Properties of Concrete Subjected to Impact", Journal of Structural Engineering, Vol. 109, No. 7, July 1983.

[123] Young Soo Chung, Christian Meyer, and Masanobu Shinzuka, "Modelling of Concrete Damage", ACI Structural Journal, Vol. 86, No. 3, pp. 259-271, May-June 1989.

[124] Soroushian P., Ki-Bong C. and Alahmad A., "Dynamic Constitutive Behaviour of Concrete", ACI Jounal, March-April pp. 251-259, 1986.

[125] Reji John and Surendra P. Shah, and Yeou-Shang Jenq, "A Fracture Mechanics Model to Predict the Rate Sensitivity of Mode 1 Fracture of Concrete", Cement and Concrete Research, Vol. 17, pp. 249-262, 1987.

[126] Syamonds, P. S., "Behaviour of Materials under Dynamic Loading" , Ed. N. J. Huffington, ASME, pp. 106-124, 1965.

[127] Owen, D. R. J. and Hinton E., "Finite Element In Plasticity: Theory and Practice", Pineridge Press, U.K., 1980.

[128] Albertini, C. and Montagnani, M., "Testing Techques Based on the Split Hopkinson, Mechanical Properties of High Rates of Stain, Conferences series No. 21, The Institute of Physics, London, 1974.

[129] Rao S. S., "The Finite Element Method in engineering", Pergamon Press ,1982.

[130] Hinton E. and Roger Owen, "Computational Modelling of Reinforced Concrete Structures", Department of Civil Engineering, University of Swansea, U.K. 1986.

[131] Zienkiewicz O. C. and Taylor R. L., "The Finite Element method", McGraw-Hill Book Company, 1989.

[132] Cook R. D., Malkus D. and Plesha M. E., 'Concepts and Applications of Finite Element Analysis', Third Edition, John Wiley and Sons, 1989.

[133] 'Finite Element analysis of reinforced concrete', Published by; The American Society of Civil Engineers, 345 East 47th Street, New York 10017, 1982.

[134] Zienkiewicz, O. C., Taylor, R. L., and Too, J. M., "Reduced Integration Technique in General Analysis of Plates and Sheels", International Journal for Numerical Methods in Engineering., Vol. 3, pp. 275-290, 1971.

[135] Malkus D. S. and Hughes T. J. R., "Mixed Finite Element Methods-Reduced and Selective Integration: A Unification of Concepts", Com. Meth. Appl. Mech. and Engng. V. 15, p.63-81, 1978.

[136] Bicanic, N. J. N., "Non-Linear Finite Element Transient Response of Concrete Structures", Ph.D. Thesis, University. of Wales, Swansea, 1979.

[137] Clough R. W., "Analysis of Structural Vibration and Response", in Recent Advances in Matrix Methods of Structural Analysis and Design (Eds. Gallagher R. H., Yamata Y. and Oden, J. T.) First U.S-Japan Seminar, 1969,

Alabama Press, pp.441-482, 1971.

[138] Hinton, E., Rock T., and Zienkiewicz O. C., "A Note on Mass Lumping and Related Processes in the Finite Element Method", Earthquake Engineering Dynamics, Vol. 4, pp. 245-249, 1976.

[139] Rock T., "Dynamic Analysis of Civil Engineering Structures", Ph.D. Thesis, University of Wales, Swansea, 1977.

[140] Clough R. W. and Mojtahedi, Soheil, "Earthquake Response Analysis Considering Non-Proportional Damping", Earthquake Engineering and Structural Dynamics, Vol. 4, pp. 489-496, 1976.

[141] Inman, Daniel J., "Vibration with control measurement and stability". Department of Mechanical and Aerospace Engineering State University of New York at Buffalo, Buffalo, New York, Prentice-Hall International, Inc., 1967.

[142] Thomson, William T., "Theory of Vibration With Applications", Second Edition, George Allen and Unwin LTd., 40 Museum Street, London, WCIA 1LU., 1966.

[143] Wilson E. L. and Penzien J., "Evaluation of Orthogonal Damping Matrices", International Journal For Methods in Engineering, Vol. 4, pp. 5-10, 1972.

[144] Clough R. C. and Joseph Penzien, "Dynamic of Structures", McGraw-Hill Book Company, 1975.

[145] Constantino C. J., "Finite Element Approach to Stress Wava Problems", 1967, in, Belytschko T., Chiapetta R. L. and Bartel H. D., "Efficient Rarge Scale Non-Linear Transient Analysis by Finite Elements", International Journal for Numerical Methods in Engineering, V. 10, pp. 579-596, 1976.

[146] Wilson E. L., "A Computer Program For the Dynamic Stress Analysis of Underground Structures ", International Journal for Numerical Methods in Engineering, V. 10, pp. 579-596, 1976.

[147] Farhoomand and Wilson E. L., "A Non-Linear Finite Element Code For Analysing the Blast Response Of Underground Structures", in, in, Belytschko T., Chiapetta R. L. and Bartel H. D., "Efficient Rarge Scale Non-Linear Transient

Analysis by Finite Elements", International Journal for Numerical Methods in Engineering, V. 10, pp. 579-596, 1976.

[148] Vashi K. M., "Computation of Seismic Response From Higher Frequency Modes.", Journal of Presure Vessel Technology, V. 103, pp.16-19, February 1981.

[149] Mackie R. I., "Improving Finite Element Prediction of Modes of Vibration", International Journal for Numerical Methods in Engineering, V. 33, pp. 333-344, 1992.

[150] Cronin D. C., "Eigenvalue and Eigenvector Determination For Non-Classically Damped Dynamic System", Computers and Structures, V. 36, No. 1, pp. 133-138, 1990.

[151] Lin., Jerry I., "An Element Eigenvalue Theorem and it's Application for Stable Time Steps", Computer Methods In Applied Mechanic and Engeering V. 73, pp. 283-294, 1989.

[152] Shrikrishna M. Kulkarni and Ng. S. F., "Inclusion of Higher Modes In the Analysis of Non-Classical Damped Systems", Earthquake Engineering and Structures, Vol. 21, pp. 543-549, 1992.

[153] Maddox N. R., "On The Number of Modes Necessary for Accurate Response and Resulting Forces in Dynamic Analyses", Journal of Applied Mechanics, pp. 516-517, July 1975

[154] Leger P. and Dussault S., "Non-Linear Seismic Response Analysis Using Vector Superposition Method", Earthquake Engineering and Structural Dynamics, V. 21, pp. 163-176, 1992.

[155] McDonald, Jr. P. H. Raleigh N. C., "Non-Linear Dynamic Coupling in a Beam Vibration", ASME, Applied Mechanics Division, No. 55-APM-23, pp. 573-578, January 1955.

[156] McDonald P. H., "Nonlinear Dynamic of A Beam ", Computers and Structures , V. 40, No. 5, pp. 1315-1320, 1991.

[157] Pui Shumb B. Shing and Stephen A. Mahin, "Computational Aspects of A seismic Performance Test Method Using On-Line Computer Control", Earthquake engineering and Structural Dynamics, Vol. 13, pp. 507-526, 1985.

[158] Lambert J. D., "Computational Methods in Ordinary Differential Equations", Wiley, 1973.

[159] Felippa C. A. and Park K. C.,"Computational Aspects of Time Integration Procedures In Structural Dynamics", Journal of Applied Mechanics, V. 45, pp. 595-602, September 1978.

[160] Tomasz Kucharski, "A Numerical Method For Dynamic Response Analysis of Discrete Systems", Computers and Structures, V. 28, No. 6, pp. 723-727, 1988.

[161] Newmark N. M., "A method of Computation For Structural Dynamics", ASCE EMS, pp.67-94, 1959.

[162] Warburton G. B., "Some recent Advances in Structural Vibrations", in 'A Survey of Direct Time Integration Methods In Computational Structural Dynamics', Edited by; Dokainish M. A. and Subbaraj K., Computers and Structures, V. 32 No. 6, pp. 1371-1386, 1989.

[163] Chan S. P., Cox H. L. and Benfield W. A.,"Transient Analysis of Forced Vibrations of Complex Structural Mechanical Systems", Journal of R. Aeronaut Soc. V. 66, pp. 457-460, 1962.

[164] Zienkiewicz O. C., "A New Look at The newmark, Houbolt and Other Time-stepping Formulae. A Weighted Residual approach", Civil Engineering. Department, Report C/R/273/76. University. of Wales, Swansea.

[165] Thomas R. and Gladwell I., "On The Properties of the Zienkiewicz Weighted Residual Methods", Numerical Analysis Report No. 27. Department of Mathematics, University.

[166] Wood W. L., Bossak, M. and Zienkiewicz O. C. 'An aplha modification of Newmark's method.', Int. J., Num. Meth. Eng. 15, pp. 1562-1566, 1891.

[167] Houbolt J. C., "A Recurrence Matrix Solution For The Dynamic response of Elastic Aircraft", Journal of R. Aeronaut. Sci. V. 17, pp. 540-550, 1950.

[168] Hans M. Hilber, Thomas J. R. Hughes and robert L. Taylor, "Improved Numerical Dissipation For Time Integration Algorithms In Structural Dynamics",

Earthquake Engineering and Structural Dynamics, V. 5, pp. 283-292, 1977.

[169] Hoff C. and Pahl P. J., "Development of an Implicit Method With Numerical Dissipation From A Generalized Single-Step Algorithm for Structural Dynamics", Computer Methods In Applied Mechanic and Engeering V. 67, pp. 367-385, 1988.

[170] Krieg R. D., "Unconditionally Stability in Numerical time integration Methods", Journal of Applied Mechanics, V. 40, pp. 417-420, 1973.

[171] Warburton G. B., "Some Recent Advances in Structural Vibrations", in 'A Survey of Direct Time-Integration Methods in Computational Structural Dynamics-I Explicit Methods' edited by; Dokainish M. A. and Subbaraj K., Computers and Structures, V. 22, pp. 1371-1386, 1989.

[172] Belystschko T., "A Survey of Numerical Methods and Computer Programs for Dynamic Structural Analysis", Nucl. Engng. V. 37, pp. 23-34, 1976.

[173] Belyischko Ted and Engelmann, Bruce E., "Explicit Time integration With Enhanced Stability For Structural Dynamics", Computer and Structures, V. 29, No. 4, pp. 587-590, 1988.

[174] Hamming R. W., "Numerical Methods For Scientists and Engineers", McGraw-Hill Book Company, London, 1962.

[175] Philips G. M. and Taylor P. J., "Theory and Applications of Numerical Analysis", Academic Press, London and New York, 1973.

[176] Richard L. Burden and Douglus J. Faires., "Numerical Analysis", Third Edition, Prindle, Weber and Schmidt, Boston., 1985.

[177] Thomas J. R. Heghes, Pister Karl S. and Robert L. Taylor, "Implicit-Explicit Finite Elements in Non-Linear Transient Analysis", Computer Methods in Applied Mechanics and Engineering, 17/18 pp. 159-182, 1979.

[178] Hughes T. J. R. and Liu W. K., "Implicit-Explicit Finite Elements in Transient Analysis: Stability Theory", ASME Journal of Applied Mechanics Division, V. 45, pp. 371-374, June 1978.

[179] Clough R. W., "The Finite Element In Plane Stress Analysis", Procs. ASCE Conf. On Electronic Computation, Pittsburgh, Pa., September. 1960.

[180] Bathe K. J.,"An Assessment of Current Finite Element Analysis of Non-Linear Problems In Solid Mechanics", in Numerical Solution of Partial Differential Equations, 111, B. Hubbard (ed.), Academic Press, pp. 117-164, 1976.

[181] Nilson, A. H., 'Nonlinear Analysis of reinforced Concrete by the Finite Element Method', ACI Journal, V. 65, pp. 757-766, 1968.

[182] Matthies H. and Strang G., "The Solution of Nonlinear Finite Element Equations", 1JUME, 14 pp. 1613-1626, 1979.

[183] Reed M. B., "Newton-Like Methods With Limited Storage, for the Solution of Elasto-Viscoplasticity", International Journal for Numerical Methods In Engineering, Vol. 35, pp. 223-240, 1992.

[184] Gopalakrishna H. S. and Lowell T., "Newton-Raphson Procedure for the Sensitivity Analysis of Nonlinear Structural Behaviour", Computers and Structures, V. 30, No. 6, pp. 1263-1273, 1988.

[185] Chen C. N., "An Acceleration Method in Elasto-Plastic Finite Element Computation", Computers and Structures V.44, No. 1/2, pp. 125-131, 1992.

[186] Liu Wing Kam, Ted Belytschko and Zhang Y. F., "Implementation and Accuracy of Mixed-Time Implicit-Explicit Methods for Structural Dynamics", Computer and Structures, V. 19, No. 4, pp. 521-530, 1984.

[187] Argyris J. M. Scharpf D. W., "Methods of Elasto-Plastic Analysis", ISD, ISSC Symp. on Finite Element Tech. Stuttgart, 1969.

[188] Phillips G. M., and Taylor P. J., "Theory and Applications of Numerical Analysis", Academic Press, London and New York, 1973.

[189] Bathe K. J. and Wilson E. L., "Numerical Methods In Finite Element Analysis", Prentice Hall, 1976.

[190] Mullen R. and Belytschko T., "An Analysis of An Unconditionally Stable Explicit Method", Computers and Structures, V. 16, pp. 691-696, 1983.

[191] Belytschko R. and Mullen R., "Explicit Integration of Pronlems in Finite Elements in Non-Linear Mechanics", in 'A Survey of Direct Time Integration Methods In Computational Structural Dynamics', Edited by; Dokainish M. A. and Subbaraj K., Computers and Structures, V. 32 No. 6, pp. 1371-1386, 1989.

[192] Cryer C. W., "A New Class of Highly Stable Methods: A_0 Methods", in "Some Transient and Coupled Problems - A State-of Art-Review", Wood W. L.,(edt.), of "Numerical Methods for Transient and Coupled Problems", John Wiley and Sons Ltd. 1987.

[193] Dahlquist G. G., "A Special Stability Problem for Linear Multistep Methods",in, "Some Transient and Coupled Problems - A State-of Art-Review", Wood W. L.,(edt.), of "Numerical Methods for Transient and Coupled Problems", John Wiley and Sons Ltd. pp. 993-1001, 1987.

[194] Gordon R. Johnson and Howard I Epstein, "Short Duration Analytical Earthquake", Journal of the Structural Division, Vol. 102, No. ST5, May 1975.

[195] Zienkiewicz O. C., Bicanic N. and Fejzo R. "Substitute short duration earthquake accelelograms for non-linear analysis", Journal of Dams and Earthquake, TTL, London, pp. 17-21, 1981.